



# ASIAN-PACIFIC ASTRONOMY

*Proceedings of the 6th Asian-Pacific Regional  
Meeting on Astronomy of the International  
Astronomical Union*

**Editors**

**V. K. KAPAHI**

**N. K. DADHICH ★ G. SWARUP ★ J. V. NARLIKAR**

**A Supplement to  
*Journal of Astrophysics and Astronomy***



**1995**

**INDIAN ACADEMY OF SCIENCES**

**Bangalore 560 080**

© 1995 by the Indian Academy of Sciences  
A Supplement to *Journal of Astrophysics and Astronomy*, Vol. 16, 1995

**Phototypeset at Thomson Press (India) Ltd., New Delhi and printed  
at Lotus Printers, Bangalore - 560 044 for the Indian Academy of Sciences.**

# Contents

Preface.....	xiii
--------------	------

## Invited Discourses

1. The Beauty and Danger of Comets and Asteroids (Vainu Bappu Lecture) .....	<b>T. Gehrels</b> 1
2. Meghnad Saha's Influence in Astrophysics (Meghnad Saha Lecture) .....	<b>D. DeVorkin</b> 35

★★★★★

## The Early Universe and Structure Formation

3. Inflation and Cosmic No-hair Conjecture (Invited Talk).....	<b>K. Sato</b> 37
4. Cosmology Today: Models and Constraints (Invited Talk).....	<b>T. Padmanabhan</b> 47
5. Confrontation of a Double Inflationary Cosmological Model with Ob- servations of the Large Scale Structure.....	<b>J. P. Mücke &amp; S. Gottlöber</b> 59
6. Cosmological Solutions in Two-Component Nonlinear Sigma Model .....	<b>S. V. Chervon</b> 65
7. Perturbative Growth of Cosmological Correlations.....	<b>S. Bharadwaj</b> 69
8. The Formation and Evolution of Voids in the Universe.....	<b>V. Sahni, B. S. Sathyaprakash &amp; S. F. Shandarin</b> 73
9. Nonlinear Evolution of Density Perturbations.....	<b>J. S. Bagla &amp; T. Padmanabhan</b> 77
10. Neutral Hydrogen at High Redshifts as a Probe of Structure Formation .....	<b>A. Kumar, K. Subramanian &amp; T. Padmanabhan</b> 83
11. Quasi Steady State Cosmology.....	<b>J. V. Narlikar, F. Hoyle &amp; G. Burbidge</b> 87
12. On Non-Singular Cosmological Models.....	<b>N. Dadhich, R. Tikekar &amp; L. K. Patel</b> 93



**Abstracts**

13. Nonexistence of Nonstatic Sourceless Abelian Gauge Strings in a Robertson-Walker Universe with $k = 1$ .....	<b>D. Bhattacharyya &amp; S. Banerji</b>	99
14. Some Exact Solutions in Bianchi III and VI <sub>0</sub> String Cosmology.....	<b>R. Tikekar &amp; L. K. Patel</b>	99
15. A Rigorous Proof of the Inflationary Spectrum.....	<b>Jai chan Hwang</b>	100



**Observational Cosmology**

16. The Lyman Alpha Absorbers Probes of the High Redshift Universe (Invited Talk).....	<b>R. W. Hunstead, D. P. Mar &amp; M. Pettini</b>	103
17. Radio Observations of the Anisotropy in the Cosmic Microwave Background (Invited Talk).....	<b>R. Subrahmanyam</b>	111
18. Faint Blue Galaxies and Gravitational Lensing by Clusters of Galaxies (Invited Talk).....	<b>P. Guhathakurta</b>	119
19. Cosmological Evolution of Linear Sizes and the Unification of Quasars and Radio Galaxies.....	<b>V. K. Kapahi, R. M. Athreya, C. R. Subrahmanya, R. W. Hunstead, J. C. Baker, P. J. McCarthy &amp; W. van Breugel</b>	125
20. A New Population of Gravitationally Lensed Radio Arcs in Distant Abell Clusters.....	<b>J. Bagchi &amp; V. K. Kapahi</b>	131
21. Chemical Evolution of High Redshift Galaxies.....	<b>P. Khare &amp; N. C. Rana</b>	137
22. Cross-correlation Analysis of $\gamma$ -ray Burst Time Profiles.....	<b>P. D. Gupta &amp; A. N. Ramaprakash</b>	141

**Abstracts**

23. Radio Source Counts at 232 MHz.....	<b>Z. Xizhen</b>	145
24. On the Reality of the Physical Association Between QSOs and Galaxies .....	<b>A. K. Sapre &amp; V. D. Mishra</b>	146
25. The Quasar-Galaxy Pair 3C 232/NGC 3067.....	<b>P. K. Das</b>	147
26. Dark Matter Around Binary Galaxies: Disruption of Shells and Formation of Flows.....	<b>J. Anosova &amp; B. Anandarao</b>	147
27. Cosmological Limits on the Detection Range of the TeV $\gamma$ -ray Telescope 'TACTIC'.....	<b>A. K. Mitra &amp; C. L. Bhat</b>	148
28. Assessing Fluctuations Using Small Samples.....	<b>D. G. Banhatti</b>	149

29. Large Scale Structure of the Universe: Cluster-void Fine Structure .....	<b>J. Anosova, S. Iyer &amp; R. K. Varma</b>	149
30. Cosmographic Methods.....	<b>D. G. Banhatti</b>	150

★★★★★

## Active Galactic Nuclei

31. Unified Schemes for Radio-loud Active Galactic Nuclei (Invited Talk) .....	<b>Gopal-Krishna</b>	153
32. Neutral Hydrogen 21 cm Quasar Absorption Line Systems (Invited Talk).....	<b>C. L. Carilli</b>	163
33. Accretion Disks in Quasars and Active Galactic Nuclei (Invited talk) .....	<b>P. Ghosh</b>	171
34. Halo Model for Low and Intermediate Redshift, Heavy Element, Quasar Absorption Lines.....	<b>P. Khare &amp; R. Srianand</b>	181
35. Aspect Dependent Optical Continuum Emission in Radio Quasars..... .....	<b>J. C. Baker, R. W. Hunstead, V. K. Kapahi &amp; C. R. Subrahmanya</b>	185
36. Anisotropic Emissions from Blazars.....	<b>K. K. Ghosh &amp; S. Soundararajaperumal</b>	189
37. Ionized Gas in Elliptical Galaxies.....	<b>K. P. Singh, T. P. Prabhu, A. K. Kembhavi &amp; P. N. Bhat</b>	195

## Abstracts

38. A Head-Tail Source Found with Miyun Synthesis Radio Telescope .... .....	<b>Z. Xizhen, T. A. Th. Spoelstra &amp; W. Yumin</b>	201
39. A VLA 20 and 90 centimeter Radio Survey of Distant Abell Clusters with Central cD Galaxies.....	<b>J. Bagchi &amp; V. K. Kapahi</b>	202
40. Variability in Southern BL LAC Objects at cm Wavelengths..... .....	<b>Don Bramwell</b>	203
41. Multi-Waveband Studies of the Molonglo 1-JY Sample of Radio Gala- xies.....	<b>V. K. Kapahi, R. M. Athreya, C. R. Subrahmanya, P. J. McCarthy &amp; W. van Breugel</b>	203
42. Twin Jets in an FR II Radio Galaxy.....	<b>L. Saripalli, R. Subrahmanyan &amp; R. Hunstead</b>	204
43. Compact Groups of Galaxies: Interactions and Radio Emission..... .....	<b>V. R. Venugopal, K. S. V. S. Narasimhan &amp; S. M. Alladin</b>	204
44. A Jet Model of Plasma Turbulence Acceleration for AGNs..... .....	<b>Tong Yi &amp; Li Qingkang</b>	204

45. BVRI Imaging of the Disturbed Spiral Galaxy NGC 2701 .....	<b>S. K. Pandey, A. K. Kembhavi &amp; V. Mohan</b>	205
46. Multicolour Investigations of Shells, Dust and Other Features in Elliptical Galaxies.....	<b>N. Thakur, D. Sahu, S. K. Pandey &amp; A. K. Kembhavi</b>	205
47. Surface Photometry of the Elliptical Galaxies NGC 1600 and NGC 507 .....	<b>A. Mahabal, A. K. Kembhavi, K. P. Singh &amp; R. Green</b>	206
48. Surface Photometry of Seyfert Galaxies NGC 2992, NGC 3227 and NGC 7172.....	<b>G. C. Anupama, A. K. Kembhavi, M. Elvis &amp; R. Edelson</b>	206
49. Detection of Microvariability in Polarization in a BL LAC Object OJ287.....	<b>M. R. Deshpande &amp; U. C. Joshi</b>	206
50. Dynamics of Stellar Content of Hot-Spot Regions of Active Galaxies .....	<b>V. Korchagin, A. K. Kembhavi, D. Mayya &amp; T. Prabhu</b>	207
51. Quasar-Galaxy Interactions: A Possible Mechanism for Formation of cD-Galaxies and Gravitational Lenses.....	<b>J. Anosova &amp; M. K. Deshpande</b>	207
52. The Merger Time of Interacting Galaxies – Its Dependence on Energy and Angular Momentum.....	<b>G. M. Ballabh, K. S. V. S. Narasimhan &amp; S. M. Alladin</b>	208



## Pulsars

53. New Lessons from Old Pulsars (Invited Talk).....	<b>M. Bailes</b>	209
54. Pulsars in Globular Clusters (Invited Talk).....	<b>A. Ray</b>	215
55. Pulsar Observations with the GMRT (Invited Talk).....	<b>A. A. Deshpande</b>	225
56. Evolution of the Magnetic Fields of Neutron Stars in Low-mass Binary Systems.....	<b>M Jahan Miri &amp; D. Bhattacharya</b>	231
57. Millisecond Pulsars as Sources of $\gamma$ -rays for Globular Clusters and Galactic Background.....	<b>V. B. Bhatia, S. Mishra &amp; N. Panchapakesan</b>	235
58. A Digital Signal Pre-processor for Pulsar Search using Ooty Radio Telescope.....	<b>P. S. Ramkumar, T. Prabu, M. Girimaji &amp; G. Markandeyulu</b>	239
59. Coherent Dedispersion System for GMRT.....	<b>S. Izhak, Y. Gupta &amp; C. R. Subrahmanya</b>	243
60. Pulsar Observations with the 512 Channel Correlator at ORT.....	<b>M. Vivekanand</b>	247
61. Evolution of the Magnetic Field of an Accreting Neutron Star.....	<b>S. Konar, D. Bhattacharya &amp; V. Urpin</b>	249

**Abstracts**

62. Refractive Interstellar Scintillation Studies of Pulsars.....	251
..... <b>Y. Gupta, B. J. Rickett, R. Bhat &amp; M. Vivekanand</b>	
63. Pulsational Mode and Detection of Gravitational Wave Source.....	251
..... <b>R. K. Parui</b>	
64. A Search for TEV $\gamma$ -rays from PSR 0355 + 54.....	252
..... <b>V. K. Senecha, C. L. Bhat, R. C. Rannot, R. K. Kaul,</b>	
..... <b>M. L. Sapru, A. K. Tickoo &amp; H. S. Rawat</b>	
65. Unique Observations of PSR 0950 + 08 and Possible Terrestrial Effects	253
..... <b>M. R. Deshpande, H. O. Vats, P. Janardhan, A. D. Bobra,</b>	
..... <b>H. Chandra &amp; G. D. Vyas</b>	

**Interstellar and Interplanetary Medium**

66. Mass Loss in AGB Stars – Recent Observational Developments.....	255
..... <b>R. Sahai</b>	
67. Cold, Warm and Hot Gas in the Merged Galaxy-Pair NGC 7252.....	259
..... <b>P. Guhathakurta, J. E. Hibbard, J. H. Van Gorkom &amp;</b>	
..... <b>F. Schweizer</b>	
68. Molecular, Atomic and Ionized Gas towards Cas-A.....	261
..... <b>N. G. Kantharia, K. R. Anantharamaiah, W. C. Erickson &amp;</b>	
..... <b>H. E. Payne</b>	
69. Radio Synthesis Imaging of Scatter-broadening at Small Solar Elongations.....	265
..... <b>K. R. Anantharamaiah, P. Gothoskar &amp; T. J. Cornwell</b>	
70. Ionized Gas in the Inner Galaxy.....	269
..... <b>K. R. Anantharamaiah, F. J. Lockman, N. G. Kantharia &amp;</b>	
..... <b>A. D. Roshi</b>	
71. Radio Recombination Lines from External Galaxies.....	273
..... <b>K. R. Anantharamaiah, J. H. Zhao, W. M. Goss &amp; F. Viallefond</b>	
72. The Interstellar Medium Surrounding the Vela Supernova Remnant	275
..... <b>T. P. Saravanan, A. A. Deshpande &amp; G. Srinivasan</b>	
73. Bright-rimmed Molecular Clouds Near Massive Stars.....	277
..... <b>C. Indrani &amp; T. K. Sridharan</b>	
74. Star Formation in Giant Extragalactic HII Regions.....	281
..... <b>Y. D. Mayya</b>	
75. EGRET Observations of the Galactic Diffuse Gamma Ray Emission	285
..... <b>P. Sreekumar</b>	
76. Short Time Scale Variability in the Solar Wind.....	289
..... <b>P. Gothoskar &amp; A. P. Rao</b>	

**Abstracts**

77. Recombination Line Observations of the Galactic Centre Region near 325 MHz.....	<b>A. Roshi, T. Velusamy &amp; K. R. Anantharamaiah</b>	293
78. Structure in Interstellar HI in the Directions of PSR 1557-50 and PSR 1641-45.....	<b>A. A. Deshpande, W. E. Wilson, E. R. Davis, D. McConnell &amp; P. M. McCulloch</b>	293
79. Non Equilibrium Ionization and Elemental Abundances in Two Supernova Remnants.....	<b>K. P. Singh &amp; J. P. Hughes</b>	294
80. Instability of Gravitating Grainy Plasma.....	<b>B. Kaur &amp; G. L. Kalra</b>	294
81. The Neutral Hydrogen Subsystem in the Milky Way: The Movements and the Structure.....	<b>I. V. Petrovskaya</b>	295
82. The Effect of Time Dependent Tidal Forces on Molecular Clouds.....	<b>M. Das and C. J. Jog</b>	295
83. Dynamics of Clumps in Molecular Clouds.....	<b>U. Gorti, H. C. Bhatt &amp; I. P. Williams</b>	296
84. Cosmic Rays and Interstellar Medium.....	<b>S. Biswas</b>	296
85. Interplanetary Scintillation Measurements and Deformation of Heliospheric Current Sheet.....	<b>B. Bala &amp; S. R. P. Nayar</b>	297
86. Effects of Two Types of High Speed Solar Wind Stream on Cosmic Ray Intensity and on Geomagnetic Disturbances.....	<b>P. K. Shrivastava &amp; R. P. Shukla</b>	297
87. A 327 MHz Interplanetary Scintillation Survey of Radio Sources over 6 Steradian.....	<b>V. Balasubramanian, P. Janardhan &amp; S. Ananthakrishnan</b>	298
88. Estimation of Solar Coronal Plasma Density by IPS Observations.....	<b>H. O. Vats &amp; M. R. Deshpande</b>	298
89. The Geminga Supernova and the High and Intermediate Velocity Neutral Hydrogen Concentrations.....	<b>V. R. Venugopal</b>	299
90. Infrared Emission from HII Regions: An Analysis of IRAS Data.....	<b>D. B. Vaidya &amp; B. G. Anandarao</b>	299

★★★★★

**Stars and Stellar Physics**

91. Mass Loss from Wolf-Rayet Stars (Invited Talk).....	<b>B. Hidayat</b>	301
92. Evidence for Mass Loss in Close Binaries and its Implications (Invited Talk).....	<b>A. H. Batten</b>	309

93. Lithium Abundances as Clues to Stellar Mixing.....	<b>S. Balachandran</b>	313
94. SN 1993J in M 81: Photometry and Spectrophotometry.....	<b>T. P. Prabhu</b>	317
95. Observations of SN 1993j in BAO.....	<b>Li Qibin &amp; Wang Lifan</b>	323
96. Emission Line Spectrum of the Hot R Cr B Type Star MV Sgr.....	<b>G. Pandey, N. K. Rao &amp; D. L. Lambert</b>	327

## ***Abstracts***

97. Infrared Spectroscopy of Accretion Disks in Young Stars.....	<b>J. S. Carr &amp; A. T. Tokunaga</b>	331
98. Polarization Variability in Isolated T Tauri Stars.....	<b>M. V. Mekkaden</b>	332
99. Angular Diameter of Carbon Star TX Piscium from Lunar Occultation Observations in the Near Infrared.....	<b>S. Ragland, T. Chandrasekhar &amp; N. M. Ashok</b>	332
100. CCD Photometry of the Young Open Cluster NGC 366.....	<b>A. K. Pandey, B. C. Bhatt, V. Mohan, D. C. Paliwal &amp; H. S. Mahra</b>	333
101. Theoretical Models of Starspots.....	<b>J. S. Park &amp; H. S. Yun</b>	334
102. Effects of Differential Rotation and Tidal Distortion on the Periods of Small Adiabatic Oscillations of Stellar Models.....	<b>V. P. Singh &amp; M. K. Sharma</b>	336
103. Stochastic Radial Pulsation of Gaseous Masses.....	<b>A. K. Chaudhary, M. K. Das, R. K. Tavakol &amp; V. B. Bhatia</b>	336
104. Non-Linear Stability of a Cluster of Stars Sharing Galactic Rotation .....	<b>K. B. Bhatnagar &amp; P. P. Hallan</b>	338
105. Some Unidentified Features in the IRAS LRS Spectra of Cool Peculiar Stars .....	<b>M. S. Vardya &amp; K. S. Krishna Swamy</b>	339
106. Short Time-Scale Monitoring of SiO Maser Sources.....	<b>A. Joseph &amp; C. S. Shukre</b>	340
107. Coulomb Excitation and Production of P-elements.....	<b>H. L. Duorah &amp; K. Duorah</b>	341



## **Sun and the Solar System**

108. Probing the Solar Interior (Invited Talk).....	<b>S. M. Chitre</b>	343
109. Physics of the Solar Corona and Flares Revealed by <i>Yohkoh</i> (Invited Talk).....	<b>T. Kosugi</b>	359

110. Solar Flare Observations with the <i>Yohkoh</i> Hard X-ray Telescope (Invited Talk).....	<b>T. Kosugi</b>	367
111. Dynamical Structures of Uranian Rings.....	<b>Y. Kozai</b>	373
112. Structures in Saturn's Magnetosphere.....	<b>J. C. Bhattacharyya</b>	377

### ***Abstracts***

113. A Study of Active Region Magnetic Field Structure Using VLA-Radio, <i>Yohkoh</i> X-ray and Mess-Optical Observations.....	<b>N. Gopalswamy</b>	381
114. H $\alpha$ Intensity Oscillations Observed in Solar Flares.....	<b>R. Jain &amp; S. C. Tripathy</b>	381
115. 2-Dimensional Velocity Field Measurement of Eruptive Prominence Observed on January 14, 1993.....	<b>A. Bhatnagar &amp; S. C. Tripathy</b>	382
116. Three-Dimensional Velocity Structure of Surge and Quiescent Prominences.....	<b>N. Srivastava &amp; S. K. Mathew</b>	382
117. Direct Observational Evidence for the Heating of the Solar Chromosphere .....	<b>R. Kariyappa, K. R. Sivaraman &amp; M. N. Anandaram</b>	383
118. Spectroscopic Analysis of Prominence H $\alpha$ CaII H & K and HeI 10830 Lines.....	<b>Y. D. Park, H. S. Yun &amp; K. Ichimoto</b>	384
119. Solar Observations using Lithium Niobate Fabry-Perot Etalon.....	<b>A. Bhatnagar, C. Debi Prasad &amp; S. K. Mathew</b>	384
120. Study of Solar Flares Observed in Hard X-ray and Soft X-ray Emissions .....	<b>V. K. Verma &amp; M. C. Pande</b>	385
121. Eruptive Prominence Associated with Limb Flare of 25 January 1991 .....	<b>Wahab Uddin &amp; V. K. Verma</b>	385
122. Eruption of Helical Prominence of December 15, 1992.....	<b>Wahab Uddin, V. P. Gaur &amp; M. C. Pande</b>	386
123. Eruption of a Large Quiescent Prominence on January 14, 1993.....	<b>Wahab Uddin &amp; K. R. Bondal</b>	386
124. Recurrent Surge Activity from Active Region NOAA 6368.....	<b>Wahab Uddin, V. K. Verma &amp; M. C. Pande</b>	387
125. Mass Transfer and Surge Activity of 14 May 1993.....	<b>V. K. Verma &amp; Wahab Uddin</b>	387
126. On the Periodicity of Solar Wind Phenomena.....	<b>V. K. Verma &amp; G. C. Joshi</b>	387
127. Coronal Mass Ejections and the Critical Ionization Velocity Phenomenon .....	<b>E. Golbraikh, M. Filippov &amp; R. Steinitz</b>	388
128. Masked Coronal Mass Ejections: An Attempt to Demask Them.....	<b>M. Filippov, E. Golbraikh &amp; R. Steinitz</b>	388

129. Diamagnetic Abundance Differentiation.....	<b>R. Steinitz &amp; E. Kunoff</b>	389
130. Misconceptions Concerning the Vanishing Average of the Diamagnetic Effect.....	<b>R. Steinitz</b>	389
131. Diamagnetic Acceleration of the Solar Wind....	<b>B. Sekeles &amp; R. Steinitz</b>	390
132. Energy Transport to the Solar Corona by Magnetic Kink Waves.....	<b>A. R. Choudhuri, M. Dikpati &amp; D. Banerjee</b>	390
133. The Evolution of Weak Magnetic Fields of the Sun in Relation to Dynamo Theory.....	<b>M. Dikpati &amp; A. R. Choudhuri</b>	391
134. Magneto-Convection in Sunspot Penumbra.....	<b>S. G. Tagare &amp; P. Murali</b>	391
135. Helioseismic Determination of Sound Speed in the Sun.....	<b>S. Basu &amp; H. M. Antia</b>	392
136. On the Relation of AAA Asteroids and Comets.....	<b>S. Siregar</b>	392
137. Formation and Regression of the Martian North Polar Cap in 1992-1993 from Image Processed CCD and Photographic Images and Drawings.....	<b>K. Iwasaki, S. M. Larson, E. Panjaitan, I. Radiman T. Akabane &amp; S. Ebisawa</b>	393
138. On the Dust Torus around the Orbit of Phobos.....	<b>A. V. Krivov &amp; V. B. Titov</b>	394
139. Imaging Polarimetry of Comet Austin.....	<b>U. C. Joshi, J. S. Chauhan, M. R. Deshpande, A. K. Sen &amp; A. K. Bhatnagar</b>	395
140. Physical Structure and Stability of Cometary Nuclei.....	<b>B. S. Sandhu &amp; M. Sölc</b>	395



## Instrumentation

141. New Observing Facilities and Recent Progress in China (Invited Talk).....	<b>Ye Shuhua</b>	397
142. Plans for a Large Indian Telescope (Invited Talk).....	<b>S. N. Tandon</b>	403
143. Subaru: An 8-m Optical/IR Telescope Project (Invited Talk).....	<b>N. Kaifu</b>	411
144. Concept and Status of the ESO Very Large Telescope Project (Invited Talk).....	<b>D. Enard</b>	419
145. The Giant Metrewave Radio Telescope (GMRT) (Invited Talk).....	<b>S. Ananthakrishnan</b>	427



146. New Nobeyama Radioheliograph (Invited Talk).....	<b>H. Nakajima <i>et al.</i></b>	437
---	----------------------------------	-----

## ***Abstracts***

147. Project GRACE – A New Ground-based Facility for Gamma-ray Astrophysics Cerenkov Experiments.....	<b>C. L. Bhat, R. Koul, R. C. Rannot, M. L. Sapru &amp; A. K Tickoo</b>	443
148. 1.2 m Infrared Telescope at Gurushikar.....	<b>M. R. Deshpande</b>	444
149. Lucifers: A Photoelectric Radial-Velocity Spectrometer at Mt John University Observatory.....	<b>J. B. Hearnshaw, L. C. Watson &amp; D. M. Ward</b>	444
150. High Angular Resolution Imaging using a Rotational Shear Interferometer.....	<b>J. K. Rajagopal &amp; N. Udayashankar</b>	445
151. Image Restoration by Blind Iterative Deconvolution: Results Obtained from VBT.....	<b>S. K. Saha &amp; P. Venkatakrishnan</b>	446
152. An Imaging Polarimeter for Astronomical Observations.....	<b>A. K. Sen &amp; S. N. Tandon</b>	446
153. Sheikh Tahir Astronomical Centre: The Birth of an Idea and Beyond.....	<b>M. Ilyas</b>	447
154. The Mauritius Radio Telescope.....	<b>K. Golap, N. H. Issur, R. Somanah, R. G. Dodson, M. Modgekar, S. Sachdev, N. Udayashankar &amp; Ch. V. Sastry</b>	447
155. Gauribidanur Radio Heliograph.....	<b>K. R. Subramanian, M. S. Sundara Rajan, R. Ramesh &amp; Ch. V. Sastry</b>	448
156. IPS Radio Telescopes at Thaltej and Rajkot.....	<b>H. O. Vats, M. R. Deshpande, A. D. Bobra, K. S. Lali, N. S. Nirman &amp; P. Venat</b>	449
157. Prime Focus Feeds for GMRT Antennas.....	<b>G. Sankarasubramanian, G. Swarup, S. Ananthakrishnan, M. R. Sankararaman, S. Suresh Kumar &amp; S. M. Izhak</b>	450
158. Low Noise Multi-Frequency Front-ends for the GMRT.....	<b>A. Praveen Kumar, A. C. Chiplunkar, S. Nayak &amp; N. G. Sreedharan</b>	451
159. Local Oscillator, IF and Baseband Systems for GMRT.....	<b>T. L. Venkatasubramani, B. Ajithkumar, R. Somasekhar, K. S. Saini &amp; G. Chattopadhyay</b>	451
160. Analog Optical Fibre Network for GMRT.....	<b>D. S. Sivaraj, M. R. Sankararaman &amp; S. Suresh Kumar</b>	452
161. Control and Monitor System for GMRT.....	<b>R. Balasubramanian, C. Asodekar &amp; A. Ramakrishna</b>	452

162. The Correlator System for GMRT.....	
.....C. R. Subrahmanya, A. Dutta, V. M. Tatke, U. S. Puranik, A. Dixit & S. Joardar	453

★★★★★

## Astronomy in Antarctica

163. Discussion Meeting on Astronomy in Antarctica.....	R. D. Cannon	455
164. Astronomy in Antarctica -- India's First Attempt.....	G. S. D. Babu	457
165. On the Possibility of 200 $\mu$ m Observations in Antarctica.....	G. B. Sholomitskii	461

★★★★★

## Regional Co-operation in Astronomy

166. Panel Discussion.....		465
----------------------------	--	-----

★★★★★

## Teaching of Astronomy

167. Star Watching Programme: An Effective Way to Teach the Importance of Astronomy.....	S. Isobe	473
---	----------	-----

★★★★★

Author Index.....	475
-------------------	-----



# Preface

The 6th Asian-Pacific Regional Meeting on Astronomy of the International Astronomical Union was held during 16th – 20th August, 1993 at the Inter-University Centre for Astronomy and Astrophysics (IUCAA) in Pune, India. Jointly hosted by IUCAA and the National Centre for Radio Astrophysics (NCRA) of the Tata Institute of Fundamental Research, the meeting was attended by over 300 astronomers and astrophysicists from 20 countries; about 200 of them from the host country.

The scientific programme of the meeting was divided into seven broad areas covering a wide spectrum of topics in astrophysics. Plenary sessions consisting mainly of invited talks on various themes were held in the forenoons and two parallel workshop sessions were generally held in the afternoons. The workshops consisted of a mixture of invited and contributed papers as well as poster presentations. Apart from the scientific workshops, there were discussion meetings on astronomy in Antarctica; regional co-operation in astronomy and on the teaching of astronomy. Other important scientific events included invited discourses to commemorate two well-known Indian names in astronomy and astrophysics, viz., Meghnad Saha and Vainu Bappu. The Meghnad Saha centenary lecture was delivered by D. DeVorkin, titled '*Saha's Influence on Modern American Astrophysics*', and the Vainu Bappu lecture was delivered by Tom Gehrels on the topic '*The Beauty and Danger of Comets and Asteroids*'.

We are indebted to the authors of all the papers presented at the Meeting the proceedings of which comprise this book. A large fraction of the poster papers is included in the proceedings though only in the form of abstracts. We are thankful to the co-ordinators of different workshops for their help in reviewing and selecting the posters for inclusion in the proceedings.

We would also like to acknowledge the financial support provided for the meeting by the International Astronomical Union, the Third World Academy of Sciences, the University Grants Commission and the Department of Science and Technology of the Government of India.

Our grateful thanks to the **Indian Academy of Sciences** and the editorial board of the *Journal of Astrophysics and Astronomy* for agreeing to bring out these proceedings as a Supplement issue.

V. K. Kapahi, N. Dadhich, G. Swarup & J. V. Narlikar.



## The Beauty and Danger of Comets and Asteroids

### *Vainu Bappu Lecture*

Tom Gehrels *University of Arizona, Space Science Building, Tucson, Arizona 85721, USA*

**Abstract.** This paper follows the transcribed text of the Vainu Bappu Lecture presented on 17 August 1993 to the 6th Asian-Pacific Regional Meeting on Astronomy of the International Astronomical Union. The topic is on comets and asteroids, the role they played in our origins, and the danger of impacts still today. There is more beauty than danger, as even the hazards are being brought under control. Astronomers are in the lead, because the menacing asteroids have to be discovered first, which is done with optical telescopes.

**Key words:** Comets—asteroids—CCD.

I first met Vainu Bappu in 1952, long ago, but clearly remembered as he made a distinct impression. That happened in Pasadena, California, where he was a Research Associate. He had broad interests, not just in science but also in his country and its progress after Independence. I had been in India and he invited me to come back, as have his successors, for which I am deeply grateful, and for the opportunity to deliver this lecture in memory of Vainu Bappu. As a student he had discovered a comet and computed its orbit. He would have enjoyed being here, participating in these thoughts about the beauty and danger of comets and asteroids, as I am inviting you to do now.

Danger, yes. It is real and it is frightening. But even within that danger lies a beauty because we are on our way to solving the problem. It is a major problem for humanity, but we are beginning to take care of it. It may even become an example of solving global problems. The interesting part for us as astronomers is that we are in the forefront of the solution because the dangerous objects have to be found first, and that is an astronomical challenge. It is discussed in detail in the book *Hazards Due to Comets and Asteroids* that I am editing (Gehrels 1994), as are some answers to the question of what to do if we find a dangerous asteroid.

The greatest beauty, however, lies in our research as astrophysicists. The comets and asteroids are left over from their participation in the formation of the solar system, as a part of the aggregation of dust and gas from the interstellar medium. The Milky Way is seen because of its many stars, but there also are dark regions where starlight is obscured by opaque clouds of gas and dust (see Fig. 1). The individual particles are so small that if you had one in your hand, your eyes would not be able to resolve it because its size is near a micron, a thousandth of a millimeter. From such nebulae, the stars are formed, and so was the solar system. The mechanisms are complex; they are described in the book *Protostars and Planets III*, edited by Levy and Lunine (1993).

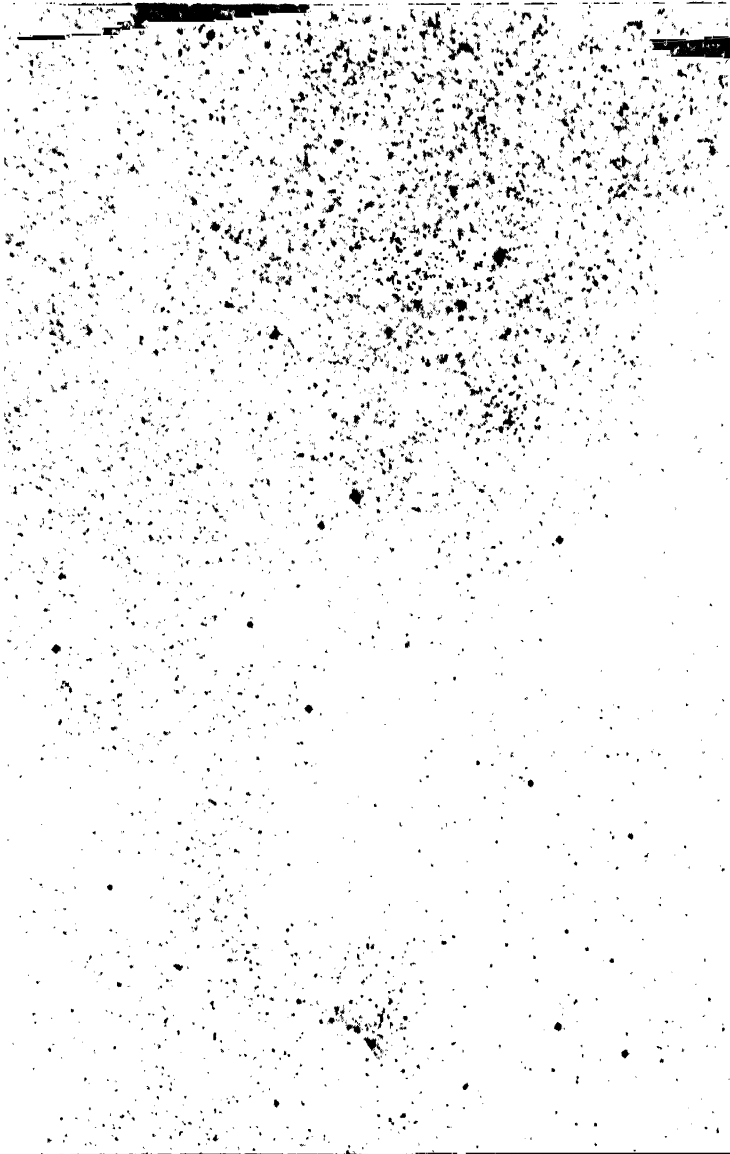


**Figure 1.** The 'North America' nebula.

The solar nebula had, among its dust and gas, nature's next step up in size that we refer to as a planetesimal, of kilometer dimensions. Yet later in solar-system formation we call it a comet or asteroid. The Earth was formed by the accumulation of dust and gas and planetesimals; the bombarding accretion increased progressively as Earth's mass and gravity increased. Some awesomely noisy spectacle that must have been! As

the impacts became more energetic, the temperature increased and in the end, the Earth probably was a molten globe. The bombardment stopped when the material of the inner solar nebula was used up. This occurred gradually some 4,000 million years ago. A cooling stage followed, from the outside inward, with the crust of the Earth solidifying. Yet other waves of impacts followed later when the outer parts of the solar system were taking final form. Comets and asteroids had made the cores of the outer planets, which then completed their accretion mostly with gas, to become the gaseous giants Jupiter, Saturn, Uranus and Neptune.

Eventually, a steady state was reached in the solar system with the asteroids left over in the main belt, generally between 2.2 and 3.3 astronomical units (AU; see Fig. 2). That is in the inner part of the solar system where, with the Sun coming on through the clearing space, temperatures had been rising such that the volatiles and gases had evaporated; asteroids consist mostly of sandy siliceous materials (Fig. 3).

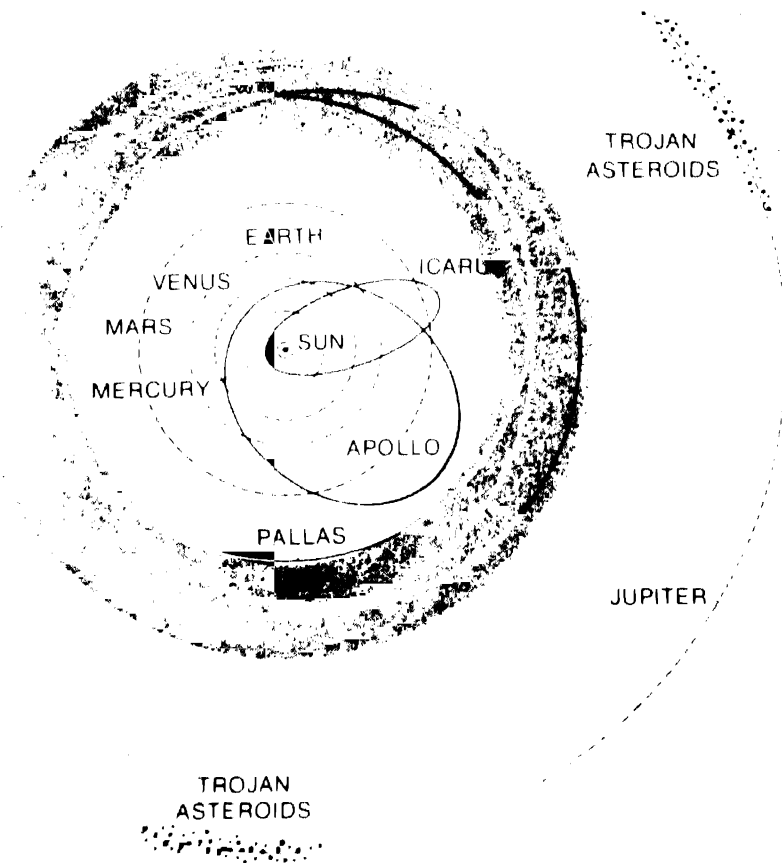


**Figure 2.** The asteroid belt and a few planet-crossing asteroids.





**Figure 3.** Asteroid (951) Gaspra, observed by the Galileo spacecraft in 1992.

In the outer parts of the solar system, at distances on the order of  $10^5$  AU, a storage remained for cometary cores that we call the Oort Cloud, after Professor Jan Oort, who derived this model in a classical paper. The cloud is tenuous, but large, having some  $10^{13}$  objects (see Fig. 4). Because of low temperature at this great distance from the Sun, they still contain snows, gases and ices among the dust. We call them dirty snowballs, that probably are dark aggregates of hundreds of kilometer-sized planetesimals tenuously held together; their composition is mostly carbonaceous, organic.

Back on Earth, we see in the geological layering successively the slow stages of making primitive life, followed by, about 400 million years ago, the onset of rapid evolution of more advanced species. Larger mammals appeared, like the dinosaurs, who roamed the Earth for some 200 million years. And then, in a few-thousand years, they were gone. It has now been fairly well proven that their demise was due to impact of an asteroid or comet about 12 km in diameter. From where had it come?

The orbits of the cometary nuclei in the Oort Cloud may be perturbed by the gravitational attraction of stars or massive nebulae passing by the solar system

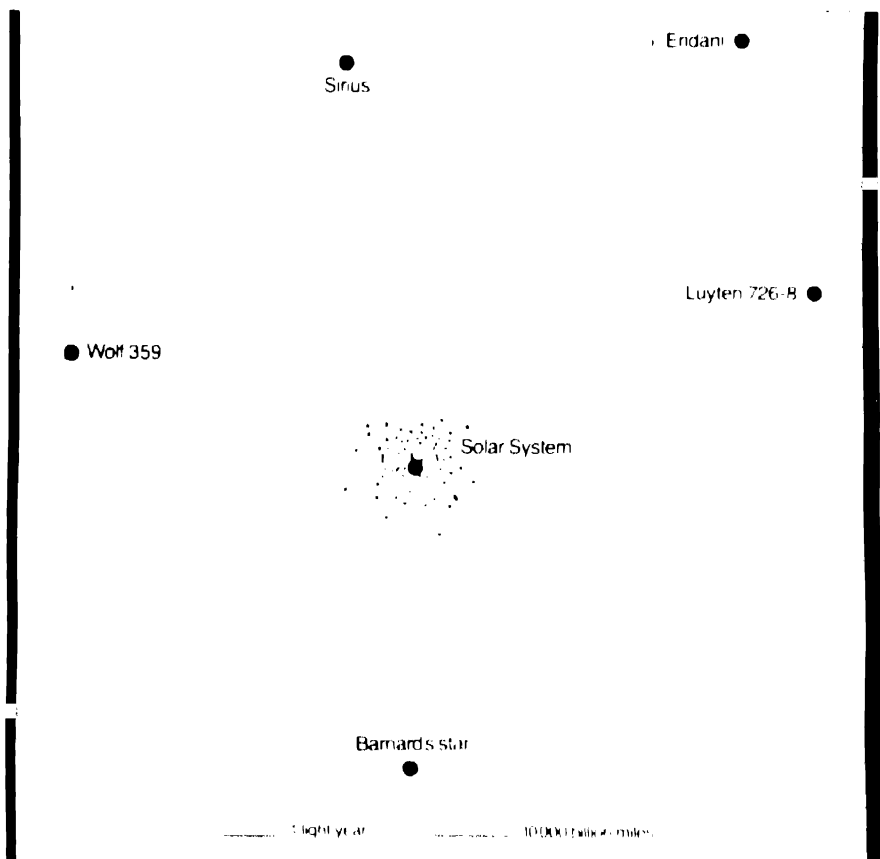


**Figure 4.** A comparison of the distances to a few of the nearer stars with the size of the Oort Cloud of cometary nuclei surrounding the Sun. This figure is reproduced from the back of the book edited by Smoluchowski *et al.* (1986).

(Fig. 4). The effects of such distant encounters have been modeled to show that the cometary orbits may be decircularized such that they come towards the inner part of the solar system. We can then see them as active comets: as they come closer to the heat of the Sun, evaporation of the contained gases and volatiles brings forth the coma and tails (see Figs. 5 and 6). When the material heats up, the gas comes out of the nucleus in huge jets as from a jet engine or a volcano. Together with the gases, dust particles are thrown out so that a dust tail as well as a tail of ionized gas may be seen.

Returning to the asteroid belt, its members generally have stable orbits, but there are so many of them that collisions occur. If such collisions take place where there are rhythmic resonance encounters with Jupiter, complex interactions take place. Jupiter's gravity causes the collisional fragments to be either tossed out of the solar system or to be brought into elliptical orbits toward the inner regions of the solar system, the domain of the terrestrial planets.

This is a steady state again, with a balance of supply and demand. The supply is due to the collisions and perturbations, while the demand is caused by gravitational collection of the planets. The lifetime of comets and asteroids that approach the Earth is typically  $10^7$  years. Eventually they will all collide anyway, with either Mars, the Earth-Moon system, Venus, or Mercury.

So, the primary beauty of comets and asteroids is that they participated in the original formations, in our very own origins and well-being. Without them, we would not have had this Earth, we would not have been here ourselves. The subsequent beauty is that the Darwinian gradual evolution of life was impacted. Discontinuities, mass extinctions, are seen in the geological record. For instance, the voracious dinosaurs were eliminated so that our type of mammals had a chance to evolve, and here we are.

A further beauty lies in the opportunity for sending space missions to comets and asteroids, eventually landing on them, sampling their surfaces for detailed study. This is treated in the book *Resources from Near-Earth Space* (Lewis et al. 1993). The first mission to a near-Earth asteroid is called 'Clementine', to fly by the Moon and by Asteroid (1620) Geographos in 1994. There is a need for more target candidates, particularly with a low differential velocity, a low delta-V, between the objects in its elliptical orbit and the Earth in its nearly circular one. In August 1993, we knew of only 180 objects that may come close to the Earth, and these would mostly require exorbitant amounts of fuel for an extended encounter, a 'rendezvous' with the spacecraft. Much more work at astronomical telescopes is needed in order to find suitable targets.

My final beauty is a simple one to behold: it is fun to hunt them. It is a challenge to develop new techniques for finding the elusive bodies. The discovery of new objects, new types of objects, brings unforgettable moments for the observer!

In 1969 the idea sprouted to build a telescope that would be dedicated to the small objects in the solar system, the comets, asteroids, and satellites. A most encouraging colleague is Aden Meinel, who was then Director of the Optical Sciences Center of the University of Arizona. For instance, he helped in the acquisition for India of the 1.2-m telescope at Osmania University, which may now also be used for the 'Kalki Program' to observe asteroids (Table 1). In 1969, Meinel acquired for our telescope a 1.8-m mirror blank, a reject or surplus from a 'spy in the sky' type of program, but a precious piece of optics, as it is of lightweight construction made of lowest expansion material,



**Figure 5.** The nucleus of periodic Comet Halley, from images made by the Giotto spacecraft.

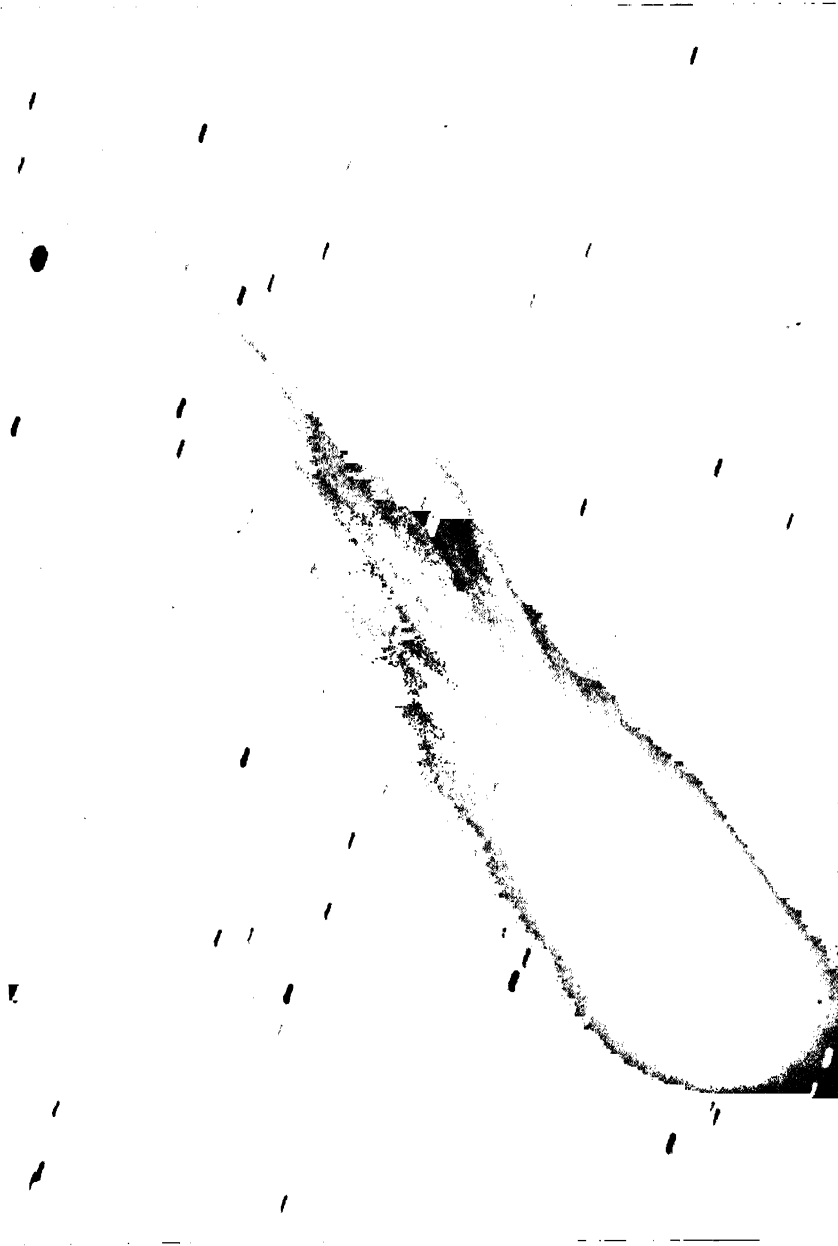


Figure 6. Periodic comet Mrkos.

**Table 1.** Overview of personnel for CCD scanning.

T. Gehrels	Observer, Principal Investigator.
R. S. McMillan	Instrumentation.
M. L. Perry	Engineering.
J. V. Scotti	Observer, Astrometry.
R. Jedicke	Observer, Analysis.
T. H. Bressi	Student Assistant.
T. C. Metcalfe	Student Assistant.

quartz! I had it sagged to  $f/2.7$ , but that is as far as we got. The idea of a dedicated Asteroid Telescope was too far ahead of its time; few people were active in these fields at that time. When it became obvious that there was not going to be an Asteroid Telescope very soon, Aden borrowed the mirror back for the Multi-Mirror Telescope (MMT; see Fig. 7). It was used for at least a decade in the MMT, biding its time to work on exciting objects...asteroids! For that it was returned in January 1993, when we were indeed beginning to build the dedicated 1.8-m Scannerscope.

To develop scanning techniques with charge-coupled devices (CCDs), a venerable 0.9-m Newtonian telescope had been made available in 1981 (see Figs. 8–10). The background of this program and studies of comets and asteroids are discussed in Gehrels (1988). It was the original Steward Observatory Telescope erected in 1921 on the campus, and moved to Kitt Peak in 1964. We now call it the 'Spacewatch Telescope' (see Gehrels 1991). On Kitt Peak, 50 km west of Tucson, there are some 19 telescope systems in operation, mostly under the control of the Kitt Peak National Observatory. The University of Arizona has a site of its own for a few telescopes such as the 0.9-m Newtonian.

The crew for asteroid work is shown in Table 1. It is a small team, but dedicated to not only keeping the 0.9-m in operation 18 nights per month, but also to guiding the fabrication of the 1.8-m Spacewatch Telescope. For the latter, Mr. Larry Barr joined us who is a senior telescope designer with a fine record at Kitt Peak, Mauna Kea, and other observatories.

An early design for the 1.8-m is shown in Fig. 11, namely as a straight prime-focus reflector. Because of shortage in funding, we make the telescope more compact as seen in Fig. 12. It saves in cost, particularly in the size of the dome seen in Fig. 13. The result is a 'folded prime focus' which is accomplished with a flat mirror at the top, 76 cm in diameter. This causes a light loss of about 6% more than would have been obscured at straight prime focus, the price we will have to pay indefinitely for an affordable telescope. It is a stiff structure allowing observations made into 60 km/hr winds, which occur at Kitt Peak particularly in the spring. Neither could we have executed the imaginative design by Mr. Barr, of Fig. 14. So, it is hereby left for posterity.

In addition to the small crew, Spacewatch has collaborations for the interpretation of its observations [Table 2; see Gehrels (1991)]. A present collaboration concerns our findings in the outer parts of the solar system (described below); it is mostly done by James Scotti in a Ph.D. Program with Mark Bailey at John Moores University in Liverpool, England. Another active collaboration is with David Rabinowitz, who used to be a Research Associate at Spacewatch, after which he moved to the Carnegie

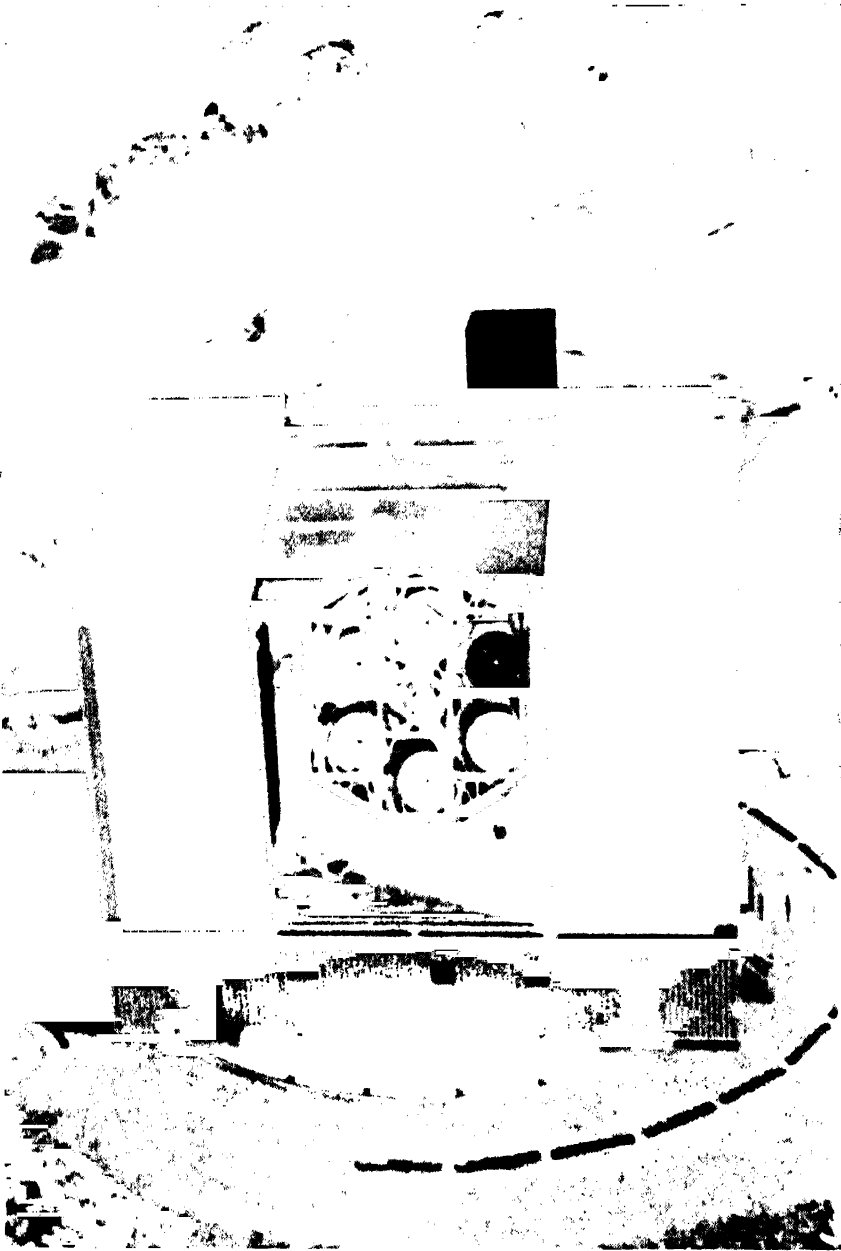


Figure 7. The Multi-Mirror Telescope on Mount Hopkins, Arizona.

Institution near Washington, D.C.; his work is on the 10-m objects found near the Earth (also described below). Let me now describe the work at the 0.9-m Spacewatch Telescope.

At the north port of the Newtonian telescope, McMillan *et al.* (1994) take the light into a fiber down to a temperature-controlled spectrometry room on the ground floor.



**Figure 8.** A partial view of Kitt Peak with the Arizena area in the foreground, the domes of its 2.2-m and 0.9 m telescopes.





**Figure 9.** The 0.9-m Spacewatch Telescope.

This is done during about nine nights centered on full moon each month for their program of determining radial velocities of stars that may show a periodicity due to the rotation about them of a massive planet. In addition to the fiberhead of McMillan's planet detection program, we have a dewar, also permanently installed, on the

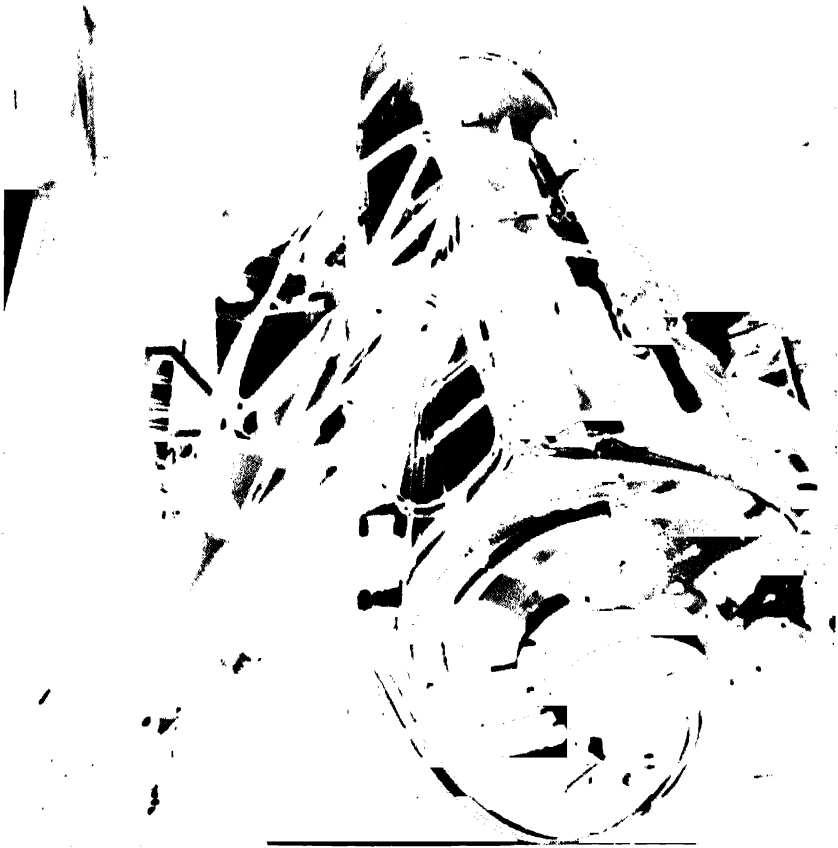


**Figure 10.** The Spacewatch Telescope at night.

south port (Fig. 15). This contains a Tektronix  $2048 \times 2048$  CCD of about 70% quantum efficiency with pixel size 24 microns. This is for the discovery of asteroids and comets.

The automatic detection has required about eight man-years of computer programming. The charge-coupling property of the CCD is used to transfer the charges from row to row when the telescope drive is turned off whereby there is a scanning on the sky. The full width of the CCD thereby moves across in 146.53 seconds, at zero declination. The principle is that of a 'bucket brigade' in firefighting, handing over from the pixel capacitors the light converted photo-electrically into charges. From the last readout row, the end register, the data are read into a Solbourne Sun-Station system. Three scans are made for each region on the sky, of about half a degree width

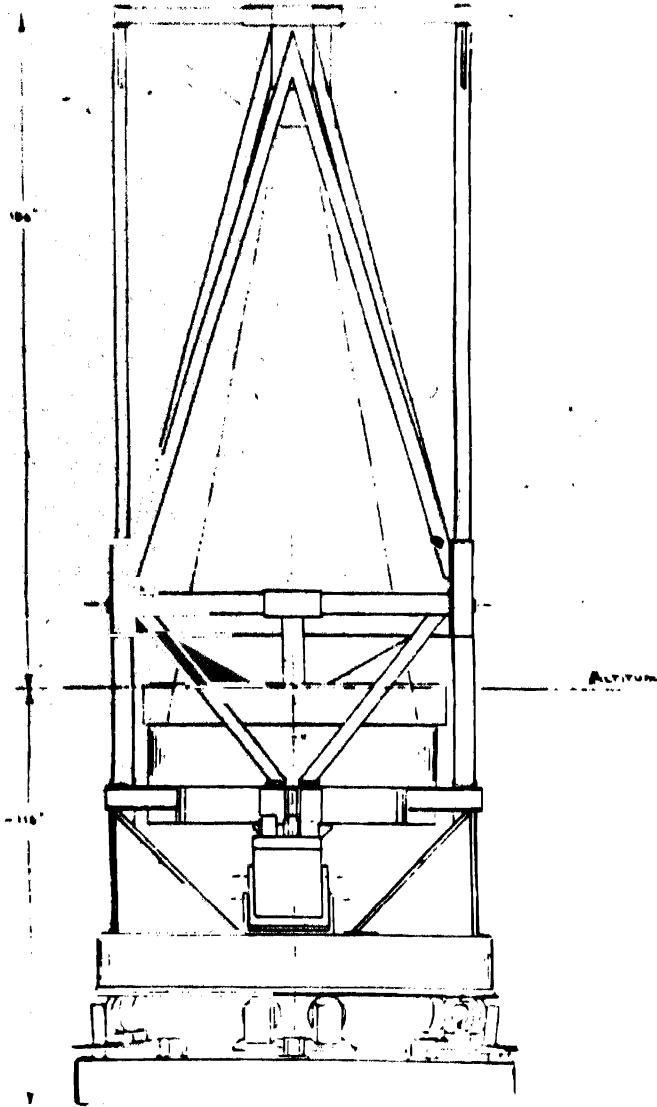


**Figure 11.** An early design of the 1.8-meter alt-az Spacewatch Telescope.

and usually about 10 degrees length. In intricate bookkeeping, the computer lists the pixel coordinates of as many as 40,000 stars and asteroids in the scan. By comparing the listings obtained during the three scans, the computer finds the moving objects. There also is a routine for 'streak detection' of the very fast-moving objects that will make a trail on the exposure of  $146.53/\cos \delta$  secs duration. In addition, the observer watches the scan go by, because the human eye is so efficient at discovering very faint

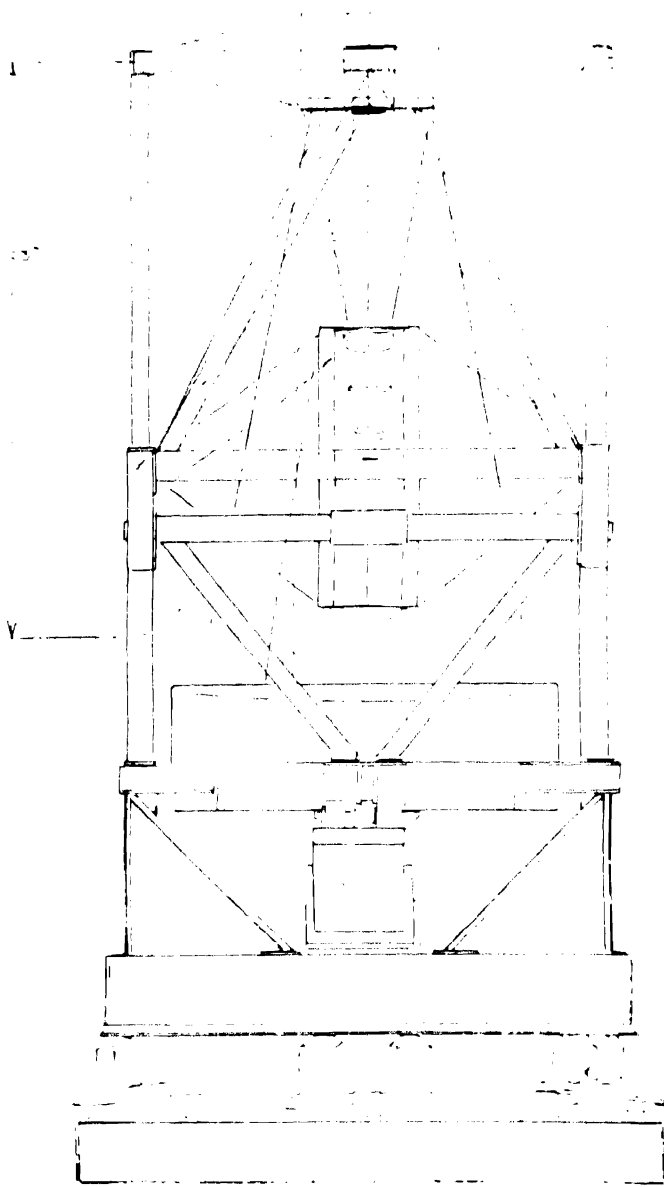


**Figure 12.** The 1.8-m Spacewatch Telescope in its 'folded prime focus' configuration.

trails. While the computer is set to discover trails down to a level of confidence or precision of 3.5-sigma, long trails are reliably recognized by eye and brain even at the 1-sigma level.

The work schedule of the observer is demanding. On a winter night he gets into the dome by about 6 p.m. and is finished by about 6:30 a.m. It is a vigilant operation with little time off. The first and second scans are watched carefully, looking for faint trails

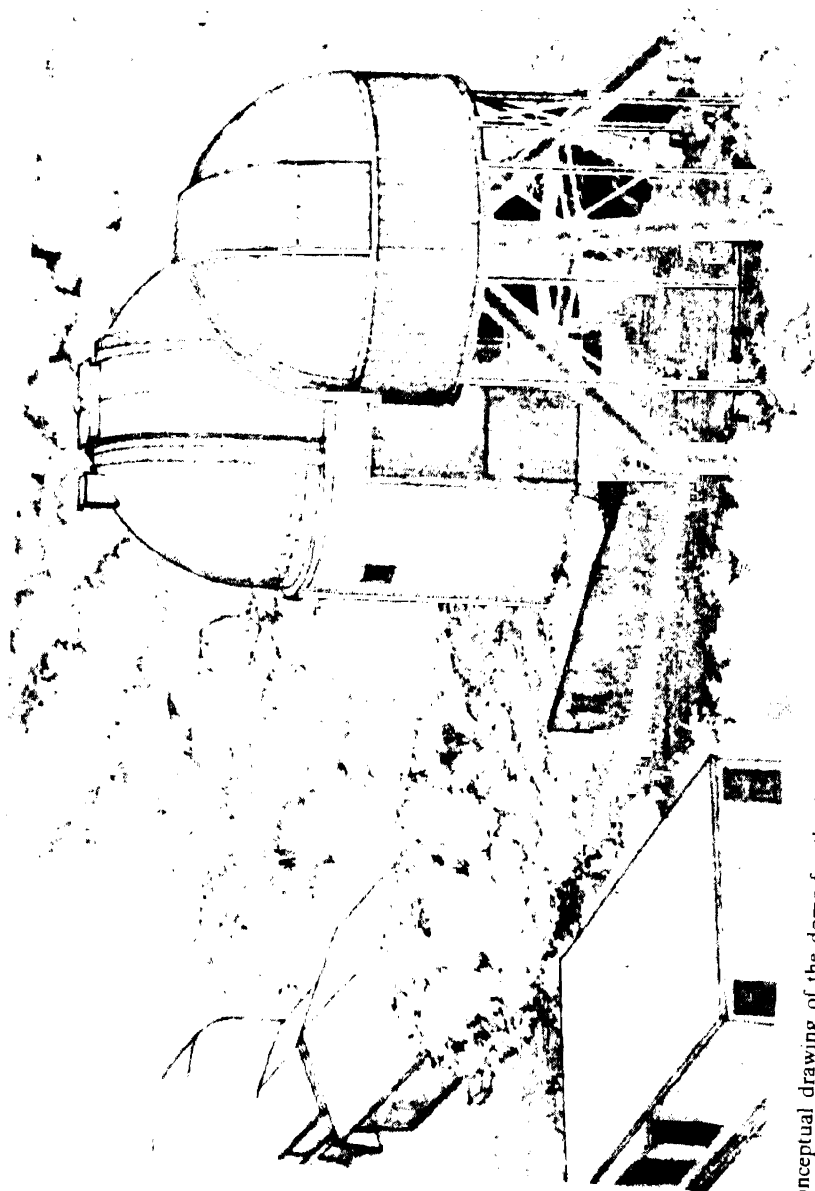


**Figure 13.** Conceptual drawing of the dome for the 1.8-m Spacewatch Telescope immediately north of the 0.9-m Spacewatch Telescope. This is, however, too close together; a better site was made available.

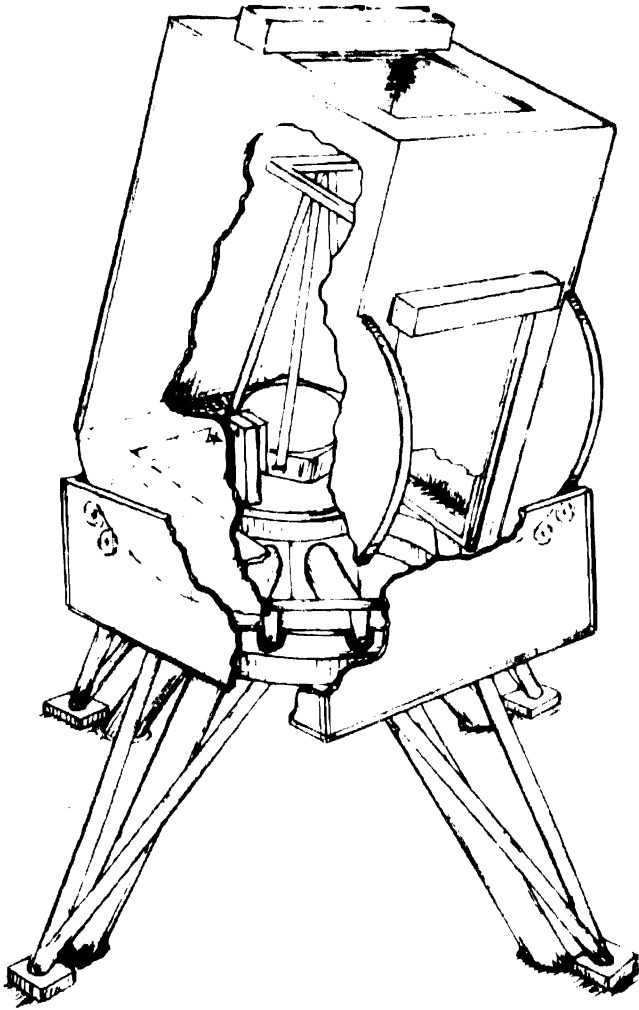


**Figure 14.** An early design of the shelter for the 1.8-m Spacewatch Telescope, a truss-mounted, 2-axis rotating enclosure (L. D. Barr, personal communication, 1993).

and comets. The third scan is exciting because of the new discoveries by the motion-detection routine, and visually deciding against the reality of about one-third of the new discoveries reported by the computer. We could diminish the computer errors by setting the sigma level of detection higher than 3.5 sigma, but that could be at the cost of losing a real discovery. At 7 a.m. the computer begins the analysis of the discoveries, by calling up snapshots for each one of the discovered objects (Fig. 16). This is a large number, for a good winter's night on the order of 4500 snapshots. The observer then needs several hours in the daytime to sort out the discoveries, which becomes a thrill when a special object is discovered. That could be a comet, or a near-Earth object, or a distant one such as the so-called Centaurs that move in the space of Saturn-Neptune.

**Table 2.** Overview of Spacewatch collaborations.

Identification	Collaborators
Planet detection	R. S. McMillan.
Gamma Ray bursters	N. Gehrels.
Satellites of asteroids	J. D. Drummond.
Synchronous debris	F. Vilas.
Search for planet X	J. D. Anderson.
Brown dwarfs survey	F. J. Low.
CCD scanning on spacecraft	M. Ya. Marov.
Astrometry	B. G. Marsden.
Comet recovery	B. G. Marsden.
Comet diameters	E. Roemer.
Orbit software	D. J. Tholen.
Follow up	E. L. G. Bowell <i>et al.</i>
Project Kalki	R. Rajamohan.
Cometesimals	L. A. Frank.
Comet trails	M. V. Sykes.
Arjuna	D. L. Rabinowitz.
Centaur	M. E. Bailey.
P/Shoemaker-Levy 9	H. J. Melosh.

During a good winter's night as many as nearly a thousand asteroids in the main belt may be discovered. Their positions, which are good to about  $\pm 0.5$  arcsecs, are put on e-mail to whomever wants to receive this information. We ourselves are not following up astrometrically on these asteroids; we do that only for the special objects.

To distinguish the object's distance from its rates, we use a simple principle, which is best illustrated by an airplane flying nearby where it has great angular velocity. When it flies at greater distance, it has a lower angular rate, even when its linear velocity is the same. Similarly, when a comet or asteroid is at great distance from us, its angular rate is low. Except for a very close object that makes a long trail, the observed motion is primarily a reflex of the Earth's predominant angular velocity. So, by observing the angular rate, a first indication is obtained of distance. This works only near opposition, the direction opposite the sun, but there it works quite well as is shown in Fig. 17 (Rabinowitz 1991, 1993).

Figure 18 shows a screen typical for a part of a first or second scan. Some of the stars are so bright that their light appears to spill over into adjacent pixels so that they appear large. Their images are not round but show four peaked extensions which are diffraction spikes from the support vanes of the Newtonian secondary mirror. The bright vertical lines are due to hot pixels, while there also are a few dark lines due to dead pixels.

Figure 18 has a bright trail of an asteroid that moves so fast that it produces a trail in the  $146.53/\cos \delta$  secs exposure time. Since the trail is brighter than the limit set for the computer, the 'streak detection' software recognized this object, 1992 JD. Figure 18 also shows that we can make a snapshot in order to keep the image for detailed inspection after it has scrolled off the screen. The rates of motion are computed so that the observer can find the object again in a new set of scans. Of course, the direction of motion is not known, and both directions may have to be tried before the object is recovered.

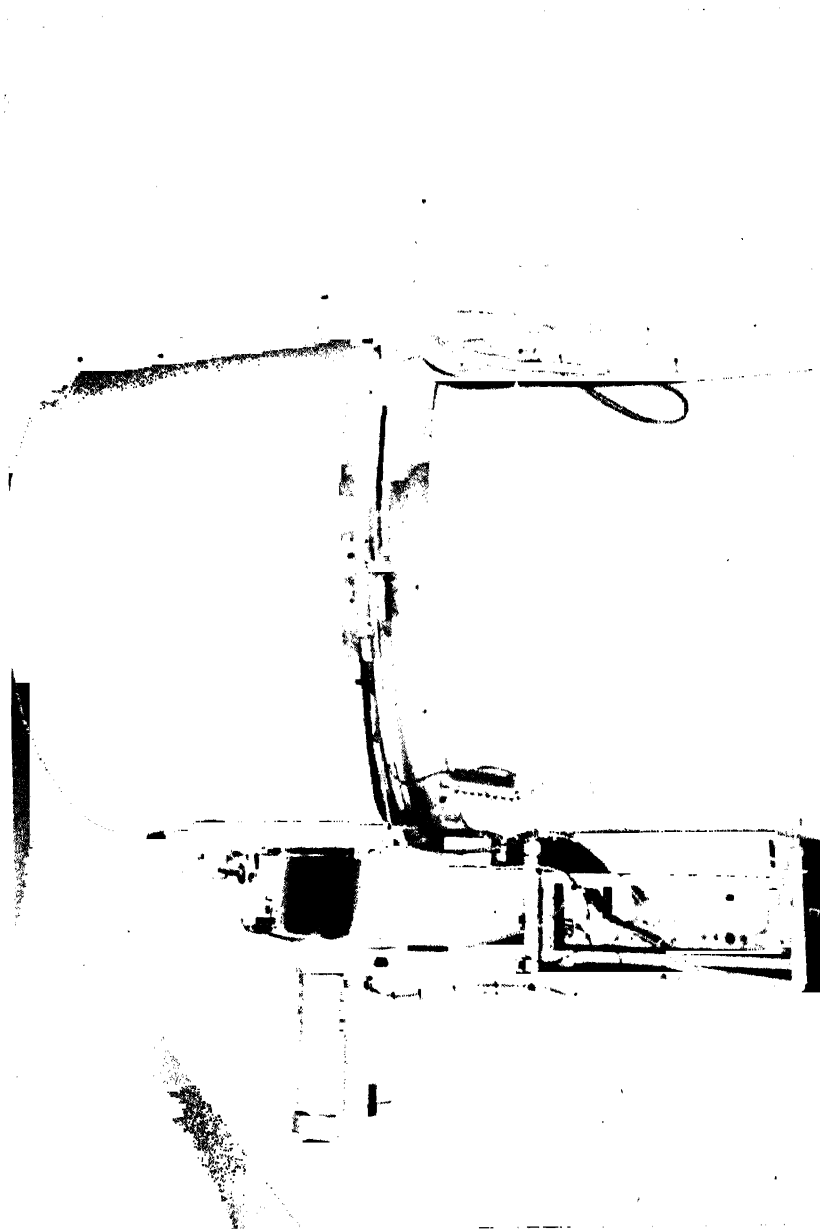


**Figure 15.** At the south port of the Newtonian telescope, there is the  $2048 \times 2048$  CCD with its controller underneath.



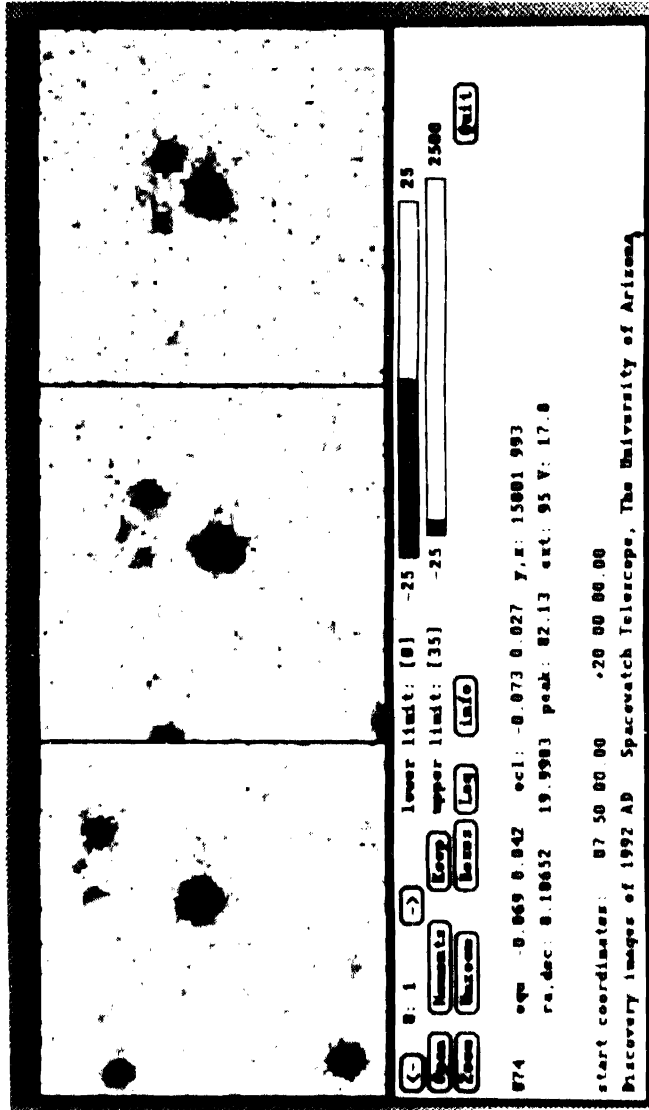
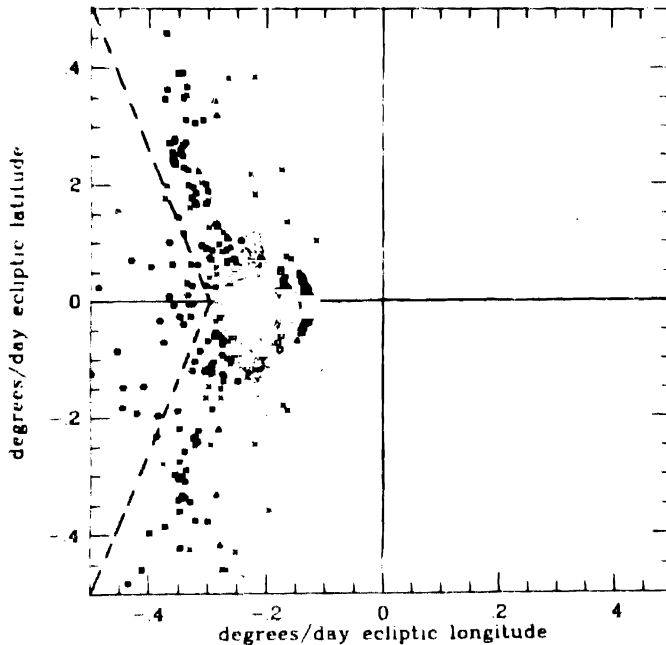


Figure 16. In the reviews, in the daytime, the frames of the three scans are displayed.

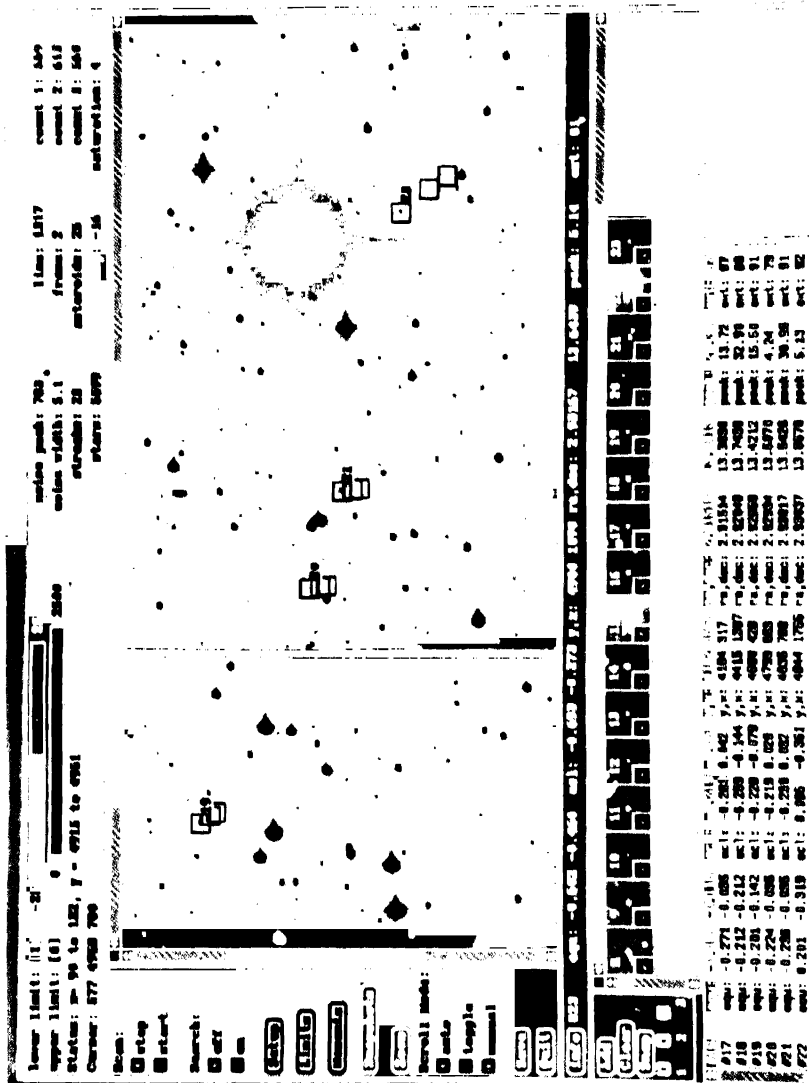


**Figure 17.** Expected angular rates of various asteroids. The dashed lines bound on the left the area for Earth-approachers. Other asteroid groups represented are, from right to left: Trojans, Hildas, and the ones in the main belt. The ones distributed over high rates in ecliptic-latitude rates are the Hungaries.

Trail-detection-by eye has yielded the smallest, closest and fastest object that we have found so far, 1993 KA2, which moved 29 degrees per day when it was discovered, but only 12 deg/day at the end of that night of May 21, 1993. If the discovery scan had been made only about 45 minutes earlier, the object would have moved 45 deg/day, too fast and too faint to have been seen at all. This behavior is understood by considering the airplane again, now flying overhead at high angular rate, which diminishes as it disappears in the distance. Indeed, the afternoon before that night, 1993 KA2 came to its closest distance to the Earth, about 150,000 kilometers, travelling at a rate of 12 degrees per hour. The diameter of 1993 KA2 is about 6 meters, a parameter we know only to within some  $\pm 50\%$  because we do not determine reflectivities. The object could be of a carbonaceous type of material, quite dark, and then have a diameter of 9 m, or it could be bright as a more silicaceous type, and it would be only 3 m. These compositional types are determined in surface spectrometry with special equipment and at large telescopes. Such determinations are made by a few experts; they have identified several dozens of different materials by comparison with meteorites.

Figure 19 shows a third CCD scan. An image that may have looked stellar has been identified as belonging to a moving object, with a square around that image. The computer also draws two other squares, for the positions of the object in the previous scan and in the scan before that, respectively the second and first scans. For further reference and inspection, the object is kept in the image gallery, below the star field,





and the computer provides other parameters such as the rate of motion in ecliptic and equatorial coordinates, and a brightness parameter. The position is computed by comparison with certain stars in the field for which the coordinates are provided by the Guide Star Catalog of the Hubble Space Telescope. The scans, typically 10 degrees long and half-a-degree wide, have several dozens of stars from that catalog.

Figure 19 shows the discovery of several main-belt asteroids and then another one is seen at wider spacing; this is the near-Earth asteroid 1991 VG. It is the one we are not entirely certain of, as it could be a man-made object. It has by far the lowest delta-V of all, as it is in a circular orbit closely resembling that of Earth.

Our scientific results of Spacewatch are, of course, the most important. Dozens of publications, by us and others, have already appeared. Soon after the automatic detection began, we found small objects, smaller than 100 meters in diameter, more rapidly than predicted. This is seen in Fig. 20 which shows an extrapolation of the size-frequency relation for the near-Earth asteroids over the range of 0.3–10 km. For the large asteroids, the points were determined from Shoemaker and Spacewatch data. The extrapolation with the straight solid line caused us to expect a certain rate of discovery for smaller objects. Instead, the frequency seems to be taking off beginning at about 100 meters; we are finding an extra large number of asteroids of the smaller sizes. That it is a large effect is seen in the logarithmic ordinate scale such that at the 7-m size we are finding 40 times the expected numbers.

We actually observe magnitude-frequency relations, and the transformation to sizes depends on an adoption of the reflectivity for an average composition. Essential for the interpretation of Fig. 20 is that the same reflectivity is used for the smaller as for the larger objects. It is known from military reconnaissance (Tagliaferri *et al.* 1994) that objects of 10-m size hit the Earth's atmosphere a few times per year. However, most of them do not penetrate the atmosphere. Only the metallic ones come through to make craters, as observed by Gene and Carolyn Shoemaker, who not only are active as astronomers in finding these objects at Palomar (Table 4), but also as geologists in exploring the frequency and composition of objects that made well-preserved craters in the Australian deserts.

We already have a name for that exceptional population of small objects, namely the *Arjuna*s after the Pandava prince in the Bhagavad Gita, in the discussion of our dharma, a determination to see our predicament through. Concerning the hazards, the predicament is to find and study these objects, and to build the best possible telescope.

The excess has been summarized by Rabinowitz *et al.* (1993), but a referee objected to the name *Arjuna*s as it has not been approved as yet by the International Astronomical Union. About the origin of the *Arjuna*s we are divided ourselves. Four different origins are being considered. There is a possibility that these objects are boulders, boules, being ejected by comets. Around volcanoes on the Earth, boules are found, round objects of similar size near 1/3 m in diameter. Perhaps for the comets the same could happen. In comparison with the cometary conditions of low density, near  $0.1 \text{ gm/cm}^3$ , a 10-m size might be expected.

These objects could be secondary debris from the Moon, Mars, or from secondary collisions of the near-Earth objects. First, the collisions in the asteroid belt occur, and Jupiter brings the fragments to the inner part of the solar system. The magnitude-frequency relation follows the one expected for fragmentation, even in the case of a hammer hitting a rock and breaking it up in small pieces. Towards smaller sizes

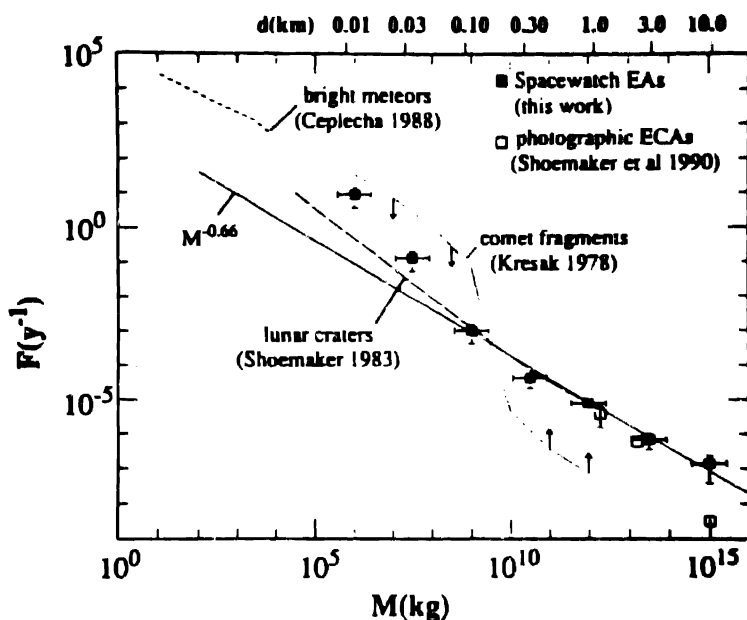


**Figure 20.** Rate of terrestrial impacts as a function of diameter, or mass (Rabinowitz 1993).

there is a rapid increase in the number of objects, a factor of 2.5 per astronomical magnitude. At about the 10-m size, the collision probabilities among themselves are sufficient to get secondary collisions in less than  $10^8$  years, appreciably less than the lifetime of the solar system. Near-Earth asteroids show a preference for having perihelia near the Earth or Venus. In other words, it appears that in addition to Jupiter also the receiving planets Earth and Venus play a role in the gravitational interaction with planet-crossing comets and asteroids.

Another major result of the Spacewatch program is the discovery of two objects, (5145) Pholus and 1993 HA2, with a semimajor axis near 22 AU, eccentricity about 0.6 and inclination near 20 degrees. They are in chaotic orbits; a chance encounter with Uranus, for instance, can greatly affect the orbit (Bailey *et al.* 1992). The surprising result is that they are by far the most reddish objects in the solar system, which is interpreted with tholins, organic material, on their surface. They differ from (2060) Chiron which is not so reddish and has a more circular orbit, near those of Saturn and Uranus. Chiron had, with number 2060, received an asteroid identification because at first no evidence of coma was found. Several years after its discovery, however, cometary activity was observed so that Chiron is now considered to be a large comet.

The Spacewatch crew has had excitement with periodic comet Shoemaker-Levy 9. Figure 21 was a startling picture the likes of which had not been known before. It was found by Gene and Carolyn Shoemaker together with David Levy who is known as the biographer of Tombaugh and Bok (Levy 1991, 1993) and as a great discoverer of comets. Immediately after the discovery they called Jim Scotti at the Spacewatch Telescope, who verified that it was a cometary object. Its dust is seen to the one side in Fig. 21, which is brighter than the other. Over three months, we obtained a set of observations, of which Scotti and Melosh made an analysis (1993). The nodules kept

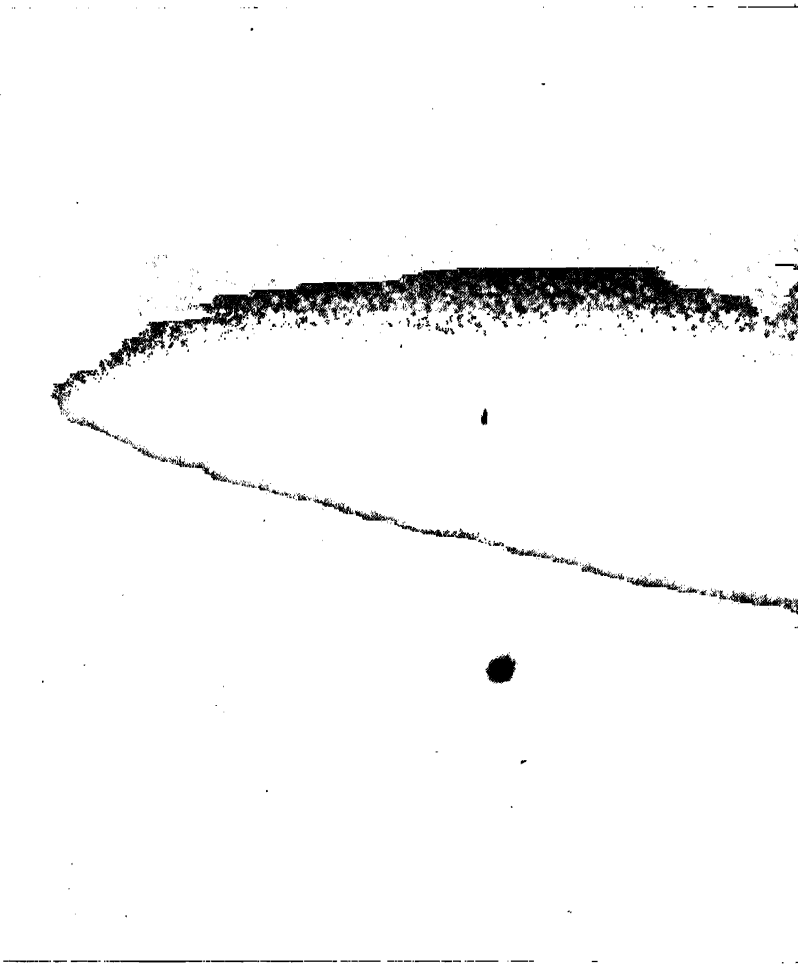


**Figure 21.** Periodic Comet Shoemaker-Levy 9.

stretching farther apart, and this was projected backwards. The nodules were together at a distance of only 1.6 kilometers at the time of the closest approach to Jupiter, on July 8, 1992. This therefore indicates at least a lower limit to the diameter of the original comet, which apparently broke up at the closest approach to Jupiter. The original comet had come too close to Jupiter, within the so-called Roche limit named after a Frenchman who studied such effects first. Comets generally have very low mass density,  $0.1 \text{ gm/cm}^3$  (Melosh and Schenk 1993). When the comet got too close, it was pulled apart by the differential gravity of Jupiter, which is known to depend strongly on the distance from Jupiter, with the third power of the distance. An indication that the analysis is correct follows from the alignment of the nodules at the time of the closest approach, pointed toward the center of Jupiter, an orientation that was maintained in space.

This analysis is, however, an issue of lively discussion among various scientists. If the comet had an appreciable rotation, then the objects could have flown farther

apart. In summary, it appears that the size of the original comet is at least 2 km, but it could be as large as 10 km. From the observations in 1993 it was also derived that the nodules will hit Jupiter within six days centered on July 21, 1994. The effects on the Jovian atmosphere may be observable from the Galileo spacecraft and also, but at low resolution, from Voyager II. Soon after the event, the rotation of Jupiter will bring the impact area into view from Earth. So, in our lifetime we will be observing an impact on Jupiter. How about impacts on Earth?

Concerning the hazards due to comets and asteroids, it is an unpleasant topic that we became aware of slowly. I have been showing Table 3 for 15 years, but it is only during the last few years that I really began to realize the horror of such impacts. This tardiness seems rather naive now. The hazards have always been with us! Meteorites have come falling down such as at Dhajala, west of Ahmedabad, India (see Fig. 22). The school declared a holiday after the noisy crash and break-up of the object, and the children searched the area. Even though it was a stony meteorite, which looks similar to rocks, these children know the desert so well that they found a large number of the pieces.

Figure 23 shows a physician with his patient in Alabama in 1954. She had been hit by a meteorite while lying on the sofa in her living room, hurt quite badly as you can see. The funny story about this is that she wanted to keep the meteorite, but she was living in a rented house and its owner, pointing at the holes in roof and ceilings, also made a claim so that he could sell it to recover his expenses. A court session was scheduled at which the State of Alabama reportedly entered a claim that this was an act of God, the State represents such High Authority, so the State should have the meteorite. The judge wisely assigned the meteorite to the woman because she had the most intimate knowledge of it.

As we move on to larger impacts, there is the crater in Northern Arizona (Fig. 24). When you come to Arizona, don't just go see the Grand Canyon, but also walk around this crater for a memorable experience. It was made by a 35-m metallic object some 30,000 years ago. The kinetic energy was about 100 'Hiroshimas', 100 times the energy used at Hiroshima in August 1945. I use the Hiroshima comparison with due respect for the horror of that event. An asteroid impact would not have the radiation effects that were so terrible in Hiroshima and Nagasaki.

Another reminder of collisions is the one at Tunguska, Siberia, in 1908 (Fig. 25), with a blast in the upper atmosphere that was heard as far away as London. Fortunately, no people were killed. This would have been different if it had been over the cities shown in Fig. 25, which would have been obliterated by the blast and subsequent fires.

Table 3 shows the statistics of the hazards; it is only approximately correct, but the numbers are given to be easy to remember. We know the statistics a little better such

**Table 3.** Approximate statistics for the larger near-earth objects impacting on Earth.

Diameter (kilometers)	Number of objects	Impact probability (years between impacts)	Impact energy (Hiroshimas)
10	10	$10^8$	$10^9$
1	1,000	$10^6$	$10^6$
0.1	100,000	$10^4$	$10^3$





**Figure 22.** School children near Dhajala village, India.



**Figure 23.** The only documented case of a meteorite hitting a person, namely at Sylacauga, Alabama on 30 November, 1954.

that it may not be exactly 1,000 that are larger than 1 km; the number presently stands at  $1,700 \pm 500$ . The largest near-Earth asteroids are about 10 km in diameter. That is good, because the ones in the main belt between Mars and Jupiter orbits are as large as 1,000 km and if any one of those would hit the Earth, life would have been entirely obliterated. Furthermore, the observation that the largest are near 10 km appears to confirm that we are dealing with fragments, from collisions in the asteroid belt.

The number of years between impacts of 10-km objects has been modeled by various scientists at approximately 100 million years. But please do not say that if something like this happens only once in a 100-million years, you are not going to worry about it. It is merely a statistical expression. The chance of it happening tomorrow is just as great or just as small as some tomorrow 100-million years from now. Furthermore, it is essential to take the last column into account, which gives the impact energy. It is straightforward to compute the kinetic energy,  $1/2 mv^2$ , assuming a density typical for meteorites of  $3 \text{ gm/cm}^3$ . Again, I compare with Hiroshima in 1945 ( $5 \times 10^{20}$  ergs, 13,000 tons of TNT), as this seems the only way to give people a feeling of the calamity.

As we move down in Table 3 to a factor of 10 smaller in size, the number increases by a factor of 100. This is well established for the magnitude-frequency law in the



Figure 24. The 'Meteor' Crater in northern Arizona.

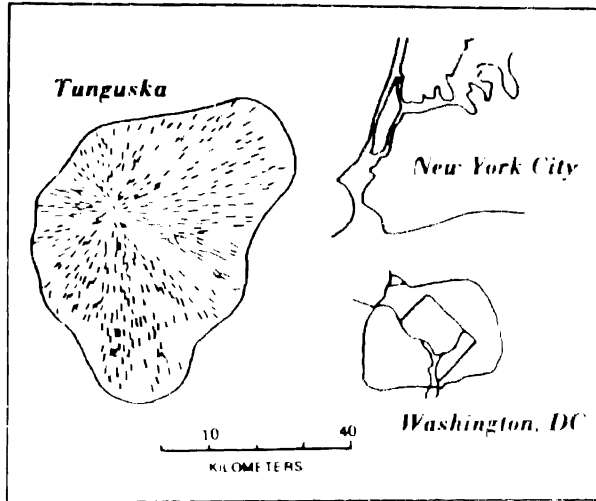


**Figure 25.** The Tunguska impact area compared with those of New York City and Washington, D.C. (J. Pike, personal communication 1992) For Tunguska the directions of the felled trees are indicated.

asteroid belt, and it is also theoretically understood as the fragmentation law. A first indication for the near-Earth objects themselves, confirms this, as is discussed with Fig 20.

That middle line of Table 3 is considered to separate global and regional disasters. Modeling, by various groups of scientists, of disasters and consequences indicates that the asteroids larger in diameter than about 1 km, depending on composition, can cause global devastation; the smaller ones, for instance the ones of Arizona and Tunguska, cause 'only' limited devastation.

What do we mean by a global hazard? An extreme case has been studied in detail. It happened 65 million years ago, clearly marked by a discontinuity in the geological strata between the Cretaceous and the Tertiary periods. It is referred to by German initials as the K-T event. After years of searching, the K-T crater was identified. It is 380 km in diameter in the Yucatan Peninsula of Mexico, the largest crater found on Earth or Moon. The impact explosion of the 12-km object threw enormous quantities of dust from the ground, and some from the object itself, up high into the Earth's stratosphere. First, there was total darkness for at least half-a-year, during which most of that dust settled in a layer a few centimeters thick between the Cretaceous and Tertiary deposits. The composition of that layer has been identified as non-terrestrial. Below it, the evidence for dinosaurs is found. Above it, three-fourths of previously living species are now missing. The dinosaurs too?

It was an exceptionally large object and an exceptionally bad place for an impact, namely within only about 2% of the Earth's surface having a deep layer of limestone. The 2% occur in equatorial regions, where 200-400 million years ago there had been tropical rain forests. Another example would be the Barrier Reef of Australia. By the impact explosion, the carbon and nitrogen in the limestone were brought into the Earth's atmosphere where they combined with the oxygen into CO<sub>2</sub> etc., the gases that cause greenhouse effects. That global warming was to at least 10 degrees

Centigrade, lasting a few-thousand years. That finally is the answer! Paleontologists had been arguing that the dinosaurs were extinguished over thousands of years, not in that first half-year of darkness. Plankton, for instance, could have been eliminated by the darkness, but not the large and tough animals like the dinosaurs.

It is all being studied in further detail, and summarized in the book *Hazards Due to Comets and Asteroids* (Gehrels 1994). Study meetings have been held, at Aspen, Colorado in 1981, and four other conferences, 1991–1993. The *Hazards* book appears in the Space Science Series of the University of Arizona Press, designed to produce texts for advanced graduate students and source books for scientists and engineers. Some of the special procedures are to combine authors from various backgrounds to write a certain chapter together, and this is followed by helpful refereeing and editing. This book has 46 chapters with 120 participating authors, about half of them planetary scientists, and the other half not. They bring a wide experience in the detection and mitigation of these objects, their statistics and characteristics, and a variety of techniques that could be used to avoid a disaster. The required energies are large because the square enters in of the velocity of the impactor, about 20 kms per second. The tremendous energies needed to push the thing aside may require more than conventional explosives. When the warning time is short, and the masses are always large, a small engine on the asteroid or even chemical explosion may not be sufficient. We may have to resort to the greatest forces that can be unleashed, nuclear weapons, neutron bombs. We therefore asked, already in 1981, the people familiar with nuclear engineering to help us with these problems. There is sufficient clarity such that in an emergency a mitigation system could be put together and launched within several months. A nuclear warhead would be exploded at a short distance from the object in order to ignite surface material so that the burn-off, similar to cometary jet effects, would yield an impulse away from the explosion. We must be aware, however, of the hazards on Earth due to the preparation and application of such powerful weapons.

Curious for us as astronomers, who have so long been in an ivory tower, satisfied with the remoteness of our subjects, is the realization that we have to lead this practical problem. We have to find those 1,700, of diameters of 1 km and larger, that could cause global demise. The Spacewatch Telescope, with its CCD scanning, is at the forefront of trying new techniques by which it may be possible to find the 1,700 with a fair degree of completion within the next 25 years. An international network of some six telescopes has been suggested in the so-called *Spaceguard* plan. These studies and plans have been stimulating. In actual practice the ones of Table 4 are in operation, partly still with photographic techniques, or appear to come on-line before the year 2000. The work at the venerable Palomar Schmidt may be discontinued, by 1995. On the other hand, the Schmidt of the European Southern Observatory, in Chile, may be used. Some of the numbers are my own estimates, particularly in the columns for the area coverage per year and the years it took, or will take, to bring the system into full operation. Each program will continue to be improved, as was the case for Spacewatch which found one near-Earth asteroid in 1989, 15 in 1991, and 25 in 1993.

The most urgent first step is to find the 1,700. Once we have orbits for them, the uncertainty is removed, and the problem solved, because then we can make predictions for the globally disastrous objects. The network of telescopes would probably continue to look for new comets that could come in from the Oort Cloud. We are

**Table 4.** Programs for detection of near-earth objects.

Coming on line	Telescope Aperture m	Identification
1973-1983	0.4	Palomar.
1984-1990	0.9	Spacewatch.
1990-1995	1.0	Côte d'Azur
1990-1995	1.2	Anglo-Australian Obs.
1994-1996	0.6	Lowell Observatory.
1994-1997	1.0	U.S. Air Force.
1995-1997	1.8	Spacewatch.

searching for objects that would be hitting the Earth within the next century or so; these are our problem. Beyond that, our grandchildren will accept the challenge. The chance of finding such a menace is on the order of 1 in 6,000. So the chance is small, but we must get to that stage in order to remove the uncertainty that it can happen anytime. Once we have these orbits, we can rest assured, and by that time also the techniques of what to do about them will be better established.

In conclusion, I thank my hosts and the Smithsonian Institution for making this presentation possible.

## References

- Bailey, M. E., Chambers, J. E., Hahn, G., Scotti, J., Tancredi, G., 1992, Transfer Probabilities Between Jupiter and Saturn-Family Orbits: Application to 1992 AD = 5145, in *Observations and Physical Properties of Small Solar System Bodies*, Eds. J. Surdej & J. C. Gerard, Proc. 30th Liège Int. Astrophys. Coll., Univ. of Liège, Belgium, pp. 285-287.
- Gehrels, T., 1988, *On the Glassy Sea, an Astronomer's Journey* (New York: American Institute of Physics), 349 pp.
- Gehrels, T., 1991, Scanning with Charge-Coupled Devices; *Space Sci. Rev.*, **58**, 347-375.
- Gehrels, T. (Ed.), 1994, *Hazards Due to Comets and Asteroids* (Tucson: University of Arizona Press), (in press).
- Levy, D., 1991, *Clyde Tombaugh: Discoverer of Planet Pluto* (Tucson: University of Arizona Press).
- Levy, D., 1993, *The Man Who Sold the Milky Way: A Biography of Bart Bok* (Tucson: University of Arizona Press).
- Levy, E. H., Lunine, J. I. (Eds.), 1993, *Protostars and Planets III* (Tucson: University of Arizona Press), 1596 pp.
- Lewis, J. S., Matthews, M. S., Guerrieri, M. (Eds.), 1993, *Resources of Near-Earth Space* (Tucson: University of Arizona Press), 977 pp.
- McMillan, R. S., Moore, T. L., Perry, M. L., Smith, P. H., 1994, Long, Accurate Time Series Measurements of Radial Velocities of Solar-Type Stars; *Astrophys. Space Sci.* (in press).
- Melosh, H. J., Schenk, P., 1993, Split Comets and the Origin of Crater Chains on Ganymede and Callisto; *Nature*, **365**, 731-733.
- Rabinowitz, D. L., 1991, Detection of Earth-Approaching Asteroids in Near Real Time; *Astr. J.*, **101**, 1518-1559.
- Rabinowitz, D. L., 1993, The Size Distribution of the Earth-Approaching Asteroids; *Astrophys. J.*, **407**, 412-427.
- Rabinowitz, D. L., Gehrels, T., Scotti, J. V., McMillan, R. S., Perry, M. L., Wisniewski, W., Larson, S. M., Howell, E. S., Mueller, B.E.A., 1993, Evidence for a Near-Earth Asteroid Belt; *Nature*, **363**, 704.

- Scotti, J. W., Melosh, H. J. 1993, Tidal Break-up and Dispersion of P/Shoemaker-Levy 9: Estimate of Progenitor Size; *Nature*, **365**, 733-735.
- Smoluchowski, R., Bahcall, J. N., Matthews, M. S. (Eds.), 1986, *The Galaxy and the Solar System* (Tucson: University of Arizona Press), 485 pp.
- Tagliaferri, E., Erlich, A., Jacobs, C., Spalding, R., Worden, S. P. 1994, Detection of Meteoroid Impacts by Optical Sensors in Earth Orbit, in *Hazards Due to Comets and Asteroids* (Tucson: University of Arizona Press), (in press).

## Meghnad Saha's Influence in Astrophysics

### *Meghnad Saha Lecture*

David DeVorkin *Smithsonian Institution, Department of Space History, Washington DC 20560, USA*

**Abstract.** Commemorative seminars and celebrations have been taking place in India this year to mark the 100th birthday of the physicist Meghnad Saha, who was born on October 6, 1893. Saha was a lower caste Vaishya, born into a poor shopkeeper's family whose focus was rural Bengalese village life on the periphery of colonial Calcutta. From these unlikely beginnings, Saha became a significant catalyst for the transformation of astrophysics circa 1921 when, in a quartet of papers appearing in the *Philosophical Magazine* and in the *Proceedings of the Royal Society*, he showed how the quantum theory could be applied to stellar atmospheres through his theory of thermal ionization equilibrium. He was the first to show, on the basis of physical theory, that the Harvard spectral sequence was a temperature sequence.

*Key words:* History of Astronomy – stellar spectroscopy – Saha equation.

In 1924, E. A. Milne described the state of affairs in spectroscopic astronomy before Saha's papers had appeared.

It was known that some spectral lines could be produced, in the laboratory, only at high temperatures or under intense discharges, and that such lines were often only to be found in stars with high effective temperatures. But it was not known why this was so, or why the same line tended to disappear at still higher temperatures; and of quantitative explanation there was none. There appeared to be a definite relation between effective temperature and type of spectrum, but the connection was empirical. There was a gap in the logical argument (Milne 1924).

Saha had been excited by modern physics for some time, and was actively exploring the nature of the atom and how it behaved under a variety of conditions relevant to problems in physics and astronomy when he decided to attack the problem of linking the spectra of the sun and stars to Bohr's theory of the atom. He may well have been influenced by Professor D. N. Mallik, one of his teachers at the Sir T. N. Palit College of Science. Mallik had previously provided "kind help and encouragement" when Saha performed a theoretical study of mechanical action between two electrical systems (Meghnad 1917). And at the time, Mallik himself was performing experiments on ionization phenomena, which may well have drawn Saha's attention<sup>1</sup>.

---

<sup>1</sup>'High Vacuum-Spectra of Gases', which was communicated directly by Mallik as resulting from a paper delivered at the Third All-India Science Congress, 1916. In this paper, the two draw attention to their studies of gases like hydrogen under low pressure, and the spectroscopic study of gas discharge phenomena under low pressure.



In its original form, Saha's theory required much elucidation, both to firm up its theoretical foundations, and to refine the observational databases upon which it depended. His combining the concept of heat balance with Bohr's atomic model was innovative, but was not accepted by British theorists, whereas such formalisms were of less concern to Americans who wished mainly to exploit the consequences of his theory. Although Saha's theory of thermal ionization was rapidly absorbed into astrophysics, at first there was a question in Saha's mind whether he would be accepted as the creator of the theory unless he remained active in the field. Some at first merely called it the ionization equilibrium equation, and a few called it the Eggert-Saha equation. Some British patriots much later even called it the Eggert-Saha-Milne-Fowler equation.

Though it was Saha who set much of spectroscopic astrophysics along the new path, it was Henry Norris Russell in America, as well as E. A. Milne, R. H. Fowler, C. H. Payne, and others in the West, who were at the right place at the right time to take it through its course. Together they provided for the first time quantitative knowledge of compositions, density distributions, and temperatures, that resulted in the binding together of physics and astronomy in a manner that persists today. Saha, unable to compete in Calcutta due to indifference from the West, and political rivalries at home, could only watch what he set in motion.

By the 1930s Saha's political activism, present since 1905 when he was a protester in the wake of the partition of Bengal, emerged as he founded the 'Science & Culture' group, centered on a journal bearing the name. Though an ardent believer in independence, Saha nevertheless disagreed with Gandhi and Nehru's policies, feeling that it was essential for India to acquire, adapt, and apply the technical and scientific expertise of the West, and to make it Indian, in order to build a strong independent nation. Buying technology was not enough; growing a domestic infrastructure was essential. In 1938 Saha turned from spectroscopy to accelerator physics, campaigning that India had to compete in this new arena to become a truly modern, competitive nation, when it was freed from British bondage. These sentiments and his continuing activism won him a seat in Parliament after Independence.

How Saha attempted to remain active in astrophysics, and the details of his reception in the West, are discussed extensively elsewhere (DeVorkin 1994).

## References

- DeVorkin, David, 1994 *Saha's Influence in the West: A Preliminary Account*, Saha Commemoration Volume (Calcutta: forthcoming).
- Meghnad, Saha, 1917, On Maxwell's Stresses, *The Philosophical Magazine* 6th S. 33 March 256-261.
- Milne, E. A., 1924, Recent Work in Stellar Physics, *Proceedings of the Physical Society, London*, 36 pp. 94-113; quote from p. 95. quoted in DeVorkin and Kenat QMI p. 110.

# **The Early Universe and Structure Formation**



## Inflation and Cosmic No-Hair Conjecture

**Katsuhiko Sato** *Department of Physics, Faculty of Sciences, The University of Tokyo, Tokyo 113, Japan.*

**Abstract.** Recent developments of the study of cosmic no-hair conjecture are reviewed. Although strict no-hair conjecture does not hold within the limit of classical physics, there are some anisotropic or inhomogeneous solutions which evolve to inflationary universe. This suggests that the class of these solutions is rather large. It seems, however, no-hair conjecture holds effectively, provided that the universe itself does not collapse, since black holes and worm holes, which were formed as the consequence of evolution of initial inhomogeneities, evaporate away in the early universe, and the spacetime reduces to a homogeneous one.

*Key words:* Early universe -- inflationary model -- cosmology.

### 1. Introduction

In 1992 April, Smoot *et al.* (1992) announced that COBE-DMR group discovered the finite fluctuations in the cosmic microwave background radiation. Although the amplitude of the temperature fluctuations  $\Delta T/T$  at ten degree was only of the order of  $10^{-5}$ , this was the discovery which remains history, since by this discovery, it was justified that the seeds of the structure of the universe existed surely at the cosmic time, 300,000 years. At this time, the universe cleared up because of the recombination of hydrogen atoms. The standard scenario of structure formation in the big bang model becomes essentially indubitable by this discovery. The second important issue is that this discovery supports the inflationary universe model strongly, since the spectrum of the fluctuations was very consistent with the prediction of the inflationary universe model (Hawking 1982; Guth & Pi 1982; Starobinsky 1982; Bardeen *et al.* 1983). The careful comparison of the observation with the prediction from the inflationary universe models were done by many people after the discovery taking into account the tensor mode (for example Steinhardt 1993 and papers cited therein).

Originally, an exponentially expanding universe model was proposed as a consequence of grand unified theories (GUTs) by Sato (1981a, 1981b); Kazanas (1980) and Guth (1981). Sato (1981a, 1981b) considered this model in order to solve a problem of the formation of seeds of cosmic structure. In the standard FRW model, the seeds of the structure or the density fluctuations were created in the very early universe. The severe problem of this scenario is that spatial size of the seeds must be much greater than the particle horizon when they were formed, since the horizon in the FRW model becomes smaller and smaller with going back to the early universe. Sato (1981a, 1981b) showed that if the seeds are formed by phase transition of vacuum predicted by GUTs, the size of the seeds can be enlarged by the subsequent exponential expansion of the universe. As a consequence, the size of the fluctuations

becomes much greater than the horizon in the FRW model. Independently of GUTs, Starobinsky (1980) pointed out the universe expands exponentially as a consequence of  $R^2$  gravity which might arise by a quantum gravity effect. This exponentially expanding universe model was named as Inflationary Universe Model by Guth (1981) and he stressed that the inflationary universe model solves the flatness and horizon problems which were essential difficulties in the Standard Big Bang Model. Original model based on the first order phase transition of vacuum, however, has severe problems that phase transitions never terminate (Sato 1981b; Guth & Weinberg 1983), and the universe becomes extremely bumpy by the formation of huge bubbles, which conflicts with large-scale homogeneity of the present universe. In order to solve this problem, various modified models were proposed. 'New' Inflationary Model (Albrecht & Steinhardt 1982; Linde 1982), Chaotic Inflationary Model (Linde 1983) and Extended Inflation Model (La & Steinhardt 1989) are representative ones. Although many interesting models such as Soft Inflation Models (Berkin *et al.* 1990) and Scalar Neutrino Model (Murayama *et al.* 1993) are proposed, there has not yet been a definite model for Inflation. For recent developments, see reviews, Olive (1990), Goldwirth & Piran (1992).

The horizon problem is to question why our universe is so homogeneous over the horizon. Paradoxically, however, inflationary Universe models were proposed in the context of Robertson-Walker metric which is homogeneous and isotropic metric. People criticized that the above consequence is nothing but the assumption. In order to answer this criticism, inflationary model should be analyzed for more general universe models and it must be shown that the universe becomes isotropic and homogeneous by inflation independently of the initial conditions. The conjecture that all the inhomogeneous and anisotropic universes with cosmological constants (the vacuum energy density) evolve towards the deSitter universe is called cosmic no hair conjecture (Gibbons & Hawking 1977). Until now, many investigations on this conjecture have been done. In this paper, recent developments on this problem is reviewed.

## 2. Cosmic no-hair conjecture in anisotropic universe

First investigation of no-hair conjecture was done for the anisotropic but homogeneous universe model, because this is the most simple case. Wald (1983) showed that all the Bianchi types except IX evolve exponentially towards the deSitter solution. He also showed that it is the case that even Bianchi types IX model provided that  $\Lambda/^{(3)}R > 1/2$ , where  $\Lambda$  is the cosmological constant and  $^{(3)}R$  is three curvature. Extension of Wald's work was carried out by many people, Moss & Sahni (1986), Turner & Widrow (1986), Jensen & Stein-Schabes (1986), Rothman & Ellis (1986), Martinez-Gonzales & Jones (1986), Belinski *et al.* (1985). Recent investigation of Kitada & Maeda (1992) is one of the most interesting extensions of Wald's work. They investigated cases for the power-law inflation driven by scalar field  $\phi$  with the potential  $V(\phi) = V_0 \exp(-\lambda \kappa \phi)$ , and found a general condition for Bianchi types IX model, where  $\kappa^2 = 8\pi G$ . In the limit  $\lambda \rightarrow 0$ , (exponential expansion), the sufficient condition for inflation reduces to  $\Lambda/^{(3)}R > 1/3$  instead of the value  $1/2$  given by Wald (1983). For more progress in anisotropic homogeneous models, see a review of Maeda (1994) and papers cited therein.

### 3. Evolution of inhomogeneous inflationary universe

For the case of inhomogeneous universes, Starobinsky (1983) first found the solution of the inhomogeneous universe which evolves towards the deSitter solution. Barrow & Gron (1986) and Stein-Schabes (1987) also found solutions which evolve to homogeneous and isotropic universe. Shinkai & Maeda (1993) investigated for the plane wave mode of gravitational wave. Jensen & Stein-Schabes (1987) showed that any inhomogeneous universe will tend towards the deSitter solution if the following three conditions are satisfied, i.e., 1) the dominant energy condition,  $\rho > 0$ , 2) the strong energy condition,  $\rho + 3p > 0$ , and 3) the scalar spatial curvature is not positive in all the spacetime. The first and second conditions are very general, but the third condition cannot be accepted generally because usually density fluctuations contain positive curvature regions. The justification given by them is, therefore, limited in a very narrow class of cosmological models. In spite of these efforts, we can show a simple counter example against the cosmological no hair conjecture. That is the existence of the Schwarzschild-deSitter solution, which describes black holes in the deSitter universe. The metric is given by

$$ds^2 = -[1 - 2M/r - (r/l)^2]dt^2 + [1 - 2M/r - (r/l)^2]^{-1}dr^2 + r^2d\Omega^2, \quad (1)$$

where  $l$  is the horizon length of the deSitter universe, which is given by

$$l = (8\pi G\rho_v/3)^{-1/2} = (\Lambda/3)^{-1/2}, \quad (2)$$

where  $\rho_v$  is the vacuum energy density and  $\Lambda$  is the cosmological constant. If a black hole exists from the initial of the universe, it never disappears within classical physics. Furthermore even if no black hole exists from the initial, we can set an inhomogeneity which evolves towards a black hole. It is obvious that once black holes are formed, the universe cannot evolve to a homogeneous state within the classical physics. We may, therefore, conclude that no-hair conjecture does not hold in principle. Practically, however, it is very important to find a condition that inhomogeneous universes evolve towards the deSitter solution, and make clear whether the condition is satisfied in wide class or not, even if no-hair conjecture does not hold strictly.

Piran & Williams (1986) carried out the numerical simulation of the evolution of inhomogeneous universe by using  $[3+1]$  Regge calculus formalism. In their model, the universe is composed of 5 vertex and 10 edges. They showed that anisotropies and inhomogeneities are considerably decreased by inflation, but they have frozen during the inflation. In spite that, this is a pioneering work, the result is not clear and it is obvious that our universe cannot be described by only 5 vertexes. A severe problem of this formalism is that the Hamiltonian constraint and the evolution equation are inconsistent in inhomogeneous cases.

Furihata & Sato (1993) extended 5 cell model to 16 cell model, and investigated evolution of the anisotropic but homogeneous universe, since the inconsistency between the Hamiltonian constraint and the evolution equation disappears in homogeneous models. In our model,  $^3S$  universe is subdivided into 16 tetrahedra, and is composed of 8 vertex and 24 edges as shown in Fig. 1. In order to represent anisotropy, we made a tetrahedron composed of two types of edges with the length of  $\sqrt{a}$  and  $\sqrt{b}$ .

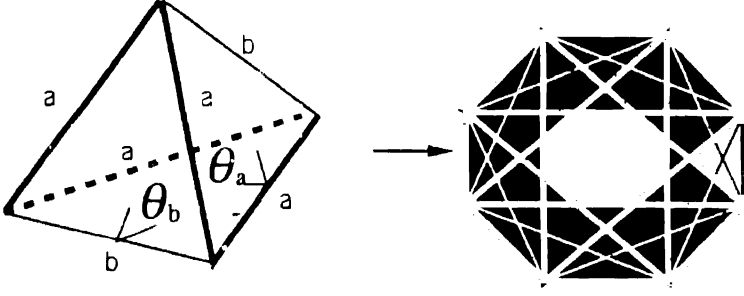


**Figure 1. Left:** An elementary tetrahedron. The four bold lines and the two thin lines have squared edge lengths  $a$  and  $b$ , respectively. **Right:** 16 cell homogeneous anisotropic model. All tetrahedra are equivalent.

As a scalar potential, chaotic inflation type model,  $V(\phi) = m^2 \phi^2/2$ , was employed. As initial models, we took  $a = b$  and  $\phi = 0$ , but expansion rates are different,  $\dot{\phi} \neq 0$ , where  $\omega \equiv \sqrt{a/b}$ . Under these initial conditions, the evolution equations are solved numerically. We have found all the models which satisfy the condition  $\Lambda_i^{(3)} R > 1/3$  evolve towards the deSitter solution. With decreasing the value of  $\Lambda_i^{(3)} R \ll 1/3$ , most of the models tend to recollapse, although some models still can go into inflationary phase successfully. This result is consistent with Kitada & Maeda (1992). We also found that with increasing the initial shear energy, which is defined as  $\dot{\phi}^2/6$ , universe evolves towards deSitter solution even if the initial vacuum energy  $V(\phi_i)$  is small. Extension to the inhomogeneous models is under progress, although it is hard to remove the inconsistency between the Hamiltonian constraint and the evolution equation.

At present, it is difficult to get reliable results by numerical simulation. Then, how can the fate of the very inhomogeneous universe be investigated? In order to investigate this problem, daring simplification or idealization is necessary. In the present talk, we discuss assuming that high density regions are spherical symmetric and the densities in them are spatially constant. The evolution of the spacetime structure of the bumpy universe was investigated in the original inflationary universe model (the first order phase transition model, Sato 1981a, b; Guth 1981) in detail in a series of papers, Sato *et al.* (1981, 1982), Sato 1987, Maeda *et al.* (1982), Kodama *et al.* 1981. When the amplitude of the density fluctuations is very large, the evolution of the spacetime structure in the inflationary universe is essentially the same even if the origin of the fluctuations is classical or quantum. Therefore the result obtained in the phase transition model essentially describes the evolution of the spacetime structure in the new inflation model (Linde 1982; Albrecht & Steinhardt 1981) and chaotic inflation model (Linde 1982) also. Here let's discuss the evolution by using a phase transition model.

### 3.1 Spacetime structure in a bubble or a low density hollow

As is well known, phase transition proceeds by nucleation of bubbles and subsequent expansion of bubbles. Let's assume the vacuum energy of the false vacuum to be  $\rho_1$ .

and the vacuum energy density in bubbles to be  $\rho_2$ . We can consider that these bubbles correspond to low density regions in the new inflation model and chaotic inflation model. By virtue of generalized Birkoff theorem, the metric in a spherical symmetric bubble (a hollow) must be the Schwarzschild-deSitter solution (equation 1), but with  $M=0$ , i.e., the metric is the deSitter metric with the cosmological constant  $\Lambda_2 = 8\pi G\rho_2$ , which is smaller than that of the outer high density region.

### 3.2 Spacetime structure of a high density region surrounded by bubbles

In the phase transition model, there exist infinite size networks of the false vacuum (the high energy state) in the early stage of the phase transition. However, in the cause of the phase transition, the high density vacuum regions ( $\rho_1$ ) are eventually divided into pieces and surrounded by bubbles. This also occurs in the new inflationary universe model and the chaotic inflation model with inhomogeneities in the cause of rolling down of the scalar field. In order to make clear the metric, let's consider the following simplified model: At  $t = t_0$ , infinite number of bubbles are created on the sphere of radius  $r = r_0$ . Then the universe is divided into three regions as shown in Fig. 2a region A is the inner high density ( $\rho_1$ ) vacuum region. The metric in this region is given by usual deSitter metric. The region B is the shell like low density vacuum region (bubble region), and the inner surface  $W_-$  and outer surface  $W_+$  of this region are expanding at light velocity. The metric is the Schwarzschild-deSitter metric (equation 1) with the mass  $M = 4\pi r_0^3 \rho_1 / 3$  and the cosmological constant  $\Lambda_2 = 8\pi G\rho_2$ . The region C is the outer high density vacuum region, and the metric is described by usual deSitter metric. As shown in Fig. 3, black holes are formed when the initial radius  $r_0$  is smaller than the horizon length of the deSitter universe,  $l = (8\pi G\rho_1/3)^{-1/2}$ , irrespective of the density contrast  $x \equiv \rho_1/\rho_2$ . The most interesting case is that wormhole structure is formed. As shown in Fig. 3, wormholes are produced when the density contrast  $\rho_1/\rho_2$  is greater than three and

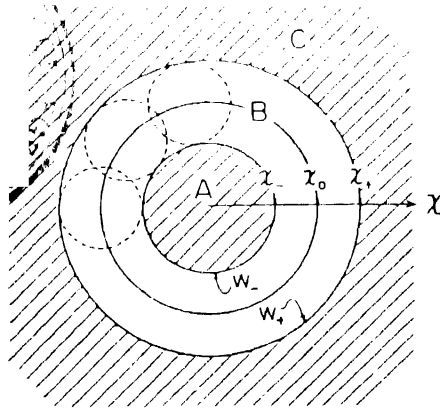


**Figure 2a.** A simplified model for high density vacuum region A, which is surrounded by low density vacuum region (bubble region) B.



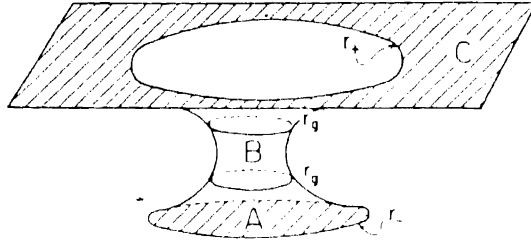


**Figure 2b.** A schematic picture of wormhole created from the large amplitude inhomogeneities. Because the region A is causally disconnected from the original universe, we can call the region A as 'a child universe' and the original universe C as 'mother universe'.

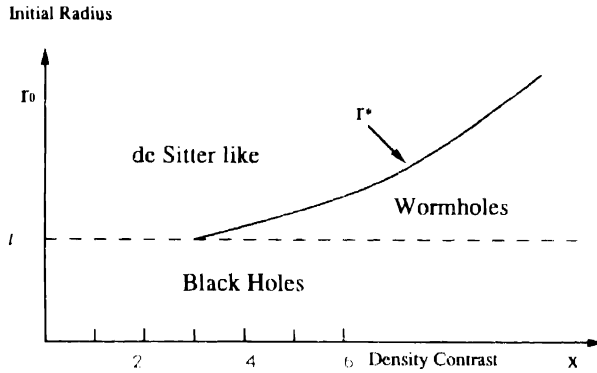


**Figure 3.** Summary of the final spacetime structure as a function of two parameters, the initial radius  $r_0$  and the density contrast  $x \equiv \rho_1/\rho_2$ .

also the initial radius  $r_0$  is greater than the horizon length  $l$  but smaller than the critical radius which is defined as

$$r^* = 3^{-1/2} (2/(x^2 - 1))^{1/3} x l. \quad (3)$$

In Fig. 2b, a space like hypersurface with constant conformal time is shown schematically. As shown in this figure, the inner region A remains as an ever-expanding deSitter like sub-universe connected with the outer universe C by an Einstein Rosen (wormhole) bridge B. Because the region A is causally disconnected from the original universe, we called the region A as 'a child universe' and the original universe C as 'mother universe' (Sato *et al.* 1981, 1982).

Recently Nambu & Siino (1992) carried out numerical simulation of the evolution of spherical symmetric false vacuum. Their results show good agreement with the present analytic result. Sakai & Maeda (1993) extended this bubble dynamics in generalized Einstein Theories.

Obviously no-hair conjecture breaks down in classical level, since these holes never disappear, and spacetime remains very inhomogeneous as discussed in preceding sections.

#### 4. Fate of inhomogeneous inflationary universe and evaporation of holes

In the preceding section, we showed that trapped high density regions evolve to wormholes by assuming that the spatial structure is spherical symmetric. In reality, the high density regions are highly asymmetric and new bubbles are nucleated (in the phase transition scenario) or low density regions are formed (in the new or chaotic inflation scenarios) therein. However the essential feature of the above model is still applicable to the actual situation. The very reason why black holes and wormholes are created is that the high density regions are trapped by low density vacuum. In case the relative size of the trapped domain to the surrounding low density region is small when it is formed, the domain wall continues to contract at light velocity and the energy released by the rolling over of the scalar field may well be concentrated in a very small region. Hence a black hole is generally created regardless of the initial shape of the high density domain. On the other hand, in case the domain size is larger than the horizon length, the domain wall continues to expand to infinity and consequently the universe attains to have two asymptotic (flat) regions. This anomalous structure occurs independent of the domain shape and strongly indicates the general formation of wormhole-bridge structure. Now we can speculate the evolution of the spacetime structure of the very inhomogeneous universe:

i) If wormholes, which are produced from the inhomogeneities, evaporate as black holes do, the Einstein-Rosen bridge disappears and child universes will become entirely spatially disconnected. Here 'spatially disconnected' means that there is a connected space like slice of the universe such that it does not intersect with the causal boundary of the universe and its causal future.  $J_+(\Sigma)$  is composed of topological disconnected components.

ii) The child-universes also expand exponentially, and phase transition (in the phase transition scenario) or inhomogeneous rolling over of scalar field (in the new and chaotic inflation scenarios) proceeds also therein. As a result grand-child universes are formed. This sequential production of universes may continue on and on. Now we easily arrive at an idea of multi-production of the universe; although the creator might have made a unitary universe, the universe itself is capable of bearing child-universes, which are again capable of bearing universes and so on (Sato 1981a, b, Sato *et al.* 1982). Linde's eternally existing self-reproducing chaotic inflationary universe model (1986) is an application to chaotic inflation, in which density contrast is generated by quantum gravitational effects. Blau, Guendelman & Guth (1987) and Farhi & Guth (1987) discussed the creation of wormholes taking into account the effects of the shell energy density more generally, but essential scenario is the same one of previous investigation (Sato *et al.* 1981; Kodama *et al.* 1981; Maeda *et al.* 1982; Sato *et al.* 1982).

Now let's discuss whether or not cosmic no-hair conjecture holds in this scenario. Typical mass of black holes and wormholes is of the order of

$$M = \frac{4\pi l^3}{3} \rho_v \approx \begin{cases} 1 \text{ kg} & \text{for GUT scale} \\ m_{\text{pl}} & \text{for Planck scale,} \end{cases} \quad (4)$$

where  $m_{\text{pl}}$  is the Planck mass. Then evaporation time of holes can be estimated as

$$t_{\text{ev}} = \left( \frac{M}{m_{\text{pl}}} \right)^3 t_{\text{pl}} \approx \begin{cases} 10^{-19} \text{ sec} & \text{for GUT scale} \\ t_{\text{pl}} & \text{for Planck scale,} \end{cases} \quad (5)$$

where  $t_{\text{pl}}$  is the Planck time. This evaporation time is much earlier than the nucleosynthesis era. The spacetime evolves towards a homogeneous one by the evaporation without conflicts with cosmological observations. We may conclude that no-hair conjecture holds effectively, provided that the universe itself does not collapse.

## 5. Summary

In the present talk, we reviewed recent development of the study of cosmic no-hair conjecture. It is clear that strict no-hair conjecture does not hold within the limit of classical physics. There are simple counter examples against this conjecture. If black holes and wormholes were formed once, they never disappear and the spacetime remain inhomogeneous. On the other hand, however, there are some inhomogeneous solutions which evolve to homogeneous isotropic universe. This suggests that the class of these solutions is rather large, as shown in homogeneous but anisotropic universe models. In order to make clear the condition for this 'weak no-hair conjecture' to hold, more careful investigation including numerical simulations is necessary (see for example, Goldwirth & Piran 1992). It seems, however, no-hair conjecture holds effectively, provided that the universe itself does not collapse, since black holes and wormholes, which were formed as a consequence of the evolution of initial inhomogeneities, evaporate away in the early universe, and the spacetime would reduce to a homogeneous one.

## Acknowledgements

The author thanks Y. Furihata, Y. Kitada and K. Maeda for stimulating discussion on problems of the cosmic no-hair conjecture. This work was partly supported by the Japanese Grant-in-Aid for Science Research Fund of the Ministry of Education, Science and Culture (No. 05640449, No. 05243103).

## References

- Albrecht, A., Steinhardt, P. J. 1982, *Phys. Rev. Lett.*, **48**, 1220.
- Bardeen, J. M., Steinhardt, P. J., Turner, M. S. 1983, *Phys. Rev.*, **D28**, 679.
- Barrow, J. D., Gron, O. 1986, *Phys. Lett.*, **182B**, 25.
- Belinsky, V. A., Grishchuk, L. P., Khalatnikov, I. M., Zeldovich, Ya. B. 1985, *Phys. Lett.*, **155B**, 232.
- Berkin, A. L., Maeda, K., Yokoyama, J. 1990, *Phys. Rev. Lett.*, **65**, 141.
- Blau, S. K., Guendelman, E. I., Guth, A. H. 1987, *Phys. Rev. D.*, **35**, 1747.
- Farhi, E., Guth, A. H. 1987, *Phys. Lett.*, **183B**, 149.
- Furihata, Y., Sato, K. 1993, *Class. Quantum Grav.*, **10**, 1147.
- Goldwirth, D. S., Piran, T. 1992, *Phys. Rep.*, **214**, 223.
- Gibbons, G. W., Hawking, S. W. 1977, *Phys. Rev.*, **D15**, 2738.
- Goldwirth, D. S., Piran, T. 1992, *Phys. Rep.*, **214**, 223.
- Guth, A. H., Pi, S.-Y. 1982, *Phys. Rev. Lett.*, **49**, 1110.
- Guth, A. H. 1981, *Phys. Rev.*, **D23**, 347.
- Guth, A. H., Weinberg, E. 1983, *Nucl. Phys.*, **B212**, 321.
- Hawking, S. W. 1982, *Phys. Lett.*, **B115**, 295.

- Jensen, L. G., Stein-Schabes, J. A. 1987, *Phys. Rev.*, **D35**, 1146.
- Kazanas, D. 1980, *Astrophys. J.*, **241**, L59.
- Kitada, Y., Maeda, K. 1992, *Phys. Rev.*, **D45**, 1416.
- Kodama, H., Sato, K., Sasaki, M., Maeda, K. 1981, *Prog. Theor. Phys.*, **66**, 2052.
- La, D., Steinhardt, P. J. 1989, *Phys. Rev. Lett.*, **62**, 376.
- Linda, A. D. 1982, *Phys. Lett.*, **108B**, 389.
- Linde, A. D. 1983, *Phys. Lett.*, **129B**, 177.
- Linde, A. D. 1986, *Phys. Lett.*, **175B**, 395.
- Maeda, K., Sato, K., Sasaki, M., Kodama, H. 1982, *Phys. Lett.*, **108B**, 98.
- Maeda, K. 1993, *Proceedings of the 37th Yamada Conference on the Evolution of Universe and its Observational Quest*, Ed. K. Sato (Tokyo: Universal Academic Press)
- Martines-Gonzalez, E., Jones, B. J. T. 1986, *Phys. Lett.*, **167B**, 37.
- Moss, I., Sahni, V. 1986, *Phys. Lett.*, **178B**, 156.
- Murayama, H., Suzuki, H., Yanagida, T., Yokoyama, J. 1993, *Phys. Rev. Lett.*, **70**, 1912.
- Nambu, Y., Siino, M. 1992, *Phys. Rev.*, **D46**, 5367.
- Olive, K. A. 1990, *Phys. Rep.* **190**, 307.
- Piran, T., Williams, R. M. 1986, *Phys. Rev.*, **D33**, 1622.
- Rothman, T., Ellis, G. F. R. 1986, *Phys. Lett.*, **108B**, 19.
- Sakai, N., Maeda, K. 1993, *Prog. Theor. Phys.*, **90**, 1001.
- Sato, K. 1981a *Mon. Not. R. astr. Soc.*, **195**, 467.
- Sato, K. 1981b, *Phys. Lett.*, **99B**, 66.
- Sato, K., Sasaki, M., Kodama, H., Maeda, K. 1981, *Prog. Theor. Phys.*, **65**, 1443.
- Sato, K., Sasaki, M., Kodama, H., Maeda, K. 1982, *Phys. Lett.*, **108B**, 103.
- Shinkai, H., Maeda, K. 1993, *Proceedings of the 37th Yamada Conference on the Evolution of Universe and its Observational Quest*, Ed. K. Sato (Tokyo: Universal Academic Press)
- Smoot, G. F. et al. 1992, *Astrophys. J.*, **396**, L1.
- Starobinsky, A. A. 1980, *Phys. Lett.*, **B91**, 99.
- Starobinsky, A. A. 1982, *Phys. Lett.*, **B117**, 175.
- Starobinsky, A. A. 1983, *JETP Lett.*, **37B**, 66.
- Steinhardt, P. J. 1993, *Proceedings of the 37th Yamada Conference on the Evolution of Universe and its Observational Quest*, Ed. K. Sato (Tokyo: Universal Academic Press)
- Stein-Schabes, J. A. 1987, *Phys. Rev.*, **D35**, 2345.
- Turner, M. S., Widrow, L. M. 1986, *Phys. Rev. Lett.*, **57**, 2237.
- Wald, R. M. 1983, *Phys. Rev.*, **D28**, 2118.



## Cosmology Today: Models and Constraints

**T. Padmanabhan** *Inter-University Centre for Astronomy and Astrophysics, Post Bag Ganeshkhind, Pune 411 007, India*

**Abstract.** Cosmological models for structure formation are severely constrained by several of the recent observational results. We now have observations which probe the power spectrum of fluctuations from about  $0.5 h^{-1} \text{ Mpc}$  to  $3000 h^{-1} \text{ Mpc}$ . These probes and the constraints they imply on models for structure formation are reviewed.

**Key words:** Cosmology — large scale structure.

### 1. Recipe for the universe

Models for structure formation assume that small perturbations in the energy density existed at very early epochs. These perturbations can then grow via gravitational instability leading to the structures we see today. Inflationary models – which are probably the most successful ones (Guth & Pi 1982; Hawking 1982; Starobinsky 1982; Padmanabhan *et al.* 1989; for a review see Narlikar & Padmanabhan 1991) in this regard produce density perturbations with an initial power spectrum  $P_{\text{in}}(k) \simeq Ak$ . Since each logarithmic interval in  $k$  space will contribute to the energy density an amount  $\Delta_p^2(k) \equiv d\sigma^2/d(\ln k) = (k^3 P(k))/(2\pi^2)$  we find that  $\Delta_p^2 \propto k^4$  for  $P \propto k$ . The contribution to gravitational potential from the same range will be  $\Delta_\phi^2 = \Delta_p^2 (9H_0^4/4k^4 a^2)$  which is independent of  $k$  if  $\Delta_p^2 \propto k^4$ . All these models need to be fine-tuned to keep the amplitude of the fluctuations small upto, say,  $z \gtrsim 10^3$ .

Given a Friedmann model with small inhomogeneities described by a power spectrum  $P(k, z_{\text{in}})$  at a high redshift  $z = z_{\text{in}}$ , we can predict unambiguously the power spectrum  $P(k, z_D)$  at  $z \approx z_D \approx 10^3$ , since we can use linear perturbation theory during this epoch. The shape of the spectrum at  $z = z_D$  will depend on the composition of dark matter in the universe (for a detailed discussion of these effects, see Padmanabhan 1993).

The fact, that one can compute the power spectrum at  $z \approx z_D$  analytically, allows one to predict large scale anisotropies in CMBR unambiguously in any given model. Comparing this prediction with the anisotropy observed by COBE one can fix the amplitude  $A$  of the power spectrum. For a wide class (Padmanabhan & Narasimha 1992) of the models,  $\Delta(k) \simeq 10^{-3} (kL)^2$  with  $L \simeq (24 \pm 4) h^{-1} \text{ Mpc}$  for  $k^{-1} \gtrsim 80 h^{-1} \text{ Mpc}$ . For CDM like models the function  $\Delta(k)$  flattens out at larger  $k$  and is about unity around  $k^{-1} \simeq 8 h^{-1} \text{ Mpc}$ . In pure HDM models,  $\Delta(k)$  has a maximum value of  $\Delta_m \simeq 0.42 h^{-2} (m/30 \text{ eV})^2$  at  $k_m \simeq 0.11 \text{ Mpc}^{-1} (m/30 \text{ eV})$  and decreases exponentially at  $k \gtrsim k_m$ .

The evolution of the power spectrum after decoupling (for  $z < z_D$ ) is more difficult to work out theoretically. In general, the power spectrum grows in amplitude

(preserving the shape), as long as the perturbations are small (Padmanabhan 1993). Fig. 1 shows the density contrast  $\sigma(R)$  computed from the linearly extrapolated power spectrum  $\Delta_0(k)$  in four different models. The density contrast  $\sigma(R)$  measures the rms fluctuations in mass within a randomly placed sphere of radius  $R$ ; upto factors of order unity,  $\sigma(R) \simeq \Delta(k \simeq R^{-1})$ .

At small scales, the true power  $\Delta_{true}(k)$  will be larger than  $\Delta_0(k)$  due to nonlinear effects. Fig. 2 shows the actual nonlinear evolution of the power spectrum with redshift based on numerical simulations. For a wide class of models, one can relate (Bagla & Padmanabhan 1994) the nonlinear and linear density contrasts by a set of power laws of the form:  $\sigma_{NL}^2(a, x) = A[\sigma_L^2(a, l)]^n$  with  $l^3 = x^3(1 + \sigma_{NL}^2)$  where  $A = n = 1$  for  $\sigma_L^2 \leq 1.2$ ;  $A = 0.794$ ,  $n = 2.9$  for  $1.2 \leq \sigma_L^2 \leq 6.0$  and  $A = 9.12$ ,  $n = 1.55$  for  $\sigma_L^2 \geq 6.0$ . This relation shows that  $\sigma_{NL}$  is steeper than  $\sigma_L$ .

In fact, for  $k^{-1} \gtrsim 2h^{-1} \text{ Mpc}$ , one can even neglect the evolution of the gravitational potential and study the motion of the particles in a potential 'frozen' in time. Such an approximation reproduces (Bagla & Padmanabhan 1994) the results of exact N-body simulations quite accurately for  $k^{-1} \gtrsim 1h^{-1} \text{ Mpc}$ . Fig. 3 shows the results of such a simulation. We see that the central effect in cosmological clustering is the motion of particles towards the minimum of the initial potential field.

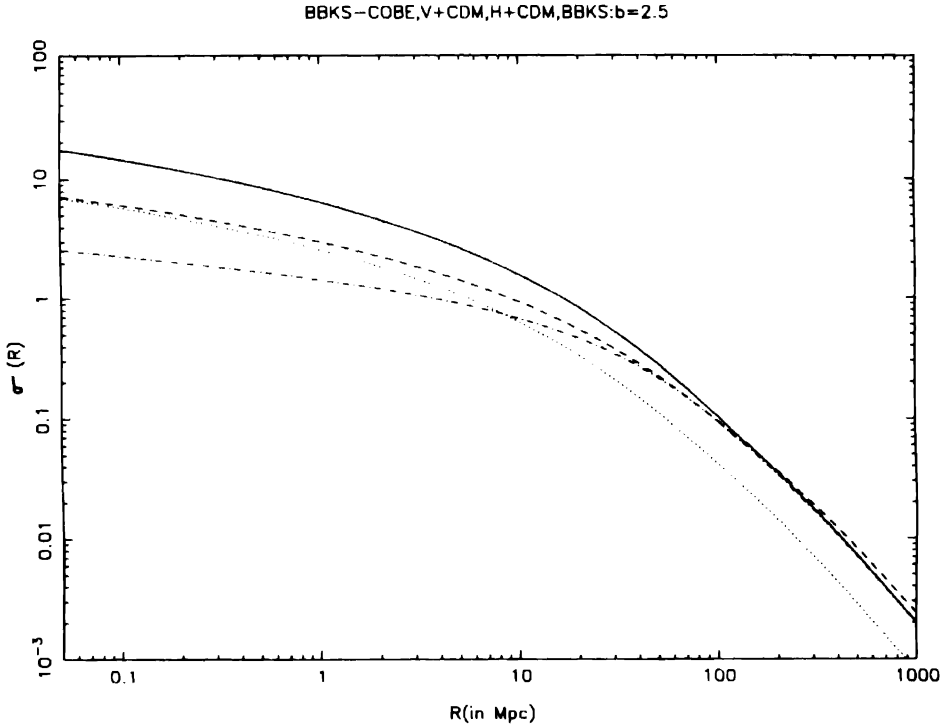


**Figure 1.** The linearly extrapolated density contrast, filtered by a sphere of radius  $R$ , in four different models. All models are for  $\Omega_i = 1$ , and normalised by COBE. Solid line: CDM model; Dashed line:  $\Lambda + \text{CDM}$  model with  $\Omega_v = 0.8$ ,  $\Omega_{\text{CDM}} = 0.2$ ,  $h = 0.8$ ; Dash-dot line: C + HDM model with  $\Omega_{\text{CDM}} = 0.7$ ,  $\Omega_{\text{HDM}} = 0.3$ ; Dotted line: CDM model with  $b = 2.5$ .

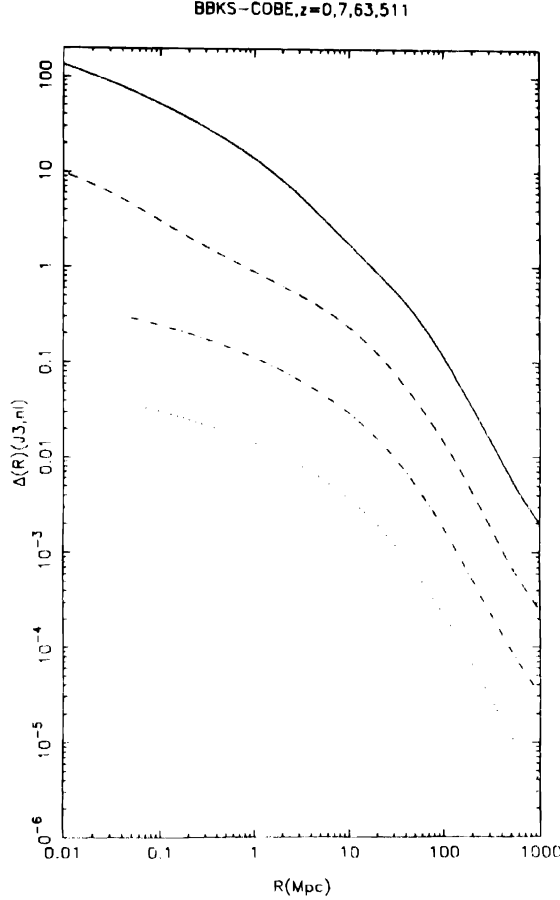


**Figure 2.** Non-linear evolution of the power spectrum based on N-body simulations.

At still smaller scales, it is important to understand gas dynamical processes before one can compare theory and observations. Since baryons can dissipate energy and sink to the minima of the dark matter potential wells, the statistical properties of visible galaxies and dark matter halos could be quite different. It is usual to quantify our ignorance at these scales by a ‘bias’ (acronym for ‘Basic Ignorance of Astrophysical Scenarios’) factor  $b$  and write  $\xi_{\text{gal}}(r) = b^2 \xi_{\text{mass}}(r)$ . Such a parameterisation is useful if  $b$  is independent of scale and morphology of galaxies. This seems to be somewhat unlikely.

## 2. Probing the power spectrum

One of the direct ways of constraining the models is to estimate the density contrast  $\sigma_{\text{obs}}(R)$  from observations at different scales and compare it with the theoretically predicted values. We shall discuss the probes of different scales in the decreasing order.



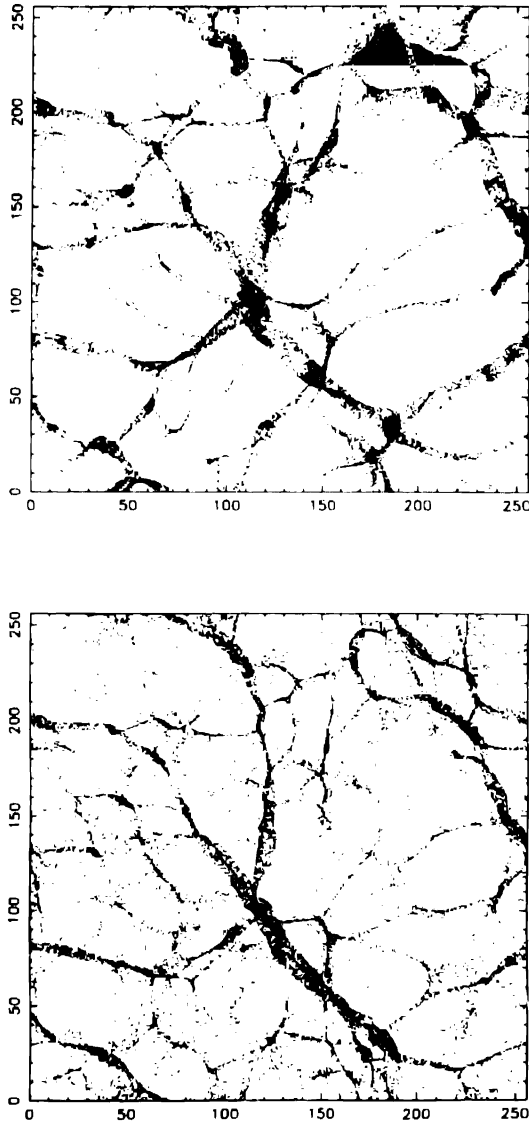


**Figure 3.** (a) (Top) A slice of the universe for a power spectrum  $P(k) \propto k^{-1}$  in 2D. This is obtained by moving the particles in a potential which is frozen in time. (b) (Bottom) The corresponding slice of the universe obtained from exact N-body evolution. The similarity between (a) and (b) shows that the key feature of cosmological evolution is in moving the particles towards the minima of the potential.

### 2.1 Near horizon scales: $(300-3000)h^{-1} \text{ Mpc}$

**COBE DMK:** These scales are so large that the best way to probe them is by studying the MBR anisotropy at angular scales which correspond to these linear scales. Since

a scale  $L$  subtends an angle  $\theta(L) \cong 1^\circ (L/100h^{-1} \text{ Mpc})$  at  $z \cong z_D$ , the  $(\Delta T/T)$  observations at  $(3^\circ - 30^\circ)$  probe these scales. The COBE-DMR observations (Smoot 1992) of  $(\Delta T/T)_{\text{rms}}$  and  $(\Delta T/T)_Q$  allow one to obtain the following conclusions: (i)  $\sigma(10^3 h^{-1} \text{ Mpc}) \cong 5 \times 10^{-4}$  (ii) The power spectrum at large scales is  $P_\eta(k) \cong Ak^n$  with  $n \cong 1.1 \pm 0.6$  and if we take  $\Omega = 1$ ,  $n = 1$ , then  $A^{1/4} \cong (24 \pm 4) h^{-1} \text{ Mpc}$  (iii) In this (Bagla & Padmanabhan 1993) range,  $\sigma(R) \cong (24 \pm 4 h^{-1} \text{ Mpc}/R)^2$ .

*Primordial gravity waves:* A large class of inflationary models also predict the existence of a stochastic background of gravitational waves which can be used to probe scales  $L \cong H_0^{-1} \cong 3000 h^{-1} \text{ Mpc}$ . The expected energy density of these waves is about  $\Omega_g \cong 3 \times 10^{-9}$ , and the spectrum is scale-invariant (Fabbri & Pollock 1983; Starobinsky 1985). Unfortunately, the current generation of gravity wave detectors cannot observe this background.

### 2.2 Very large scales: $(80 - 300) h^{-1} \text{ Mpc}$

*CMBR probes:* These scales span  $(0.8^\circ - 3^\circ)$  in the sky at  $z \cong z_D$ . Several ground based and balloon-borne experiments to detect anisotropy in MBR probe this scale. For example, the UCSB South Pole experiment has recently reported (Schuster 1993) a preliminary 'detection' of  $(\Delta T/T) \cong 10^{-5}$  at  $1.5^\circ$  scale, and a 95% confidence level bound of  $(\Delta T/T) < 5 \times 10^{-5}$ . This translates into the constraint of  $\sigma(10^2 h^{-1} \text{ Mpc}) \leq 5 \times 10^{-2}$ .

*CfA2 survey:* Some galaxy surveys notably CfA2 survey and pencil-beam surveys probe scales which are about  $10^2 h^{-1} \text{ Mpc}$  in depth (Broadhurst *et al.* 1990; Vogeley *et al.* 1992). Unfortunately, the statistics at these large scales is not good enough for one to obtain  $\sigma(R)$  directly from these surveys.

### 2.3 Large scales: $(40 - 80) h^{-1} \text{ Mpc}$

*CMBR probes:* The scales correspond to  $\theta_{\text{MBR}} \sim (24' - 48')$  and are probed by the experiments looking for small angle anisotropies in MBR. The claimed detection (Cheng *et al.* 1993) by MIT-MASM of  $(\Delta T/T) \cong (0.5 - 1.9) \times 10^{-5}$  at  $\theta \cong 28'$ , if confirmed, will give a bound of  $\sigma(50 h^{-1} \text{ Mpc}) \leq 0.3$ .

*Galaxy surveys:* Several galaxy surveys in particular the IRAS-QDOT and APM surveys, give valuable information about this range (Rowan-Robinson *et al.* 1990; Efsthathiou *et al.* 1990; Saunders *et al.* 1991). The angular correlation of galaxies, measured by APM survey is  $\omega(\theta) \cong (1 - 5) \times 10^{-3}$  at  $\theta \cong 14'$ . This corresponds to  $\sigma(50 h^{-1} \text{ Mpc}) \cong 0.2$ . What is more important, these surveys give valuable information about the shape of the power spectrum in this range.

*Large scale velocity field:* Using distance indicators which are independent of Hubble constant, it is possible to determine the peculiar velocity field  $v(R)$  of galaxies upto about  $80 h^{-1} \text{ Mpc}$  or so. The motion of these galaxies can be used to map the underlying gravitational potential at these scales. Careful analysis of observational data shows (Bertschinger & Dekel 1989; Dekel *et al.* 1990; Bertschinger *et al.* 1990) that  $v(40 h^{-1} \text{ Mpc}) \cong (388 \pm 67) \text{ kms}^{-1}$  and  $v(60 h^{-1} \text{ Mpc}) \cong (327 \pm 82) \text{ kms}^{-1}$ . From these values it is possible to deduce that  $\sigma(50 h^{-1} \text{ Mpc}) \cong 0.2$ . These observations also

allow us to determine the value of the parameter  $(\Omega^{0.6}/b_{\text{IRAS}})$  where  $b_{\text{IRAS}}$  is the bias factor with respect to IRAS galaxies. One finds that  $(\Omega^{0.6}/b_{\text{IRAS}}) = 1.28^{+0.75}_{-0.59}$  which implies that if  $\Omega = 1$ , then  $b_{\text{IRAS}} = 0.78^{+0.66}_{-0.29}$  and if  $b_{\text{IRAS}} = 1$  then  $\Omega = 1.51^{+1.74}_{-0.97}$ .

*Clusters and voids:* The cluster-cluster correlation function and the spectrum of voids in the universe can, in principle, tell us something about these scales. Unfortunately, the observational uncertainties are so large that one cannot yet make quantitative predictions.

It should be noted that a straight extrapolation of COBE-DMR result  $\sigma(R) \cong (24h^{-1} \text{ Mpc}/R)^2$  to  $R = 50h^{-1} \text{ Mpc}$  gives  $\sigma_{\text{COBE}}(50h^{-1} \text{ Mpc}) \cong 0.2$ . This is consistent with the result from large scale streaming  $\sigma_{\text{LSV}}(50h^{-1} \text{ Mpc}) \cong 0.2$ , which is not surprising since both probe the gravitational potential of dark matter. However, the result of galaxy surveys – based on visible matter – also gives  $\sigma_{\text{APM}}(50h^{-1} \text{ Mpc}) \cong 0.2$ . This suggests that observations are consistent with the conclusion that biasing is unimportant at  $R \cong 50h^{-1} \text{ Mpc}$ .

#### 2.4 Intermediate scales: $(8-40)h^{-1} \text{ Mpc}$

These scales span the angular scales of  $\theta_{\text{MBR}} \cong (4.8' - 24')$  and contain a background mass of  $M_{\text{smooth}} \cong (1.2 \times 10^{15} - 1.5 \times 10^{17})\Omega h_{50}^{-1} M_{\odot}$ . Note that the finite duration of the recombination epoch ( $\Delta z \cong 80$ ) wipes out anisotropies at angular scales smaller than  $\theta_{\text{min}} \cong 8'\Omega^{1/2}h$ . However, it is possible to probe these scales directly.

*Galaxy surveys:* The galaxy-galaxy correlation function  $\xi_{\text{gg}} \cong [r/5.4h^{-1} \text{ Mpc}]^{-1.8}$  is fairly well determined at these scales. Direct observations suggest that  $\sigma_{\text{gal}}(8h^{-1} \text{ Mpc}) \cong 1$  but the  $\sigma_{\text{DM}}$  and  $\sigma_{\text{gal}}$  at these scales can be quite different because of biasing.

*Cluster surveys:* There have been several attempts to determine the correlation function of clusters of different classes. It is generally believed that  $\xi_{\text{cc}} \cong (r/L)^{-1.8}$  with  $L \cong 25h^{-1} \text{ Mpc}$ . The index  $n = 1.8$  is fairly well determined though the scale  $L$  is not; in fact,  $L$  seems to depend on the richness class of the cluster. The quantity  $(\xi_{\text{cc}}/\xi_{\text{gg}})^{1/2}$  can be thought of as measure of the relative bias between cluster and galaxy scales. Observations suggest (Dalton *et al.* 1992; Nicol *et al.* 1992; Bahcall & West 1992; Postman *et al.* 1992) that this quantity depends on the cluster class and varies in the range (2-8). The observational uncertainties are still quite large for this quantity to be of real use: but if the observations improve we will have valuable information from  $\xi_{\text{cc}}$ .

*Abundance of rich clusters:* The scale  $R = 8h^{-1} \text{ Mpc}$  contain a mass of  $1.2 \times 10^{15} \Omega h_{50}^{-1} M_{\odot}$ . When this scale becomes nonlinear, it will reach an overdensity of about  $\delta \cong 178$ , or – equivalently – it will contract to a radius of  $R_f \cong (8h^{-1} \text{ Mpc})/(178)^{1/3} \cong 1.5h^{-1} \text{ Mpc}$ . A mass of  $10^{15} M_{\odot}$  in a radius of 1.5 Mpc is a good representation of Abell clusters we see in the universe. This implies that the observed abundance of Abell clusters can be directly related to  $\sigma(8h^{-1} \text{ Mpc})$ ; Several people have attempted to do this (White *et al.* 1993); the final results vary depending on the modelling of Abell clusters, and give  $\sigma(8h^{-1} \text{ Mpc}) \cong (0.5-0.7)$ . Since  $\sigma_{\text{gal}}(8h^{-1} \text{ Mpc}) \cong 1$ , this shows that  $b \cong (1.23-2)$  at  $8h^{-1} \text{ Mpc}$ .

It is possible to give this argument in a more general context (Subramanian & Padmanabhan 1994). Suppose that the contribution to critical density from collapsed

structures with mass larger than  $M$  is  $\Omega(M)$ , at a given redshift  $z$ . Then one can show that

$$\Omega(M) = \text{erfc} \left[ \frac{\delta_c(Hz)}{\sqrt{2}\sigma_0(M)} \right]$$

where  $\delta_c = 1.08$  and  $\text{erfc}(x)$  is the complementary error function. Figure 4 shows  $\Omega(M)$  as a function of  $\sigma_0(M)$  for various values of  $z$ . The Abell clusters (at  $z = 0$ ) contribute in the range  $\Omega \simeq (0.001-0.02)$ . Even with such a wide uncertainty, we get  $\sigma_{\text{clus}} \simeq (0.5-0.7)$ .

### 2.5 Small scales: $(0.05-8)h^{-1} \text{ Mpc}$

These scales correspond to structures with  $M_{\text{smooth}} \simeq (3 \times 10^8 - 1.2 \times 10^{15})\Omega h_{50}^{-1} M_\odot$ , and we have considerable amount of observational data covering these scales. Unfortunately, it is not easy to make theoretical predictions at these scales because of nonlinear, gas dynamical, effects.

*Epoch of galaxy formation:* Observations indicate that galaxy-like structures have existed even at  $z \simeq 3$ . This suggests that there must have been sufficient power at small

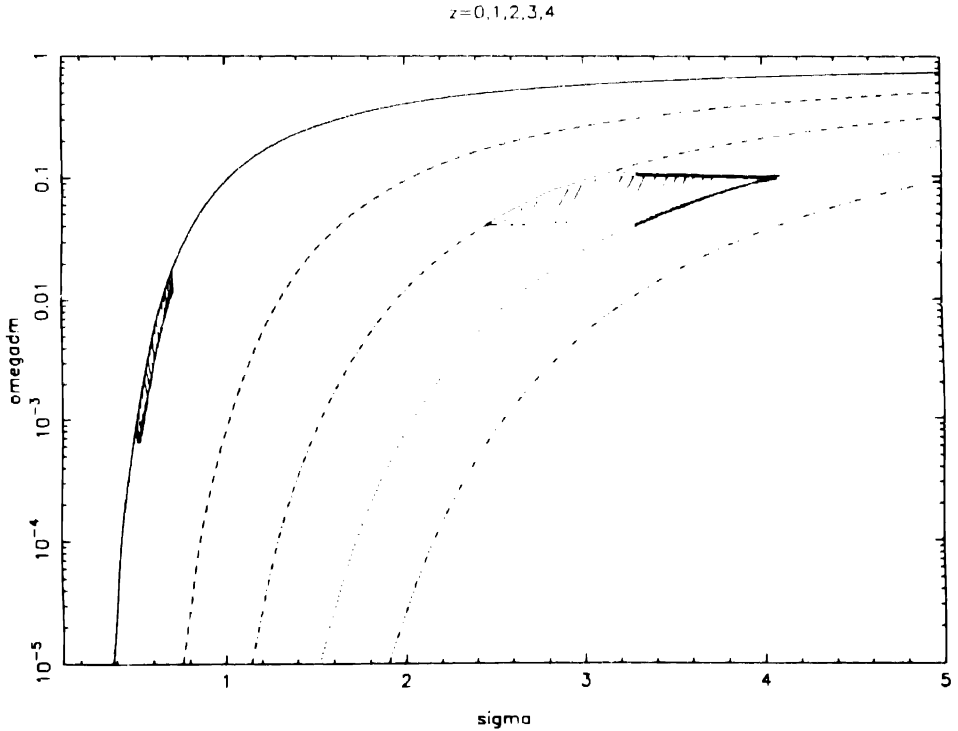


**Figure 4.** The contribution  $\Omega(M)$  due to collapsed objects at different redshifts as a function of  $\sigma(M)$ . Since Abell clusters (at  $z = 0$ ) contribute  $\Omega \simeq (0.001-0.02)$  we need  $\sigma(M) \simeq (0.5-0.7)$  at cluster scales. Similarly, since damped Lyman alpha systems contribute  $\Omega \simeq (0.04-0.1)$  in the redshift range of  $z \simeq (2-3)$  we need  $\sigma(M) \simeq (2.5-4.1)$  at the mass scales of  $M \simeq (10^{11}-10^{12})M_\odot$ .

scales to initiate galaxy formation at these high redshifts. Unfortunately, we do not have reliable estimate for the abundance of these objects at these redshifts and hence we cannot directly use it to constrain  $\sigma(R)$ .

*Abundance of quasars:* The luminosity function of quasars is fairly well determined upto  $z \approx 4$ . If the astrophysical processes leading to quasar formation are known, then the luminosity function can be used to estimate the abundance of host objects at these redshifts. Though these processes are somewhat uncertain, most of the models for quasar formation suggest (Hachneht 1993) that we must have  $\sigma(0.5^{-1} \text{ Mpc}) \gtrsim 3$ .

*Absorption systems:* The universe at  $1 \lesssim z \lesssim 5$  is also probed by the absorption of quasar light by intervening objects. These observations suggest that there exists significant amounts of clumped material in the universe at these redshifts with neutral hydrogen column densities of  $N_{\text{HI}} \simeq (10^{15} - 10^{22}) \text{ cm}^{-2}$ . We can convert these numbers into abundances of dark matter halos by making some assumptions about this structure. We find that (Subramanian & Padmanabhan 1994) in the redshift range of  $z \simeq (1.7 - 3.5)$  damped Lyman alpha systems contribute a fractional density of  $\Omega_{\text{Ly}} \simeq (0.06 - 0.23)$ . This would require  $\sigma(10^{12} M_{\odot}) \simeq (3 - 4.5)$ . This is also shown in Fig. 4.

*Gunn-Peterson bound:* While we do see absorption due to *clumped* neutral hydrogen, quasar spectra do not show any absorption due to smoothly distributed neutral hydrogen. Since the universe became neutral at  $z \lesssim z_p \simeq 10^3$ , and since galaxy formation could not have made all the neutral hydrogen into clumps, we expect the IGM to have been ionised sometime during  $5 \lesssim z \lesssim 10^3$ . It is not clear what is the source for these ionising photons. Several possible scenarios (quasars, massive primordial stars, decaying particles etc.) have been suggested in the literature though none of these appears to be completely satisfactory (Gunn & Peterson 1965; Steidel & Sargeant 1987; Schneider *et al.* 1989; Shapiro & Giroux 1987; Couchman & Rees 1986; Miralda-Escudé & Ostriker 1990). In all these scenarios, it is necessary to form structures at  $z \gtrsim 5$  so that an ionising flux of about  $J = 10^{-21} \text{ ergs cm}^{-2} \text{ s}^{-1} \text{ Hz}^{-1} \text{ sr}^{-1}$  can be generated at these epochs. Once again, it is difficult to convert this constraint into a firm bound on  $\sigma$  though it seems that  $\sigma(0.5 h^{-1} \text{ Mpc}) \gtrsim 3$  will be necessary.

*Direct observation 21 cm line:* It will be possible to observe the neutral hydrogen at  $z \gtrsim 3$  by observing the redshifted 21 cm line. The searches performed so far have not led to reliable detections. In a standard CDM model one would expect fluxes of (1.5-3) mJy from protocondensates with abundances of  $N \simeq (10^{-8} - 10^{-7}) \text{ Mpc}^{-3}$  at  $z = 3.3$ . These fluxes should be detectable (Subramanian & Padmanabhan 1993) in the near future with GMRT.

The constraints discussed in this section are summarised in Fig. 5.

### 3. Scorecard for the models

The simplest models one can construct will contain a single component of dark matter, either cold or hot. Such models are ruled out by the observations. The HDM models, normalised to COBE result will have maximum power of  $\Delta_m \simeq 0.42 h^{-2} (m/30 \text{ eV})^2$  at  $k = k_m = 0.11 \text{ Mpc}^{-1} (m/30 \text{ eV})$ . In such a case, structures could have started forming only around  $(1 + z_c) \simeq (\Delta_m/1.68) \simeq h_{50}^2 (m/30 \text{ eV})^2$  or at  $z_c \simeq 0$ . We cannot explain a host

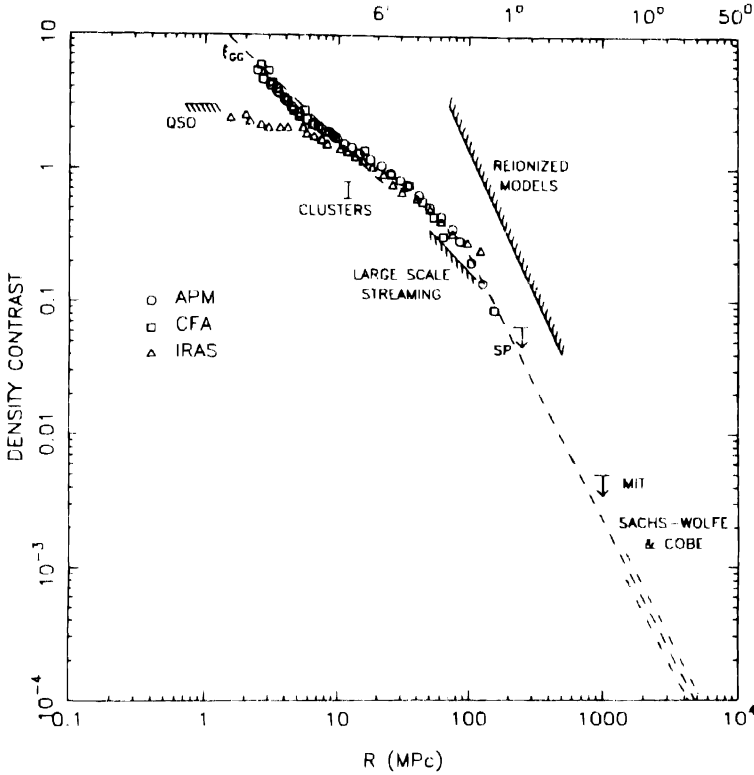


**Figure 5.** Constraints on  $\sigma(R)$  from different observations. See text for the discussion.

of high- $z$  phenomena with these models. The pure CDM models face a different difficulty. These models, normalised to COBE, predict  $\sigma_8 \simeq 1$ , which is too high compared to the bounds from cluster abundance. When nonlinear effects are taken into account, one obtains  $\xi_{\text{RG}} \propto r^{-2.2}$  for  $h = 0.5$  which is too steep compared to the observed value of  $\xi_{\text{RG}} \propto r^{-1.8}$ . In other words, CDM models have wrong shape for  $\xi(r)$  to account for the observations.

The comparison of CDM spectrum with observations suggests that we need more power at large scales and less power at small scales. This is precisely what happens in models with both hot and cold dark matter or in models with nonzero cosmological constant. These models have been extensively studied during the last year, and they fare well as far as large and intermediate scale observations are concerned. However, they have considerably less power at small scales compared to CDM model. As a result, they do face some difficulty (Subramanian & Padmanabhan 1994) in explaining the existence of high redshift objects like quasars. For example (Pogosyan *et al.* 1993), a model with 30% HDM and 70% CDM will have  $\sigma_{0.5} \simeq 1.5$ ; to explain the abundance of quasars comfortably one needs  $\sigma_{0.5} \simeq 3.0$ . If we use a more liberal criterion of  $\sigma(10^{11} M_\odot) \gtrsim 2$  [which corresponds to  $\sigma_{0.4} \gtrsim 2$  for  $h = 0.5$ ] then one is left with a very narrow window in the  $(\Omega_c - h)$  plane which accounts for all observations. Demanding that  $\sigma(10^{12} M_\odot) > 2$

[which is equivalent to saying that  $10^{12} M_{\odot}$  objects must have collapsed at a redshift of  $z_{12} = (2/1.68) - 1 \simeq 0.2$ ] will completely rule out this model.

Similar difficulties exist (Kofman *et al.* 1993) in models with cosmological constant. On demanding that: (i) the age of the universe is between (13–15) Gyr; (ii) the galaxy survey results are reproduced; (iii)  $\sigma_8$  is at an acceptable range and (iv) the large scale streaming motions are correctly reproduced, one finds that no acceptable window exists in the  $(\Omega_{\text{CDM}} - h)$  plane for a model with  $\Omega_{\text{CDM}} + \Omega_{\Lambda} = 1$ . If the constraint (iv) is relaxed to a  $2\sigma$  level then a narrow window exists in this plane.

The comparison of models show that it is not easy to accommodate all the observations even by invoking two components to the energy density. (These models also suffer from serious problems of fine-tuning.) By and large, the half-life of such quick-fix model seem to be about 2–3 years. One is forced to conclude that to make significant progress it is probably necessary to perform a careful, unprejudiced analysis of: (a) large scale observational results and possible sources of error and (b) small scale astrophysical processes.

### Acknowledgements

I thank J. S. Bagla, O. Lahav, M. Rees, K. Subramanian and S. D. M. White for useful discussions.

### References

- Bagla, J. S., Padmanabhan, T. 1994 in preparation; Hamilton, A. J. S. *et al.* 1991, *Astrophys. J.*, **374**, L1.
- Bagla, J. S., Padmanabhan T. 1994 *Mon. Not. R. astr. Soc.*, **266**, 227; Bagla, J. S., Padmanabhan, T., 1994, (this volume).
- Bertschinger, E., Dekel, A. 1989 *Astrophys. J.*, **364**, 349; Bertschinger, E. *et al.* 1990, *Astrophys. J.*, **364**, 370.
- Broadhurst, T. *et al.* 1990, *Nature* **343**, 726; Vogeley, M. S. *et al.* 1992, *Astrophys. J. Letts.*, **391**, L5.
- Cheng, E. S. *et al.* 1993, preprint.
- Dalton, G. D. *et al.* 1992, *Astrophys. J. Letts.*, **390**, L1; Nicol, R. C. *et al.* 1992, *Mon. Not. R. astr. Soc.*, **255**, 21p; Bahcall, N., West, M. 1992, *Astrophys. J.* **270**, 70; Postman, M. *et al.* 1992, *Astrophys. J.*, **384**, 404.
- Fabbri, R., Pollock, M. D. 1983, *Phys. Lett. B.* **125**, 445; Starobinsky, A. A. 1985, *Sov. Astron. Letts.*, **9**, 302.
- Gunn, J. E., Peterson, B. A. 1965, *Astrophys. J.*, **142**, 1633; Steidel, C. C., Sargent, W. L. W. 1987, *Astrophys. J. Letts.*, **318**, L11; Also see Schneider *et al.* 1989, *Astr. J.*, **98**, 1951; See eg. Shapiro, P. R., Giroux, M. L. 1987, *Astrophys. J. Letts.*, **321**, L107; Couchman, H. P. M., Rees, M. J. 1986, *Mon. Not. R. astr. Soc.*, **221**, 1513; Miralda-Escudé, J., Ostriker, J. P., 1990, *Astrophys. J.*, **350**, 1.
- Guth, A., Pi, S. Y. 1982, *Phys. Rev. Lett.*, **49**, 1110; Hawking, S. W. 1982, *Phys. Lett.*, **B115**, 295; Starobinsky, A. A. 1982, *Phys. Lett.*, **B117**, 175; Padmanabhan, T., Seshadri, T. R., Singh, T. P. 1989, *Phys. Rev.*, **D39**, 2100. For a review see Narlikar, J. V., Padmanabhan, T. 1991, *Annu. Rev. Astron. Astrophys.*, **29**, 325.
- Hachnelt, M. G. 1993, IOA preprint.
- Kofman, L. *et al.* 1993, CITA preprint.
- Padmanabhan, T., Narasimha, D. 1992, *Mon. Not. R. astr. Soc.*, **259**, 41p.
- Padmanabhan, T. 1993, *Structure formation in the Universe* (UK: Cambridge University Press), chap. 4.

- Pogosyan, D. Yu, Starobinsky, A. A. 1993, IOA preprint.
- Rowan-Robinson, M. *et al.* 1990, *Mon. Not. R. astr. Soc.*, **247**, 1; Efsthathiou, G. *et al.* 1990, *Mon. Not. R. astr. Soc.*, **247**, 10p; Saunders, W. *et al.* 1991, *Nature*, **349**, 32.
- Smoot, G. F. *et al.* 1992, *Astrophys. J.*, **396**, L1.
- Schuster, J. *et al.* 1993, *Astrophys. J.*, **412**, L47.
- Subramanian, K., Padmanabhan, T. 1993, *Mon. Not. R. astr. Soc.*, **265**, 101.
- Subramanian, K., Padmanabhan, T. 1994, IUCAA preprint S'94.
- White, S. D. M. *et al.* 1993, *Mon. Not. R. astr. Soc.*, **262**, 1023.





## Confrontation of a Double Inflationary Cosmological Model with Observations of the Large Scale Structure

J. P. Mückel & S. Gottlöber *Astrophysikalisches Institut Potsdam, An der Sternwarte 16, 14482 Potsdam, Germany*

**Abstract.** We consider the non-scale invariant perturbation spectra originated by a double inflationary cosmological model. The predictions of the derived spectra are compared with the results of large scale observations as bulk flow velocity, mass variances, counts-in-cells analysis applied to the Stromlo-APM redshift survey and the determination of cosmic Mach numbers. This comparison strongly restricts the possible parameter space and allows for the determination of a very few fitting models.

*Key words:* Cosmology - large scale structure.

### 1. Introduction

During the last years observations seem to indicate that the predictions of the standard CDM model at very large scales and on small scales are incompatible. Although the cold dark matter model (CDM) with biasing ( $b_q \simeq 1.5 - 2.5$ ) and  $n = 1$  for the spectrum (Harrison-Zeldovich spectrum) of the primordial density perturbations ( $\delta_k^2 \propto k^n$ ) leads to results remarkably close to the observational data, recent observations of such structures as the Great Attractor (Lynden-Bell *et al.* 1988; Dressler 1991) and the Great Wall (de Lapparent *et al.* 1986), the large-scale clustering in the redshift survey of IRAS galaxies (Efsthathiou *et al.* 1990; Saunders *et al.* 1991), and the angular correlation function of the deep APM galaxy survey (Maddox *et al.* 1990, see also Loveday *et al.* 1992) imply that at scales larger than approximately  $10 h^{-1} \text{ Mpc}$  there is more power in the perturbation spectrum than expected in the standard model. The spectrum of perturbations observed at the present time is a product of an initial (primordial) spectrum and some transfer function  $T(k)$ . The latter results from the transition from the radiation-dominated era to the matter dominated one at redshifts  $z \sim 10^4$  and depends on the structure of the dark matter. Thus, any deviation from the standard model may be explained either by changing the initial flat spectrum, or by changing the transfer function  $T(k)$  in accordance with a more complicated matter content. For a model with mixed dark matter one can find observational constraints in a similar way as discussed here (Pogosyan & Starobinsky 1993, see also for further references). Following Gottlöber, Mückel & Starobinsky (1993) we investigate here nonflat primordial perturbation spectra within the standard CDM model. These spectra are generated in a double inflationary cosmological models (Gottlöber, Müller & Starobinsky 1991). The standard CDM model contains one free parameter, namely the normalization constant. The attempts to modify the power spectrum due to an effective change of matter content introduces one more

parameter. In the result of our model the shape of the initial perturbation spectrum is modified. This leads to three parameters of the models to be defined. The resulting spectra are of Harrison-Zeldovich-Type only in the limiting cases of very small and very large scales. In the intermediate range the effective exponent  $n$  is a function of the scale. The spectra are characterized by the parameter  $\Delta$  which is approximately equal to the ratio of the power at large and at small scales and by a typical wave number  $k_b$  denoting the onset of the step like behaviour in the spectra towards the large scale end. The quantity  $\Delta$  mainly depends on the parameters characterizing the inflationary stages (the mass of the scalar particle and the coupling constant of the higher order terms) whereas  $k_b$  depends on the energy density of the scalar field at the onset of the second inflation.

Inflation leads to a flat homogeneous universe with adiabatic perturbations of the metric in terms of the peculiar gravitational potential. The Fourier components of the Gaussian fluctuations  $\phi_k$  determine the shape of the primordial perturbation spectrum  $\phi_k^2 k^4 \propto \delta_k^2$ .

The principal shape of the considered spectra can be given with good approximation by the fit formula

$$\phi_k = \begin{cases} \left[ \frac{A}{k^{3/2}} \left[ \log \left( \frac{k_b}{k} \right) \right]^i + \frac{B}{k^{3/2}} \left[ \log \left( \frac{k_1}{k_b} \right) \right]^\theta \right] & \text{if } k \leq k_b \\ \left[ \frac{B}{k^{3/2}} \left[ \log \left( \frac{k_1}{k} \right) \right]^\theta \right] & \text{if } k > k_b. \end{cases} \quad (1)$$

Then the power spectrum is  $P(k) = \phi_k^2 k^4 T(k)$  where a good fit for the transfer function  $T(k)$  is given by Bond & Efstathiou (1984).

## 2. Comparison with observations

For the obtained perturbation spectra we have calculated the mean square expectation values  $C_l$  of the background temperature fluctuations (Gottlöber & Mückel 1993). With the measured  $\sigma(10') = 1.1 \times 10^{-5} \times (1 \pm 0.17)$  (Smoot *et al.* 1992) the free

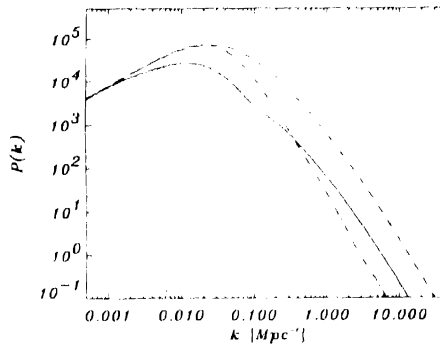


**Figure 1.** COBE normalized perturbation spectra of the standard CDM model (dashed line), a MDM model (30% hot and 70% cold dark matter, dash dotted line), a model with nonzero cosmological constant (dotted line) and the best fit model ( $k_{\text{break}}^{-1} = 7 \text{ Mpc}$ ,  $\Delta = 3$ , solid line).

normalization constant for the calculated spectra has been determined and using the linear transfer function  $T(k)$  of the standard CDM model (Bond & Efstathiou 1984) the power spectrum of the density fluctuations at the present epoch  $P(k)$  can be calculated. The shape of the different density perturbation spectra is shown in Fig. 1.

By help of the density perturbation spectrum  $P(k)$  we are able to compute the variance of the mass fluctuation  $\sigma_M^2(R) = (\delta M/M)^2$  in a sphere of length scale  $R$ . By comparison with  $\sigma_8$  from galaxy observations we estimate the bias factors, i.e. the relation between dark matter mass distribution and the galaxy distribution. The different bias factors obtained for the considered spectra are within the range between 1.5 and 4.4. We present the permitted region in the parameter space for the bias factors in the  $\Delta - k_b^{-1}$  plane (Fig. 2). Somewhat smaller bias we obtain by fitting the angular correlation functions for the different spectra to the angular correlation function obtained for the APM data (Maddox *et al.* 1990). Next we have investigated our spectra with respect to the bulk-flow studies by Bertschinger *et al.* (1990) and more recently by Courteau *et al.* (1993). We have estimated the velocity variance  $\sigma_v(R)$  for our models. The predicted velocities are marginally less than the observed ones. However, it seems likely that the actual values of the bulk flow velocities at our location of the universe are larger than the average values which should be compared

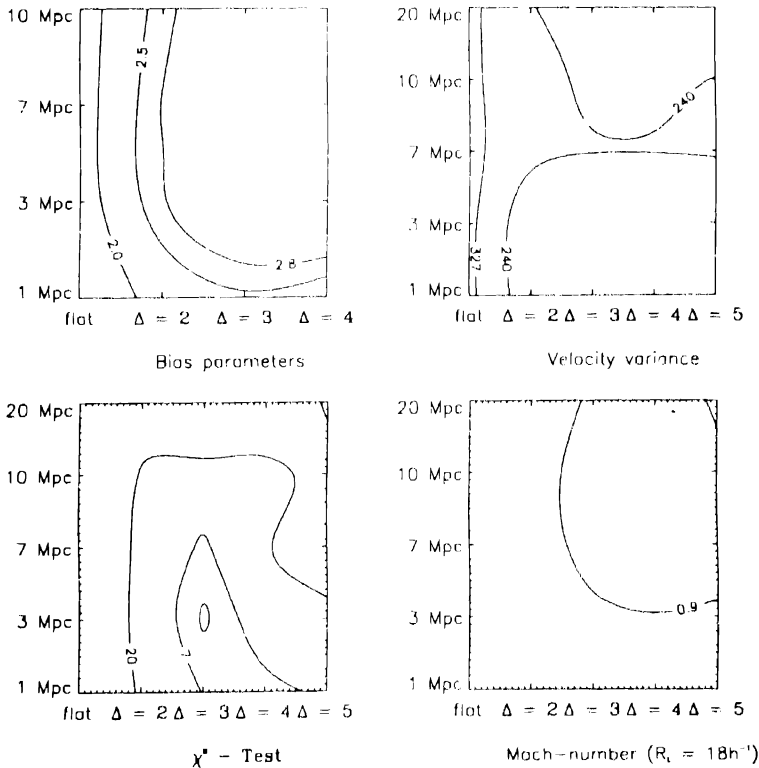


**Figure 2.** The permitted regions in the  $\Delta - k_b^{-1}$  parameter space fitting the observational data obtained for the bias parameters, the bulk velocities, the counts-in-cells analysis and for the cosmic Mach number test.

with the model predictions. Taking into account both uncertainties in the COBE normalization and in the determination of the bulk velocities as well as the predictions of the best fitting models ( $k_h^{-1} \leq 7$  Mpc) are within the error boxes (Fig. 2).

Further we compare the predicted variances  $\sigma_i^2$  for the counts-in-cells analysis of large-scale clustering in the newly completed Stromlo-APM redshift survey (Loveday *et al.* 1992) by a  $\chi^2$ -test spectra. In Fig. 2 we show the labels of  $\chi^2(\Delta, k_0) = \text{const.}$  where we adopt (the formal degree of freedom is equal to 7) that  $\chi^2 \approx 3$  is a very good fit, the fits are reasonable up to  $\chi^2 \approx 7$  and above  $\chi^2 \approx 20$  the fits are bad. For the flat standard CDM model we get  $\chi^2 = 47.5$ . Finally, we provide the Mach number test for our models. This test is independent of the normalization of the spectrum and of all considerations concerning the mass variance as well (Ostriker & Suto 1990). We compare the predicted values for our models with the Mach numbers  $M$  obtained from observational analysis  $M_1 = (4.2 \pm 1.0)$ ,  $M_2 = (2.2 \pm 0.5)$ , and  $M_3 = (1.3 \pm 0.4)$  at the scales  $R_L = 4 h^{-1}$  Mpc,  $8 h^{-1}$  Mpc, and  $18 h^{-1}$  Mpc, respectively. For the function  $M_3(\Delta, k_0)$  we draw the allowed region given by the error bar labels from observationally obtained Mach numbers in the  $\Delta - k_h^{-1}$  plane (Fig. 2).

### 3. Conclusions

The comparison of all provided tests yields a nonzero parameter space for our models. The results from the counts-in-cell analysis for the APM-Stromlo survey and the Mach number test are most restrictive. Especially from the  $\chi^2$ -test we conclude that the spectrum with an amplitude at large scales three times of the amplitude for the standard flat CDM model and an onset of the strongest deviation from the flat spectrum between  $20 h^{-1}$  Mpc and  $50 h^{-1}$  Mpc represents the best fit of the observational data. The best fit spectra will be reproduced quite well by (1) with the parameters  $k_h = 0.1$ ,  $k_1 = e^{60}$ ,  $A = 788$ ,  $B = 60.6$ , and  $\gamma = 0.5$  and  $\beta = 0.66$ . For these spectra we obtain bias factors between 2.0 and 2.7. In order to get stronger limitations on the theoretical models more observational data are needed. Especially positive measurements of the CBR anisotropy at smaller angular scales ( $\theta \leq 1^\circ$ ) would make the existing models more distinguishable (Gottlöber & Mückel 1993).

### Acknowledgement

We wish to thank Alexei A. Starobinsky initiating the work on this subject for valuable discussion and helpful remarks.

### References

- Bertschinger, E., Dekel, A., Faber, S. M., Dressler, A., Burstein, D. 1990, *Astrophys. J.*, **364**, 370.
- Bond, J. R., Efsthathiou, G. 1984, *Astrophys. J.*, **285**, L45.
- Courteau, S., Faber, S. M., Dressler, A., Willick, J. A. 1993, *Astrophys. J.*, **1**, L1.
- Dressler, A. 1991, *Nature* **350**, 391.
- de Lapparent, V., Geller, M., Huchra, J. 1986, *Astrophys. J.*, **202**, L1.
- Efsthathiou, G., Kaiser, N., Saunders, W., Lawrence, A., Rowan-Robinson, M., Ellis, R. S., Frenk, C. S. 1990, *Mon. Not. R. astr. Soc.*, **247**, 10p.

- Gottlöber, S., Mückel, J. P. 1993, *Astr. Astrophys.*, **272**, 1–7.
- Gottlöber, S., Mückel, J. P., Starobinsky, A. A. 1993, preprint *AIP* 93–11.
- Gottlöber, S., Müller, V., Starobinsky, A. A. 1991, *Phys. Rev. D*, **D 43**, 2510.
- Loveday, J., Efstathiou, G., Peterson, B. A., Maddox, S. J. 1992, *Astrophys. J. Letters*, **400**
- Lynden-Bell, D., Faber, S. M., Burstein, D., Davies, R. L., Dressler, A., Terlevich, R. J., Wegner, G. 1988, *Astrophys. J.*, **326**, L9.
- Maddox, S. J., Efstathiou, G., Sutherland, W. J., Loveday, J. 1990, *Mon. Not. R. astr. Soc.*, **242**, 43p.
- Ostriker, J., Suto, Y. 1990, *Astrophys. J.*, **348**, 378.
- Pogosyan, D. Yu., Starobinsky, A. A. 1993, *Mon. Not. R. astr. Soc.*, in print.
- Saunders, W., *et al.* 1991, *Nature*, **349**, 92.
- Smoot *et al.* 1992, *Astrophys. J.*, **396**, L1.



## Cosmological Solutions in Two-Component Nonlinear Sigma Model

S. V. Chervon\* *Inter-University Centre for Astronomy and Astrophysics, Post Bag 4, Ganeshkhind, Pune 411 007, India*

**Abstract.** The general features of the exact solutions for the two-component nonlinear sigma model in the framework of spatially flat Friedman-Robertson-Walker, de Sitter and Bianchi-I type universes are discussed.

**Key words:** Cosmology—early universe.

### 1. Nonlinear sigma model

The nonlinear sigma model or chiral model represents the theory of several scalar fields, where the interaction is introduced by the constraint on the values of free scalar fields (Perelomov 1987). It was shown (Chervon 1992), that the nonlinear sigma model (NSM) is a possible candidate to the inflationary universe scenario as a generalization from the self-interacting scalar field (SSF) theory and multiple inflationary models. The SSF theory with any type of potential  $V(\phi)$  can be obtained from the two-component NSM by imposing special restrictions on derivatives of the chiral fields. That is why this model looks very attractive in the framework of inflation scenarios. The exact solutions for the two-component NSM minimally coupled to gravity within the context of cosmological spaces will be discussed in the present paper.

Let us consider the self-gravitating NSM (Ivanov 1983) in the presence of the cosmological constant. The corresponding action is

$$S = \int_M d^4x \sqrt{g} \left\{ \frac{R + 2\Lambda}{2\kappa} + \frac{\alpha}{2} h_{AB} \varphi_i^A \varphi_k^B g^{ik} \right\}. \quad (1)$$

Here  $x = (x^1, \dots, x^4)$  are the local coordinates of space-time  $(M, g_{ik})$ ;  $\varphi = (\varphi^1, \dots, \varphi^n)$  is the multiplet of scalar fields which lies in a target or chiral space  $N$  with the metric  $h_{AB}$ ;  $\alpha$  is a coupling constant;  $g = |\det(g_{ik})|$ ;  $\varphi_{,k} := \varphi_{,k} := \partial_k \varphi$ . Where repeated indices occur the summation convention is assumed.

Starting from the surface of rotation

$$dS_\sigma^2 = d\phi^2 + 2P(\phi)d\chi^2, \quad \varphi^1 = \phi, \varphi^2 = \chi \quad (2)$$

as a target space, it is possible to rewrite (1) in the form

$$S = \int_M d^4x \sqrt{g} \left\{ \frac{R + 2\Lambda}{2\kappa} + \frac{\alpha}{2} [\phi_i \phi^i + 2P(\phi)\chi_i \chi^i] \right\}. \quad (1^*)$$

\* On leave of absence from the Moscow State University Branch in Ulyanovsk, 42, Leo Tolstoy St., Ulyanovsk 432700, Rossija.



By varying the action (1\*) with respect to  $\varphi^A$  one can obtain the equations of motion

$$\frac{1}{\sqrt{g}} \partial_i (\sqrt{g} \phi^i) - \frac{dP}{d\phi} \chi_i \chi^i = 0, \quad (3a)$$

$$\frac{1}{\sqrt{g}} \partial_i (\sqrt{g} 2P(\phi) \chi^i) = 0. \quad (3b)$$

The components of the energy momentum tensor are

$$T_{ik} = \alpha \{ \phi_i \phi_k + 2P(\phi) \chi_i \chi_k \} - \frac{\alpha}{2} g_{ik} \{ \phi_j \phi^j + 2P \chi_j \chi^j \}. \quad (4)$$

To get the equation of motion corresponding the SSF theory

$$S_{SSF} = \int_M d^m x \sqrt{g} \left\{ \frac{1}{2} \phi_i \phi_k g^{ik} - V(\phi) \right\}, \quad (5)$$

one needs to introduce the following constraints:

$$(i) \chi_i \chi^i P(\phi) = -V(\phi); \quad (ii) \chi(x) \text{ is the solution of (3b)}. \quad (6)$$

As a rule in the context of inflation scenarios the potential of self-interaction  $V(\phi) > 0$ . Then the condition (i) implies that the chiral potential  $P(\phi)$  should be more or less than zero depending on the sign of the  $\chi_i \chi^i$ .

It should be noticed here, that under restriction (6) the dynamical equations for the NSM (3) and for the SSF theory (5) will be the same. But the energy momentum tensors are different. Namely, the right-hand part of (4) can never be reduced to the energy momentum tensor of the SSF

$$T_{ik}^{SSF} = \phi_i \phi_k - \frac{1}{2} g_{ik} [ \phi_j \phi^j - 2V(\phi) ]. \quad (7)$$

Therefore, the sources of gravitational field are always different, even when the conditions (6) hold.

## 2. Isotropic and homogeneous universes

Let us now turn our attention to the gravitational field produced by the two-component NSM (1\*). For the spatially flat space-times with the metric

$$dS_M^2 = (dt)^2 - K^2(t) \{ (dr)^2 + r^2 [(d\theta)^2 + \sin^2 \theta (d\varphi)^2] \}. \quad (8)$$

there exist three exact solutions:

$$\Lambda = 0; \quad K^2(t) = a_0 t^{2/3}; \quad \varepsilon = \frac{1}{3\kappa t^2};$$

$$\Lambda > 0; \quad K^2(t) = b_0 \{ \cosh \tau \}^{2/3}; \quad \tau = t \sqrt{3\Lambda}; \quad \varepsilon = -\frac{\Lambda}{\kappa \cosh^2(\tau)}; \quad (9)$$

$$\Lambda < 0; \quad K^2(t) = c_0 |\cos \eta|^{2/3}; \quad \eta = -\sqrt{-3\Lambda}t; \quad \epsilon = -\frac{\Lambda}{\kappa \cos^2 \eta}.$$

$$(a_0, b_0, c_0 = \text{constants})$$

All these solutions are independent of the chiral potential  $P(\phi)$  and correspond to extremely stiff matter with the equation of state:  $p = \epsilon$ . The fact that the scalar factor  $K^2(t)$  is independent of the chiral potential  $P(\phi)$  means that the deformation, saving the rotational symmetry of the internal space (in our case, target space) does not affect on the gravitational field.

Thus, we have got an exponentially ((9),  $\Lambda > 0$ ) and power law ((9),  $\Lambda = 0$ ) expansion of the universe (8), what usually needs for inflationary scenario. Besides, the oscillating type of the universe ((9),  $\Lambda < 0$ ) is also obtained. The solutions for the chiral fields, corresponding to (9), will be presented elsewhere.

### 3. Anisotropic universe

The possibility of inflation in the anisotropic models of the universe has been considered by many authors (see, for example, Rothman & Ellis 1986; Moss & Sahni 1986; Lidsey 1992). Let us consider the case of Bianchi-I type universe with the line element

$$dS_M^2 = dt^2 - B^2(t)dr^2 - C^2(t)\{d\theta^2 + d\varphi^2\}. \quad (10)$$

The exact solution below indicate the possibility of power law expansion of the universe (10), when cosmological constant is absent.

$$dS^2 = dt^2 - t^{2c/(c+2)}dr^2 - t^{2/(c+2)}\{d\theta^2 + d\varphi^2\},$$

$$p = \epsilon = \frac{\beta}{\kappa t^2}, \quad \beta = (2c+1)(c+2)^{-2}c \neq -2,$$

$$\phi = c_3 \ln t + \phi_0, \quad \chi = c_4 \ln t + \chi_0,$$

$$P(\phi) = P_0 = \text{const}, \quad \frac{2\beta}{\kappa\alpha} = c_3^2 + 2P_0 c_4^2. \quad (11)$$

The solution (11) is an example of anisotropic inflationary model (Kofman, Sahni & Starobinsky 1983). This solution corresponds to 'slow rolling' regime (Linde 1990) because the chiral fields' equations (3) lead to the restriction  $P = P_0 = \text{const}$ . Under this restriction the universes (9) are also permitted.

### 4. Conclusion

The cosmological solutions (9), (11) of the two-component nonlinear sigma model are independent of the chiral potential  $P(\phi)$  and correspond to extremely stiff matter. The exponential and power law expansion of deSitter and Friedman-Robertson-Walker universes are possible for the model under consideration as well as power law expansion for Bianchi-I type anisotropic universe.

### References

- Chervon, S. V. 1992, *Preprint IUCAA 15/92*, October 1992.
- Ivanov, G. G. 1983, *Teoreticheskaja i Matematicheskaja Fizika* **57**, No. 1, 45 (in Russian).
- Kofman, L. A., Sahni, V., Starobinsky, A. 1983, *JETF* **58**, 1090.
- Lidsey, J. E. 1992, *Class. Quantum Grav.*, **9**, 1239.
- Linde, A. 1990, *Particle Physics and Inflationary Cosmology*, (New York: Gordon and Breach).
- Moss, I., Sahni, V. 1986, *Phys. Lett.* **B178**, 159.
- Perelomov, A. M. 1987, *Phys. Rep.*, **146**, No. 3, 135.
- Rothman, T., Ellis, G. F. R. 1986, *Phys. Lett.* **B180**, 19.

## Perturbative Growth of Cosmological Correlations

Somnath Bharadwaj *Raman Research Institute, Bangalore 560 080, India*  
and *Joint Astronomy Program, Indian Institute of Science, Bangalore 560 012, India*

**Abstract.** We briefly describe the results of our recent detailed analysis, using the BBGKY hierarchy, of the perturbative evolution of correlation functions in cosmological models. The equations for the evolutions of the two and three point correlation functions that are discussed here can be used to study the growth of clustering in the weakly nonlinear regime for various kinds of initial conditions. They can also be used to test approximation schemes which are currently used to describe the nonlinear growth of density perturbations. As an example, we present the form of the three point correlation function that arises from Gaussian initial conditions in an  $\Omega = 1$  universe. This does not have the ‘hierarchical’ form often assumed.

**Key words:** Cosmology: large scale structure of the universe—Galaxies: clustering.

Here we shall discuss in brief some results, a detailed derivation and discussion of which are presented elsewhere (Bharadwaj 1993). The reader is also referred to Peebles (1980) for a comprehensive discussion of this subject.

We consider deviations of the matter distribution in the universe from the homogeneous and isotropic state. Correlation functions describe the statistical properties of these disturbances. We wish to study the evolution of the correlation functions due to gravitational instabilities in an expanding universe.

The correlation functions only contain information about the spatial distribution of the matter. They have no velocity information. To study the dynamics one has to use distribution functions on phase space. The evolution of these quantities is governed by the BBGKY hierarchy.

We choose initial conditions where the deviation of the matter distribution from the homogeneous and isotropic state is small, and is characterized by a small parameter  $\epsilon$ . All peculiar motions are also of this order. Then, by taking velocity moments of the first three equations of the BBGKY hierarchy we derive equations for perturbatively evolving the irreducible two and three point correlation functions.

We display below the equation for perturbatively evolving the two point correlation function  $\xi$ . The parameter  $\lambda$  is defined as

$$d\lambda = \frac{dt}{a(t)^2},$$

where  $a(t)$  is the scale factor and  $t$  the cosmic time. Using this simplifies the equations

$$\frac{\partial^3}{\partial \lambda^3} \xi - 8\pi G\rho \left[ a \frac{\partial}{\partial \lambda} \xi + \frac{\partial}{\partial \lambda} (a\xi) \right] = f \quad (1)$$

In the equation above  $f$  is a function (which is rather lengthy and not shown here) of order  $v^3$  and higher which depends on the three point correlation function and the third velocity moment of the two particle distribution function. To the lowest order i.e.  $v^2$ , ' $f$ ' is zero and the equation for  $\xi$  gives the results we expect from the linear theory of density perturbations. To go further, the evolution of the function  $f$  has to be considered.

We have a similar equation for the three point correlation function also. To order  $v^3$  this reproduces the results of linear theory.

These equations can be used to perturbatively study the growth of cosmological clustering beyond the linear regime. They may also be used to test various approximation schemes used to describe the nonlinear growth of density perturbations. The perturbative approach will only work in the weakly nonlinear regime. It is hoped that a better understanding of the growth of clustering in the weakly nonlinear regime may motivate schemes to close the BBGKY hierarchy and get some understanding of the highly nonlinear regime.

Next, we restrict ourselves to Gaussian initial conditions in a universe with  $\Omega = 1$ . Many scenarios for the generation of the initial perturbations predict Gaussian initial conditions. In this case there is no initial three point correlation function. We use the equation for the three point correlation function to calculate the induced three point correlation function that arises from the two point correlation function due to gravity. In the calculation we have kept only the growing mode. The irreducible three point correlation function that arises takes the form

$$\begin{aligned} \zeta(1, 2, 3, t) = \sum_{a,b,c} \left[ \frac{1}{7}(5 + 2\cos^2\theta)\xi(x)\xi(y) + \cos\theta \frac{d}{dx}\xi(x)y\bar{\xi}(y) \right. \\ \left. + \frac{4}{7}(1 - 3\cos^2\theta)\xi(x)\bar{\xi}(y) + \frac{2}{7}(9\cos^2\theta - 3)\bar{\xi}(y)\bar{\xi}(x) \right], \end{aligned} \quad (2)$$

where

$$\bar{\xi}(x) = \frac{1}{x^3} \int_0^x \xi(x')x'^2 dx' \quad (3)$$

In the equation above

$$x = |x^a - x^b|$$

$$y = |x^a - x^c|,$$

and

$$\cos\theta = \frac{x_\mu y_\mu}{xy}$$

where the subscript  $\mu$  refers to the cartesian components. The superscripts  $a, b$  and  $c$  refer to the points between which the correlation is being evaluated and are summed over the values shown in the table below.

$a$	1	1	2	2	3	3
$b$	2	3	3	1	1	2
$c$	3	2	1	3	2	1

The three point correlation is of order  $\epsilon^4$ .

In the linear theory the evolution is local. Here we see the first signs of nonlocality developing. The three point correlation function  $\zeta$  does not depend only on the values of the two point correlation function  $\xi$  at the separations occurring in  $\zeta$ . It depends on the two point correlation at all scales smaller than the scales where the three point correlation function is being evaluated.

Fry (1984) has calculated the three point correlation function for the special case of power-law initial two point correlation function

$$\xi(x) = Ax^{-n}. \quad (4)$$

The result shown above agrees with Fry's result when 'n' is less than three. For higher values of 'n' the integral of the two point correlation function diverges and deviations from the power law behaviour are required at small separations to obtain meaningful results.

The expression for the three point correlation function presented here can in principle be used to test the assumption of Gaussian initial conditions against observations. This can only be done at large scales where the perturbations are still weakly nonlinear.

### Acknowledgements

We would like to thank Prof. Rajaram Nityananda for his advice and encouragement.

### References

- Bharadwaj, S. 1993, preprint.  
 Fry, J. N. 1984, *Astrophys. J.*, **279**, 499.  
 Peebles, P. J. E. 1980, *The Large Scale Structure of the Universe*, (Princeton: Princeton University Press).



## The Formation and Evolution of Voids in the Universe

Varun Sahni & B. S. Sathyaprakash *Inter-University Centre for Astronomy and Astrophysics, Post Bag 4, Ganeshkhind, Pune 411 007, India.*

Sergei F. Shandarin *Department of Physics and Astronomy, University of Kansas, Lawrence, Kansas 66045, U.S.A.*

**Abstract.** The formation and evolution of voids in the Universe are discussed using the semi-analytic approach of the adhesion model of structure formation.

**Key words:** Large scale structure – voids – adhesion model.

The distribution of galaxies in the sky is marked by the presence of coherent large scale structures such as clusters and superclusters of galaxies, as well as vast underdense regions spanning volumes of order  $10^4 \text{ Mpc}^3$ , commonly called *voids*. Since the discovery of the colossal Bootes void (volume  $\sim 10^6 \text{ Mpc}^3$ ) (Kirshner *et al.* 1981) the presence of voids in the large scale distribution of galaxies has been spectacularly confirmed both by redshift, as well as pencil beam surveys of the Universe. Indeed the most comprehensive void catalogue to date records an estimated 129 voids belonging to both galactic hemispheres (Kauffmann & Fairall 1991).

The fact that voids might provide a key to understanding the large scale structure of the Universe was emphasised more than a decade ago, by Zeldovich & Shandarin (1982). Since then voids have been studied both analytically as well as numerically in a number of theoretical treatments (see Sahni *et al.* 1993 and references therein). In the present study we discuss the formation and evolution of voids in the Universe using a semi-analytic approach known as the adhesion model (Gurbatov, Saichev & Shandarin 1989). The adhesion model has been known to provide a very accurate treatment of nonlinear gravitational instability at very late times and for a wide variety of cosmological models including the currently popular *Cold Dark Matter* (henceforth CDM) model. Using the adhesion model we have attempted to answer such important questions as:

Do voids evolve with time? (Ans. Yes they do.) Are voids necessarily empty? (Ans. No, not always, our simulations show that there exists a finite probability of a void having one or more mini-pancake running through it.)

To substantiate these claims we show the results of our simulations (which average three realisations of the CDM spectrum using  $128^3$  particles, in a 128 Mpc box with periodic boundary conditions), for the present epoch, in Fig. 1. The right panel in this figure shows the number fraction of voids  $n(D_i)/N$  where  $n$  is the number of voids having a diameter  $D_i$ ,  $N = \sum_i n(D_i) \simeq 1500$  is the average number of voids in our simulation. The left hand panel shows the associated void volume fraction  $v(D_i)/V = (n(D_i) \times \pi D_i^3/6)/V$ ,  $V = \sum_i V(D_i)$ . We find that the volume spectrum of voids shows a fairly uniform spread for voids having diameters in the range  $10 \leq D \leq 30 \text{ Mpc}$  where  $D$  is the void diameter. Approximately 65% of the total volume in voids is



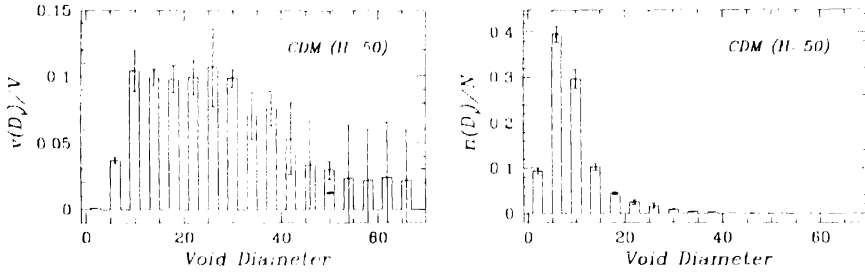


**Figure 1.** Number fraction of voids in a certain diameter class (left hand panel) and the corresponding volume fraction (right hand panel) for the CDM model.

contained in voids lying within this range. By contrast, the number spectrum of void sizes has a well defined peak on scales of  $\sim 6$  Mpc, indicating that the most abundant voids in our simulation ( $\sim 40\%$ ) are of this size. However, the net contribution from such small size voids, to the overall void volume, is a tiny  $\sim 4\%$ .

We also find that the void spectrum evolves with time and that the average size of a void in the CDM model grows approximately as  $\bar{D}(z) = \bar{D}_0 / \sqrt{1+z}$ , where  $\bar{D}_0 \simeq 14$  Mpc, is the mean diameter of a void today and  $z$  is the cosmological redshift. (We would like to caution the reader that our results may be biased towards smaller void sizes simply because our simulations were performed with a limited dynamical range spanning a rather small  $\sim 128$  Mpc toroidal Universe. Larger simulations being planned by us will help verify whether 14 Mpc is indeed a typical length scale for voids in a *realistic* (viz. effectively unbounded) CDM Universe).

As mentioned earlier we find that voids can be populated by substructure such as mini-Zeldovich pancakes. A measure of substructure is provided by the average *genus* characteristic per void, which is the total number of mini-pancakes within voids of a certain diameter class divided by the total number of voids belonging to that class. Our results for the CDM model shown in Fig. 2 show that (a) larger voids have higher mean genus, and (b) roughly one out of every twenty voids is likely to be populated by a mini-pancake at the present epoch. In addition, we find that as voids grow older they also become progressively more empty and have less substructure within them.

Our simulations also show the existence of a distinct correlation between the sizes of voids, and the value of the linear gravitational potential at void centers, the

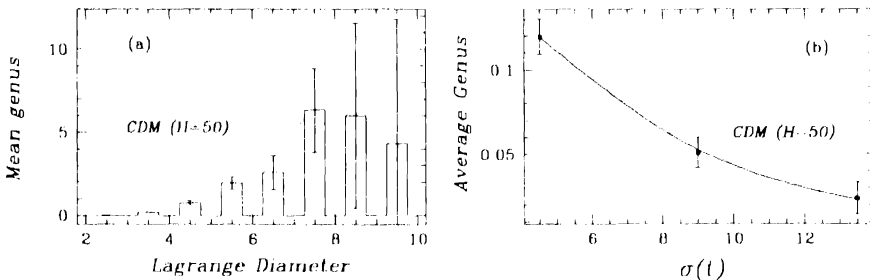


**Figure 2.** Genus characteristic of voids for the CDM model: (a) Mean genus as a function of void size and (b) Genus averaged over all voids as a function of epoch.

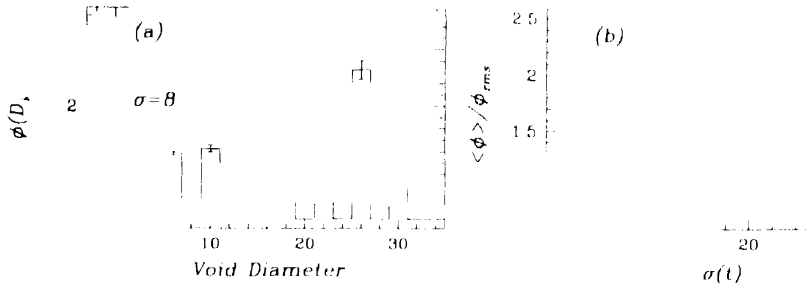


**Figure 3.** Value of the primordial gravitational potential as a function of (a) void size and (b) epoch, for power-law spectrum  $n = 1$ . (See the text for details.)

correlation becoming very significant at late times. In Fig. 3 we show this dependence of gravitational potential (a) on void size for a fixed epoch, and (b) on epoch corresponding to different values of  $\sigma(t)$  which is defined in units of the r.m.s. linear density contrast on the grid scale:  $\sigma(t) = [a^2 \int_0^t P(k) k^2 dk]^{1/2} \propto a(t)$ ; where  $a(t)$  is the scale factor of the Universe;  $P(k) = \langle |\delta_k|^2 \rangle \propto k^n$ , is the power spectrum and  $|\delta_k|$  is the spatial Fourier transform of the density contrast. The phases of the Fourier components are randomly distributed, so that the gravitational potential  $\phi(x)$  has the statistical properties of a Gaussian random field. A cutoff was introduced into the spectrum by requiring that  $P(k) = 0$  for  $k > k_c$ . (Physical processes which can give rise to such a cutoff include the free streaming of weakly interacting massive particles (WIMP's) such as massive neutrinos.) The figures correspond to  $n = 1$ . We find that not only is the value of the gravitational potential in general higher in the center of a larger void (Fig. 3a), but that the average value of the gravitational potential evaluated at void centers increases with time roughly as  $\langle \phi \rangle / \phi_{rms} \propto \sqrt{\sigma(t)}$  (Fig. 3b). This observation could help us to reconstruct the primordial form of the potential from an observation of void sizes.

Our results also show that, far from being a constant, the number of voids in the Universe evolves, first increasing to a maximum value and then decreasing steadily. This behaviour of the void population reflects the growth of large scale structure in the Universe which proceeds in two complementary epochs. During the first, pancakes and filaments form, giving rise to the cellular structure of the Universe. During this period matter moves steadily along pancakes into filaments (which form at the intersections of pancakes) and then along them into knots (which form at the intersection of filaments). The second stage witnesses the gravitational attraction of filaments and knots towards each other, resulting in their merger and the subsequent disruption of the cellular structure formed during the previous epoch.

## References

- Gurbatov, S. N., Saichev, A. I., Shandarin, S. F. 1989, *Mon. Not. R. astr. Soc.*, **236**, 385.  
 Kauffmann, G., Fairall, A. P. 1991, *Mon. Not. R. astr. Soc.*, **248**, 313.  
 Kirshner, R. P., Oemler, A. Jr., Schechter, P. L., Shectman, S. A. 1981, *Astrophys. J.*, **248**, L57.  
 Sahni, V., Sathyaprakash, B. S., Shandarin, S. F. 1993, *Astrophys. J.*, (submitted).  
 Zeldovich, Ya. B., Shandarin, S. F. 1982, *Soviet astr. Lett.*, **8**, 67.



## Nonlinear Evolution of Density Perturbations

**J. S. Bagla & T. Padmanabhan** *Inter-University Centre for Astronomy and Astrophysics,  
Post Bag 4, Ganeshkhind, Pune 411 007, India*

**Abstract.** From the epoch of recombination ( $z \approx 10^3$ ) till today, the typical density contrasts have grown by a factor of about  $10^6$  in a Friedmann universe with  $\Omega = 1$ . However, during the same epoch the typical gravitational potential has grown only by a factor of order unity. This fact can be exploited to provide a new, powerful, approximation scheme to study the formation of nonlinear structures in the universe by evolving the initial distribution of matter using a gravitational potential frozen in time. We carry out this scheme for several standard models and discuss the results.

**Key words:** Galaxies: formation – large scale structure of Universe.

It is believed that structures like galaxies and clusters of galaxies formed out of small inhomogeneities via gravitational instability. In this paper we discuss a new approximation scheme called Frozen Potential Approximation (hereafter FPA) (Bagla & Padmanabhan 1994a; Brainerd *et al.* 1993) for studying the nonlinear growth of inhomogeneities and to summarise the results.

The exact trajectory of a particle in a Friedmann universe is described by the equations:

$$\frac{d^2 \mathbf{x}}{da^2} + \frac{3}{2a} \frac{d\mathbf{x}}{da} = -\frac{3}{2a} \nabla\psi; \quad \nabla^2\psi = \frac{\delta}{a}, \quad (1)$$

where  $a(t)$  is the expansion factor,  $\mathbf{x}$  is the comoving coordinate,  $\rho_b$  is the background matter density, and  $\psi$  is the scaled gravitational potential  $\psi = (2/3H_0^2)\phi$ . In Zeldovich approximation (ZA) (Zeldovich 1970; Shandarin & Zeldovich 1989), it is assumed that the velocity of a particle remains constant along its trajectory thereby leading to the trajectory  $\mathbf{x}(a) = \mathbf{x}_{in} - a\nabla\psi|_{in}$ . Zeldovich ansatz can be used to show that the first structures to form in a generic gravitational collapse are planar surfaces of high density, the so called pancakes. The unrealistic part of dynamics in ZA is that particles continue to move (after collapsing and forming a pancake) with the same velocity leading to thickening of pancakes.

It is possible to generate a better approximation (Bagla & Padmanabhan 1994a; Brainerd *et al.* 1993) by freezing the potential at the initial value and evolving the density perturbations to mildly non-linear density contrasts with much more realistic dynamics. The trajectories are now evolved using (1) but with a fixed potential:

$$\frac{d^2 \mathbf{x}}{da^2} + \frac{3}{2a} \frac{d\mathbf{x}}{da} = -\frac{3}{2a} \nabla\psi(a_{in}). \quad (2)$$

In FPA, the particles move towards the minima of the potential and then oscillate about it with a decaying amplitude due to the expansion of the Universe. We now discuss several results of this approximation.

The two approximations are compared visually in Fig. 5 which gives slices [with dimensions  $(96 \times 96 \times 15) (h^{-1} \text{Mpc})^3$ ] of the universe in these schemes at different epochs for CDM normalised to COBE. It is obvious that at early stages ( $z \gg 1$ ) of structure formation, all approximations give similar results, while at later stages ( $z \approx 0$ ) the differences are quite prominent. Pancakes do not thicken in FPA and, at late stages, clumpy structures dominate. In Fig. 1 we have shown the density contrast  $\sigma(r)$  defined as  $\sigma^2 \equiv \bar{\xi}$  with  $\bar{\xi}(r) = 3J_3(r)/r^3$  for three redshifts for standard CDM using FPA. For comparison we have also plotted the N-body result at  $z = 0$ .

The FPA can be quite useful in studying the evolution of voids in the universe. One way of estimating the sizes of voids is to compute the rms displacement of particles in a simulation (Shandarin 1992) which can be related to the average diameter of voids by  $D_{\text{void}} = 2kd_{\text{rms}}$  where (for spherical voids)  $k = 1.3$ . The thick line in Fig. 2 shows the evolution of  $d_{\text{rms}}$  for CDM and HDM. For the standard CDM model, we find that  $d_{\text{rms}} \approx 9h^{-1} \text{Mpc}$  at  $z = 0$ . The behaviour of  $d_{\text{rms}}$  can also be studied analytically in some special cases (Bagla & Padmanabhan 1994b). Consider, for example, the motion of particles near a local density minima. The density profile away from the centre of a low density void can be approximated as  $\delta = -(r/L)^{-n}$  where  $n$  is a positive constant. In this case, equation of motion has one simple solution:

$$r = \left[ \frac{3n^2}{(3-n)(n+2)} \right]^{1/n} La^{1/n}. \quad (3)$$

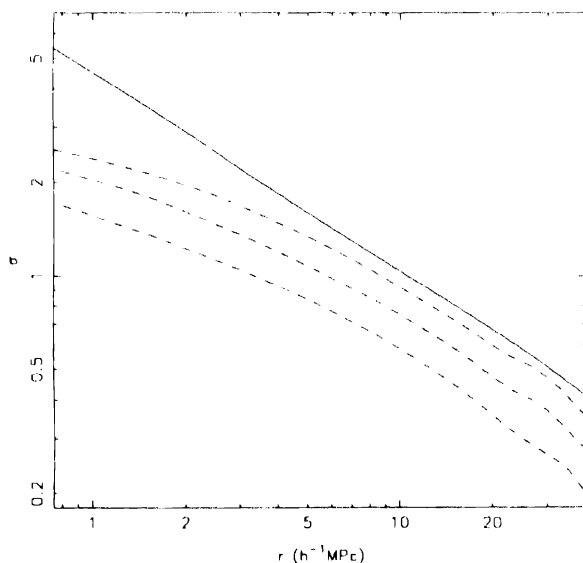


**Figure 1.** Evolution of density contrast in the Frozen Potential Approximation. Also drawn here is the curve for density contrast obtained from N-Body for  $z = 0$ . Here the density contrast is defined as  $\sigma \equiv \sqrt{\bar{\xi}}$ .

which holds for  $n < 3$ . For a gaussian random field, the profile of density around a density extrema is a power law with the same index as the correlation function (Bardeen *et al.* 1986 (BBKS)). For our universe, the index of the correlation function is about 1.8, and we expect the voids to grow as  $a^{1/1.8}$  or  $(1+z)^{-1/1.8}$  in the late stages. However, in the linear limit, we expect the void radius to grow as  $a$ . While calculating  $d_{rms}$  from simulations, we average over regions with different index  $n$  and hence expect  $d_{rms}$  to grow at a rate intermediate between  $a$  and  $a^{1/1.8}$ . These features are clearly seen in Fig. 2. The two dot-dash lines indicate growth proportional to  $a$  and  $a^{1/1.8}$  and have intercepts chosen to match with  $d_{rms}$  for CDM.

Finally, let us consider the accuracy and limitations of FPA. It can be shown that the relation between true density contrast  $\sigma^2$  and the linear density contrast  $\sigma_L^2$  (Hamilton *et al.* 1991; Nityananda *et al.* 1993) is well approximated by:

$$\sigma^2(x, a) \propto \begin{cases} \sigma_L^2(l, a) & (\text{for } \sigma^2 \lesssim 1) \\ [\sigma_L^2(l, a)]^3 & (\text{for } 3 \lesssim \sigma^2 \lesssim 50) \\ [\sigma_L^2(l, a)]^{3/2} & (\text{for } 50 \lesssim \sigma^2), \end{cases} \quad (4)$$

where  $l = x(1 + \sigma^2)^{1/3}$  (Bagla & Padmanabhan 1994b). Taking  $\sigma_L^2(l, a) \propto a^2 l^{-(n+3)}$  where  $n$  is a local index, we get for  $(\sigma/a)$ :

$$\frac{\sigma(x, a)}{a} \propto \begin{cases} a^{-1(n+1)/(n+4)} & 10 \lesssim \sigma^2 \lesssim 50 \\ a^{-1(n+2)/(n+5)} & 50 \lesssim \sigma^2. \end{cases} \quad (5)$$

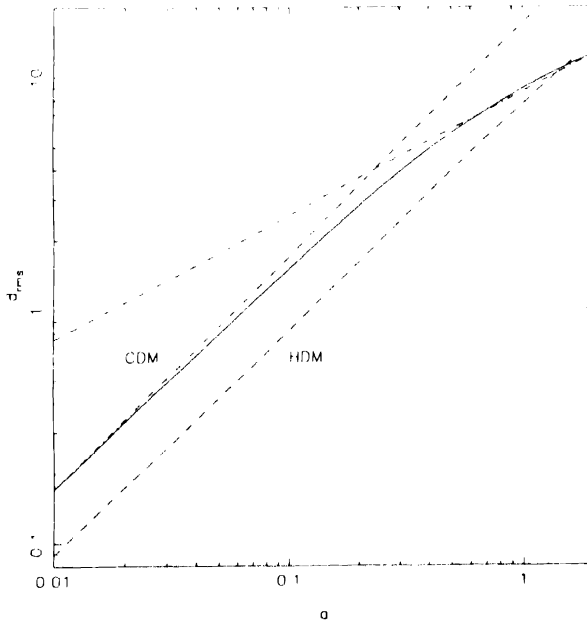


**Figure 2.** Evolution of  $d_{rms}$ . Here  $d_{rms}$  is plotted as a function of the scale factor, the continuous line is for CDM and the dashed line corresponds to HDM model. Dot-dashed lines have been drawn for the power law solutions,  $a$  and  $a^{1/1.8}$  for early and late times respectively, as discussed in the text.

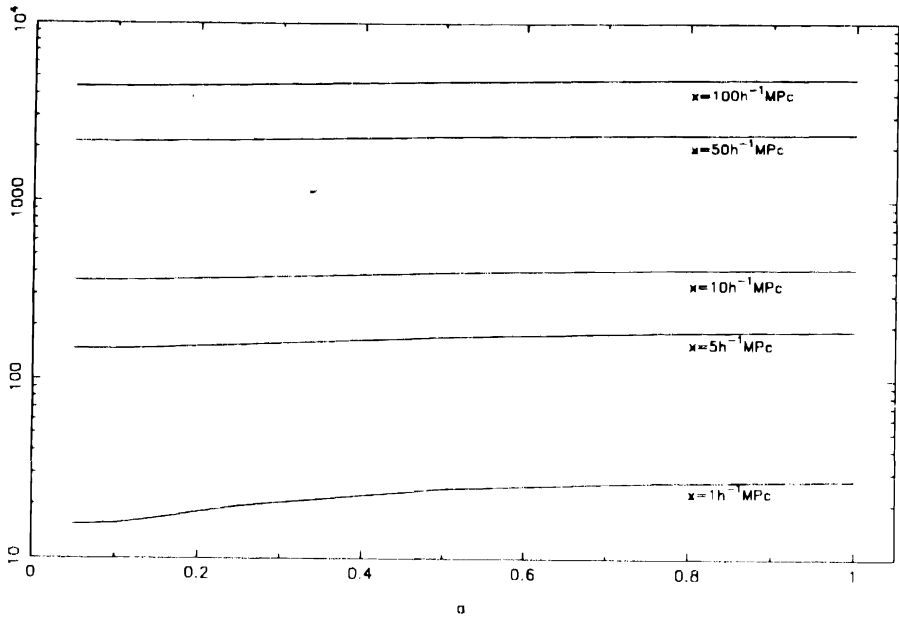


**Figure 3.** Variation in potential with scale factor. We have plotted the variance of potential  $\zeta$  as a function of the scale factor for  $r = 1, 5, 10, 50$ , and  $100 h^{-1} \text{ Mpc}$ .

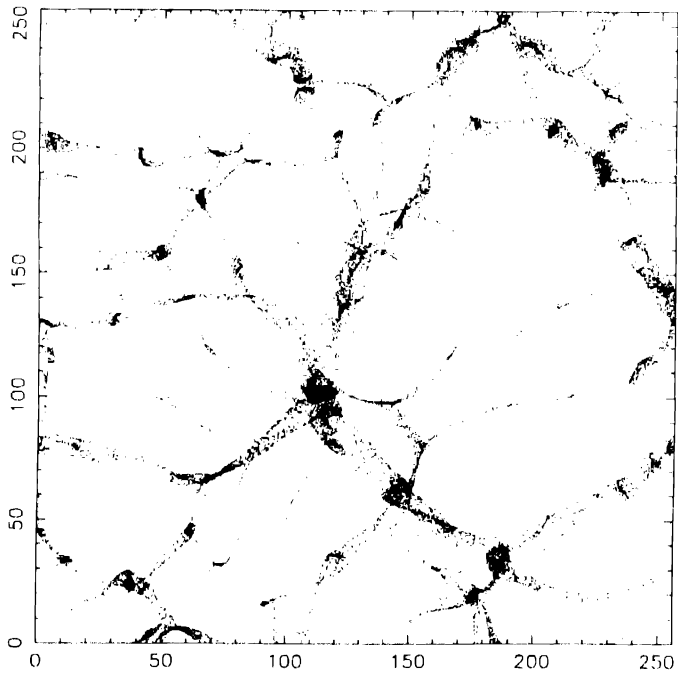


**Figure 4a.** An FPA simulation in two dimensions.

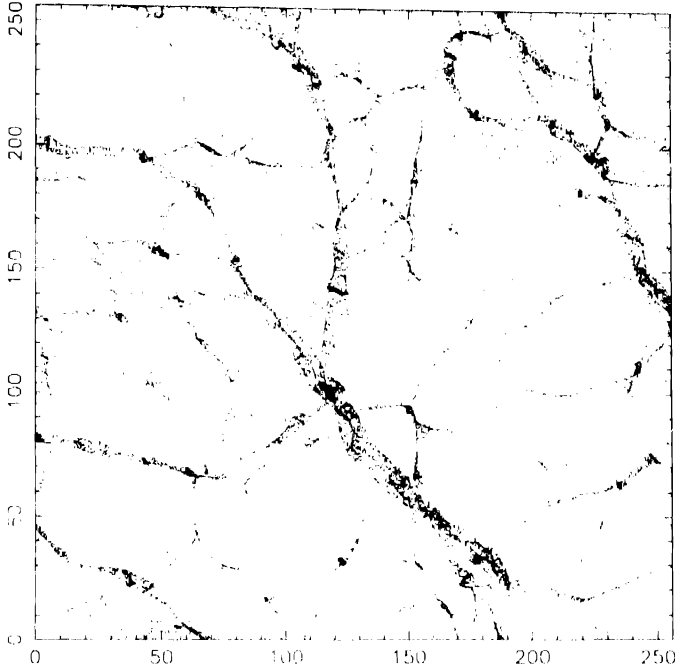


**Figure 4b.** An  $N$ -body frame from a 2-d simulation for the same initial potential as that used in Fig. 5a. The pancakes are much thinner than the ones in the FPA simulation. Also notice the shift of pancakes in this case.

In the standard CDM model  $n \simeq -2$  in the nonlinear domain ( $\sigma^2 \gtrsim 50$ ) and  $n \simeq (-1$  to  $-2)$  in the quasilinear regime. From (5) we see that  $(\sigma/a)$  remains constant for  $n = -1$  and  $n = -2$  in the quasilinear and nonlinear regimes respectively. Hence in CDM like spectra, there is a conspiracy of indices ensuring that there is very little change in the gravitational potential. Fig. 3 shows  $\psi$  at four different length scales in standard CDM model, as a function of scale factor. It is clear that constancy of  $\psi$  is a reasonable approximation for CDM like spectra.

The FPA, however, is not accurate at small scales, for a different reason. If the streaming velocity at a (large) length scale  $L$  is  $v(L)$  then structures at this scale would have, on the average moved a distance of  $H_0^{-1}v(L)$ . In CDM models at scales  $L \simeq 50 h^{-1} \text{ Mpc}$ ,  $v \simeq 200 \text{ km s}^{-1}$ ; hence these structures could have moved about  $H_0^{-1}v \simeq 2 h^{-1} \text{ Mpc}$  by now. Thus at scales smaller than about  $1 h^{-1} \text{ Mpc}$  we would expect the approximation to show some inaccuracy due to motion of pancakes.

These aspects can be clearly seen in Fig. 4a,b which compares FPA with exact  $N$ -body simulations in 2D. The pancakes in  $N$ -body simulations are thinner than those in FPA (due to deepening of potential wells) and are also slightly shifted with respect to those in FPA.

The FPA is a powerful approximation which can be used to obtain approximate results, numerically as well as analytically. A very strong point in favour of this approximation is that it contains full information about velocities and therefore it can be used to study various models in the redshift space.



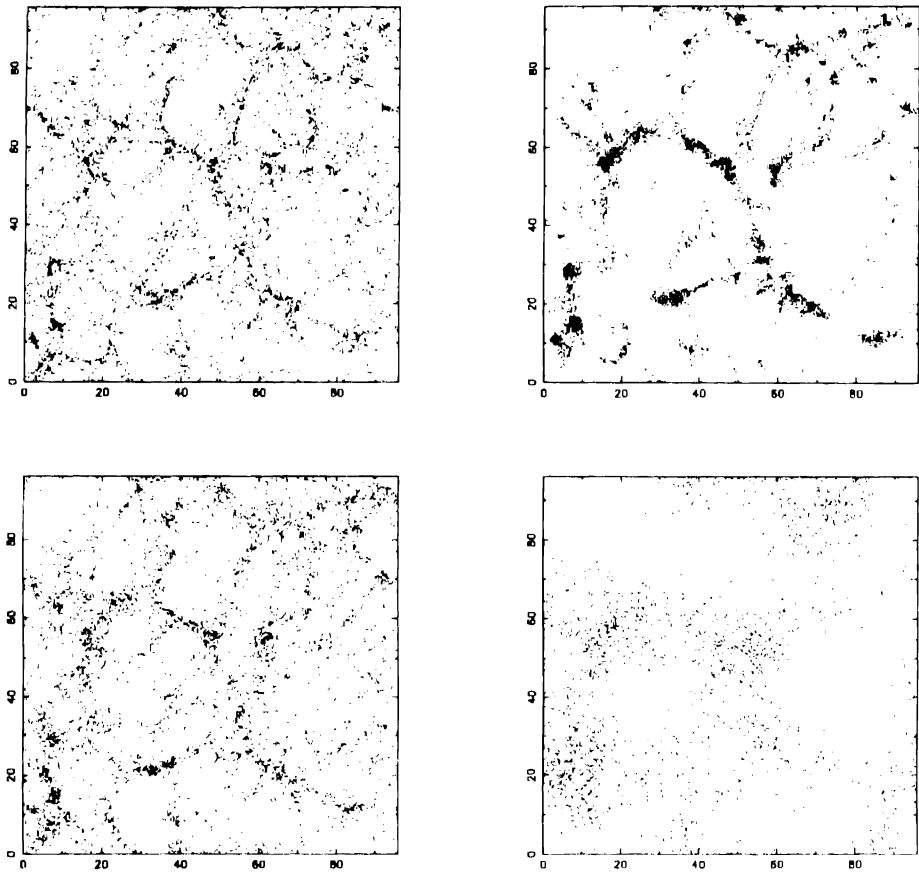


**Figure 5.** Evolution of density perturbations in CDM for Frozen Potential and Zeldovich approximation. These frames, from left to right, correspond to  $a = 0.25$  and  $1.0$  respectively. The top row of frames is for FPA and the bottom row is for ZA.

## References

- Bagla, J. S., Padmanabhan, T. 1994a, *Mon. Not. R. astr. Soc.*, **226**, 227.  
 Bagla, J. S., Padmanabhan, T. 1994b, (in preparation).  
 Bardeen, J. M. *et al.* 1986, *Astrophys. J.*, **304**, 15 (BBKS).  
 Brainerd, T. G. *et al.* 1993, *Astrophys. J.*, **418**, 570.  
 Hamilton, A. J. S. *et al.* 1991, *Astrophys. J.*, **374**, L1.  
 Nityananda, R., Padmanabhan, T. 1993, *Scaling Properties of Gravitational Clustering in the Non-linear regime*, IUCAA-12/93, preprint; submitted to *Mon. Not. R. astr. Soc.*  
 Shandarin, S. F. 1992, *Large Scale Structure of the Universe*. Lectures delivered at IUCAA (Dec. 1992)  
 Shandarin, S. F., Zeldovich, Ya. B. 1989, *Rev. Mod. Phys.* **61**, 185.  
 Zeldovich, Ya. B. 1970, *Astr. Astrophys.* **5**, 84.

## Neutral Hydrogen at High Redshifts as a Probe of Structure Formation

**A. Kumar & K. Subramanian** *National Centre for Radio Astrophysics, Tata Institute of Fundamental Research, Pune University Campus, Ganeshkhind, Pune 411 007.*

**T. Padmanabhan** *Inter-University Centre for Astronomy and Astrophysics, Pune University Campus, Ganeshkhind, Pune 411 007.*

**Abstract.** Structure formation at  $z \lesssim 10.0$  can be detected and studied using the 21 cm line emission from the neutral hydrogen. Two of us (Subramanian & Padmanabhan 1993, Paper I) had earlier computed the expected abundance of protoclusters as a function of the flux density at various redshifts, in the Cold dark matter (CDM) and the Hot dark matter (HDM) models. Here we work out in detail how the HI line profile from a single spherically symmetric protocluster evolves as it decouples from hubble expansion and collapses. We find peak fluxes of the HI line profile to be typically of order 0.4–0.8 mJy while the widths (FWHM) are of order 0.6–1.5 Mhz. Such protoclusters could be detectable by the Giant Metrewave Radio Telescope (GMRT) which is being built in India.

*Key words:* Structure formation – protoclusters – GMRT.

### 1. Introduction

Galaxies and large scale structures in the universe may originate by the growth of small initial perturbations via gravitational instability. In this picture it should be possible to detect neutral hydrogen in the protocondensates by observing the redshifted 21 cm line (Sunayev & Zeldovich 1972, 1974). The GMRT presently being constructed in India is expected to provide a sensitive instrument for detecting such protocondensates (Swarup 1984). It is, therefore, interesting to work out the expected flux of redshifted 21 cm emission in various models of structure formation and compare the results with the expected sensitivity limits of future instruments like GMRT.

In Paper I two of us had computed the expected abundance of protocondensates which will emit a flux higher than  $S$ , at various redshifts, in the CDM and HDM models, normalised using the COBE results. Here we complement the study in Paper I by working out in detail how the HI line profile from a single protocluster evolves as it decouples from hubble expansion and collapses. Our calculations assume that: (i) The protocluster consists of small scale clumps of HI gas, as is likely in hierarchical clustering theories of galaxy formation (Paper I and Subramanian & Swarup 1992). (ii) The density profile of the protoclusters is spherically symmetric and the density contrast is a decreasing function of the radius. We will also test the sensitivity of the results to changes in the assumed density profile.

## 2. Evolution of the line profile

Consider a spherically symmetric perturbation with excess density contrast  $\delta_i(r_i)$  monotonically decreasing with  $r_i$ . As the protocluster evolves, shells at larger and larger radii decouple from the hubble expansion, turn around and collapse. The 21 cm line emission from different volume elements will be redshifted differently because of the peculiar velocity of the elements and hence will be observed at different frequencies. By properly adding them, we can obtain the energy emitted by such a condensate as a function of the observed frequency.

In the spherical model the time evolution of a shell of radius  $r$  in the condensate is given by  $r(t) = (3x/10\bar{\delta}_0(x)) (1 - \cos\psi)$  where  $t = (3/5)^{3/2} (3/4) (t_0/\bar{\delta}_0(x)^{3/2}) (\psi - \sin\psi)$ . Here  $x = [a(t_0)/a(t_i)] r_i = (1 + z_i) r_i$  is the comoving radius of the shell and  $\bar{\delta}_0(x) = \langle \delta_0(x) \rangle = (3/5) (1 + z_i) \bar{\delta}_i(r_i)$  is the average excess density contrast within the shell, extrapolated to the present epoch  $t_0$ . (We have also assumed a flat universe with  $\Omega = 1$ .) From these equations it is simple to work out how the velocity and density profile of the protocluster evolves (Peebles 1980; Padmanabhan & Subramanian 1992).

The energy emitted per unit time in 21 cm line radiation from a small volume  $dxdydz$  of the protocondensate is  $dE = (3/4) A_{21} h\nu_p (\rho_{\text{III}}(x, y, z)/m_p) dxdydz$ . Here  $A_{21}$  is the spontaneous emission rate,  $\nu_p$  is the frequency of the 21 cm photon,  $m_p$  the proton mass and  $\rho_{\text{III}}$  the neutral hydrogen density which we take to be a fraction,  $f$  say, of the total mass density. To compute the luminosity per unit frequency interval,  $du(v)/dv$ , from the protocondensate, we transform  $dE$  from  $(x, y, z)$  to the  $(x, y, v)$  (sky-frequency) co-ordinates, and integrate the emission over the sky. This transformation introduces a Jacobian factor of  $\partial v/\partial z \propto \partial v_z/\partial z$  in the denominator. Knowing the expressions for  $\rho(x, y, z, t)$ , and  $v_z(x, y, z, t)$ , we can explicitly compute the evolution of the line profile at various redshifts.

In particular we have taken here the spherically symmetric form for  $\rho(r, t)$  and  $v(r, t)$  calculated as above. In this case it is more convenient to use  $(r, \phi, \theta)$  co-ordinates and transform  $\theta$  to  $v$  using  $v = (v_c/(1 + z_c)) (1 - (v(r, t)\cos\theta/c))$  where  $z_c$  is the redshift of the protocluster. We then have

$$\frac{du(v)}{dv} = \frac{3\pi}{2} A_{21} h c (1 + z_c) \int \frac{\rho_{\text{III}}(r, t) r^2 dr}{m_p v(r, t)}. \quad (1)$$

In evaluating  $du/dv$  we should keep in mind that (at a fixed  $v$ ), only those values of  $r$  satisfying the above  $v - \theta$  relation for some  $\theta$  will contribute to the integral in (1). We can also compute the observed flux as a function of frequency by dividing (1) by  $4\pi D_L^2$ , where  $D_L$  is the luminosity distance of the  $\Omega = 1$  FRW Universe.

For explicit computations we have adopted an initial density profile of the form:  $\delta_0(x) = \delta_0(0) [1 + (x/a)^2]^{-\alpha}$  for  $x < R$  and zero for  $x > R$ . We have chosen  $R = 15.09$  Mpc corresponding to a protocluster of mass  $10^{15} M_\odot$ , and  $a = 3$  Mpc. We have calculated the line profile for three different density profiles  $\alpha = 1, 3/2, 5/2$  and also for the top hat profile  $\delta_0(x) = \text{constant}$ . The central density contrast  $\delta_0(0)$  is chosen so that the excess density contrast of the protocondensate is  $n \times \sigma_{\text{CDM}}(R)$  where  $n = 1.0, 2.5$ , and  $\sigma_{\text{CDM}}^2(R)$  is the mean square fluctuation in the sphere of radius  $R$  in the CDM model normalised to the COBE results (note that this is the only model we consider here). The neutral fraction  $f$  is somewhat uncertain and we have taken it to be 0.025 (see also Paper I and Subramanian & Swarup 1992). Further we have cut off the contributions to the flux from

shells which have collapsed to a radius more than half their turn around radius. This is to take account of the possible ionisation of HI once collapse and virialisation occurs.

In Fig. 1 we plot the emitted luminosity per unit velocity range ( $v_z$ ) (in units of  $10^{25} \text{erg s}^{-1} \text{Hz}^{-1}$ ) at different stages of the evolution ( $z = 8.5, 5.1, 3.34$ ) of the protocondensate for  $\alpha = 1$  and taking it to be a  $1\sigma$  fluctuation. As shells at larger and larger radii turnaround, the peak luminosity increases, while the half width decreases. Indeed, the peak flux can become arbitrarily high, since there could be a caustic in the velocity space. However, the internal velocities of the small scale clumps in the protocluster will in general lead to the smoothing of the line and so a peak of finite height. To take this into account, we convolve the emission profile with a gaussian of dispersion  $\sigma_v = 100 - 200 \text{ km s}^{-1}$ , velocity widths typical of luminous galaxies.

The raw and the convolved ( $\sigma_v = 200 \text{ km s}^{-1}$ ) line profiles (flux vs frequency) are shown in Fig. 2 for  $z = 3.34$ , one of the redshifts which will be probed by the GMRT, for both a  $1\sigma$  and a  $2.5\sigma$  fluctuation (solid and dashed lines correspond to the

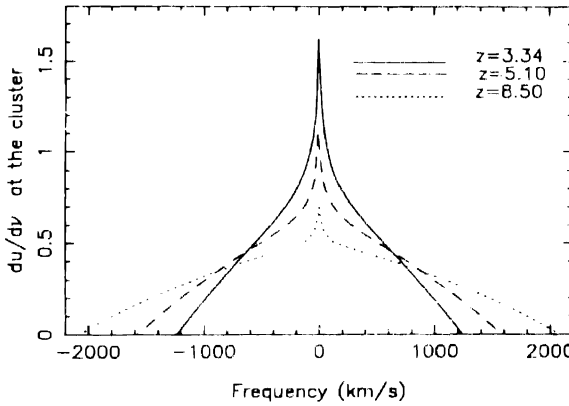


**Figure 1.** The emissivity line profile at different stages of the evolution ( $z = 8.5, 5.1, 3.34$ ) of the protocondensate for  $\alpha = 1$  and taking the protocondensate to be a  $1\sigma$  fluctuation.

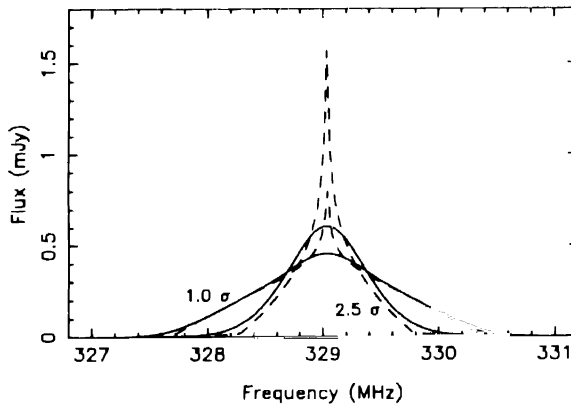


**Figure 2.** The raw and the convolved ( $\sigma_v = 200 \text{ km s}^{-1}$ ) line profiles (flux vs frequency) for  $z = 3.34$ , for both a  $1\sigma$  and a  $2.5\sigma$  fluctuation. Solid and dashed lines correspond to the convolved and raw profiles respectively.

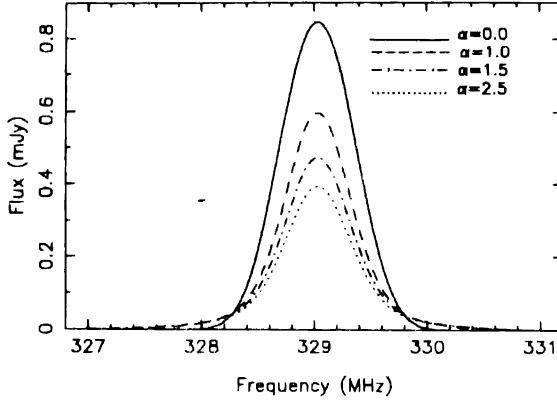


**Figure 3.** The convolved line profile for different initial density profiles ( $\alpha = 0, 1, 3/2, 5/2$ ) taking the protocluster to be a  $3\sigma$  fluctuation.

convolved and raw profiles respectively). The peak fluxes of the convolved line profiles that we have looked at are typically of order  $0.4 - 0.8$  mJy while the widths (FWHM) are of order  $0.6 - 1.5$  MHz, depending on  $\sigma_v$  and the value of  $n$ . If one considers a protocondensate with twice the mass adopted above the fluxes also correspondingly increase by a factor  $\sim 2$ . Note that the expected  $\sigma_{\text{rms}}$  due to the thermal noise in GMRT at the corresponding frequency (327 MHz), for 10 hour integration and say a bandwidth of 300 KHz is about 0.16 mJy. This assumes the source to be within the synthesised beam, which typically encompasses a mass  $\sim 5 \times 10^{14} M_{\odot}$ . Also  $\sigma_{\text{rms}}$  increases very little for a factor of two increase in the beam size (R. Subrahmanyam, private communication). So typical protoclusters could indeed be detectable by the GMRT. Finally in Fig. 3 we illustrate the effect of assuming different initial density profiles ( $\alpha = 0, 1, 3/2, 5/2$ ) for a protocluster which is a  $3\sigma$  fluctuation. One sees that changing  $\alpha$  from 0 to  $5/2$  leads to a decrease of the peak flux by a factor  $\sim 2$ .

The parameters of a protocluster which we have adopted here appear to us to be quite reasonable. We have taken a protocondensate with the mass corresponding to a rich cluster and considered  $1 - 3\sigma$  fluctuations in a COBE normalised CDM model. The major uncertainty in our calculations is the neutral fraction  $f$  which we have taken here to be 2.5% of the total mass. For a different value of  $f$  one has to simply scale the flux in Figs. 2 and 3 by  $f/(0.025)$ . Our results indicate that typical protocondensates in the CDM model could be detectable by the GMRT.

## References

- Peebles, P. J. E. 1980, *Large Scale Structure of the Universe*, (Princeton: Princeton University Press).  
 Padmanabhan, T., Subramanian, K. 1992, *Bull. Astr. Soc. India*, **20**, 1.  
 Sunyaev, R. A., Zeldovich, Ya. B. 1972, *Astr. Astrophys.*, **20**, 189.  
 Sunyaev, R. A., Zeldovich, Ya. B. 1974, *Mon. Not. R. astr. Soc.*, **171**, 375.  
 Swarup, G. 1984, *Giant Metre-Wavelength Radio Telescope Proposal*, Radio Astronomy Centre, TIFR, India.  
 Subramanian, K., Swarup, G. 1992, *Nature*, **359**, 512.  
 Subramanian, K., Padmanabhan, T. 1993, *Mon. Not. R. astr. Soc.*, **265**, 101 (paper I).

## Quasi Steady State Cosmology

Jayant V. Narlikar *Inter-University Centre for Astronomy and Astrophysics, Post Bag 4, Ganeshkhind, Pune-411 007, India*

F. Hoyle *102 Admirals Walk, Bournemouth BH2 5HF, UK.*

G. Burbidge *Centre for Astrophysics and Space Sciences and Department of Physics, University of California at San Diego, La Jolla, CA 92093-011 USA.*

**Abstract.** Because of a number of unsatisfactory features of the standard hot big bang cosmology, it is argued that there is a case for exploring alternative approaches to cosmology. The approach described here called the quasi steady state cosmology (QSSC), uses a field theoretic description of matter creation within the framework of general relativity.

A cosmological solution with the universe expanding exponentially along with cycles of expansion and contraction arises from mini-creation events taking place near the event horizons of highly collapsed massive objects. The now familiar phenomena like QSOs, AGN, radio sources, etc. are the manifestations of matter creation in such events. In this way cosmology is seen to be related to high energy astrophysics in a very direct way. The QSSC can explain the abundances of light nuclei and the microwave background, the observed large scale features of the universe like the  $m-z$  relation, the source count, the angular size-redshift relation, as well as observed distribution of the ages of galaxies.

**Key words:** Cosmological models— creation of matter— steady state cosmology.

### 1. Introduction

Despite a widespread support for the standard big bang cosmology, the theory has failed to resolve some of the basic issues of cosmology such as (i) determination of the temperatures of the microwave background, (ii) the relationship of its very small anisotropy to large scale structures in the universe, (iii) a workable theory of structure formation consistent with observations of dark matter and the large scale streaming motions, (iv) the relation of discrete source populations to a realistic view of the evolving universe, (v) the awkward observations of the very old and very young systems of galaxies, globular clusters etc., (vi) the lack of any link between the primordial big bang and the smaller and relatively recent origin of violent phenomena like the QSOs and AGN and (vii) the theoretical problem of describing the big bang event within conventional physics.

For details of these points see earlier work of Arp *et al.* (1990) and Hoyle *et al.* (1993). Our main purpose here is to argue that despite the popularity enjoyed by the big bang cosmology today, the above list is sufficient to motivate an alternative approach to

cosmology, an approach that does at least as well as the big bang and is better able to deal with the above issues.

## 2. Local creation of matter and cosmology

In 1948 Bondi & Gold (1948) and Hoyle (1948) had independently proposed the steady state theory as an alternative to the big bang cosmology. Bondi & Gold had adopted the Perfect Cosmological Principle as the starting point of their approach while Hoyle had taken a field theoretic description of matter creation as the main motivation. Here we will follow the second approach but with some significant modification.

The field equations are derived from an action principle. Although Hoyle *et al.* (1993) considered a direct particle interaction approach motivated by Mach's Principle, the following simplified derivation essentially reproduces their equations in the more familiar field theory format. Thus the classical Hilbert action leading to the Einstein equations is modified by the inclusion of a scalar field  $C$  of zero rest mass whose derivatives with respect to the spacetime coordinates  $x^i$  are denoted by  $C_{,i}$ . For the notation followed and further details see Narlikar (1993). To allow for explicit description of creation the worldline of a typical matter particle has a beginning at a finite point in spacetime.

Thus, if the worldline of particle  $a$  begins at point  $A$ , then the action principle gives a necessary condition for creation of mass  $m_a$  as

$$C_i C^i = m_a^2 c^4. \quad (1)$$

This is the 'creation threshold' which must be crossed for particle creation.

Calculations show that a highly collapsed object of mass  $M$  and radius  $R$  (say) can achieve this condition close to its surface. For,  $C_i C^i$  increases as  $(1 - 2GM/c^2 r)^{-1}$  as  $r \rightarrow R \approx 2GM/c^2$ . So it is possible for the creation threshold to be reached *near* a massive collapsed object even if it is *below* the threshold far away from it. Thus, instead of a single big bang event of creation, we have mini-creation events (MCEs) near collapsed massive objects.

The  $C$ -field tensor has negative stresses which lead to the expansion of spacetime, as in the case of inflation. The formalism described here is essentially that used by Hoyle & Narlikar (1962, 1966a, b) in the 1960s to produce inflation type solution (which, of course predated Guth's inflationary cosmology by 15 years!).

Since the  $C$ -field is a global cosmological field, we expect the creation phenomenon to be globally cophased. Thus, there will be phases when the creation activity is large, leading to the generation of the  $C$ -field strength in large quantities. However, the  $C$ -field growth because of its large negative stresses leads to a rapid expansion of the universe and a consequent drop in its background strength. When that happens creation is reduced and takes place only near the most collapsed massive objects thus leading to a drop in the intensity of the  $C$ -field. The reduction in  $C$ -field slows down the expansion, even leading to local contraction and so to a build-up of the  $C$ -field strength. And so on!

We can describe this up and down type of activity as an oscillatory solution superposed on a steadily expanding deSitter type solution of the field equations by

a scale factor that varies with cosmic time  $t$  as follows:

$$S(t) = \exp\left(\frac{t}{P}\right) \left\{ 1 + \alpha \cos \frac{2\pi t}{Q} \right\}. \quad (2)$$

Note that the universe has a long term secular expanding trend, but because  $|\alpha| < 1$ , it also executes non-singular oscillations around it. We can determine  $\alpha$  and our present epoch  $t = t_0$  by the observations of the present state of the universe. Thus an acceptable set of parameters is  $\alpha = 0.75$ ,  $t_0 = 0.85Q$ ,  $Q = 4 \times 10^{10}$  yr.,  $P = 20Q$ . Although the set is not unique and there will be a *range* of acceptable values, we will work with this set to illustrate the performance of the model.

### 3. The origin of nuclei and the microwave background

We have as yet not said what particle is being created by the C-field. The answer is, the Planck particle whose mass is  $m_p \approx (3\hbar/4\pi G)^{1/2} \sim 10^{-55}$  g. This particle, however, has a very short lifetime  $\sim 10^{-44}$  s. It decays ultimately into the baryon octet and radiation. Most members of the octet except  $n$  and  $p$  are also short-lived and decay into protons. Only the neutron and the proton combine into stable helium nuclei. Thus approximately 25% by mass (2 out of 8 baryons) combine to form helium.

A more careful calculation gives the helium mass fraction to be around 23%, with a tiny fraction of 1–2% in the form of metals. This type of nucleosynthesis also generates  $^2\text{H}$ ,  $^3\text{H}$ ,  $^3\text{He}$ ,  $^6\text{Li}$ ,  $^7\text{Li}$ ,  $^9\text{Be}$ ,  $^{10}\text{Be}$  etc. in small amounts that are in agreement with the observations and in fact, lead to a better agreement than in the big bang model.

There is one further important consequence. In the big bang model the required production of deuterium imposes a stringent upper limit on the present day baryon density. This limit forces us to assume that the dark matter component of the universe must be largely nonbaryonic. In the QSSC, there is no such density limit from deuterium abundance and thus the dark matter component *can be baryonic*. We will discuss this point further in the following section.

What about the microwave background? The QSSC obtains it in the following way. First, each Planck particle decay is like a fireball: it produces lot of energy, including baryons ( $\sim 10^{19}$  per Planck particle) and radiation. Bulk of the fireball energy goes into expansion. However, some radiation remains as relic of the fireball. Together with the starlight generated in the preceding oscillatory cycles this energy is to be thermalized to provide the microwave background. Does it provide enough radiant energy to give a 2.7 K background? Is the background thoroughly thermalized to produce a black body spectrum? Also, is it homogeneous to the extent given by COBE (Smoot *et al.* 1992) and other measurements? Quantitative studies (see Hoyle *et al.* 1993: preprint) answer all these questions in the affirmative.

Quantity-wise the starlight from several past generations of stars is sufficient to maintain a steady background of radiation whose present temperature is calculated to be  $\sim 2.7$  K, provided, some agency is available to thermalize it. The agency proposed is dust in the form of metallic needles, mostly of iron which absorb the ambient radiation and reradiate it in the microwaves. Provided this has gone on long enough, the radiation spectrum will have an accurate black body form. Calculation shows that



indeed the thermalization has occurred through as many as  $10^3$  absorptions and remissions by iron whiskers sufficient to ensure an extremely close approximation to the black body curve. The iron whiskers are typically  $\sim 1$  mm in length and  $10^{-6}$  cm in radius of cross section. The iron itself is produced partly from stellar nucleosynthesis in supernovae and partly from the decay of the Planck particle. The required density in the form of such whiskers is only  $\sim 10^{-35}$  g cm $^{-3}$ ; well within the observed cosmic abundances of iron. Further, it can be shown that the background produced will be very smooth with a patchiness of density of the order of  $10^{-5}$ . Fluctuations of density and temperature of this or larger order get smoothed out by redistribution of iron grains by the radiation pressure. For fluctuations on smaller scales the dynamical smoothness-restoring forces are too small to make the radiation smooth. Thus, the COBE finding  $\Delta T/T \sim 10^{-5}$  is consistent with the above picture.

#### 4. Relationship to cosmology and Astrophysics

We highlight here the performance of the QSSC in the three classic tests of cosmology.

(i) *The redshift-magnitude relation:* For the oscillatory steady state model the apparent magnitude is not a monotonic function of distance; nor so is the redshift. Both  $m$  and  $z$  decrease as we go past the last oscillatory minimum. At magnitudes fainter than, say 24, we may see moderately blueshifted sources from the previous cycle.

(ii) *The counting of radio sources:* In the source count curve calculated for a typical low frequency survey there is a super-Euclidean slope at high flux levels arising from contributions of sources from previous cycle in addition to those from the present cycle. Indeed, this and other features of the source count curve observed over a wide range of flux densities from  $\sim 10$  mJy to  $\sim 100$  Jy (see for example Kellermann & Wall 1986) can be matched by our theoretical curve without recourse to any evolutionary parameters. A source may be located several cycles back and yet have a modest redshift. Optically such a source may be unobservable, but in the radio it would still have a detectable flux density and may be classified as an *empty field*.

(iii) *The angular size-redshift relation:* This test first proposed by Hoyle (1959) has not, however, yielded any clearcut answer as there are several observational uncertainties. A detailed working out of Hoyle's formula for the QSSC shows it also to be compatible with Kellermann's (1993) findings for compact radio sources. For the larger sources considered by Kapahi (1987) and others the linear size would be expected to be more and more compressed as we go more and more towards the oscillatory minimum. Calculations by Hoyle *et al.* (1993; preprint) show that this leads to a fall off not very different from the  $1/z$  law found by Kapahi.

The minicreation events (MCEs) have several points of contact with astrophysics. We briefly enumerate a few:

(i) *Gravity wave sources:* The explosive creation near compact massive objects makes them potential sources of gravity waves, provided the events are sufficiently anisotropic. Narlikar & Das Gupta (1993) have shown that such events in the mass range of  $100$ – $1000 M_{\odot}$  can be detected by the laser interferometric detectors being planned worldwide. Further, the gravity wave background created by such MCEs may also detectably affect the timing mechanism of millisecond pulsars.

(ii) *High energy sources*: The explosive nature of energy generation in QSOs and AGN as well as in the gamma ray burst sources makes the MCEs ideal candidates for these energy sources. This is in keeping with Ambartsumian's conjecture (1958, 1965) that the AGN are likely sites for matter creation in explosive form.

(iii) *The age of the universe*: According to QSSC the universe is infinitely old but the average age of astronomical objects is  $1/3 P \sim 3 \times 10^{11}$  yrs. This makes many clusters much older than hitherto assumed. Even our Galaxy might have age of this order with several generations of stars formed, evolved and burnt out. The dark matter component in the Galaxy may be largely made of burnt out stars.

## 5. Concluding remarks

In this alternative cosmology there is considerable scope for inputs from high energy particle physics, in particular (i) in giving a quantum formalism of the  $\bar{C}$ -field (which is described here only classically) and (ii) in working out the details of how the created Planck particle decays to baryons.

Some of the main predictions that distinguish the QSSC from big bang cosmology are (i) the existence of faint blue shifted galaxies (ii) the dark matter turning out to be baryonic (iii) the existence of very old and very young galaxies (iv) the detection of gravity waves from the MCEs, and (v) the evidence for matter creation in sources of high energy astrophysics.

## References

- Ambartsumian, V. A. 1958, 1965, *Proc. of the Solvay Conference on The Structure of the Universe*, p. 241, and *Proc. of the Solvay Conference on The Structure and Evolution of the Galaxies*, p. 1
- Arp, H. C., Burbidge, G., Hoyle, F., Narlikar, J. V., Wickramasinghe, N. C. 1990, *Nature*, **346**, 807.
- Bondi, H., Gold, T. 1948 *Mon. Not. R. astr. Soc.*, **108**, 252.
- Hoyle, F. 1948 *Mon. Not. R. astr. Soc.*, **108**, 372.
- Hoyle, F. 1959, *Paris Symposium on Radio Astronomy*, Ed. R.N. Bracewell (Stanford University Press), p. 529.
- Hoyle, F., Narlikar, J. V. 1962 *Proc. R. Soc.*, **A270**, 334.
- Hoyle, F., Narlikar, J. V. 1966a *Proc. R. Soc.*, **A290**, 143.
- Hoyle, F., Narlikar, J. V. 1966b *Proc. R. Soc.*, **A290**, 162.
- Hoyle, F., Burbidge, G., Narlikar, J. V. 1993, *Astrophys. J.*, **410**, 437.
- Kapahi, V. K. 1987, *Observational Cosmology, IAU Symp. No. 124*, Ed. A., Hewitt, G. Burbidge & L. Z. Fang, (Dordrecht: D. Reidel), p. 251.
- Kellermann, K. 1993 *Nature*, **361**, 134.
- Kellermann, K., Wall, J. V. 1987 *Observational Cosmology, IAU Symp. No. 124* (1987, Ed. A. Hewitt, G. Burbidge & L. Z. Fang), (Dordrecht: D. Reidel), p. 545
- Narlikar, J. V. 1993 *Introduction to Cosmology*, 2<sup>nd</sup> Edition, (Cambridge).
- Narlikar, J. V., Das Gupta, P. 1993 *Mon. Not. R. astr. Soc.*, **264**, 489.
- Smoot, G. F. et al. 1992 *Astrophys. J.*, **396**, L1.



## On Non-Singular Cosmological Models

**N. Dadhich** *Inter-University Centre for Astronomy and Astrophysics, Post Bag 4, Ganeshkhind, Pune 411 007, India*

**R. Tikekar** *Department of Mathematics, Sardar Patel University, Vallabh Vidyanagar 358 120, India*

**L. K. Patel** *Department of Mathematics, Gujarat University, Ahmedabad 380 009, India*

**Abstract.** We argue that a simple and natural inhomogenisation and anisotropisation of the Friedman-Robertson-Walker (FRW) open model leads to the family of non-singular cosmological models. Further for cylindrically symmetric metric separable in time and radial coordinates, the identified family forms the complete set of non-singular perfect fluid solutions of Einstein's equations.

**Key words:** Singularity free models   non-singular models   cosmology - cylindrical symmetry.

For the description of the present state of our Universe, the standard FRW model is generally believed to be quite successful and adequate. It prescribes a homogeneous and isotropic distribution for its matter content. It is realised, though, that such a character cannot be sustained at all scales, particularly at very early stages of evolution when dissipative processes can no longer be ignored. Consideration of inhomogeneity and anisotropy at early times is also justified for avoidance of special initial conditions and for formation of large scale structures in the Universe.

The well-known examples of anisotropic models are the Bianchi models, which have in recent times received considerable attention in the context of quantum cosmology and early Universe. Inhomogeneity has also been considered by several authors (Wainwright & Goode 1980; Feinstein & Senovilla 1989; Patel & Dadhich 1992a, 1993a). The singular beginning of cosmological models is considered as the characteristic of the Einsteinian cosmology. All these models suffer from the singularity at  $t = 0$  irrespective of their isotropy and homogeneity properties. This view is strongly aided by the powerful singularity theorems (Hawking & Ellis 1973) that predict inevitability of occurrence of singularity so long as GR and reasonable physical conditions are adhered to. Thus a folklore had come to stay that the big-bang singularity is an essential feature of the relativistic cosmology and it can only be avoided by invoking unusual physical properties for matter or quantum and other fields or modifying GR. Several such models have been considered where singularity is managed by introducing one or more of these features (Bekenstein & Meisels 1980; Murphy 1973).

On this background it was very remarkable when Senovilla (1990) found an exact solution of Einstein's equations which was free of singularity and had a physically acceptable behaviour for matter ( $\rho = 3p > 0$ ). It gave a big jolt to the folklore. Here is

an exact GR solution with regular behaviour for physical and geometrical invariants and free of singularity of any kind. Thus GR does admit non-singular cosmological solutions with physically reasonable behaviour for its matter content. It was subsequently shown that, not only geometrical and physical invariants are finite and regular, the spacetime is geodesically complete (Chinea *et al.* 1992). That is particle trajectories will never meet catastrophic conditions leading to their termination for arbitrary evolution in their proper time. This was the first non-singular solution, true to GR and confirming to all physically acceptable conditions.

Now the question arises how does this solution escape the wrath of powerful singularity theorems that have been established for very general framework? The theorems are based on the four basic assumptions that guarantee regular and smooth behaviour for spacetime manifold, positivity of energy density (that produces gravity), proper causality conditions (prohibiting violation of causality) and existence of closed trapped surfaces. Except the last one, the first three seem quite natural and obvious. Let us first see what do we mean by trapped surface? In physical terms it means a surface that traps photons, i.e. both in and out going wavefronts move inwards. That is gravitational field becomes so strong that photons get trapped. This may be a plausible state for collapse of a body under gravity but certainly not so for cosmology. Even for collapse this should arise as a consequence of the field equations rather than a priori assumption. This concept has though played a very crucial role in defining a black hole but its role in cosmology is not at all obvious. It is doubtful whether it has any. For FRW model has the big-bang singular beginning but there occurs no trapped surfaces in the past and only the closed universe will encounter them in the future. By dropping the trapped surfaces assumption, the theorems can be rendered ineffective without loss of any physical and geometrical desirable features. This is exactly what the Senovilla model does (Chinea *et al.* 1992).

In the cosmological context it is justified to take the spacetime metric to be separable in space and time coordinates and fluid motion to be irrotational. Under these conditions it is easy to see that acceleration can be non-zero only if shear is non-zero (Raychaudhuri 1993). From the Raychaudhuri (1955) equation, it is clear that for avoidance of singularity acceleration (pressure gradient that counter-acts gravitational attraction) must be non-zero. In this situation acceleration can only arise from shear, i.e. both shear (which though helps collapse) and acceleration must be present. The former arises out of anisotropy and the latter from inhomogeneity. Thus anisotropy and inhomogeneity become the essential ingredients of non-singular cosmological models.

The obvious choice then would be to anisotropise and inhomogenise FRW metric. It will not work straight away because FRW is spherically symmetric that cannot sustain shear with separability. We should hence give up spherical symmetry. This is what we propose to do in the following way: transform FRW metric in cylindrical coordinates and then anisotropise and inhomogenise it. Now it works (Dadhich *et al.* 1993a,b) and the resulting spacetime is the identified family of non-singular cosmological solutions (Ruiz & Senovilla 1992).

We begin with the FRW metric for the open Universe,

$$ds^2 = dt^2 - T^2(t) \left( \frac{dr^2}{1+r^2} + r^2 d\theta^2 + r^2 \sin^2 \theta d\phi^2 \right) \quad (1)$$

and transform it into cylindrical coordinates

$$ds^2 = dt^2 - T^2(t) \left( \frac{dr^2}{1+r^2} + (1+r^2)dz^2 + r^2 d\phi^2 \right) \quad (2)$$

by the transformation

$$r = (\sinh^2 z + r^2 \cosh^2 z)^{1/2}, \tan \theta = \frac{\bar{r}}{\sinh z \sqrt{1+r^2}}. \quad (3)$$

Further writing  $m\bar{r} = \sinh(m\hat{r})$  and then dropping caps to write

$$ds^2 = dt^2 - T^2(t)(dr^2 + \cosh^2(mr)dz^2 + m^{-2} \sinh^2(mr)d\phi^2). \quad (4)$$

Let us now inhomogenise and anisotropise the FRW metric by writing

$$ds^2 = T^{2a} \cosh^{2a}(mr)(dt^2 - dr^2) - T^{2b} \cosh^{2b}(mr)dz^2 - m^{-2} \sinh^2(mr) T^{2c} \cosh^{2c}(mr)d\phi^2 \quad (5)$$

where we have used the coordinate freedom to write  $g_{rr} = |g_{rr}|$ . We could have as well used the form (2). Taking the natural field  $u = T^2 \cosh^a(mr)dt$ , the isotropy of fluid uniquely determines

$$T = \cosh(kt), \alpha = \gamma. \quad (6)$$

With this the metric (5) is the family of singularity free models identified by Ruiz & Senovilla (1992).

Notice that  $m^{-2} \sinh^2(mr)$  is simply to ensure  $2\pi$  periodicity for the angle  $\phi$  and elementary flatness near the axis and hence it does not participate in the inhomogenisation and anisotropisation process. Ruiz & Senovilla (1992) have taken  $\beta + \gamma = 1$  and different undetermined function of  $r$  in place of  $\cosh(mr)$  and have found that all functions are expressible as powers of the same function  $\cosh(mr)$ . For time dependence  $T = \cosh(kt)$  is the general solution. Even if we take  $\beta + \gamma = 1$  and different  $T(t)$  functions, it turns out that they can all be given as the powers of the single function, as given by (6). Thus the metric (5) with (6) forms the complete set of singularity free solutions of cylindrically symmetric metric with separable functions of  $r$  and  $t$  (Dadhich *et al.* 1993b).

For singularity free models, both Weyl and Ricci curvatures should be regular and their regularity for the metric (5) also demands  $\alpha = \gamma$ . The isotropy of pressure constrains the parameters and it can be shown that the only two following cases give rise to singularity free models:

- (i)  $b = c, \alpha = \gamma, \alpha + \beta = 1, a = -b/(1 + 2b), k = (1 + 2b)m$ ,
- (ii)  $b + c = 1, \alpha = \gamma, \alpha + \beta = 1, a = -b(1 - b), k = 2m$ .

In the former case there does not occur an equation of state  $\rho = \mu p$  in general, however for  $b = -(1/3)$  we obtain the Senovilla radiation model with  $\rho = 3p$ . In the latter case it is always  $\rho = p$  giving the stiff matter model (Patel & Dadhich 1993b). The matter free limit ( $\rho = 0$ ) of the stiff matter model yields two distinct singularity free vacuum solutions. It may be noted that all these are the general solutions in the given setting.

For the case  $b = c$ , the pressure and density are given by

$$8\pi\rho A^2 = \frac{b^2(1-2b)}{(1+2b)^3} k^2 \cosh^{-2}(mr) - \frac{(3b+1)(b+1)}{(1+2b)^2} k^2 \cosh^{-2}(kt), \quad (7)$$

$$8\pi p A^2 = \frac{b(2b-1)(2+3b)}{(1+2b)^3} k^2 \cosh^{-2}(mr) - \frac{(3b+1)(b+1)}{(1+2b)^2} k^2 \cosh^{-2}(kt), \quad (8)$$

and expansion, shear and acceleration parameters read as follows:

$$\theta = (\alpha + 1)k \sinh(kt) \cosh^{-\alpha-1}(kt) \cosh^{-a}(mr) \quad (9)$$

$$\sigma^2 = \frac{2}{3}(2\alpha - 1)^2 k^2 \sinh^2(kt) \cosh^{-2(\alpha+1)}(kt) \cosh^{-2a}(mr) \quad (10)$$

$$\dot{u}_r = -am \sinh(mr) \cosh^{-a}(kt) \cosh^{-a-1}(mr), \quad (11)$$

where  $A = \cosh^a(kt) \cosh^a(mr)$ . It is clear that both physical as well as kinematic parameters are regular and finite for whole of spacetime.

The metric (5) has been shown to be geodesically complete (Dadhich & Patel 1993c) in general without reference to any matter distributions with the parameters constrained as  $\alpha \geq 0$ ,  $\alpha + \beta \geq 0$ ,  $\alpha \geq \beta$ ,  $a \geq 0$ ,  $a + b \geq 0$ ,  $a \geq b$  and  $b \leq 0$ .

The overall behaviour of the model is similar to the Senovilla radiation model. At  $t \rightarrow \pm \infty$  spacetime curvature and physical as well as kinematic parameters tend to zero though the metric does not go over to the Minkowski form. At  $t \rightarrow -\infty$  the Universe has vanishingly low density, as  $t$  increases it contracts and becomes dense until  $t = 0$  is reached. At any given  $r$ ,  $\rho$  is maximum at  $t = 0$  and at any instant  $\rho$  is maximum at  $r = 0$ . The density is absolute maximum at  $t = 0$  and  $r = 0$ , which can arbitrarily be prescribed by choosing the free parameter  $k$ . At  $t = 0$  contraction turns into expansion and shear also changes its sense. The acceleration does not let the universe to collapse into a singularity. For  $t > 0$  it expands and attains the low density state again as  $t \rightarrow \infty$ .

The metric (5) with (6) can as well be cast in the form

$$ds^2 = (1 + k^2 t^2)^{\alpha-1} (1 + m^2 r^2)^a dt^2 - (1 + k^2 t^2)^2 (1 + m^2 r^2)^{a-1} dr^2 \\ - (1 + k^2 t^2)^b (1 + m^2 r^2)^b dz^2 - r^2 (1 + k^2 t^2)^a (1 + m^2 r^2)^c d\phi^2, \quad (12)$$

which reduces to the FRW form (2) for  $\alpha = \beta = 1$ ,  $a = c = 0$  and  $b = 1$  where  $T(t) = (1 + k^2 t^2)$ . It is interesting that if one just uses hyperbolic or  $(1 + k^2 t^2)$  functions, which are clearly the obvious choice for singularity free spacetime, one ends up with the family of singularity free models.

One may ask the question, how robust is the singularity free framework in relation to accommodating other force fields? It turns out that viscosity cannot be included without sacrificing positivity of viscosity coefficients for all time (Patel & Dadhich 1992b) while the radial heat flow can easily be included (Patel & Dadhich 1983c). Both the cases above can be generalised to have radial heat flow. Note that for  $\rho = \mu p$ ,  $\mu$  can have the only two discrete values ( $\mu = 1, 3$ ). If we introduce massless scalar field alongwith perfect fluid in the case (i), the resulting fluid can have an equation of state,  $4 > \mu > 3$ , opening out a narrow window for  $\mu$ .

We are now investigating a general diagonal metric without any symmetry but separable in space and time coordinates for non-singular cosmological solutions. It turns out that when the metric depends upon all the three space coordinates, the isotropy of fluid pressure requires vanishing of shear and hence only singular solutions can emerge because acceleration vanishes. The family of non-singular solutions discussed above has the only one space coordinate dependence. For two coordinates dependence we can have shear and consequently acceleration non-zero, that means there may occur another family of singularity free solutions. This is what we are currently trying to find.

Finally the most pertinent question for the singularity free models is: how to evolve them into the (present day) FRW models? The question is inherently very difficult because the former are cylindrically symmetric wherein a direction is singled out while the latter are spherical having no identifiable direction. It may be noted that the ratio of shear to expansion, that measures the anisotropy, is a constant for these models. This means anisotropy will not decay but stay for all times. Since the discovery of these solutions it is for the first time some sort of linkage to the physically interesting FRW model has been pointed out. The affirmative answer to the above question will undoubtedly have a very important bearing on our overall cosmological perception of the Universe and particularly for the early Universe cosmology.

### Acknowledgement

We thank A. K. Raychaudhuri for helpful communication. L. K. Patel and R. Tikekar thank IUCAA for hospitality.

### References

- Bekenstein, D., Meisels, A. 1980, *Astrophys. J.* **237**, 342.  
 Chineza, F. J., Fernandez-Jombrina, L., Senovilla, J. M. M. 1992, *Phys. Rev.*, **D45**, 481.  
 Dadhich, N., Patel, L. K., Tikekar, R. 1993a, Preprint: IUCAA 19/93.  
 Dadhich, N., Tikekar, R., Patel, L. K. 1993b, *Curr. Sci.*, **65**, 694.  
 Dadhich, N., Patel, L. K. 1993c, Preprint: IUCAA 20/93.  
 Feinstein, A., Senovilla, J. M. M. 1989, *Class Quantum Grav.* **6**, 189.  
 Hawking, S. W., Ellis, G. F. R. 1973, *The Large Scale Structure of the Universe*, (Cambridge University Press).  
 Murphy, J. M. 1973, *Phys. Rev.*, **D8**, 4231.  
 Patel, L. K., Dadhich, N. 1992a, *Astrophys. J.*, **401**, 433.  
 Patel, L. K., Dadhich, N. 1992b, Preprint, IUCAA-21/92.  
 Patel, L. K., Dadhich, N. 1993a, *J. Math. Phys.*, **34**, 1927.  
 Patel, L. K., Dadhich, N. 1993b, Preprint: IUCAA-1/93.  
 Patel, L. K., Dadhich, N. 1993c, *Class. Quantum Grav.* **10**, L85.  
 Raychaudhuri, A. K. 1955, *Phys. Rev.*, **98**, 1123.  
 Raychaudhuri, A. K. 1993, Private communication.  
 Ruiz, E., Senovilla, J. M. 1992, *Phys. Rev.* **D45**, 1995.  
 Senovilla, J. M. M. 1990, *Phys. Rev. Lett.*, **64**, 2219.  
 Wainwright, J., Goode, S. W. 1980, *Phys. Rev.*, **D22**, 1906.





## Abstracts

### Nonexistence of Nonstatic Sourceless Abelian Gauge Strings in a Robertson-Walker Universe with $k = 1$

D. Bhattacharyya & S. Banerji *The University of Burdwan, Burdwan 713 104, India.*

A model of a sourceless Abelian gauge string was examined by Morris in a Robertson-Walker universe with flat space ( $k = 0$ ) and showed that it could be created or destroyed by energy flow. We generalised the result to a Robertson-Walker universe with spatial curvature  $k = \pm 1$  and found that creation or destruction of the string was possible only when  $k = 0.1$  but no nonstatic solution consistent with the boundary conditions exists when  $k = -1$ . This however, is true when the gauge field structure is separable in space and time coordinates. A more detailed account is given in *Bull. Astr. Soc. India*, **21**, 421 (1993).

**Key words:** Gauge strings—Universe.

★ ★ ★ ★ ★

### Some Exact Solutions in Bianchi III and VI<sub>0</sub> String Cosmology

Ramesh Tikekar *Department of Mathematics, Sardar Patel University, Vallabh Vidyanagar, 388 120, India.*

L. K. Patel *Department of Mathematics, Gujarat University, Ahmedabad 380 009, India.*

Assuming the expression  $T_{ik} = \rho u_i u_k - \lambda w_i w_k + 1/4\pi[-g^{lm}F_{il}F_{km} + \frac{1}{4}g_{ik}F_{lm}F^{lm}]$ ,  $u_i u^i = -w_i w^i = 1$ ,  $u_i w^i = 0$ , for the energy momentum tensor of a cloud of string dust, in presence of magnetic field some exact solutions of Einstein's field equations  $R_{ik} - (\frac{1}{2})Rg_{ik} = -8\pi T_{ik}$  in Bianchi III and VI<sub>0</sub> string cosmology have been obtained. The metrics along with the relevant features of the solutions are specified below:

#### Bianchi III space time solutions

The Bianchi III type solutions have the metric

$$ds^2 = dt^2 - A^2(t)dx^2 - B^2(t)\exp(-2ax)dy^2 - C^2(t)dz^2. \quad (1)$$

**Solution 1:** With  $A = B = [\alpha(t - t_0) - (K^2/\alpha)]$ ,  $C = 1$ ,  $\alpha > a^2$ , (1) describes a model beginning with a singularity at  $t = t_0 + (K/\alpha)$ , which at  $t = t_0 + K/\alpha[3(\alpha - a^2)/(\alpha - a^2)]^{1/2}$ , represents a dust filled universe with a magnetic field.

**Solution 2:** With  $A = B = C^{2/n}$ ,  $C = (\alpha + \beta t^2)^{n/4}$ , we get a model with a singularity at  $t = -(-\beta/\alpha)^{1/2}$  undergoing expansion till  $t = 0$ , followed by a contraction till  $t = (-\beta/\alpha)^{1/2}$

**Solution 3:** The metric of this solution is  $ds^2 = A^9 d\tau^2 - A^2[dx^2 + e^{-2ax} dy^2] - A^n dz^2$  where  $A = [(\beta + \alpha\tau) - K^2 \tau^2 / 2(n+1)]$  and  $n = [3 + (33)^{1/2}]$ . It is a generalization of a Bianchi I model of string cosmology.

**Solution 4:** With  $A = (\alpha t + \beta)^{(n+1)/(n^2+n+1)}$ ,  $C = A^n$ , (1) describes a distribution of geometric strings on putting  $n = 0$ ,  $\alpha = 1$  &  $\beta = 0$ . The model has an initial singularity at  $t = 0$  and unchecked expansion. For  $a = 0$  it reduces to Friedman dust model with zero curvature.

### Bianchi VI<sub>0</sub> space time solutions

The metric of Bianchi VI<sub>0</sub> type solutions have the form

$$ds^2 = A^2(t)(dt^2 - dx^2) - B^2(t)e^{2mx} dy^2 - C^2(t)e^{-2mx} dz^2. \quad (2)$$

**Solution 5:** With  $A = B^2 = C^2 = A_0 \exp[2(m^2 - K)^{1/2} t]$ ,  $A_0 = \text{const.}$  (2) describes an expanding model without singularity.

**Solution 6:** With  $A = B^2 = C^2 = (\alpha t)^\rho$ ,  $\alpha = \text{const.}$ ,  $m^2 = K^2$ , (2) provides a model with a singularity at  $t = 0$  complying with requirement  $\rho > 0$  until  $t = 3/K \sqrt{5/2}$ , where  $\rho = 0$ . It is physically significant for weak magnetic fields.

**Solution 7:** With  $A^2 = \exp(m^2 t^2 + 2at)$ ,  $B = C = t$ ,  $a = \text{const.} (> 0)$ , (2) provides a singularity free model undergoing expansion.

**Solution 8:** For  $A = \exp(\alpha t)$ ,  $B = C = \exp(mt)$ ,  $\alpha = \text{const.}$  (2) leads to a singularity-free model with  $\rho > 0$ ,  $\rho_p > 0$  for  $m < \alpha$  and the equation of state  $\rho = (1 + W)\lambda$ , with  $W = 4(m - \alpha)/(2\alpha - 3m)$ , characterizing Takabayashi strings if  $2\alpha < 3m$  so that  $W > 0$ . If  $\alpha = m$ ,  $\rho = \lambda$ .

★★★★★

## A Rigorous Proof of the Inflationary Spectrum

Jai-chan Hwang *Korea Astronomy Observatory, Daejeon, S. Korea.*

**Keywords:** Early universe— inflationary spectrum.

We consider an early acceleration (inflation) phase supported by a minimally coupled scalar field. The equation of motion is

$$\phi_a^{;a} - V_{,\phi} = 0. \quad (1)$$

Concerning the scalar-type mode, without losing any generality, we can take a uniform-curvature gauge which leads to a metric

$$ds^2 = -(1 + 2\alpha)dt^2 - 2\chi_{,\alpha} dt dx^\alpha + a^2(t)\delta_{\alpha\beta} dx^\alpha dx^\beta. \quad (2)$$

From equation (1) and using the Einstein's equation we can derive a closed form equation for the perturbed scalar field as:

$$\delta\ddot{\phi} + 3H\delta\dot{\phi} + [V_{,\phi\phi} + 2\frac{\dot{H}}{H}\left(3H - \frac{\dot{H}}{H} + 2\frac{\ddot{\phi}}{\dot{\phi}}\right) - \frac{1}{a^2}\nabla^{(3)2}] \delta\phi = 0. \quad (3)$$

There are two points we would like to make in this short summary. First, in the large scale equation (3) allows an integral form solution valid for general  $V(\phi)$

$$\delta\phi(\mathbf{x}, t) = \frac{\dot{\phi}}{H} \left[ -C(\mathbf{x}) + D(\mathbf{x}) \int^t \frac{H^2}{a^3 \dot{\phi}^2} dt \right]. \quad (4)$$

Second, for a power-law (includes the exponential case) expansion stage supported by the background scalar field, there arises a curious cancellation which reduces equation (3) to the widely studied form:

$$\delta\ddot{\phi} + 3H\delta\dot{\phi} - a^{-2}\nabla^{(3)2}\delta\phi = 0. \quad (5)$$

With these two steps, which are only available in this newly found uniform curvature gauge choice, we can provide a rigorous analytic proof of the inflationary spectrum. In short, equation (5) makes the classical evolution part simple, whereas equation (3) allows us to calculate the generated quantum fluctuations completely taking the accompanying metric fluctuations into account. The derived spectrums for general vacuum states can be written, for the exponential and the power-law cases respectively, as:

$$\begin{aligned} \mathcal{P}_c^{1/2} &= \frac{H}{|\dot{\phi}|} \mathcal{P}_{\delta\dot{\phi}}^{1/2} \\ &= \frac{H}{|\dot{\phi}|} \frac{H}{2\pi} |c_2(k) - c_1(k)|, \quad \frac{H}{|\dot{\phi}|} \frac{\Gamma(v)}{\pi^{3/2} a |\eta|} \left( \frac{k|\eta|}{2} \right)^{3/2-v} |c_2(k) - c_1(k)|. \end{aligned} \quad (6)$$

The notation, derivation and also implications of these results can be found in Hwang 1993.

## Reference

Hwang, J. 1993, *Phys. Rev. D.*, **48**, 3544.

★★★★★



# **Observational Cosmology**



## The Lyman Alpha Absorbers – Probes of the High Redshift Universe

Richard W. Hunstead & David P. Mar *School of Physics, University of Sydney, NSW 2006, Australia.*

Max Pettini *Royal Greenwich Observatory, Cambridge CB3 0EZ, UK.*

**Abstract.** The Lyman  $\alpha$  absorption lines in the spectra of high-redshift QSOs probe a pervasive but poorly understood component of the early universe. The discrete nature of the absorption lines implies that the neutral hydrogen is concentrated into ‘clouds’ which are immersed in a medium transparent to Lyman  $\alpha$ . The issue of whether the Lyman  $\alpha$  forest clouds are distributed randomly in space or show evidence for clustering is of great relevance for studies of structure formation in the universe. We have found evidence of possible large-scale structure at  $z \approx 2$  in the distribution of *weak* Lyman  $\alpha$  lines in the QSO Q1101–264 on scales  $\sim 115 h^{-1}$  Mpc. The features seen in the two-point correlation function may indicate a characteristic clustering length, or may possibly result from non-uniform ionisation of the intergalactic medium.

At the opposite end of the distribution of H I column densities are the damped Lyman  $\alpha$  systems. Measurements of the abundances of zinc and chromium in a recently completed survey of 17 damped Lyman  $\alpha$  systems spanning the range  $z_{\text{abs}} = 1.78\text{--}3.03$  show that at  $z \approx 2$  (a) the typical metallicity [Zn/H] of the damped Lyman  $\alpha$  galaxies is approximately 1/10 solar, (b) there is a large spread in metallicity at essentially the same epoch, and (c) the bulk of the Cr is depleted from the gas phase and incorporated into dust grains. The low metal abundances confirm earlier, less precise estimates and the wide dispersion suggests that the damped Lyman  $\alpha$  lines may arise in sightlines through galaxies of widely differing masses and rates of evolution. The presence of dust in the damped Lyman  $\alpha$  absorption systems, even at these low metallicities, probably accounts for the low incidence of Lyman  $\alpha$  emission from the absorbers, and may also explain the failure of deep searches for primeval galaxies.

**Key words:** Lyman alpha forest — QSOs — cosmology.

### 1. Introduction

The radiation from distant objects such as QSOs has to negotiate many obstacles before reaching our ground-based or orbiting telescopes. These obstacles might consist of regions of neutral gas, ionised gas, dust, magnetic fields, gravitational fields and, of course, the terrestrial atmosphere and clouds. Passage of the radiation through such regions may affect its spatial, spectral and polarisation properties, and cause time variations in its intensity. In other words, each region intercepted by the radiation will leave a characteristic imprint on the recorded signal. If we are able to interpret these



clues correctly they can yield information about the physical and chemical environments along a path stretching back as far as 90% of the age of the universe. As a result, the detailed study of high- $z$  QSOs and galaxies is proving to be a uniquely powerful cosmological tool.

Although our observations (in most cases) give us no direct clues to the morphology or lateral extent of the intervening obstacles, the evidence points increasingly towards them arising in galaxies which happen to fall on the line of sight. Moreover, the serendipitous nature of such alignments means that we are probably sampling 'normal' examples of intervening galaxies, as distinct from the more pathological objects (QSOs and radio galaxies) we might be using as the background probes. If the sightline passes sufficiently close to a galactic nucleus, or the centre of a cluster of galaxies, we may observe multiple images or arc-like distortions as a result of gravitational lensing (Blandford & Narayan 1992). Likewise, if the sightline encounters a region of ordered magnetic fields we might expect to record excess Faraday rotation measure (Perry *et al.* 1993 and references therein) in the radio emission. For radio sources of sufficiently small angular size we might also observe intensity variations due to refractive scintillation as the wavefront passes through ionised regions of the local interstellar medium (Rickett 1986).

The most obvious indication of intervening material, however, and the best documented, is the plethora of discrete absorption lines seen in the spectra of all high- $z$  QSOs. These absorption lines are presumed to originate in discrete 'clouds' which are scattered along the line of sight and embedded in a medium transparent in Lyman  $\alpha$ . Observations at intermediate and high spectral resolution have identified three main classes of absorbers, characterised principally by their column densities of neutral hydrogen: (i) the damped Lyman  $\alpha$  systems, with  $N(\text{H I}) > 10^{20} \text{ cm}^{-2}$ , (ii) the so-called 'metal-line' systems, with  $10^{15} < N(\text{H I}) < 10^{20} \text{ cm}^{-2}$ , and (iii) the Lyman  $\alpha$  forest 'clouds' with  $N(\text{H I}) \leq 10^{15} \text{ cm}^{-2}$ . It is still not clear whether these three broad classes represent different sightlines through basically similar objects, presumably galaxies, or whether they originate in fundamentally different systems. In either case, QSO absorption line spectroscopy remains a unique probe of gas phase abundances, dust and molecular fraction in these remote systems, and can give us estimates of other parameters such as temperature, star formation rate and transverse size of the absorbing regions.

In this brief presentation we will concentrate on some recent results from high resolution spectroscopy of high- $z$  QSOs, with specific emphasis on the Lyman  $\alpha$  forest and damped Lyman  $\alpha$  absorbers.

## 2. The Lyman $\alpha$ forest

The Lyman  $\alpha$  clouds are by far the most numerous 'objects' at high redshifts accessible to detailed study with ground-based telescopes, allowing trends to be examined statistically. Their macroscopic properties have been defined by studies at intermediate resolution ( $\sim 1 \text{ \AA}$ ), showing that the stronger Lyman  $\alpha$  absorbers - those with rest-frame equivalent widths  $W_0 > 320 \text{ m\AA}$  - (a) are distributed cosmologically, (b) evolve strongly in number density with redshift ( $dn/dz \propto (1+z)^\gamma$ ,  $\gamma \sim 2.4$ ; Murdoch *et al.* 1986), and (c) show no convincing evidence for clustering on scales  $\Delta v > 300 \text{ km s}^{-1}$ , this being the smallest separation which can be sampled at intermediate resolution.

The lack of clustering is a characteristic feature distinguishing the Lyman  $\alpha$  clouds from the metal-rich absorption systems (see discussion in Bechtold & Schectman 1989). Their apparently isotropic but random distribution in space has led to the interpretation of the Lyman  $\alpha$  clouds as an intergalactic population not associated with galaxies, at least at high redshifts. On the other hand, their mere ubiquity from  $z \sim 0$  out to the highest redshifts ( $z \sim 5$ ) probed to date makes it extremely unlikely that they are 'innocent bystanders' during the epoch of galaxy formation, and this should be reflected at some level in their physical properties and spatial distribution. In support of this view, there have been several recent reports claiming a non-random distribution of absorbers along the sightlines to some QSOs (e.g. Dobrzycki & Bechtold 1991 and references therein) as well as evidence for large-scale structure among the stronger Lyman  $\alpha$  lines (e.g. Francis & Hewett 1993; Mo *et al.* 1992, and references therein).

Our picture of the Lyman  $\alpha$  clouds and their relationship to other objects is gradually improving as we obtain spectroscopic data of better quality and resolution, and extend the studies to lower redshift using data from HST. However, we still have only a very sketchy picture of the physical conditions within the Lyman  $\alpha$  clouds and in the surrounding intergalactic medium.

The highest spectral resolution currently applied to QSO absorption line research is  $\sim 7 \text{ km s}^{-1}$  FWHM, obtained with the University College London echelle spectrograph on the 3.9 m Anglo-Australian Telescope (Pettini *et al.* 1990). At this resolution the H I lines are all resolved, as are most of the heavy-element lines, and there is virtually no line blending, at least for  $z \sim 2-3$ . In the case of the bright  $z = 2.14$  QSO Q1101-264 (Hunstead, Pettini & Mar 1994, in preparation) this has brought to light some new and interesting results. With signal-to-noise ratios ranging from  $\simeq 20$  at the longest wave-lengths to  $\simeq 7$  at the UV limit, we can detect Lyman  $\alpha$  lines as weak as  $W_0 = 6-20 \text{ m}\text{\AA}$  at the  $3\sigma$  level: the S/N is substantially higher than that obtained for the same QSO by Carswell *et al.* (1991) with the same instrumental setup but shorter integration time. In the region covered,  $3389-3848 \text{ \AA}$  (with small inter-order gaps), we identify 63 absorption lines as Lyman  $\alpha$  after an exhaustive search for metal-line systems. The two-point correlation function for this sample shows an excess of line splittings near  $\Delta v \simeq 20000 \text{ km s}^{-1}$ , corresponding to a comoving scale  $\sim 115 h^{-1} \text{ Mpc}$  (Einstein-deSitter model,  $H_0 = 100 h \text{ km s}^{-1} \text{ Mpc}^{-1}$ ).

At first sight it seems extraordinary that such a clustering signal has not been seen before, since such large scales are adequately covered even by low-resolution spectra. However, most clustering analyses have been carried out on samples of Lyman  $\alpha$  lines much stronger than those considered here (e.g. Sargent *et al.* 1980; Bi *et al.* 1991), leading us to suspect that the features detected in the two-point correlation function may be due to the *weaker* lines in the Q1101-264 sample. Indeed, when the sample is split at the median equivalent width,  $W_0 = 89 \text{ m}\text{\AA}$ , we find that there is little or no evidence for clustering of the stronger lines, in accord with previous results. The structure in the two-point correlation function seems to arise solely from the weaker lines; this result is illustrated in Fig. 1. It is important to stress that no previous analysis of clustering in the Lyman  $\alpha$  forest has reached such low equivalent widths.

Assessment of the formal significance of the signal in Fig. 1 is no longer straightforward when the line distribution is evidently non-random; standard Poissonian errors will tend to underestimate the true uncertainties. Less-biased error estimates have been investigated, for example the bootstrap resampling technique (Barrow *et al.*

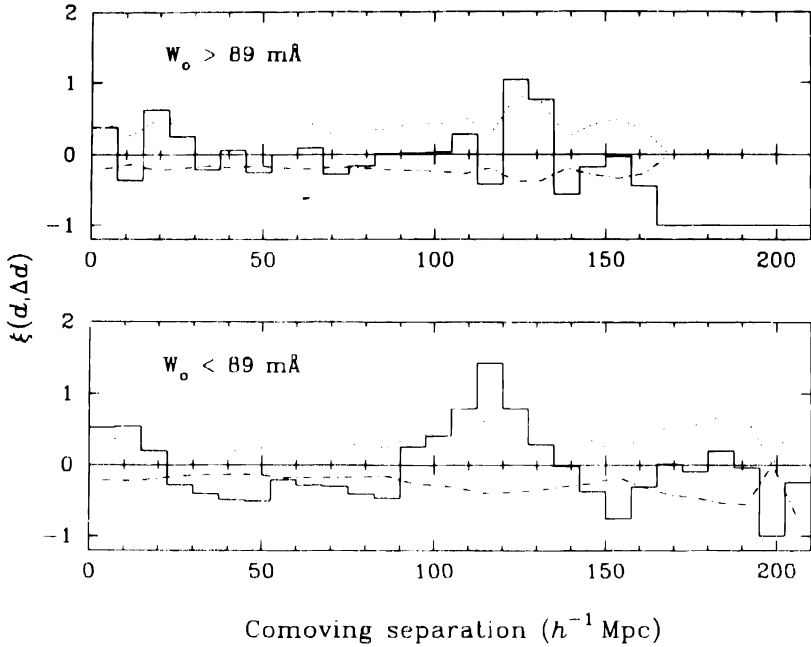


**Figure 1.** Two-point correlation functions, shown as a function of comoving separation, for the two sub-samples of Lyman  $\alpha$  lines in Q 1101–264 obtained by dividing the full sample at the median equivalent width of 89 mÅ. **Upper panel:** Lines with  $W_0 > 89$  mÅ. **Lower panel:** Lines with  $W_0 < 89$  mÅ. Only the weak lines show significant structure in the two-point correlation function. Two  $1\sigma$  error estimates are shown on each plot; the upper, dotted line refers to the best estimate errors, given by a non-Poissonian ensemble formula for  $\xi < 1$ , and bootstrap resampling estimates when  $\xi \geq 1$  (see text); the lower, dot-dash line gives conventional Poisson errors.

1984) and non-Poissonian formulae (Mo, Jing & Börner 1992), and we have also carried out Monte Carlo simulations to test how likely it is that the observed two-point correlation results could have arisen by chance. The excess of points near  $115 h^{-1}$  Mpc and the run of negative points spanning  $30$ – $80 h^{-1}$  Mpc still appear significant with the revised estimates. For the lower panel in Fig. 1 the random trials gave a chance probability of  $< 0.3\%$  for line configurations having  $\xi(r, \Delta r)$  results with  $\chi^2 \geq \chi^2_{\text{observed}}$ .

A further test was to devise a simple 1-dimensional clustering model which mimicked the observed structure, and to investigate its robustness. The outcome was a 3-parameter model with gaussian line clumps superimposed on a uniform background. The best-fitting values (defined to  $\sim 20\%$ ) were a clump separation of  $115 h^{-1}$  Mpc, clump  $\sigma$  of  $10 h^{-1}$  Mpc and a peak overdensity of five times the background. It is interesting to note that the clump size and separation from this simple model correspond well with the typical correlation scales for rich clusters and superclusters, respectively (Bahcall 1988), while the overdensity is directly comparable with that of present-day galaxies in superclusters.

However, it is not clear whether the non-uniform redshift distribution of the weak Lyman  $\alpha$  lines in Q 1101–264 represents a characteristic clustering length or

simply reflects non-uniformities in the metagalactic ionising flux on large scales. Since these low- $N$  Lyman  $\alpha$  clouds are expected to be easily destroyed, it is most likely that they trace the deepest voids in the galaxy distribution where the ionising flux is lowest.

Despite the low chance probability noted above, these results must still be considered tentative (a) because of the small sample of lines, and (b) because the large scale structure implied by Fig. 1 spans more than half the wavelength range covered in the AAT spectrum. On the other hand there is mounting evidence that weak Lyman  $\alpha$  lines evolve more slowly than the strong lines considered in earlier studies, creating a consistent (but not necessarily correct) picture in which weak Lyman  $\alpha$  lines are the unexpected tracers of large-scale structure at early epochs. Confirmation of this picture requires the detection of similar clustering in other QSO sightlines.

### 3. Heavy element abundances in the damped Lyman $\alpha$ systems

While direct searches for high-redshift galaxies have been singularly unproductive, we routinely detect 'galaxies' (or at least gas which we suspect to reside in galaxies) out to  $z > 4$  via the metal absorption lines they produce in the spectra of background QSOs. A subset of the metal systems, the damped Lyman  $\alpha$  systems (Wolfe 1990), are receiving increasing attention because, although rare, they account for most of the neutral hydrogen seen at high redshifts, a total mass density comparable with stars in present day galaxies. This similarity has led to the suggestion that the damped Lyman  $\alpha$  systems may be the high- $z$  counterparts of present day galaxies like our own, observed prior to the bulk of star formation, at a time when the gas fraction was high and gravitational contraction was still underway.

Since 1987 we have been conducting a survey aimed at measuring the metallicities, dust content and star-formation rates in the galaxies responsible for the damped Lyman  $\alpha$  systems (Pettini *et al.* 1994). The strategy we have adopted for measuring the degree of metal enrichment is to target the resonance lines of the singly-ionised trace elements Zn and Cr. In Galactic and Magellanic Cloud stars both Zn and Cr track Fe over a wide range of metallicities. However, in the local interstellar medium Zn, unlike other iron-peak elements, is not readily incorporated into dust grains and remains in the gas phase at close to solar abundance (within a factor 2-3) even in the densest clouds. On the other hand, Cr is amongst the most heavily depleted elements, with typically only  $\sim 1\%$  remaining in the gas phase. Both elements are predominantly singly-ionised in H I regions and the total column density of neutral hydrogen can be determined accurately by profile fitting to the damping wings of Lyman  $\alpha$ . The column density ratio  $N(\text{Zn}^+)/N(\text{H I})$  then measures directly the overall level of metal enrichment of the damped Lyman  $\alpha$  galaxies, while  $N(\text{Cr}^+)/N(\text{Zn}^+)$  gives a measure of the depletion of refractory elements onto dust. Finally, in the black cores of the damped Lyman  $\alpha$  lines the light from the QSO is completely extinguished, allowing the possibility of detecting Lyman  $\alpha$  emission from H II regions in the intervening galaxy and thereby inferring a star-formation rate.

At the redshifts of most known damped systems ( $z \sim 1.7-3.5$ ), Zn II  $\lambda\lambda 2025, 2062$  and Cr II  $\lambda\lambda 2055, 2061, 2065$  are shifted into a convenient spectral region where

detector sensitivity is high. Moreover, the absorption lines are expected to be weak, even at large  $N(\text{H I})$ , so line saturation is unlikely to be a problem, as it is for the resonance lines of the more abundant elements. For this reason reliable column densities can be derived directly from measured equivalent widths.

In our survey of 15 damped Lyman  $\alpha$  systems, we have used the 3.9 m Anglo-Australian Telescope, the 4.2 m William Herschel Telescope and the 5 m Hale telescope at resolutions of 0.8–1.4  $\text{\AA}$  FWHM and exposure times ranging from 16 000–40 000 s. Details of the observations and data reduction are given by Pettini *et al.* (1994). Fig. 2 presents a montage of the damped Lyman  $\alpha$  line and Zn II and Cr II lines in the  $z_{\text{abs}} = 1.7764$  system towards the QSO 1331 + 170. This illustrates the quality of the spectroscopic data and, in particular, the high signal-to-noise ratio needed to detect the Zn and Cr lines.

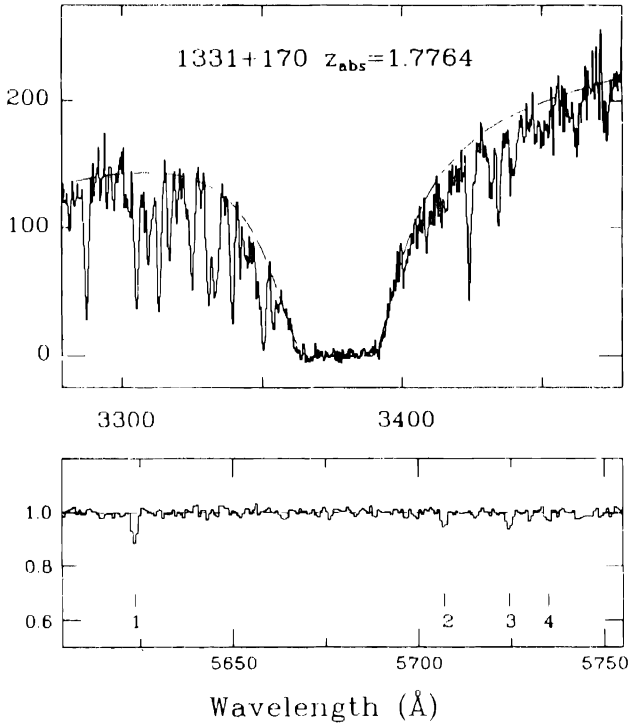


**Figure 2.** Spectra of the Lyman  $\alpha$  and Zn/Cr regions in the  $z_{\text{abs}} = 1.7764$  damped Lyman  $\alpha$  system in 1331 + 170. **Upper panel:** Damped Lyman  $\alpha$  line showing the adopted profile fit (dashed line) and the many narrow absorption lines, mostly due to the Lyman  $\alpha$  forest. The ordinate scale is in photon counts. **Lower panel:** Region encompassing the Zn II and Cr II absorption lines at the redshift of the damped Lyman  $\alpha$  system. Vertical ticks mark the expected positions of the lines. Line 1: Zn II  $\lambda 2025.484$ ; line 2: Cr II  $\lambda 2055.596$ ; line 3: Cr II  $\lambda 2061.575$  + Zn II  $\lambda 2062.003$  (blended) and line 4: Cr II  $\lambda 2065.501$ . The QSO spectrum has been normalised to the underlying continuum; note the expanded vertical scale. The derived abundance of zinc in the  $z_{\text{abs}} = 1.7764$  system is 24 times below solar; chromium is 170 times below solar.

The principal findings of this survey are as follows:

- (1) At  $z \sim 2-3$ , damped Lyman  $\alpha$  galaxies are generally metal-poor, with a medium metallicity of 1/10 solar, implying that the process of metal enrichment through stellar nucleosynthesis had not proceeded far in most galaxies by  $z \approx 2$ .
- (2) At a given redshift, there is a considerable spread in the degree of metal enrichment amongst the different damped Lyman  $\alpha$  galaxies; the range may extend over at least two orders of magnitude, suggesting that the damped Lyman  $\alpha$  absorption systems may arise in sightlines through galaxies of widely differing masses and evolution rates.
- (3) Cr is consistently less abundant than Zn by factors ranging from 3.5 to  $> 13$ ; this is unlikely to be a departure from solar relative abundances, and is taken as evidence for dust in the damped Lyman  $\alpha$  systems. However, there is substantially less dust in these distant galaxies at  $z \approx 2$  than found in the Galactic interstellar medium today.
- (4) The majority of damped Lyman  $\alpha$  absorbers shows no spectroscopic evidence for Lyman  $\alpha$  emission in the black core of the damped line; the interpretation of this result has been either in terms of dust extinction of Lyman  $\alpha$  (Charlot & Fall 1993) or a low duty cycle for massive star formation (Valls-Gabaud 1993).

#### 4. Future work

The new results presented here are the outcome of substantial allocations of observing time on 4-m class telescopes. They were difficult observations, stretching the instrumentation to the limit and requiring the support of time assignment committees over several observing seasons. With the forthcoming generations of 8-10 m telescopes, it will be possible to obtain data of similar quality in shorter time allocations. However, observers are urged to use the much greater light-gathering power to improve S/N ratios as well as extending such studies to more difficult regions of observational parameter space, such as higher redshift and higher spectral resolution.

One aspect of QSO absorption line studies which will benefit from increased collecting area will be the determination of the lateral sizes of absorbing regions using the multiple images from gravitationally lensed QSOs. At present the fainter lensed images cannot be observed at the high spectral resolution necessary to overcome line blending and extend the investigation to weaker lines. An alternative approach which holds promise is to use the extended Lyman  $\alpha$  emission from high- $z$  radio galaxies as a background probe for investigating the transverse sizes of Lyman  $\alpha$  absorbers. In this case, the weakness of the continuum emission means that the inverse (or proximity) effect can be safely ignored (Murdoch *et al.* 1986; Bajtlik *et al.* 1988) and absorption can be probed over the entire Lyman  $\alpha$  emission profile.

#### Acknowledgements

We thank Linda Smith and David King for permission to include the main results of our damped Lyman  $\alpha$  study. R. W. H. would like to thank the Local Organising Committee for making the meeting so enjoyable and fruitful, and the Indian transportation system for a 5 $\sigma$  experience. R. W. H. also acknowledges financial assistance for the observational program from the Australian Research Council.

## References

- Bahcall, N. A. 1988, *Ann. Rev. Astr. Astrophys.*, **26**, 631.
- Bajtlik, S., Duncan, R. C., Ostriker, J. P. 1988, *Astrophys. J.*, **327**, 570.
- Barrow, J. D., Bhavsar, S. P., Sonoda, D. H. 1984, *Mon. Not. R. astr. Soc.*, **210**, 19 p.
- Bechtold, J., Schectman, S. A. 1989, in *Active Galactic Nuclei*, Eds. D. E. Osterbrock & J. S. Miller (Dordrecht: Kluwer) p. 549.
- Bi, H. G., Börner, G., Chu, Y. 1991, *Astr. Astrophys.*, **247**, 276.
- Blandford, R. D., Narayan, R. 1992, *Ann. Rev. Astr. Astrophys.*, **30**, 311.
- Carswell, R. F., Lanzetta, K. M., Parnell, H. C., Webb, J. K. 1991, *Astrophys. J.*, **371**, 36.
- Charlot, S., Fall, S. M. 1993, *Astrophys. J.*, **415**, 580.
- Dobrzycki, A., Bechtold, J. 1991, *Astrophys. J.*, **377**, L69.
- Francis, P. J., Hewett, P. C. 1993, *Astr. J.*, **105**, 1633.
- Mo, H. J., Jing, Y. P., Börner, G. 1992, *Astrophys. J.*, **392**, 452.
- Mo, H. J., Xia, X. Y., Deng, Z. G., Börner, G., Fang, L. Z. 1992, *Astr. Astrophys.*, **256**, L23.
- Murdoch, H. S., Hunstead, R. W., Pettini, M., Blades, J. C. 1986, *Astrophys. J.*, **309**, 19.
- Perry, J. J., Watson, A. M., Kronberg, P. P. 1993, *Astrophys. J.*, **406**, 407.
- Pettini, M., Hunstead, R. W., Smith, L. J., Mar, D. P. 1990, *Mon. Not. R. astr. Soc.*, **246**, 545.
- Pettini, M., Smith, L. J., Hunstead, R. W., King, D. L. 1994, *Astrophys. J.*, in press.
- Rickett, B. J. 1986, *Astrophys. J.*, **307**, 564.
- Sargent, W. L. W., Young, P. J., Boksenberg, A., Tytler, D. 1980, *Astrophys. J.*, **42**, 41.
- Valls-Gabaud, D. 1993, *Astrophys. J.*, **419**, 7.
- Wolfe, A. M. 1990, in *The Interstellar Medium in Galaxies*, Eds. H. A. Thronson & J. M. Shull. (Dordrecht: Kluwer) p. 387.

## Radio Observations of the Anisotropy in the Cosmic Microwave Background

Ravi Subrahmanyan *NCRA, Tata Institute of Fundamental Research, Poona University Campus, Post Bag 3, Ganeshkhind, Pune 411 007, India.*

**Abstract.** Angular anisotropy in the sky temperature of the relict cosmic microwave background (CMB) is commonly believed to originate in the coupling of density perturbations and inhomogeneities in matter to the radiation. Observations of the spectrum of temperature anisotropy constitutes a probe of structure formation in the universe and of astrophysical processes in galaxy formation. The experimental techniques commonly used to measure the CMB anisotropy, their relationship to the sky fluctuation spectrum and the current status of the measurements are reviewed.

**Key words:** Methods: observational—galaxies: formation—cosmic microwave background—cosmology: observations.

### 1. Introduction

The standard hot big bang cosmology is generally accepted as the best model we have today for the thermal history of the universe. Within this framework, the radiation is expected to be in thermodynamic equilibrium with the baryonic matter in the early universe. As the thermodynamic temperature of the expanding universe dropped past a value of about 3000 K, recombination of the primeval baryonic plasma would result in a decoupling of the radiation from the predominantly neutral baryonic matter. Subsequently, the relict photons would free-stream essentially unscattered by the residual electrons. In this model, the recombination epoch represents the last scattering surface for the relict photons: the quasi-static ionization equilibrium during the universal expansion results in this surface located at about  $z = 10^3$  having a width of  $\Delta z = 10^2$  in redshift space. When we observe the cosmic microwave background, we see the universe at the recombination epoch.

Structure formation in the universe is generally believed to be the gravitational growth of primordial density perturbations. The coupling of these perturbations to the radiation field – due to fluctuations in the gravitational potential (Sachs-Wolfe effect), due to the adiabatic nature of the fluctuations and due to Doppler velocities in the scattering particles – cause *primary anisotropies* in the CMB. These primary anisotropies are imprinted at the recombination epoch.

Standard recombination theory predicts the last scattering surface to be located at redshift  $z_r \approx 1100$ . The horizon scale at  $z_r$  subtends an angle of about  $1^\circ$  on the sky. Models for structure formation that adopt the initial density fluctuation spectrum to have a power-law form  $P(k) \sim k^n$ , with  $n = 1$ , predict an angular anisotropy in the CMB  $\Delta T/T$  that peaks at about  $1^\circ$ . Observations of  $\Delta T/T$  anisotropy on angular scales  $\gtrsim 1^\circ$  will probe the primordial density perturbation spectrum on scales  $\gtrsim 100$  Mpc



and primarily through the Sachs-Wolfe effect. Observations on angular scales  $\lesssim 1$  arcmin will probe  $\Delta\rho/\rho$  on scales  $\lesssim 1$  Mpc. The finite depth of the last scattering surface essentially erases primary CMB anisotropies on angular scales  $\lesssim 8$  arcmin.

Dissipative collapse during galaxy formation is expected to release energy that most likely reionized the intergalactic baryons and renewed the coupling between the baryonic matter and relict radiation. At the epoch of galaxy formation, processes like the inverse-Compton scattering off hot gas in gravitational potential wells and the Doppler scattering off bulk flows due to these potentials result in *secondary anisotropies* in the CMB. However, reionization at redshifts  $z \gtrsim 10$  can shift the last scattering surface to more recent epochs and consequently primary anisotropies upto the horizon scale at the new last scattering surface may be erased upto angular scales of  $5^\circ$ .

CMB anisotropies are inevitable in a causal universe where structure forms by the growth of seed fluctuations. Observations of CMB anisotropy, therefore, are a probe of (a) the initial density perturbation spectrum  $\Delta\rho/\rho$  at the recombination epoch  $z_r$  and (b) the subsequent dynamical and astrophysical evolution of the universe.

## 2. Characterization of CMB anisotropy

The distribution of the CMB temperature fluctuations over the celestial sphere,  $\Delta T(p) = T(p) - \langle T(p) \rangle$ , can be decomposed in a spherical harmonic expansion:

$$\frac{\Delta T(p)}{\langle T \rangle} = \sum_{lm} a_{lm} Y_{lm}(p), \quad (1)$$

$p$  denotes a unit vector to the celestial sphere,  $Y_{lm}$  are the spherical harmonic functions and  $a_{lm}$  are the coefficients. The basis functions for this decomposition consist of the dipole ( $l = 1$ ), quadrupole ( $l = 2$ ) and higher order multipoles;  $l$  denotes the multipole order. The coefficients  $a_{lm}$  are a measure of the power in the different harmonics and constitute a discrete power spectrum of the sky distribution.

The angular autocorrelation function (ACF) of the CMB sky temperature fluctuations may be computed:

$$C(\phi) = \frac{\langle \Delta T(p) \times \Delta T(p+r) \rangle}{\langle T(p) \rangle^2}, \quad (2)$$

where  $r$  is a vector on the celestial sphere and  $|r| = \phi$ . The ACF is defined over a finite range 0 to  $\pi$  radians. Equivalently, the sky fluctuations may be described by a power spectrum  $P(Q)$  which is the radial Fourier transform of the ACF  $C(\phi)$ :

$$P(Q) = 2\pi \int_0^2 \omega C(\omega) J_0(Q\omega) d\omega, \quad (3)$$

where  $\omega = 2 \sin(\phi/2)$ . When characterizing the anisotropy on small angular scales on small sky patches, where the ACF  $C(\phi)$  may be assumed to rapidly approach zero for large angles, the transform may be written as an infinite integral:

$$P(q) = 2\pi \int_0^\infty \phi C(\phi) J_0(2\pi\phi q) d\phi. \quad (4)$$

Here  $q$  represents the wavenumber (in  $\text{Mpc}^{-1}$ ) and  $\alpha = 2c/(\Omega_0 H_0)$ . The spectrum  $P(q)$  decomposes the power over wavenumbers  $q$  which is related to the multipole order by  $l = 2\pi\alpha q$  for large orders.

### 3. Characterization of the observing technique

The CMB sky fluctuations are generally presumed to have a Gaussian distribution in temperature and characterizable by a power spectrum. All the radio observations together aim to measure the power spectrum.

An observation consists of an experiment done with a particular telescope configuration and involves a specific observing and data reduction procedure. This complete observation may be characterized by an effective telescope filter function (TFF). The observation views the CMB sky through this filter several times and obtains a number of estimates for the CMB temperature. All these values together lead to an estimate for the CMB variance, as viewed through the TFF specific to the observation.

Different observational configurations are characterizable by different TFFs and these selectively detect CMB power  $P(Q)$  in different regimes of  $Q$ -space. Collectively, the CMB power spectrum is measured by a bank of filters whose characteristics (band shapes) are dissimilar. Any specific model for the CMB spectrum may be tested by computing the expected response for each experimental TFF and comparing with the measurements of sky variances. However, independent of models for  $P(Q)$ , the observations may all be combined to place limits on the coefficients of the spherical harmonics or any alternate decomposition. Effectively, this would be making the filterbank uniform in characteristics.

#### 3.1 Single-dish radio observations

When the sky is viewed with a telescope beam, the sky fluctuations are effectively smoothed by the beam profile. Assuming the beam to have a Gaussian form and with dispersion  $\phi_0$ , fluctuations with small angular scales with multipole order  $l \gtrsim (1/\phi_0)$  are erased and the TFF has the form

$$F(l) \sim \exp(-l^2 \phi_0^2). \quad (5)$$

The TFF is a low-pass filter in  $l$ -space.

To avoid errors due to instrumental gain instabilities, the telescope beams are normally position-switched rapidly on the sky and difference measurements are made. Single beam-switching between two positions separated by an angle  $\phi_s$  will be insensitive to sky fluctuations on angular scales well-exceeding  $\phi_s$  and consequently such an observing strategy would effectively have no response to multipoles on small orders  $l \lesssim (1/\phi_s)$ . The TFF for the single beam-switching difference measurements will be

$$F(l) \sim \exp(-l^2 \phi_0^2) \times [1 - J_0(l\phi_s)]. \quad (6)$$

The TFF is a band-pass filter in  $l$ -space. The upper cutoff is determined by the beam dispersion  $\phi_0$  and the lower cutoff is determined by the switching angle  $\phi_s$ .

Double beam-switching is sometimes adopted to cancel gradients in atmospheric emission. This is a combination of two single-switched difference measurements. The beam switching in the two single-switched cases are done between a common field ( $ON$ ) and reference fields located on opposite sides ( $OFF1$  and  $OFF2$ ). The single differences ( $ON - OFF1$ ) and ( $ON - OFF2$ ) are averaged to obtain ( $ON - OFF1/2 - OFF2/2$ ). The double switching measurement has additional sensitivity on angular scales corresponding to twice the switching angle:  $2\phi_s$ . The TFF is proportional to

$$F(l) \sim \exp(-l^2 \phi_0^2) \times \left[ \frac{3}{2} - 2J_0(l\phi_s) + \frac{1}{2}J_{\text{circ}}(2l\phi_s) \right] \quad (7)$$

Several beam-switching experiments adopt the basic single beam-switching technique between field-pairs with fixed separation, but select the sky fields so that the difference between any arbitrary pair can be computed as a linear combination of the single beam-switched measurements. The measurements can then be analysed to obtain estimates of CMB fluctuations on scales up to the maximum field separation ( $\phi_m$ ). Different linear combinations will give estimates of CMB variance as viewed through different TFFs, and the TFFs can have peak sensitivities in the  $l$ -space range from  $(1/\phi_m)$  to  $(1/\phi_0)$ . The experiment, as a whole, will be a simultaneous measurement of CMB power over this broad range.

### 3.2 Fourier synthesis techniques

Interferometric radio observing techniques have also been adopted in attempts to *image* CMB anisotropy. As compared to observations with single-dish techniques, interferometers are insensitive to uniform atmospheric and other sky background emissions. The interferometric fringes provide rejection to spurious signals like groundspillover and man-made radio interference. Sky fluctuations due to discrete radio sources can also be subtracted in the imaging observations. Multiple interferometer baselines simultaneously provide measurements of CMB fluctuations on a range of angular scales. Fourier synthesis observations are characterized by a primary beam (the antenna pattern of a single interferometer element) and a synthetic beam (which determines the resolution of the synthesized image). The synthesized image may be thought of as obtained by firstly multiplying the true sky by the primary beam, then convolving this product by the synthetic beam.

The TFF corresponding to any image produced by Fourier synthesis is then dependent on position in the image. At any position, the TFF is the radial transform of the product beam ( $B_{sp}$ ) at that position – the product beam at a position is the product of the synthetic beam centred at that position with the primary beam centered on the field centre. Since the beams (especially the synthetic beam) generally do not have circular symmetry, one takes a circumferential average of the 2-D Fourier transform:

$$F(q) = \int \int B_{sp}(\theta, \phi) J_0(2\pi xqr) d\theta d\phi, \quad (8)$$

where  $r = \sqrt{\phi^2 + \theta^2}$ .

#### 4. Observations of CMB anisotropy

Observations may be classified on the basis of the angular scale at which they attempt to detect CMB anisotropy. On large angular scales exceeding several degrees, the observations probe  $l \lesssim 10$ . Both the MIT and COBE experiments have detected anisotropy on these scales. The TENERIFE experiment probes  $15 \lesssim l \lesssim 30$ . On intermediate angular scales of order 1 degree, corresponding to  $l \sim 10^2$  there is possible detection of CMB fluctuations by the UCSB group at the south pole. On small angular scales  $\lesssim 1$  arcmin, experiments probe  $l \gtrsim 10^3$ . On these scales there are no detections to date, with lower limits to fluctuations being set by the OVRO, ATCA and VLA observations.

##### 4.1 Large scale anisotropy

The MIT group (Meyer *et al.* 1991) made an image of one-third of the sky with a resolution of  $3.8^\circ$  FWHM at a frequency of 168 GHz. The observations were made during a 10 hr balloon flight using a bolometer scanning the sky by pointing at a zenith angle of  $44^\circ$  and rotating at 1.5 rpm. The map was initially calibrated using an internal temperature reference, however, accurate calibration of the fluctuations was possible post-imaging by assuming the detected CMB dipole amplitude to be 3.3 mK. The observations detected significant fluctuations above the instrument noise on coherence scales 3–22 degrees with the excess CMB-sky rms estimated to be  $30\text{--}80\ \mu\text{K}$ .

The COBE-DMR experiment (Smoot *et al.* 1992) produced all-sky maps at 31.5, 53 and 90 GHz with beams of  $7^\circ$  FWHM. The satellite-borne differential radiometers actually differenced sky regions  $60^\circ$  apart. However, over a 6 month period, the difference measurements enabled any arbitrary sky direction to be related to any other region and these were collectively analysed to produce all-sky maps. The dipole amplitude was determined to be  $3.36 \pm 0.1\ \text{mK}$  and the quadrupole term  $Q_{\text{rms}}$  was estimated to be  $13 \pm 4\ \mu\text{K}$ . Subtracting the dipole and smoothing the images to a resolution of  $10^\circ$ , the residual CMB fluctuations were estimated to have an rms of  $30 \pm 5\ \mu\text{K}$ .

The MIT 168 GHz and COBE-DMR images have been shown to be strongly correlated (Ganga *et al.* 1993) suggesting that the two independent experiments have detected the same sky structures. More importantly, the correlation between the images at the widely separated frequencies confirms the thermal nature of the sky fluctuations.

The TENERIFE observations (Watson *et al.* 1993) scanned a sky strip at 14.9 GHz with a double switched beam. The beam had a  $5.6^\circ$  FWHM and the throw angle was  $8^\circ.1$ . No CMB fluctuations are reported detected, with the rms CMB fluctuations on a coherence scale of  $4^\circ$  determined to be less than  $49\ \mu\text{K}$  with 95 per cent confidence.

##### 4.2 Intermediate scale CMB anisotropy

The best results to date on degree scale CMB fluctuations have come from the UCSB group observing from the south pole. The observations generally cover a linear sequence of  $N$  equi-spaced fields on the sky and  $(N - 1)$  difference measurements are made between all pairs of adjacent fields by sinusoidal single beam switching.

The experiment at about 30 GHz (Schuster *et al.* 1993) made 13 difference measurements in each of four frequency bands over the range 25 to 35 GHz. The beam had a  $1.5^\circ$  HPBW and throw 3 $^\circ$ . The difference measurements were made with an instrument rms noise as low as  $13.5 \mu\text{K}$  and detected an excess rms of  $24 \mu\text{K}$  at a coherence scale of  $1.5^\circ$ .

At the higher frequency of 91 GHz (Meinhold & Lubin 1991), 9 difference measurements were obtained on a sequence of adjacent fields with a beam of 30 arcmin HPBW and  $1.4^\circ$  throw. No significant excess variance was detected above the instrument rms noise of  $60 \mu\text{K}$  and a 95 per cent confidence upper limit of  $96 \mu\text{K}$  was placed on the rms of CMB fluctuations with 20–30 arcmin coherence scales.

### 4.3 Small scale anisotropy

No CMB anisotropy has been detected to date on these scales. The OVRO double beam switching observations of fields close to the north celestial pole (Readhead *et al.* 1990) were made at a frequency of 20 GHz and with a beam  $1.8^\circ$  HPBW and throw  $7.15^\circ$  arcmin. The difference measurements had an instrument rms noise of  $30 \mu\text{K}$  and placed an upper limit of  $58 \mu\text{K}$  on CMB fluctuations with  $2.6^\circ$  arcmin coherence scale.

Fourier synthesis observations with the VLA (Formalont *et al.* 1992) of a field at 8.44 GHz produced a  $7^\circ$  arcmin size image of a sky patch with a resolution of  $80^\circ$  arcsec. Discrete sources were detected by making a high resolution ( $10^\circ$  arcsec) image of the field and subtracted. The low-resolution image shows excess (above that expected from instrument noise) variance that falls off away from the primary-beam pointing centre as would be expected if the variance originates in the sky. An extrapolation of the  $\log N - \log S$  source counts to levels below the flux limit to which discrete sources were detected and subtracted suggested that the excess variance is due to fainter sources that have not been subtracted. Therefore, the observations were used to place an upper limit of  $50 \mu\text{K}$  on the rms of CMB fluctuations in imaging with  $80^\circ$  arcsec resolution.

The most sensitive observations of arcmin scale CMB structure have been made by the Australia Telescope (ATCA; Subrahmanyan *et al.* 1993). The five 22-m diameter antennas were configured in an ultra compact 122-m array to maximize the brightness sensitivity. The antennas were placed in an equi-spaced linear configuration and only baselines between adjacent antennas were used to make the high brightness sensitive image of the field. An image of an  $8^\circ$  arcmin field with  $2^\circ$  arcmin resolution at 8.7 GHz was made with a brightness sensitivity of  $36 \mu\text{K}$ . The image was expected to be confusion limited (due to discrete radio sources in the sky) with the confusion rms noise estimated to be  $70\text{--}160 \mu\text{K}$ . Data obtained on longer baselines between the antennas in the array were used to derive a model for the confusion and this was subtracted. The resulting image is shown in Fig. 1 and places an upper limit of  $25 \mu\text{K}$  on CMB fluctuations in sky patches imaged with  $2^\circ$  arcmin resolution.

## 5. Implications

The COBE detection of CMB fluctuations may be used to normalize the amplitude of density fluctuations at the recombination epoch. With this normalization, the standard  $\Lambda$ CDM model requires a biasing factor  $b \approx 0.9$  to match the observed present-day

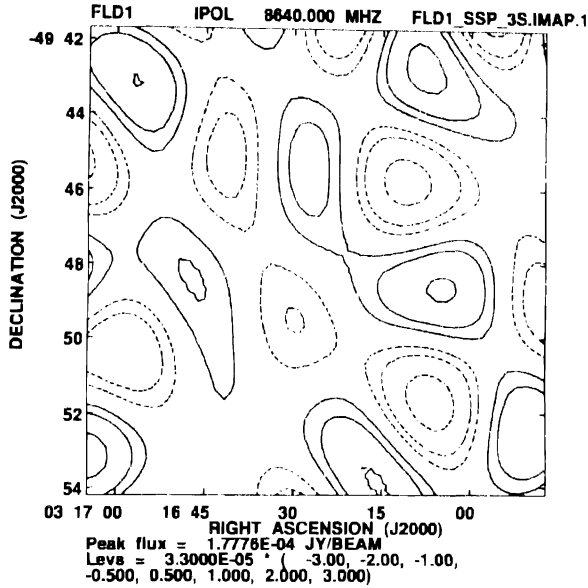


**Figure 1.** Image of a sky patch made with the Australia Telescope. Discrete source confusion has been modelled and subtracted before synthesizing the image. Contours are in units of  $\mu\text{Jy beam}^{-1}$ .  $1\text{-}\sigma$  rms noise of  $33 \mu\text{Jy beam}^{-1}$  corresponds approximately to  $36 \mu\text{K}$  in sky brightness temperature.

galaxy distribution. The COBE detection also constrains the index of a power-law form initial density perturbation spectrum  $P(k) \sim k^n$  to be  $n = 1 \pm 0.6$ .

Extrapolation of the  $n = 1$  spectrum with COBE normalization to smaller scales leads to an expectation for the CMB fluctuation on  $1'$  scale that appears to be in conflict with the UCSB south pole results (Gorski *et al.* 1993). This may be interpreted as implying a  $n < 1$  density perturbation spectrum. Alternately, CMB anisotropy on small scales up to degree scales might be attenuated as a result of early reionization post recombination. However, this would be expected to result in enhanced CMB fluctuations on arcmin scales as a result of the generation of secondary anisotropies. The isocurvature/baryon dark matter (BDM) models for galaxy formation predict enhanced fluctuations on arcmin scales and the ATCA results appear to rule out the standard BDM (Hu *et al.* 1993).

With the large angular scale anisotropy level presumably measured by COBE, and with measurements on degree scales possibly close to becoming confirmed detections, improved effort towards detecting arcmin-scale anisotropy is needed to give the complete spectrum of CMB anisotropy. The Australia Telescope Compact Array, with the new upgrade to its receivers, seems best suited to achieve this end.

## References

- Formalont, E. B., Partridge, R. B., Lowenthal, J. D., Windhorst, R. A. 1992, *Astrophys. J.*, **404**, 8  
 Ganga, K., Cheng, E., Meyer, S., Page, L. 1993, *Astrophys. J.*, **410**, L57.  
 Gorski, K. M., Stompor, R., Juszkievicz, R. 1993, *Astrophys. J.*, **410**, L1.

- Hu, W., Scott, D., Silk, J. 1993, *Phys. Rev. D*, submitted.
- Meinhold, P., Lubin, P. 1991, *Astrophys. J.*, **370**, L11.
- Meyer, S. S., Cheng, E. S., Page, L. A. 1991, *Astrophys. J.*, **371**, L7.
- Readhead, A. C. S. *et al.* 1989, *Astrophys. J.*, **346**, 566.
- Schuster, J. *et al.* 1993, *Astrophys. J.*, **412**, L47.
- Smoot, G. F. *et al.* 1992, *Astrophys. J.*, **396**, L1.
- Subrahmanyan, R., Ekers, R. D., Sinclair, M., Silk, J. 1993, *Mon. Not. R. astr. Soc.*, **263**, 416.
- Watson, R. A. *et al.* 1993, *Nature*, **357**, 660.

## Faint Blue Galaxies and Gravitational Lensing by Clusters of Galaxies

Puragra Guhathakurta<sup>1</sup> *Princeton University Observatory, Peyton Hall, Princeton, NJ 08544-1001, USA.*

**Abstract.** This talk is divided into two parts: the first part discusses the nature of faint blue field galaxies, while the second describes an ongoing project to study the effects of gravitational lens distortion of the faint blue galaxies by rich galaxy clusters in the foreground, and thereby investigate the distribution of (mostly dark) matter in these clusters.

Faint field galaxy counts and their redshift distribution suggest a specific form for the evolution of the overall galaxy luminosity function, one where the faint end was steeper in the past than it is today. Recent studies have shown these faint galaxies to be weakly clustered. A few different scenarios for galaxy evolution are examined in the light of these observational facts. Extensive merging at moderate redshifts (less than unity) appears to be disfavored. The counts may be dominated by a new population of blue galaxies that are mostly invisible at the present epoch.

Clusters of galaxies are a class of massive objects—a substantial number of which have been identified at  $z \lesssim 1$ . Studying the most massive and compact of these objects, especially those at moderate to high redshifts, can provide important constraints on theories for the formation of large scale structure. Gravitational lensing by rich clusters can be useful probes of the amount of matter they contain. Light rays passing near the dense cluster core are deflected resulting in distorted images of background galaxies, the most extreme examples of these being giant luminous arcs. In this paper, I describe an ongoing project to measure (in a statistical sense) the distortion caused by lensing and thereby determine cluster masses.

*Key words:* Gravitational lensing—clusters of galaxies—cosmology.

### 1. Faint blue galaxies

Deep photographs, and more recently CCD images, of the sky have shown that there is a high surface density of faint blue galaxies (FBGs) all over the sky (Kron 1980; Tyson 1988). The properties of FBGs may provide useful insight into the evolutionary history of galaxies like our own. Over the last five years, much observational data have been gathered but the intrinsic nature of these galaxies remains something of an enigma. These new data include:

<sup>1</sup> Hubble Fellow.



- Ultra-deep counts in the optical *BVR*I bands to  $B > 26$  (Tyson 1988; Guhathakurta *et al.* 1990; Lilly *et al.* 1991) and in the near-ultraviolet (Guhathakurta 1991).
- An extension of the count data into the  $2.2\ \mu\text{m}$  *K*-band (Lilly *et al.* 1991).
- Spectroscopic redshift surveys that probe the bright end of the FBG distribution (with limiting magnitudes in the range  $B = 22\text{--}24$ ) (Broadhurst *et al.* 1988; Colless *et al.* 1990; Lilly *et al.* 1991). -
- Studies of the galaxy-galaxy angular correlation function  $w(\theta)$  on arcminute scales (Efsthathiou *et al.* 1991).

The observed galaxy surface density, particularly that at shorter wavelengths (*UBV*) appears to be significantly in excess of the no-evolution prediction. The *B* counts show an excess of about a factor of five, although the exact amount depends on how the model prediction is normalized (and on the cosmological model, of course). This is generally thought to be a sign of evolution, in the sense that galaxies were brighter in the past (cf. Koo 1986). The recent redshift surveys, however, show the FBGs to be at quite modest redshifts, with  $N(z)$  peaking at  $z = 0.3$  even for limiting magnitudes as faint as  $B = 23\text{--}24$ . This led Broadhurst *et al.* (1988) to conclude that the *shape* of the galaxy luminosity function (LF) at high  $z$  is different from that at  $z = 0$ , with the faint end being more prominent in the past. While it has been argued that the increased prominence of intrinsically faint galaxies may be purely due to their being bluer and consequently having smaller *K*-corrections than the bright early-type galaxies (all within the context of the standard evolutionary scenario) (Koo & Kron 1992), it is more likely that  $N(m)$  and  $N(z)$  can only be explained simultaneously if there is a real change in the shape of the LF. Colless (private communication) has stressed that the standard model predicts  $z > 1$  for the bluest galaxies with  $B \sim 23$  but even these are observed to be at much lower redshifts.

Further, in order to push the predicted  $N(z)$  towards lower  $z$ , the standard model requires a low density universe ( $\Omega \sim 0.2$ ). This is in apparent contradiction with the low density of galaxies on *K*-band images, the latter being consistent with an Einstein-deSitter cosmology (Lilly *et al.* 1991). The interpretation of the *K* counts, however, is not easy. The redshifts probed by the *K* data are not very high (similar to the *B* data) so that the  $2.2\ \mu\text{m}$  *K* band in effect samples the near-IR portion of the FBG spectra in their rest frame. Unfortunately, very little is known about the local galaxy LF at these wavelengths so that even a no-evolution model is difficult to construct.

Several authors have considered alternatives to the standard evolutionary model. In one of these scenarios, present-day bright galaxies are formed by the merging of several smaller objects in the past, so that LF is heavily weighted towards the faint end at earlier epochs (Broadhurst *et al.* 1992). It should be noted that even in this scenario it is necessary for the *specific* luminosity of galaxies to have been higher in the past—mergers with conserved luminosity would lead to a galaxy count slope of 0.4 and this is shallower than that observed in the *B* band (0.45). However, galaxies that are about to merge are expected to be strongly clustered. This is exactly the opposite of what is observed for FBGs in the range  $B = 24\text{--}26$  (Efsthathiou *et al.* 1991).

In fact, the observed amplitude of  $w(\theta)$  is significantly lower than that expected for  $L^*$  galaxies in an Einstein-deSitter universe. Could this imply that we live in a low density (or cosmological constant-dominated) universe or that the intrinsic clustering of galaxies evolves more rapidly than the stable clustering case (Melott 1992)? As mentioned earlier, the low density cosmological model appears to be in conflict with the *K*-band counts.

Further, in either case, the  $w(\theta)$  amplitude would be suppressed achromatically – i.e. for galaxies selected in any bandpass. This is not observed to be the case. The amplitude of the angular correlation function decreases towards shorter wavelengths in going from the  $I$ - to the  $U$ -band. This is unlikely to be due to differences in the amount of projection in the  $U$ -,  $B$ -,  $R$ -, and  $I$ -selected samples since all of these appear to lie in approximately the same redshift range ( $z \approx 0.5$ –1).

Thus, one is led towards the conclusion that the steepening of the faint end of the LF at high  $z$  (implied by the  $B$  counts and the redshift distribution) is caused by a new population of galaxies – i.e. by number evolution. In this picture, the FBGs are present in abundance at  $z \sim 1$ , but would have had to have faded or otherwise destroyed themselves (e.g. Babul & Rees 1992) by the present epoch in order to escape detection. This population must clearly be quite blue (close to flat spectrum) since their dominance of the galaxy counts seems to increase towards shorter wavelengths. They would also have to be weakly clustered (correlation length  $r_0 < 5.5 h^{-1}$  Mpc) relative to bright galaxies. The FBGs are not extreme dwarfs; their luminosity is about  $0.1 L^*$  (for those with measured redshifts) and recent high-resolution imaging (Colless, private communication) shows late-type morphology.

## 2. Gravitational lensing by galaxy clusters

### 2.1 Sources and lenses

Our study is somewhat unusual compared to other lensing studies, most of which start with image plane morphology (e.g. double quasars and radio Einstein rings) resulting in unknown lens selection functions. We use faint blue galaxies ( $B_J \sim 24$ –27) as the sources behind the lens. These objects, with their high surface density and isotropic properties (Tyson 1988; Lilly *et al.* 1991), serve as the perfect ‘cosmic wallpaper’. Of the brighter examples of these galaxies ( $B_J \leq 23$ ), about half lie in the redshift range 0.3–0.9 (Colless *et al.* 1990). The median redshift for our fainter ‘source plane’ galaxies is expected to be higher ( $\bar{z} \gtrsim 0.5$ ). We then pick a candidate lens, a foreground ( $z = 0.2$ –0.5) rich galaxy cluster, known *a priori* to be a massive object. We usually select X-ray bright clusters ( $L_X \gtrsim 10^{44}$  erg s $^{-1}$ ), since  $L_X$  is a good indicator of the depth of the cluster potential well, and those having a concentration of optically bright galaxies within the central  $\sim 100$  kpc. Deep multiband CCD imaging of the cluster (down to a threshold of  $29 B_J$  mag arcsec $^{-2}$ ) is used to study the distortion in the shapes of the background galaxies caused by gravitational lensing.

The discovery of giant luminous arcs in clusters (Soucail *et al.* 1988; Lynds & Petrosian 1989) led to the suggestion that these are amplified images of background faint galaxies that happen to lie on a caustic associated with the lensing cluster. This has been confirmed by spectroscopic redshift determination of several arcs by the Toulouse group: in every case, the arc lies well behind the cluster. The cluster mass gives rise to a shear that causes the background galaxies to be stretched along circles centred on the cluster. The separation of background galaxies from cluster members is relatively simple. The former are quite blue (mean  $B_J - R \sim 0.5$  over the range  $B_J = 24$ –27), while cluster ellipticals are very red ( $B_J - R = 1.5$ –2). The distant blue galaxies show a continuum of morphologies going from the giant arcs (e.g. in Abell 370 and

CL 2244 02) through smaller arclets to only slightly elongated galaxies which are preferentially aligned tangentially relative to the cluster centre.

## 2.2 Simulations and mass determination

In order to relate the observed distortion of background galaxies to the amount of mass in the cluster, we carry out realistic simulations in which we use an actual image of the distant galaxies (in a randomly chosen part of sky *not* containing a foreground cluster) as the background 'screen'. The cluster mass is modelled as a smooth soft-core isothermal lens, while each of the bright cluster ellipticals is assigned a truncated isothermal scaled to its Faber-Jackson mass. The 'screen' is then distorted by this model gravitational lens and the effects of seeing and noise are added. The distortion is quantified by first computing an ellipticity vector for each galaxy (using its intensity-weighted second moments) and then integrating over all background galaxies. This distortion measure in the simulated image is compared to that in the actual CCD image in order to derive lens parameters.

For three of the better studied clusters (Tyson *et al.* 1990; Tyson 1991) that show strong lensing effects, Abell 1689, 3C295 (CL 1409), CL 0024 + 16, the inferred depth of the smooth cluster potential, expressed in terms of an equivalent line-of-sight velocity dispersion, is about  $\sigma = 1100 - 1500 \text{ km s}^{-1}$ . The derived core radius of the mass distribution ranges from  $40 - 70 h^{-1} \text{ kpc}$  but is somewhat more uncertain. Most of the mass ( $\sim 80\%$ ) must be in the smooth extended component (rather than concentrated inside the ellipticals), since the long arcs and arclets are mostly seen centred on the cluster as a whole; rarely do the background galaxies form arcs around individual cluster galaxies.

## 3. Discussion

Gravitational lensing can thus be a useful probe of the (mostly dark) matter in the inner few 100 kpc of clusters. Unlike the mass derived from direct kinematical measures of  $\sigma$ , the estimate from lensing is independent of dynamical assumptions (i.e. whether the cluster is virialized) and possible projection of (unbound) foreground or background galaxies. For those clusters with reliable kinematically determined velocity dispersions (e.g. Abell 1689), the measured value of  $\sigma$  and value estimated from lensing distortion are usually in reasonable agreement or the latter is slightly smaller, indicating that the above biases on the kinematical estimate are small. Moreover, the lensing value may be a slight underestimate because of the effects of seeing, the possibility that some fraction of field galaxies are very compact and unresolved, imperfect separation of cluster members from the field population, etc. The high velocity dispersions found in clusters (now confirmed through these two independent techniques) may be a problem for the standard biased cold dark matter model (Peebles *et al.* 1990). We have studied 26 clusters to date and find that all the optically rich and/or compact ones show appreciable lensing. The matter core sizes derived from lensing for these objects are usually smaller than the X-ray core radii. An extension of this technique, using large-area deep CCD imaging to measure the shapes and orientations of distant galaxies, can be used to map foreground dark matter clumps not associated with galaxies.

### Acknowledgements

It is a pleasure to acknowledge Tony Tyson and Gary Bernstein and other collaborators for stimulating discussions. Support for this work was provided by NASA through grant number HF-1033.01-92A from the Space Telescope Science Institute, which is operated by the Association of Universities for Research in Astronomy, Inc., under NASA contract NAS 5-26555.

### References

- Babul, A., Rees, M. J. 1992 *Mon. Not. R. astr. Soc.*, submitted.
- Broadhurst, T. J., Ellis, R. S., Shanks, T. 1988, *Mon. Not. astr. R. Soc.*, **235**, 827.
- Broadhurst, T. J., Ellis, R. S., Glazebrook, K. 1992, *Nature*, **355**, 55.
- Colless, M. M., Ellis, R. S., Taylor, K., Hook, R. N. 1990, *Mon. Not. R. astr. Soc.*, **244**, 408.
- Efstathiou, G., Bernstein, G., Katz, N., Tyson, J. A., Guhathakurta, P. 1991, *Astrophys. J. Lett.*, **380**, L47.
- Guhathakurta, P. 1991, in *Early Observable Universe from Diffuse Backgrounds*, Ed. B. Rocca-Volmerange *et al.* (Editions Frontieres), p. 155.
- Guhathakurta, P., Tyson, J. A., Majewski, S. R. 1990, *Astrophys. J. Lett.*, **357**, L9.
- Koo, D. C. 1986, *Astrophys. J.*, **311**, 651.
- Koo, D. C., Kron, R. G. 1992, *A. Rev. Astr. Astrophys.*, **30**, 613.
- Kron, R. G. 1980, *Astrophys. J. Suppl.*, **43**, 305.
- Lilly, S. J., Cowie, L. L., Gardner, J. P., 1991, *Astrophys. J.*, **369**, 79.
- Lynds, R., Petrosian, V. 1989, *Astrophys. J.*, **336**, 1.
- Melott, A. L. 1992, *Astrophys. J. Lett.*, **393**, L45.
- Peebles, P. J. E., Daly, R. A., Juszkievicz, R. 1990, *Astrophys. J.*, **347**, 563.
- Soucail, G., Mellier, Y., Fort, B., Mathez, G., Cailloux, M. 1988, *Astrophys. J.*, **191**, L19.
- Tyson, J. A. 1988, *Astrophys. J.*, **96**, 1.
- Tyson, J. A. 1991, in *Proceedings of the 1990 Texas/ESO-CERN Symposium*, in press.
- Tyson, J. A., Valdes, F., Wenk, R. A. 1990, *Astrophys. J.*, **349**, L1.



## **Cosmological Evolution of Linear Sizes and the Unification of Quasars and Radio Galaxies**

V. K. Kapahi, R. M. Athreya & C. R. Subrahmanya *National Centre for Radio Astrophysics, TIFR, Pune 411 007, India*

R. W. Hunstead & J. C. Baker *University of Sydney, NSW 2006, Australia.*

P. J. McCarthy *Observatories of the Carnegie Institution of Washington, Pasadena, Ca 91101, USA*

W. van Breugel *IGPP, Livermore, Ca 94550, USA.*

**Abstract.** We have investigated the linear size distributions of sources in the new Molonglo quasar sample with a limiting flux density of 0.95 Jy at 408 MHz, a factor of  $\sim 5$  deeper than 3CR sample. The relatively low radio frequency of the finding survey, together with near-completeness with regard to deep optical identifications and spectroscopy, make this a very good sample for testing the unification of quasars and radio galaxies based on orientation effects. We find that even though of lower radio luminosity, Molonglo quasars in different redshift ranges are typically larger than 3CRR quasars. This is contrary to the known behaviour of radio galaxies of similar radio luminosity, and is difficult to understand in unification schemes based only on orientation.

**Key words:** Cosmological evolution    unification of radio galaxies and quasars.

### **1. Introduction**

The linear sizes of powerful double radio sources appear to be a function of the cosmic epoch as well as of the radio luminosity of the sources. Attempts to disentangle the two effects using samples covering a wide range in flux density have met with considerable success in recent years as far as radio galaxies are concerned. It is now generally agreed (Kapahi 1986, 1989; Oort *et al.* 1987; Singal 1988, 1993a; Subramanian & Swarup 1990) that over a wide range in redshift ( $z$ ) and radio luminosity ( $P$ ), the median linear sizes ( $l_m$ ) of radio galaxies can be expressed as  $l_m \propto P^\beta (1+z)^{-n}$ , with  $\beta \sim 0.3$  and  $n \sim 3$ . In the case of quasars on the other hand, there is little evidence for such a relation; existing data appear to indicate a weaker dependence on epoch ( $n \sim 0$  to 2) and possibly an inverse dependence on  $P$  (e.g. Barthel & Miley 1988; Singal 1988, 1993a). It is not clear if various selection effects and biases in the quasar samples (possibly induced by relativistic beaming and other orientation dependent effects on the radio and optical continuum radiation) could be responsible for the apparently different behaviour of quasars and radio galaxies. The matter is of considerable significance to the ‘unified scheme’ of Barthel (1989) which has attracted a great deal of attention in recent years. The scheme postulates that

radio galaxies and quasars are intrinsically similar; those seen at small-angles ( $\leq 45^\circ$ ) to their jet axes being classified as quasars and the others as radio galaxies. It therefore requires that the projected linear sizes of quasars should be systematically smaller than those of radio galaxies, but both should show similar dependences on  $z$  and  $P$ .

Complete and unbiased samples selected at low radio frequencies (where most sources are lobe-dominated and therefore not seriously affected by orientation biases due to relativistic beaming effects in the parsec-scale nuclear jets) are clearly necessary to compare the linear size statistics of radio galaxies and quasars in the context of the unified scheme. The relative numbers and projected size distributions of radio galaxies and quasars in different redshift ranges in the 3CRR sample with  $S_{1.78} \geq 10$  Jy (Laing *et al.* 1983), which is the only sample with complete optical identification and spectroscopic data, appear to be in conflict with Barthel's unification scheme even if the range of viewing angles dividing the two classes is allowed to evolve with epoch or radio luminosity (Kapahi 1990; Singal 1993b). In view of the relatively small number of quasars in the 3CRR sample, however, it is important to investigate a larger independent sample. We report here the preliminary results from a new and almost 'complete' sample of quasars formed from the Molonglo Reference Catalogue.

## 2. The Molonglo Quasar Sample (MQS)

The Molonglo quasar sample (MQS) was initially defined on the basis of optical identifications with stellar objects on the UK Schmidt III aJ plates (complete down to a limiting magnitude of  $B_J \sim 22.5$ ) of about 550 radio sources with  $S_{4.85} \geq 0.95$  Jy,  $-30^\circ < \delta < -20^\circ$  and RA ranges of  $20^h - 6^h$  and  $9.5^h - 14^h$  in the Molonglo Reference Catalogue (MRC; Large *et al.* 1981), based on radio positions determined with the Molonglo Observatory Synthesis Telescope at 843 MHz (Hunstead & Subrahmanya, in preparation) or taken from the MRC. Follow-up work has included high resolution radio imaging at 5 GHz using the Very Large Array and optical spectroscopy with the Anglo-Australian Telescope (see Baker *et al.* 1994 for some preliminary results based on optical spectroscopy). Some more quasars have subsequently got added to the initial sample as a result of deep CCD optical imaging (with the 2.3 m Dupont telescope of the Las Campanas Observatory) and spectroscopy (with the 4 m telescope of the Cerro Tololo Inter-American Observatory) that some of us have been carrying out on the complete sample of 550 Molonglo sources (McCarthy *et al.* 1990).

The MQS at present consists of 81 quasars with spectroscopic redshifts. Of the remaining candidate identifications without spectroscopy, we estimate that another 5 to 10 objects may get confirmed as quasars after spectroscopy. This small incompleteness of the sample is however unlikely to have any serious effect on our analysis reported here as the missing quasars do not form any special group as far as their apparent radio and optical properties are concerned.

## 3. Comparison of Molonglo and 3CRR quasars

Assuming a typical spectral index of 0.9, the Molonglo quasars go about a factor of 5 deeper in flux density than the 3CRR quasars. The principal difference in the redshift distributions of the two samples (Fig. 1) is the presence of a somewhat longer tail at  $z > 2$  in the Molonglo sample.

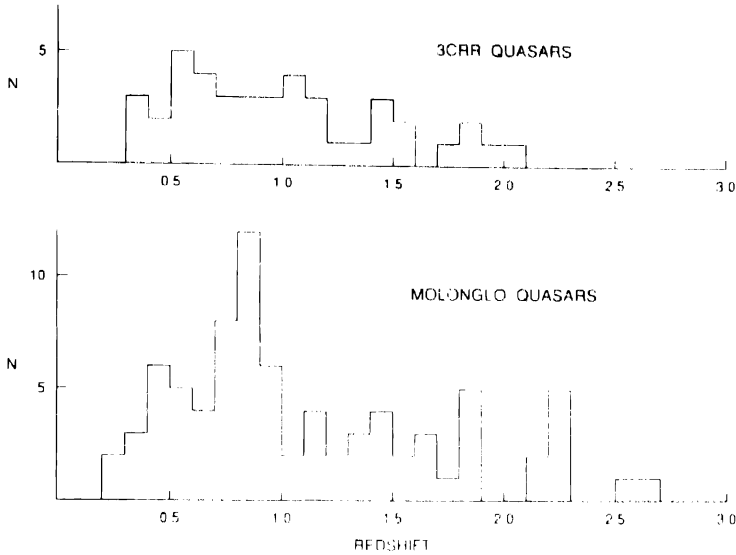


**Figure 1.** Redshift distribution of 3CRR and Molonglo quasars.

The linear size distributions of quasars in the two samples are compared in Fig. 2. The Molonglo sample is seen to have a larger fraction of compact unresolved sources ( $l \lesssim 20$  kpc, assuming  $H_0 = 50 \text{ km s}^{-1} \text{ Mpc}^{-1}$  and  $q_0 = 0$ ) of both the flat spectrum ( $\alpha < 0.5$ ; core-dominated) and the steep-spectrum ( $\alpha > 0.5$ ) varieties. Reasonable arguments can be made for excluding such objects from both the samples in comparing the linear size distributions of extended radio quasars. The larger fraction of core-dominated objects in MQS is probably related to the higher selection frequency and a consequent increase in their selection probability due to the doppler boosting of the flux density in their radio cores because of relativistic beaming effects (Orr & Browne

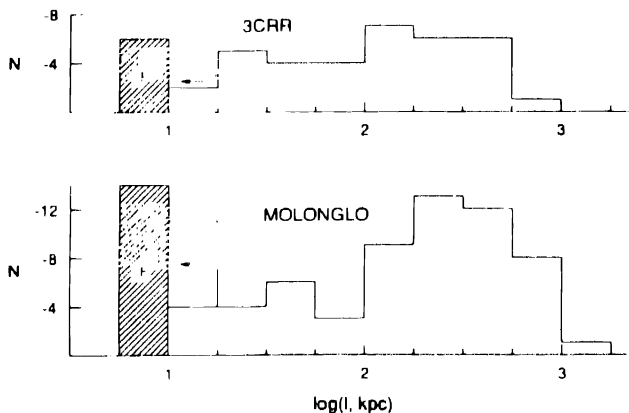


**Figure 2.** Distributions of linear sizes of all quasars in the 3CRR and Molonglo samples. Shaded area refers to core-dominated flat spectrum quasars.



1982). The overall spectral shapes of many of these core-dominated quasars indicate that they would not qualify to be in the sample at  $S_{408} > 0.95$  Jy if only the unbeamed flux in their lobes is considered. The incidence of compact steep-spectrum sources is also known to increase with increasing frequency of selection due to low frequency turnovers in their radio spectra (e.g. Kapahi 1981). Their radio structures and linear sizes do not also appear to show a continuity with the more extended double quasars. In the subsequent comparison we have therefore excluded the core-dominated as well as all steep spectrum quasars with a total linear size  $< 20$  kpc.

For the extended steep spectrum sources the values of  $l_m$  (median linear size) in the 3CRR and Molonglo samples are 133 kpc and 237 kpc respectively. Even though the average radio luminosity of the Molonglo quasars is a factor of  $\sim 5$  lower than that of the 3CRR quasars, their linear sizes appear to be considerably larger. This is contrary to expectation if quasar sizes also depended directly on radio luminosity as in the case of radio galaxies. If we subdivide the samples into two different redshift ranges, viz.  $0.5 < z < 1.0$  and  $1.0 < z < 2.0$ , the median linear sizes are consistently larger for the Molonglo quasars in both the ranges (Fig. 3 and Table 1), indicating an inverse correlation of  $l$  with  $P$ . The number of extended quasars at  $z < 0.5$  is too small (4 in 3CRR and 7 in Molonglo) to make a meaningful comparison but the estimated values of  $l_m$  of 316 kpc and 274 kpc respectively are not inconsistent with the above trend due to the larger errors in  $l_m$ .

It is also interesting to compare the linear size distributions of Molonglo quasars with those for 3CRR radio galaxies at similar redshifts. In the range of  $0.5 < z < 1.0$  where the numbers involved are reasonably large (25 quasars vs. 32 galaxies) the value of  $l_m = 268$  kpc (Kapahi 1990) for the 3CRR radio galaxies is actually smaller than the value of 331 kpc for the Molonglo quasars. The galaxies in this comparison have considerably higher luminosity than the quasars, and since the sizes of radio galaxies are expected to be even smaller at luminosities corresponding to the Molonglo quasar luminosities, the data appear to be in serious conflict with the predictions of the unified scheme.

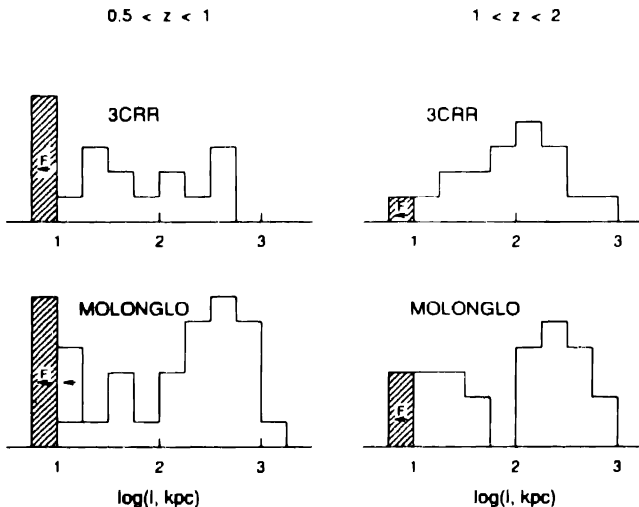


**Figure 3.** Distributions of linear sizes in two different redshift ranges.

**Table 1.** Median linear sizes of extended steep-spectrum quasars in the 3CRR and Molonglo samples.

Redshift range	3CRR			Molonglo		
	No. of quasars	$\log P_{\text{med}}$ 408 MHz ( $\text{WHz}^{-1}$ )	$l'_{\text{med}}$ kpc	No. of quasars	$\log P_{\text{med}}$	$l_{\text{med}}$ kpc
$z < 0.5$	4	27.8	$316^{+185}_{-116}$	7	27.4	$274^{+180}_{-109}$
$0.5 < z < 1$	13	28.6	$100^{+95}_{-50}$	25	27.8	$331^{+109}_{-81}$
$1 < z < 2$	16	29.1	$115^{+45}_{-32}$	20	28.7	$200^{+75}_{-55}$

At present our spectroscopic observations of Molonglo radio galaxies are not complete enough to make a direct comparison of the sizes of Molonglo quasars and Molonglo galaxies in the same redshift ranges. There are 72 radio galaxy identifications in our Molonglo sample that have a spectroscopic redshift  $z > 0.5$ . Of the remaining objects, if we make the reasonable assumption that those without any optical identifications on the sky survey plates are likely to be radio galaxies at  $z > 0.5$ , we can make an approximate comparison of radio galaxies and quasars at  $z > 0.5$  in the Molonglo samples. For this we further assume the unidentified objects to have  $z \approx 1$  for converting the measured angular size into a linear size (the fairly flat  $\theta - z$  relation at  $z > 0.5$  implies that the errors thus introduced are not likely to be very serious). A comparison thus carried out shows that the  $z > 0.5$  radio galaxies have  $l_{\text{med}} \sim 153$  kpc as compared to  $l_{\text{med}} \sim 251$  kpc for the  $z > 0.5$  quasars in the Molonglo sample. This is indeed hard to understand in the context of the unified scheme. It is also hard to imagine any strong biases or selection effects in our samples that can make the quasars look larger than the galaxies.

#### 4. Conclusions

Based on the statistics of linear sizes in the new Molonglo 1-Jy quasar sample, which is nearly complete from the point of view of deep optical identifications and spectroscopy, we have presented evidence that the redshift and luminosity dependence of radio quasars is quite different from what has been inferred for radio galaxies. There is also a preliminary suggestion in our data that the median linear size of extended steep spectrum quasars is actually larger than the median size for radio galaxies in the Molonglo sample at  $z > 0.5$ . If confirmed, our results would pose a major challenge to the models that use orientation effects alone to unify radio galaxies and quasars.

#### References

- Baker, J. C., Hunstead, R. W., Kapahi, V. K., Subrahmanya, C. R. 1995, *J. Astrophys. Astr.* (Suppl.), **16**, 185–188.  
 Barthel, P. D. 1989, *Astrophys. J.*, **336**, 606.  
 Barthel, P. D., Miley, G. K. 1988, *Nature*, **333**, 319.

- Kapahi, V. K. 1981, *Astr. Astrophys. Suppl.*, **43**, 381.
- Kapahi, V. K. 1986, *Highlights of Astr.*, **7**, 371.
- Kapahi, V. K. 1989, *Astr. J.*, **97**, 1.
- Kapahi, V. K. 1990, in 'Parsec-Scale Radio Jets' Eds. J. A. Zensus & T. J. Pearson, (Cambridge University Press) p. 304.
- Laing, R. A., Riley, J. M., Longair, M. S. 1983, *Mon. Not. R. astr. Soc.*, **204**, 151.
- Large, M. I., Mills, B. Y., Little, A. G., Crawford, D. F., Sutton, J. M. 1981, *Mon. Not. R. astr. Soc.*, **194**, 693.
- McCarthy, P. J., Kapahi, V. K., van Breugel, W., Subrahmanya, C. R. 1990, *Astr. J.*, **100**, 1014.
- Oort, M. J. A., Katgert, P., Steeman, F. W. M., Windhorst, R. A. 1987, *Astr. Astrophys.*, **179**, 41.
- Orr, M. J. L., Browne, I. W. A. 1982, *Mon. Not. R. astr. Soc.*, **200**, 1067.
- Singal, A. K. 1988, *Mon. Not. R. astr. Soc.*, **233**, 870.
- Singal, A. K. 1993a, *Mon. Not. R. astr. Soc.*, **263**, 139.
- Singal, A. K. 1993b, *Mon. Not. R. astr. Soc.*, **262**, L27.
- Subramanian, K., Swarup, G. 1990, *Mon. Not. R. astr. Soc.*, **247**, 237.

## A New Population of Gravitationally Lensed Radio Arcs in Distant Abell Clusters

J. Bagchi & V. K. Kapahi *National Centre for Radio Astrophysics, TIFR, Pune 411 007, India.*

**Abstract.** We report the discovery of a population of faint, and possibly gravitationally lensed, radio sources near the centres of distant Abell clusters from sensitive VLA maps made at 21 cm  $\lambda$  of a statistical sample of 46 distant ( $0.1 < z < 0.3$ ) clusters containing dominant cD galaxies. Sources down to  $\approx 1$  mJy in flux density were detected near the field centres. There appears to be a statistically significant, non-random orientation of faint radio sources with their major axes close to the tangential directions with respect to the radius vectors from the cluster centres, strongly suggestive of gravitational lensing by the cluster potential. Maximum distortions were found to be present within  $0.25 R_A$  ( $R_A$ , the Abell radius = 3Mpc) from cluster centres. Several of the tangentially oriented sources have large angular sizes ( $\approx 10''$ – $35''$ ) but possess flat radio spectra (spectral index  $\alpha \lesssim 0.5$  between 0.3 and 1.4 GHz). These properties further strengthen the gravitational lensing hypothesis. A preliminary analysis of the data is reported in which we discuss the possible applications of this finding in the study of gravitating mass distribution in clusters of galaxies and in employing these cluster gravitational telescopes to study the faint radio galaxies in the distant universe.

*Key words:* Clusters of galaxies—gravitational lensing—arclets—cosmology.

### 1. Introduction

The gravitational lensing (GL) effect is emerging as a new tool of observational cosmology. The discovery of giant luminous arcs (GLAs) in two clusters of galaxies (Lynds & Petrosian 1986; Soucail *et al.* 1987) and the suggested interpretation of the phenomenon as gravitational lensing (Paczynski 1987) generated the exciting possibility of using clusters as gravitational lenses. The redshifts of these arcs were found to be much greater than the cluster redshifts, confirming the GL interpretation (Soucail *et al.* 1988). Realizing that these GLAs are examples of strong lensing due to favourably placed distant galaxies, Grossman & Narayan (1988) predicted the existence of numerous smaller arclets for each GLA. Such small optical arclets were indeed seen in the cluster A370 and A2218 (Fort *et al.* 1988; Pello-Descyrcy *et al.* 1988). Ultra-deep CCD imaging of a few clusters by Tyson *et al.* (1990) has revealed populations of arclets that are extremely faint ( $B \approx 25$ – $27$ ), unusually blue ( $B-R \approx 0.3$ ), and are mostly tangentially placed relative to cluster centres (see Fort, 1991 for a review). Due to their extreme faintness, no redshift measurement of these arclets has been possible with

current technology. However, on the basis of unambiguous colour redshifts of a few arclets, Fort (1991) derived a probable redshift range of 0.7–1.3. We report here the statistical evidence for a new population of faint radio images detected near the centres of distant Abell clusters. The near tangential alignment of these sources indicates that these are possibly the gravitationally lensed radio arclets. A preliminary analysis of this result is presented here (we have used  $H_0 = 50 \text{ km s}^{-1} \text{ Mpc}^{-1}$ , and  $q_0 = 0.5$ ).

## 2. The cluster sample

We searched for signals of GL in a radio survey (Bagchi 1992) of a nearly complete sample of 46 Abell clusters of distance class  $D \geq 5$  ( $0.1 \leq z_{\text{estimated}} \leq 0.3$ ) and with a Bautz-Morgan morphological class I or I: (i.e. containing a first ranked cD galaxy; Leir & van Den Bergh 1977). The clusters were observed with VLA in the snapshot mode at wavelengths of  $20 \text{ cm } \lambda$  and  $90 \text{ cm } \lambda$ . We attained the completion limits of  $\sim 1 \text{ mJy}$  and  $\sim 15\text{--}25 \text{ mJy}$  at the two wavelengths respectively (for point sources near field centres). The FWHM sizes of the circular gaussian beams were  $30'' \times 30''$  at  $20 \text{ cm } \lambda$ , and  $60'' \times 60''$  at  $90 \text{ cm } \lambda$ . The results of this VLA survey, relating in particular to the radio properties of the cD galaxies, are presented in Bagchi & Kapahi (1994).

## 3. The radio arclets

The radio sources associated with cluster member galaxies are a potential source of confusion in looking for radio arclets. To reduce this, we disregard the radio sources found to be associated with the cD galaxies on the basis of good positional agreement. The orientations of the remaining radio sources were calculated by measuring the angle  $\phi$  of the major axes of the sources with respect to the radius vectors from the cluster centres (the acute angle was taken). To this end, two dimensional elliptical gaussians were fitted to sources detected on the  $20 \text{ cm } \lambda$  radio maps. Only radio sources that have deconvolved largest angular sizes  $\geq 8''$  and have their major axes P.A. known with an accuracy better than  $30^\circ$  were used to avoid dilution of the GL signal by many ‘round’ sources (the P.A. errors have a standard error of  $\approx 5^\circ$ ).

A composite radio-source orientation map of 40 usable sources in 28 clusters is shown in Fig. 1. The common centre of all the clusters is on the ‘+’ symbol and the circle is the boundary  $0.25 R_A$  ( $R_A$ , the Abell radius  $= 3 \text{ Mpc}$ ). We have assumed the optical centres of the clusters to be the barycentres for GL. The major-axes of the sources are drawn as lines of equal length regardless of their actual sizes. This distribution of the orientation angles  $\phi$  in intervals of  $10^\circ$  is presented in Fig. 2. The distribution clearly shows an excess of sources tending to be tangential with respect to cluster centres. The median value of the orientation angle is found to be  $61^\circ \pm 5^\circ$  as against  $45^\circ$  expected for a randomly oriented population. A Kolmogorov-Smirnov (K-S) test shows the distribution to be non random at the  $\approx 98\%$  level of confidence, while a  $\chi^2$ -test gives a confidence level of  $> 99\%$ . The distance of  $0.25 R_A$  (or  $780 \text{ kpc}$ ) from cluster centres defines the region of most significant tangential alignment and has no intrinsic physical significance. In fact, a significant excess of nearly tangentially oriented radio sources of larger angular sizes ( $> 15''$ ) could be detected even upto  $0.7 R_A$  ( $2.1 \text{ Mpc}$ ) from cluster centres. Most of the sources causing the tangential

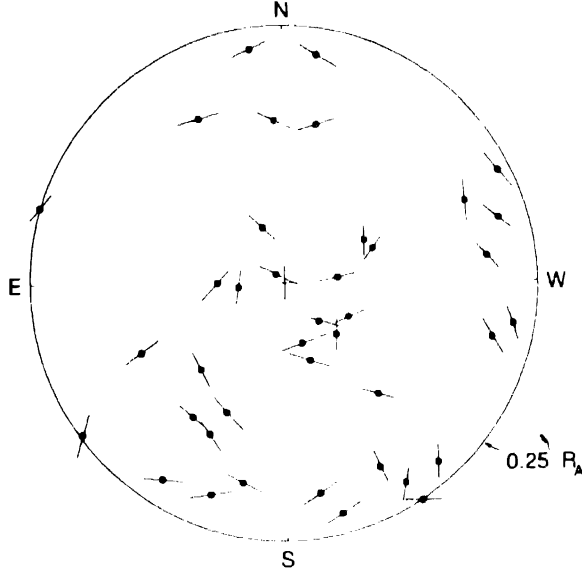


**Figure 1.** A composite radio-source orientation map of 40 sources in 28 clusters of galaxies. The common centre of all the clusters is on the '+' symbol and the circle is the boundary of  $0.25 R_A$ . The major-axes of the sources are drawn as vectors of equal length regardless of their actual sizes.

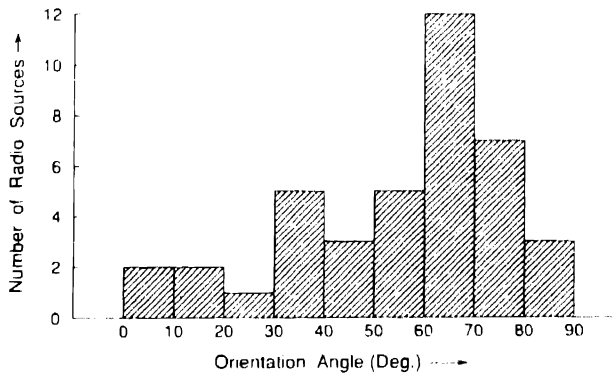


**Figure 2.** A histogram of the distribution of orientation angles with respect to the radius vectors for the sources shown in Fig. 1.

alignment were found to possess a rather flat radio spectrum with  $\alpha \lesssim 0.5$  between 0.3 and 1.4 GHz.

#### 4. Discussion and conclusion

We have detected a significant tangential alignment of radio images near cluster cores and interpret it as due to gravitational lensing of background sources by massive clusters (e.g.

Smail *et al.* 1991; Tyson 1992). The fact that the peak in the orientation distribution occurs in the range of  $60\text{--}70^\circ$ , could be related to the elliptical distribution of mass in the clusters. No information regarding the velocity dispersion ( $\sigma$ ) of these clusters is available in literature. However, using the  $\sigma$  vs. richness ( $R$ ) correlation for Abell clusters (e.g. Girardi *et al.* 1993), we can roughly estimate their efficiency as lenses. About 40% are expected to have the velocity dispersion  $\sigma \approx 1000 \text{ km s}^{-1}$  ( $R = 2, 3$ ) and the rest 60% should have  $\sigma \approx 700\text{--}800 \text{ km s}^{-1}$  ( $R = 1$ ). In order to produce a significant excess of tangentially oriented sources over distances  $\sim 5'$  from centres, the central surface mass density ( $\Sigma$ ) in a majority of lenses should approach the critical value ( $\Sigma_c$ ) needed for multiple imaging i.e.,  $\Sigma/\Sigma_c \sim 1$ , where

$$\Sigma = (9\sigma^2)(2\pi Gr_c)^{-1} = 0.69 (\sigma/10^3 \text{ km s}^{-1})^2 (r_c/100 \text{ kpc})^{-1} \text{ gm cm}^{-2}.$$

Here  $r_c$  is the core-radius of the assumed isothermal density distribution (Turner, Ostriker & Gott 1984) and  $\Sigma_c = (c^2/4\pi G) \cdot (D_s/D_l \cdot D_l)$  for the angular-diameter distances  $D_l$  (to lens),  $D_s$  (to source) and  $D_{ls}$  (lens to source) respectively (e.g. Kovner 1989). Placing the lenses at  $z_l = 0.1$  and sources over the range  $z_s = 0.5$  to  $3.0$ , the critical density spans a rather high range of  $\Sigma_c \approx 1 - 0.75 \text{ gm cm}^{-2}$ . This implies that clusters with  $\sigma \approx 800 \text{ km s}^{-1}$  and near  $z_l \sim 0.1$  are marginal lenses unless their core radii  $r_c \leq 50 \text{ kpc}$ . On the contrary, clusters at  $z_l = 0.2 - 0.3$  and having  $\sigma > 800 \text{ km s}^{-1}$  can act as efficient lenses for the sources of redshifts  $z_s \geq 0.8$  ( $\Sigma_c \leq 0.6 \text{ gm cm}^{-2}$ ) if they have core radii  $r_c \leq 75 \text{ kpc}$ . Thus, if the gravitating mass is spherically distributed, it is necessary that a significant fraction of lensing clusters have compact cores ( $r_c \approx 50\text{--}75 \text{ kpc}$ ). Assuming average values of  $\bar{z}_l = 0.15$ ,  $\bar{\sigma} = 800 \text{ km s}^{-1}$  and  $\bar{r}_c \approx 60 \text{ kpc}$  over the sample population of lenses, a lower limit of  $z_s > 0.7$  can then be obtained for the source population, thereby implying that the parent population of the radio-arclets is possibly the radio-galaxies and quasars at cosmological distances.

The detection of tangential alignment of radio images upto  $\sim 2 \text{ Mpc}$  from cluster centres generates the possibility of mapping the shape and scale of the dark-matter distribution in clusters using the statistical information on the distortions of a sufficiently large number of images. By surveying  $\sim 20$  Abell clusters to a depth of  $\sim 0.3 \text{ mJy}$  (about 3 times deeper than the present data), it should be possible to obtain a large sample of  $\sim 1200$  faint radio sources (upto  $3 \text{ Mpc}$  from cluster centres for  $z_l \approx 0.15$ ) for the purpose of statistical analysis. It is also possible that a few radio analogues of giant arcs have been detected in our sample. We are trying to identify these using higher resolution VLA observations. Due to the large amplification of fluxes and the angular sizes of the sources, the detection of such a giant radio arc holds the exciting possibility of showing the details of an extremely distant and normally unobservable radio source. In conclusion, a detailed study of the gravitationally lensed radio-arclet population has important implications for the study of clusters and for cosmology.

## References

- Bagchi, J. 1992. Ph. D. Thesis, Indian Institute of Science, Bangalore.  
 Bagchi, J., Kapahi, V. K. 1994, *J. Astrophys. Astr.*, **15**, 275–308.  
 Fort, B., Prieur, J. L., Mathez, G., Mellier, Y., Soucail, G. 1988, *Astr. Astrophys.*, **200**, L17.  
 Fort, B. 1991, *Proc. of a Conference on Gravitational Lenses held in Hamburg, Germany*, 9–13 Sept. 1991, **267** (Springer-Verlag).

- Girardi, M., Biviano, A., Giuricin, G., Mardirossian, I., Mezzetti, M. 1993, *Astrophys. J.*, **404**, 38.
- Grossman, S. A., Narayan, R. 1988, *Astrophys. J.*, **324**, L37.
- Kovner, I. 1989, *Astrophys. J.*, **337**, 621.
- Leir, A. A., Van Den Bergh, S. 1977, *Astrophys. J. Suppl.*, **34**, 381.
- Lynds, R., Petrosian, V. 1986, *Bull. AAS*, **18**, 1014.
- Paczynski, B. 1987, *Nature*, **325**, 572.
- Pello-Descayre, R., Soucail, G., Sanahuja, B., Maltez, G., Ojero, E. 1988, *Astr. Astrophys.*, **190**, L11.
- Smail, I., Ellis, R. S., Fitchett, M. J., Norgaard-Nielsen, H. U., Hansen, L., Jorgensen, H. E. 1991, *Mon. Not. R. astr. Soc.*, **252**, 19.
- Soucail, G., Fort, B., Mellier, Y., Picat, J. P. 1987, *Astr. Astrophys.*, **172**, L14.
- Soucail, G., Mellier, Y., Fort, B., Mathez, G., Cailloux M. 1988, *Astr. Astrophys.*, **191**, L19.
- Turner, E. L., Ostriker, J. P., Gott, J. R. 1984, *Astrophys. J.*, **284**, 1.
- Tyson, J. A., Valdes, F., Wenk, R. A. 1990, *Astrophys. J.*, **349**, L1.
- Tyson, J. A. 1992, *Phys. Today*, **45**(6), 21.





## Chemical Evolution of High Redshift Galaxies

Pushpa Khare *Department of Physics, Utkal University, Bhubaneswar 751 004, India.*

N. C. Rana *Inter-University Centre for Astronomy and Astrophysics, Ganeshkhind, Post Bag 4, Pune, India.*

**Abstract.** We have determined the rate of chemical evolution of galaxies from  $z = 4$  to 2, from the observed redshift distributions of C IV and Lyman limit absorption systems in the spectra of quasars.

**Key words:** Chemical evolution—galaxies—quasar absorption lines.

The observed redshift distribution of the Lyman limit systems (LLS) and C IV absorption systems, is usually parameterised as

$$N(z) \propto (1+z)^\gamma, \quad (1)$$

$N(z)$  being the number of absorption systems of a given kind per unit redshift interval per line of sight,  $\gamma$  being the evolutionary parameter. Observations of a large number of quasars give

$$\gamma_{\text{LLS}} = 0.68 \pm 0.54 \quad 0.67 < z < 3.6 \quad (2)$$

$$\gamma_{\text{C IV}} = -1.2 \pm 0.56 \quad 1.5 < z < 4.0 \quad (3)$$

(Sargent *et al.* 1988; Steidel 1990). The LLS are characterized by a neutral hydrogen column density  $N_{\text{H I}} \geq 2 \times 10^{17} \text{ cm}^{-2}$ , while the C IV line sample used for the above analysis has a column density of C IV,  $N_{\text{C IV}} \geq 6 \times 10^{13} \text{ cm}^{-2}$ . Assuming the comoving number density of galaxies to be unchanging with redshift, the above values of  $\gamma$  give the effective radii of the galactic halos for detection as LLS and as C IV systems as,

$$R_{\text{eff}}^{\text{LLS}}(z) = \text{constant} \quad (4)$$

$$R_{\text{eff}}^{\text{C IV}}(z) = (1+z)^{-0.85}. \quad (5)$$

We assume the halos to be spherical with radius  $\sim 50 \text{ kpc}$  and assume a diffuse background UV radiation field increasing with  $z$  as  $(1+z)^2$  upto  $z = 2.0$  and as  $(1+z)^{0.2}$  thereafter (Miralda-Escude & Ostriker 1990). The column density of H I and C IV along any line of sight through the halo is obtained by constructing photo-ionization models assuming plane parallel slabs. The effective radii of the galaxies for LLS & C IV systems are the largest impact parameters of the lines of sight through the halo, producing  $N_{\text{H I}} \sim 2 \times 10^{17} \text{ cm}^{-2}$  and  $N_{\text{C IV}} \sim 6 \times 10^{13} \text{ cm}^{-2}$ . Constancy of  $R_{\text{eff}}^{\text{LLS}}$  implies an increase in the mass of the gas in the halo at least as  $(1+z)^{0.75}$ . This along with the observed dependence of  $R_{\text{eff}}^{\text{C IV}}$  on  $z$  gives the rate of change of abundance of carbon,  $X_c(z)$ , with redshift in the galactic halos. This is shown in Fig. 1, which also shows the effect of the presence of an abundance gradient ( $X_c(r) = X_c(0)e^{-br}$ ) in the galactic halo, on the rate of chemical evolution. The effect of variation in redshift

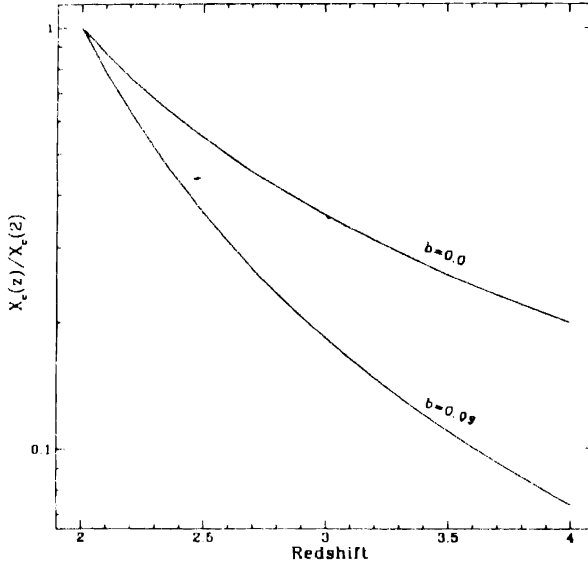


**Figure 1.** Abundance of carbon vs  $z$ , with and without abundance gradient  $b$  is in  $\text{Kpc}^{-1}$ .

dependence of UV radiation for  $z \geq 2$  on the rate of chemical evolution is shown in Fig. 2.

In conclusion we have shown that (1) the mass of the gas in the galactic halos was higher in the past by a factor  $\geq 3$  at  $z = 4$  than at present and (2) the abundance of carbon increased 5–20 times from  $z = 4$ –2.

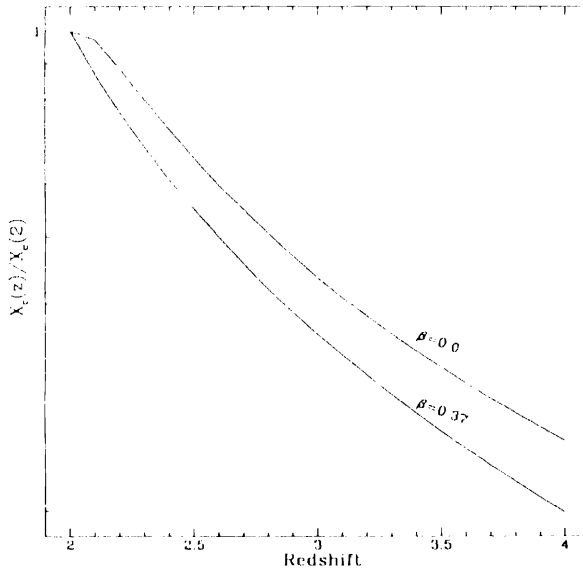


**Figure 2.** Effect of  $z$  dependence of UV field for  $z > 2$  on the abundance of carbon.

### **References**

- Miralda-Escude, Ostriker, J. P. 1990, *Astrophys. J.*, **350**, 1  
Sargent, W. L. W., Boksenberg, A., Steidel, C. C. 1988, *Astrophys. J. Suppl.*, **68**, 539.  
Steidel, C. C. 1990, *Astrophys. J. Suppl.*, **74**, 37.



## Cross-correlation Analysis of $\gamma$ -ray Burst Time Profiles

Patrick Das Gupta *Department of Physics and Astrophysics, University of Delhi, Delhi.*

A. N. Ramaprakash *Inter-University Centre for Astronomy and Astrophysics, Post Bag 4, Ganeshkhind, Pune 411 007, India.*

**Abstract.** We develop the formalism to use cross-correlation techniques to identify gravitationally lensed burst events among dissimilar-looking, faint bursts occurring in the same error box in the sky. The technique is verified using actual burst time profiles.

**Key words:** Gamma-ray bursts—gravitational lenses—cross-correlation analyses.

### 1. Introduction

One of the major issues pertaining to Gamma-ray Bursters (GRBs) is the question whether they are Galactic or extragalactic in origin. Though several Galactic (Proc. Los Alamos Workshop 1990), cosmological (Usov & Chibisov 1975; Paczynski 1986a) and mixed (Lingenfelter & Higdon 1992) models had been suggested, none of them have so far been able to establish successfully, the distance at which the bursts originate. A potential observation that can settle the controversy of burst locations, is that of detecting a gravitationally lensed event (Paczynski 1986b). If the GRBs are extragalactic in origin, the probability that a burst is lensed by an intervening galaxy or clusters of galaxies increases with the distance to the event. Hence, the fainter bursts are statistically more likely to be lensed, in which case it is important to develop methods that will allow us to determine when two faint burst events seen in the same error box are lensed images of a single burst. Recently, J. Wambsganss (1993) has studied the complementary problem of developing a method to distinguish between two burst time profiles that appear similar.

In this paper, we develop a method that studies the time profiles corresponding to two burst events originating in the same error box, but separated in time, using cross-correlation techniques.

### 2. Formalism

The observed counts  $C_1(i)$  and  $C_2(j)$ , corresponding to two burst events lying in the same error box,  $i$  and  $j$  being the time bin indices, also contain background noise so that

$$C_\alpha(i) = S_\alpha(i) + n_\alpha(i). \quad (1)$$

Hereafter  $\alpha = 1, 2$  stands for the appropriate quantity corresponding to the first and second event respectively. In equation (1),  $S_\alpha$  are the intrinsic time profiles of the two events, while  $n_\alpha$  are the background noise counts that are mutually uncorrelated and

are assumed to be stationary. Choosing equal lengths for the two data trains, we cross-correlate these to obtain

$$(O_1 \circ O_2)(i) = \sum_{j=1}^N O_1(j) O_2(j+i); \quad \text{where} \quad O_a(i) = C_a(i) - \frac{1}{N} \sum_{k=1}^N C_a(k). \quad (2)$$

are the observed counts less their averages.

The background noise counts at different time bins are assumed to be uncorrelated so that

$$\langle n_a(i) n_a(j) \rangle = \sigma_a^2 \delta_{ij} + \mu_a^2, \quad (3)$$

where  $\mu_a$  and  $\sigma_a^2$  are the means and variances of  $n_a$ , with  $\langle \rangle$  representing an ensemble average. The cross-correlation signal and noise are given by

$$S(i) \equiv \langle (O_1 \circ O_2)(i) \rangle = \sum_{j=1}^N S'_1(j) S'_2(j+i) \quad (4)$$

and

$$\begin{aligned} N(i) &\equiv \sqrt{\langle (O_1 \circ O_2)^2(i) \rangle - \langle (O_1 \circ O_2)(i) \rangle^2} \\ &= \sqrt{N \sigma_1^2 \sigma_2^2 + \sigma_1^2 \sum_{j=1}^N S_1'^2(j) + \sigma_2^2 \sum_{j=1}^N S_2'^2(j+i)}, \end{aligned} \quad (5)$$

respectively, where

$$S'_a(i) \equiv S_a(i) - \frac{1}{N} \sum_{j=1}^N S_a(j). \quad (6)$$

The signal-to-noise ratio then is given by

$$\frac{S(i)}{N(i)} = \frac{\sum_{j=1}^N x_j y_{j+i}}{\sqrt{N + \sum_{j=1}^N x_j^2 + \sum_{j=1}^N y_{j+i}^2}}, \quad \text{where} \quad x_j \equiv \frac{S'_1(j)}{\sigma_1} \quad \text{and} \quad y_j \equiv \frac{S'_2(j)}{\sigma_2}. \quad (7)$$

Applying Schwarz inequality to the above expression, it is easy to see that the signal-to-noise ratio is maximized when  $y_{j+i} \propto x_j$ .

The above results tell us that if the two intrinsic time profiles are the same except for an overall scalefactor and time lag (which will be the case if the burst is gravitationally lensed), then the cross-correlation will result in a sharp peak when these time profiles sit exactly on top of each other.

### 3. Results

We apply the method described in the previous section by simulating faint bursts. For this, we scale the time profile of the burst corresponding to trigger number 179, down by a factor 1.87, so that the peak counts are just  $3\sigma$  above the mean background noise. The scaled time profile  $S_{179}$ , having length 17 s is then assumed to be the intrinsic burst signal for our analysis. The burst counts are then obtained as

$$C_1(i) = n_1(i) + S_{179}(i) \quad \text{and} \quad C_2(i) = n_2(i) + A S_{179}(i - L), \quad (8)$$

**Table 1.** BURST 179-1 scaled down by 1.87; lag = 300 bins.

Ampli. factor	Corr. peak	Time of peak(s)	FWHM of peak(s)	Noise N
1.0	$3.45 \times 10^7$	17.216	1.024	$2.12 \times 10^6$
0.5	$1.63 \times 10^7$	17.216	1.04	$1.8 \times 10^6$
0.25	$7.77 \times 10^6$	17.024	0.576	$1.71 \times 10^6$

where  $A$  is a de-amplification factor lying in the range (0, 1),  $L$  is the time lag index in number of bins, while  $n_1$  and  $n_2$  are statistically independent background noise counts. The question, then, is: How far can we decrease  $A$  and still maintain a sharp peak in  $O_1 \circ O_2$  with a sufficiently high S/N ratio?

The results we have obtained are shown in Table 1. The time lag index was taken to be  $L = 300$ , which corresponds to a time delay of 17.216 s. From Table 1, it is clear that cross-correlation indeed show high peaks at or very close to 17.216 s. Therefore, this technique not only helps in identifying lensed time profiles but also in determining accurate value of the time-delay. Upto  $A \sim 0.3$ , the cross-correlation shows a distinct peak with a full width at half maxima (FWHM) of 0.5 s and S/N ratio of 5. For  $A$  less than 0.2,  $O_1 \circ O_2$  starts becoming noisy. What this implies is that in the case of a lensed event, if one of the images is detected with a burst peak at  $3\sigma$  above the average background noise while the other is with a peak only at  $1\sigma$  above the mean noise, it is still possible to say with a high degree of confidence that both these events correspond to the same burst.

A similar analysis has also been carried out for the burst 451, for which we find that upto  $A \sim 0.1$  the cross-correlation peak is distinct with a S/N ratio over 3. This verifies the effectiveness of this technique in identifying faint lensed events. Since for the numerical evaluation of cross-correlations, standard algorithms use fast Fourier transforms, our method turns out also to be computationally efficient.

### Acknowledgements

It is a pleasure to thank Prof. P. N. Bhat and Dr. Macomb for providing the time history data for the gamma ray bursters.

### References

- Lingenfelter, R. E., Higdon, J. C. 1992, *Nature*, **356**, 132.  
Paczynski, B. 1986a, *Astrophys. J.*, **308**, L51.  
Paczynski, B. 1986b, *Astrophys. J.*, **308**, L43.  
*Proc. of the Los Alamos Workshop on Gamma-ray Bursts, Observations, Analyses and Theories*, 1990, Ed. C. Ho, R. I. Epstein & E. E. Fenimore (Cambridge Univ. Press) p. 494.  
Usov, V. V., Chibisov, G. V. 1975, *Soviet Astr.-AJ*, **19**, 115.  
Wambsganss, J. 1993, *Astrophys. J.*, **406**, 29.





## Abstracts

### Radio Source Counts at 232 MHz

Zhang Xizhen *Beijing Astronomical Observatory, CAS, Beijing 100080, China*

The Miyun Synthesis Radio Telescope (MSRT) has been used in a moderately deep meter-wave survey at 232 MHz, covering the sky area north of declination  $+30^\circ$ . The first results on the source counts are presented in this paper. The sample consists of three sub-samples which correspond to high, middle, and low galactic latitude. The log N–log S curves for steep spectra sources and flat sources were obtained. An interesting result is discussed.

The catalogue of the Miyun 232 MHz Survey is complete down to 0.25 Jy (Zhang *et al.* 1993). For source count purpose, three small samples were taken from this survey. The characteristics of the samples are listed in Table 1.

In Miyun 232 MHz survey, a lot of ‘new’ sources were catalogued first. Among the ‘new’ sources, whose flux density is less than 0.3 Jy and no counterpart found from other catalogue, were not included in the samples. The number removed is  $<0.5\%$  for sub-sample A and B, and  $<1\%$  for sub-sample C. The spectral indices were derived between 232 MHz and 4.85 GHz. The flux densities at 4.85 GHz were taken from 87GB catalogue (Gregory 1990). For sources without 4.85 GHz counterparts, the spectral-indices were calculated by two methods: one is to extrapolate according to other frequency data; another, if no other frequency data was available, to assume the 4.85 GHz flux density to be the lower limit of 4.85 GHz catalogue.

The sample covers about  $1200 \text{ deg.}^2$  sky area and the total number is about 3500. The interesting thing is that there is a source excess around flux density of 0.4 Jy. To check this excess, several tests had been carried out. The log N–log S curves of the three sub-samples for flat and steep sources were obtained separately. The preliminary results of the counts, the excess around 0.4 Jy is always there. The excess either appears in the curves of flat spectrum sources or appears in the curves of steep sources depending on how to calculate the spectra-indexes for sources without high frequency counterparts. The interesting thing is to study why so many strong sources are found at low frequency survey only.

The variation of source number as galactic latitude may be explained by the irregularity of the large scale structure of the universe, the absorption of the Galaxy, and the distribution to the super-galactic-coordinates. Further research and explanation on the excess will be given later.

**Table 1.** The characteristics of the sample.

Sub-sample A	Sub-sample B	Sub-sample C
$b > 50$ deg.	20-50	$b < 15$ deg.
400(sq. deg.)	500(sq. deg.)	300(sq. deg.)
1144(sources)	- 1507(sources)	839(sources)

**References**

Gregory, P. C. *et al.* 1990, *NRAO Preprint*, **90/91**.  
Zhang, X. *et al.* 1993, *Astr. Astrophys. Suppl.*, **99**, 545.



**On the Reality of the Physical Association between QSOs and Galaxies**

A. K. Sapre & V. D. Mishra *School of Studies in Physics, Pt. Ravishankar Shukla University, Raipur 492 010, India*

In order to provide an independent evidence that QSOs lying close to galaxies with very different redshifts are physically associated with the galaxies, Burbidge (1979) found that if  $\theta (< 1'')$  is the angular separation between such a QSO and a galaxy and  $z_g$  is the redshift of the galaxy then  $(\log \theta, \log z_g)$  pairs for a sample of such QSO-galaxy cases are statistically correlated and that the regression coefficient for linear regression of  $\log \theta$  on  $\log z_g$  is close to  $-1.0$  implying that these QSOs are physically associated with the galaxies and that the redshifts of such QSOs are largely non-cosmological. If this is indeed the case then  $[V_q, \log (cz_q)]$  plot for such QSOs should be a complete scatter diagram without any statistically significant correlation between  $V_q$  and  $\log (cz_q)$ . In order to test this we have considered a sample of 58 QSOs drawn from the catalogue of Hewitt & Burbidge (1980) such that  $\theta < 600''$  and  $(z_q - z_g) > 0.5$ . For this sample we have found that the correlation coefficient  $r = 0.56$  and that the correlation is statistically significant at 99% confidence level. However, regression coefficient for the linear regression of  $V_q$  on  $\log (cz_q)$  is  $b = 3.72 \pm 0.09$  which is not consistent, at 99% confidence level, with the value of 5.0 expected theoretically if the redshifts of these QSOs are cosmological. But such a sample, being magnitude limited, suffers from the well-known Malmquist bias. On removing this we get a sub-sample of 31 QSOs for which  $r = 0.85$  and  $b = 4.86 \pm 0.11$ . Thus we find that the correlation between  $V_q$  and  $\log (cz_q)$  for these QSOs is statistically significant at 99% confidence level and that the departure of 'b' from the theoretically expected value of 5.0 (if the redshifts of the QSOs are cosmological) is not statistically significant at 95% confidence level. Thus our results raise doubts about the reality of the physical association between such close pairs of QSOs and galaxies.

**References**

Burbidge, G. R. 1979, *Nature*, **282**, 451.  
Hewitt, A., Burbidge, G. R. 1980, *Astrophys. J. Suppl. Ser.*, **43**, 1.



## The Quasar-Galaxy Pair 3C 232/NGC 3067

P. K. Das *Indian Institute of Astrophysics, Bangalore 560034, India*

An explanation for the observed bridge of matter apparently connecting the spiral NGC 3067 and the quasar 3C 232 is sought in terms of a model for the anomalous redshift for quasars put forward by Narlikar and Das which is based on the Machian theory of gravitation of Hoyle and Narlikar. In this scenario the high redshift quasar is hypothesised to have been 'born' in and ejected from the nucleus of the associated low redshift parent galaxy. The quasar has an anomalous redshift component and the particle masses in it grow with time. It is shown that by a suitable choice of initial conditions the observed configuration of 3C 232 and NGC 3067 can be achieved. Further the other observed features such as low redshift emission and absorption features associated with the quasar and the severely disturbed state of the galaxy can be qualitatively accounted for in this scenario.

★ ★ ★ ★ ★

## Dark Matter Around Binary Galaxies: Disruption of Shells and Formation of Flows

J. Anosova & B. Anandarao *Physical Research Laboratory, Ahmedabad, India*

We study the dynamics of extended shells around binary systems by computer simulations in the framework of the restricted three-body problem.

We consider superpositions of many initial conditions for this problem. Initially the zero-mass particles are distributed uniformly randomly on a sphere with a radius  $R$  and have the same radial velocities  $V$  with respect to the centre of mass of a binary. The components of a binary with masses  $M_1$  and  $M_2$  move in a circular orbit.

We apply this model to galaxy binary systems surrounded by shells containing small mass particles (e.g. a shell may consist of particles of dark matter – massive black holes, globular clusters, molecular clouds etc.). We consider the model of cosmological expansion of a shell with different radial velocity.

It is shown, that initially a shell extends homogeneously, later the particles rest; after this they come back, zones of compressed matter is then formed. At some moment we have collapse of these particles. They approach with big-mass components of binaries: all matter there is inside binary system. After this numerous particles quickly escape from the system. We consider five models with different values of parameters: the masses  $M_1$  and  $M_2$  of the members of binaries, radius  $R$  of shells around them, and the initial velocity  $V$  of zero-mass particles.

For models with small  $R$  and  $V$ , about half of particles escape from the system. For large values of  $R$  and  $V$  the shell is completely disrupted. The escaped particles form a wide flow. The position of the flow and the direction of motion of the zero-mass particles depend on the position of the big-mass bodies at the moment of closest approach of the bodies as well as on a ratio of their masses. In the model with the equal-

mass components of a binary, we find that most particles do not escape from the system but form the strong stable flow crossing the centre of inertia of a binary. The resulting flows move mainly in the plane of orbit of galaxy binary.

**Key words:** Dark matter -- binary systems -- shells -- flows.

\*\*\*\*\*

## Cosmological Limits on the Detection Range of the TeV $\gamma$ -ray Telescope 'TACTIC'

A. K. Mitra & C. L. Bhat *Bhabha Atomic Research Centre, Nuclear Research Laboratory, Trombay, Bombay 400 085, India.*

We are presently engaged in building a high-sensitivity VHE  $\gamma$ -ray telescope, TACTIC, for carrying out detailed studies of cosmic  $\gamma$ -ray sources in the energy bracket 0.2–10 TeV (Bhat *et al.* 1993a, 1993b). A Crab Nebula-like d.c. signal (CRAB) can be detected at the  $5\sigma$ -significance level in under 1 hour of observations, while a signal, a factor of  $\sim 50$  weaker, can be recovered with the same confidence level in  $\sim 200$  h.

The high-energy  $\gamma$ -ray experiment EGRET on board the Compton Observatory has so far detected at least 16 active galaxies (Fitchell 1993). Of these, 2 objects have a red-shift  $< 0.2$ , while 14 others have  $z$  between 0.54–2.17. Only one BL-Lac object, MK-421, ( $z = 0.03$ ), has so far been detected in the VHE region, while brighter (and more distant), high-energy EGRET sources have so far eluded detection at higher energies (Punch *et al.* 1992). One plausible explanation for this apparently contradictory behaviour is that the TeV signals from these sources suffer significant attenuation due to recessional effects and  $\gamma$ - $\gamma$  interactions with the optical/infrared photon fields in the metagalactic space (Stecker *et al.* 1992). In view of this possibility, it is desirable that an estimate be made of the cosmological detection capability of TACTIC also.

For this, we closely follow the treatment given by Stecker *et al.* (1992). For the model of the universe with  $\Omega = 1$  and incorporating similar values for other parameters, we parameterize the optical thickness for attenuation of a photon of energy  $E_\gamma$  as

$$\tau = n \left[ \frac{E_\gamma}{0.5 \text{ TeV}} \right]^{1.55} [(1+z)^{4.8} - 1], \quad (1)$$

where  $n$  has a value between 0.16 and 0.40, depending upon the actual value of the metagalactic infra-red photon field density. Assuming the cosmic source to have a  $\gamma$ -ray luminosity of  $L_\gamma$  in the (0.5–5 TeV) band with a power law index  $= 2.0$ , the photon flux recorded by a detector with threshold 0.5 TeV may be written as

$$F_\gamma \approx \frac{L_\gamma}{4\pi d^2} \frac{1}{(1 \text{ TeV})} \int_{0.5 \text{ TeV}}^{5 \text{ TeV}} e^{-\tau(E)} dE_\gamma, \quad (2)$$

where the luminosity distance  $d(\Omega = 1)$  may be written as

$$d = 8000 [(1+z) - \sqrt{1+z}] \text{ Mpc}, \quad (3)$$

Now assuming a canonical value of  $L_\gamma = 10^{45} \text{ erg s}^{-1}$ , from the foregoing equations, we

find that TACTIC, with its minimum detectable value of  $F_\gamma = 1.4 \times 10^{-12} \text{ cm}^{-2} \text{ s}^{-1}$  (0.02 Crab), would be able to probe upto  $z \approx 0.21 - 0.275$  ( $d \approx 900 - 1200 \text{ Mpc}$ ). There are only two known  $\gamma$ -ray-loud galaxies lying within this range of  $z$ , and, therefore, serious thought needs to be given to extend this range further by working at a lower threshold energy ( $\sim 0.1 \text{ TeV}$ ) without compromising on the background rejection capability of TACTIC.

### References

- Bhat, C. L. *et al.* 1993a, This proceedings.  
 Bhat, C. L. *et al.* 1993b, *Proc. 'Towards a Major Atmospheric Cerenkov Detector-II'*, Calgary, (in press).  
 Fitchel, C. E. 1993, preprint no. 93-39, NASA, GSFC, Maryland.  
 Punch, M. *et al.* 1992, *Nature*, **358**, 478.  
 Stecker, F. W. *et al.* 1992, *Astrophys. J.*, **390**, L49.

★ ★ ★ ★ ★

### Assessing Fluctuations Using Small Samples

D. G. Banhatti *School of Physics, Madurai-Kamaraj University, Madurai 625 021, India*

I discuss the assessment of fluctuations for their deviation from the mean of a small statistical sample, with an example of counting radio sources in the sky. If the fluctuation being assessed is large, one may exclude it in calculating the sample mean and standard deviation (or rms). To look for a fluctuation comparable to the sample rms, excluding it from the mean and rms calculation is a biased procedure. For a sample of size  $N$ , the maximum any instance can deviate from the mean in units of the rms is  $(N-1)/N^{1/2}$ . Thus, for example, it is not correct to talk of a  $3\sigma$  deviation for an instance in a sample of 10, since the maximum possible deviation is only  $2.85\sigma$ . Also, the assessment of a given deviation using the  $\chi^2$  test is valid only for sufficiently large  $N$ , so that the underlying population may be approximated to normal (i.e., Gaussian). To assess fluctuations in a small sample of a normally distributed random variable, the following question must be answered: If  $x$  is normally distributed, what is the distribution of the deviation of a single instance, say  $x_j$ , from the mean  $\langle x \rangle$  of a sample of size  $N$  (containing  $x_j$ ) in units of  $s \equiv [\sum_{i=1}^N (x_i - \langle x \rangle)^2 / (N-1)]^{1/2}$ ? In other words, what is the distribution of the sample statistic  $\delta_j \equiv (x_j - \langle x \rangle)/s$ ?

★ ★ ★ ★ ★

### Large Scale Structure of the Universe: Cluster-Void Fine Structure

J. Anosova, S. Iyer & R. K. Varma *Physical Research Laboratory, Ahmedabad, India*

Using the objective criterion developed by one of the authors (Anosova 1987) we carry out a statistical clustering analysis of the distribution of galaxies. We consider an area

of the sky with coordinates approximately given by  $0^\circ < \alpha < 1^\circ$  and  $-90^\circ < \delta < +90^\circ$ , and study a distribution of galaxies in the CFA-Catalogue. The number of galaxies with known redshifts inside this area is 115.

We identify the confident and probable non-chance galaxy groups and clusters on the whole and their components as well as probable and confident chance ones. For every galaxy we define the probability that this galaxy belongs to a cluster or it is a single (isolated) object of the field. We have found 19 confident and probable galaxy groups with multiplicity  $n < 7$  and with physical connection of members, one 'super-cluster' with  $n = 31$  containing a few small clusters. 75.0% of the galaxies under study are members of these clusters. The other 29 galaxies in the field are confident single ones, 15 of them have nearest neighbours with confident or probable chance connection. The average confidence level for determining the members of the galaxy clusters is  $P_{\text{rch}} = 0.932 \pm 0.067$ ; and for voids it is  $P_{\text{rch}} = 0.995 \pm 0.014$ .

It is shown that between all clusters and single galaxies there are confidently determined empty regions (voids). We also found two confident non-chance compact galaxy groups with large differences of radial velocities for their members, approximately 2000 km/s. For every cluster and the sample of single galaxies we define the average values of basic characteristics.

Therefore, we conclude that in the examined part of the Universe the normal galaxy field with randomly distributed galaxies does not exist. We obtain here the cluster-void structure of the Universe. Sometimes we observe in the field one or a few close clusters, connected with each other; sometimes we observe one or two single galaxies. Between these clusters and single galaxies we have voids with an average confidence level  $P_{\text{rch}} = 0.987 \pm 0.028$ .

*Key words:* Galaxy distribution functions—galaxy clusters—voids—chance and non-chance groups.

★★★★★

## Cosmographic Methods

D. G. Banhatti *School of Physics, Madurai-Kamaraj University, Madurai 625 021, India*

Cosmographic methods are surveyed, giving examples of results on the large-scale structure in the universe using these methods. Showing structure upto few 100 Mpc, the distribution of light tends to uniform random (i.e. Poisson) beyond that scale. In particular, binning or counting radio sources to estimated depths  $z < 1$  shows uniform random distribution, confirmed by power-spectrum analysis and its Fourier dual method of covariance function analysis (or use of two-point correlation functions) on radio source surveys at similar depths and on angular scales from tenths of a degree to tens of degrees. Shallower optical surveys (to  $z = 0.1$ ) show galaxies to be clustered, with the clusters arranged in sheetlike superclusters enclosing voids, the more distant voids being bigger. Percolation studies of these optical surveys of galaxies also bring out this structure of connected clusters. In projection, some of these sheets appear like filaments, whose 'objectivity' has been confirmed by graph theoretical methods. Probabilities of finding different numbers of objects in regions of a given size or of

finding a given number of objects in regions of different sizes, called distribution functions, can be compared with the predictions for relaxed gravitational clustering to determine the ratio of the gravitational correlation energy to the kinetic energy of peculiar motion, the expected ratio being zero for no clustering (i.e., uniform random distribution) and 2 if all objects are clustered. Application to surveys to different depths gives  $1.40 \pm 0.05$  on 1 to 10 Mpc scales,  $0.58 \pm 0.08$  on 10 to 50 Mpc scales and  $0.02 \pm 0.01$  scales  $> 100$  Mpc, in consonance with results using other methods. Fractal geometry may be applied on these scales (i.e., from a few Mpc to a few 100 Mpc) to give a power-law of slope  $-1.7$  for the average density of visible matter against the averaging scale, consistent with the slope of the two-point correlation function, and giving the fractal dimension  $1.3 (= 3 - 1.7)$ . Deeper optical and radio surveys show that this hierarchical (or fractal) structure gives way to a uniform random distribution beyond a few 100 Mpc. Topological methods have shown that the galaxy distribution becomes less choppy (or smoother) when averaged over larger and larger volumes, in agreement with results using other methods. Currently available surveys of large-scale structure in the universe may be listed in order of increasing depth as Zwicky, CfA, Giovanelli and Haynes, Abell, QDOT/ QIGC, IRAS, APM, X-ray, radio and COBE; the last being a survey of the 2.73 K cosmic relic background radiation, the deepest possible that can be probed with photons.

★ ★ ★ ★ ★





# **Active Galactic Nuclei**



## Unified Schemes for Radio-loud Active Galactic Nuclei

Gopal-Krishna *National Centre for Radio Astrophysics, TIFR, Pune 411 007, India.*  
Also *Max-Planck-Institut f. Radioastronomie, D-53010 Bonn, Germany*

**Abstract.** We briefly review the background and the current observational framework of the unification scheme according to which classification of a radio-loud AGN is determined principally by its aspect. After summarizing the extensive observational support to the scheme, arising through different wavebands, we focus here on addressing certain questions and potential problems emerging from recent studies of powerful radio sources, involving the measurements of their radio sizes and VLBI polarimetry of their nuclear jets. Possible resolutions of these issues are discussed.

**Key words:** Radio galaxies – quasars – relativistic jets – blazars.

### 1. Introduction

In the simplest terms, an AGN is perceived to be a strong, essentially isotropic emitter of ionizing photons arising from dissipative processes within the disk of material being accreted towards the galactic centre. Both the featureless continuum (FC) of these photons and the surrounding broad-line-emitting region (BLR) ionized by them are believed to be directly observable in the case of AGN classified as quasars and Seyfert 1 galaxies (Antonucci 1993; Osterbrock 1993). Although such a gravitational engine can occur both in spiral and elliptical galaxies, the latter alone seem capable of ejecting energetic jet pair needed to produce giant, double-lobed radio sources (Blandford 1990; Bridle 1992). Broadly, such radio-loud AGN are classified as radio galaxies (RGs), quasars (QSRs) and blazars. Some proposals to relate (i.e., ‘unify’) them mainly through orientation effects are briefly discussed here (see, Antonucci 1993, for a detailed review and fuller literature coverage). Confining mainly to powerful radio sources, I aim to focus here on certain new issues arising from their radio observations. Recent reviews of the unified schemes for radio-weak AGN can be found in Osterbrock (1993), Antonucci (1993) and Wilson (1992).

### 2. Radio-loud AGN: Classification and phenomenology

Standard taxonomy of radio-loud AGN, which are  $\simeq 10\%$  of all AGN, enlists BL Lacs, core-dominated quasars (CDQs), lobe-dominated quasars (LDQs), broad-line radio galaxies (BLRGs) and narrow-line radio galaxies (NLRGs). Although radio-loud AGN, especially their radio-powerful subset characterized by a double-lobed radio morphology, are rather rare and remote, their accessibility through the additional (radio) window offers unique possibilities. These include the feasibility of imaging the

nuclear outflow (jets) and magnetic field configuration on the parsec scale by VLBI, as well as the availability of (statistical) orientation indicators for the large-scale radio structure, such as: lobe-separation, core-to-lobe flux ratio ( $R$ ), core polarization, jet-counterjet brightness ratio and lobe-depolarization asymmetry (section 3.2). Further, bright radio emission seems to be generic to rapidly varying AGN (e.g., Impey *et al.* 1991; Wills *et al.* 1992; Perlman & Stocke 1993). Known as blazars, such AGN are sub-classified as 'BL Lacs' if the optical emission lines are very weak (or, absent); otherwise, they are called 'optically-violently-variables (OVVs)', or 'Highly-polarized-quasars (HPQs)'. Indeed, most CDQs are now believed to be potential blazars (Fugmann & Meisenheimer 1988; Impey *et al.* 1991; Wills *et al.* 1992; Witzel *et al.* 1993).

Moderately powerful radio sources ( $\log P < 25.5 \text{ WHz}^{-1}$  at 1 GHz, taking  $H_0 = 50 \text{ km s}^{-1} \text{ Mpc}^{-1}$ ) are usually dominated by a roughly symmetric pair of jets broadening & fading away from the nucleus (FR1 type). Their luminous counterparts (FR2 type), i.e., powerful radio galaxies (PRGs) & quasars (QSRs), typically exhibit bright 'hotspots' near the extremities of their radio lobes (see, Bridle 1992).

Are the various classes of AGN physically different, or their diversity is merely a result of viewing the same type of objects from different directions? As discussed below, this urge to unify through orientation effects has been remarkably successful in stemming the tide of diversification. Some alternative, possibly viable scenarios for unification, invoking a temporal evolution of nuclear activity (Neff & Hutchings 1990), or a strong jet-environment interaction (Norman & Miley 1984), come out with less sharp verifiable predictions and are not discussed here.

### 3. Orientation-dependence: Obscuration and relativistic beaming

Two processes on the innermost parsec scale render the nuclear emission anisotropic:

- Obscuration of the nuclear FC and BLR by a dusty torus of cool gas (Antonucci 1984; Antonucci & Miller 1985; Krolik & Begelman 1986), or by a warped gaseous disk (Sanders *et al.* 1989)
- Relativistic beaming of the jet's nonthermal continuum (Blandford & Rees 1978).

#### 3.1 Some evidences for the obscuring tori in radio-loud AGN

- From spectro-polarimetry: An early evidence came from the NLRG 3C234 with the detection of FC and BLR emission strongly polarized perpendicular to the radio axis (in a frequency-independent manner). This and an analogous result for the narrow-line Seyfert NGC1068 were interpreted by postulating a quasar type nucleus whose FC and BLR emission is obscured by a surrounding dusty torus, but escapes through its polar openings (along the radio jets) and is then partly scattered towards us by thermal electrons (Antonucci & Miller 1985; Krolik & Begelman 1986). Similar evidence is now available for a few more NLRGs (Antonucci 1993).
- From imaging polarimetry: For several NLRGs, the rest-frame UV/optical/IR emission coming from the central parts, or from the off-nuclear patches is found to be substantially polarized perpendicular to the radio axis. This is expected in the

obscuring torus scenario (e.g., de Serego Alighieri *et al.* 1993; Tadhunter *et al.* 1992; Antonucci & Barvainis 1990).

■ From the deficit of ionizing photons: The extended emission-line region (EELR) in several NLRGs has been found to require for its excitation a nuclear UV source directing a much greater intensity towards the EELR than in our direction. This is consistent with the obscuring torus-cum-relativistic beaming model for the anisotropic nuclear continuum (e.g., Heckman *et al.* 1992).

### 3.2 Evidences for the relativistic jets in radio-powerful AGN

Although superluminally moving radio knots in the parsec-scale nuclear jets of powerful radio sources are a well known indicator of relativistic bulk motion (Lorentz factor  $\Gamma \gg 1$ ), several other evidences are now available:

- VLBI of a few blazars has yielded brightness temperatures of  $1 - 3 \cdot 10^{12}$  K (Linfield *et al.* 1990), i.e. well above the inverse Compton limit, thus requiring  $\Gamma \gg 1$ . Relativistic motion can also explain the enormous brightness temperatures ( $10^{16} - 10^{18}$  K) inferred for the intra-day variable blazars (Witzel *et al.* 1993).
- For the nuclear jets of many blazars,  $\Gamma \gg 1$  is also inferred from the apparent deficit of X-rays compared to the synchro-self-Compton flux densities predicted from the jets, assuming them to be stationary (Ghisellini *et al.* 1993).
- The observed intense and rapidly varying  $\gamma$  ray emission from several blazars mandates  $\Gamma \gg 1$  for the nuclear jets, or else the  $\gamma$  rays would be self-absorbed in photon-photon collisions (e.g., Dermer & Schlickeiser 1993).
- The strong anti-correlation observed for QSRs between the  $[OII]3727$  line equivalent-width and the radio core-to-lobe flux ratio ( $R$ ) argues for relativistic beaming of the nuclear optical continuum as well (Baker *et al.*, 1995, this volume, 185–188), since the  $[OII]3727$  line is isotropically emitted (Hes *et al.* 1993). The question whether  $R$  is indeed a statistical measure of relativistic beaming in the nuclei of powerful radio sources has been investigated in the past by looking for its anti-correlation with (i) linearity of the VLBI jet, (ii) overall radio size, and (iii) arm-length symmetry (see, Readhead *et al.* 1978; Hine & Scheuer 1980; Gopal-Krishna *et al.* 1980; Gopal-Krishna 1980). Such tests were carried out more effectively using large samples of QSRs (Kapahi & Saikia 1982; Browne & Perley 1986) and have indicated consistency with  $\Gamma \simeq 5$  estimated by Orr & Browne (1982) from the source counts of flat-spectrum QSRs (see, also, Kapahi & Kulkarni 1986).
- The apparent one-sidedness of the parsec-scale jets can be easily understood in terms of relativistic beaming. Furthermore, the strong tendency for both the parsec-scale and kiloparsec-scale jets to appear brighter on the same side of the nucleus argues for the relativistic bulk flow persisting out to kiloparsec-scale, at least in intrinsically powerful jets (Scheuer 1984; Bridle 1992).
- The case for relativistic beaming in kiloparsec-scale jets is further strengthened by the spectacular finding that in QSRs, the brighter appearing jet is nearly always on the side of the lobe which is less depolarized at long wavelengths (and is, thus, likely to be on the near side from us) (Garrington *et al.* 1988; Laing 1988).
- There is growing evidence that the optical (and also X-ray) emission from QSR nuclei consists of two components. Of these, one correlates strongly with the radio jet emission and should, likewise, be relativistically beamed (e.g., Impey *et al.* 1991; Wills *et al.* 1992; Kembhavi 1993).

#### 4. Steps towards the unification of radio-loud AGN

The abundant evidence for anisotropic nuclear radiation (section 3) implies that in any classification scheme for radio sources a key parameter to consider is the angular separation,  $\theta$ , between the line-of-sight and the principal axis of the source, defined by the jet/torus axis. In 1978, Blandford & Rees interpreted the extreme variability and core-dominance of BL Lacs by identifying them as the double sources whose jets are pointed nearly in our direction. This concept was expanded upon to 'unify' CDQs and LDQs, taking the latter to be the 'parent population' (Orr & Browne 1982; see Kapahi & Saikia 1982 for independent arguments) (section 3.2d). However, the presumed lack of orientation bias in this postulated parent population was questioned by the subsequent detection of: (i) unexpectedly large radio lobes associated with superluminal CDQs (Schilizzi & de Bruyn 1983; see, however, Antonucci 1993), (ii) large jet/counter-jet brightness asymmetry in every QSR, including the largest ones (Barthel *et al.* 1989), (iii) superluminal motion in the cores of even the largest known QSRs (Barthel *et al.* 1989; Porcas 1981), and (iv) a striking depolarization asymmetry of QSR radio lobes (Laing 1988; Garrington *et al.* 1988). The implied dearth of QSRs with jets near the sky plane paved the way for a more comprehensive unifying scheme (Barthel 1989; Scheuer 1987; Peacock 1987; Morisawa & Takahara 1987) in which the nuclear emission is anisotropized by the torus, too (section 3) and, furthermore, PRGs are perceived as the parent population of both QSRs and blazars. Two main versions of this scheme are:

##### 4.1 *The unified scheme for radio-mediocre sources (FR1 type)*

Consensus has increasingly favoured identification of the FR1 NLRGs as the misaligned BL Lacs. Firstly, the two are found to be statistically matched in terms of aspect-independent properties, such as the lobe radio emission, as well as the host galaxy's light and its cluster environment (Browne 1983; Antonucci & Ulvestad 1985; Ulrich 1989; Smith & Heckman 1990; Perlman & Stocke 1993; Falomo *et al.* 1993). Secondly, it was shown that the observed RLF of BL Lacs can be successfully modelled, starting with the RLF of the (randomly-oriented) FR1 NLRG population, taking a characteristic  $\Gamma \simeq 7$  (Urry *et al.* 1991). This implies a critical viewing angle  $\theta_* \simeq 10^\circ$  within which a FR1 NLRG would be identified as a BL Lac.

##### 4.2 *The unified scheme for high-luminosity radio sources (FR2 type)*

Here the alignment is postulated to improve along the NLRG(FR2)-LDQ-CDQ sequence. A modelling similar to the above yields  $\Gamma \simeq 11$  and  $\theta_* \approx 38^\circ$  and  $\approx 14^\circ$ , respectively for the LDQs and CDQs, taking PRGs (i.e., FR2-type NLRGs) as the parent population (Padovani & Urry 1992). The estimated critical angle of  $\approx 38^\circ$  for QSRs is close to  $\theta_* \approx 44^\circ$  estimated earlier by Barthel (1989) simply from the relative numbers of PRGs and QSRs at intermediate redshifts ( $0.5 < z < 1$ ) in the 3CRR sample where the sources have been selected by their lobe emission and are therefore expected to be almost randomly oriented. Interestingly, a similar value of  $\theta_*$  has recently been inferred also from radio variability (Lainela & Valtaoja 1993).

## 5. Consistency checks on the orientation-based FR2 unified scheme

### 5.1 Statistical properties related to the radio jets and lobes:

- Compared to PRGs of the same average lobe power, QSRs exhibit more prominent jets on all scales, relative to the lobes (e.g., Bridle 1992).
- Nuclear (VLBI) jets in LDQs exhibit slower motion than those in CDQs (Hough *et al.* 1993).
- Compared to QSRs, PRGs show a much weaker lobe depolarization asymmetry (Garrington & Conway 1991).
- Both PRGs and QSRs follow the same relationship between the EELR ([OIII] line) luminosity and intrinsic jet power (Rawlings & Saunders 1991).

### 5.2 Statistical clues arising from orientation-independent properties

- EELRs associated with  $z \simeq 0.5$  3CR PRGs and QSRs (matched in lobe radio power) are comparably luminous in the [OII]3727 line (Hes *et al.* 1993).
- Hosts: According to the most recent study, the host galaxies of PRGs and QSRs sampled near  $z \simeq 0.5$  are found to be statistically indistinguishable in optical luminosity (Veron-Cetty & Woltjer 1990). Likewise, the hosts of distant QSRs fall on the 'near-IR Hubble diagram' for PRGs (Lehnert *et al.* 1992). A mid-IR comparison of the 3CR QSRs and PRGs with  $z \simeq 1$  shows that the former are 2–3 times stronger, on average (Heckman *et al.* 1992). However, at these wavelengths the nuclear emission is expected to be anisotropic (Pier & Krolik 1993) and, hence, the above difference may not be intrinsic.
- The cluster environments around PRGs and QSRs are shown to be similar, at least upto  $z \simeq 0.6$  (Hill & Lilly 1991). Further, the galaxy 'companions' of the two seem to have similar luminosity functions (Smith & Heckman 1990).

## 6. Some major recent challenges to the FR2 unified scheme

From radio data, two potentially serious problems have been posed recently:

### 6.1 The linear size 'paradox'

The simple orientation-based unified scheme predicts that all those members of the PRG parent population would be classified as QSRs whose nuclear FC and BLR emission is directly visible to us, a condition fulfilled whenever the nuclear axis is pointed to within an angle  $\psi$  from the observer's direction,  $\psi$  being the typical half-angle of the viewing cone through the torus (Barthel 1989). Thus, for a flux-limited sample populated by randomly oriented FR2 sources with a characteristic value of  $\psi$ , one can predict both the number ratio ( $x$ ) of PRGs and QSRs, and the ratio ( $y$ ) of their observed median linear sizes ( $l$ ). For the FR2 subset of the 3CRR sample in the redshift range 0.5 to 1, the  $\psi \simeq 44^\circ$  inferred from the observed  $x = 2.6$ , predicts a  $y = 1.8$  which agrees with the observed  $y = 2.2 \pm 0.8$  (Singal 1993a; Barthel 1989). However, such a consistency is not found for  $z < 0.5$ , i.e., for intrinsically weaker 3CRR sources. The lower value of  $\psi (\simeq 36^\circ)$  inferred in their case (which presents a scenario whereby LDQs



would become increasingly rare among intrinsically weaker radio sources) predicts a  $y = 2.2$ , which is discrepant from the observed  $y = 1.3 \pm 0.3$ . This 'incompatibility' with the simple unified scheme has been highlighted by Singal (1993a) and Kapahi (1990). As a possible cause for this, we have indicated the unrealistic basic assumption that the radio jets remain perfectly aligned with the torus axis, all the way out to the hotspots (which define the radio axis). The predicted value of  $y$  would be  $\simeq 30\%$  lower (and, thus, consistent with the observations), if one allows for an average misalignment of  $20^\circ$  to  $30^\circ$  between the torus axis and the radio axis. Such a modest misalignment is expected on theoretical and observational grounds, except perhaps for extremely energetic jets (see, Gopal-Krishna *et al.* 1993).

Linear-size data for larger, *albeit* incomplete samples of powerful steep-spectrum radio sources have also been used to verify the unified scheme. As a supporting evidence, we thus found the upper envelopes of the  $l-z$  diagrams for PRGs and QSRs to show very similar slopes, after normalizing the radio sizes to a fixed radio luminosity ( $P$ ), assuming identical  $l-P$  dependences for PRGs and QSRs (Gopal-Krishna & Kulkarni 1992). This assumption is based on the observed similarities between their host galaxies, as well as their environments (section 5.2) (in case this assumption turned out to be flawed, the simple unified scheme would anyway lose its *locus standi* and all tests would be superfluous).

Further tests of the unified scheme using still larger samples have been reported in two recent papers where opposite conclusions have been reached, despite an unprecedentedly large coverage of the  $P-z$  plane (Singal 1993b, Nilsson *et al.* 1993). In contrast to Singal (though in conformity with the unified scheme), Nilsson *et al.* find no evidence that towards lower redshifts ( $z < 0.5$ ) QSRs begin to appear larger in radio size, compared to PRGs of the same average lobe power, or that the two show different  $l-P/z$  relationships. The contradictory outcomes of these two studies are probably rooted in the different sample selection procedures adopted, in particular, the emphasis of Nilsson *et al.* on preserving the morphological purity of the sample by excluding all sources whose existing maps do not show a clearly resolved FR2 structure. The extent of subjectivity introduced by this well meaning approach is unclear. In any case, the crucial requirement of clubbing *all* BLRGs with QSRs cannot be realized for either of these large samples, given the limited spectroscopic information available currently. The situation is expected to improve with the availability of a new Molonglo sample (Kapahi *et al.*, this volume).

## 6.2 The parsec-scale 'dichotomy' between the blazar subclasses

BL Lacs are often perceived as being, almost exclusively the aligned versions of low-power (FR1) radio galaxies (e.g., Murphy *et al.* 1993; Urry *et al.* 1991), while their powerful 'analogues', the HPQs, are thought to be the aligned subset of the PRG parent population. Recent work, however, has revealed distinctly FR2-type powerful radio lobes in a significant fraction of BL Lacs (Kollgaard *et al.* 1992). Such intrinsically powerful BL Lacs are then expected to be, together with HPQs, the closely aligned versions of the PRG parent population, with LDQs representing the cases of intermediate alignment. This important, seemingly natural extension of the FR2 unified scheme has been challenged by two recent findings:

- Polarimetric VLBI shows that whereas the magnetic field in the radio knots of even powerful BL Lacs is generally perpendicular to the jet, HPQs show no such trend

(Gabuzda *et al.* 1992). This has led to the claim that BL Lacs and HPQs are intrinsically different types of AGN (e.g., Kollgaard *et al.* 1992).

■ By comparing the predicted synchro-self-Compton X-ray flux with measurements, it is inferred that even in powerful BL Lacs, the jets have systematically lower Doppler factors compared to those in HPQs (see, Ghisellini *et al.* 1993).

We have recently argued that it is possible to reconcile both these results with the simple unified scheme by considering a physically plausible two-component model for the VLBI knots which are commonly identified with the planar shocks inside the relativistic jet flow (Gopal-Krishna & Wiita 1993). The two components are: (i) A front layer of freshly excited plasma of the shock-front (region A) where the magnetic field component perpendicular to the jet has been enhanced due to compression, and (ii) a second, much larger and roughly spherical region B with slightly lower  $\Gamma$  and diminished emissivity. The synchrotron plasma expands from region A backwards into region B and, thereby, a *partial realignment* of the magnetic field along the jet occurs. To observers located close to the jet direction, the strongly boosted region A with a higher  $\Gamma$  and perpendicular magnetic field configuration would appear to dominate (simulating the BL Lac characteristics). To somewhat less well-aligned observers, the substantially relaxed region B at the rear of the superluminal knot, with its lower  $\Gamma$  and hence a wider radiation pattern, would appear dominant (yielding the HPQ characteristics). Further, according to this picture, Ghisellini *et al.* (1993) would have systematically underestimated the Doppler factors for BL Lacs (section 6.2b) because of having assumed a spherical geometry for region A, which implies a much greater volume than the more plausible layer-like geometry. Another potential consequence of our model is that due to both  $\Gamma$  and magnetic field being lower in the region B, compared to region A, the synchrotron self-Compton X-ray flux would be enhanced relative to the softer-spectrum synchrotron X-rays. This could explain the tendency of HPQs to show a flatter X-ray spectrum, compared to BL Lacs (as reported by Worrall & Wilkes 1990).

## 7. Conclusions

To summarize, the simple orientation-dominated unified schemes for radio-loud AGN have been remarkably assertive of their strength in the face of the extensive, multi-wavelength verification campaign. The still unproven obscured quasar nucleus in Cyg-A continues to be an irritant (Jackson & Tadhunter 1993), though some evidence for it exists (Djorgovski *et al.* 1991). It is conceivable that physically meaningful refinements to these simple schemes will be mandated by increasingly subtle tests in future, not to mention the possibility of some major holes in the currently popular AGN paradigm itself (e.g., Kinney 1992; Fernandes & Terlevich 1993; Binette *et al.* 1993). Nonetheless, the mounting evidence that the diversity of AGN has been grossly exaggerated in the past constitutes a healthy prognosis for the future.

## References

- Antonucci, R. R. J. 1984, *Astrophys. J.*, **278**, 499.
- Antonucci, R. 1993, *A. Rev. Astr. Astrophys.*, **31**, 473.
- Antonucci, R., Barvainis, R. 1990, *Astrophys. J. Lett.*, **363**, L17.
- Antonucci, R., Miller, J. 1985, *Astrophys. J.*, **297**, 621.

- Antonucci, R., Ulvestad, J. 1985, *Astrophys. J.*, **294**, 158.
- Barthel, P. D., Hooimeyer, J. R., Schilizzi, R. T., Miley, G. K., Preuss, E. 1989, *Astrophys. J.*, **336**, 601.
- Barthel, P. D. 1989, *Astrophys. J.*, **336**, 606.
- Binette, L., Fosbury, R., Parker, D. 1993, *Publ. astr. Soc. Pacific*, **105**, 1150.
- Blandford, R. D. 1990, in *Active Galactic Nuclei*, Eds T. J. -L. Courvoisier & M. Mayor (Springer-Verlag), p. 161.
- Blandford, R. D., Rees, M. J. 1978, in *Proc. Pittsberg Conf. on BL Lacs*, Ed. A. M. Wolfe (Pittsberg University Press), p. 328.
- Bridle, A. H. 1992, in *Testing the AGN Paradigm*, Eds S. Holt, S. G. Neff & C. M. Urry (AIP), p. 386.
- Browne, I. W. A. 1983, *Mon. Not. R. astr. Soc.*, **204**, 23.
- Browne, I. W. A., Perley, R. A. 1986, *Mon. Not. R. astr. Soc.*, **222**, 149.
- Dermer, C. D., Schlickeiser, R. 1993, *Astrophys. J.*, **416**, 458.
- di Serego Alighieri, S., Cimatti, A., Fosbury, R. 1993, *Astrophys. J.*, **404**, 584.
- Djorgovski, S., Weir, N., Matthews, R., Graham, J. 1991, *Astrophys. J. Lett.*, **372**, L67.
- Falomo, R., Pesce, J. E., Treves, A. 1993, *Astr. J.*, **105**, 2031.
- Fernandes, R. C., Terlevich, R. 1993, *Astrophys. Space Sci.*, **205**, 91.
- Fugmann, W., Meisenheimer, K. 1988, *Astr. Astrophys. Suppl.*, **76**, 145.
- Gabuzda, D. C., Cawthorne, T. V., Roberts, D. H., Wardle, J. F. C. 1992, *Astrophys. J.*, **388**, 40.
- Garrington, S. T., Leahy, J. P., Conway, R. G., Laing, R. A. 1988, *Nature (London)*, **331**, 147.
- Garrington, S. T., Conway, R. 1991, *Mon. Not. R. astr. Soc.*, **250**, 198.
- Ghisellini, G., Padovani, P., Celotti, A., Maraschi, L. 1993, *Astrophys. J.*, **407**, 65.
- Gopal-Krishna 1980, *Astr. Astrophys.*, **86**, L1.
- Gopal-Krishna, Kulkarni, V. K. 1992, *Astr. Astrophys.*, **257**, 11.
- Gopal-Krishna, Kulkarni, V. K., Mangalam, A. V. 1993, *Mon. Not. R. astr. Soc.*, in press.
- Gopal-Krishna, Preuss, E., Schilizzi, R. T. 1980, *Nature (London)*, **288**, 344.
- Gopal-Krishna, Wiita, P. J. 1993, *Nature (London)*, **363**, 142.
- Heckman, T. M., Chambers, K. C., Postman, M. 1992, *Astrophys. J.*, **391**, 39.
- Hes, R., Barthel, P. D., Fosbury, R. A. E. 1993, *Nature (London)*, **362**, 326.
- Hill, G. J., Lilly, S. J. 1991, *Astrophys. J.*, **367**, 1.
- Hine, R. G., Scheuer, P. A. G. 1980, *Mon. Not. R. astr. Soc.*, **193**, 285.
- Hough, D. H., Vermeulen, R. C., Readhead, A. C. S. 1993, in *Subarc-second Radio Astronomy*, Eds R. J. Davis & R. S. Booth (Cambridge University Press), p. 193.
- Impey, C. D., Lawrence, C. R., Tapia, S. 1991, *Astrophys. J.*, **375**, 46.
- Jackson, N., Tadhunter, C. N. 1993, *Astr. Astrophys.*, **272**, 105.
- Kapahi, V. K. 1990, in *Parsec-scale Radio Jets*, Eds J. A. Zensus & T. J. Pearson (Cambridge University Press), p. 304.
- Kapahi, V. K., Saikia, D. J. 1982, *J. Astrophys. Astr.*, **3**, 465.
- Kapahi, V. K., Kulkarni, V. K. 1986, in *IAU Symp. No. 124 "Quasars"*, Eds G. Swarup & V. K. Kapahi (Dordrecht: D. Reidel), p. 207.
- Kapahi, V. K., Athreya, R. M., Subrahmanya, C. R., Hunstead, R. W., Baker, J. C., McCarthy, P. J., van Breugel, W. 1995, *J. Astrophys. Astr. Suppl.*, **16**, 125-130.
- Kembhavi, A. 1993, *Mon. Not. R. astr. Soc.*, **264**, 683.
- Kinney, A. L. 1992, in *Testing the AGN Paradigm*, Eds S. S. Holt, S. G. Neff & C. M. Urry (AIP), p. 139.
- Kollgaard, R. I., Wardle, J. F. C., Roberts, D. H., Gabuzda, D. C. 1992, *Astr. J.*, **104**, 1687.
- Krolik, J., Begelman, M. 1986, *Astrophys. J. Lett.* **308**, L55.
- Lainela, M., Valtaoja, E. 1993, *Astrophys. J.*, **416**, 485.
- Laing, R. A. 1988, *Nature (London)*, **331**, 149.
- Lehnert, M., Heckman, T., Chambers, K. C., Miley, G. K. 1992, *Astrophys. J.*, **393**, 68.
- Linfield, R. P., Levy, G., Edwards, C., Ulvestad, J., Ottenhoff, C. 1990, *Astrophys. J.* **358**, 350.
- Morisawa, K., Takahara, F. 1987, *Mon. Not. R. astr. Soc.*, **228**, 745.
- Murphy, D. W., Browne, I. W. A., Perley, R. A. 1993, *Mon. Not. R. astr. Soc.*, **264**, 298.
- Neff, S. G., Hutchings, J. 1992, *Astr. J.*, **100**, 1441.
- Nilsson, K., Valtonen, M., Kotilainen, J., Jaakkola, T. 1993, *Astrophys. J.*, **413**, 453.
- Norman, C., Miley, G. K. 1984, *Astr. Astrophys.*, **141**, 85.

- Orr, M., Browne, I. W. A. 1982, *Mon. Not. R. astr. Soc.*, **200**, 1067.
- Osterbrock, D. E. 1993, *Astrophys. J.*, **404**, 551.
- Padovani, P., Urry, C. M. 1992, *Astrophys. J.*, **387**, 449.
- Peacock, J. 1987, in *Astrophysical Jets and Their Engines*, Ed W. Kundt (Dordrecht: Reidel), p. 185.
- Perlman, E. S., Stocke, J. T. 1993, *Astrophys. J.*, **406**, 430.
- Pier, E. A., Krolik, J. 1993, preprint.
- Porcas, R. W. 1981, *Nature (London)*, **294**, 47.
- Rawlings, S., Saunders, R. 1991, *Nature (London)*, **349**, 138.
- Readhead, A. C. S., Cohen, M., Pearson, T., Wilkinson, P. 1978, *Nature (London)*, **276**, 768.
- Sanders, D., Phinney, E., Neugebauer, G., Soifer, B., Matthews, K. 1989, *Astrophys. J.*, **347**, 29.
- Scheuer, P. A. G. 1984, in *Proc. IAU Symp. No. 110*, p. 197.
- Scheuer, P. A. G. 1987, in *Superluminal Radio Sources*, Eds J. Zensus & T. J. Pearson (Cambridge University Press), p. 104.
- Schilizzi, R., de Bruyn, A. 1983, *Nature (London)*, **303**, 26.
- Singal, A. K. 1993a, *Mon. Not. R. astr. Soc.*, **262**, L27.
- Singal, A. K. 1993b, *Mon. Not. R. astr. Soc.*, **263**, 139.
- Smith, E. P., Heckman, T. M. 1990, *Astrophys. J.*, **348**, 38.
- Tadhunter, C., Scarrott, S., Draper, P., Rolph, C. 1992, *Mon. Not. R. astr. Soc.*, **256**, 53p.
- Ulrich, M. H. 1989, in *BL Lac Objects*, Ed L. Maraschi, T. Maccacaro & M. H. Ulrich (New York: Springer), p. 45.
- Urry, C. M., Padovani, P., Stickel, M. 1991, *Astrophys. J.*, **382**, 501.
- Veron-Cetty, M. P., Woltjer, L. 1990, *Astr. Astrophys.*, **236**, 69.
- Wills, B., Wills, D., Breger, M., Antonucci, R., Barvainis, R. 1992, *Astrophys. J.*, **398**, 454.
- Wilson, A. S. 1992, in *Physics of Active Galactic Nuclei*, Eds W. J. Duschl & S. J. Wagner (Springer-Verlag), p. 307.
- Witzel, A., Wagner, S., Wegner, R., Steffen, W., Krichbaum, T. 1993, in *Subarcsecond Radio Astronomy*, Eds R. J. Davis & R. S. Booth (Cambridge University Press), p. 159.
- Worrall, D., Wilkes, B. 1990, *Astrophys. J.*, **360**, 396.



## Neutral Hydrogen 21 cm Quasar Absorption Line Systems

C. L. Carilli *National Radio Astronomy Observatory, P.O. Box O, Socorro, NM, 87801*  
and *Sterrewacht Leiden, Postbus 9513, RA 2300 Leiden, Nederland*

**Abstract.** Studies of redshifted neutral hydrogen 21 cm absorption towards radio loud quasars are reviewed.

**Key words:** Quasars – absorption lines – neutral Hydrogen.

### 1. Introduction

Observations of redshifted 21 cm absorption towards quasars and AGN has contributed in a unique way to our understanding of many astrophysical questions, including: the formation and evolution of galaxies, the physical conditions in diffuse gas in nearby and distant galaxies, and the origin of heavy element quasar absorption line systems in general. The most recent review of this topic was by Briggs (1988). This review will follow along the lines of that by Briggs, with an emphasis on results since 1988.

The 21 cm absorbers are at the high end of the column density distribution function for quasar absorption line systems, with typical values of  $N(\text{HI}) \geq \text{few} \times 10^{19} \text{ cm}^{-2}$  (Tytler 1987; Lanzetta *et al.* 1991). For comparison, the Ly  $\alpha$  forest lines correspond to  $N(\text{HI}) = 10^{13} - 10^{17} \text{ cm}^{-2}$ , and the MgII and Ly limit systems correspond to  $N(\text{HI}) \geq 10^{17} \text{ cm}^{-2}$ . Values of  $N(\text{HI}) \geq \text{few} \times 10^{19} \text{ cm}^{-2}$  are also indicative of the damped Ly  $\alpha$  absorbers, and of absorption by low ionization states of cosmically less abundant ions, such as CaII and NaI. These high column density absorbers are relatively rare: there is roughly one absorption system between  $10^{19} - 10^{20} \text{ cm}^{-2}$  for every 500 systems between  $10^{13} - 10^{14} \text{ cm}^{-2}$  (Tytler 1987).

Although rare, the 21 cm absorbers provide a number of unique tools for studying quasar absorption lines. First, radio observations typically are made with velocity resolutions of order  $1 \text{ km sec}^{-1}$ , or two orders of magnitude higher than most optical spectroscopic studies. Hence, 21 cm observations allow for a study of the detailed kinematics of the absorbing clouds. Second, radio interferometry allows for resolutions ranging from arcseconds down to milliarcseconds. Coupled with the fact that the background radio sources typically have structure from pc to kpc scales, 21 cm observations then provide the best opportunity for studying the spatial structure of the absorbing clouds. Lastly, comparison of column densities derived using 21 cm observations with those derived from other means provides an estimate of the spin temperature,  $T_s$ , of the gas (cf. Dickey & Lockman 1990). For most astrophysical circumstances  $T_s$  is a good estimate of the gas kinetic temperature (Field 1959a), although the possibility of departures of  $T_s$  from the kinetic temperature have been discussed for regions of very low density (Field 1959b) and for regions of intense radiation (Wolfe *et al.* 1982).

Neutral hydrogen 21 cm absorption through the optical disks of nearby spiral galaxies (i.e.  $z \leq 0.15$ ) has been studied extensively. This includes study of gas in our own galaxy (cf. Dickey & Lockman 1990), study of associated absorption towards low

$z$  AGN (e.g. van Gorkom *et al.* 1989; Dickey 1986; Schmelz *et al.* 1986), and study of disk gas in a few nearby spiral galaxies using background radio sources (e.g. Dickey *et al.* 1992; Braun & Walterbos 1992). Likewise 21 cm emission searches towards low  $z$  Ly  $\alpha$  forest systems (van Gorkom *et al.* 1993), intermediate  $z$  MgII systems (Yanny *et al.* 1993), and at very high redshifts (Wieringa *et al.* 1992; Uson *et al.* 1991) are in progress. A complete review of all these studies is beyond the scope of this paper. Herein we concentrate on absorption by the higher  $z$  systems ( $z \geq 0.25$ ), and by intervening low  $z$  systems in which the absorbing gas is well outside the optical disk of the parent galaxy.

Table 1 is an updated version of the list of 21 cm quasar absorption lines listed in Briggs (1988). Multiple systems are listed as  $N \times \Delta v$ , where  $N$  is the multiplicity,  $\Delta v$  is the typical width of the components. The total velocity spread is listed parenthetically. The reference numbers are listed at the end of the paper, and systems previously listed in Briggs (1988) are referenced as such. The highest  $z$  system (towards 0902 + 343) is an absorbing cloud associated with a radio galaxy, and hence is not really in line with this review. However, it is an object of current interest and hence has been included in the list along with appropriate references.

There are a number of methods which have been used to select targets for 21 cm absorption searches. A standard approach is to target known optical heavy element systems. The ground-based 'optical window' then implies the selection of CaII systems at low  $z$  ( $0 \leq z \leq 1.3$ ), MgII systems at intermediate  $z$  ( $0.4 \leq z \leq 2.2$ ), and damped Ly  $\alpha$  systems at high  $z$  ( $z \geq 2$ ). The 'detection efficiency' of 21 cm absorption for systems selected using the different ion species is clearly going to be different: only  $\approx 10\%$  of the MgII systems show 21 cm absorption when searched to optical depths of a few percent (Briggs & Wolfe 1983), while for damped Ly  $\alpha$  systems with columns  $\geq 10^{21} \text{ cm}^{-2}$  the efficiency is 100% (Briggs 1988). The CaII systems show a similarly high detection efficiency, although the availability of sensitive receivers in the lower  $z$  range makes for somewhat deeper searches towards the CaII systems (Carilli & van Gorkom 1992). Other methods include: blind searches in redshift (Brown & Fisher 1993), observing quasar-galaxy pairs (Boisse *et al.* 1988; Womble 1992; Corbelli & Schneider 1990), and observing red gravitational lenses (see below).

## 2. On the parent objects

The low  $z$  (CaII) systems are important since they provide the most direct means of studying the parent galaxy with which the absorbing clouds are associated, and the relationship between the clouds and the galaxies. These low  $z$  systems had often been used as examples of absorption by gas clouds in the 'halos' of spiral galaxies (cf. Boksenberg & Sargent 1978). Subsequent deep imaging in the optical and in HI 21 cm emission have shown that the parent galaxies of the low  $z$  21 cm absorption line systems are gravitationally disturbed galaxies, and that the extended gas seen in absorption towards the quasars results directly from these tidal disturbances (Carilli & van Gorkom 1992; Sargent & Steidel 1990). In retrospect this conclusion is not surprising since these systems were selected for having cool gas well outside the optical parent galaxies (as seen in absorption). Observations of the HI emission from nearby spiral galaxies show that the neutral hydrogen extent in galaxies is a strong function of environment: galaxies in mergers, pairs, or small groups typically have large cross sections, while isolated spirals and galaxies in dense clusters have small HI sizes. The

Table 1. The 21 cm absorbers.

Source	$Z_Q$	$Z_A$	$N(\text{HI})$ $10^{18} T_s \text{ cm}^{-2}$	$T_s$ K	FWHM $\text{km sec}^{-1}$	Method of selection	Reference
0959 + 685	0.773	-0.00047	0.13	< 90	2	CaII	1
3C275.1	0.557	0.0021	0.07	< 530	5	QG pair	4
3C368.4	1.4	0.0033	2		$2 \times 30$ (180)	QG pair	2
3C232	0.513	0.0047	0.21	< 300	3.6	QG pair	3
1327 - 206	1.17	0.018	0.36	240	$2 \times 10$ (250)	CaII	5
2020 - 370	1.050	0.029	0.40	700	10	CaII	3
0248 + 430	1.316	0.051	1.2		44	CaII	6
1413 + 135	?	0.245	13		18	Grav. Lens?	7
1229 - 021	1.038	0.395	3		12	MgII	3
3C196	0.871	0.437	4		40	21 cm	3
0235 + 164	0.94	0.524	30		$5 \times 8$ (120)	MgII	3
0218 + 357	0.94?	0.685	4		43	Grav. Lens	8
3C286	0.849	0.692	3		9	21 cm	3
1331 + 170	2.081	1.776	2.7	1000	20	Ly $\alpha$	3
1157 + 014	1.986	1.944	20	1500	42	Ly $\alpha$	3
0458 - 020	2.286	2.038	20	600	$2 \times 8$ (30)	Ly $\alpha$	3
0902 + 343	3.395	3.597	4.4		270	21 cm	9, 10



general point can be made that quasar absorption line systems provide a cross-section weighted view of objects in the universe, and for the nearby universe, the galaxies of largest cross section are gravitationally interacting systems.

The intermediate  $z$  (MgII) systems are distant enough that direct study of the parent galaxies is difficult. The 'classic' paper which attempted to interpret the 21 cm systems in the general context of the MgII systems was by Briggs & Wolfe (1983). They hypothesized a 'two-phase' model for absorption by spiral galaxies: a cold, quiescent disk of dimension similar to the optical disk, embedded in a warm, turbulent halo with a radius a few times that of the optical disk. Lines-of-sight through just the halo give rise to MgII absorption, while those through the disk and the halo give rise to both MgII and 21 cm absorption. This model explains in a neat way both the relative statistics of MgII and 21 cm absorption (see above), and the different velocity structures: the 21 cm lines are typically narrow ( $\leq 40 \text{ km sec}^{-1}$ ), while the large equivalent widths observed for the saturated MgII lines imply multiple components typically spread over  $> 100 \text{ km sec}^{-1}$ . Follow-up optical imaging and spectroscopy of the parent objects of these systems has basically been consistent with this simple picture (Bergeron & Boisse 1991). However room remains for a contribution to the statistics by clusters of gas rich, star forming dwarf galaxies (Yanny *et al.* 1990), and the lack of such extended halos of absorbing clouds around nearby galaxies, including our own, requires that there must be significant evolution in the nature of galaxy halos from intermediate to low  $z$  (Bergeron & Boisse 1991). Also, parallel studies have shown that not all galaxies at intermediate redshifts have such halos of absorbing clouds, and hence that the statistics may be different than originally proposed (Bechtold & Ellingson 1992).

The highest  $z$  systems (damped Ly  $\alpha$ ) probe physical conditions when the universe was less than 1/5 its present age. Hence, dramatic evolutionary effects may be invoked. Wolfe (1988) has proposed that the damped Ly  $\alpha$  systems arise in gas in 'proto-disk galaxies', with radii roughly a factor of two larger than present day spirals, which eventually evolve into the spiral galaxies seen today. This conclusion is based on a number of facts. First, the column densities implied are comparable to lines-of-sight through the disks of spiral galaxies. Second, the statistics require absorbers larger than present day spirals. And third, the implied cosmic mass density in the damped Ly  $\alpha$  systems at  $z > 2$  is comparable to that in luminous matter in the disks of present day spirals:  $\Omega \approx 0.0014 h^{-1}$  (Lanzetta *et al.* 1991). To date, the only direct supporting evidence for the proto-disk hypothesis is a VLBI observation of redshifted 21 cm absorption associated with the damped Ly  $\alpha$  system at  $z = 2.038$  towards 0458+020 by Briggs *et al.* (1989). Using the Arecibo-to-Greenbank interferometer, Briggs *et al.* (1989) were able to set a lower limit to the size of the absorbing cloud of  $\approx 8 h^{-1} \text{ kpc}$ , based on the similarity of the single dish and interferometric absorption profiles towards this extended radio source. This fact, coupled with the narrow line widths, implies that the cloud cannot support itself as a spherical, virialized system. They hypothesize a flattened, rotating gas distribution, i.e. a 'proto-disk'. This fundamental conclusion is based on a single visibility, and hence is inherently ambiguous. More complete VLBI imaging in the redshifted 21 cm line of this and other such systems is in order.

### 3. Physical conditions

The equations for converting observed line parameters such as FWHM ( $\Delta v$  in

km sec<sup>-1</sup>), peak optical depth ( $\tau$ ), rest frame equivalent width (EW in Angstroms), or surface brightness ( $I$  in Jy arcsecond<sup>-2</sup>), to HI column density ( $N(\text{HI})$  in cm<sup>-2</sup>), for various observing techniques are:

$$21 \text{ cm absorption: } N(\text{HI}) = 1.8 \times 10^{18} T_s \tau \Delta r$$

$$21 \text{ cm emission: } N(\text{HI}) = 1.3 \times 10^{24} I \Delta r$$

$$\text{damped Ly } \alpha \text{ absorption: } N(\text{HI}) = 1.9 \times 10^{18} \text{EW}^2$$

$$\text{normal Ly } \alpha \text{ absorption: } N(\text{HI}) = 7.6 \times 10^{11} \tau \Delta r.$$

The  $T_s$  dependence for  $N(\text{HI})$  derived from 21 cm absorption comes from a significant contribution by stimulated emission. Hence, a comparison of  $N(\text{HI})$  derived from 21 cm absorption with that derived using other methods yields an estimate of  $T_s$ . Of course, if there are multiple temperature phases in the absorbing gas then the derived values of  $T_s$  is strictly an upper limit to the temperature in the coldest phase. Temperatures for some of the low  $z$  systems have been derived by comparing 21 cm absorption with 21 cm emission, and the values are given in table 1. Temperatures for the damped Ly  $\alpha$  systems have been derived from comparison of 21 cm absorption with damped Ly  $\alpha$  absorption, and these are also given in table 1. Note that three of the low  $z$  systems (0959 + 683, 3C275.1 and 3C232) have lines that are narrow enough to set physically interesting upper limits to  $T_s$  by assuming a thermal origin for the line width:  $T_s = 22 \times (\Delta r)^2 \text{K}$ . The broader lines in most systems are likely a blending of narrow components. Lastly, Corbelli & Schneider (1990) and Stocke *et al.* (1991) have used observations of 21 cm emission and absorption, or the lack thereof, in quasar-galaxy pairs to set an upper limit to the soft X-ray background.

While the explicit dependence of  $N(\text{HI})$  on  $T_s$  makes 21 cm absorption of limited use for determining abundances or dust-to-gas ratios, we briefly consider these quantities in the 21 cm absorbing clouds as derived using other probes. For the low  $z$  systems Womble (1992) has made an empirical comparison of the observed EW of the CaII lines with  $N(\text{HI})$  derived from emission studies. She finds that CaII depletion onto dust grains is typically lower by an order of magnitude or more compared to normal Galactic disk gas, as has been seen for some Galactic high velocity clouds. For the damped Ly  $\alpha$  systems various optical spectroscopic techniques have been used to determine the abundances and dust-to-gas ratios (cf. Meyer & Roth 1990; Pei *et al.* 1991). Abundances of about 10% solar, and dust-to-gas ratios of about 10% ISM are typical, suggesting chemically young galaxies at high  $z$ . Pei *et al.* (1991) also conclude from the lack of a '2175 Angstrom extinction bump' that the dust properties at  $z > 2$  must differ considerably from Galactic. Lastly, Foltz *et al.* (1988) have a tentative detection of H<sub>2</sub> molecular absorption associated with the damped Ly  $\alpha$  absorber at  $z = 2.80$  towards 0528 + 250. They find a ratio of molecular to atomic hydrogen of  $\approx 10^{-3}$ .

Detection of high  $z$  21 cm absorption has been limited almost exclusively to selecting for previously known damped Ly  $\alpha$  absorption. Implicit in this is that the quasar be fairly bright in the optical. Heisler & Ostriker (1988) suggest that dust obscuration may have a rapid onset with  $\tau \propto (1+z)^{2.5}$ , and hence that there may be a population of quasars beyond  $z \approx 3$  which are effectively obscured in the optical. Two consequences of this idea are that the low dust-to-gas ratios in the known systems may simply be

a selection effect, and that the damped Ly  $\alpha$  surveys may miss the highest column density systems. A search for redshifted HI 21 cm absorption towards flat spectrum radio sources with very faint, or absent, optical counterparts would shed light on this interesting question.

The general question of reddening in quasar absorption lines systems, and the possibility of a population of optically obscured quasars, leads to the final topic of this review: red gravitational lenses. We have begun a search of HI 21 cm absorption towards red gravitational lenses (cf. McMohan *et al.* 1993). These are sources which have radio morphologies, and other properties, consistent with their being gravitationally lensed, but for which either no, or a very red, optical counterpart has been detected. One idea to explain such sources is that the optical quasar is obscured by dust in the lens (Stocke *et al.* 1992). A test of this idea is to search for HI 21 cm absorption, to verify the existence of cold gas on the line-of-sight to the background source. Thus far two such sources have shown strong 21 cm absorption (0218 + 357 and 1413 + 135). These detections demonstrate a new technique for determining lens redshifts in otherwise difficult circumstances. Further, the potential exists for imaging the HI distribution in the lens in absorption towards the extended background radio source, and hence for 'mapping' the gravitational potential of the lens in a way independent of lens models, thereby providing a fundamental test of gravitational lens theory.

#### 4. The future

Observing redshifted 21 cm absorption and emission is difficult work for these reasons. First, the limited total bandwidths available with existing spectrometers makes searches laborious. Second, the interference environment outside the protected radio bands becomes worse every year. And third is the general lack of available receivers in these frequency ranges at most large telescopes. Fortunately, the future looks very bright. Instrumentation and techniques are being developed for dealing with transient interference (Fisher 1991). Wide-band, many channel spectrometers are being built. And a number of large telescopes with state-of-the-art, frequency agile feeds and receivers are being constructed (the GMRT and the GBT), or significantly up-graded (Arecibo and the WSRT).

#### Acknowledgements

The author would like to thank Drs. Elvis and Kembhavi for asking him to come to India, the local organizing committee and NRAO for financial support, and Drs. J. van Gorkom, R. Braun, and A. G. de Bruyn for comments and discussions on this and related topics. The NRAO is operated by Associated Universities Inc., under cooperative agreement with the NSF.

#### References

- Bechtold, J., Ellingson, F. 1992, *Astrophys. J.*, **396**, 20.
- Bergeron, J., Boisse, P. 1991, *Astr. Astrophys.*, **243**, 344.
- Boisse, P., Dickey, J., Kazes, I., Bergeron, J. 1988, *Astr. Astrophys.* **191**, 193.
- Boksenberg, A., Sargent, W. 1978, *Astrophys. J.*, **220**, 42.

- Braun, R., Walterbos, R. 1992, *Astrophys. J.*, **386**, 120.
- Briggs, F., Wolfe, A. 1983, *Astrophys. J.*, **268**, 76.
- Briggs, F. 1988, in *QSO Absorption Lines*, Eds. J. C. Blades, D. Turnshek & C. Norman. (Cambridge University Press) p. 275 (ref. 3).
- Briggs, F. *et al.* 1989, *Astrophys. J.*, **341**, 650.
- Briggs, F., Sorar, E., Taramopoulos, A. 1993, *Astrophys. J. Lett.*, **415**, L99 (ref. 10).
- Brown, R., Fisher, R. 1993, in preparation.
- Carilli, C., van Gorkom, J. 1992, *Astrophys. J.*, **399**, 373 (ref. 5).
- Carilli, C., Perlman, E., Stocke, J. 1992, *Astrophys. J. Lett.*, **400**, L13 (ref. 7).
- Carilli, C., Rupen, M., Yanny, B. 1993, *Astrophys. J. Lett.*, **412**, L59 (ref. 8).
- Corbelli, E., Schneider, S. 1990, *Astrophys. J.*, **356**, 14 (ref. 4).
- Dickey, J. 1986, *Astrophys. J.*, **300**, 190.
- Dickey, J., Lockman, F. J. 1990, *A. Rev. Astr. Astrophys.* **28**, 215.
- Dickey, J., Brinks, E., Puche, D. 1992 *Astrophys. J.*, **385**, 501.
- Field, G. 1959a, *Astrophys. J.*, **129**, 551.
- Field, G. 1959b, *Astrophys. J.*, **129**, 536.
- Fisher, R. 1991, *Spectral Processor Manual*, NRAO, Greenbank, WV.
- Foltz, C., Chaffee, F., Black, J. 1988 *Astrophys. J.*, **324**, 267.
- Haschick, A., Crane, P., Baan, W. 1983, *Astrophys. J. Lett.*, **269**, L43 (ref. 2).
- Heisler, J., Ostriker, J. 1988, *Astrophys. J.*, **332**, 543.
- Lanzetta, K. M. *et al.* 1991, *Astrophys. J. Suppl.*, **77**, 1.
- McMohan, P. *et al.* 1993, in preparation.
- Meyer, D., Roth, K. 1990, *Astrophys. J.*, **363**, 57.
- Pei, Y. C., Fall, S. M., Bechold, J. 1991, *Astrophys. J.*, **378**, 6.
- Schmelz, J., Baan, W., Haschick, A., Eder, J. 1986, *Astr. J.*, **92**, 1291.
- Sargent, W., Steidel, C. 1990, *Astrophys. J. Lett.*, **359**, L37.
- Stocke, J., *et al.* 1992, *Astrophys. J. Lett.*, **400**, L1.
- Stocke, J. T. *et al.* 1991, *Astrophys. J.*, **374**, 72.
- Tytler, D. *Astrophys. J.*, **321**, 49.
- Uson, J., Bagri, D., Cornwell, T. 1991, *Phys. Rev. Lett.*, **67**, 3328 (ref. 9).
- Uson, J., Bagri, D., Cornwell, T. 1991, *Astrophys. J. Lett.*, **377**, L65.
- van Gorkom, J. H. *et al.* 1989, *Astr. J.*, **97**, 708.
- van Gorkom, J. H., Bahcall, J., Jannuzi, B., Schneider, D. 1993, *Astr. J.*, in press.
- Wieringa, M., de Bruyn, A., Katgert, P. 1992, *Astr. Astrophys.*, **256**, 331.
- Wolfe, A., Davis, M., Briggs, F. 1982, *Astrophys. J.*, **259**, 495.
- Wolfe, A. 1988, in *QSO Absorption Lines*, Eds. J. C. Blades, D. Turnshek & C. Norman (Cambridge University Press) p. 297.
- Womble, D. S. 1992, *Ph.D. Thesis*, UCSD (ref. 6).
- Womble, D., Sargent, W., Carilli, C. 1993, in preparation (ref. 1).
- Yanny, B., York, D., Williams, T. 1990, *Astrophys. J.*, **351**, 377.
- Yanny, B., Rupen, M., Carilli, C., York, D. 1993, in preparation.



## Accretion Disks in Quasars and Active Galactic Nuclei

Pranab Ghosh *Tata Institute of Fundamental Research, Bombay 400 005, India*

**Abstract.** I review the observational evidence for accretion disks in QSOs and AGNs. Spectral evidence, such as the blue/UV bump, reprocessed line emission, and X-ray reflection signature, are discussed. Evidence coming from short- and long-term variability is evaluated, as is that obtained from reverberation mapping techniques. I summarize the statistical studies, and describe the recent HST observations of the outer parts of a possible accretion disk in NGC 4261. Finally, I tabulate the characteristics of accretion disks in QSOs and AGNs inferred from these considerations.

*Key words:* Quasars—active galaxies—accretion disks—black holes.

### 1. Introduction

It is now generally believed (see, e.g., Blandford & Rees 1992 and the references therein) that black holes with masses  $\sim 10^6$ – $10^9 M_\odot$ , fed by accretion disks are the central powerhouses of quasars and active galactic nuclei (AGNs). An essential component of this 'standard' model is the accretion disk, thin or thick, cold or hot, gas- or radiation-pressure dominated, and with its source of opacity in different parts provided by electron scattering, free-free or free-bound absorption, or by molecules or grains. The disk extends from an inner radius which cannot be any smaller than that of the last stable orbit around the black hole ( $= 3R_g$  for a Schwarzschild black hole, in units of  $R_g \equiv 2GM/c^2$ , the gravitational radius), to an outer radius which is not estimated very well, but is currently thought to be  $\geq 10^4 R_g$ , where the self-gravitation of the disk first begins to drive it unstable. A schematic view of a possible configuration of the accretion disk and the emission regions is shown (Collin-Souffrin 1992) in Fig. 1 for illustrative purposes; other configurations have also been proposed (see Perry, these proceedings, and references therein).

In this review, I concentrate on the observational evidence for the existence of accretion disks in quasars and AGNs. The lines of evidence come from (a) the spectral properties, (b) the time variability, (c) the statistical properties, and, (d) direct observations with high spatial resolution, e.g., with the Hubble Space Telescope (see § 5). In § 2, I discuss the evidence gathered from various aspects of the optical, UV and IR emission properties of quasars and AGNs, including their continuum, line emission, and polarization characteristics, as well as that obtained from the recent X-ray studies of AGNs. In § 3, I present the evidence provided by studies of the time variability of AGNs on both short and long timescales. Section 4 deals with evidence coming from statistical studies of AGN samples, while § 5 describes the recent, pioneering observation of the outer parts of the accretion disk in NGC 4261. The basic characteristics of accretion disks in quasars and AGNs, as inferred from these observed properties, are summarised in § 6.

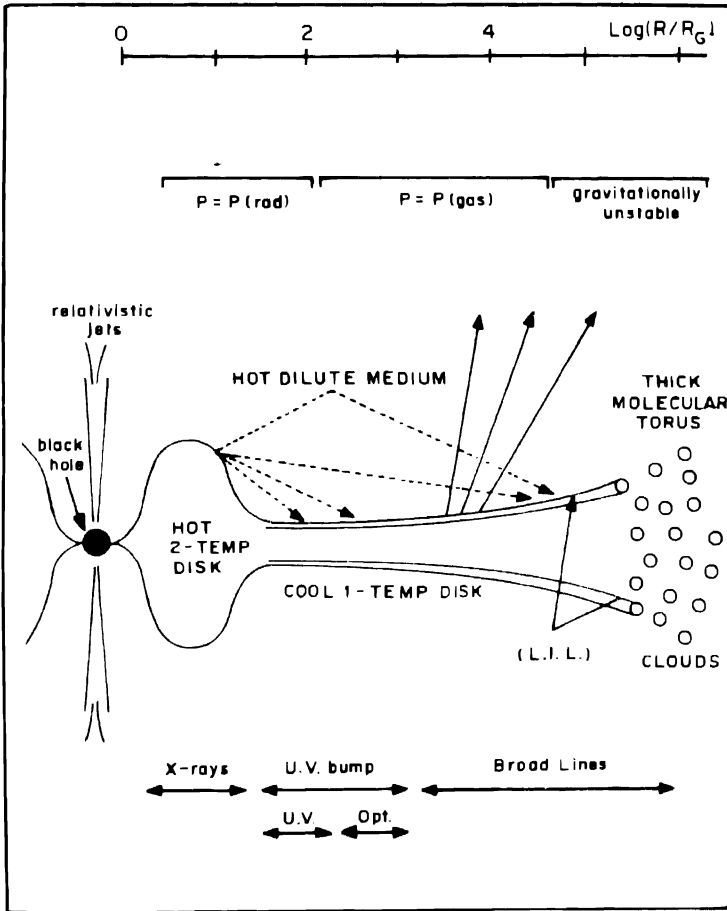


**Figure 1.** A possible accretion disk configuration in AGNs, showing the hot inner parts, cool outer parts, and cold, gravitationally unstable, outermost parts. Also indicated are the length scales and emission characteristics of the different parts. (After Collin-Souffrin (1992)).

## 2. Spectral properties

### 2.1 The big blue bump

A schematic broadband spectrum of AGNs is shown in Fig. 2. The emitted power is roughly constant over many decades of frequency, except for a broad peak covering the blue/UV range, the so-called 'big blue bump'. This bump is usually interpreted as thermal emission from the accretion disk (Shields 1978; Malkan & Sargent 1982; Sun & Malkan 1989 and the references therein), although alternative models have also been proposed (Guilbert & Rees 1988; Barvainis 1993). The general argument (Collin-Souffrin 1992) in favour of the accretion disk model is that it produces in a natural way the  $\sim 10^5$  K optically-thick gas required for emitting the UV bump, with

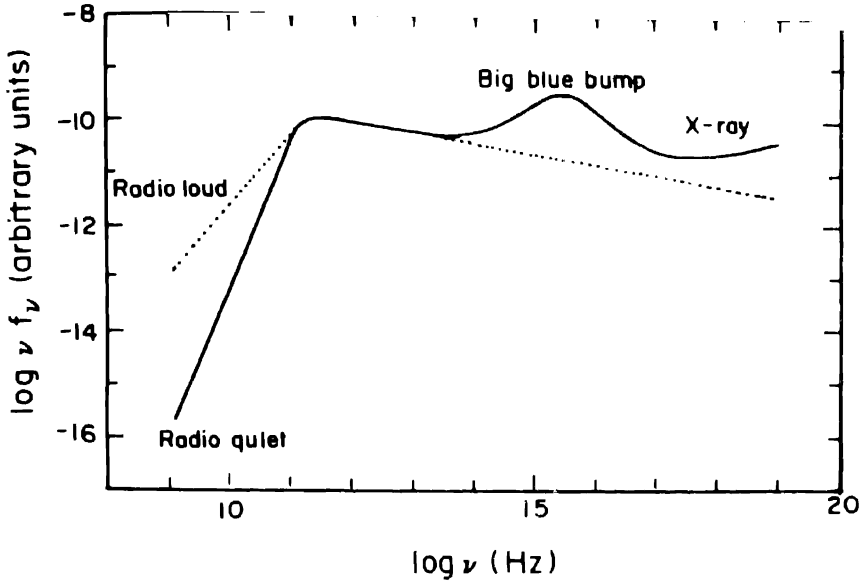


**Figure 2.** Schematic representation of the broadband continuum spectra of QSOs and AGNs, showing the blue/UV bump. (After Nandra (1991)).

the column-densities compatible with the small or nonexistent Lyman edges implied by observation (Antonucci *et al.* 1989).

Extensive fitting of the blue bump with continuum emission spectra of thin accretion disks (Shakura & Sunyaev 1973) has been carried out by Malkan and his associates (Malkan 1983; Sun & Malkan 1987, 1989), taking into account the effects of relativity (including those of gravitational focusing, Doppler boosting and gravitational redshift), inclination angle, and detailed opacities (Laor & Netzer 1989). These fits have yielded masses for the central black hole in the range  $M \sim 10^8 - 10^9 M_\odot$  and accretion rates in the range  $\dot{M} \sim 0.01 - 40 M_\odot \text{ yr}^{-1}$ , the inferred masses being smaller and the accretion rates higher for the Schwarzschild metric than for the Kerr metric.

## 2.2 Reprocessed radiation from the accretion disk

The emission lines from QSOs & AGNs can be divided into two categories, 'High Ionization Lines' (HIL), e.g.,  $\text{Ly}\alpha$ , C IV, Si IV, ... and 'Low Ionization Lines' (LIL), e.g. Balmer lines, Fe II, Mg II, .... The LIL are emitted by extended, weakly ionized regions which are thought to be ionized by hard X-ray continuum. The high total luminosity of the LIL, and so the large amount of power necessary to excite them (compared to the HIL), constitute one of the most convincing arguments (Ulrich 1989) for the LIL being produced by reprocessing of hard X-rays intercepted by the accretion disk. The X-rays, coming from a central region of size  $\lesssim 10 R_g$ , say, can illuminate the disk (a) directly, at small radii, (b) due to 'flaring' of the disk, at large radii, and (c) due to back-scattering by a hot corona surrounding the disk.



Detailed calculations of reprocessing by Collin-Souffrin and her associates (Collin-Souffrin & Dumont 1990; Dumont & Collin-Souffrin 1990a, b; Collin-Souffrin 1991) have shown that a large variety of line profiles, including double-peaked ones, can be produced, depending on the outer radius of the disk and the viewing angle. Most of the reprocessing is thought to occur in the region  $10^3 R_g \leq R \leq 10^4 R_g$ . The reprocessing model provides a natural explanation of the large line widths ( $\sim$  Keplerian velocity in the disk), as also for the large column densities and coverage factors required for the LIL emitting regions (Collin-Souffrin 1992).

### 2.3 Double-peaked emission lines

Broad, double-peaked H $\alpha$  lines are seen in many radio-loud AGNs, and are obvious candidates for double-peaked emission lines characteristic of rotating material. Following the classic case of Arp 102B which was fitted to simple relativistic Keplerian disk models (Chen, Halpern & Filippenko 1989), about a dozen such disk-fitted profiles are known now (Eracleous & Halpern 1993), and one example is showed in Fig. 3.

### 2.4 Lyman edges

The drastic increase in opacity shortward of 912 Å (in the rest frame of the AGN) should produce a Lyman edge at the appropriately redshifted frequency, but only partial edges are expected. Further, any narrow absorption line accompanying the edge indicates that it could not have originated in a disk (Kinney 1992). From the study by Antonucci *et al.* (1989) of high-redshift quasars, and that by Koratkar *et al.* (1992) of low- to medium-redshift quasars, the conclusion is that only  $\sim 15\%$  of the objects show the expected signature of accretion disks.

### 2.5 Polarization

Thin accretion disks are expected to emit most of the polarized radiation in the far UV, and detailed calculations including relativistic effects (Laor *et al.* 1990) suggest the following picture. A broad polarization feature near the Lyman edge, and a rise in the degree of polarization towards shorter wavelengths. Observations (Antonucci 1992) do not however, show this. Significant polarization is absent for some objects, and the percentage polarization does not show the expected frequency dependence in those objects for which detection is significant.

### 2.6 X-ray signatures

Recent X-ray observations (Nandra 1991) of AGNs have shown that the 2–30 KeV spectra have the following features: (a) a power-law behaviour with a photon index  $\sim 0.7$ , together with (b) a hard tail above  $\sim 10$  KeV, and (c) Fe fluorescence line at 6.4 KeV. These features have been successfully interpreted as due to reflection of an intrinsic power-law spectrum from a slab of cold material, which naturally produces fluorescence lines and Comptonization tails, as shown in Fig. 4 (Lightman & White

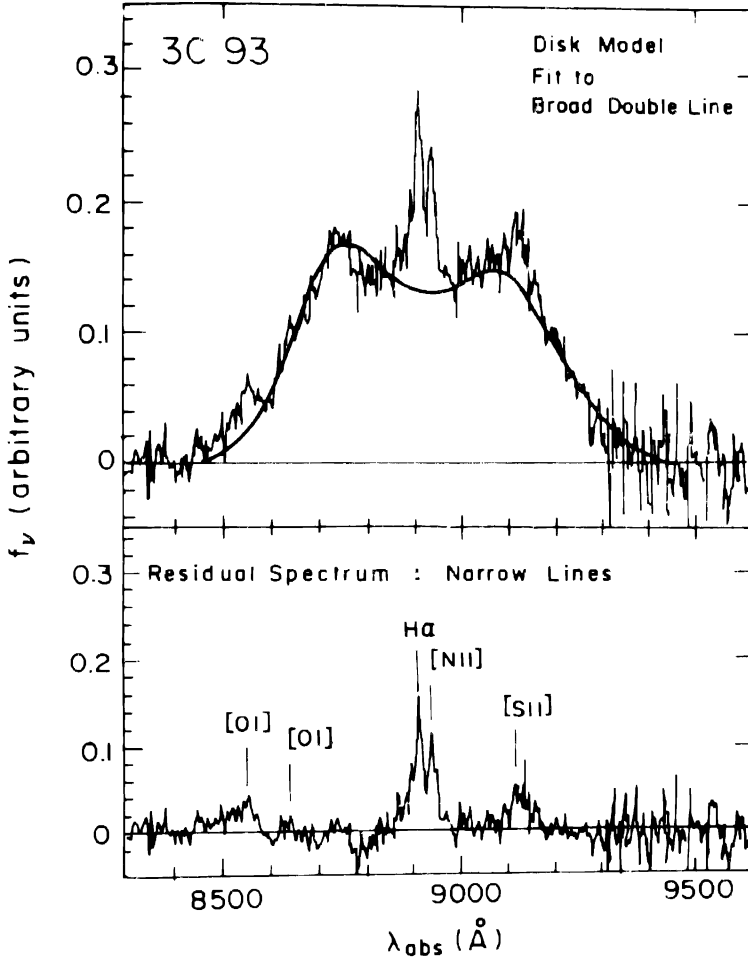


**Figure 3.** An example of broad, double-peaked H $\alpha$  profiles, fitted by the relativistic Keplerian disk model. The lower panel shows the residual spectrum (narrow lines) obtained by subtracting the model profile from the observed one. (After Eracleous & Halpern (1993)).

1988; Fabian *et al.* 1989; George & Fabian 1991; Matt *et al.* 1991). The reflecting slab is identified with the accretion disk.

### 3. Time variability

Optical, UV, X-ray and  $\gamma$ -ray fluxes from QSOs and AGNs show variability on a wide range of timescales, which can be roughly classified as light travel timescale ( $t \lesssim 10^3$  s.), and the dynamical ( $10^3$  s.  $\lesssim t \lesssim 10^5$  s.), thermal ( $10^5$  s.  $\lesssim t \lesssim 10^7$  s.), and viscous ( $t \gtrsim 10^7$  s.) timescales of accretion disks (Abramowicz 1991). Studies of these variabilities can be used to constrain the viscosity parameter  $\alpha$  of AGN accretion disks (Siemiginowska & Czerny 1989).

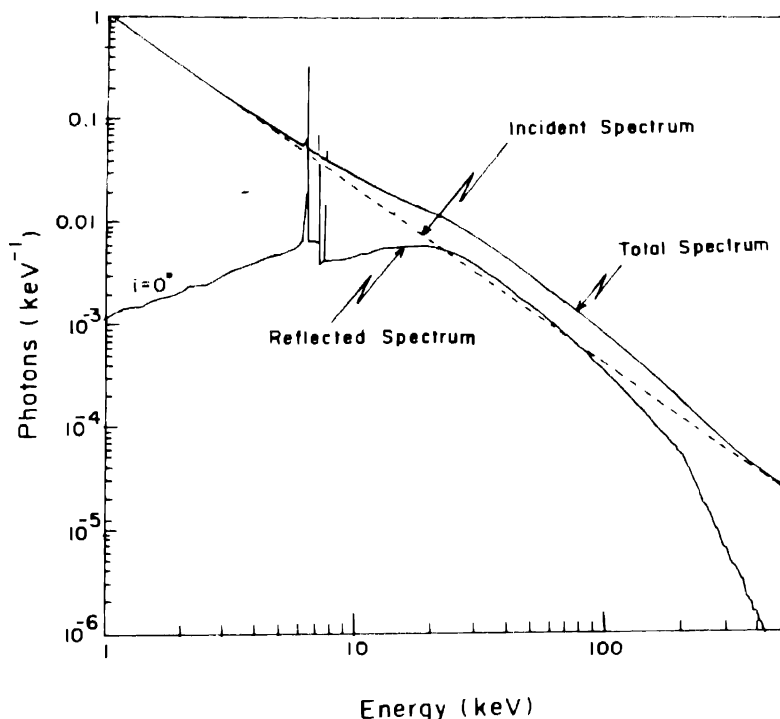


**Figure 4.** Monte Carlo simulations of the spectra of X-rays reflected from cold plasma slabs. Shown are: (a) the incident power-law spectrum of index 0.7 (dashed line), (b) the reflected spectrum (lower solid line), showing 6.4 KeV Fe  $K_{\alpha}$  and other fluorescence lines, and a continuum which is much flatter than the incident one, and, (c) the composite spectrum (upper solid line) which shows these lines and a 'hard tail' above  $\sim 10$  KeV, as observed. (After Nandra (1991)).

### 3.1 Short-term variability

On dynamical timescales, the power spectrum of AGN variability is featureless, and can be approximated by a power law of index between  $-1$  and  $-2$  (Abramowicz 1991). The only exception, i.e., the claimed periodicity of NGC 6814 at  $\sim 1.2 \times 10^4$  s, has recently been shown to be due to an unrelated stellar source, possibly a cataclysmic binary system, in the same field of view (Madejski *et al.* 1993). This power spectrum has been explained in terms of the emission from a distribution of relativistically rotating 'spots' or inhomogeneities on the surface of the accretion disk (Abramowicz *et al.* 1991).

### 3.2 Long-term variability

Power spectra at smaller frequencies is poorly determined at present, but also consistent with a featureless power-law, and possibly with a roll-over at low frequencies (Abramowicz 1991). A basic mechanism for variability on these timescales could be the limit-cycle oscillations of accretion disks (Abramowicz *et al.* 1988, 1989; Honma *et al.* 1991a, b). The effects of advective cooling, horizontal pressure gradient, and deviation from Keplerian flow are very important near the sonic point which occurs in the

innermost parts of the accretion disk. Addition of these to the standard thin-disk theory (Shakura & Sunyaev 1973) results in 'slim' disk models, which have a three-branched S-shaped characteristic curve, the middle branch being unstable. Thus the disk can undergo oscillations on the thermal timescale between the (stable) uppermost and lowermost branches.

### 3.3 Reverberation mapping

Using the observed time-variability of reprocessing emission lines (He II, C IV, O I, ...) against the known time-variation of the ionizing continuum flux to extract information about the structure of the reprocessing region is a powerful technique in principle (Blandford & McKee 1982), but limited in practice by poor-quality data. Recent application of maximum-entropy deconvolution methods (Krolik *et al.* 1991) to the UV data on NGC 5548 has shown how interesting and useful information can still be obtained by this technique. So far, the main robust result has been that the size of the reprocessing region is  $\sim 15-30$  light-days. Whereas this is obviously consistent with the sizes implied by the disk models outlined in § 2, more work is required to establish the shape of the region.

## 4. Statistical evidence

Examples of this line of evidence are the colour-magnitude study of Caditz (1993) and the study of the correlation between line/continuum ratio and inclination angle by Netzer *et al.* (1992). In the former study, it is shown that a sample of  $\sim 200$  QSOs and AGNs over a limited range of redshifts occupy a well-defined region in the (U - B) colour vs B-magnitude diagram. The lower boundary of the region corresponds to accretion at the critical Eddington rate,  $\dot{M}_{\text{Edd}}$  and the upper boundary, to a maximum black hole mass  $M \sim 10^{9.5} M_{\odot}$ . Contours of constant  $\dot{M}$  and  $M$  obtained from accretion disk models (see § 2) map out the region well (Caditz 1993).

## 5. Direct observation

Pioneering work with the Planetary Camera on the Hubble Space Telescope has yielded what may be the first direct image of the very outer parts of the accretion disk in NGC 4261 (Jaffe *et al.* 1993). Note, however, that the size of the observed disk-like object is  $\sim 10^{20}$  cm., i.e.,  $\sim 10^7 R_g$  for a  $\sim 10^8 M_{\odot}$  black hole. By contrast, the sizes of the accretion disks discussed above are  $\lesssim 10^5 R_g$ , i.e. within the unresolved point-like nucleus in the HST image. Thus the observed disk is likely to be the mass-supply disk lying outside the accretion disk (see Fig. 1), in which self-gravitational instabilities break up the disk at first into clouds and then into gaseous bars (Begelman *et al.* 1989).

## 6. Conclusions

In Table 1, I summarize the information on the basic characteristics, e.g. black hole mass, accretion rate, size, viscosity, of AGN accretion disks obtained from considera-

**Table 1.** Inferred characteristics of AGN accretion disks.

Characteristic	Inferred values	Method(s) involved
Mass of central black hole ( $M$ )	$10^8 \lesssim M/M_\odot \lesssim 10^{9.5}$	a) Disk model fits to big blue bump. b) Statistical study in colour-magnitude diagram.
Mass accretion rate ( $\dot{M}$ )	$10^{-1} < \dot{M}(M_\odot \text{ yr}^{-1}) < 10$	Disk model fits to big blue bump.
Size of reprocessed line emission region ( $R$ )	$10^3 \lesssim R/R_G \lesssim 10^4$ $6M_g \lesssim R/\text{light-days} \lesssim 60M_g$	a) Detailed modelling of reprocessed line emission. b) Relativistic disk modelling of double-peaked H $\alpha$ lines. c) Reverberation mapping.
Viscosity parameter ( $\alpha$ )	Here, $M_g \equiv M/(10^8 M_\odot)$ $10^{-3} \lesssim \alpha \lesssim 10^{-1}$	Disk modelling of variability timescales.

tions described in the earlier sections. Although accretion disk models for QSOs and AGNs continue to be very popular, they are not without their problems. Future work will undoubtedly focus on the resolution of these, perhaps through the recognition of essential components of the model in addition to accretion disks.

## References

- Abramowicz, M. A. 1991, in *Variability of Active Galaxies*, Ed. W. J. Duschl *et al.* (Heidelberg: Springer) p. 255.
- Abramowicz, M. A., Bao, G., Lanza, A., Zhang, X. H. 1991, *Astr. Astrophys.*, **245**, 454.
- Abramowicz, M. A., Czerny, B., Lasota, J. P., Szuszkiewicz, E. 1988, *Astrophys. J.*, **332**, 646.
- Abramowicz, M. A., Kato, S., Matsumoto, R. 1989, *Publ. astr. Soc. Japan*, **41**, 1215.
- Antonucci, R. 1992, in *Testing the AGN Paradigm*, Ed. S. S. Holt *et al.* (New York: American Inst. of Physics), p. 486.
- Antonucci, R. R. J., Kinney, A. L., Ford, H. C. 1989, *Astrophys. J.*, **342**, 64.
- Barvainis, R. 1993, *Astrophys. J.*, **412**, 513.
- Blandford, R. D., McKee, C. F. 1982, *Astrophys. J.*, **255**, 419.
- Blandford, R. D., Rees, M. J. 1992, in *Testing the AGN Paradigm*, Ed. S. S. Holt *et al.* (New York: American Inst. of Physics), p. 3.
- Begelman, M. C., Frank, J., Shlosman, I. 1989, in *Theory of Accretion Disks*, Ed. F. Meyer *et al.* (Dordrecht: Kluwer), p. 373.
- Caditz, D. 1993, *Astrophys. J.*, **411**, 103.
- Chen, K., Halpern, J. P., Filippenko, A. V. 1989, *Astrophys. J.*, **339**, 742.
- Collin-Souffrin, S. 1991, *Astr. Astrophys.*, **249**, 344.
- Collin-Souffrin, S. 1992, in *Testing the AGN Paradigm*, Ed. S. S. Holt *et al.* (New York: American Inst. of Physics), p. 119.
- Collin-Souffrin, S., Dumont, A. M. 1990, *Astr. Astrophys.*, **229**, 292.
- Dumont, A. M., Collin-Souffrin, S. 1990a, *Astr. Astrophys.*, **229**, 302.
- Dumont, A. M., Collin-Souffrin, S. 1990b, *Astr. Astrophys.*, **229**, 313.
- Eracleous, M., Halpern, J. P. 1993, *Astrophys. J. Suppl.*, in press.
- Fabian, A. C., Rees, M. J., Stella, L., White, N. E. 1989, *Mon. Not. R. astr. Soc.*, **238**, 729.
- George, I. M., Fabian, A. C. 1991, *Mon. Not. R. astr. Soc.*, **249**, 352.
- Guilbert, P. W., Rees, M. J. 1988, *Mon. Not. R. astr. Soc.*, **233**, 475.

- Honma, F., Matsumoto, R., Kato, S., 1991a, *Publ. astr. Soc., Japan*, **43**, 147.
- Honma, F., Matsumoto, R., Kato, S., Abramowicz, M. A. 1991b, *Publ. astr. Soc. Japan*, **43**, 261.
- Jaffe, W., *et al.* 1993, *Nature*, **364**, 213.
- Kinney, A. L. 1992, in *Testing the AGN Paradigm*, Ed. S. S. Holt *et al.* (New York: American Inst. of Physics), p. 139.
- Koratkar, A. P., Kinney, A. L., Bohlin, R. C. 1992, *Astrophys. J.*, **400**, 435.
- Krolik, J. H., *et al.* 1991, *Astrophys.*, **371**, 541.
- Laor, A., Netzer, H. 1989, *Mon. Not. R. astr. Soc.*, **238**, 897.
- Laor, A., Netzer, H., Piran, T. 1990, *Mon. Not. R. astr. Soc.*, **242**, 560.
- Lightman, A. P., White, T. R. 1988, *Astrophys. J.*, **335**, 57.
- Madejski, G. M., *et al.* 1993, *Nature*, **365**, 626.
- Malkan, M. A. 1983, *Astrophys. J.*, **268**, 582.
- Malkan, M. A., Sargent, W. L. W. 1982, *Astrophys. J.*, **254**, 22.
- Matt, G., Perola, G. C., Piro, L. 1991, *Astr. Astrophys.*, **247**, 27.
- Nandra, K., 1991, Ph.D. Thesis, Leicester University.
- Netzer, H., Laor, A., Gondhalekar, P. M. 1992, *Mon. Not. R. astr. Soc.*, **254**, 15.
- Shakura, N. I., Sunyaev, R. A. 1973, *Astr. Astrophys.*, **24**, 337.
- Shields, G. A. 1978, *Nature*, **272**, 706.
- Siemiginowska, A., Czerny, B. 1989, *Mon. Not. R. astr. Soc.*, **239**, 289.
- Sun, W. H., Malkan, M. A. 1987, in *Supermassive Black Holes*, Ed. M. Kafatos (Cambridge: Cambridge University Press), p. 273.
- Sun, W. H., Malkan, M. A. 1989, *Astrophys. J.*, **346**, 68.
- Ulrich, M. H. 1989 in *Theory of Accretion Disks*, Ed. F. Meyer *et al.* (Dordrecht: Kluwer), p. 3.



## Halo Model for Low and Intermediate Redshift, Heavy Element, Quasar Absorption Lines

P. Khare & R. Srianand *Department of Physics, Utkal University, Bhubaneswar 751 004, India*

**Abstract.** A model for galactic halos is shown to explain several observed properties of the heavy element absorption lines in the spectra of quasars.

**Key words:** Quasars: heavy element absorption lines—galactic halos.

Galactic halos, responsible for producing QSO absorption lines, are assumed to have radii  $\simeq 50$  kpc and contain identical, randomly moving clouds which are responsible for producing multiple components of the metal lines observed in the high resolution observations. The number of clouds per unit volume is assumed to be distributed in the halo as,

$$n_c(r) = \frac{n_{c0}}{\left(1 + \frac{r^2}{r_c^2}\right)}, \quad r_c \simeq 6 \text{ kpc}. \quad (1)$$

The metal abundance in the clouds is assumed to depend on the cloud distance from the galactic centre as,

$$X(r) = X(0)e^{-br}, \quad b \simeq 0.09 \text{ kpc}^{-1}. \quad (2)$$

Photoionization models are constructed for the clouds. Cloud sizes ( $N_H \sim 10^{20} - 10^{21} \text{ cm}^{-2}$ , for ionization parameter,  $\Gamma$ , between 0.01–0.001 and  $X(0) = 0.1-0.5$ ) are chosen so as to give the Mg II column density in the central cloud as  $10^{14} \text{ cm}^{-2}$ . The abundance gradient gives the column density in the clouds near the edge  $\sim 10^{12} \text{ cm}^{-2}$ . The range of Mg II column densities is consistent with the observed range (Petitjean & Bergeron 1990). Equivalent width for Mg II lines is calculated for line of sight through individual clouds and then added to give the equivalent width due to all clouds along lines of sight,  $W(P)$ , with given impact parameter  $P$ .

The value of  $n_{c0}\sigma_0$  at  $z \sim 0.5$ , ( $\sigma_0$  being the cross section of individual clouds), is chosen so as to give best fit for the observed (Bergeron & Boisse 1991) values of  $W(P)$  for different  $P$  values at these redshifts as shown in Fig. 1. The equivalent width distribution of Mg II lines, given by the model is shown to be well represented by a power law with slope between  $-1.6$  and  $-1.9$  which agrees well with the observed value of  $-1.65$  (Steidel & Sargent 1992). The column density distribution of neutral hydrogen is shown to roughly agree with the observed distribution, which is not very well known in the range of interest ( $10^{18} - 2 \times 10^{19} \text{ cm}^{-2}$ ). The distribution of individual clouds with different Mg II column densities is also well explained by the model.



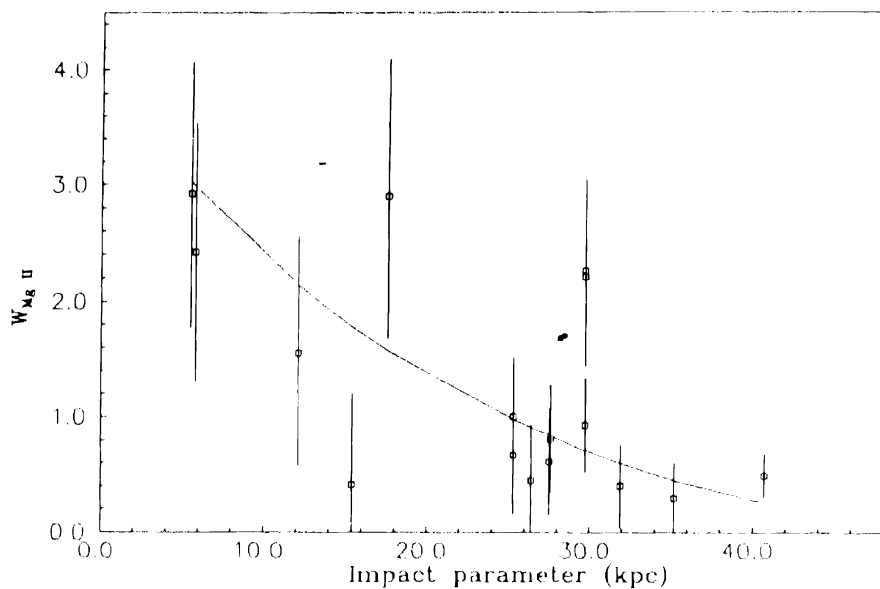


**Figure 1.** Observed restframe equivalent widths of MgII vs impact parameter and the model best fit.

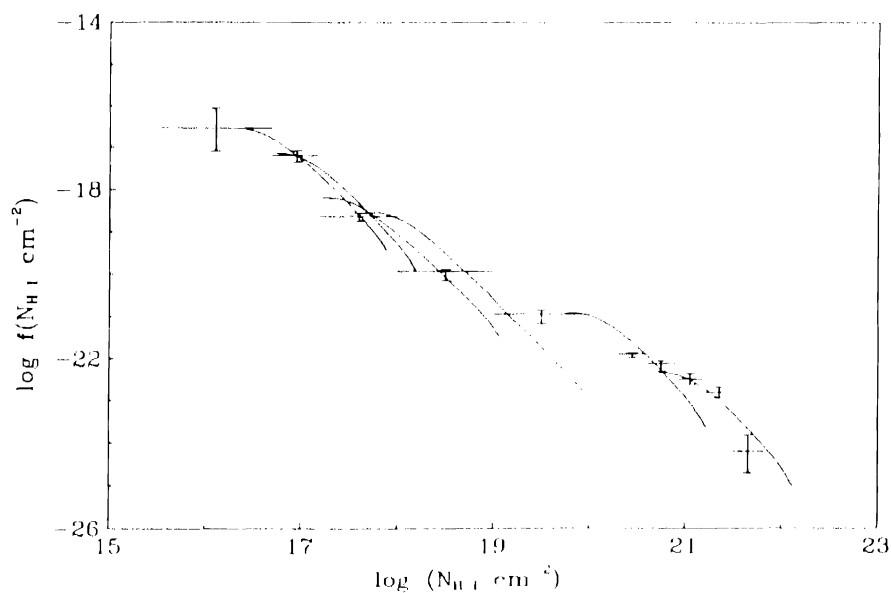


**Figure 2.** Observed neutral hydrogen column density distribution compared with the predictions of models with a range of input parameters.

This model is then extended to higher redshifts,  $z = 1-2$ . More information is available at these redshifts as both C IV and Mg II are observable. The range of parameters  $N_H$ ,  $\Gamma$  and  $X(0)$  used above is shown to reproduce (i) Equivalent width distribution of C IV and Mg II, (ii) Doublet ratio of C IV and Mg II as a function of  $W$ , (iii) Equivalent width ratios of several lines, (iv) Neutral hydrogen column density distribution for  $N_H = 10^{16} - 10^{22} \text{ cm}^{-2}$  (shown in Fig. 2). Depending on the impact parameter the models reproduce, damped Lyman alpha systems, Lyman limit systems with and without accompanying C IV lines, Lyman limit systems without metal lines and systems with neutral hydrogen column density below that of the LLS.

The cloud sizes vary from 0.3–3.0 kpc and have a volume filling factor of  $\sim 0.02-0.2$ . The total number of clouds in the halo is between 700–70,000 giving it a total mass of  $10^{10} - 10^{11} M_\odot$ .

### References

- Bergeron, J., Boisse, P. 1991, *Astr. Astrophys.*, **243**, 344.  
Petitjean, P., Bergeron, J. 1990, *Astr. Astrophys.*, **231**, 309.  
Steidel, C. C., Sargent, W. L. W. 1992, *Astrophys. J. Suppl.*, **80**, 1.



## Aspect Dependent Optical Continuum Emission in Radio Quasars

J. C. Baker & R. W. Hunstead *Department of Astrophysics, University of Sydney, NSW 2006, Australia*

V. K. Kapahi & C. R. Subrahmanya *National Centre for Radio Astrophysics, TIFR, Pune 411 007, India*

**Abstract.** We have defined a new, complete, low-frequency selected sample of southern radio quasars, the Molonglo Quasar Sample, with the aim of studying the aspect dependence of the radio and optical emission. As a test for enhancement of the optical continuum, we find that the narrow [O II] and [O III] emission line equivalent widths decrease systematically with radio core dominance. This effect is consistent with the optical continuum being relativistically boosted at angles close to the line of sight. However, such an interpretation seems to be in conflict with the aspect independent behaviour of the broad lines, most notably H $\beta$ .

**Key words:** Quasars: emission lines – optical spectroscopy – radio sources – active galaxies.

### 1. Introduction

Statistical studies have suggested that radio core-dominated quasars are on average over one magnitude brighter in the optical than their lobe dominated counterparts (Browne & Wright 1985; Kapahi & Shastri 1987; Wills *et al.* 1992). Since radio core dominance is believed to arise from Doppler boosting of a forward-directed relativistic jet seen at small angles to the line of sight, such a difference in optical magnitudes can be understood if the optical continuum also depends on viewing angle and is enhanced along with the radio core emission. If so, then virtually all existing QSO samples will contain a significant orientation bias. We have attempted to minimize this bias by selecting a new sample at low radio frequency, where the flux density is dominated by the unbeamed extended emission, and by ensuring that optical identifications are complete down to the limit of deep sky survey Schmidt plates.

### 2. The Molonglo Quasar Sample (MQS)

Initially,  $\sim 700$  sources with  $S_{408} > 0.95$  Jy, in a  $10^\circ$  declination strip ( $-30^\circ < \delta < -20^\circ$ ) and in the RA ranges  $20^{\text{h}}-06^{\text{h}}$  and  $09^{\text{h}}-14^{\text{h}}$ , were selected from the 408 MHz Molonglo Reference Catalogue (Large *et al.* 1981). The sources were mapped at 843 MHz with the Molonglo Observatory Synthesis Telescope in snapshot mode, and optical identifications of stellar counterparts were made from the UK Schmidt IIIaJ plates, complete down to the limiting magnitude  $B_J \sim 22.5$ . Follow-up radio imaging

has been undertaken at the VLA at 5 GHz for all the QSO candidates. Optical spectroscopy at the Anglo-Australian Telescope has provided us with redshifts ( $0.1 < z < 2.9$ ), continuum slopes and emission line data.

### 3. The equivalent width test

A widely used test for the enhancement of the optical continuum has been the comparison of narrow emission line equivalent width,  $W_\lambda$ , with radio core dominance parameter,  $R$  (Wills & Browne 1986);  $R$  is usually defined as the ratio of core to extended flux density at a given emitted frequency (we use 10 GHz). If the optical continuum is brighter in quasars viewed at small angles to their radio jet axis then, for an isotropically emitted line,  $W_\lambda$  will decrease with increasing  $R$ . This has been observed by Browne & Murphy (1987) for a collection of X-ray selected quasars using the narrow [O III]  $\lambda 5007$  line. The same effect is observed with the MQS (Baker *et al.* 1993). However, Jackson & Browne (1990) presented evidence, from a comparison of [O III] luminosities for a matched set of radio galaxies and quasars, that the [O III] line is significantly stronger in the quasars and may not be emitted isotropically.

Recent studies suggest that, unlike [O III], the distribution of [O II]  $\lambda 3727$  luminosity is the same for both radio galaxies and quasars (Bremer *et al.* 1992; Hes *et al.* 1993), consistent with the quasar-radio galaxy unification picture (Barthel 1989). This suggests that [O II] might be emitted more isotropically than [O III] and, therefore, be a better line to use as a benchmark.

Our preliminary plot of  $W_\lambda$ [O II] against  $R$  is shown in Fig. 1(a). A strong decrease in  $W_\lambda$  with  $R$  is evident, spanning four orders of magnitude, and is remarkably

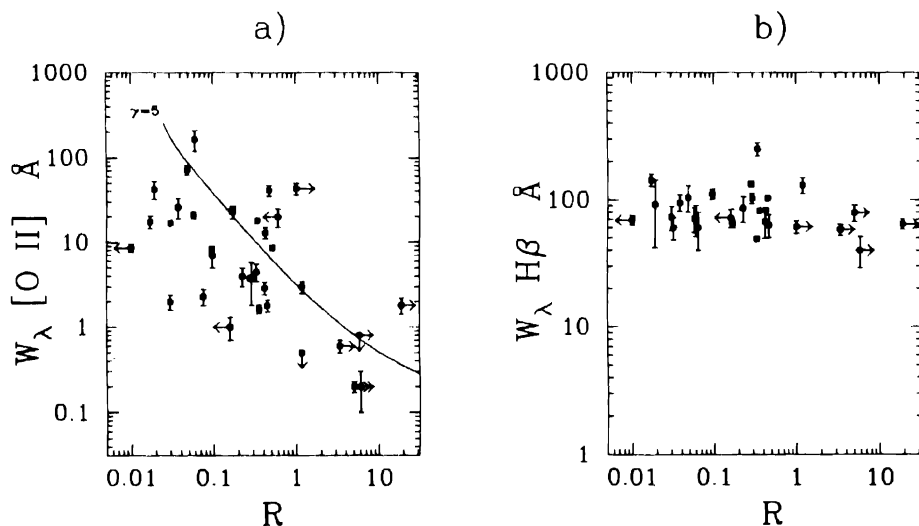


**Figure 1.** Preliminary plots of  $W_\lambda$  versus  $R$  for (a) [O II]  $\lambda 3727$  showing a strong anticorrelation consistent with the  $\gamma = 5$  Doppler boosted continuum model shown (Browne & Murphy 1987), and (b) H $\beta$   $\lambda 4861$  showing  $W_\lambda$  to be independent of  $R$ .

consistent with a simple relativistically beamed continuum model (Browne & Murphy 1987). Such a strong anticorrelation cannot be attributed solely to a decrease in [O II] line luminosity, which has a range of only one order of magnitude, comparable with the scatter. We therefore believe that the trend is most readily explained by a progressive enhancement of the optical continuum emission with increasing  $R$ .

#### 4. Broad line equivalent widths

In contrast to the narrow line results, we observe little or no anticorrelation between  $W_\lambda$  and  $R$  for the broad lines C IV and C III]. Perhaps Mg II shows a weak anticorrelation, although the scatter is large. The lack of a strong trend for the broad lines can be understood in terms of partial obscuration of the BLR, leading to anisotropy in the line emission.

The result for H $\beta$  is intriguing (Fig. 1b), the equivalent width being independent of  $R$  over the range  $R = 0.01 - 10$ , with very little dispersion. The narrow range in equivalent width can be interpreted alternatively as a direct proportionality between the H $\beta$  line and continuum luminosity, a correlation which appears to hold for all kinds of AGN except BL Lac objects (Yee 1980; Miller *et al.* 1992). The tightness of this correlation (and its wide applicability) suggests that it is telling us something fundamental about the emission mechanism.

H $\beta$  itself cannot be relativistically beamed, because it is not observed to be blue-shifted with respect to the narrow forbidden lines. Could the line-to-continuum proportionality imply that aspect dependence is in fact caused by obscuration and not relativistic beaming? It appears as though H $\beta$  emanates from a region with precisely the same opening angle as the optical continuum. On the other hand, the [O II] plot in Fig. 1(a) seems to show very strong orientation effects and these are difficult to explain with current geometric models.

#### 5. Conclusions

We have presented evidence that, on the one hand, the optical continuum of radio quasars is strongly aspect dependent and consistent with a simple Doppler beaming model. On the other hand, this straightforward interpretation appears inconsistent with the narrow distribution of H $\beta$  equivalent width over a wide range in  $R$ , which suggests a common angular dependence for the Balmer lines and optical continuum. It is hoped that these apparently conflicting results will stimulate further theoretical work on modelling the physics and geometry of quasar emission regions.

#### Acknowledgements

JCB is grateful for a postgraduate scholarship from the Research Centre for Theoretical Astrophysics, Sydney University, and RWH acknowledges financial support from the Australian Research Council.

## References

- Baker, J. C., Hunstead, R. W., Kapahi, V. K., Subrahmanya, C. R. 1993, in *The Nature of Compact Objects in AGN*, Eds. A. Robinson, R. J. Terlevich, C.U.P., (in press).
- Barthel, P. D. 1989, *Astrophys. J.*, **336**, 606.
- Bremer, M. N., Crawford, C. S., Fabian, A. C., Johnstone, R. M. 1992, *Mon. Not. R. astr. Soc.*, **254**, 614.
- Browne, I. W. A., Murphy, D. W. 1987, *Mon. Not. R. astr. Soc.*, **226**, 601.
- Browne, I. W. A., Wright, A. E. 1985, *Mon. Not. R. astr. Soc.*, **213**, 97.
- Hes, R., Barthel, P. D., Fosbury, R. A. E. 1993, *Nature*, **362**, 326.
- Jackson, N., Browne, I. W. A. 1990, *Nature*, **343**, 43.
- Kapahi, V. K., Shastri, P. 1987, *Mon. Not. R. astr. Soc.*, **224**, 17p.
- Large, M. I., Mills, B. Y., Little, A. G., Crawford, D. F., Sutton, J. M. 1981, *Mon. Not. R. astr. Soc.*, **194**, 693.
- Miller, P., Rawlings, S., Saunders, R., Eales, S. 1992, *Mon. Not. R. astr. Soc.*, **254**, 93.
- Wills, B. J., Browne, I. W. A. 1986, *Astrophys. J.*, **302**, 56.
- Wills, B. J., Wills, D., Breger, M., Antonucci, R. R. J., Barvainis, R. 1992, *Astrophys. J.*, **398**, 454.
- Yee, H. K. C. 1980, *Astrophys. J.*, **241**, 894.

## Anisotropic Emissions from Blazars

K. K. Ghosh & S. Soundararajaperumal *Indian Institute of Astrophysics, Vainu Bappu Observatory, Kavalur 635 701, India*

**Abstract.** Radio through X-ray continuum emission spectra of 30 blazars are presented. A new bimodal nature of blazar's distribution, in the radio–X-ray luminosity plane, shows the differences between BL Lac objects and highly polarized quasars or optically violent variables.

**Key words:** Galaxies: nuclei— BL Lac objects — quasars — radiation mechanisms.

### 1. Introduction

Optically Violent Variables (OVVs), Highly Polarized Quasars (HPQs), Flat Spectrum Radio Quasars (FSRQs) and BL Lac objects have been classed as 'blazars'. Blazars are radio-loud objects where relativistic jets close to the line of sight are thought to cause blazar characteristics like rapid variability, high polarization, high luminosity, and in many cases, superluminal motion. If the relativistic jets are real, the identification of the isotropic and non-isotropic emission components from the blazars may be used as a statistical indicator of orientation relative to the line of sight and also to probe the geometry of the nuclear region. In this paper we present the X-ray (0.04–10 keV) observations of 30 blazars. Also we present the radio through X-ray continuum emission spectra of these objects.

### 2. Observations, analysis and results

#### 2.1 X-ray observations

X-ray spectra of 30 blazars were obtained with the EXOSAT X-ray satellite using low- (0.04–2 keV) and medium- (2–10 keV) energy (LE and ME) detectors. Details of observations have been described in earlier papers (Ghosh & Soundararajaperumal 1992a, b). The XSPEC (X-ray Spectral Fitting) software package was used to analyse the combined LE and ME spectra of the blazars. Power-law plus the uniform absorption model was used to fit the spectra, but the derived values of the hydrogen column densities ( $N_H$ ) for most of the sources are smaller than the corresponding galactic  $N_H$  values. Next we fitted the spectra using the power-law plus the fixed absorption model which provided reasonably good fit to the spectra. The fit parameters suggest that the BL Lac objects are relatively steeper than the HPQs, OVVs. The values of the X-ray spectral indices ( $\alpha$ ) of HPQs/OVVs are in the range of 0.4–1.0 and that for BL Lacs are in the range of 1.0–2.2. From the measured LE and ME count rates we have computed the X-ray hardness ratio (HR, defined as the ratio between the



average ME count rate and the average count rate in the CMA + thin Lexan filter) of these blazars and we have found that the BL Lac objects are relatively X-ray softer ( $HR < 5$ ) than the HPQs/OVV s ( $HR > 5$ ). Also we have carried out the ME flux variability studies of the present blazar sample and have found that only BL Lacs have displayed rapid variability (on time scales of few hours).

## 2.2 Multifrequency spectra

For the multifrequency continuum emission spectra (radio through X-ray) of blazars, the far-infrared and ultraviolet fluxes were obtained from the IRAS and IUE databases and the radio, mm, infrared and optical fluxes were obtained from the literature. Figs. 1a, b show the multifrequency spectra of a BL Lac (Mkn 501) and a HPQ (AO 0235 + 164), respectively. From these figures it may be seen that the radio through X-ray spectra of BL Lacs and HPQs/OVV s may be fitted with a single and double parabolic curves, respectively. Multifrequency spectra of HPQs/OVV s display spectral discontinuity between UV and X-ray bands.

## 2.3 Spectral indices and luminosities

Two point spectral indices between radio and optical bands ( $\alpha_{R-O}$ ) and between optical and X-ray bands ( $\alpha_{O-X}$ ) show the bimodal nature of the distribution of blazars in the present sample (Fig. 2) which is similar to the ones found in other samples (Ledden & O'Dell 1985; Stocke *et al.* 1985, 1988; Worrall *et al.* 1987). This supports against the

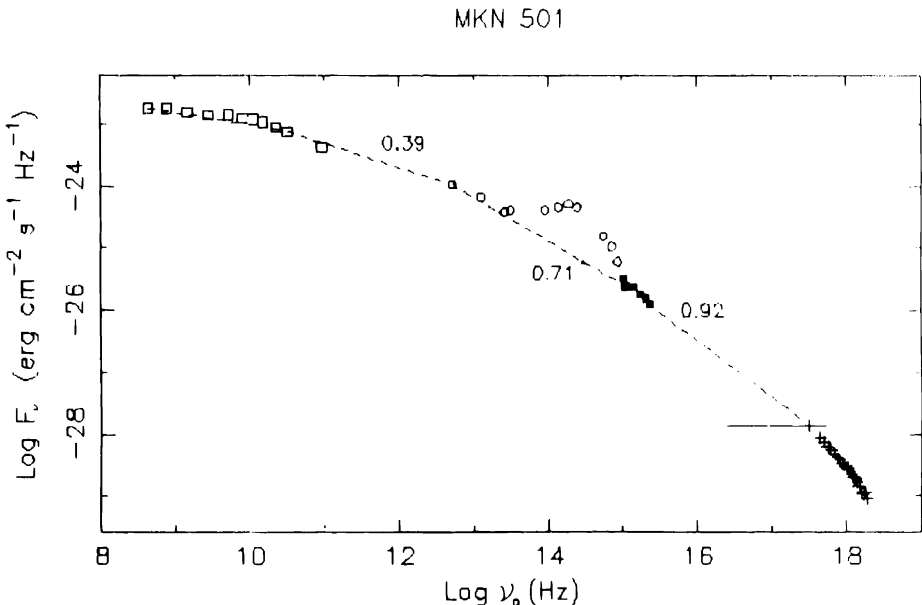


Figure 1a. Broad-band spectrum of Mkn 501.

AO 0235 + 164

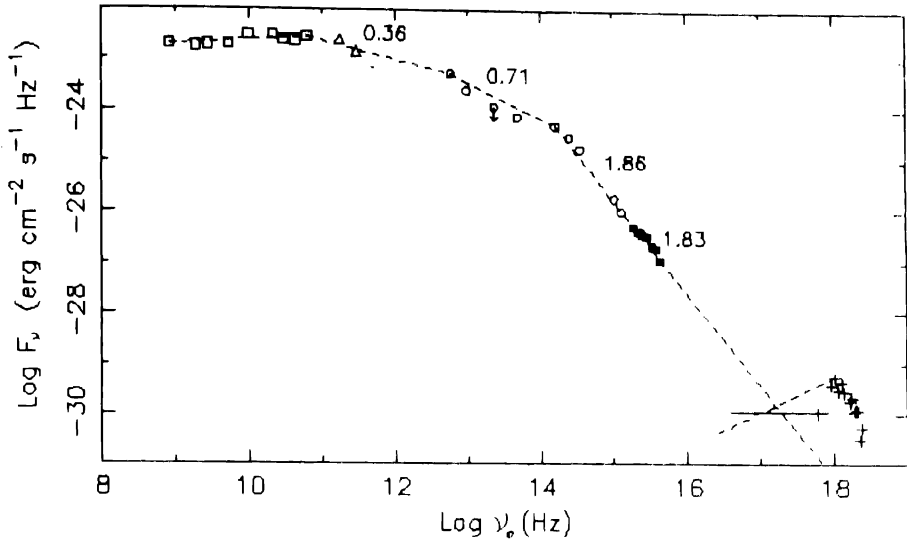


Figure 1b. Broad-band spectrum of AO 0235 + 164.

biasness of the present sample. Also we have found that the UV spectral indices of HPQs/OVV are much steeper than the BL Lacs.

From the statistical studies of luminosities of blazars in different energy bands (radio, mm, FIR, IR, optical, UV and X-ray) we find that the luminosities of the adjacent bands (i.e.  $L_{\text{radio}}$  vs.  $L_{\text{mm}}$ ;  $L_{\text{mm}}$  vs.  $L_{\text{FIR}}$ ; etc.) are strongly correlated, but no correlation is present between UV and X-ray luminosities. A new bimodal nature of blazar's distribution in the  $L_{\text{radio}} - L_{\text{X}}$  plane has been detected which can be seen from Fig. 3. Also we have found that, over radio through X-ray frequencies, BL Lacs and HPQs/OVV output most of their radiations in the IR-Optical and X-ray bands, respectively.

### 3. Discussion

Multifrequency spectra of BL Lacs can be fitted with a smooth curve (broken power laws) which suggests that radio through X-rays are due to synchrotron mechanism. However, two-components are required to fit multifrequency spectra of HPQs/OVV. Also the observed X-rays from HPQs/OVV are much above the extrapolation of the spectrum from lower frequencies (radio through UV), which is in agreement with the results obtained by Worrall (1989) for a different sample of blazars. These results suggest that radio through UV spectra of HPQs/OVV are from synchrotron radiation and X-rays are from self-Compton photons. Also, our new bimodal nature of blazar's distribution (see Fig. 3) suggest that different radiation mechanisms may play important roles in BL Lacs and HPQs/OVV. We have also noted that the sources of two-component spectra (HPQs/OVV) are superluminal radio sources. Relativistic jet

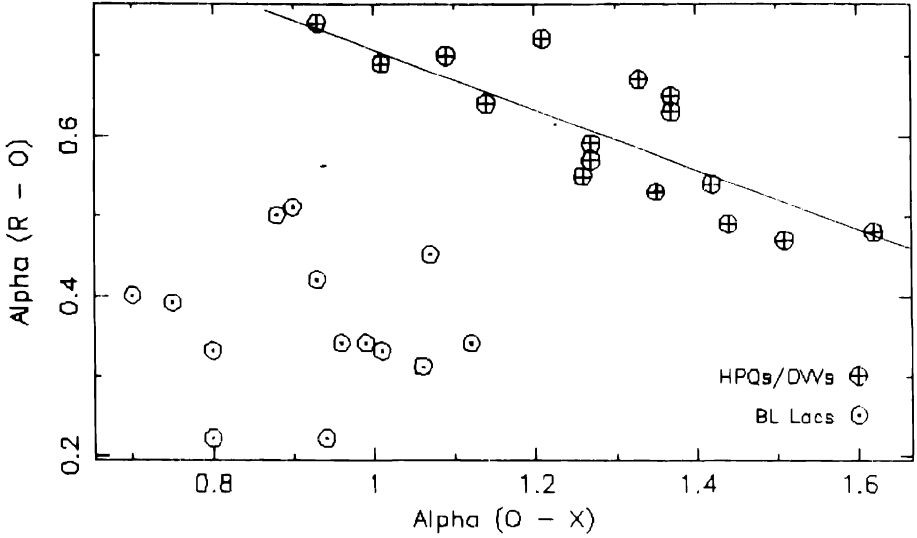


**Figure 2.** Plot of two-point spectral indices of 30 blazars between radio and optical band ( $\alpha_{R-O}$ ) and between optical and X-ray band ( $\alpha_{O-X}$ ).

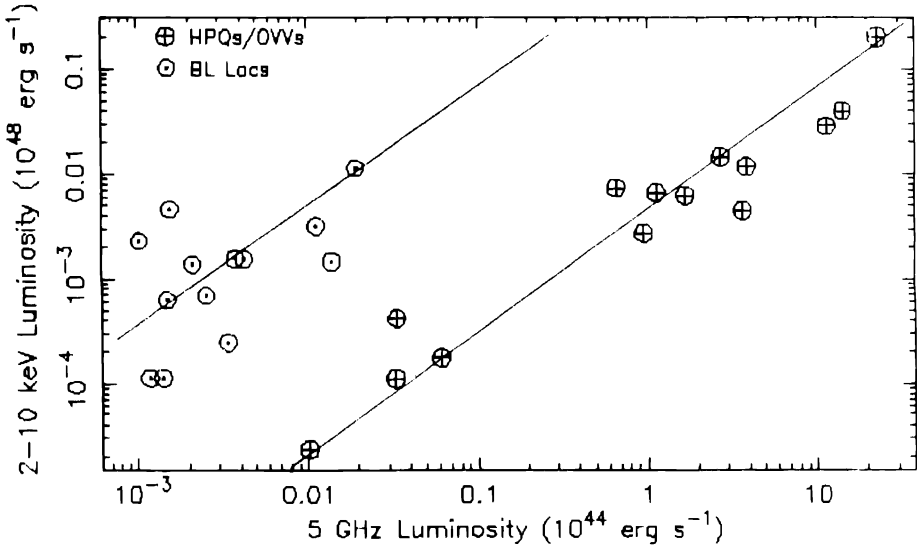


**Figure 3.** Radio (5 GHz) luminosity versus X-ray (2-10 keV) luminosity of blazars.

models (Konigl 1989 and references therein) have been proposed to explain the observed properties of various classes of blazars and it is generally believed that the dominant radiation from blazars are due to the jets. However, the jet models have their own limitations. Simultaneous multifrequency observations of these objects are strongly encouraged to understand the anisotropic emissions from blazars.

## References

- Ghosh, K. K., Soundararajaperumal, S. 1992a, *Astrophys. J.*, **389**, 179.  
Ghosh, K. K., Soundararajaperumal, S. 1992b, *Astrophys. J.*, **398**, 501.  
Konigl, A. 1989, *BL Lac Objects*, Eds. L. Maraschi, T. Maccacaro, M. -H. Ulrich (Berlin: Springer) p. 321.  
Ledden, J. E., O'Dell, S. L. 1985, *Astrophys. J.*, **298**, 630.  
Stoeckle, J. T., Liebert, J., Schmidt, G., Gioia, I. M., Maccacaro, T., Schild, R. E., Maccagni, D., Arp, H. 1985, *Astrophys. J.*, **298**, 619.  
Stoeckle, J. T., Morris, S. L., Gioia, I. M., Maccacaro, T., Schild, R. E., Wolter, A. 1988, *Optical Surveys for Quasars*, Ed. P. Osmer, A. C. Porter, R. Green, C. Foltz, (San Francisco: Astronomical Society of the Pacific) p. 311.  
Worrall, D. M., Giommi, P., Tananbaum, H., Zamorani, G. 1987, *Astrophys. J.*, **313**, 596.  
Worrall, D. M. 1989, *BL Lac Objects*, Eds. L. Maraschi, T. Maccacaro, M. -H. Ulrich, (Berlin: Springer) p. 303.



## Ionized Gas in Elliptical Galaxies<sup>1</sup>

K. P. Singh<sup>2</sup>, T. P. Prabhu<sup>3</sup>, A. K. Kembhavi<sup>4</sup> & P. N. Bhat<sup>2</sup>

<sup>2</sup> *Tata Institute of Fundamental Research, Bombay 400 005, India.*

<sup>3</sup> *Indian Institute of Astrophysics, Bangalore 560 034, India.*

<sup>4</sup> *Inter-University Centre for Astronomy & Astrophysics, Pune 411 007, India.*

**Abstract.** We report observations of H $\alpha$  nebulosities in the X-ray bright elliptical galaxies which are members of nearby groups of galaxies or clusters. Our sample includes NGC 1399, NGC 1600, NGC 2563, NGC 3607, NGC 4203, NGC 4636, NGC 4753 and NGC 5044. Some of these galaxies have X-ray cooling flows. The results are based on CCD surface photometry carried out using the broad band filters *V* and *R*, and a narrow band filter appropriate for the red-shifted H $\alpha$  + [N II] emission. We present the integrated H $\alpha$  luminosities in these galaxies and examine various emission mechanisms. Photoionization by young stars is a viable mechanism. New features like dust and shells with blue colours have been discovered in some galaxies. The presence of the 10<sup>4</sup> K gas is associated with the presence of such features indicative of galaxy-galaxy interactions. In NGC 3607, rings or a disk of dust surrounds the ionized gas. In NGC 4753, a very complex system of dust lanes is observed. We suggest that the dust and associated gas in NGC 3607 is acquired from an interacting neighbour NGC 3608. Accretion events or mergers may be common in these galaxies.

**Key words:** Elliptical galaxies—surface photometry—galaxy-galaxy interactions; ionization; gas; dust.

### 1. Introduction

Optical spectroscopic observations have revealed that nearly 40% of the elliptical galaxies show faint emission lines (Phillips *et al.* 1986). These emission line spectra have the characteristic of LINERS (Low Ionization Nuclear Emission Regions) wherein the lines from singly ionized species are strong relative to HII regions and higher ionization lines are weak relative to AGNs. This has led to the suggestion that such spectra are typically produced by low velocity ( $< 100 \text{ km s}^{-1}$ ) shocks or photo-ionization by a dilute power-law continuum (Heckman 1987). In particular, H $\alpha$  and [NII] emission lines are seen in the central regions of the elliptical galaxies indicating the presence of warm (10<sup>4</sup> K) ionized gas. The origin of the gas, its ultimate fate, and excitation mechanisms are not fully understood, however. The investigation of the above questions can be extremely interesting as it covers many topics e.g., inter-relationship of different gas phases, theory of cooling flows, frequency and relevance of mergers in

<sup>1</sup> Based on observations using Vainu Bappu Telescope, VBO, Kavalur.

galaxy evolution, stellar evolution, star formation etc. It is with the aim of getting an insight on these problems that we are imaging the faint emission nebulosities and studying the properties of the warm gas viz., mass, luminosity, extent, structure and shape with respect to the stellar component, association with dust and shells etc.

We have targeted the X-ray bright elliptical galaxies (Fabbiano *et al.* 1992) which are members of nearby groups of galaxies or clusters (Table 1). Diffuse X-ray emission and 'cooling flows' have been resolved in some of these galaxies (Thomas *et al.* 1986).

## 2. Observations

The galaxies were imaged using a GEC P8603 front-illuminated CCD at the prime focus of the 2.3 m Vainu Bappu Telescope (VBT) at Kavalur. The images were obtained through broadband *V* and *R* filters as well as narrow band filters selected appropriately for the target galaxy based on its redshift so as to cover the H $\alpha$  emission. Spectrophotometric standard stars (Stone 1977) in the neighbouring regions of the sky were observed for calibrating the narrow band filter data. The standard stars in the 'dipper asterism' region of M67 (Bhat *et al.* 1992), from Landolt (1983) and Kilkenny & Menzies (1989) were observed for calibrating the *V* and *R* data. The details of the CCD camera and its standardization using the M67 star cluster have been reported by Bhat *et al.* (1990 & 1992), and Anupama *et al.* (1993). Briefly, the image scale on the CCD is 0.6 arcsec pixel<sup>-1</sup> at the *f*/3.25 prime focus of the VBT and the field of view is  $5.7 \times 3.8$  arcmin<sup>2</sup>. The read-out noise of the CCD is  $\sim 10$  electrons and the gain setting corresponds to  $\sim 4$  electrons per CCD count (ADU) (Prabhu, Mayya & Anupama 1992).

## 3. Results

In Fig. 1, we show two representative contour maps of the surface brightness of H $\alpha$  and [NII] emission from NGC 1600 and NGC 3607 derived using the *R* and narrow-band filter data (for details see Singh *et al.* 1993). All galaxies in our sample, except NGC 2563, were detected to have significant line emission. The emission is concentrated in the central regions. The sizes are in the range 2.0–2.5 kpc in NGC 3607, 4203, 4636 and 4753, and 4–6 kpc in NGC 1399, 1600 and 5044. The total H $\alpha$  + [NII] luminosities are given in Table 1. The ratio of these luminosities to their total X-ray luminosities ranges from  $\sim 2 \times 10^{-2}$  to  $\sim 1$ . X-rays may be absorbed considerably in the dust of NGC 4753, thus leading to very low observed  $L_x$ . From the *V* and *R* data we detect many *new features like rings and lanes reddened due to dust in NGC 3607 and 5044, and residual shells which are distinctly blue in NGC 4203 and 4636* (Table 1).

## 4. Discussion

We have examined various emission mechanisms, such as recombination in cooling flows, heating of neutral gas associated with dust found in most of these galaxies, and ionization due to stars. Ionization in cooling flow fails to account for the observed emission nebulosities unless the recombination rate is increased by  $10^2$  to  $10^3$  times. Heat conduction, though adequate in some galaxies with small ratio of  $L_{H\alpha + [NII]}$  to  $L_x$

Table 1.

Galaxy name NGC	Type (RC3) <sup>6</sup>	Blue magnitude (RC3) <sup>6</sup>	Distance <sup>1</sup> (Mpc)	$\log L_{H\alpha}^{2}$ (nm) (ergs s <sup>-1</sup> )	$\log L_x^1$ (ergs s <sup>-1</sup> )	Other information <sup>3,4,5</sup> (Dust & shell features <sup>2</sup> )
1399	E1	10.55	27.2	40.98	42.31	Fornax Cluster, CF, shell.
1600	E3	11.93	90.3	40.36	41.95	Group, CF, shells.
2563	SO	13.24	96.1	-----	42.12	Cancer cluster, CF, shells.
3607	SO	10.82	32.0	40.63	40.88	HG56, dust rings.
4203	SAB0	11.80	15.6	40.82	40.96	GH94, Blue shell.
4636	E0	10.43	27.3	40.20	41.65	HG41, CF, Blue shell.
4753	I0	10.85	24.3	40.55	40.08	HG41, Dust lanes.
5044	E0	11.72	62.5	41.66	43.17	HG39, CF, Dust lane.

<sup>1</sup> Distances and  $L_x$  are from Fabbiano *et al.* (1992).

<sup>2</sup> Present work.

<sup>3</sup> HG: Group of galaxies from the Catalog by Huchra & Geller (1982).

<sup>4</sup> GH: Group of galaxies from the Catalog by Geller & Huchra (1983).  
(Also see Vennik (1986) for the N 3607 group).

<sup>5</sup> CF: Cooling Flow galaxies (Thomas *et al.* 1986).

<sup>6</sup> RC3: de Vaucouleurs *et al.* (1993).



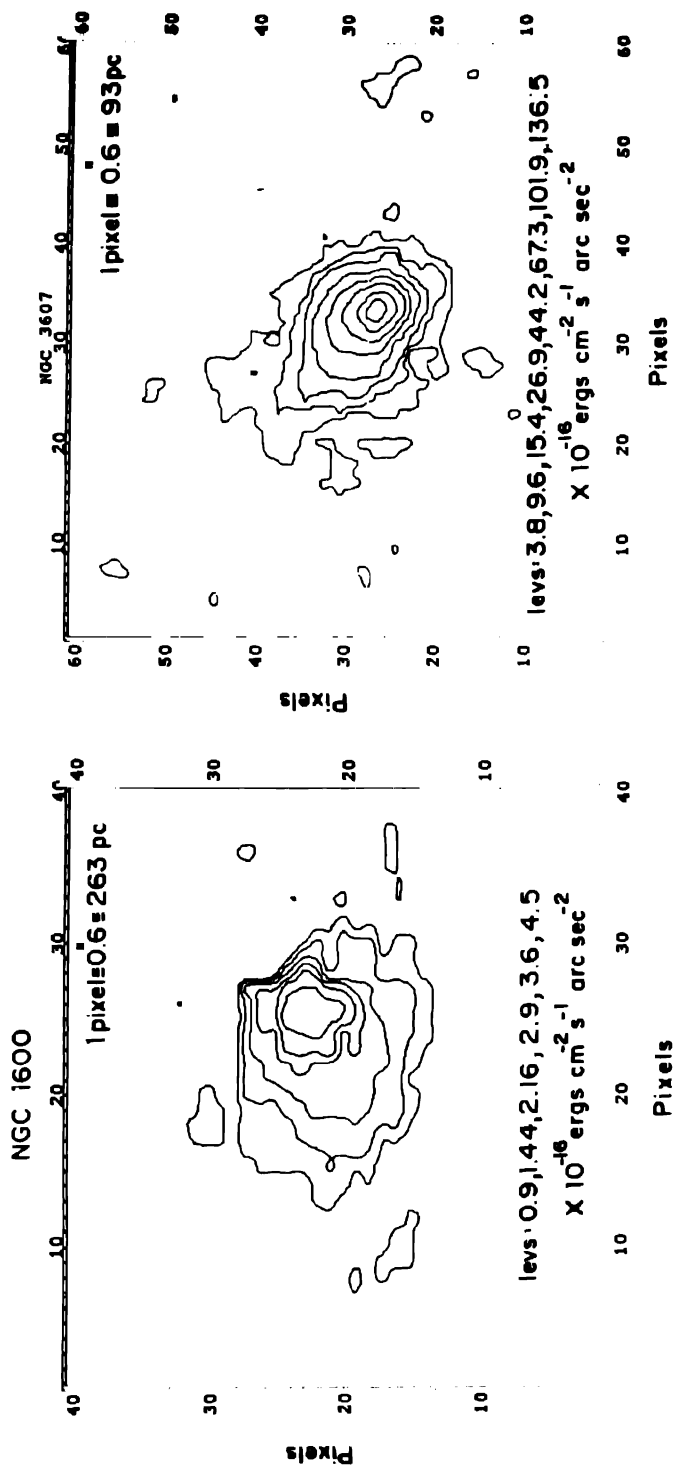


Figure 1. Surface brightness maps of  $\text{H}\alpha + [\text{NII}]$  emission in NGC 1600 and NGC 3607. Contour levels are indicated in the figure. East is towards the top and North is towards the right approximately.

as in NGC 4696 (Sparks, Macchetto & Golombek 1989), is found to be insufficient to match the cooling rate of the  $10^4$  K gas in NGC 3607 (Singh *et al.* 1993), NGC 4203 and 4753 (Singh *et al.* (in prep.)). If the ionization is due to stars, bursts of star formation and top heavy star formation are needed (Singh *et al.* 1993). In addition, the cooling timescales of the warm gas are very short and the dust cannot survive for too long in these environments. Therefore, both dust and neutral gas need to be replenished frequently. In case of NGC 3607, there is good evidence, from its rotation curve, of interaction with the gas rich neighbour NGC 3608 (Jedrzejewski & Schechter 1988) which could also be the supplier of gas and dust. The presence of shells in most galaxies (particularly those with blue colours) indicates significant ongoing merger activity and star formation. In conclusion, it appears that accretion and merger effects are common and are also the cause of enhanced star formation and ionization in these galaxies.

### Acknowledgements

We are grateful to the staff of Indian Institute of Astrophysics, Bangalore for the maintenance of the VBT and CCD system. We thank G. Selvakumar and M. Ganesan for their assistance during the observations.

### References

- Anupama, G. C., Kembhavi, A. K., Prabhu, T. P., Singh, K. P., Bhat, P. N. 1993, *Astr. Astrophys.*, (in press).
- Bhat, P. N., Kembhavi, A. K., Patnaik, K., Patnaik, A. R., Prabhu, T. P. 1990, *Indian J. Pure & Applied Phys.*, **28**, 649.
- Bhat, P. N., Singh, K. P., Prabhu, T. P., Kembhavi, A. K. 1992, *J. Astrophys. Astr.*, **13**, 293.
- de Vaucouleurs, G., de Vaucouleurs, A., Corwin, Jr., H. G., Buta, R. J., Paturel, G., Fouque, P., 1993, *Third reference Catalogue of Bright Galaxies*, Springer-Verlag. (RC3).
- Fabbiano, G., Kim D.-W., Trinchieri, G. 1992, *Astrophys. J. Suppl.*, **80**, 531.
- Geller, M. J., Huchra, J. P. 1983, *Astrophys. J. Suppl.*, **52**, 61.
- Heckman, T. M. 1987, *IAU Symposium 121, Observational Evidence of Activity in Galaxies*, Ed. E. Khachikian, K. Fricke & J. Melnick, (Dordrecht: Reidel), p. 421.
- Huchra, J., Geller, M. 1982, *Astrophys. J.*, **257**, 423.
- Jedrzejewski, R., Schechter, P. L. 1988, *Astrophys. J.*, **330**, L87.
- Kilkenny, D., Menzies, J. W. 1989, *South African Astr. Obs. Circ. No.*, **13**, 25.
- Landolt, A. U. 1983, *Astr. J.*, **88**, 439.
- Phillips, M. M., Jenkins, C. R., Dopita, M. A., Sadler, E. M., Binette, L. 1986, *Astr. J.*, **bf 91**, 1062.
- Prabhu, T. P., Mayya, Y. D., Anupama, G. C. 1992, *J. Astrophys. Astr.*, **13**, 129.
- Singh, K. P., Prabhu, T. P., Kembhavi, A. K., Bhat, P. N. 1993, *Astrophys. J.*, (submitted).
- Sparks, W. B., Macchetto, F., Golombek, D. 1989, *Astrophys. J.*, **345**, 153.
- Stone, R. P. S. 1977, *Astrophys. J.*, **218**, 767.
- Thomas, P. A., Fabian, A. C., Arnaud, K. A., Forman, W., Jones, C. 1986, *Mon. Not. R. astr. Soc.*, **222**, 655.
- Vennik, J. 1986, *Astr. Nachr.*, **307**, 157.



## Abstracts

### A Head-Tail Source Found with Miyun Synthesis Radio Telescope

Zhang Xizhen<sup>1</sup>, T. A. Th. Spoelstra<sup>2</sup> & Wang Yumin<sup>1</sup>

<sup>1</sup>*Beijing Astronomical Observatory, CAS, Beijing 100080, China*

<sup>2</sup>*NFRA, Postbus 2, 7990 AA Dwingeloo, The Netherlands*

**Key words:** Radio source—multi-wavelength observations—cD galaxy

A new head-tail radio source was found using the MSRT in 1988 at 232 MHz, in one of the fields of the Miyun 232 MHz radio survey, i.e. centered at  $\alpha_{(1950.0)} 0^{\text{h}}41^{\text{m}}$  and  $\delta_{(1950.0)} 41^{\circ}12'$ . The source appears as a large diffuse tail ( $\sim 20'$ ) with two other known sources north of it. The source is not present in the B3 catalog (Ficarra, A. *et al.* 1985). It is located at  $R.A. 00^{\text{h}}50^{\text{m}} 17.1^{\text{s}}$ , Dec.  $43^{\circ}18'23.9''$ . It does not appear in the IRAS point source catalog and IRAS weak source catalog. It has also no UV counterpart in the IUE database. Only a Zwicky cluster (ZC0050 + 4325) is found within the field of view of the MSRT but it is far from the source. With the MSRT resolution of  $3.8 \times 3.8$  the source cannot be resolved, but gives a peak flux of 0.44 Jy and an integrated flux density of 0.7 Jy at 232 MHz.

To resolve the source, observations with the VLA at frequencies 1.4 GHz, 4.9 GHz, and 8.4 GHz have been made. At 1.4 GHz it is seen as a source with two bending tails, while at higher frequency it appears to have a single tail with a nucleus. VLA observations provided accurate positions and resolved the source complex into several components as summarized in Table 1. In order to study changes of spectral index in the source complex the 4.8 GHz map has been convolved to resolution of the 1.4 GHz map. The results are also given in Table 1.

We also obtained maps with about  $1'$  resolution at 151 MHz and 327 MHz from Cambridge and WSRT, respectively. Both of them show complex morphologies and tendencies like that at 1.4 GHz.

The optical observation was obtained in October 1991 with Xinlong 2.16 m telescope, Beijing Astronomical Observatory, and the CCD direct-imaging camera. A  $14''$  galaxy was found at the position of the head of the new head-tail source. Its coordinates are  $\alpha 00^{\text{h}}50^{\text{m}} 13.45^{\text{s}}$ ,  $\delta 43^{\circ}18'43.5''$  (1950.0). There is an empty field at the position of the component 2.

This peculiar source may be either a member of a cluster of galaxies or a cD galaxy. There is not so much evidence for the first possibility, because this galaxy is rather isolated, i.e. not clearly related to a cluster or group of galaxies. A cD galaxy with two radio tails and angle between the tails of less than  $90^{\circ}$  had not been found in literature. Is this the first one? The source was also identified by Peng (Peng 1993) as a possible variable.

We wish to thank Prof. Chen Jianshen for granting us telescope time and giving us much useful direction. We are indebted to Drs. W. M. Goss, J. P. Ge, and P. Warner for their observations of the interesting sources.

**Table 1.** The spectral indices list.

Component	Position(1950.0)	Spectra index(1417–4885)
Tail A		– 0.97
Tail B		– 0.79
Head(H)	005013.6 + 431842.4	– 0.16
Component 1	005024.1 + 431901.6	– 0.2
Component 2	005018.5 + 431813.6	– 0.6

### References

- Ficarra, A., Grueff, G., Tomassetti, G. 1985, *Astr. Astrophys. Suppl.*, **59**, 255.  
 Peng Bo 1993, *Thesis of Beijing Astronomical Observatory*, **97**.

★★★★★

## A VLA 20 and 90 centimetre Radio Survey of Distant Abell Clusters with Central cD Galaxies

J. Bagchi & V. K. Kapahi *National Centre for Radio Astrophysics, TIFR, Pune 411 007, India*

Results of an extensive imaging radio survey of a statistical sample of the most distant Abell clusters ( $0.1 < z < 0.3$ ) of galaxies dominated by cD galaxies are reported. In order to understand the origin and evolution of radio sources in these clusters, about 50 cluster fields were mapped at 1.4 GHz, and about 35 of these were mapped both at 1.4 GHz and 330 MHz, all with the VLA. The main results are as follows:

- The radio luminosity function (RLF) of the cD galaxies is found to agree quantitatively with the RLF of giant elliptical galaxies (located in less richer galactic environment) for 1.4 GHz radio luminosity  $< 10^{24.5} \text{ WHz}^{-1}$ . However, beyond this limit, cD galaxies are more likely to be radio sources than ellipticals. This behaviour of the RLF can be understood in terms of the correlation between radio and optical luminosity of the giant elliptical systems.
- No significantly large population of steep spectrum radio sources with spectral index  $\alpha > 1.2$  between 330 and 1400 MHz is found in these clusters. The median spectral index of the cD galaxies is only  $0.70 \pm 0.13$ , very similar to the median value for non cluster radio galaxies.
- A re-examination of the radio and X-ray data on the nearby ( $0.03 < z < 0.15$ ) Abell clusters with cD galaxies reveals a significant negative correlation between the radio luminosity of the cD galaxy and the cooling time of the hot intra-cluster-medium. As many as 70% of the radio emitting cD galaxies (with 1.4 GHz radio luminosity  $> 10^{22.7} \text{ WHz}^{-1}$ ) are found to be located at the focii of 'cooling-flows'. This implies that the majority of the radio-loud cDs detected by us in distant Abell clusters could be associated with massive 'cooling-flows'. Physical models of the confinement of the radio plasmas and the fuelling of central energy sources of cDs are examined to understand the effect.

- (d) The radio-emitting cD galaxies are found to be located close to the centres of their host clusters, while the radio-quiet cDs are not centrally located. The possibility of the dynamical evolution of clusters causing this effect is considered.
- (e) A significant excess in the surface number density in the central 1 Mpc of the clusters is detected over the isotropic radio source background. No such departure is found in the outer parts of the same clusters, implying clustering of radio sources near cluster centres.

★★★★★

## Variability in Southern BL LAC Objects at cm Wavelengths

Don Bramwell *Hartebeesthoek Radio Astronomy Observatory, South Africa*

The behaviour of the most variable objects is discussed in comparison with active northern sources and with the less active objects in the sample.

★★★★★

## Multi-Waveband Studies of the Molonglo 1-JY Sample of Radio Galaxies

V. K. Kapahi, R. M. Athreya & C. R. Subrahmanya *National Centre for Radio Astrophysics, TIFR, Pune 411 007, India*

P. J. McCarthy *Observatories of the Carnegie Institution of Washington, Pasadena, USA*

W. van Breugel *IGPP, Lawrence Livermore National Laboratory, Livermore, USA*

The current status of the project to identify and study radio galaxies in a complete sample of over 500 radio sources from the Molonglo Reference Catalogue with  $S \geq 0.95$  Jy at 408 MHz is described. Radio maps of the entire sample have been made with resolutions between 1 and 5 arcsec at 5 GHz using the Very Large Array. The maps are being used to make optical identifications from deep R-band CCD imaging using the 2.5 m Du Pont telescope at Las Campanas. Spectroscopic observations of identified objects are being made with the 4 m telescope at Cerro Tololo. The project has already led to the identification of about 50 galaxies at  $z > 1$ . About 20 of these have  $z > 2$ , including two at  $z = 3.13$  and  $3.04$  respectively, which are the most distant galaxies known in the southern hemisphere. Our results confirm the correlation between radio spectral index and redshift, as most of the high redshift galaxies have rather steep radio spectra.

Many of the galaxies are also being imaged in the g, I, J, H and K wavebands in order to determine the spectral energy distributions. The results are discussed in the context of the observed alignment between the radio, optical and IR emission.

★★★★★

## **Twin Jets in an FR II Radio Galaxy**

**Lakshmi Saripalli** *Universität Bonn, Germany*

**Ravi Subrahmanyan** *National Centre for Radio Astrophysics, Pune 411 007, India*

**Richard Hunstead** *University of Sydney, NSW 2006, Australia*

Using the Australia Telescope, we have discovered a bright jet and counter-jet in a radio galaxy that has an edge-brightened structure. These quasi-continuous jets are the longest astrophysical jets seen to date. We present the observations and implications for the unifying theory for PRGs and quasars.

★★★★★

## **Compact Groups of Galaxies: Interactions and Radio Emission**

**V. R. Venugopal, K. S. V. S. Narasimhan & S. M. Alladin** *Inter-University Centre for Astronomy and Astrophysics, Pune 411 007, India*

Menon (1992, *Mon. Not. R. astr. Soc.*, **255**, 41) has shown that in the case of radio-loud E & SO galaxies in the Hickson compact groups the distances of the nearest neighbours are less than those for radio-quiet galaxies and they are predominantly the first ranked ones. We attempt to interpret these results in terms of the compactness of the groups and the tidal radii of the galaxies (radio sources) and their nearest neighbours and their merger times.

★★★★★

## **A Jet Model of Plasma Turbulence Acceleration for AGNs**

**Tong Yi & Li Qingkang** *Beijing Normal University, Beijing 100875, China*

The jet stream is an important phenomenon for active galactic nuclei. One of the most important problems about jets is why they can go from pc scale to several hundred kpc scale, while remaining collimated. It is possible that jets have been accelerated while they spurt from the nozzles. Many of the models have been suggested to discuss jets and some results have been obtained.

In this paper we put forward the possibility that particles are accelerated by plasma turbulence waves. Using the conservation equation of the wave action density, the state equation, the conservation equation for momentum, the continuity equation and the conservation equation of magnetic flux, we obtain the solution for jet velocity and the

results are coincident with the observational evidence (such as high velocity of jets). So we think that the plasma turbulent wave is an efficient mechanism to accelerate jets.

★★★★★

## **BVRI Imaging of the Disturbed Spiral Galaxy NGC 2701**

**S. K. Pandey** *Ravishankar University, Raipur 492 010, India*

**A. K. Kembhavi** *Inter-University Centre for Astronomy and Astrophysics, Pune 411 007, India*

**V. Mohan** *Uttar Pradesh State Observatory, Nainital 263 129, India*

We present the results of BVRI imaging of the disturbed spiral galaxy NGC 2701 taken at the f/13 Cassegrain focus of the one metre telescope at UPSO, Nainital, India. NGC 2701 is classified as a SAB(rs)c type galaxy having a relatively large and elongated companion at 8' South. Its structure is rather complex, and it is difficult to derive the surface brightness, ellipticity and position angle distributions in the usual manner by fitting ellipses to the observed isophotes. We present these profiles as well as two dimensional colour maps of the galaxy. We also present the decomposition of the galaxy into its bulge and disc components, put limits on a possible central point source, and discuss the residual structure present after a smooth model of the galaxy is eliminated.

★★★★★

## **Multicolour Investigations of Shells, Dust and Other Features in Elliptical Galaxies**

**Neeharika Thakur, Devendra Sahu & S. K. Pandey** *Ravishankar University, Raipur 492 010, India*

**A. K. Kembhavi** *Inter-University Centre for Astronomy and Astrophysics, Pune 411 007, India*

We present results of CCD observations of several elliptical galaxies obtained in *B*, *V* and *R* bands at the prime focus of the 2.3 metre Vainu Bappu Telescope (VBT) at Kavalur, India. We have examined these galaxies for the presence of shells, dust and other features by constructing colour maps, and residuals obtained by subtracting a smooth model of the underlying galaxy from the original image. We confirm the presence of features in NGC 2476 and NGC 4374 which have been studied earlier by other workers, and report on features in other ellipticals for the first time. We provide estimates of the fluxes and colours of various features.

★★★★★



## **Surface Photometry of the Elliptical Galaxies NGC 1600 and NGC 507**

**Ashish Mahabal & A. K. Kembhavi** *Inter-University Centre for Astronomy and Astrophysics, Pune 411 007, India*

**K. P. Singh** *Tata Institute of Fundamental Research, Bombay 400 005, India*

**Richard Green** *National Optical Astronomy Observatories, P.O. Box 26732, Tucson, USA*

We present results of CCD direct imaging of the two elliptical galaxies NGC 1600 and NGC 507, which are known X-ray sources and are members of interacting pairs. We have used various techniques to examine these galaxies for the presence of shells, structure and other features. We examine properties of the features found and compare these with the features in ellipticals reported by other workers. We also examine the regions between and around the members of the group.

★ ★ ★ ★ ★

## **Surface Photometry of Seyfert Galaxies NGC 2992, NGC 3227 and NGC 7172**

**G. C. Anupama & A. K. Kembhavi** *Inter-University Centre for Astronomy and Astrophysics, Pune 411 007, India*

**M. Elvis** *Harvard-Smithsonian Centre for Astrophysics, Cambridge, Ma, USA*

**R. Edelson** *National Aeronautics and Space Administration, Washington DC 20546, USA*

Broad band images of NGC 2992, NGC 3227 and NGC 7172, selected from a larger sample of hard X-ray loud Seyfert galaxies, the Piccinotti sample, have been analysed. We present here the results of surface photometry. The radial luminosity profile is decomposed into point source, bulge and disc components. An estimate is made of the extinction in these galaxies, as also the mass of dust and neutral hydrogen present in the galaxy.

★ ★ ★ ★ ★

## **Detection of Microvariability in Polarization in a BL LAC Object OJ287**

**M. R. Deshpande & U. C. Joshi** *Physical Research Laboratory, Ahmedabad 380 009, India*

One of the important studies related to AGN is to detect rapid variations in the flux and polarization to assess the size of the source and possibly the physical processes taking place in the nuclei of AGNs. Recently we have detected 6.3 min variations in polarization

from a BL Lac object OJ287, which was subsequently confirmed by others. The importance of these observations on the energetics in the central engine/jet will be discussed.

★★★★★

## **Dynamics of Stellar Content of Hot-Spot Regions of Active Galaxies**

**V. Korchagin & A. K. Kembhavi** *Inter-University Centre for Astronomy and Astrophysics, Pune 411 007, India*

**D. Mayya & T. Prabhu** *Indian Institute of Astrophysics, Bangalore 560 034, India*

We investigate self-regulated propagation of star formation in molecular clouds fragmented to cold dense structures with masses lying near or above the Jeans mass. Strong UV radiation of newborn massive stars heating and compressing nearby dense inhomogeneities could be a triggering mechanism for the formation of a new generation of stars. Once initiated, star formation propagates with a velocity determined by the parameters of cloud inhomogeneities.

The UV flux from newly born stars leads to evaporation of protostellar inhomogeneities which produce stars, and when the UV flux reaches a critical value, propagation of star formation has to stop. So star formation in galaxies has a built in self-regulatory mechanism.

The propagating, self-regulated star forming activity manifests itself as hot-spots in various galactic regions. We determine theoretically an integral stellar mass spectrum in stellar complexes in such a hot spot scenario, and compare it with results from other scenarios of star formation.

★★★★★

## **Quasar-Galaxy Interactions: A Possible Mechanism for Formation of cD-Galaxies and Gravitational Lenses**

**J. Anosova & M. K. Deshpande** *Physical Research Laboratories, Ahmedabad 380 009, India*

Tidal effects of disruption and merger of a massive perturber-quasar on a galaxy cluster have been studied by computer simulations using Aarseth's N-BOBY 2 code. The model consists of a spherical N-body galaxy cluster and a point-mass perturber. A wide range of the initial conditions (the ratios of masses of the objects, virial coefficient  $q$  of N-body system, pericentric distances and eccentricities of the orbit) have been used.

It is shown that for small pericentric distance, parabolic orbits and values of virial coefficients  $q > 0.5$ , collisions of objects can result in their merger. Products of such merger have properties of the cD-galaxies or gravitational lenses.

★★★★★

## **The Merger Time of Interacting Galaxies – Its Dependence on Energy and Angular Momentum**

G. M. Ballabh, K. S. V. S. Narasimhan & S. M. Alladin *Osmania University, Hyderabad 500 007, India*

An analytical expression for the merger time  $t_m$ , of interacting galaxies is deduced in terms of their orbital energy,  $E$ , and angular momentum,  $L$ , from the tidal forces estimated by neglecting the internal structure and motion. This relation gives results which are consistent with those obtained by detailed N-body simulations. It is noted that  $t_m$  depends very strongly on  $L$  ( $t_m \propto L^6$ ). Energy-angular momentum plots for different masses and merging time are given according to the analytical relations obtained.

★★★★★

# **Pulsars**



## New Lessons from Old Pulsars

**Matthew Bailes** *Australia Telescope National Facility, CSIRO, PO Box 76, Epping, Australia, 2121.*

**Abstract.** The recently awarded Nobel prize for physics to Prof. J. H. Taylor and Prof. R. Hulse for the discovery of the binary pulsar PSR 1913 + 16, reinforces the fact that even 25 years after their discovery, radio pulsars continue to appear at the forefront of modern astrophysical research. The most exciting advances over the past decade have come from observations of old pulsars which have been given a second lease of life due to mass transfer from a binary companion. The study of these so-called 'recycled' pulsars has taught us a great deal, not only about these exciting systems, but also about the evolution of the 'normal' pulsars.

**Key words:** Pulsars; binary—neutron stars.

### 1. Introduction

In the early 1980's the bulk of the radio pulsar population consisted of what I will refer to as 'normal' pulsars. These pulsars were characterised by strong magnetic field strengths ( $\sim 10^{12}$  G), rotation periods of between 33 ms and 4 seconds, with the bulk of the population within a factor of a few of 1 second. They typically lay at distances of a few kpc and appeared to be migrating from the galactic plane with velocities of  $\sim 100 \text{ km s}^{-1}$  (Lyne, Anderson & Salter 1982). However a new class of pulsars were emerging, the so-called 'millisecond' pulsars. These were characterised by much lower magnetic field strengths  $\sim 3 \times 10^8$  G, and rotation periods measured in terms of milliseconds. The first of these PSR 1937 + 21, discovered by Backer *et al.* (1982) remains the most rapidly rotating neutron star known with a rotation period of only 1.55 ms. After the completion of the second Molonglo survey (Manchester *et al.* 1978), which discovered 155 pulsars, the sample of 'normal' pulsars was adequate for most statistical studies, and the millisecond pulsar injected new life into radio pulsar studies and surveys.

In this paper I will first of all outline the standard model of radio pulsar evolution at the time when only a handful of millisecond pulsars were known, which is largely the model of Lyne, Manchester & Taylor (1985). Then I will take the reader through the significant advances in our understanding which took place largely as the result of the discovery of millisecond and recycled pulsars. For a more complete work on the recent pulsar discoveries interested readers should consult Bailes & Johnston (1993).

### 2. Normal pulsar evolution circa 1985

In a landmark paper only a few years after their discovery Gunn & Ostriker (1970) described a model of the pulsar population which remained in vogue for almost 20 years. At the time there were only about 40 pulsars known and less than half of these

possessed measured period derivatives. The product of a pulsar's period  $P$  and period derivative  $\dot{P}$  gives an indication of its magnetic field strength  $B$ , and in convenient units:

$$B_{12} \sim \sqrt{P\dot{P}_{-15}} \quad (1)$$

here  $B_{12}$  is the magnetic field strength in units of  $10^{12}$  G,  $P$  the period in seconds, and  $\dot{P}_{-15}$  is the period derivative in the conventional pulsar units of  $10^{-15} \text{ s s}^{-1}$ . The characteristic age of a pulsar  $\tau$  is usually defined as

$$\tau = \frac{P}{2\dot{P}} \quad (2)$$

and is close to the true age provided that the initial spin period is small compared to the current one, the magnetic field does not decay and the braking index is 3. The main conclusions of Gunn & Ostriker (1970) were as follows:

- Pulsars live for about  $4 \times 10^6$  years and perish due to the decay of their magnetic field strength  $B$ , with the radio luminosity being proportional to  $B^2$ .
- The beaming fraction is about 20%.
- The birthrate is about one per 30 years in the Galaxy.
- The average velocity of pulsars at birth is  $100 \text{ km s}^{-1}$ .
- Pulsars arise from stars greater than  $4 M_{\odot}$ .

Fifteen years after this paper, Lyne, Manchester & Taylor (1985) repeated the analysis of Gunn & Ostriker (1970) with a much larger ( $\sim 300$ ) and more complete sample of the radio pulsar population. In this paper a new distance model was derived and many of the conclusions of Gunn & Ostriker (1970) appeared to stand the test of time. The birthrate derived was between one per 30 years and one per 120 years. The field decay constant derived was 9 Myrs and the velocities measured for pulsars by Lyne, Anderson & Salter (1982) using interferometry  $\sim 200 \text{ km s}^{-1}$  were shown to be largely consistent with their observed  $z$ -distribution.

### 3. New lessons from old pulsars

The refined model of Gunn & Ostriker (1970) presented by Lyne, Manchester & Taylor (1985) has now undergone substantial revision. This is almost solely due to the discovery of the recycled pulsars both in the disk and globular clusters.

#### 3.1 *Discovery of the millisecond pulsar: Implications for pulsar radio luminosity*

The millisecond pulsar PSR 1937 + 21 had a magnetic field strength 4 orders of magnitude lower than the bulk of the pulsar population. This pulsar was extremely luminous and as a result it was immediately obvious that the luminosity of (at least millisecond) pulsars did not follow the  $L \propto B^2$  law proposed by Gunn & Ostriker (1970) and used by Lyne, Manchester & Taylor (1985) in their analyses of the pulsar population. Prószyński & Przybycień (1984) and others such as (Narayan 1987; Chevalier & Emmering 1986) attempted to use relations of the form

$$L_{\text{rad}} \propto P^{\alpha} \dot{P}^{\beta} \quad (3)$$

to describe a radio pulsar's radio luminosity ( $L_{\text{rad}}$ ), where  $\alpha$  and  $\beta$  were constants. These fits to the observed data argued strongly against the  $\alpha = \beta = 1$  used by Gunn & Ostriker (1970) and Lyne, Manchester & Taylor (1985), and suggested a negative value for  $\alpha$  was more appropriate. Despite this, there remains an enormous scatter about any power law relation relating pulsar radio luminosity to  $P$  and  $\dot{P}$  (Lorimer *et al.* 1993).

### 3.2 Birthrate of millisecond pulsars: Implications for magnetic field decay

The discovery of the low-luminosity millisecond pulsar PSR 1855 + 09 meant that the birthrate of these objects was much higher than their assumed progenitors, the Low-mass X-ray binaries, even if the millisecond pulsars lived forever (Narayan 1987; Kulkarni & Narayan 1988). This meant that pulsar magnetic fields must cease decaying if millisecond pulsars were long-lived objects. On the other hand if millisecond pulsars were once 'normal' pulsars, their magnetic fields *must* have decayed.

### 3.3 Optical identification of the companion of PSR 0655 + 64: Implications for field decay

Kulkarni (1986) successfully detected the optical companion of the binary pulsar PSR 0655 + 64. It was a very cool white dwarf with a cooling age near that of the characteristic age of the pulsar. This meant that the magnetic field of PSR 0655 + 64 was no longer decaying and lead Kulkarni to propose a two-component model for pulsar magnetic fields. In his model the core field was non-decaying and the crustal field decayed on shorter timescales. Srinivasan & Bhattacharya (1987) proposed that there was a minimum value of magnetic field strength for the millisecond pulsars, and that the fields would not decay below this level. The field of PSR 0655 + 64 was a factor of 30 higher than the millisecond pulsars, and so the core field strength had to vary between pulsars by a considerable amount.

### 3.4 The globular cluster pulsars: Implications for field decay

After the initial discovery of the pulsar in M28 by Lyne *et al.* (1987), several surveys of nearby globular clusters were undertaken. This resulted in a large number of radio pulsar detections. Because type II supernova explosions ceased in globular clusters shortly after their formation, it is widely believed that the neutron stars present there are either at least several billion years old, or have been formed by some alternative formation mechanism, such as the relatively recent accretion-induced collapse of a white dwarf star. If the former is true, the observed large range of field strengths in the cluster pulsars meant that the core fields of pulsars range by three and a half orders of magnitude, which makes the two-component theory somewhat less palatable.

The kinematic evidence for field decay was shown to be less secure than originally thought by Bailes (1989), and when Bhattacharya *et al.* (1992) demonstrated via a statistical treatment of the pulsar population that there was no need for field decay to explain their observed distribution, the evidence for field decay in the absence of mass accretion became scarce. Now models in which pulsar magnetic fields do not decay, unless they accrete matter are more in vogue, as argued by Taam & van den Heuvel (1986), van den Heuvel (1986) and Bailes (1989). The theoretical basis for such models are however, far from secure. Some examples of such models are Srinivasan *et al.* (1990) and Romani (1990).



### 3.5 The pulsar distance model

The millisecond pulsars in globular clusters clearly demonstrated a problem with the almost universally-accepted distance model of Lyne, Manchester & Taylor (1985) in that it underestimated the distances to the globular cluster pulsars. This is now understood to be because of the finite layer of free electrons in the Galaxy. Prior to the discovery of the globular cluster pulsars it was virtually impossible to obtain reliable distances to pulsars at high  $z$ . The globular cluster pulsars made it possible to estimate the maximum possible  $DM \sin b$  in the galaxy, where  $DM$  is the pulsar's dispersion measure and  $b$  is its galactic latitude.

A parallax measurement using high-precision timing of the millisecond pulsar PSR 1855 + 09 increased the number of local pulsars which possessed reliable distance measurements, and it became clear that the pulsar distance model in fact underestimated the distance to most nearby pulsars. Most pulsars are now almost a factor of two further away than previously thought (Taylor & Cordes 1993). This has decreased their birthrate and increased their mean velocities.

## 4. In retrospect

Although there no longer appears to be any strong evidence for pulsar magnetic field decay in the absence of accretion, a revision of the evolution of pulsar theory makes it clear how the belief in magnetic field decay arose, and how it was reinforced. When Gunn and Ostriker attempted to derive a luminosity law they restricted their parameterization to one variable, the magnetic field  $B$ . *Once it had been postulated that  $L \propto B^2$ , the only way a pulsar could die was to have its field decay!* The observation by Lyne, Ritchings & Smith (1975) that the *observed*, (as opposed to underlying), distribution of pulsars in the  $P - \dot{P}$  plane was consistent with field decay, and that the kinetic ages of pulsars were also consistent with this, further reinforced this belief. Finally, the infinite extent of the Galactic free-electron layer in the Lyne, Manchester & Taylor (1985) model meant that the derived  $z$ -distances of all pulsars were less than 1 kpc. This meant that all pulsars were believed to die before reaching larger  $z$ -heights. If the luminosity was related to the magnetic field strength and period, then pulsars either had to slow down to very long periods by the time they reached a  $z$ -height of 1 kpc, or have their fields decay. The slow-down rate was constrained by the magnetic field strength distribution and equation (1), and therefore field decay was a necessity.

Thus, in a subtle way, the pulsar distance model induced apparent field decay in statistical analyses of the radio pulsar population such as Narayan & Ostriker (1990). Without the globular cluster pulsars, our knowledge of the galactic free electron layer would not have improved and theoretical models of the pulsar population would still require some artificial method of reducing pulsar lifetimes, such as field decay.

## References

- Backer, D. C., Kulkarni, S. R., Heiles, C., Davis, M. M., Goss, W. M. 1982, *Nature*, **300**, 615.  
 Bailes, M., Johnston, S. 1993, in *Review of Radio Science 1990-1992* Ed. W. R. Stone (Oxford University Press) p. 677.

- Bailes, M. 1989, *Astrophys. J.*, **342**, 917.
- Bhattacharya, D., Wijers, R. A. M. J., Hartman, J. W., Verbunt, F. 1992, *Astr. Astrophys.*, **245**, 198.
- Chevalier, R. A., Emmering, R. T. 1986, *Astrophys. J.*, **304**, 140.
- Gunn, J. E., Ostriker, J. P. 1970, *Astrophys. J.*, **160**, 979.
- Kulkarni, S. R., Narayan, R. 1988, *Astrophys. J.*, **355**, 755.
- Kulkarni, S. R. 1986, *Astrophys. J.*, **306**, L85.
- Lorimer, D. R., Bailes, M., Dewey, R. J., Harrison, P. A. 1993, *Mon. Not. R. astr. Soc.*, **263**, 403.
- Lyne, A. G., Anderson, B., Salter, M. J. 1982, *Mon. Not. R. astr. Soc.*, **201**, 503.
- Lyne, A. G., Brinklow, A., Middleditch, J., Kulkarni, S. R., Backer, D. C., Clifton, T. R. 1987, *Nature*, **328**, 399.
- Lyne, A. G., Manchester, R. N., Taylor, J. H. 1985, *Mon. Not. R. astr. Soc.*, **213**, 613.
- Lyne, A. G., Ritchings, R. T., Smith, F. G. 1975, *Mon. Not. R. astr. Soc.*, **171**, 579.
- Manchester, R. N., Lyne, A. G., Taylor, J. H., Durdin, J. M., Large, M. I., Little, A. G. 1978, *Mon. Not. R. astr. Soc.*, **185**, 409.
- Narayan, R., Ostriker, J. P. 1990, *Astrophys. J.*, **352**, 222.
- Narayan, R. 1987, *Astrophys. J.*, **319**, 162.
- Prószyński, M., Przybycień, D. 1984, in *Millisecond pulsars* Eds. S. P. Reynolds & D. R. Stinebring (NRAO, Green Bank) p. 151.
- Romani, R. W. 1990, *Nature*, **347**, 741.
- Srinivasan, G., Bhattacharya, D. 1987, in *IAU Symposium No. 125: The origin and evolution of neutron stars*. Eds. D. J. Helfand & J. Huang (Dordrecht: Reidel) p. 109.
- Srinivasan, G., Bhattacharya, D., Muslimov, A. G., Tsygan, A. I. 1990, *Curr. Sci.*, **59**, 31.
- Taam, R. E., van den Heuvel, E. P. J. 1986, *Astrophys. J.*, **305**, 235.
- Taylor, J. H., Cordes, J. M. 1993, *Astrophys. J.*, **411**, 674.
- van den Heuvel, E. P. J. 1986, in *The Origin and Evolution of Neutron Stars*, *IAU Symposium No. 125* Eds. D. J. Helfand & J. Huang (Dordrecht: Reidel) p. 393.



## Pulsars in Globular Clusters

A. Ray *Tata Institute of Fundamental Research, Bombay 400 005, India*

**Abstract.** Nearly three dozen pulsars discovered in the globular clusters (GCs) have shown that these pulsars are not only quite numerous but also have somewhat different characteristics from those of the pulsars appearing near the galactic disk. Here I discuss the issues about the formation and evolution of pulsars in the globular cluster systems. In particular the question regarding the total population of these pulsars and their possible progenitor systems is addressed. The implication of the presence of a number of slow pulsars in some of the GCs is mentioned.

**Key words:** Pulsars -- binary and multiple stars -- globular clusters in the Milky Way.

### 1. Observational data on globular cluster pulsars

The number of currently confirmed pulsars in the globular clusters (GCs) is 33. A list of these pulsars with their spin periods and characteristic ages together with the dynamical properties of the GCs they appear in are given in Table 1. The GC pulsars, observed so far, have important differences from those of the galactic disk pulsars in several respects: 1) While the vast majority of more than  $\approx 600$  pulsars in our galaxy located in the galactic disk have periods between 200 ms to 2 seconds, most of the pulsars discovered so far in the GCs (all but 8) have spin periods  $P_{\text{spin}} \leq 25$  ms. 2) Similarly, while the characteristic age  $\tau_c = P/(2\dot{P})$  of the galactic disk pulsars range (mostly) between 1 to  $10 \times 10^6$  yrs, out of the pulsars in GCs which have determined characteristic ages only about three come even close to being as young as the disk pulsars. 3) The magnetic fields of the GC pulsars (assumed to be of dipolar structure) are found to span a wider range of values ( $5 \times 10^8 \leq B \leq 10^{12}$  G) with most pulsars having low field compared to those in the galactic disk where most pulsars have fields in the range of  $10^{11} \leq B \leq 10^{12}$  G (there is however uncertainty in some of the GC pulsars' fields and intrinsic spin period derivatives as the acceleration of the pulsars in the GC and the resultant contamination to  $\dot{P}$  are difficult to model due to uncertainties in the cluster parameters – see e.g. Biggs *et al.* 1994). 4) More than one-third of the GC pulsars are in binary systems and roughly 40% of the ‘millisecond’ pulsars (with  $P_{\text{spin}} \leq 25$  ms) in GCs are in binary systems. Table 2 gives the orbital period distribution of GC pulsars in binary systems. For the currently available data, the number of binary systems with short orbital periods ( $P_{\text{orb}} \leq 1d$ ) is the same as the number of systems with long orbital periods.

Table 1. Pulsars in globular clusters.

Globular cluster	Dist <sup>(1)</sup> (kpc)	PSR B	$\log \rho_c^{(1)}$ ( $M_\odot/\text{pc}^3$ )	$V_{\text{disp}}^{(1)}$ (km/s)	No. of PSR	No. of binaries	$P_{\text{spin}}$ (ms)	$\tau_c = P/(2\dot{P})$ (Gyr)	$B$ ( $10^9 C_i$ )	Ref.
47Tuc	4.6	0021-72	5.0	13.1	11P	4 +	C 5.76			2
							D 5.36	> 3.5	< 0.5	3, 4
							E 3.53			3
							F 2.62			3
							G 4.04			3
							H 3.21			3
							I 3.48			3, 5
							J 2.10			3
							L 4.34			3
							M 3.67			3
M15	9.7	2127 + 11	Core collapsed <sup>2(1)</sup>		8P	1	N 3.05			5
							A 110.66	> 0.13'	< 38'	6, 7
							B 56.13	> 0.062'	< 28'	6, 7
							C 30.53	0.096	12	8
							D 4.80	> 0.18'	< 1.4'	7, 8
							E 4.65	> 0.16'	< 1.4'	7, 8
							F 4.03	> 0.4'	< 0.8'	7
							G 37.66	> 0.13'	< 13'	7
							H 6.74	> 0.11'	< 2.6'	7
NGC6624	8.0	1820 - 30	Core collapsed <sup>2(1)</sup>		2P	—	A 5.44			9
							B 378.6	0.2	110	9
M5	7.6	1516 + 02	4.1	8.4	2P	1	A 5.5	> 1	< 0.74	10, 19
							B 7.9			10
M13	7.1	1639 + 36	3.6	7.8	2P	1	A 10.0	> 0.9	< 1.2	11
							B 3.5			12

Terzan 5	7.1	1744 – 24A	6.4	11.8	1P	—	11.56	> 2*	< 9.8*	13, 19
NGC6440	7.1	1746 – 20	5.7	13	1P	—	288.6			14
M28	5.8	1821 – 24	4.7	10.6	1P	—	3.05	0.032	2.17	15
NGC6760	4.1	1908 + 00	4.3	5.8	1P	1	3.62	> 0.006	< 6	16
NGC6539	3.1	1802 – 07	4.2	4.5	1P	1	23.1	> 1.5*	< 1.6*	17
NGC6342	11.6	1718 – 19	4.2	4.5	1P	1	1004	0.01	1500	18
M4	2.1	1620 – 26	3.9	5.1	1P	1	11.07			20
M53	18.5	1310 + 18	3.2	6.5	1P	1	33.16			11
Total					33P	13 +				

**References:** 1) Webbink 1985; 2) Manchester *et al.* 1990; 3) Manchester *et al.* 1991; 4) Robinson *et al.* 1993; 5) Manchester 1993; 6) Anderson *et al.* 1990; 7) Anderson 1992; 8) Prince *et al.* 1991; 9) Biggs *et al.* 1994; 10) Wolszczan *et al.* 1989; 11) Kulkarni *et al.* 1991; 12) Deich *et al.* 1992; 13) Nice & Thorsett 1992; 14) Manchester *et al.* 1989; 15) Foster *et al.* 1988; 16) Deich *et al.* 1993; 17) D'Amico *et al.* 1993; 18) Lyne *et al.* 1993; 19) Phinney 1992; 20) Thorsett *et al.* 1993; 21) Hut *et al.* 1992.

\* Binary pulsar but no  $P_{\text{orb}}$  available; hence does not appear in Table 2.

\*  $P$  contaminated by PSR acceleration in GC field.  $\tau_c$  reported is the cluster model dependent lower limit due to Phinney 1992 or D'Amico *et al.* (1993) or Anderson (1992).

**Table 2.** Orbital period distribution.

Globular cluster	Pulsar	$P_{\text{spin}}$ (ms)	$P_{\text{orb}}$ (d)	$c$	$M_c^\dagger$ ( $M_\odot$ )	$B_p$ ( $10^9$ G)
$P_b \lesssim 1d$						
Ter 5	1745 – 24 <sup>a)</sup>	11.56	0.075	$< 0.0012$	(0.09)	$< 9.8$
47Tuc	0021 – 72J	2.10	0.12	$< 0.03$	(0.02)	
NGC6760	1908 + 00	3.62	0.14	$< 0.01$	(0.02)	$< 6$
47Tuc	0021 – 72I	3.48	0.23		(0.22)	
NGC6342	1718 – 19 <sup>a)</sup>	1004	0.258	$\leq 0.005$	(0.12)	1500
M15	2127 + 11C	30.53	0.335	0.681	1.3	12
$P_b \gtrsim 1d$						
M13	1639 + 36B	3.5	1.26		(0.16)	
47Tuc	0021 + 72E	3.53	2.22	$< 0.08$	(0.16)	
NGC6539	1802 – 07	23.10	2.62	0.21	(0.30)	$< 1.6$
M5	1516 + 02B	7.94	6.8*	0.127*	(0.11)	
M4	1620 – 26	11.07	191.44	0.025	(0.28)	
M53	1310 + 18	33.16	255.84	$< 0.01$	(0.31)	

<sup>†</sup> Assumed value of  $\sin i = 1$ ,  $M_{\text{PSR}} = 1.4 M_\odot$  when companion mass is enclosed in brackets.

<sup>a)</sup> Eclipsing pulsar.

\* Provisional parameters; full timing solution unavailable; Wolszczan (1993) private communication.

## 2. Formation and evolution of the pulsars

The presence of a number of pulsars with characteristic ages considerably smaller than the GC ages (typically  $\approx 10^{10}$  yr) suggests that either these neutron stars were formed recently in the accretion induced collapse (AIC) of massive white dwarfs (Chanmugam & Brecher 1987; Michel 1987) or that some old neutron stars have been recently spun up to short periods by accretion of matter. In both cases, presence of a companion star in a binary orbit is suggested. Given the large number of binary pulsars in GCs – many of them with ‘millisecond’ spin periods ( $P_{\text{spin}} \leq 25$  ms) the ‘standard’ model of accretion spin up with low magnetic field neutron stars seemed attractive. However there are a number of single pulsars as well in the GCs and some of them have relatively long spin periods. The implications of the presence of these latter ones (Michel 1993) will be mentioned later.

The preponderance of bright X-ray sources in the globular cluster systems (GCs) (where approximately 10% of all known bright X-ray sources are associated with  $\approx 10^{-4}$  of the total mass of the galaxy) had led workers to suggest that these sources are X-ray binaries formed by the tidal capture of a non-compact star by a neutron star in the dense stellar environment of the GC cores (Fabian, Pringle & Rees 1975). Since transfer of mass and angular momentum from the companion star to the neutron star can lead to a substantial spin up of the neutron star (which at a subsequent stage can appear as a rapidly rotating radio pulsar – see e.g. Alpar *et al.* 1982) it was natural to expect that the GCs could be abundant with fast pulsars as well (Ray, Kembhavi & Antia 1987; van-den Heuvel 1988). In the tidal capture process, a close passage of a compact star near a main sequence or a giant star (a ‘normal’ star) sets up tidal

oscillations in the extended envelope of the normal star, which as a dynamical process takes up sufficient energy to lead to the formation of a bound system. In some of the tidal captures there is scope for much viscous dissipation of energy in the (convective) envelope of the normal star so that the latter may undergo substantial structural changes (Ray, Kembhavi & Antia 1987). The subsequent outcome depends on a variety of somewhat uncertain timescales of viscous dissipation and orbit contraction due to frictional drag in circumstellar (or common) envelope and that of envelope ejection (where applicable). Thus the system might evolve into either 1) a Low Mass X-ray Binary (LMXB) directly, or 2) a detached binary after envelope ejection, or 3) a Thorne Zytkov supergiant or 4) a neutron star surrounded by a massive disk comprising of the stellar debris of the erstwhile companion. A spun up pulsar might result through channels 1) and 4) and in the latter channel, an isolated and 'fast' pulsar may materialize. It is therefore unlikely that the two-body tidal capture alone produces all the recycled pulsars in the GCs via either of the possibilities 1) or 4) listed above since even in a number of low density clusters like M13 or NGC 6760 'millisecond' pulsars have been observed. Clusters like these and M53 differ from the dense clusters like M15 by almost a 1000 times in density and yet their detected pulsar populations do not scale by the same factors.

In low density clusters especially, the effect of exchange interaction between primordial binaries and neutron stars could be a source of binary or recycled pulsars in globular clusters (Hills 1976). Spectroscopic and eclipsing binaries started being discovered in the globular clusters in the mid to late 1980s (see Hut *et al.* 1992, for a recent review where the binary fraction in globular clusters is suggested to be 20–35%). The cross section for a neutron star to exchange *into* a hard binary with semi major axis  $a_{\text{AU}}$  given in astronomical units (with  $a \gg R_*$ ) can be roughly  $100 a_{\text{AU}}$  times the two body tidal capture cross section (Hut & Bahcall 1983). The rate of formation of binary pulsars via the exchange mechanism thus depends on the size of the orbit and the fraction of the *incident* binary, which may be higher in the cluster core due to mass segregation effects.

The maximum orbital period  $P_i$  following two-body tidal capture (after orbit circularization due to tidal effects, assumed to take place without angular momentum loss from the system), when the target star has approximately the cluster turn-off mass (below which it is on the main sequence) is less than a day. To attain a longer orbital period, the binary has to expand via mass transfer from a giant companion overfilling its Roche lobe where the nuclear evolution of the companion's core leads to an expansion of the envelope corresponding to the star's ascent of the giant branch (Webbink, Rappaport & Savonije 1983). The requirement that the secondary has to evolve substantially in the cluster lifetime indicates that the companion has to be more massive than the cluster turn-off mass. But if the binary has an initial period of  $P_i \approx 1d$  then after the full nuclear evolution of the companion and a transfer of  $\approx 0.6 M_{\odot}$  to the compact star the orbital period increases to only  $\approx 10$  days. While *some* of the first four binary pulsars (with the exception of PSR 1802-07 in NGC6539) with  $P_{\text{orb}} \geq 1d$  listed in Table 2 may belong to this category, the last two such as PSR 1310 + 18 in M53 and PSR 1620 - 26 in M4 (whose orbital periods are an order of magnitude larger than 10 days) are not easily explained on the basis of two body tidal capture and subsequent evolution of a main sequence dwarf companion to the red giant stage. Instead these are more likely to be the result of capture of a giant star or of a star with developing degenerate core by the compact star where the initial period after capture may have



been larger. The first four binary systems (except PSR 1802 – 07) in Table 2 with  $P_{\text{orb}} \geq 1d$  have orbital periods and companion masses which are consistent with past Roche lobe overflow from erstwhile giant companions which developed degenerate cores of mass corresponding to the current companions (Sweigart & Gross 1978). On the other hand a system like PSR 2127 + 11C which is a binary containing two neutron stars with  $P_{\text{orb}} = 0.335d$  and eccentricity = 0.68 and is similar to the well known binary PSR 1913 + 16 may have evolved from an exchange collision involving a single neutron star and a binary containing a neutron star with a main sequence or a giant companion (see Phinney 1992 for a detailed discussion).

Note that among the binary pulsars listed in Table 2 with  $P_{\text{orb}} \leq 1d$ , a majority have very low mass companions (except for PSR 2127 + 11C in M15), whereas the ones with larger orbital periods have somewhat more massive companions. The mass range of the companions of the wider binaries are broadly consistent with remnant masses of cores of nuclear evolving companions undergoing Roche lobe overflow and mass transfer onto the compact star as outlined by Webbink *et al.* (1983). A plot of the binary pulsars of Table 2 on the  $P_{\text{orb}} - P_{\text{spin}}$  plane clearly separates out the ultra-low mass binary pulsars from the moderately massive companioned ( $0.1 - 0.3 M_{\odot}$ ) pulsars – suggesting different evolutionary mechanisms. The spread in the spins of the two classes are comparable but the orbital range of the latter class is much wider.

There are a number of binary pulsars with orbital periods less than a day that have small mass functions and (implied) ultra-low mass companions. One of them PSR 1744 – 24 in Ter 5 is an eclipsing pulsar with  $P_{\text{spin}} = 11.6$  ms in the GC Terzan 5 and has an orbital period of  $P_b = 1.81$  h with a  $0.089 (M_{\odot}/\sin i)$  companion (Lyne *et al.* 1990). Kluzniak *et al.* (1992) have argued that the possible evolutionary histories of eclipsing pulsar PSR 1744 – 24 allow the Ter 5 pulsar to be the progenitor of a PSR 1957 + 20 type system. More generally, a system like this could be reincarnated many times as a LMXB and a radio-pulsar binary, with the two phases alternating. In fact, X-ray burst sources in globular clusters could have had as their progenitors binary millisecond radio pulsars similar to this one. If a pulsar is as energetic as the PSR 1957 + 20, then energetic radiation from the pulsar can lead to a gradual evaporation of the companion (Kluzniak *et al.* 1988). However, it is likely that this mechanism is not operating in the case of PSR 1744 – 24, since the spin-down luminosity of this pulsar is expected to be substantially smaller than that of PSR 1957 + 20 as the former has a spin period almost an order of magnitude larger than that of the latter. Instead, the orbit of PSR 1744 – 24 should be decaying because of gravitational radiation losses and at a future date this pulsar can become an X-ray binary like 4U 1916 – 05 or 4U 1820 – 30.

PSR 1718–19 discovered in NGC 6342 (Lyne *et al.* 1993) is a long spin period ( $P_{\text{spin}} = 1.004$  sec) pulsar in a 6.2 hr binary system and has a strong magnetic field implied from its spin down rate ( $B = 1.5 \times 10^{12}$  G). It is also undergoing long eclipses of the pulsar and the binary seems embedded in a cloud of material originating from the companion star which is (currently)  $0.1 - 0.2 M_{\odot}$  in mass. Zwitter (1993) has argued that the companion is a stripped main sequence star which started out with turn off mass but is currently a star of  $0.2 - 0.4 M_{\odot}$  in shell hydrogen burning phase which has grown a helium core of  $\approx 0.1 M_{\odot}$ . The existence of PSR 1718–19 shows that the range of magnetic fields spanned in GCs is all the way from low fields characteristic of disk ‘millisecond’ pulsars to that of the canonical pulsars in the disk whose magnetic fields range mainly between  $10^{11}$  to  $10^{12}$  Gauss. Since any neutron star which was born in the

first generation of Supernova explosion of massive stars in the GCs must necessarily be very old, the presence of this high field pulsar would imply that either a) neutron star fields do not decay with time or b) neutron stars must also be forming relatively recently, perhaps not through the canonical process of implosion of the cores of massive stars, but through the AIC of white dwarfs. The AIC route has been favoured by Ergma (1993) while Wijers & Paczynski (1993) have argued preferentially in support of a tidal capture of a low mass star (with a somewhat uncertain upper limit of  $0.35 M_{\odot}$ ) by an old neutron star which is currently in a phase between the capture and onset of a low mass X-ray binary phase (see also Kluzniak *et al.* 1992). Furthermore, Wijers and Paczynski suggest that the two different channels of formation may be distinguished by a search for the companion in the I-band and the expected difference of the luminosity of the companions in the two channels. The slow pulsars must be having relatively strong magnetic fields to be detected at the distances of GCs due to limiting flux levels (Michel 1993). Since it is less likely to find such a pulsar which remains detectable for a small fraction of the GC lifetime, there could be a large number of predecessor pulsars in the GCs which have formed previously but are currently too faint.

### 3. Pulsar population and birthrate in globular clusters

When the first pulsar PSR 1821 – 24 was discovered in GC M28 (Lyne *et al.* 1987) it was realised that this pulsar represented only the ‘tip of the iceberg’ and that there should be many more pulsars in the GC systems (Kulkarni, Narayan & Romani 1990; hereafter KNR). This was because of the high radio luminosity of this pulsar ( $L_{400\text{ MHz}} \approx 700 \text{ mJy kpc}^2$ , which is typically three orders of magnitude greater than the minimum luminosity of pulsars,  $\approx 1 \text{ mJy kpc}^2$  (Dewey *et al.* 1985)). KNR estimated  $N_{\text{psr}} \approx 1500(1 + \beta)/f_b$  (total number of GC pulsars  $\approx 10^4$ ). As the number of detected pulsars both in totality in the GCs as well as in a few clusters like M15 and 47Tuc are much larger now than the sample size used by KNR, some authors have simulated the spin period distributions in a given cluster like M15 or 47Tuc (Michel 1993). Michel’s figure 2 as well as tables 3 and 4 taken together imply that the number of pulsars detected plus the ones which have become undetectable is about 7000 which is broadly consistent with the analysis of KNR as well as Johnston, Kulkarni & Phinney (1992; JKP). However, the binary pulsar detected recently by Lyne *et al.* (1993) in NGC 6342 having a spin period of 1.004 sec and a field of  $10^{12}$  Gauss would have a large weighting factor and would imply that there are a large number of systems like this which have formed in the past and are now too faint to be detected. If one repeats Michel’s analysis with the twelve GC pulsars occurring solely in binaries a magnetic field distribution very similar to his figure 2 results, only slightly displaced parallelly. This diagram for GC binary pulsars has a gap between inferred magnetic fields of  $10^{10}$  to  $10^{12}$  Gauss, but this is most likely due to the small number statistics of the spin period distribution of binary pulsars. It has been argued in the literature (Chen, Middleditch & Ruderman 1993) that radio pulse profiles of most fast pulsars in the GCs are quite different from those of the fastest pulsars in the galactic disk and this is difficult to reconcile with the canonical spin up and recycling model. It is therefore possible that rather than being greatly ‘spun-up’ by accretion in a recycling scenario, some of the globular cluster pulsars are born spinning rapidly as for example in the Accretion Induced Collapse.

Abundance of neutron stars in a given globular cluster may depend on several dynamical properties of the host GC (e.g. mass of the cluster, escape velocity from the cluster) as well as the distribution of stellar masses (among which are the progenitors of the neutron stars) when the cluster forms. If the dominant process of formation of currently observed pulsars is the two body tidal capture of a neutron star by an extended star then the number of capture products can be written as a function of the values of the parameters in the GC core because neutron stars sink to the cluster centre due to mass segregation. However, there are clusters where three-body processes rather than two-body processes like above are expected to be dominant and JKP have parameterized this by an  $\alpha$  less than unity and investigated the effect of weighting function  $W \propto \rho^2 M_i$  as well as the steepness  $\gamma$  of the pulsar radio luminosity function  $dN/dL \propto L^{-\gamma}$  to find the statistically most likely distribution of pulsars in the GCs. The inferred number of pulsars produced in the GCs (whether currently active or dead) range from  $N'_p \approx 500/f_b$  to  $2500/f_b$  with  $\gamma = 2$  and  $\alpha = 1/2$ . These numbers are somewhat larger than another estimate made by Wijers & van Paradijs (1991; WvP) who estimated  $N_p$  to be less than  $300/f_b$  to  $700/f_b$ . Here  $f_b$  is the beaming fraction ( $0.2 \leq f_b \leq 1$ ). JKP have argued that Wijers and van Paradijs have obtained the number of *currently active* pulsars (born in the last  $3 \times 10^8$  yrs) whereas the KNR and JKP rates pertain to the total number of pulsars in the GCs produced so far. It is to be noted however that the JKP method does not bring into their analysis explicit restriction to any particular region of the  $B - P_{\text{spin}}$  plane whereas WvP analysis do (being an estimate of the currently active pulsars). With the discovery of the 1 s pulsar in NGC 6342, the 'allowed' region should considerably expand (corresponding to fainter luminosities). It is possible that a reanalysis of the currently available data might bridge the discrepancy between the two methods even for their preferred choice of  $\gamma$ .

The large number of pulsars in GCs was thought to pose a problem for the birthrate of pulsars with respect to that of their presumed parent population – the neutron star X-ray binaries (hereafter NS  $\times$  Bs) (KNR; Bailyn & Grindlay 1990). The birthrate of the pulsars would be nearly two orders of magnitude larger than the birthrate of their presumed progenitors – the NSXBs. There is a possibility that the LMXB progenitors of GC pulsars form a population distinct from the observed NSXBs (Ray & Kluzniak 1990). If a small fraction (say 10%) of LMXBs were long-lived ( $\tau_x \approx 10^9$  yr) whereas the remainder had a shorter lifetime (say,  $10^7$  yr), then  $\approx 90\%$  of NSXBs active at present would be of the long lived variety, whereas  $\approx 90\%$  of the pulsars ('recycled' or AIC) would derive from the more numerous short-lived LMXBs. In this way, the high accretion rates necessary for the accelerated LMXB evolution can be reconciled with the rather low accretion rates for GC NSXBs actually observed (rates of  $\approx 10^{-9} M_\odot \text{ yr}^{-1}$  are inferred from their low luminosity and from the presence of X-ray bursts). Note that as far as the short-lived systems are concerned, models for eclipsing binary pulsars (Kluzniak *et al.* 1988) involving self-sustained wind from a very low mass companion do indeed involve a strong mass transfer phase, possibly decreasing the LMXB lifetime to  $10^7$  yr.

However Kluzniak *et al.* (1992) have argued that there seems to be no compelling reason to assume that millisecond pulsars in GCs must have passed through a long lived X-ray binary phase. For example, collision of a compact star with an ordinary (primordial) binary system may result in the disruption of one of the target stars and an accretion of  $\approx 0.1 M_\odot$  on hydrodynamic timescales (Krolik, Meiksin & Joss 1984). This is not to imply that no millisecond pulsar is actually spun up in a low mass X-ray

binary. It is possible that a binary neutron star system may alternate a few times between the X-ray phase and the radio pulsar phase. This might happen in short orbital periods and rapidly spinning pulsars. The endpoint of such an evolution could be a millisecond pulsar, but so could be the starting point. This evolutionary sequence may provide a natural resolution to the statistical difficulty posed by the large number of millisecond pulsars and the small number of low mass X-ray binaries present in GC's.

## References

- Alpar, M. A. *et al.* 1982, *Nature*, **300**, 728.  
 Anderson, S. B. 1992, Ph.D. thesis, California Institute of Technology  
 Anderson, S. B. *et al.* 1990, *Nature*, **346**, 42.  
 Bailyn, C. D., Grindlay, J. E. 1990, *Astrophys. J.*, **353**, 159.  
 Biggs, J. D. *et al.* 1994, *Mon. Not. R. astr. Soc.*, **267**, 125.  
 Chanmugam, G., Brecher, K. 1987, *Nature*, **329**, 696.  
 Chen, K., Middleditch, J., Ruderman, M. 1993, *Astrophys. J.*, **408**, L17.  
 D'Amico, N. *et al.* 1993, *Mon. Not. R. astr. Soc.*, **260**, 17.  
 Deich, W. T. S. *et al.* 1993, *Astrophys. J.*, **410**, 195.  
 Deich, W. T. S. *et al.* 1992, *Bull. am. astr. Soc.*, **24**, 1229.  
 Dewey, R. *et al.* 1985, *Astrophys. J.*, **294**, L25.  
 Ergma, F. 1993, *Astr. Astrophys.*, **273**, L38.  
 Fabian, A. C., Pringle, J. E., Rees, M. J. 1975, *Mon. Not. R. astr. Soc.*, **172**, 15p  
 Foster, R. S. *et al.* 1988, *Astrophys. J.*, **326**, L13.  
 Hills, J. G. 1976, *Mon. Not. R. astr. Soc.*, **175**, 1p.  
 Hut, P. *et al.* 1992, *Publ. astr. Soc. Pacific*, **104**, 981.  
 Hut, P., Bahcall, J. N. 1983, *Astrophys. J.*, **268**, 319.  
 Johnston, H., Kulkarni, S. R., Phinney, E. S. 1992, in *Neutron stars in X-ray binaries and recycled pulsars*, Ed. E. van den Heuvel & S. Rappaport (Dordrecht: Kluwer) p. 349.  
 Kluzniak, W., Ruderman, M., Shaham, J., Tavani, M. 1988, *Nature*, **334**, 225.  
 Kluzniak, W., Czerny, M., Ray, A. 1992, in *Neutron stars in X-ray binaries and recycled pulsars*, Ed. E. van den Heuvel & S. Rappaport (Dordrecht: Kluwer) p. 425.  
 Krolik, J. H., Meiksin, A., Joss, P. C. 1984, *Astrophys. J.*, **282**, 466.  
 Kulkarni, S. R., Narayan, R., Romani, R. 1990, *Astrophys. J.*, **356**, 174.  
 Kulkarni, S. R. *et al.* 1991, *Nature*, **349**, 47.  
 Lyne, A. G. *et al.* 1993, *Nature*, **361**, 47.  
 Lyne, A. G. *et al.* 1990, *Nature*, **347**, 650.  
 Lyne, A. G. *et al.* 1987, *Nature*, **328**, 399.  
 Manchester, R. N. *et al.* 1990, *Nature*, **345**, 598.  
 Manchester, R. N. *et al.* 1991, *Nature*, **352**, 219.  
 Manchester, R. N. 1993, in *Back to the galaxy conference at University of Maryland*, AIP Conf. No. 278, Ed. S. S. Holt & F. Verter.  
 Manchester, R. N. *et al.* 1989, *IAU Circ. No. 4905*.  
 Michel, F. C. 1993, *Mon. Not. R. astr. Soc.*, **265**, 449.  
 Michel, F. C. 1987, *Nature*, **329**, 310.  
 Nice, D. J. & Thorsett, S. E. 1992, *Astrophys. J.*, **397**, 249.  
 Phinney, E. S. 1992, *Phil. Trans. R. Soc. London A* **341**, 39.  
 Prince, T. *et al.* 1991, *Astrophys. J.*, **374**, L41.  
 Ray, A., Kembhavi, A. K., Antia, H. M. 1987 *Astr. Astrophys.*, **184**, 164.  
 Ray, A., Kluzniak, W. 1990, *Nature*, **344**, 415.  
 Robinson, C. R. *et al.* 1993, as quoted by R. N. Manchester 1993.  
 Schweigart, A. V., Gross, P. G. 1978, *Astrophys. J. Suppl.*, **36**, 405.  
 Thorsett, S. E., Arzoumanian, Z., Taylor, J. H. 1993, *Astrophys. J.*, **412**, 133.  
 van den Heuvel, E. P. J. 1988, *Adv. Space Res.*, **8**, 355.  
 Webbink, R. F., Rappaport, S. A., Savonije, G. J. 1983, *Astrophys. J.*, **270**, 678

- Webbink, R. F. 1985, in *Dynamics of Star Clusters* Ed. J. Goodman & P. Hut p. 541.
- Wijers, R. A. M. J., van Paradijs, J. 1991, *Astr. Astrophys.*, **241**, L37.
- Wijers, R. A. M. J., Paczynski, B. 1993, *Astrophys. J.*, **415**, L115.
- Wolszczan, A. *et al.* 1989, *IAU Circ. No.* 4880.
- Zwitter, T. 1993, *Mon. Not. R. astr. Soc.*, **264**, L3.

## Pulsar Observations with the GMRT

A. A. Deshpande *Raman Research Institute, Bangalore 560 080, India*

**Abstract.** The Giant Meter-wave Radio Telescope (GMRT) being built by the National Centre for Radio Astrophysics of TIFR near Pune will become one of the most sensitive instruments for pulsar research. In this paper, we describe briefly the planned pulsar observations with the GMRT. We also discuss in some detail the design of instrumentation being built by RRI and NCRA for this purpose.

*Key words:* Pulsars—observations—instrumentation.

### 1. Introduction

The Giant Meter-wave Radio Telescope (Swarup *et al.* 1991), which is presently under construction, when completed will undoubtedly be one of the most sensitive instruments for search and observations of pulsars. The large effective collecting area (30 dishes of  $\sim 1000\text{ m}^2$  area per dish) and sufficiently wide bandwidth (32 MHz) that would be available, needs to be supplemented by suitable back-end instrumentation which takes into account some special requirements for pulsar observations. A major collaborative effort is on between the National Centre for Radio Astrophysics (NCRA), Pune and the Raman Research Institute (RRI), Bangalore, to design and build the required instrumentation and to develop the necessary analysis software for pulsar observations with GMRT.

The observational program envisaged by the staff of NCRA and RRI may be broadly classified as follows: 1) Pulsar Search and 2) Studies of known pulsars. In the following sections we discuss them separately as they require different strategies.

### 2. Proposed pulsar searches at GMRT

Most of the  $\sim 600$  pulsars known till date have been discovered in major surveys conducted with several single-dish telescope in the world, usually at frequencies near 400 MHz. Majority of the known pulsars lie within 3 kpc from the sun indicating that a large population that lies farther away from us is yet to be discovered and can be revealed only in relatively deeper searches.

The searches proposed with the GMRT are designed to be substantially deeper than most of the major existing surveys and to retain high sensitivity down to millisecond periods even for objects at large distances. The proposed searches include extensive surveys, one in the Galactic plane and another at high galactic latitudes, as well as many targeted searches in the directions of supernova remnants, globular clusters, steep spectrum sources etc..

The parameters in which the search is routinely made in the major existing surveys are confined to direction, period, dispersion measure and duty cycle of the pulse. In the

proposed search program, an extra dimension of the acceleration will be included for routine search to retain sensitivity for short period pulsars in relatively tight binary systems.

While conducting large scale surveys one invariably looks for a trade-off between the sensitivity and the speed of a survey. Pulsar search sensitivity depends not only on the effective collecting area, center frequency, total bandwidth, number of polarisation channels and integration time used, but also on the time and frequency resolutions. The speed of a survey on the other hand depends on the integration time per field, the sky area per field and the total sky area to be surveyed. In the case of GMRT, a trade-off between the effective collecting area and the sky area per field is the main consideration. We have considered two possible modes, namely, 'a phased array mode' where the dish outputs are added before detection to have the maximum available collecting area in the direction of the phase center, and 'an incoherent array mode' where detected outputs from the dishes are combined giving an effective collecting area of  $\sqrt{N}$  times the area of single dish (for  $N$  dishes). In the first mode, however, the field of view will always be much smaller (equal only if the array had been most compact) than  $(1/N)$  of that in the later mode. Hence, we plan to use the 'incoherent array mode' for pulsar surveys while for some targeted searches all the 30 dishes of GMRT used in the 'phased array mode' would offer a more attractive possibility.

Then, for example, a GMRT survey at high galactic latitudes ( $b_{ll} > 15^\circ$ ) would go  $\sim 3.5$  times deeper in flux density than the on-going Parkes survey (Bailes, in this volume), requiring a total of about 1000 hrs. of observing at 327 MHz (using 512 channels over 32 MHz bandwidth, 250  $\mu$ sec sampling, 2 polarization channels, and 5-minute integration per field). For searches in the galactic plane, however, observing at 610 and 1420 MHz would be more appropriate.

## 2.1 Instrumentation for pulsar search

This section describes briefly the digital instrumentation being developed for use in the proposed pulsar searches with the GMRT. The complex spectra available from each of the 30 dishes will be combined in two different ways (as discussed above) using an 'Array Combiner' designed to produce 'phased array' and 'incoherent array' outputs (Deshpande 1989). One of these two outputs will be selected and fed to a 'search preprocessor' (see Ramkumar *et al.* 1994, for details on this preprocessor) where the power spectra will be integrated in time and the fluctuations of the spectra around its long-term mean will be output for recording. Fig. 1 shows a schematic of this hardware.

The survey data per field would be typically  $\sim 1$  Gsamples from a 5 minute observation. For real-time speed of processing, 500 MFLOPS of computing power would be necessary. As an inexpensive solution to meet such demanding requirements, we are developing a special purpose pipeline processor which will have fixed functions while offering the required flexibility in the parameters of the function. The data read from a play-back system will pass through a PC where the dispersion gradient will be linearized and output to the pipeline processor. As shown in Fig. 2 the pipeline processor would consist of a memory that would store 1 Gsamples for a given field, followed by an incoherent dedisperser and a long-FFT module. The dedisperser would consist of intelligent memories and adder networks. The dedisperser working at

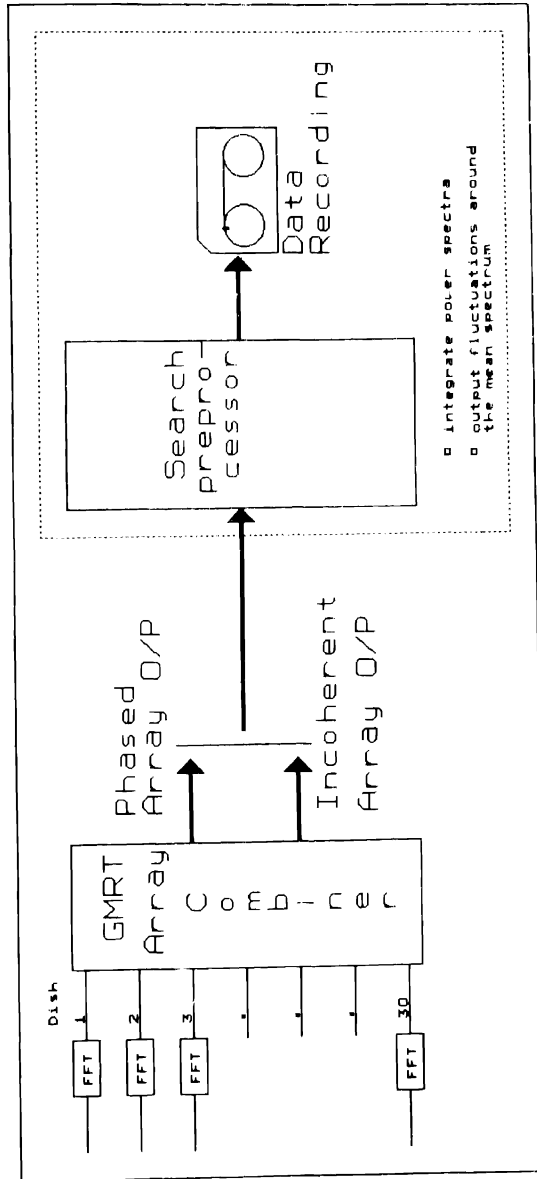
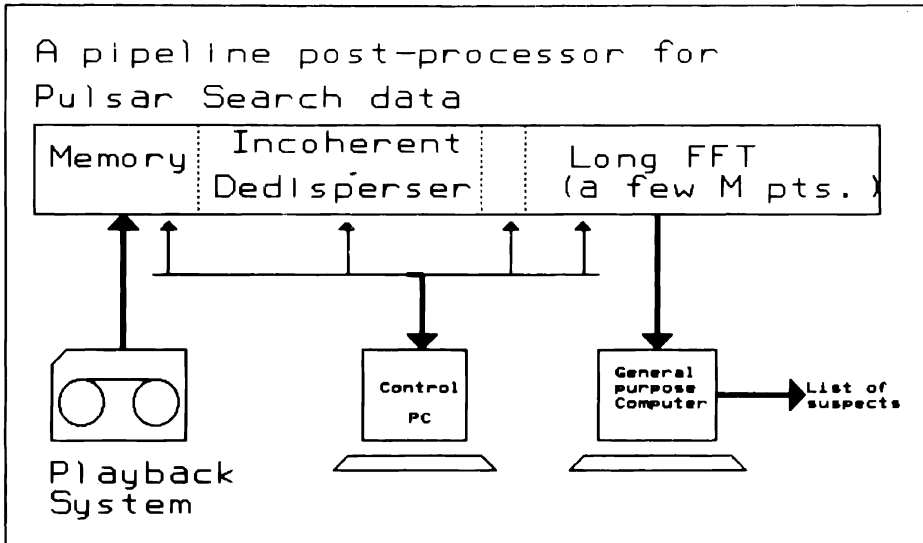


Figure 1. A schematic of the hardware (on-line) for pulsar search.





**Figure 2.** A simplified block diagram of the off-line processor for pulsar search data.

typically 3 MHz throughput rate would produce a (few) Mega-point output, corresponding to each one of (typically)  $\sim 800$  dispersion measures to be searched, every third of a second. An already dedispersed output, will be resampled corresponding to an assumed acceleration and will be Fourier transformed at a fast rate and will be sent to a general-purpose computer having moderate computing capability ( $\sim 30$ - 50 MFLOPS). All the flexibility in harmonic folding, candidate selection etc. can then be achieved through the general-purpose computer.

### 3. Studies of known pulsars

The possible studies of pulsar can be classified in three main areas of interest, namely: emission mechanism, timing of pulsars, and studies of the interstellar medium using pulsars as probes. Multi-frequency polarimetry with high time-resolution average profiles and single pulse studies including those of microstructure are of importance in the context of pulsar emission mechanism. For pulsar timing, again, high time resolution is a prime consideration while for some studies of ISM where moderate/fine spectral resolution is desirable it is possible to sacrifice time resolution. The trade-off one looks for here is between the resolutions in time & frequency and the sensitivity except when one is interested in microstructure studies.

As the considerations of field of view are unimportant while observing known pulsars, as many of the GMRT dishes as possible can be used in the 'phased array mode' to enhance the sensitivity. At high frequencies, where ionospheric phase errors are expected to be less, it should be possible to use most of the GMRT dishes in this mode.

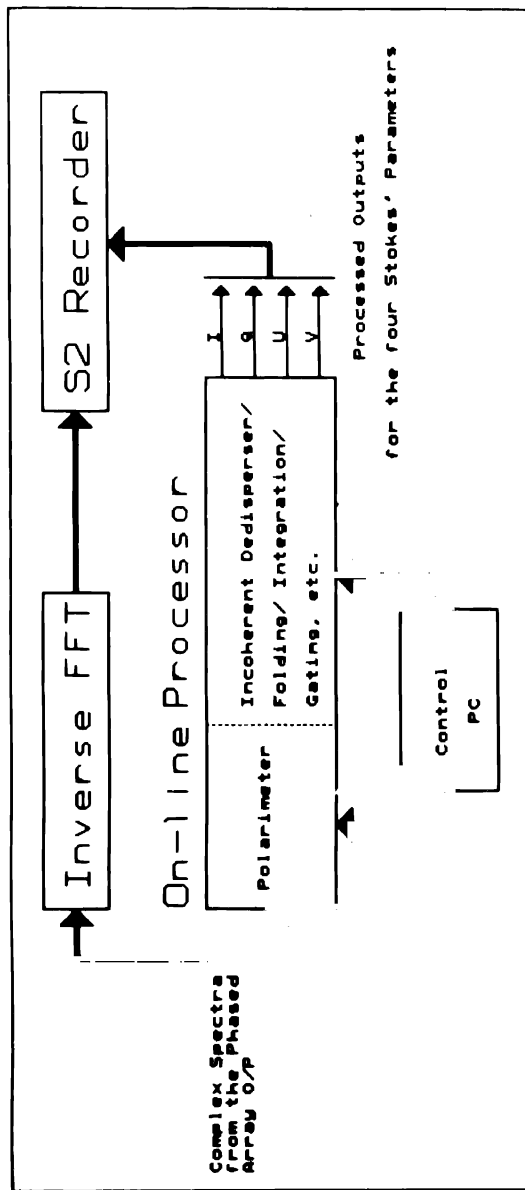


Figure 3. On-line processor for studies of known pulsars.

### 3.1 Instrumentation for pulsar observations

A state-of-art on-line digital processor is being developed to meet the signal processing requirements for most of the above studies. As shown in Fig. 3, the phased array output available from the 'Array Combiner' will be fed to the on-line digital processor. The phased array output can also be saved on to a S2 recorder after transforming the spectra back to time sequences. This provision will be used for off-line coherent dedispersion and also for VLBI experiments between GMRT and the Ooty Radio Telescope (e.g. to measure pulsar proper motions).

The on-line processor is designed to accept 4 complex voltage spectra corresponding to two side bands of 16 MHz for each of the two polarization channels. This processor consists of a full polarimeter (including a provision for corrections for differential Faraday rotation), an incoherent dedisperser, and facilities for smoothing, synchronous averaging, gating etc. The processor will be programmable and flexibly configurable to use various combinations of the processing steps. Due to the use of incoherent dedispersion the time resolution attainable with this processor (at 610 MHz) is at best 16  $\mu$ s.

An off-line coherent dedisperser is being developed by NCRA to achieve improved time resolutions necessary for microstructure studies and for timing of millisecond pulsars. More details of this system can be found in Izhak *et al.* (1994). With this system the time resolution will be improved to half a microsecond.

## 4. Progress report

A limited version of the preprocessor for search has been successfully developed and is already in use with the Ooty Radio Telescope for a survey of high galactic latitude pulsars (by NCRA and RRI). A 4-dish 'Array combiner' and a 'search preprocessor' is ready for installation at GMRT. The Array combiner for 30 dishes, the on-line processor (including the polarimeter), the off-line coherent dedisperser and the post-processor for search data are in the pipeline and are expected to be available during 1994.

## References

- Deshpande, A. A. 1989, *Pulsar Instrumentation for GMRT*, Technical Report, Raman Research Institute, Bangalore.
- Izhak, S., Gupta, Y., Subrahmanya, C. R. 1995, *J. Astrophys. Astr. Suppl.* **16**, 243–246.
- Ramkumar, P. S., Prabu, T., Girimaji, M., Markandeyulu, G. 1995, *J. Astrophys. Astr. Suppl.* **16**, 239–241.
- Swarup, G., Ananthakrishnan, S., Kapahi, V. K., Rao, A. P., Subrahmanya, C. R., Kulkarni V. K. 1991, *Curr. Sci.* **60**(2), 95.

## Evolution of the Magnetic Fields of Neutron Stars in Low-mass Binary Systems

M. Jahan Miri<sup>1,2</sup> & D. Bhattacharya<sup>1</sup>

<sup>1</sup>*Raman Research Institute, Bangalore 560 080, India*

<sup>2</sup>*Joint Astronomy Program, Indian Institute of Science, Bangalore 560 012, India*

**Abstract.** We investigate the evolution of magnetic fields of neutron stars in 'wide' low-mass binary systems due to the spin-down of the neutron star, resulting from an interaction with the stellar wind of the companion. We assume that magnetic flux from the neutron star core is expelled to the crust as the neutron star spins down due to the proposed vortex-fluxoid pinning interaction in the superfluid interior (Srinivasan *et al.* 1990). Once deposited in the crust the field will then decay due to ohmic dissipation. We construct models with a range of donor masses, orbital periods, mass-loss rates, and assumed ohmic decay timescales in the crust, and compute the final magnetic field strengths of the neutron stars. We find that the magnetic fields of millisecond pulsars, as well as other low-mass binary pulsars may be well accounted for by this mechanism if the ohmic decay timescale at the bottom of a neutron star crust is  $\sim 10^9$  years. The models seem to further indicate that an asymptotic value  $\sim 10^8$  G is the lowest possible field strength obtainable by this mechanism.

**Key words:** Neutron stars   pulsars   magnetic fields—binary systems.

### 1. Introduction

The low magnetic field strengths ( $\geq 10^8$  G) of millisecond pulsars could be due either to their progenitor neutron stars being born with such low fields or to a decay of their field strengths in course of evolution. Recent analyses of observational data suggest that magnetic fields of isolated neutron stars hardly decay in time scales  $\leq 10^8$  yr (Bhattacharya & Srinivasan 1993; Srinivasan 1991; Wakatsuki *et al.* 1992). The large preponderance of low-field pulsars in binary systems, however, indicates that the processing in a binary causes a reduction of the field strength of a neutron star (Bailes 1989; Bhattacharya *et al.* 1992).

One suggested mechanism for such a field evolution is a spin-down induced field expulsion (Srinivasan *et al.* 1990), which advocates the following scenario:

- An increase in the spin period causes the magnetic field to be expelled out of the core into the crust, where it will decay due to ohmic dissipation. The expulsion is expected as a result of the interpinning of proton superconductor fluxoids (carrying magnetic field) and neutron superfluid vortices (carrying angular momentum) in the neutron star core. With spin-down, superfluid vortices migrate outward, carrying fluxoids with them.

- In the evolution of low-mass binaries a prolonged spin-down ('propeller') phase is likely to take place, resulting in a period  $> 10^3$  sec, and a consequent reduction in the core flux.

## 2. The present work and results

In this work we model the evolution spin periods and magnetic fields of the neutron stars in wide low-mass binaries, which are believed to be the progenitors of low-magnetic-field pulsars. We adopt the above field-decay mechanism and seek the conditions under which an efficient spin-down phase (due to interaction with the stellar wind of the donor) might be realised, resulting in a low magnetic field of the descendant millisecond pulsar. We construct our evolutionary models based on the following premises:

- Wind matter can penetrate into the star's magnetosphere if ram pressure of the accretion flow ( $\dot{M}_{\text{acc}}$ ) exceeds the pressure of dipole radiation.
- At the Alfvén radius  $R_A$ , interaction of the flow and the magnetic field causes the spin period  $P$  to increase or decrease depending on the relative value of the two velocities  $V_{\text{corotation}}$  and  $V_{\text{keplerian}}$  at  $R_A$ :

$$\dot{P} \propto \xi (V_{\text{corotation}} - V_{\text{keplerian}})$$

where  $\dot{P}$  is the rate of change of  $P$  and  $\xi$  is an efficiency factor.

- The core field  $B_c$  decreases with an increase in  $P$ .
- The surface field  $B_s$  approaches  $B_c$  exponentially with a time constant  $\tau$ , and they are equal at the start.
- Instantaneous  $B_s$  and  $\dot{M}_{\text{acc}}$  determine the instantaneous  $R_A$ .
- Changes in orbital separation occur due to exchange and losses of angular momentum and mass.

We follow the coupled evolution of  $P$  and  $B_s$  and determine  $B_s$  after  $10^{10}$  yr, for the following ranges of variables: Donor Mass  $M_2$ :  $0.8 - 1.0 M_{\odot}$ ; Initial  $P$ :  $0.4 - 1.0$  sec; Initial  $B_s = B_c$ :  $10^{12} - 3 \times 10^{12}$  G;  $\tau$ :  $10^7 - 10^{10}$  yr;  $\xi$ :  $0.01 - 1.0$ ; Initial  $P_{\text{orb}}$ :  $1 - 300$  day. We confine ourselves to 'wide' binaries, with initial orbital periods greater than  $\sim 1$  day, to ensure that the entire main-sequence lifetime of the secondary is spent in a detached phase.

The results of these computations, namely the final  $B_s$  values are plotted (Fig. 1) against the initial orbital periods  $P_{\text{orb}}$ , for one set of  $\tau$ ,  $\dot{M}$ , and  $\xi$ . Circles represent the data for six observed binary pulsars (0820 + 02, 1620 - 26, 1953 + 29, 1855 + 09, J1713 + 0747, and J2019 + 2425), descended from wide low-mass X-ray binaries.

## 3. Conclusions

1. Magnetic fields of  $10^8 - 10^9$  G, similar to millisecond pulsars, can be obtained under variety of circumstances, provided  $10^{9.5} > \tau > 10^{8.5}$  yr.
2.  $B_s \sim 10^8$  G is a lower limit for the field strength of a recycled pulsar, and its value is decided by the lowest possible initial field strength and spin period of a new born neutron star.

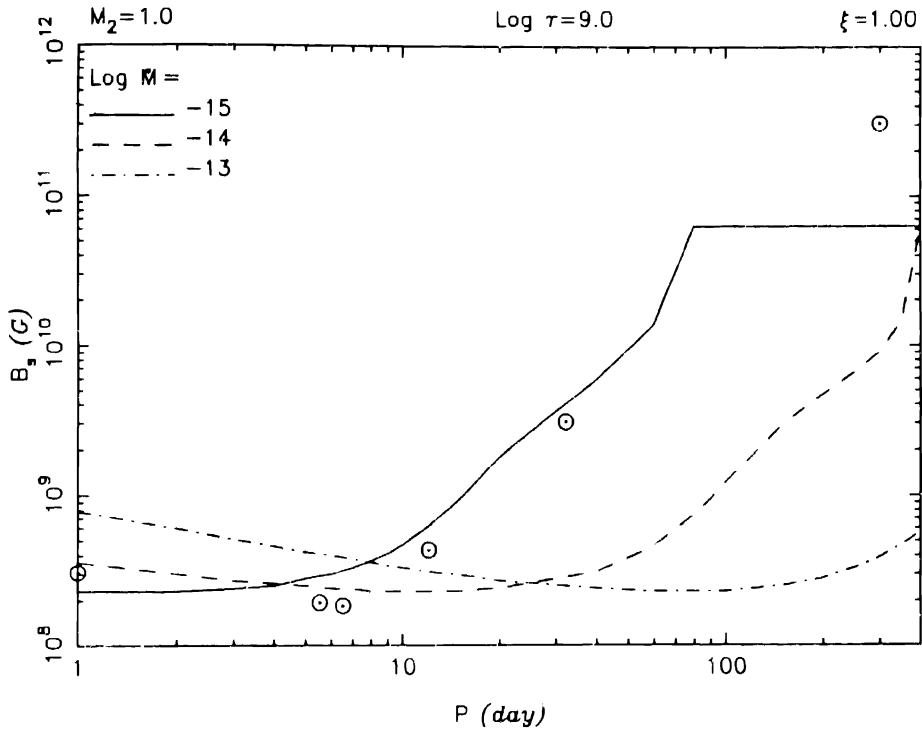


**Figure 1.** Final surface magnetic field strengths of neutron stars in low-mass binary systems with different orbital periods. Initial spin  $P = 0.4$  sec, initial surface and core  $B = 1.00 E + 12$  G.

3. Reproduction of the observed trend of final field strengths as a function of initial orbital periods is encouraging, especially in view of the wide range of possible initial conditions.
4. Old solitary neutron stars are expected to have  $B_s \sim 10^{11}$  G.
5. Extension of the work to the case of very tight orbits ( $P_{\text{orb}} < 0.5$  day), as well as the binaries with high-mass donor stars would provide further constraints on the scenario.

### References

- Bailes, M. 1989, *Astrophys. J.*, **342**, 917.  
 Bhattacharya, D., Srinivasan, G. 1993, in *X-ray Binaries* Eds. W. H. G. Lewin, J. van Paradijs & E. P. J., van den Heuvel (Cambridge University Press) in press.  
 Bhattacharya, D., Wijers, R. A. M. J., Hartman, J. W., Verbunt, F. 1992, *Astr. Astrophys.*, **254**, 198.  
 Srinivasan, G., Bhattacharya, D., Muslimov, A. G., Tsygan, A. I. 1990, *Curr. Sci.*, **59**, 31.  
 Srinivasan, G. 1991, *Ann. N.Y. Acad. Sci.*, **647**, 538.  
 Wakatsuki, S., Hikita, A., Sato, N., Itoh, N. 1992, *Astrophys. J.*, **392**, 628.



## Millisecond Pulsars as Sources of $\gamma$ -Rays for Globular Clusters and Galactic Background

V. B. Bhatia, S. Mishra & N. Panchapakesan *Department of Physics and Astrophysics, University of Delhi, Delhi 110 007, India*

**Key words:** Pulsars—gamma rays—galactic background.

### 1. Introduction

A large number of millisecond pulsars (MSPs) have been discovered in recent years in the globular clusters of the Galaxy. Some estimates say that their number may be  $10^4 \dots 5 \times 10^4$ . Many MSPs have been found in binary groups. The magnetic field of these pulsars has been estimated to be  $10^8 - 10^{10}$  G. MSPs are believed to be the resurrected run down pulsars, spinning up being due to accretion from their companions. Theory suggests that an MSP acquires period given by

$$P = B_8^{6/7} (\dot{M} \times 10^8 / M_\odot / \text{yr})^{-3/7} \text{ ms}, \quad (1)$$

where  $B_8$  is in units of  $10^8$  G. The maximum value of  $\dot{M}$  is  $M_\odot / 10^8$  per yr (Eddington rate). On the basis of observed periods, the period distribution suggested for MSPs is

$$\rho_P = (\alpha - 1) P_{\min}^{\alpha-1} P^{-\alpha}, \quad (2)$$

where  $P_{\min} = 1.6$  ms and  $\alpha = 1.4$  for  $P > P_{\min}$ . Because of short periods MSPs are expected to be the sources of  $\gamma$ -rays for the globular clusters and galactic background.

The magnetic field of a pulsar has been modelled as consisting of closed (corotating) and open field lines. Charged particles get accelerated along the open lines and emit curvature radiation. The model of Scharlemann *et al.* (1978) gives the energy acquired by an electron as

$$\gamma = 1.23 \times 10^7 R_6^{3/4} P^{-1/4} B_8^{1/4}, \quad (3)$$

where  $R_6 = R/10^6$  cm. The typical energy of a curvature photon is given by

$$E_c = 3\hbar\Omega\gamma^3/2, \quad (4)$$

the total power radiated by an electron is

$$I = 2e^2\gamma^4\Omega^2/3c, \quad (5)$$

and the total power emitted at frequency  $\nu$  is

$$P(\nu) = (\sqrt{3} e^3 B / mc^2) (\nu/\nu_c) \int d\xi K_{5/3}(\xi), \quad (6)$$



where  $B$  is the field at the point of emission and  $v_e$  corresponds to  $E_e$ . The net rate of emission of electrons from the polar caps of a pulsar is given by (Goldreich and Julian 1969)

$$\dot{N} = \Omega^2 B R^3 / 2ce. \quad (7)$$

## 2. Globular clusters

Using equations (3), (5) and (7), we get the  $\gamma$ -luminosity of a pulsar as

$$L_\gamma = 9.2 \times 10^{34} B_8^2 R_6^2 P^{-4} \text{ erg s}^{-1}. \quad (8)$$

With the help of pulsar period distribution we get the luminosity of a globular cluster:

$$L_\gamma^{\text{gc}} = 3.8 \times 10^{36} n_{500} \text{ erg s}^{-1}, \quad (9)$$

where  $n_{500}$  is the number of MSPs in a cluster. This estimate is within the range of modern detectors.

## 3. Galactic $\gamma$ -ray background

The number of photons emitted by an electron in one second in the frequency range  $v_1 - v_2$  is  $\int [P(v)/hv] dv$ . Making reasonable assumption about the lifetime of an electron, we get the  $\gamma$ s emitted per sec by an MSP in the range  $E_1 - E_2$  (measured in units of  $E_e$ ):

$$\dot{N}_\gamma = 9.7 \times 10^{36} B_8^{5/4} P^{-9/4} R_6^3 \int [F(E)/E] dE, \quad (10)$$

where  $F(E)$  stands for  $E \int d\xi K_{5/3}(\xi)$ . The local production rate of  $\gamma$ s can now be written as:

$$q = (1/4\pi) \int \dot{N}_\gamma \rho_P(P) dP. \quad (11)$$

The suggested space distribution of MSPs in galactocentric coordinates is

$$\rho(R, Z) = (N_t / 4\pi R_0^2 Z_0) \exp[-(R/R_0) - (|Z|/Z_0)], \quad (12)$$

where  $R_0 (= 4 \text{ kpc})$  and  $Z_0 (= 0.3 \text{ kpc})$  are the scale factors, and  $N_t$  is total of MSPs in the Galaxy. Equations (11) and (12) give  $\gamma$ -ray flux due to all MSPs in the galaxy:

$$F_\gamma = \int \int \int q \rho(R, Z, \theta) dR dZ d\theta. \quad (13)$$

We transform to galactic coordinate and integrate for  $l''$  between  $300^\circ$  and  $60^\circ$  for  $b'' = \pm 0, \pm 5, \pm 10, \pm 15$ .

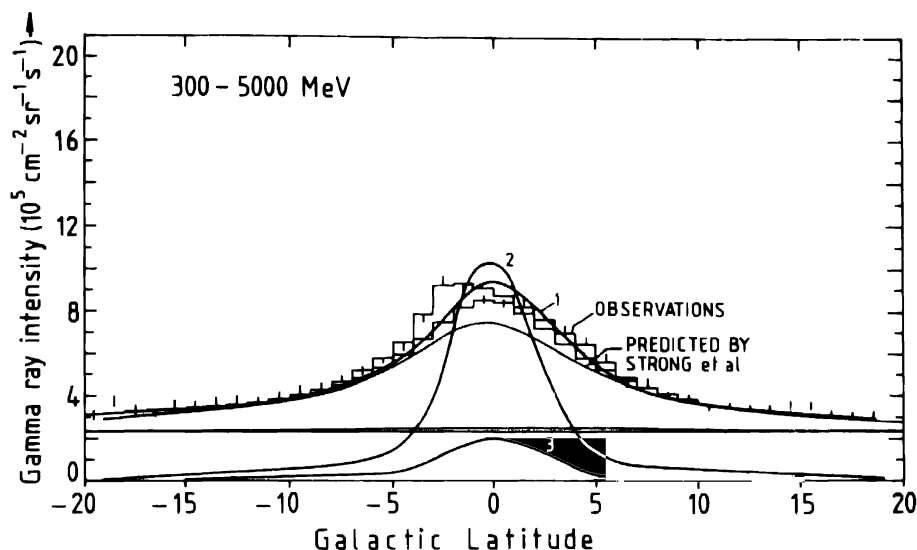


Figure 1.

#### 4. Results

Curve 2 in Fig. 1 shows the intensity for MSPs alone for  $N_t = 5 \times 10^4$  superposed on observations. Curve 3 shows the same if  $N_t = 10^4$ . Curve 1 shows the intensity due to  $N_t = 10^4$  together with contributions from other suggested processes: (i)  $\pi^0$  decay, (ii) bremsstrahlung by CR electrons and (iii) Compton scattering of microwave background photons over CR electrons. We find that  $\gamma$ -rays from MSPs in the Galaxy can explain the galactic  $\gamma$ -ray background entirely or in a substantial measure.

#### References

- Goldreich, P., Julian, W. 1969 *Astrophys. J.*, **157**, 869.  
 Scharlemann, E. T., Arons, J., Fawley, W. M. 1978, *Astrophys. J.*, **222**, 297.



## **A Digital Signal Pre-Processor for Pulsar Search using Ooty Radio Telescope**

P. S. Ramkumar, T. Prabu, Madhu Girimaji, & G. Markandeyulu<sup>†</sup> *Raman Research Institute, Bangalore 560 080, India*

<sup>†</sup> *Tata Institute of Fundamental Research, Pune 411 007, India*

**Abstract.** A fast digital signal processor has been designed and built for observation of pulsars and for pulsar search. This processor obtains spectral information over a bandwidth of 8 MHz (256 channels) every 256  $\mu$ secs. In this paper, we describe the design of this processor and present some test observations made with the Ooty Radio Telescope.

**Key words:** Pulsars—instrumentation.

### **1. Introduction**

A digital signal processing instrument suitable for pulsar observations and survey using the Ooty Radio Telescope (ORT) has been realised. The ORT consists of a phased antenna array operating at 327 MHz with a beamwidth of 0.2 sq. deg. and uses mechanical steering in hour-angle and electronic phasing for a required declination. The receiver noise temperature is about 100 K. A SSB receiver with 8 MHz bandwidth provides the video band used for our digital signal processor.

### **2. Design philosophy**

The design philosophy adopted in this exercise is aimed at reducing the cost of the machine while retaining flexibility and operational simplicity. Shortcuts to extensive, high-speed computations have been provided through the use of lookup table approach. At places where lookup table approach is not appropriate, dedicated logic has been designed, and programmed into Erasable and Programmable Logic Devices (EPLDs) which have the desired advantages. In addition, their use makes it possible to design the entire machine using only 2 layer PCBs and reduce the development time substantially.

A PC/AT is used for general control and for configuring the machine in a user selected mode. The choice of a PC/AT to setup the machine is due to the large software base available under MS-DOS in addition to the hardware flexibility.

### **3. Hardware description of the machine**

#### *3.1 Digital front-end*

The digital front-end for this machine consists of an A/D convertor which samples the baseband signal at Nyquist rate and feeds them to a FFT engine. The FFT engine

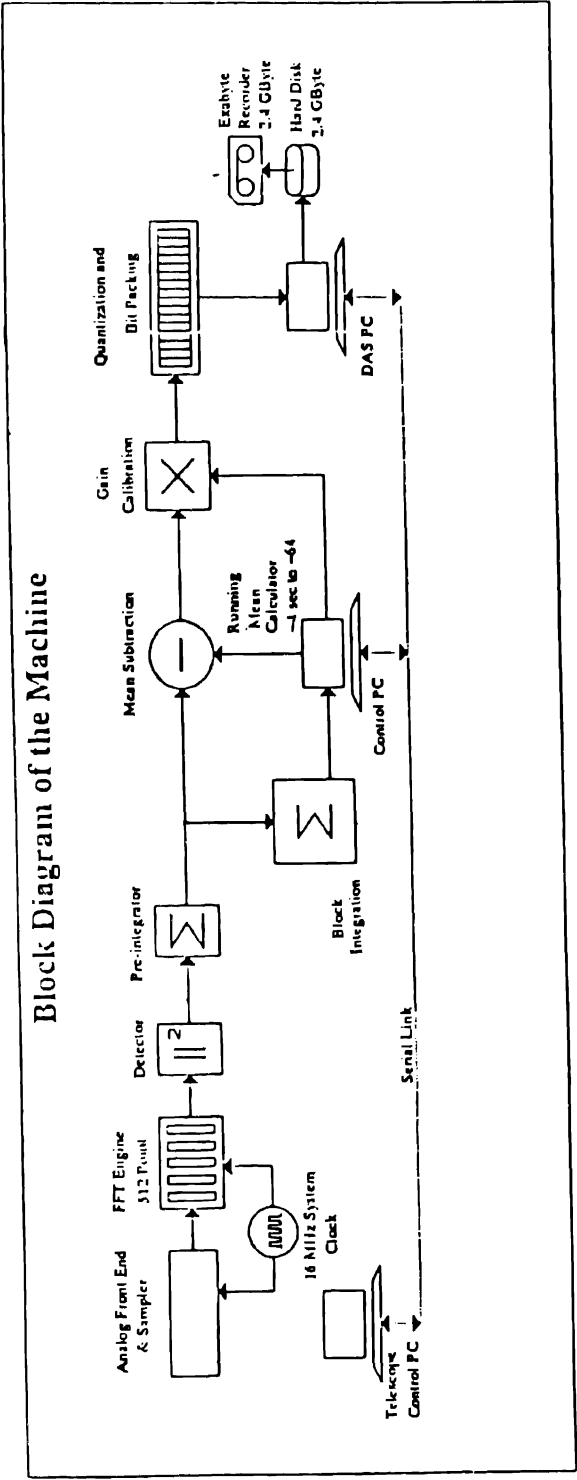


Figure 1. Block diagram of the machine.

produces an output over 256 spectral channels which are sent out serially. The FFT card is based on VLBA ASICs.

### 3.2 Search pre-processor

This is based on a part of the design of pulsar instrumentation to be built for use at GMRT (Deshpande 1989). The complex numbers representing the voltage spectrum produced by the FFT engine pass through lookup tables for conversion to a power spectrum, followed by a programmable pre-integrator, which pre-integrates between 16 and 256 samples. The pre-integrated values from each of the 256 channels are used by a control PC/AT which computes running mean over  $\approx 4$  sec to  $\approx 64$  sec. This running mean is subtracted from the pre-integrated data and the difference is quantized to 1 bit. Such quantization, although it worsens the sensitivity by a factor of 0.8 (Biggs, Lyne & Johnson 1989), helps reducing the effective data rate. A 2-bit quantization option is also provided and in this mode a lookup table based gain calibration unit is programmed by the same PC with scale factors obtained from the running mean. The quantized bits are then packed into 16-bit words and recorded onto a 2.4 GBytes hard disk drive of a PC/AT-based data acquisition system (DAS, built to handle data rates upto 128 KBytes/s). The DAS is equipped with FIFO buffer to accommodate the seek-time latency of the hard disk. The data can be periodically backed up onto an 8 mm video tape using an Exabyte Video Recorder. All the modules run through automated diagnostics while being setup by the control PC.

A set of serial links have been developed between the Control PC, the DAS-PC and a PC/AT positioning the telescope. This link has automated observational procedure substantially. Also, the total power measurement and the bandshape are recorded for calibration. A block diagram of the entire receiver is shown in Fig. 1.

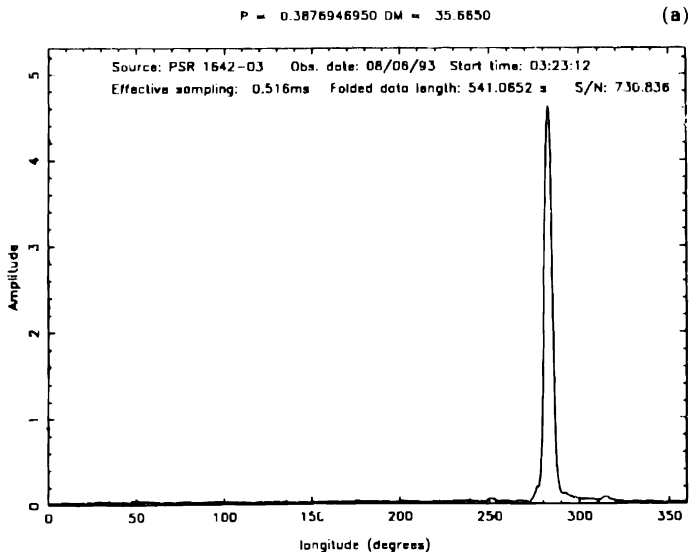
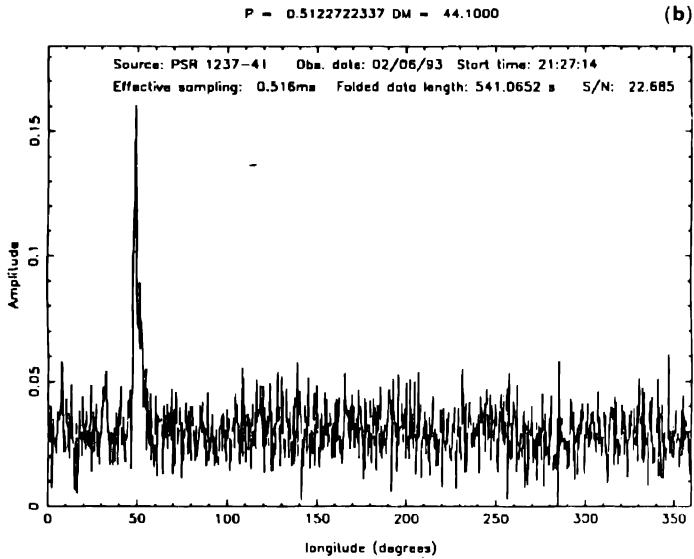


Figure 2.



**Figure 2a & b.** Pulsar profiles observed using the machine.

#### 4. Results

Several known pulsars have been observed using this instrument. Some of the profiles of the observed pulsars are shown in Fig. 2.

#### References

- Biggs, J. D., Lyne, A. G., Johnson, S. 1989, *Proc. of 23rd ESLAB Symposium*, 293.  
Deshpande, A. A. 1989, *Pulsar Instrumentation for GMRT* An internal report, Raman Research Institute.

## Coherent Dedispersion System for GMRT

S. Izhak, Y. Gupta & C. R. Subrahmanya *National Centre for Radio Astrophysics (TIFR), Postbag 3, Pune 411 007, India*

**Abstract.** A coherent dedispersion system is being built for high time resolution observations of pulsars at GMRT. Based on the requirements and the available back end, a scheme has been worked out which essentially does an offline coherent dedispersion on the time domain signal played back from the S2 recorder. The coherent dedispersor is based on high speed DSP chips. The design described here is optimized to give sub microsecond resolution at 610 MHz.

**Key words:** Pulsars – instrumentation – coherent dedispersion.

### 1. Requirements for coherent dedispersion

The dispersion of the pulsar signal can be viewed as a convolution with an impulse response characterizing the interstellar medium (Hankins & Rickett 1975). In our scheme the deconvolution required for dedispersion is done in the frequency domain, as this requires lesser computation effort than in the time domain. The length of the impulse response is given in terms of the number of samples, by the following equation (Gupta 1991):

$$N = 2 (202/f)^3 DM \delta f^2. \quad (1)$$

For a typical case of  $DM \approx 100 \text{ pc cm}^{-3}$  at center frequency  $f \approx 610 \text{ MHz}$  and bandwidth  $\delta f \approx 16 \text{ MHz}$ , the length  $N$  is  $\approx 1$  million. However for most GMRT frequencies it will not be necessary to coherently dedisperse more than 1–2 MHz, as the resolution will be limited by interstellar scattering. For the above set of parameters and for  $\delta f \approx 1.6 \text{ MHz}$ , the block length ( $N$ ) would be 16 K. For such a choice of parameters a resolution of better than  $1 \mu\text{sec}$  is obtained. The  $N$  tap deconvolution when carried out in frequency domain by overlap and save, requires  $2N$  point DFT, a  $2N$  point complex multiplication by the inverse of the transfer function of the interstellar medium and then inverse DFT of the same length. Computational bottle neck arises at the DFT/IDFT stage, the rest can be carried out easily.

### 2. Implementation

The signal will be available as the DFT of the phased array sum from 30 antennas of GMRT in four channels – two circular polarizations and two sidebands. The details of the configuration are shown in Figs. 1 and 2. The phased array sum is inverse transformed to get the time domain signal and then suitably formatted before recording on S2 recorder. The coherent dedispersion is done offline on each channel of this data



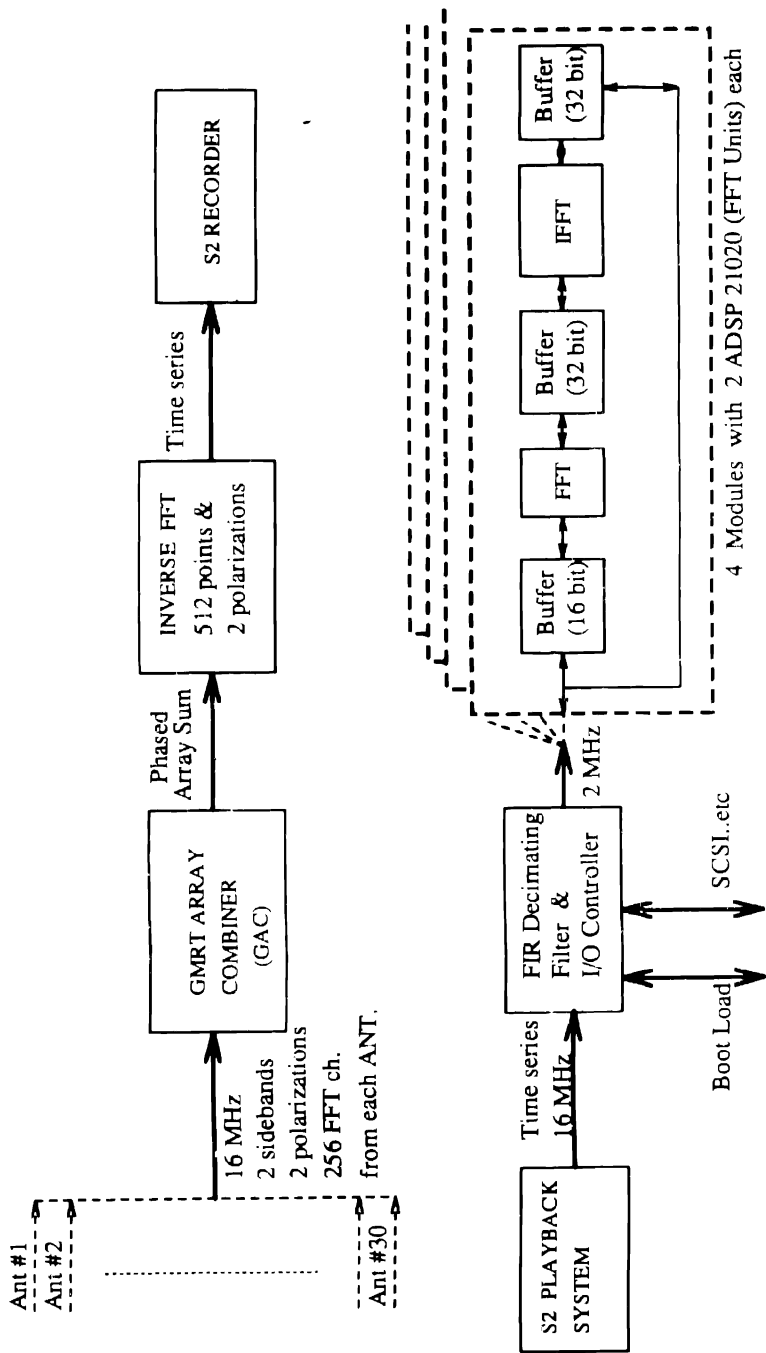


Figure 1. The functional block diagram of the Coherent Dedispersion System (CDS) for GMRT.

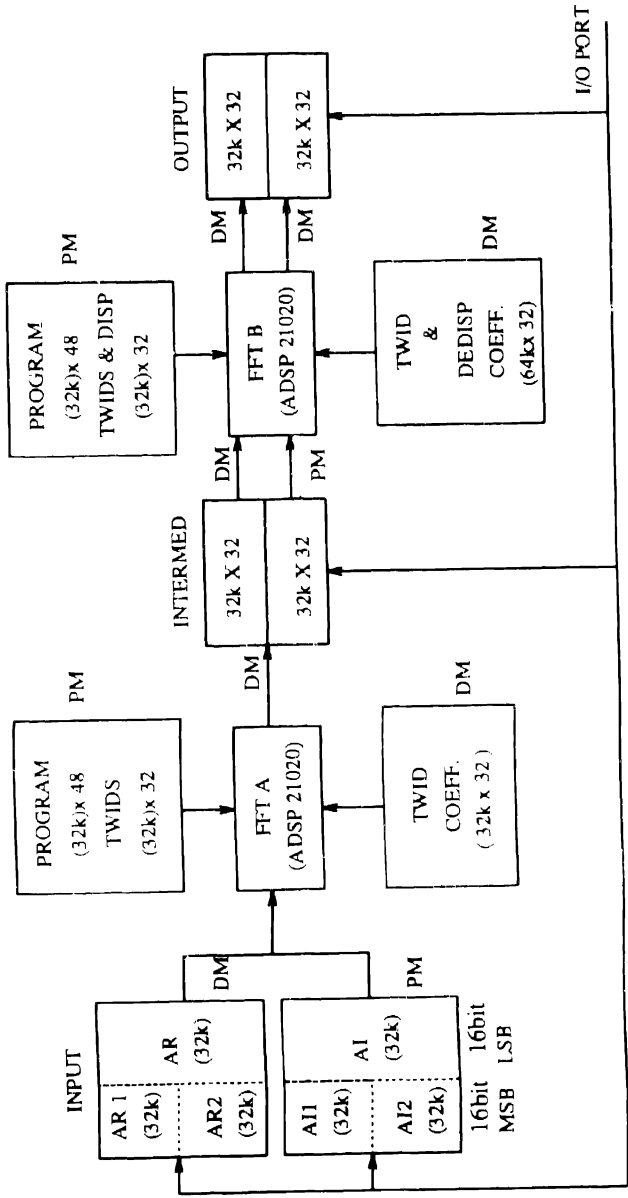


Figure 2. The details of one of the four modules of CDS.

separately, one subband at a time. The playback data is passed through a 128 tap decimating FIR filter (based on HSP 43220) to obtain a subband of about 2 MHz. This is packed as  $N$  point complex data block by the I/O node and is passed onto the four modules that make the core of the coherent dedispersion system. Each of the modules consists of two general purpose DSPs (ADSP 21020) – one devoted to performing a forward transform and the other the inverse. The multiplication of the DFT of the signal with the transfer function of the ISM is carried out by the latter DSP before performing the inverse. The modules work independently, each one processing one block of data. The dedispersed data is sent back to a standard interface for storage through the I/O node. Some amount of processing like folding can be carried out by the processor at the I/O node.

### References

- Gupta, Y. 1991, *CDS for GMRT Pulsar Machine*, GMRT Internal Technical Report.  
Hankins, T. H., Rickett, B. J. 1975, *Pulsar Signal Processing* in *Methods of Computational Physics*, vol 75, (Academic Press, 1975).

## Pulsar Observations with the 512 Channel Correlator at ORT

M. Vivekanand *NCRA, Pune University Campus, Post Bag 3, Pune 411 007, India*

**Abstract.** The 512 channel correlator at the Ooty Radio Telescope (ORT) has been in use for some time now, for pulsar observations. Three observational programs are currently under way: (a) the pulse nulling phenomenon in pulsars, (b) search for low period pulsars along specific directions in the sky, and (c) dynamic spectra of pulsars for studying refractive scintillations in the interstellar medium. A brief description of the projects is given along with some preliminary results.

*Key words:* Ooty radio telescope — pulsar — search — nulling.

### 1. Introduction

The 512 channel one-bit correlator was the main back-end at ORT, which has recently undergone considerable improvements (Vivekanand 1993). This machine has been in use for some time now for pulsar and spectral line observations. Pulsar observations require high time resolution for observing the narrow pulses, and reasonable radio frequency resolution for de-dispersing the pulsed signals. The minimum sampling interval currently available is  $\approx 3$  milli seconds, with a frequency resolution of 32 channels within the 9 MHz pass-band of ORT. Described below are three pulsar projects that are currently under way:

### 2. Targeted search for low period pulsars

Pynzar & Udaltsov (1989) have identified eight point sources in the sky as suspects for low period pulsars (periods  $\geq 10$  ms). This came out of their scintillation survey at low radio frequencies. These eight regions are currently being searched for pulsars. With a sampling interval of 3 ms, this search is sensitive to pulsars with periods  $\geq 12$  ms, and dispersion measures  $\leq 100$  pc cm $^{-3}$ , with a limiting sensitivity of 1 to 2 mJy. Five of the eight regions have been observed so far; the data is currently being analysed.

### 3. The pulse nulling phenomenon

Fifteen pulsars have been observed for their pulse nulling phenomenon, half of them being weak pulsars. The fraction of time a pulsar spends in the nulled state  $\alpha$  has been obtained for ten pulsars; for eight of them  $\alpha$  is consistent with previous estimates. The new results are:  $\alpha \leq 2.5\%$  for PSR 0149 – 16 and  $\alpha \leq 7\%$  for PSR 0942 – 13; the latter  $\alpha$  is consistent with the pulsar being of the ‘core’ kind (Rankin 1983). The rest of the pulsars could not be observed due to their highly variable radio fluxes (most probably

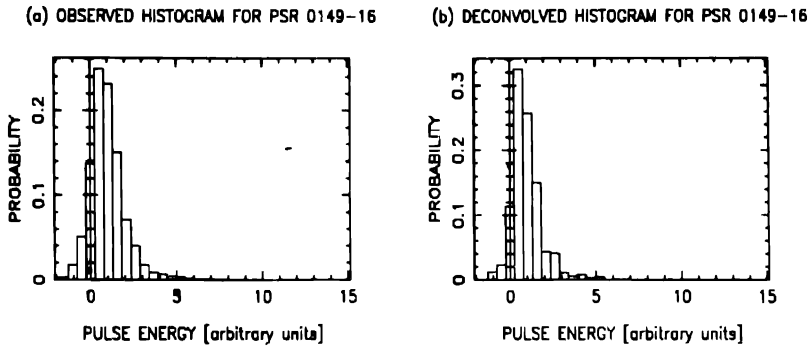


**Figure 1.** Histograms of pulse energy distribution for about 7000 periods of PSR 0149 – 16. The pulse energy is corrected for interstellar scintillations, and is in arbitrary units, with the mean pulse energy normalized to the value 1.0. (a) The observed pulse energy distribution; (b) the distribution obtained after deconvolving figure 1a with the receiver noise distribution. The percentage of nulling  $\alpha$  is obtained by subtracting, from figure 1b, different amounts of the receiver noise distribution (which is centered at zero energy), until the distribution looks smooth. In this case only an upper limit could be derived.

due to interstellar scintillations). Fig. 1a shows the probability distribution of the normalized pulse energies (i.e., after correction for interstellar scintillations) for PSR 0149 – 16; Fig. 1b is the same histogram after correction for the effect of convolution by the receiver noise distribution.

The distribution of the burst and null time-scales for PSR 0031 – 07 can be modelled in terms of two statistical processes: an exponential distribution with a typical time-scale of  $\approx 2$  to 5 periods, and a gaussian-like wider distribution with time-scales of  $\approx 20$  to 40 periods. It appears that the combination of a burst and the subsequent null forms the fundamental time-scale of the nulling phenomenon, of typical duration  $\approx 85$  periods.

#### 4. Dynamic spectra

This part has been discussed by Gupta *et al.* in this volume.

#### References

- Pynzar, A. V., Udaltsov, V. A. 1989, *Sov. Astr.*, **33**, 465.  
 Rankin, J. M. 1983, *Astrophys. J.*, **274**, 333.  
 Vivekanand, M. 1993, *Bull. Astr. Soc. India*, (to appear).

## Evolution of the Magnetic Field of an Accreting Neutron Star

Sushan Konar\*, Dipankar Bhattacharya & Vadim Urpin† *Raman Research Institute, Bangalore 560 080, India*

\*Also Joint Astronomy Program, Indian Institute of Science, Bangalore 560 012, India

†A. F. Ioffe Physical Technical Institute, St. Petersburg, Russia

*Key words.* Neutron stars—magnetic fields.

The time scale for ohmic decay of any magnetic field depends upon the electrical conductivity of the medium in which the field is embedded. Therefore, in a neutron star, owing to very different physical structure and hence different electrical conductivity of the core and the crustal matter, the field evolution time scales differ significantly from one region to another. In case of a neutron star accreting matter from a companion the crustal matter is continuously pushed into the core since the mass of the crust is finite and is limited by the elastic properties of the matter. Thus, if the magnetic flux is originally confined to the neutron star crust (Yakovlev & Urpin 1980; Blandford, Applegate & Hernquist 1983; Urpin, Levshakov & Yakovlev 1986), it is evident that the field experiences a change in decay time scale as the crustal matter undergoes a phase transition in being assimilated into the core.

We explore two possibilities: a) that the state of the newly formed core material is a normal, non-superfluid one, and b) that it goes into a superfluid state.

In either case, when the accretion takes place, the crustal material is pushed into successively more dense regions (before it is finally assimilated into the core). This, because of flux freezing, causes compression of the current loops and leads to the generation of large wavenumber components of the current. These large wavenumber modes have faster decay rates since the ohmic decay time scale is inversely proportional to the square of the wavenumber (Landau & Lifshitz 1960). Hence, the magnetic flux can decay rapidly via these modes. But once the flux frozen material is completely assimilated into the core, the mode of decay will be determined by the nature of the newly formed core material.

a) *Normal, non-superfluid  $n$ - $p$ - $e$  matter:*

For this state of matter, the conductivity has the following features (Yakovlev & Shalybkov 1991):

- 1) It is highly anisotropic in presence of magnetic field.
- 2) It is a strong function of the field strength

$$\sigma_{\perp} = \sigma_0 (1 + B^2/B_0^2)^{-1} \quad (1)$$

where

$\sigma_0$  is isotropic conductivity in absence of any field.

$B_0 = 10^8 - 10^9$  G for  $T_{\text{core}} = 10^6 - 10^7$  K.

- 3) for  $B \gg B_0$ ,  $\sigma_{\perp} \ll \sigma_{\text{crust}}, \sigma_0$ .

Since the ohmic decay time scale is proportional to the conductivity (Landau & Lifshitz 1960), a region of lower conductivity implies a faster decay for the field.

Therefore, when the crustal material, with a larger field value of the initial field, is assimilated into the core, the field undergoes a rapid decay. But this decay rate subsequently decreases as the field approaches  $B_0$  and  $\sigma_{\perp}$  approaches the very large value of the isotropic conductivity.

Hence, the field decays initially with a time scale characteristic of the initial value of the field and practically stops decaying after reaching the limiting value of  $B_0$ . For reasonable values of the core temperature (Urpin & Van Riper 1993),  $B_0$  is between  $10^8$  and  $10^9$  Gauss.

#### b) *Superfluid, superconducting matter in the core:*

In this state, after having undergone a superfluid-superconductor phase transition, the conductivity and hence the decay time scale lengthen to extremely large values. Therefore, one expects a phase of rapid decay of the field, during the early phase of the accretion (before the whole of the original crust is pushed into the core) followed by a stable phase for the field configuration.

### References

- Blandford, R., Applegate, J., Hernquist, L. 1983, *Mon. Not. R. astr. Soc.*, **204**, 1025.  
 Landau, Lifshitz 1960, *Electrodynamics of Continuous Media*, (Oxford: Pergamon Press).  
 Urpin, V. A., Levshakov, S. A., Yakovlev, D. G. 1986, *Mon. Not. R. astr. Soc.*, **219**, 703.  
 Urpin, V. A., Van Riper, K. A. 1993, *Astrophys. J.*, (in press).  
 Yakovlev, D. G., Urpin, V. A. 1980, *Soviet Astr.*, **24**, 303.  
 Yakovlev, D. G., Shalybkov, D. A. 1991, *Astrophys. Space Sci.*, **176**, 191.

## Abstracts

### Refractive Interstellar Scintillation Studies of Pulsars

Y. Gupta, B. J. Rickett<sup>a</sup>, R. Bhat & M. Vivekanand *National Centre for Radio Astrophysics, Tata Institute of Fundamental Research, Pune 411 007, India*

<sup>a</sup> *Department of Electrical and Computer Engineering, University of California, San Diego, CA 92093-0407, USA.*

The study of refractive interstellar scintillation (RISS) of pulsar signals provides useful insights into the distribution of electron density irregularities in the interstellar medium (ISM) as well as probe the long term stability of pulsar fluxes. In this context, pulsar dynamic spectra are very useful tools of study.

In the first part of this paper, we present the results from the study of the evolution of the 408 MHz dynamic spectra of eight pulsars over 16 months. The changing form of the spectra is interpreted as refractive modulation of diffractive interstellar scintillation. The correlation function versus time and frequency was computed for each observation and, by fitting a gaussian function, three parameters were estimated: the apparent decorrelation widths in frequency and in time, and the frequency drift rate of scintillation features. A model is developed for how these three parameters vary with epoch under changing angles of refraction. The model successfully describes the variations for four of the pulsars, for which the drift rate shows some sign reversals between epochs. The variability of the diffractive bandwidth fits well with the model, including its dependence on the strength of scattering. The refractive shifts are estimated from the data using the model and agree with the expected rms values. The speed estimated for the diffraction pattern compares well with the proper motion of the pulsars. Two pulsars (PSR 1642–03 and PSR 0628–28) kept a constant sign of drift rate, which we interpret as due to persistent refracting structures in their lines of sight; the inferred angle of refraction is about 0.05 mas and the implied electron density is consistent with that expected for an HII region.

New observations of pulsar dynamic spectra are underway using the Ooty Radio Telescope at 327 MHz. The aim is to monitor the evolution of the dynamic spectra over several refractive time scales. Four pulsars – PSR 1133 + 16, PSR 0823 + 26, PSR 0834 + 06 and PSR 1919 + 21 – have been observed at intervals of one to two days for durations of a few refractive time scales. Preliminary results from these observations are reported in the second part of this paper.

★ ★ ★ ★ ★

### Pulsational Mode and Detection of Gravitational Wave Source

R. K. Parui *ACS, Imphal Airport, Imphal 795 140, India*

We calculate damping rate per unit eccentricity of toroidal mode and pulsational mode



by gravitational radiation. It is found that the damping rate of the pulsational mode which becomes the quadrupole mode (emits gravitational wave) has a minima at  $e = 0.72$  for  $\gamma = 4/3$ , and  $8/5$  whereas both the pulsational mode with  $\gamma = 5/3$  and toroidal mode have no minima. Our suggestion is to measure damping rate of pulsational mode only in the programme of detection of gravity wave sources.

★★★★★

## A Search for TEV $\gamma$ -Rays from PSR 0355 + 54

V. K. Senecha<sup>1</sup>, C. L. Bhat, R. C. Rannot, R. K. Kaul, M. L. Sapru,  
A. K. Tickoo & H. S. Rawat<sup>1</sup> *Bhabha Atomic Research Centre, Nuclear Research  
Laboratory, Trombay, Bombay 400 085, India*

<sup>1</sup>Now at the Centre for Advanced Technology, Indore.

Pulsed TeV  $\gamma$ -ray emission was reported from the  $6 \times 10^5$  yr-old radio pulsar, PSR 0355 + 54 (period 156 ms), by the Pachmarhi group in 1987 (Bhat *et al.* 1990). The implied  $\gamma$ -ray luminosity ( $\sim 70\%$  of the pulsar spin-down power) points to an unusually high  $\gamma$ -ray conversion efficiency. The source was revisited by the Whipple and the Pachmarhi groups in 1988–91 and 1989–90 respectively, but no d.c. or pulsed emission was detected (Reynolds *et al.* 1993).

We have also observed the source region from 1989 November 20–December 01, using one  $3 \times 0.9$  m mirror bank of the Gulmarg atmospheric Cerenkov telescope (Koul *et al.* 1989). The observations were carried out by tracking the on-source region for 30 minutes followed by tracking an equivalent off-source region for the same duration. It needs to be noted that, although the telescope was erroneously offset by  $+1^\circ$  in declination with respect to the actual source coordinates, yet the pulsar PSR 0355 + 54 was always within the system field of view of  $4^\circ$  diameter during each on-source scan. The ambient light level seen by the telescope photomultiplier detectors was stabilized. The average event rate recorded was  $0.42 \text{ s}^{-1}$ , corresponding to a threshold primary energy of 4 TeV.

On subjecting 10 hours of 'clean' data to the pulsar analysis using contemporary pulsar contemporary ( $p, \dot{p}$ ) values, the on-source data do not show the presence of a significant pulsed component, as is also reported by the Pachmarhi and Whipple groups for the corresponding period. However, intriguingly, our overall on-source data shows a  $4.2\sigma$ -d.c. excess with respect to the corresponding off-source counts. If this apparent excess were due to VHE  $\gamma$ -rays, the corresponding flux turns out to be  $4.9 \times 10^{-11} \text{ cm}^{-2} \text{ s}^{-1}$  at  $> 4 \text{ TeV}$ . This value is a factor of  $\sim 100$  higher than (and incongruous to) what follows from the Whipple d.c. upper limit, extrapolated as per  $\sim E_\gamma^{-1}$  law (Pachmarhi group has searched for a pulsed signal only). No pulsar-associated old Supernova remnant is found in low-resolution radio surveys (Green, pers. comm.) and ROSAT X-ray searches (Trumper, pers. comm.). No other potential  $\gamma$ -ray source candidates are also found in this field. Hence we do not have a satisfactory explanation for the apparent d.c. excess at this stage.

## References

- Bhat, P. N. *et al.* 1990, *Proc. 21st ICRC Adelaide*, **2**, 325.  
Koul, R. *et al.* 1989, *J. Phys. E.*, **22**, 47.  
Reynolds, *et al.* 1993, *Astrophys. J.*, **404**, 206.

**Unique Observations of PSR 0950 + 08 and Possible Terrestrial Effects**

M. R. Deshpande, Hari Om Vats, P. Janardhan, A. D. Bobra,  
Harish Chandra & G. D. Vyas *Physical Research Laboratory, Ahmedabad 380 009,  
India*

Since the discovery of pulsars about twenty five years ago, there has been a large number of exciting events seen from several of them. PSR 0950 + 08 is a very interesting object which is regularly monitored by PRL's two radio telescopes situated at Rajkot and Thaltej. The pulsar has flux of about 3 Jy and hence it normally remains within the background noise of our telescopes, however Thaltej telescope being more sensitive, sometimes, few pulses are recorded. On July 29, 1992, this pulsar suddenly gave a very large outburst of energy and this was recorded by both radio telescopes simultaneously. The cross-correlation analysis of both these observations showed a very high degree of correlation and precise pulse frequency. The cross-correlogram and the power spectra showed that large number of pulses remained unscattered by the interplanetary medium during their passage. However, the variation of pulse intensity seems to be of two components, namely, (1) variation in pulse intensity and (2) scattering due to the irregularities in the interplanetary medium. The average flux of the pulsar during this event was  $\sim 246$  Jy (which is about 80 times the normal flux) and several pulses exceeded 850 Jy. The enhancement of the pulsar flux is very large and is seen simultaneously by both the telescopes separated by 200 kms. Moreover no enhancement was seen in any other IPS sources around the pulsar burst time. These associated observations bring out clearly that the radio burst from the pulsar is not due to the intervening media, e.g., ionosphere, interplanetary medium and interstellar medium.

There exists an indirect evidence of very intense X-ray emission which seems to have produced excess ionization in the 'D' region of the ionosphere. This evidence comes from an ionospheric sounding experiment in which pulses of HF radio waves are transmitted vertically upward and signal reflected from the ionospheric layers is received and recorded. In this there is a parameter called ' $f_{\min}$ ' which is the minimum frequency reflected by the ionosphere. The close examination of these records (usually called ionograms) reveals that on 29 July 1992, ' $f_{\min}$ ' is around 1.6 MHz in the morning and its temporal variation shows three distinct peaks of 4.0, 4.2 and 2.5 MHz (one of these peaks coincides with the local transit of the pulsar as seen by the two radio telescopes). However, it appears that pulsar was active during all the three events seen by the ionosonde, but the radio telescopes could see only one because of their narrow beam width of  $1.8^\circ$  and  $7.2^\circ$  at Thaltej and Rajkot respectively. In fact the two earlier events seen by the ionosonde on this day are stronger than the third one and hence if the radio telescope could have been tracking the pulsar, the radio burst during the first two

events would be an order of magnitude larger than the third one which is really recorded. These  $f_{\min}$  peaks are caused by the excess ionisation in the 'D' region. The ionisation in the 'D' region is produced by X-ray in the range  $1 \cdot 10 \text{ \AA}$  and the most common source is our Sun. On this day Sun was extremely quite and the observed X-ray flux was lower than  $4 \times 10^{-7} \text{ Watt/m}^2$ . The observed  $f_{\min}$  peaks require X-ray flux to be in the range  $4 \times 10^{-5}$  to  $8 \times 10^{-5} \text{ Watt/m}^2$ . From this it appears that while pulsar gave sudden outburst at 103 MHz it also gave energy at other wavelengths. This pulsar is not a known X-ray source. The amount of X-ray emission appears to be extremely large. We considered the possibility of accretion process for this event. It turns out that the energy calculations require a mass  $\sim 10^{15} \text{ kg}$  to be accreted by the pulsar during this event. This mass is almost that of a comet and thus accretion of a comet like object seems to be the cause of enhancement.

★★★★★

# **Interstellar and Interplanetary Medium**



## Mass Loss in AGB Stars – Recent Observational Developments

Raghvendra Sahai<sup>1</sup> *Jet Propulsion Laboratory, California Institute of Technology,  
MS 169-506, 4800 Oak Grove Drive, Pasadena, CA 91109, USA*

**Abstract.** Extensive mass-loss in red giant (AGB) stars, preceding and leading up to the formation of planetary nebulae, has important consequences for the evolution of the stars as well as the interstellar medium. A brief review, with focus on new studies of mass-loss envelopes involving high-spatial resolution observations made possible by recent technological advances, is presented.

**Key words:** Mass-loss – red giants – planetary nebulae – interferometry – infrared – radio – circumstellar matter.

### 1. Introduction

Extensive mass-loss (with  $dM/dt$  upto  $\sim 10^{-4} M_{\odot} \text{yr}^{-1}$ ) in intermediate mass ( $1-8 M_{\odot}$ ) stars not only affects their evolution on and beyond the asymptotic giant branch (AGB), preventing stars with masses upto  $\approx 8 M_{\odot}$  from becoming supernova, but also enriches the interstellar medium in (■) a variety of nuclides produced by CNO, 3- $\alpha$  and s-process nucleosynthesis, and (■) dust grains. The circumstellar envelopes (CSEs) resulting from the mass-loss usually have relatively simple and well-defined geometrical (spherical) and kinematical (radially-constant expansion velocity) structures, and thus constitute ideal astrophysical laboratories. Thus, some of the most difficult problems of interstellar cloud chemistry, such as the role played by dust grains, UV radiation, and shocks in the formation and destruction of different molecular species, may ultimately be solved by a study of circumstellar chemistry.

### 2. Outstanding problems

We lack a theory which can predict the basic mass-loss properties, namely, the rate ( $dM/dt$ ), expansion velocity ( $V_{\text{exp}}$ ), and the spatial distribution, from fundamental stellar parameters – luminosity, temperature, and metallicity. A number of hypotheses for mass-loss in cool red giants have been investigated (e.g. Holzer & MacGregor 1985) and a two-step process is currently favoured, whereby stellar matter is first levitated by various processes (e.g. stellar pulsation: Bowen & Willson 1991, sound waves: Pijpers *et al.* 1990) into an extended atmosphere where grains form, which are then driven outwards (dragging the gas along) under radiation pressure (e.g. Morris 1987). However important questions relating to the history (continuous or episodic) and structure

---

<sup>1</sup>Senior Resident Research Associate, National Research Council, National Academy of Sciences, Washington, DC 20418

(e.g. smooth or clumped) of the mass-loss, the formation and growth of dust grains, remain unanswered. The origin of equatorially dense structures and fast outflows ( $50\text{--}100\text{ km s}^{-1}$ ) on small angular scales seen in an increasing number of objects with extended spherically symmetric envelopes (e.g. CRL2688: Kawabe *et al.* 1987) is not clear: models involving binary companions (Morris 1987), planetary systems (Sahai *et al.* 1991), and magnetic fields (Pascoli *et al.* 1992) have been suggested.

### 3. Recent developments

Until recently, most of our knowledge about CSEs came from observations of millimeter-wave molecular lines using single telescopes. With significant increase in telescope/receiver sensitivity and the detection of thousands of AGB stars in  $12\text{--}100\text{ }\mu\text{m}$  emission by IRAS,  $\sim \text{few} \times 100$  CSEs have now been detected through systematic searches (the largest carried out with the IRAM 30-m & the SEST 15-m) in the CO  $J = 1\text{--}0$  and  $2\text{--}1$  lines (compilation by Loup *et al.* 1993). Although such studies provide useful information on the envelope-averaged  $dM/dt$  and  $V_{\text{exp}}$  necessary for studying the statistics of mass-loss, (e.g. Jura & Kleinmann 1989, and references therein) more fundamental questions relating to the nature of the mass-loss can only be addressed with high spatial resolution observations. A new self-consistent model of radiative transfer, molecular excitation, and thermodynamics which simultaneously fits the CO rotational line-emission and the far-infrared (IRAS) emission from CSEs has been developed for reliable estimates of mass-loss rates and circumstellar dust-to-gas ratios (Sahai 1990).

a) *Millimeter (& centimeter) wave interferometry*: With the advent of millimeter-wave interferometers, one can now observe a large number of circumstellar envelopes with adequate spatial resolution. Most studies have focussed on the prominent carbon-rich CSEs. Bieging, Chapman & Welch (1984) reported the first interferometric map of molecular line emission from a CSE: their map of HCN  $1\text{--}0$  in IRC + 10216 (well-studied carbon star) suggested a recent decrease in the mass-loss rate (later confirmed by analysis of CO  $4.6\text{ }\mu\text{m}$  and mm-wave line emission: Sahai 1987; Sahai & Wannier 1985). Bieging & Nguyen-Q-Rieu (1988a) find evidence for a rotating disk in the protoplanetary object CRL 2688 from HCN  $1\text{--}0$  mapping (BIMA data). VLA mapping of cm-wave line emission of  $\text{NH}_3$  &  $\text{HC}_7\text{N}$  in CRL2688 (Nguyen-Q-Rieu *et al.* 1986) reveal both disk and jet-like structures, as well as departures in the kinematics from pure expansion. Detailed information on the distribution and abundances of various molecules has been obtained for IRC10216 (VLA maps of  $\text{NH}_3$ ,  $\text{HC}_7\text{N}$  and  $\text{HC}_3\text{N}$  by Wootten *et al.* 1993, BIMA maps of SiS,  $\text{HC}_3\text{N}$ ,  $\text{C}_3\text{N}$ ,  $\text{C}_2\text{H}$ , HNC by Bieging & Nguyen-Q-Rieu 1988b, Bieging & Tafalla 1993) and CRL2688 (Nguyen-Q-Rieu & Bieging 1990), providing confirmation of some of our ideas of circumstellar chemistry, as well as raising new problems. Neri *et al.* (1992) have resolved the HCN  $1\text{--}0$  emission (PdBI data) from the unique high-velocity ( $200\text{ km/s}$ ) outflow in CRL 618 (very young PN), from which they infer that HCN is formed (on a time-scale  $< 50\text{ yr}$ ) in a post-shock region where the high-velocity outflow impacts a more slowly expanding dense envelope. Sahai & Bieging (1993) have used BIMA to map the  $J = 2\text{--}1$  ( $v = 0$ ) SiO line emission at  $86\text{ GHz}$  in oxygen-rich CSEs (see also Lucas *et al.* 1992), and find that (■) SiO is depleted rapidly beyond  $10^{15}$ , probably as a result of adhesion onto cold grains (photodissociation due to the interstellar UV becomes important at

$> 0.5 \times 10^{16}$  cm) (■) acceleration of the outflows is consistent with radiation pressure on grains condensing within 10–15 stellar radii.

(b) *Submillimeter-line observations*: Observations at submillimeter wavelengths have now become possible with the 15-m JCMT and 10 m CSO telescope allowing one to use high-excitation molecular lines as a novel probe of the inner CSEs, one which works equally well for nearby and distant objects. Sahai, Wannier & Andersson (1992) have observed a selected list of CSEs with prominent SiO  $J = 2-1$  ( $v = 0$ ) emission, in the  $J = 5-4$ ,  $6-5$ ,  $8-7$ , and  $11-10$  lines. The high- $J$  SiO line-widths at the base are only 50–75% of the CO line-widths ( $= 2 \times$  terminal envelope expansion velocity) clearly showing that the SiO lines arise in the acceleration region. A map of IRC10216 (which appears circular on arc-minute scales in CO  $J = 1-0$  and  $2-1$  line emission) in the CO  $6-5$  line made with the  $8''$  beam of the JCMT, shows that the peak emission occurs about  $6''$  south-west of the stellar position (Sahai, van der Veen & Stutzki 1993).

(c) *Molecular gas in planetary nebulae*: AGB mass-loss plays an important role in the formation of planetary nebulae (PNe). The ‘interacting-stellar-winds’ (ISW) model (Kwok 1982) successfully produces the dense ‘rims’ seen in PNe images, due to the ‘snowplow’ action of a very fast wind (1000–2000 km/s) from the central white dwarf, on the AGB envelope. Including an equatorial-to-polar density asymmetry of the AGB envelope in the ISW model (Balick 1987) naturally leads to the bipolar shapes seen in about 50% of all PNe. Until recently, it was difficult to detect the generally weak CO emission from PNe. However, CO emission has now been mapped in a number of PNe, confirming (directly or indirectly) the presence of equatorial density enhancements and/or fast outflows directed along the polar axis (NGC7027: Bieging *et al.* 1991; Jaminet *et al.* 1991, NGC3132: Sahai *et al.* 1990, IC4406: Sahai *et al.* 1991, NGC2346: Bachiller *et al.* 1989). High-resolution ( $12''$ ) CO  $J = 2-1$  maps of PNe (e.g. Bachiller *et al.* 1993 and references therein) show large-scale ( $10^{17}$  cm) fragmentation of their molecular envelopes, and the detection of molecules with large dipole moments (e.g. HCN and  $\text{HCO}^+$ ) in PNe (Sahai *et al.* 1993a) imply the presence of small ( $10^{15}$ – $10^{16}$  cm), dense ( $10^5 \text{ cm}^{-3}$ ) clumps (Sahai *et al.* 1993b).

(d) *Near-infrared imaging*: The interface between the ionised and neutral (molecular) region in PNe is a source of strong emission in the near-IR vibration-rotation lines of molecular hydrogen, which can now be mapped with high spatial and spectral resolution, with the advent of infrared CCD-array cameras and spectrometers. Images of the integrated  $\text{H}_2\text{S}(1)$  line emission at  $2.1 \mu\text{m}$  from the compact young PN NGC7027 shows an incomplete elliptical ring of knots bounding the ionised gas, and a thin shell looping around the HII region with 4-fold symmetry, coincident with the inner edge of the CO shell (Graham *et al.* 1993). Velocity-resolved (long-slit) images of the  $\text{H}_2\text{S}(1)$  line in another compact young PN, BD +  $30^\circ 3639$  (taken with the CSHELL/IRTF) show that the molecular gas is concentrated in a clumpy, tilted toroidal structure (Wannier & Sahai 1992), apparently the result of a collimated high-velocity flow excavating a bipolar cavity in an AGB CSE.

#### 4. Future prospects

A systematic survey undertaken with the upcoming Giant Meter-wave Radio Telescope (Pune, India) should produce a substantial increase in the number of AGB stars detected in HI (only 2 detected so far, see Bowers & Knapp 1988), providing the first



direct estimates for mass-loss rates, total envelope masses and ages. Increasing use of mm-wave (and future submm-wave) interferometers, infrared CCD-array cameras coupled to high-resolution spectrometers, and submillimeter telescopes, in observations of AGB stars and PNe, will lead to a detailed and comprehensive picture of the history and structure of the mass-loss during the stellar evolution.

## References

- Bachiller, R., Huggins, P. J., Cox, P., Forveille, T. 1993, *Astr. Astrophys.*, **267**, 177.  
 Bachiller, R., Planesas, P., Martin-Pintado, J., Bujarrabal, V., Tafalla, M. 1989, *Astr. Astrophys.*, **210**, 366.  
 Balick, B. 1987, *Astr. J.*, **94**, 671.  
 Bieging, J. H., Chapman, B., Welch, W. J. 1984, *Astrophys. J.*, **285**, 656.  
 Bieging, J. H., Wilner, D., Thronson, H. A. 1991, *Astrophys. J.*, **379**, 271.  
 Bieging, J. H., Nguyen-Q-Rieu 1988a, *Astrophys. J.*, **324**, 516.  
 Bieging, J. H., Nguyen-Q-Rieu 1988b, *Astrophys. J.*, **329**, L107.  
 Bieging, J. H., Tafalla, M. 1993, *Astr. J.*, **105**, 576.  
 Bowers, P. F., Knapp, G. R. 1988, *Astrophys. J.*, **332**, 299.  
 Bowen, G., Willson, L. 1991, *Astrophys. J.*, **375**, L53.  
 Graham, J. R., Serabyn, E., Herbst, T. M., Matthews, K., Neugebauer, G., Soifer, B. T., Wilson, T. D., Beckwith, S. 1993, *Astr. J.*, **105**, 250.  
 Holzer, T. E., MacGregor, K. B. 1985, *Astrophys. Space Sci. Lib.*, **117**, 229.  
 Jaminet, P. A., Danchi, W. C., Sutton, E. C., Russell, A. P. G., Sandell, G., Bieging, J. H., Wilner, D. 1991, *Astrophys. J.*, **380**, 461.  
 Jura, M., Kleinmann, S. G. 1989, *Astrophys. J.*, **341**, 359.  
 Kawabe, R., Ishiguro, M., Kasuga, T. et al. 1987, *Astrophys. J.*, **314**, 322.  
 Kwok, S. 1982, *Astrophys. J.*, **258**, 280.  
 Loup, C., Forveille, T., Omont, A., Paul, J. F. 1993, *Astr. Astrophys., Suppl. Ser.*, **99**, 291.  
 Lucas, R., Bujarrabal, V., Guilloteau et al. 1992, *Astr. Astrophys.*, **262**, 491.  
 Morris, M. 1987, *Publ. Astr. Soc. Pacific*, **99**, 621.  
 Neri, R., Garcia-Burillo, S., Guelin, M., Cernicharo, J., Guilloteau, S., Lucas, R. 1992, *Astr. Astrophys.*, **262**, 544.  
 Nguyen-Q-Rieu, Bieging, J. H. 1990, *Astrophys. J.*, **359**, 131.  
 Nguyen-Q-Rieu, Winnberg, A., Bujarrabal, V. 1986, *Astr. Astrophys.*, **165**, 204.  
 Pascoli, G., Leclercq, J., Poulain, B. 1992, *Publ. astr. Soc. Pacific*, **104**, 1.  
 Pijpers, F. P., Hearn, A. G., Habing, H. J. 1990, in *From Miras to Planetary Nebulae: Which Path for Stellar Evolution*, Eds. M. O. Mennesier & A. Omont, (Paris: Editions Frontieres) p. 131.  
 Sahai, R. 1987, *Astrophys. J.*, **318**, 809.  
 Sahai, R. 1990, *Astrophys. J.*, **362**, 652.  
 Sahai, R., Wannier, P. G. 1985, *Astrophys. J.*, **311**, 335.  
 Sahai, R., Wootten, A., Clegg, R. E. S. 1990, *Astr. Astrophys.*, **234**, L1.  
 Sahai, R., Wootten, A., Schwarz, H. E., Clegg, R. E. S. 1991, *Astr. Astrophys.*, **251**, 560.  
 Sahai, R., Wootten, A., Clegg, R. E. S. 1993a, *IAU Symposium 155, Planetary Nebulae*, Eds. R. Weinberger & A. Acker (Dordrecht: Reidel) in press.  
 Sahai, R., Wootten, A., Schwarz, H. E., Wild, W. 1993b, *Astrophys. J.*, (in press).  
 Sahai, R., van der Veen, W. E. C. J., Stutzki, J. 1993, (in preparation).  
 Sahai, R., Bieging, J. H. 1993, *Astr. J.*, **105**, 595.  
 Sahai, R., Wannier, P. G., Andersson, B-G. 1992, *Bull. Am. Astr. Soc.*, **24**, 1302.  
 Wannier, P. G., Sahai, R. 1992, *Bull. Am. Astr. Soc.*, **24**, 1179.  
 Wootten, A., Sahai, R., Nguyen-Q-Rieu, Truong-Bach 1993, in *Circumstellar Media in the Late Stages of Stellar Evolution*, The 34th Herstmonceux Conference, 12–16 July, 1993.

## Cold, Warm, and Hot Gas in the Merged Galaxy-Pair NGC 7252

Puragra Guhathakurta<sup>1</sup> *Princeton U. Observatory, Peyton Hall, Princeton, NJ 08544, USA*

John E. Hibbard & Jacqueline H. van Gorkom *Astronomy Dept., Columbia U., 538 W 120 St., New York, NY 10027, USA*

François Schweizer *Dept. of Terrestrial Magnetism, Carnegie Inst. of Washington, 5241 Broad Branch Road NW, Washington, DC 20015, USA*

This paper describes recent multi-wavelength observations of the late-stage merger remnant NGC 7252, the ‘Atoms for Peace’ galaxy. These observations are a part of a broader study of the fate of gas in a sample of interacting pairs of galaxies that are at various phases of merging (Hibbard 1994). NGC 7252 has two prominent tidal tails and a *single* central stellar body, suggesting that it is close to the final stage of the merging process. The principal conclusions of our study are summarized below (the reader is referred to Hibbard *et al.* 1994 for a more complete description):

- Radio (21 cm) spectral-line observations, using the Very Large Array of the National Radio Astronomy Observatory (in ‘D’ and ‘B/C’ configurations), of the merger remnant NGC 7252 have revealed  $2 \times 10^9 \text{ h}^{-2} M_{\odot}$  of atomic hydrogen which is located exclusively in the outer, tidal regions of the galaxy: in the two tails and in the prominent western loop that appears to wrap around the central remnant. No atomic gas is detected in the central relaxed stellar body.
- New ROSAT X-ray data (in the 0.1–2.4 keV energy range), H $\alpha$  images using the Kitt Peak 2.1-m telescope, and broadband optical *B* and *R* surface photometry (using the Cerro Tololo 0.9-m telescope) have also been obtained. In contrast to the HI distribution, the hot X-ray emitting plasma and molecular gas (mapped by Wang *et al.* 1992) are confined to the central region. Most of the H $\alpha$  appears to be associated with the inner rotating molecular-gas disk ( $r < 7''$ ), but some is seen to be associated with the base of the northwestern tail and with the western loop filling the gap between the atomic and molecular gas distributions.
- The HI data yield the first detailed map of the kinematics of the tidal tails of NGC 7252 providing important new constraints on numerical simulations of this system (Borne & Richstone 1991; Mihos *et al.* 1993). Each of the tidal features shows remarkably smooth velocity gradients. The rotation velocities as a function of position along the tail indicate that the encounter that fashioned NGC 7252 must have been prograde. We suggest that the gas at the base of the northwestern tail is on a non-circular orbit, falling back towards the main remnant body. The HI observations may provide evidence for formation of shells and ripples by late-returning tidal material, and may explain some of the peculiar kinematics (e.g. line-of-sight velocity reversals) previously recorded in this system (see Schweizer 1982).

<sup>1</sup> Hubble Fellow

- Despite the fact the HI appears to be falling in towards the central remnant, no atomic gas is detected in the remnant itself. The lack of neutral atomic hydrogen in the main body of NGC 7252, along with the presence of warm and hot ionized gas and a 'post-starburst' spectrum in this region, suggests efficient, ongoing conversion of HI into other phases.
- Prominent H $\alpha$ , HI, and stellar enhancements are seen near the end of each of the two tidal tails, each containing an amount of material similar to that seen in dwarf galaxies. Reasonable mass-to-light ratios are needed in order for these condensations to be self-bound. If these clumps are bound, they serve to support the idea originally proposed by Zwicky (1956), and verified in recent numerical simulations, that dwarf galaxies can form from tidally ejected material.
- The long, gas-rich tidal tails of the NGC 7252 system imply two spiral progenitors. This evidence, combined with the photometric properties and gas content of NGC 7252, lends strong support to Toomre's (1977) suggestion that mergers of spirals can lead to elliptical-like remnants. The radial surface brightness profile of the central remnant body follows an  $r^{1/4}$  law and NGC 7252 obeys the 'Fundamental Plane' relationships that characterize normal elliptical galaxies (Djorgovski & Davis 1987).

## References

- Borne, K. D., Richstone, D. O. 1991, *Astrophys. J.*, **369**, 111.  
 Djorgovski, S., Davis, M., 1987, *Astrophys. J.*, **313**, 59.  
 Hibbard, J. E. 1994, Ph D thesis, Columbia University.  
 Hibbard, J. E., Guhathakurta, P., van Gorkom, J. H., Schweizer, F. 1994, *Astr. J.*, (in press).  
 Mihos, J. C., Bothun, G. D., Richstone, D. O. 1993, *Astrophys. J.*, (in press).  
 Schweizer, F. 1982, *Astrophys. J.*, **252**, 455.  
 Toomre, A. 1977, in *The Evolution of Galaxies and Stellar Populations*, Eds. B. M. Tinsley & R. B. Larson (Yale University Observatory) p 401.  
 Wang, Z., Schweizer, F., Scoville, N. Z. 1992, *Astrophys. J.*, **396**, 510.  
 Zwicky, F. 1956, *Ergebnisse der Exakten Naturwissenschaften*, **29**, 344.

## Molecular, Atomic and Ionized Gas towards Cas-A

**Nimisha G. Kantharia** *Raman Research Institute, Bangalore 560 080 and Joint Astronomy Program, Physics Dept., Indian Institute of Science, Bangalore 560 012, India*

**K. R. Anantharamaiah** *Raman Research Institute, Bangalore 560 080, India*

**W. C. Erickson** *Physics Dept., Univ. of Tasmania, Tasmania 7001, Australia*

**H. E. Payne** *Space Telescope Science Institute, 3700 San Martin Drive, Baltimore, MD 21218, USA*

**Abstract.** We present a comparison of the spatial distribution of molecular gas (as determined from  $^{12}\text{CO}$ ,  $J = 1 \rightarrow 0$  line), atomic gas (as determined from 21 cm HI absorption) and ionized gas (as observed in C270 $\alpha$  recombination line) towards Cas A.

**Key words:** Radio sources: Cas A -- Radio Lines: Molecular, HI, recombination lines --ISM: Ionized carbon

### 1. Introduction

Recombination lines from highly excited Rydberg levels (principal quantum number  $n \sim 300 - 700$ ) of carbon have been detected in a number of directions. The best studied direction at various frequencies is that of the strong radio source Cas A whose line of sight intersects the Perseus and Orion arms. Though carbon recombination lines at low frequencies have been detected in many directions, it is still not clear whether the lines are associated with HI regions or molecular clouds (Payne *et al.* 1989). As a step towards resolving this question we present here a comparison of the spatial distribution of ionized carbon observed in C270 $\alpha$  recombination line with that of atomic gas observed in HI (21 cm) absorption line and the molecular gas observed in  $^{12}\text{CO}$  ( $J = 1 \rightarrow 0$ ) emission line towards the direction of Cas A. Cas A being a strong background source provides a spatial cutoff for the HI absorption and thus the study can be confined to the extent of Cas A.

### 2. Observations

The  $^{12}\text{CO}$  observations were made with an angular resolution of  $\sim 1'$  using the 10.4m telescope at the Raman Research Institute. Chopper wheel method was used for temperature calibration and frequency switching was employed for baseline correction. The spectrometer was a 256 channel filter bank of 250 kHz contiguous filters. The double sideband system temperature varied between 1000 - 1800° K depending on the weather. The C270 $\alpha$  (332.7 MHz) observations were carried out at VLA in its C and D configurations which gave an angular resolution of  $\sim 2.7' \times 2.4'$ . For the distribution of atomic gas, we have used the HI data obtained using the

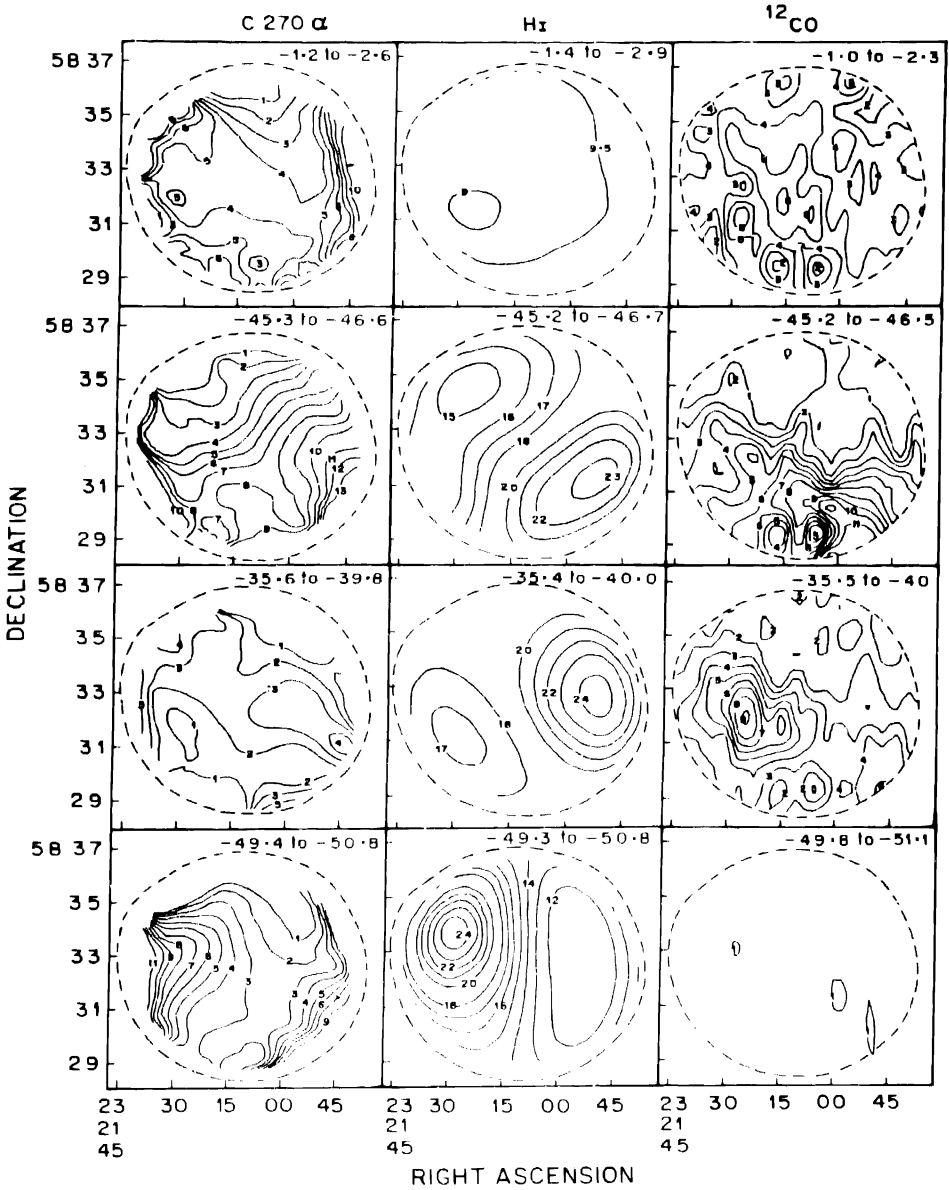


**Figure 1.** Spatial distribution of optical depths of C270 $\alpha$  recombination line and 21 cm HI absorption lines and antenna temperature ( $T_A$ ) of  $^{12}\text{CO}$  emission over the face of Cas A at four different velocities. The velocity range is indicated in each frame in km s $^{-1}$ . Contour units are C270 $\alpha$ :  $10^{-3}$ ; HI: 0.1; and  $^{12}\text{CO}$ : 0.3 K.

Westerbork Synthesis Telescope by Kalberla *et al.* (1993). The HI data was convolved to the resolution of C270 $\alpha$  observations. The spectral resolution in all these observations is  $\sim 1.5$  km/sec.

### 3. Results

The observed distribution of C270 $\alpha$ , HI and  $^{12}$ CO over the face of Cas A is presented in Fig. 1 for four velocity ranges. The top frame corresponds to the Orion arm and the other three to the Perseus arm clouds. It is clear from Fig. 1 that the distribution of C270 $\alpha$  is very similar to that of HI rather than molecular gas. This association makes it possible to construct a model in which several physical properties of the clouds can be determined by combining the recombination line and 21 cm HI measurements. Such model calculations have been recently presented by Payne *et al.* (1993).

### References

- Kalberla, P. M. W., Schwarz, U. J., Goss, W. M. 1993 (to be published).  
Payne, H. E., Anantharamaiah, K. R., Erickson, W. C. 1989, *Astrophys. J.*, **341**, 890.  
Payne, H. E., Anantharamaiah, K. R., Erickson, W. C. 1993, (submitted to *Astrophys. J.*).



## Radio Synthesis Imaging of Scatter-broadening at Small Solar Elongations

K. R. Anantharamaiah *Raman Research Institute, Bangalore 560 080, India*

Pradeep Gothoskar *National Centre for Radio Astrophysics, TIFR, Pune 411 007, India*

T. J. Cornwell *National Radio Astronomy Observatory, Socorro, NM 87801, USA*

**Abstract.** When the lines of sight to distant radio sources pass close to the Sun, the radiation from the source undergoes scattering due to electron density irregularities in the outflowing solar wind plasma and phenomenon such as intensity scintillations and angular broadening can be observed. At small solar elongations ( $\epsilon < 4^\circ$ ) the scattering is sufficiently strong that the scatter broadened image can be resolved using radio synthesis arrays such as the VLA<sup>1</sup>. The measured visibilities and the reconstructed image can be used to study the turbulence spectrum and anisotropy in the solar wind. We present here some results of observations of three strong radio sources at several elongations in the range  $0.5^\circ$ – $4^\circ$  using the A-configuration of the VLA (maximum baseline 35 km) at wavelengths of 2, 3.5, 6, and 20 cm.

*Key words:* Solar wind – synthesis imaging.

### 1. Observations and results

The radio sources 1430–155, 1437–153, and 1443–162 were observed during 2–6 Nov. 1988 when their lines of sight passed within about  $4^\circ$  of the Sun. Because of the steep gradient in the mean electron density of the solar wind ( $n_e \sim R^{-2}$  or steeper at smaller solar distance), shorter wavelength (2 and 3.5 cm) observations were more suitable at small elongations and longer wavelengths (6 and 20 cm) at larger elongations.

Each source was observed at the chosen wavelength for about 10 minutes with an integration time of 10 seconds per visibility sample. The resulting visibility data were processed using the standard method to obtain ‘clean’ images of the sources observed at different elongations. Most of the images, where broadening could be seen, are elliptical in shape indicating anisotropic scattering in the solar wind and confirms the earlier findings of Armstrong *et al.* (1990). The axial ratio of the images varies between 1.5 – 7 depending on the elongation. Fig. 1 depicts the anisotropy and the orientation of the images observed at a wavelength of 6 cm. The magnitude of the broadening is generally larger at smaller elongations, although there are several exceptions. The variation of the scattering angle (i.e. the angular size of the major axis of the image) as a function of solar distance roughly follows a  $R^{-1.6}$  law.

<sup>1</sup>VLA is part of NRAO, USA, operated by Associated Univ. Inc., under a cooperative agreement with NSF.



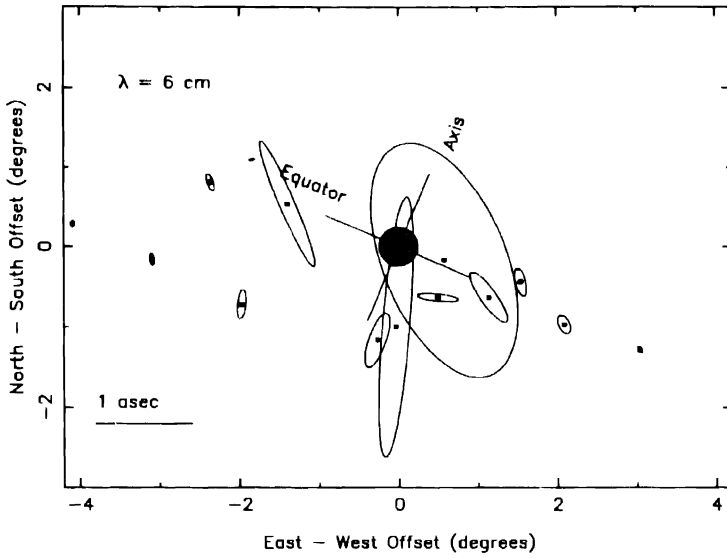


**Figure 1.** Shapes of scatter broadened images (ellipses) at different distances from the Sun (filled 0.5' circle at the centre). The scale for the images is indicated at the bottom left corner.

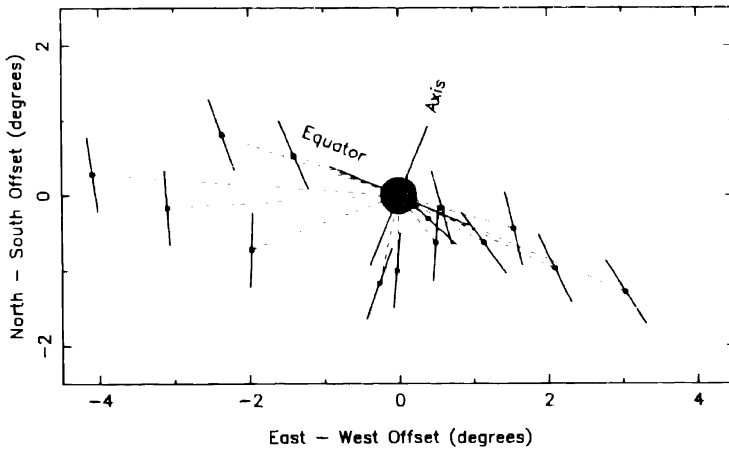


**Figure 2.** Orientation of the major axes (solid lines) of scatter broadened images with respect to the radial direction (dashed lines) from the Sun.

The anisotropy indicates that the scattering blobs are elongated in the direction perpendicular to the major axis of the image. This direction can be considered as the 'local' orientation of the magnetic field lines since density fluctuations are expected to be aligned along the field lines (Higdon 1984). Fig. 2 shows the observed orientation of

the major axis at different elongations and position angles. Clearly, the orientation is not perpendicular to the radial everywhere. The deviations are seen to be the largest near the poles, which also suggest that magnetic field lines may indeed determine the direction of elongation of the scattering blobs.

The measured visibility  $V(b)$ , on a baseline  $b$  is related to the phase structure function  $D(b)$  of the scattering screen by the simple relation  $D(b) = -2 \ln[V(b)]$ . For a power-law spectrum of density fluctuations of the form  $P(q) \propto q^{-\beta}$ , where  $q$  is the spatial wavenumber, the phase structure function has the form  $D(b) \propto b^{\beta-2}$ . Through model fits to the measured visibilities we find that  $\beta$  is in the range 1.8 to 3.0 depending on solar distance, with a median value of  $\sim 2.0$ . This applies to scale lengths in the range 1–35 km sampled by the VLA baselines. The spectrum in this range appears to be shallower compared to Kolmogorov turbulence ( $\beta = 11/3$ ) in agreement with earlier findings of Coles & Harmon (1989).

### References

- Armstrong, J. W. A., Coles, W. A., Kojima, M., Rickett, B. J. 1990, *Astrophys. J.*, **358**, 685.  
Coles, W. A., Harmon, J. R. 1989, *Astrophys. J.*, **337**, 1023.  
Higdon, J. G. 1984, *Astrophys. J.*, **285**, 109.



## **Ionized Gas in the Inner Galaxy**

**K. R. Anantharamaiah** *Raman Research Institute, Bangalore 560 080, India*

**F. J. Lockman** *National Radio Astronomy Observatory, Green Bank, WV a 24944, USA*

**Nimisha G. Kantharia** *Raman Research Institute, Bangalore 560 080, and Joint Astronomy Program, Physics Dept., Indian Institute of Science, Bangalore 560 012, India*

**Anish D. Roshi** *Radio Astronomy Centre, Ooty 643001, India*

**Abstract.** We present 90 and 20 cm radio recombination line observations of six regions in the inner galactic plane which are devoid of any discrete continuum sources.

**Key words:** Galaxy: Recombination lines, galactic plane — HII regions.

### **1. Introduction**

It has been known for about 20 years now that radio recombination lines can be observed in the inner Galaxy even from regions where there are no discrete continuum sources. The origin of these lines has been a matter of debate. It is thought that these lines could be coming from old diffuse HII regions in the inner galaxy (Shaver 1976) which cannot be identified as discrete sources in the continuum surveys or from outer envelopes of known discrete HII regions (Lockman 1979; Anantharamaiah 1986).

Anantharamaiah (1985) had detected the H272 $\alpha$  (324.99 MHz) recombination line from six ‘blank’ regions which were chosen to be devoid of any discrete continuum sources within the Ooty radio telescope beam of 2° × 6′. Example of one such blank region is shown in Fig. 1a. We have now observed these six blank regions in the H168 $\alpha$  (1.37 GHz) line using the NRAO<sup>1</sup> 43 m telescope at Green Bank. Since the beam size of the 43 m telescope is about 21′, observations were made at several positions within the Ooty beam area and the profiles were averaged with appropriate weighting to simulate the Ooty beam for the H168 $\alpha$  observations. Three of the blank regions were similarly observed in the H128 $\alpha$  line (3.1 GHz). In four of the six blank regions there is good agreement in the velocity and width of the H272 $\alpha$  and H168 $\alpha$  lines (see Fig. 1b) suggesting that the two lines originate in the same gas. In the other two cases the higher frequency line has additional components.

### **2. Properties of the ionized gas in blank regions**

Using the theory of recombination line formation and taking into account possible departure from local thermodynamic equilibrium (LTE), we have constrained the

<sup>1</sup>NRAO is operated by Associated Univ. Inc. under a co-operative agreement with the NSF.

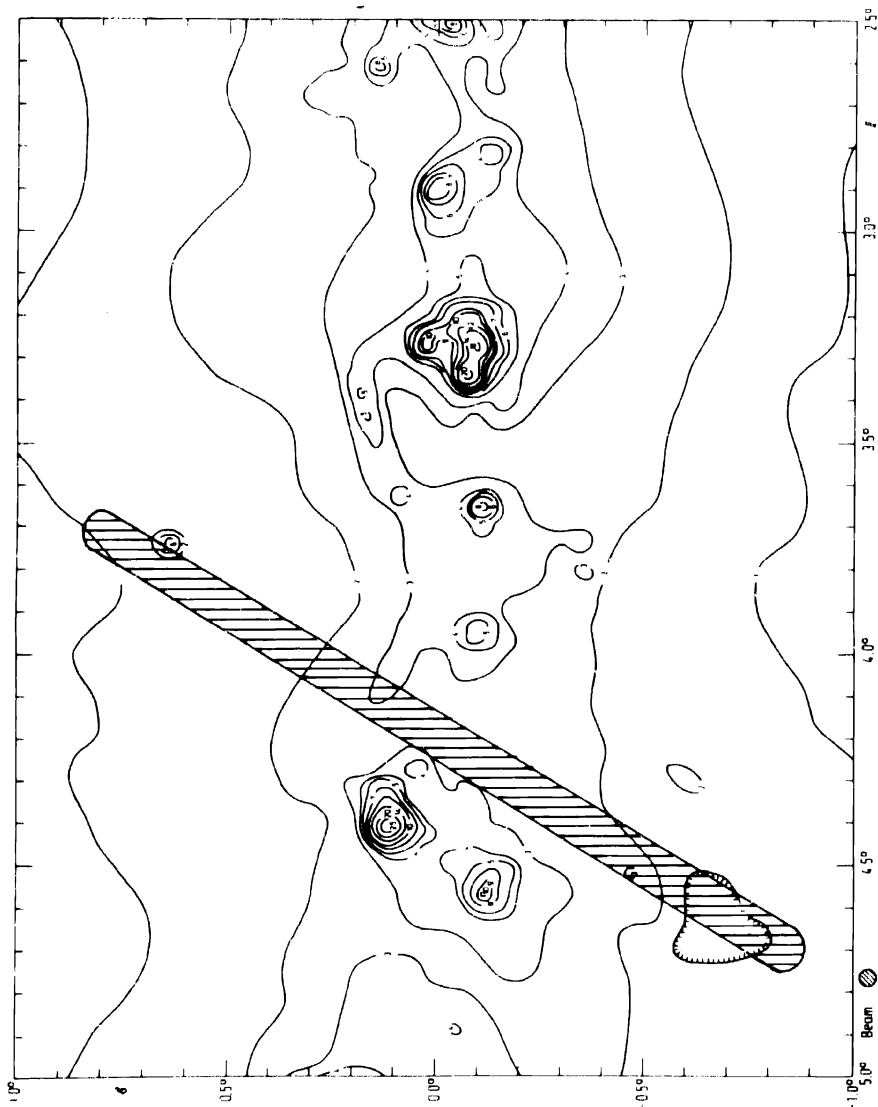


**Figure 1a.** A typical 'blank region' chosen from the 5 GHz continuum map of Altenhoff *et al.* (1978). The position of the Ooty telescope beam is shown by the hatched area.

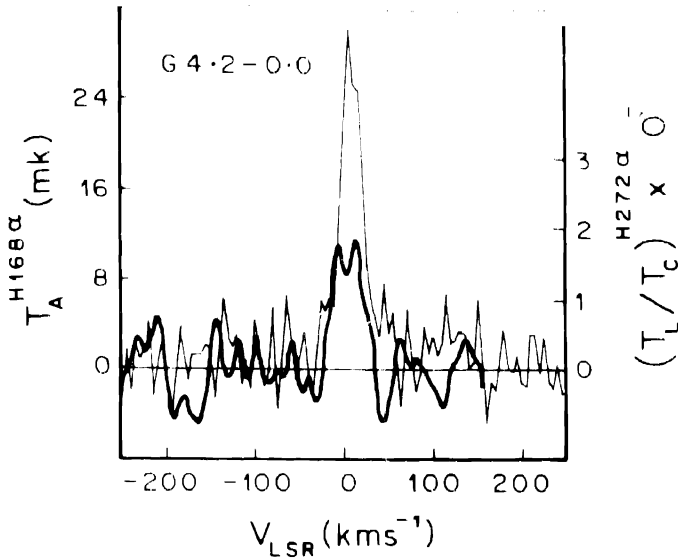


**Figure 1b.** H272 $\alpha$  (thick line) and H168 $\alpha$  (thin line) recombination lines observed from the blank region shown in (a).

electron density ( $n_e$ ), electron temperature ( $T_e$ ) and emission measure ( $n_e^2 l$ ) of the line emitting regions. Because of the very different dependence of H272 $\alpha$  and H168 $\alpha$  line intensities on electron density, the value of  $n_e$  is remarkably well constrained in all the cases irrespective of the values of  $l$  and  $T_e$ . On the other hand  $T_e$  and  $l$  are not well constrained although some handle is obtained for those cases where the H128 $\alpha$  line is also observed. In all the blank regions the electron density of the ionized gas is  $< 5 \text{ cm}^{-3}$ . If  $T_e = 5000 \text{ K}$ , then the pathlength through the gas is a few hundred parsecs except for G2.1-0.0 for which the pathlength could be several kilo parsecs. The emission measure of the gas is between a few 100 to a few 1000  $\text{pc cm}^{-6}$ .

We have also compared the radial velocity of the ionized gas observed towards the blank regions and a nearby HII region closest in velocity and seen in the 5 GHz continuum map. In three out of the 5 cases there is an HII region within  $4 \text{ km s}^{-1}$  of the central velocity observed in H272 $\alpha$ . But then, for all these three cases the derived pathlength is very large ( $> 0.5 \text{ kpc}$ ) and therefore the agreement may not suggest a physical association. We conclude, from the available evidence, that the ionized gas observed towards the blank regions is unlikely to be associated with any of the HII regions seen in the continuum surveys.

### References

- Altenhoff, W. J., Downes, D., Pauls, T., Schraml, J. 1978, *Astr. Astrophys. Suppl. Ser.*, **35**, 23.  
 Anantharamaiah, K. R. 1985, *J. Astrophys. Astr.*, **6**, 177.  
 Anantharamaiah, K. R. 1986, *J. Astrophys. Astr.*, **7**, 131.  
 Lockman, F. J. 1979, *Astrophys. J.*, **232**, 761.  
 Shaver, P. A. 1976, *Astr. Astrophys.*, **49**, 1.



## Radio Recombination Lines from External Galaxies

K. R. Anantharamaiah *Raman Research Institute, Bangalore 560 080, India.*

Jun-Hui Zhao *Harvard-Smithsonian Center for Astrophysics, Cambridge, MA 02138, USA*

W. M. Goss *National Radio Astronomy Observatory, Socorro, NM 87801, USA.*

F. Viallefond *DEMIRM, Observatoire de Paris-Meudon, 92195 Meudon Cedex, France.*

**Abstract.** Using the Very Large Array<sup>1</sup> and the Australia Telescope we have searched for the H92 $\alpha$  recombination line from 14 external galaxies and detected the line in 9 of them. All the detected galaxies have starburst nuclei and the line emission is only from the nuclear region. No line was detected in two well known Seyfert II galaxies that were searched to similar sensitivity levels.

**Key words:** Galaxies; starburst, Seyfert II — Radio recombination lines.

### 1. Introduction

For almost 14 years after the first detection of recombination lines (RRLs) from two external galaxies (M 82 and NGC 253) beyond the Magellanic clouds (Shaver, Churchwell & Rots 1977; Bell & Seaquist 1978), there were no further detections of RRLs in spite of several searches using large single dish telescopes. The next detection came in 1991 from the galaxy NGC 2146 (Puxley *et al.* 1991). Taking advantage of the high sensitivity (noise level  $\sim 100 \mu\text{Jy}$ ) and spectral dynamic range (better than 1:5000) achievable with modern synthesis telescopes such as the VLA and AT, we have begun a renewed search for RRLs from external galaxies.

### 2. Observations and results

Observations were made during October 1990 and again in February 1992 when the VLA was in the C configuration, which gives an angular resolution of  $\sim 2''.5$  at 8.4 GHz. More recently (July 1993) we observed a few southern galaxies using the AT compact array in its 750D configuration which gives a resolution of  $\sim 10''$ . The recombination line was detected at the level of 0.25–3.5 mJy from the nuclear region of 9 galaxies. The line widths are in the range 200–400  $\text{km s}^{-1}$  (FWHM). Line emission extends over a region of up to  $10''$  which corresponds to linear dimensions of a few hundred parsecs. The detected galaxies are NGC 3628, IC 694, NGC 3690, NGC 1365,

---

<sup>1</sup> VLA is a part of NRAO which is operated by Associated Univ. Inc., under a cooperative agreement with the NSF.



Arp 220, M 83, NGC 2146, NGC 4945, and the Circinus Galaxy. The strongest line is towards NGC 4945 and the weakest is from NGC 3690 (a companion of IC 694). The line was not detected in five other galaxies (NGC 262, NGC 1068, NGC 1808, NGC 6240 and NGC 3079) that were observed to a similar sensitivity level.

### 3. Nature of the ionized gas

The ionized gas that produces the observed H92 $\alpha$  line must satisfy an important constraint. In all the galaxies detected with the H92 $\alpha$  line, the radio continuum in the nuclear region has a non-thermal spectrum. The dominant non-thermal flux density in the nuclei implies that the thermal emission from the ionized region must only be a small fraction of the observed continuum flux density. This constraint rules out models with a uniform slab of ionized gas in front of the non-thermal source. However a collection of dense HII regions within the central few hundred parsecs of the galaxy can explain the observed lines. Such a model appears reasonable for a starburst nuclear region, where the HII regions could be created by the young stars born during one or more episodes of starburst and the non-thermal radiation originates in a large number of supernova remnants. Several hundred HII regions of a few parsecs in size and density of  $5-10 \times 10^3 \text{ cm}^{-3}$ , with a total mass of a few times  $10^5 M_{\odot}$  are required to account for the observed line flux density. The rate of production of Lyman continuum photons required to maintain the ionization is a few times  $10^{54} \text{ s}^{-1}$ . Much of the line emission comes from internal stimulated emission due to the continuum generated within the HII regions which account for 5–30% of the observed total continuum at 5 GHz. Results for three of the detected galaxies and model calculations are presented in Anantharamaiah et al. (1993).

### References

- Anantharamaiah, K. R., Zhao, J. H., Goss, W. M., Viallefond, F. 1993, *Astrophys. J.*, **419**, 585.  
Bell, M. B., Seaquist, E. R. 1978, *Astrophys. J.*, **223**, 378.  
Puxley, P. J., Brand, P. W. J. L., Moore, T. J. T., Mountain, C. M., Nakai, N. 1991, *Mon. Not. R. astr. Soc.*, **248**, 585.  
Shaver, P. A., Churchwell, E., Rots, A. H. 1977, *Astr. Astrophys.*, **55**, 435.

# The Interstellar Medium Surrounding the Vela Supernova Remnant

T. P. Saravanan<sup>1</sup>, A. A. Deshpande<sup>1,2</sup> & G. Srinivasan<sup>1</sup>

<sup>1</sup>*Raman Research Institute, Bangalore 560 080, India*

<sup>2</sup>*Department of Physics, University of Tasmania, Hobart, TAS Australia 7001*

**Key words:** Interstellar medium---supernova remnants.

The Vela SNR occupies a central place in the subject because of the association with the Vela pulsar. Whereas one would have expected the pulsar and its nebula (Vela X) to be near the centre of a shell, the morphology is quite complex as may be seen in Fig. 1. This has led to some controversy, and even association between the pulsar and the SNR has been questioned (Dwarakanath 1991). There may, however, be a simpler explanation for the peculiar morphology. For example, since the radio brightness of a supernova

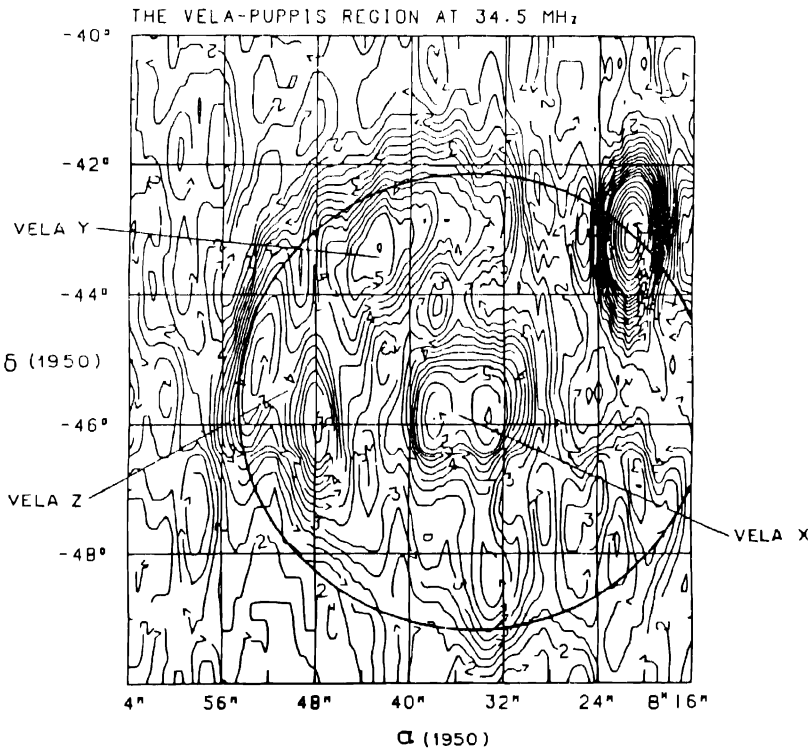


**Figure 1.** The 34.5 MHz continuum map of the Vela SNR. The contours are labelled in units of 10000 K. The bright feature in the right top corner is SNR Puppis-A and is unrelated to the Vela SNR.

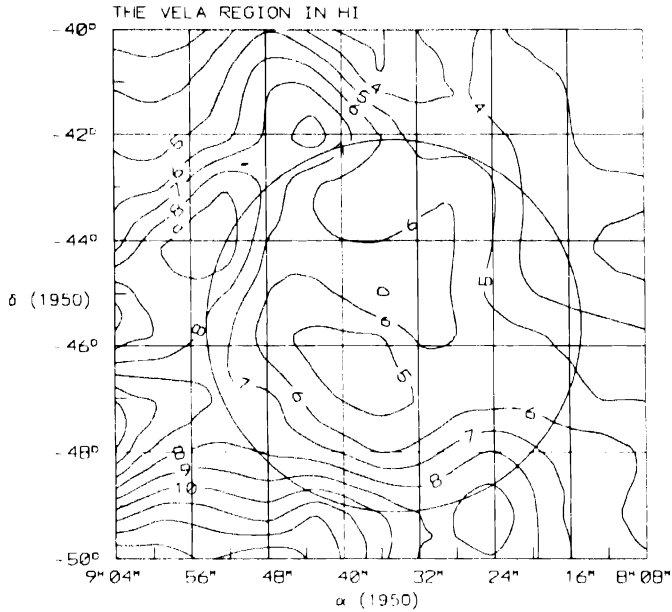


**Figure 2.** Distribution of Antenna temperature due to HI averaged over  $\sim 1$  to  $2$  km/s. This range of velocity would roughly correspond to a distance of 500 pc. The contours are labelled in units of 1 K.

remnant is related to the density of the ambient medium into which it is expanding, such an asymmetric morphology could be understood if the distribution of interstellar matter around the remnant is inhomogeneous. In order to clarify this, HI observations were made with the 26 m telescope at Mt. Pleasant Observatory, Hobart, Tasmania during July 1992. The observations were made with a bandwidth of 2.5 MHz and a 512 channel autocorrelator was used as the backend giving a velocity resolution of 1 km/s.

The HI map obtained by us is presented in Fig. 1. The distribution of HI is clearly highly inhomogeneous. The regions of higher density correlate well with the crowding of radio contours in the Vela Y, Z regions of 34.5 MHz continuum map (Fig. 2). Absence of any significant radio emission from the western half of the shell is also consistent with the lower density of HI in those directions.

Thus, our observations support the conjecture that the remnant is expanding in an inhomogeneous region of the interstellar medium resulting in an asymmetric radio surface brightness. In our opinion Vela Y and Z are parts of an incomplete shell of roughly  $7.5^\circ$  in diameter centered around the pulsar and its synchrotron nebula (Vela X) – a conclusion which is consistent with the recent ROSAT observations of this SNR (Aschenbach 1992).

### References

- Aschenbach, B. 1992, in *Highlights of Astronomy*, Ed. J. Bergeron, **9**, p. 223.  
 Dwarakanath, K. S. 1991, *J. Astrophys. Astr.*, **12**, 199.

## Bright-rimmed Molecular Clouds near Massive Stars

C. Indrani & T. K. Sridharan *Raman Research Institute, Bangalore 560 080, India*

**Abstract.** Massive stars have significant influence on the evolution of the interstellar medium. Bright rims, cometary morphology of clouds as well as their acceleration are some examples of the influence of massive stars on nearby molecular clouds. The cometary clouds in the Gum Nebula and the Rosette Nebula are very good examples. In an attempt to understand the kinematics of the clouds in such regions we have carried out CO line observations towards bright-rimmed clouds near the OB Associations Ori OB1 and Cep OB2. In the Cepheus region we find that the clouds are participating in systematic expansion from a common center whereas the motions in the Orion region appear more complicated.

**Key words:** Bright-rimmed clouds—OB associations.

### 1. Introduction

Bright-rimmed clouds are typically found in the vicinity of massive stars. They are patches of obscuration with bright rims on the side facing the stars and sometimes a tail like extension on the other side. Their peculiar morphology is believed to be caused by the effects of UV radiation and stellar winds from young stars and supernova shocks. Previous studies of such clouds in the Gum-Vela region have shown that they are expanding about a common central region containing the massive stars at  $\approx 12 \text{ km s}^{-1}$  (Sridharan 1992).

In order to find out if such motions are prevalent in other regions with massive stars, as well as to develop an evolutionary scenario, it is necessary to study regions with OB associations of different ages. As a step in this direction we studied bright-rimmed clouds near the OB associations Cep OB2 and Ori OB1 which are at distances of 450 pc and 800 pc respectively. Both these regions are younger than the Gum-Vela region. The preliminary results of this study are reported here and the complete study will appear elsewhere (Indrani & Sridharan 1993).

### 2. Observations and results

We observed about 40 clouds in the  $J = 1 \rightarrow 0$  transition of CO at 115.271 GHz using the 10.4 m millimeter-wave radio telescope at the Raman Research Institute during 1992–93. An acousto-optic spectrometer with a resolution of 50 kHz and coverage of 30 MHz was used giving a velocity resolution of  $0.12 \text{ km s}^{-1}$ . Line center velocities were obtained by fitting gaussians to the lines. The radial velocities of the clouds were thus obtained and analysed to detect any expansion.

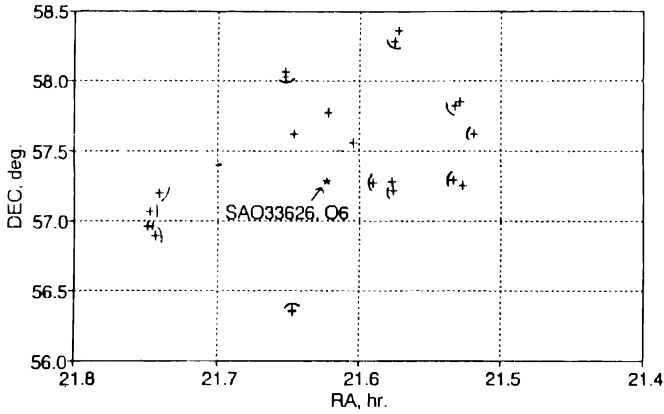


**Figure 1.** Distribution of the bright-rimmed clouds in Cep OB2 region. The arcs are the bright rims.

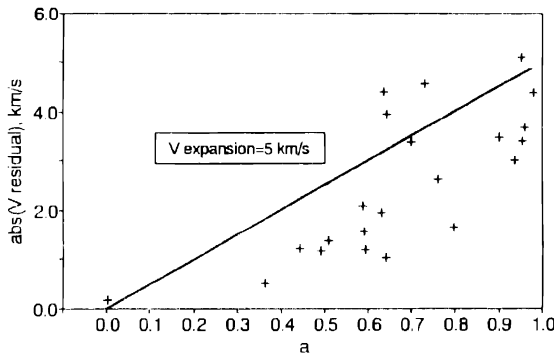


**Figure 2.** Absolute values of the residual velocities plotted against  $(1 - \sin^2 \theta / \sin^2 \theta_{\max})^{1/2} (\equiv a)$  for the region Cep OB2. The straight line shown represents a uniformly expanding shell.

For an expanding shell of bright-rimmed clouds the residual radial velocities after removing the contribution due to galactic rotation are given by the expression

$$|v_{\text{res}}| = v_{\text{exp}} (1 - \sin^2 \theta / \sin^2 \theta_{\max})^{1/2}, \quad (1)$$

where  $v_{\text{exp}}$  is the expansion velocity,  $\theta$  the angular distance of a cloud from the centre of the distribution and  $\theta_{\max}$  the maximum value of  $\theta$  (radius of the shell).

## 2.1 Cepheus OB2

Figure 1 shows the distribution of the clouds with bright rims marked. In Fig. 2 we have plotted  $|v_{\text{res}}|$  against  $\theta$ . The straight line (given by equation 1) represents a uniformly expanding shell. We used the position of the O6 star SAO33626 as the *centre* because this star dominates the association and most of the bright rims are oriented perpendicular

to the direction of this star. The data suggests an expansion velocity of  $\approx 5 \text{ km s}^{-1}$ . This gives an expansion age for the system of 4 Myr, making it younger than the Gum-Vela system, consistent with the age of the association and the smaller expansion velocity.

## 2.2 Orion OBI

The motions here are more complicated and do not fit a simple expansion picture. The association itself is large and contains many massive stars. The tail like extensions of the clouds do not point away from a common region. A more careful analysis taking into account the distribution of massive stars is needed before anything conclusive can be said.

## References

- Indrani, C., Sridharan, T. K. 1993, (in preparation).  
Sridharan, T. K. 1992, *J. Astrophys. Astr.*, **13**, 217.



## Star Formation in Giant Extragalactic HII Regions

Y. D. Mayya *Indian Institute of Astrophysics, Bangalore 560034, India*

**Abstract.** Star formation properties in Giant Extragalactic HII Regions (GEHRs) are investigated using the optical photometry and evolutionary population synthesis models. We find it necessary to have differential extinction between embedded cluster stars and the surrounding nebulosity in GEHRs, with about 50% of the cluster photons escaping the nebula unattenuated. GEHRs are found to contain hot massive stars and evolved red supergiants simultaneously, implying more than one event of star formation in the last 10 Myr. We have identified some regions on our images which may be examples of young and old regions spatially separated by 40–100 pc. Extended duration of star formation in GEHRs may be the result of a trigger from the earlier star formation event.

*Key words:* Galaxies: HII regions -- reddening -- star formation.

### 1. Introduction

GEHRs are the major sites of star formation in external galaxies. A star forming complex is characterised by an initial mass function (IMF) and its evolutionary status. Investigation of IMF and evolutionary status of GEHRs is done by indirect methods. From these studies, it is generally concluded that GEHRs are young systems containing stars mostly from a single generation with IMF slopes not very much different from Salpeter's value of 2.35 (Scalo 1986). The major sources of errors in modelling these regions in previous studies are (■) interstellar extinction correction, (■) usage of mass dependent quantities and (■) the uncertainties due to small slits often used in spectroscopic observations. With the imaging capabilities of the CCDs, the uncertainties inherent to slit spectroscopy can be eliminated and hence the IMF and evolutionary history of GEHRs can be established better. New prescription for extinction correction, usage of diagnostic diagrams involving dimensionless ratios and synthetic aperture photometry around HII regions on CCD images are some of the main improvements in the present study over the previous studies.

### 2. Data and method of analysis

CCD imaging observations carried out at the 1-m telescope at Vainu Bappu Observatory forms the main data base for the study. The photometric data on GEHRs in H $\alpha$  emission line and *BVR* continuum is obtained by synthetic aperture photometry on these images, and are catalogued in Mayya (1993). Thirty six of these regions having published spectroscopic data are used for the investigation of star formation in the present study. Metallicity, reddening and gaseous contribution within the broad *BVR* bands are estimated from the emission line ratios, from which pure cluster *B - V* and



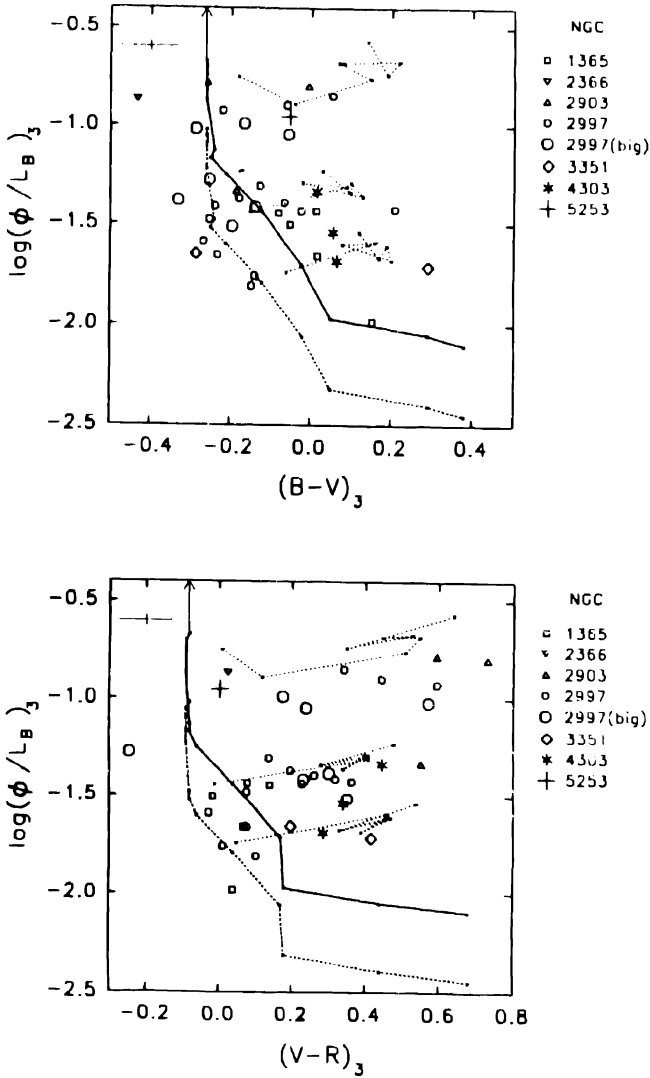


**Figure 1.** Extinction corrected regions in  $\log(\phi/L_B)$  vs  $B-V$  and  $V-R$  plane. Maximum rms errors on the observed quantities are shown by the cross at the top left corner. The evolution of a cluster with  $m_u = 60$  and  $\alpha = 2.5$  is shown by the thick line. The dots on the line are spaced 0.5 Myr apart with the dot at the bottom right being at 7 Myr. The dashed line is the model represented by thick line, with 55% of the ionizing photons escaping the nebula. A model with  $m_u = 120$  and no escape of Lyman photons begins at the tip of the arrow. Sequences with dotted lines correspond to composite models with the younger population at 0 (top), 3.5 (middle) and 5 (bottom) Myr superposed on an older population. The left-most point on these curves represents older populations at 5, 6, 6 Myr respectively. Further points are placed at increments of 1 Myr. Note that the observed regions imply the existence of two populations.

$V - R$  colours are derived. Quantity  $\frac{\phi}{L_B}$  defined as the ratio of  $H\beta$  to  $B$  band luminosity is computed from observed  $H\alpha$  and  $B$  band fluxes. This ratio resembles  $H\beta$  equivalent width, which is the ratio of  $H\beta$  flux to the underlying continuum flux. All the derived quantities are distance independent.

### 3. Discussion

Comparing observed quantities with population synthesis models (Mayya 1993) it is shown that dereddening  $B - V$  colours using Balmer decrement overcorrects the cluster colours, implying that cluster stars are not experiencing the same amount of extinction as the ionized gas. Obscuring dust closely associated with gas, which is distributed in filaments and clumps as in the case of 30 Doradus (Melnick 1992), is the most likely configuration in a majority of GEHRs. A fraction of stellar photons might escape the dust free regions between the clumps giving a net lower extinction towards stars. We estimate this fraction to be 50% for an IMF slope of 2.5. The stellar related quantities are dereddened taking this into account and are denoted by the suffix 3 in Fig. 1. The notable features on this figure are (■) Regions corresponding to a single burst young population are rare. (■) Single burst regions which are older than 3.5 Myr have their Lyman continuum flux reduced by 50%. (■)  $B - V$  and  $V - R$  colours have a large spread, with reddest regions having higher values of  $\frac{\phi}{L_B}$ . (■) An older burst of star formation of age 6–12 Myr superimposed on a younger population can explain most of the observed regions.

The absence of genuinely young regions in our sample and escape of Lyman continuum photons in moderately evolved regions might represent different stages during the evolution of GEHRs. In the young phase GEHRs are probably hidden deep inside molecular clouds. During its dynamical evolution the ionized volume may expand to a point where the ionization front bursts out providing escape routes for the ionizing photons following the 'champagne models' of Tenorio-Tagle (1979). The escaping photons may be responsible for ionization of the diffuse interstellar gas often found in sensitive imaging of disk galaxies (Dettmar 1992).

The young and old populations when separated by more than 40 pc could be identified in many star forming complexes directly on the CCD images of three of the programme galaxies. If the younger burst is due to a trigger from the older one the inferred speed of propagation of the trigger is  $4-10 \text{ km s}^{-1}$ , based on the measured separations. It may be noted that Hyland *et al.* (1992) have found direct evidence for the existence of two populations in 30 Doradus from infrared photometry, which supports our results. The observational finding of young and old populations in a majority of the regions studied here suggests that triggering of star formation may be a common phenomenon in GEHRs.

### References

- Dettmar, R.-J. 1992, *Fund. of Cosmic Phys.*, **15**, 143.  
 Hyland, A. R., Straw, S., Jones, T. J., Gatley, I. 1992, *Mon. Not. R. astr. Soc.*, **257**, 391.  
 Mayya, Y. D., 1993, *Ph. D. Thesis*, (submitted to Indian Institute of Science, Bangalore).

- Melnick, J., 1992, in *Star Formation in Stellar Systems*, eds. Tenorio-Tagle, G., Prieto, M., Sanchez, F., p. 314.
- Scalo, J. M., 1986, *Fund. of Cosmic Phys.* **11**, 1.
- Tenorio-Tagle, G. 1979, *Astr. Astrophys.*, **71**, 59.

## EGRET Observations of the Galactic Diffuse Gamma Ray Emission

P. Sreekumar<sup>1</sup> *NASA/Goddard Space Flight Center, Code 662, Greenbelt, MD 20771, USA  
(on behalf of the EGRET team).*

**Abstract.** The phase I all-sky survey in high energy gamma rays ( $E \geq 30$  MeV) carried out by EGRET aboard the Compton Observatory clearly shows the presence of diffuse gamma ray emission from the Galactic plane. This emission is generally believed to result from the interaction of cosmic rays with the interstellar medium and the interstellar radiation field. Since the interstellar medium is well observed via 21-cm line and CO observations, diffuse gamma ray observations can be used as a powerful tool to examine the nature and distribution of cosmic rays in the Galaxy. The observations can be compared with a calculation of the expected diffuse emission model from the Galaxy.

**Key words:** Gamma rays: observations: milky way- diffuse emission: cosmic rays.

### 1. Introduction

The most intense source of high energy gamma rays in our Galaxy arises from the plane of the Milky Way. This was observed in the past by the SAS-2 satellite and later studied in greater detail by the COS-B satellite. Efforts to explain the origin of the diffuse galactic emission generally assumed that these gamma rays arise from cosmic ray interactions with the interstellar gas and radiation. An important goal of this study is to use gamma ray observations to improve our understanding of the nature and distribution of cosmic rays in the Galaxy. In addition to information on cosmic rays, diffuse gamma ray observations can also provide an upper limit on the CO to H<sub>2</sub> normalization factor (X-factor). Prior to the launch of the Compton Observatory, the modeling of the COS-B data was carried out using a multiparameter fit to the observed emission, showed indications of variation of cosmic ray density with galactocentric radius as well as an upper limit of  $2.3 \times 10^{20}$  Kkms<sup>-1</sup> for the X-factor (Strong *et al.* 1988).

With the launch of EGRET aboard the Compton Observatory on April 1991, we have in orbit a high energy telescope (30 MeV to 30 GeV) with a significantly improved angular resolution, a factor of 10 or more increase in effective area over COS-B and extremely low background. Details of the instrument, its characteristics and pre- and post-flight calibration details are available in Thompson *et al.* (1993). EGRET has carried out the first all sky survey in high energy gamma rays from April 1991 to Nov 1992 (phase I). Preliminary results based on the phase I observations of the galactic diffuse emission are reported in this paper. Point sources were analyzed using a maximum likelihood analysis to determine counts and intensity. This analysis used a galac-

<sup>1</sup>Universities Space Research Association.

tic emission model of Bertsch *et al.* (1993). Point source contributions were subtracted from the observed total emission, to examine the spatial distribution and spectrum of diffuse emission from the Galactic plane.

## - 2. Discussion

The observed diffuse gamma ray emission from the plane can be compared with the model calculations of Bertsch *et al.* (1993). Fig. 1a shows the longitude dependence of the observed intensity averaged over  $\pm 10^\circ$  in latitude. The solid line represents the model of Bertsch *et al.* (1993) together with an isotropic extragalactic component of

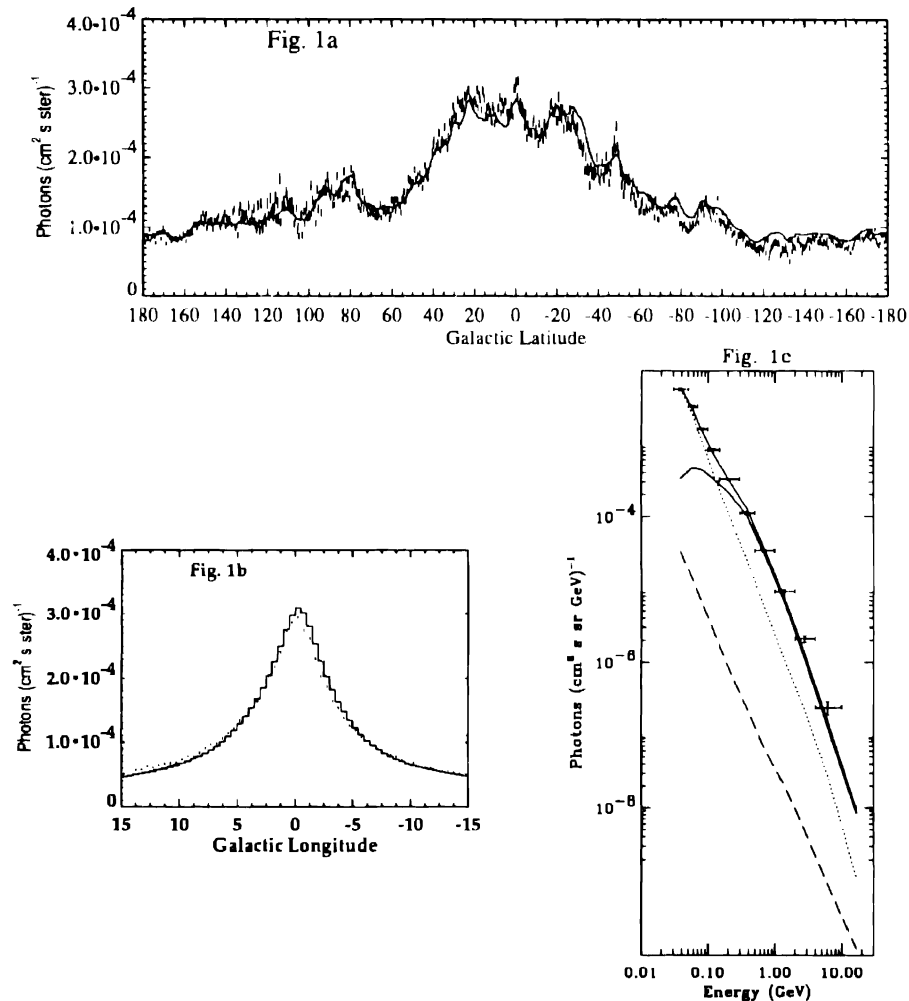


**Figure 1.** EGRET observations of the Galactic diffuse emission, showing longitude profile (figure 1a); latitude profile (figure 1b) and differential spectrum (figure 1c).

$1 \times 10^{-5}$  photons  $\text{cm}^{-2} \text{s}^{-1} \text{ster}^{-1}$  (Thompson & Fichtel 1982). It is remarkable that the model reproduces many of the spatial features at various longitudes, considering the model has only two adjustable parameters and does not force fit the observations rigorously. The assumption by Bertsch *et al.* (1993) that cosmic rays are closely tied to the interstellar gas distribution appears to have a strong basis as seen from figure 1a. The latitude distribution averaged over the whole plane, is shown in figure 1b and shows good consistency with the model predictions. The model requires an X-factor (one of the adjustable parameters of the model) of  $2.0 \times 10^{20}$  Kkms $^{-1}$  or less to be consistent with the EGRET observations. The likelihood analysis indicates that only 12% of the total observed diffuse emission from the Milky Way arise from point sources. There may still be unresolved point sources below the detection threshold of EGRET, but this is not expected to be substantial. The spectrum from the region near the Galactic center is shown in figure 1c. It shows for the first time the predicted feature from gamma rays arising from  $\pi^0$  decay. This is an important signature of cosmic ray protons in the Galaxy. Additional results on the diffuse emission from the Galactic plane will be available in Hunter *et al.* (1994).

### References

- Bertsch, D. L., Dame, T. M., Fichtel, C. E., Hunter, S. D., Sreekumar, P., Stacy, J. G., Thaddeus, P. 1993, *Astrophys. J.*, **416**, 587.  
 Hunter *et al.* 1994 (in preparation).  
 Strong, A. *et al.* 1988., *Astr. Astrophys.*, **207**, 1.  
 Thompson, D. J., Fichtel, C. E. 1982, *Astr. Astrophys.*, **109**, 352.  
 Thompson, D. J. *et al.* 1993, *Astrophys. J. Suppl. Ser.*, **86**, 629.



## Short Time Scale Variability in the Solar Wind

Pradeep Gothoskar & A. Pramesh Rao *National Centre for Radio Astrophysics  
TIFR, Poona University Campus, Pune 411 007, India*

**Abstract.** Existing observations of Interplanetary Medium (IPM) over short time scales are incomplete due to lack of steerable telescopes dedicated for such observations. Consequently, understanding of fast interplanetary disturbances and their association to the solar and geomagnetic activity has been inadequate (Neugebauer 1987). A programme of Interplanetary Scintillation (IPS) observations was, thus, initiated using the Ooty Radio Telescope (ORT), where a few strong scintillating sources were monitored over a period of one year. These observations show significant interplanetary activity over a time scale of few minutes to hours. The disturbances observed during the monitoring programme can be understood with a simple model for interplanetary scattering produced by dense plasma objects moving at high velocities. This model was used to associate the events with their origin on the Sun and subsequent geomagnetic activity produced at Earth.

**Key words:** Solar wind — solar terrestrial physics.

### 1. Observations and Model

During 1990 May to 1991 March, 6 strong scintillating sources were monitored over a wide range of elongations ( $20^\circ$ – $60^\circ$  from the Sun) and heliographic latitudes. Each source was observed for about 9 hours to obtain scintillation data. For each day, IPS power spectra were obtained with time resolution of 1–10 minutes. Total, 33 interplanetary events were detected during the programme, which were classified into slow, medium and fast events based on their morphology. For each event an estimate of Solar Wind velocity (Manoharan 1990) and scintillation index (a measure of strength of scattering and plasma density) was obtained. Two examples of the fast IPS events, observed on 31 July and 25 August 1990, are shown in Fig. 1 and Fig. 2. Both events show a remarkable increase in velocity and index in just few minutes. The event is preceded by extended precursor activity and is followed by complex post shock activity.

In order to understand these transient events, we considered IPM composed of two components namely, normal and event component. While normal component was the steady state solar wind with empirically observed properties, the event component was considered to be a dense cloud of plasma ejected radially from the Sun at high velocities. Each plasma cloud was characterized by a few parameters, such as, ejection angle  $\theta$ , opening angle  $\phi$ , density  $\rho$  and velocity  $V$  with a bow shock in front at stand off distance  $d_{\text{bow}}$ . Movement of the plasma cloud across the line of sight was used to compute the time series of scintillation index and velocity. By varying these parameters,



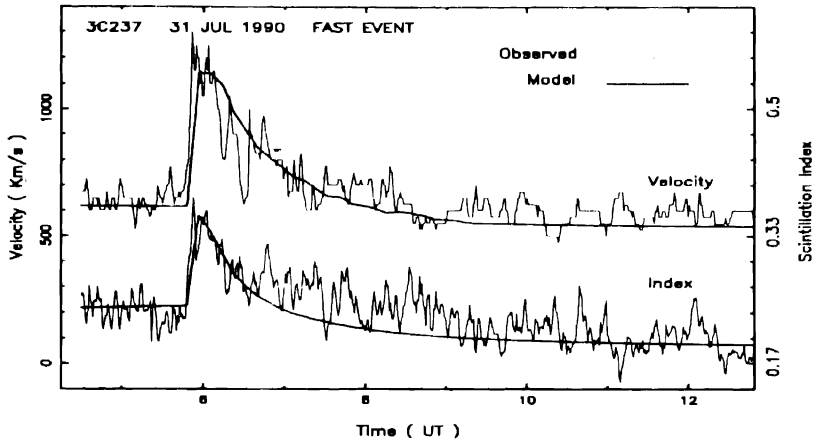


**Figure 1.** Interplanetary disturbance of 31 July 1990 was due to coronal mass ejection at 45° to the Sun-Earth line on 30 July. Extended bow shock of the event, seen here as precursor, produced sudden ionospheric commencement on 1 August.

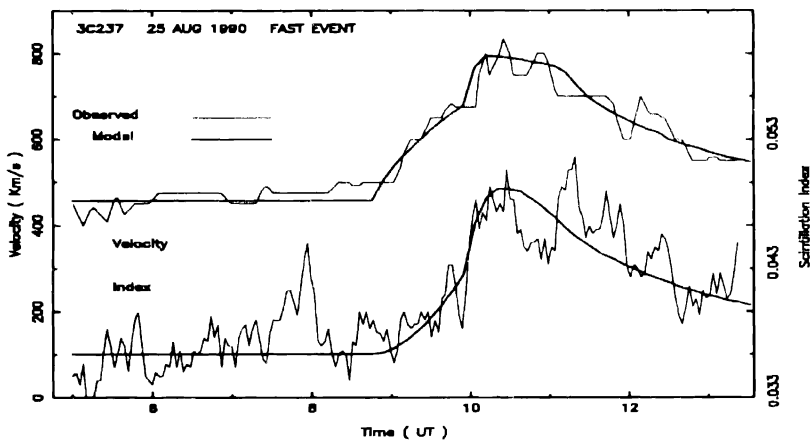


**Figure 2.** Wide spread solar flare activity on 24 August 1990 directed towards Earth produced the event of 25 August. A major geomagnetic disturbance was observed on 26 August associated with the event.

the model time series was made to reproduce the features in the observed time series. These parameters yielded a better estimate of the velocity, density and directionality of the disturbance.

## 2. Results

The model time series, for the two examples presented here, is shown in Figs. 1 and 2 (bold lines) which is superposed on the observed series of index and velocity (thin

lines). Parameters derived from these two models were, further, used to associate these events with the solar and geomagnetic activity. Event of 31 July 1990 was related to the Coronal Mass Ejection (CME) on 30 July and produced geomagnetic activity on the Earth on 1 August. The event on 25 August 1990 was due to wide spread flare activity on 24 August and was associated with the ionospheric disturbances on August 26. We have demonstrated that continuous IPS observations with high time resolution can be used to study short time scale activity in IPM. Such a data along with a simple model for mass ejection can be effectively used to associate interplanetary events with their solar origin and resulting geomagnetic disturbances.

### **References**

- Manoharan, P. K., Ananthakrishnan, S. 1990, *Mon. Not. R. astr. Soc.*, **244**, 691.  
Neugebauer, M. 1987, *Conf. Proc. Solar Wind VI*, **1**, 243.



## Abstracts

### **Recombination Line Observations of the Galactic Centre Region near 325 MHz**

Anish Roshi & T. Velusamy *Radio Astronomy Centre, Tata Institute of Fundamental Research, Udhagamandalam 643 001, India*

K. R. Anantharamaiah *Raman Research Institute, Bangalore 560 080, India*

Recombination lines (RLs) at frequencies  $< 1$  GHz are sensitive to large regions of low density ( $n_e < 50 \text{ cm}^{-3}$ ) ionized gas. Evidence for widespread presence of such gas in the inner Galaxy has come from observations of RLs at 325 MHz from selected positions in the Galactic plane (Anantharamaiah 1985) using the Ooty Radio Telescope and also RLs near 1420 MHz observed using the Green Bank and Jodrell Bank telescopes (Lockman 1976; Hart & Pedlar 1976). Taking advantage of the improved sensitivity of the Ooty radio telescope (by a factor of  $\sim 4$ ), we are preparing for a large scale survey of RLs near 325 MHz from the Galactic plane. A spectrometer which can simultaneously observe four RL transitions in two adjacent positions is under construction. A prototype of this spectrometer is currently being used for observing a single transition within the Ooty band. We present here the results of the first observations which cover a  $1 \text{ deg} \times 2 \text{ deg}$  field around the Galactic centre.

★★★★★

### **Structure in Interstellar HI in the Directions of PSR 1557–50 and PSR 1641–45**

A. A. Deshpande *Raman Research Institute, Bangalore 560 080, India.*

W. E. Wilson, E. R. Davis & D. McConnell *Australia Telescope National Facility, Narrabri NSW 2390, Australia.*

P. M. McCulloch *University of Tasmania, Physics Department, Tasmania 7001, Australia.*

A technique to investigate the spectrum of scale sizes of intervening HI using pulsars as probes has been proposed recently (Deshpande *et al.* 1992, *Mon. Not. R. astr. Soc.*, **258**, 19p). A comparison between the measurements of HI absorption spectra in the direction of PSR 1557–50 at two different epochs has indicated that structure in the HI clouds may have much smaller scale sizes than believed earlier. We reexamine the case of PSR 1557–50 in the light of our recent 21-cm measurements from the Parkes

telescope. We also examine our data in the direction of PSR 1641-45 for changes in the HI absorption spectrum and discuss the results.

★★★★★

## Non Equilibrium Ionization and Elemental Abundances in Two Supernova Remnants

K. P. Singh *Tata Institute of Fundamental Research, Bombay 400 005, India*

John P. Hughes *Harvard-Smithsonian Center for Astrophysics, Cambridge, MA 02138*

We have carried out nonequilibrium ionization (NEI) analysis of X-ray spectral data from the Einstein Observatory and EXOSAT for a number of supernova remnants (SNRs). We present results from this analysis for two SNRs viz. G292.0 + 1.8 and W44. The spectra are well described by a single temperature and single-timescale NEI model for both the SNRs. The values for the temperature and ionization time scale are  $kT = 1.71^{+0.26}_{-0.22}$  keV and  $n_e t = 4.7^{+1.1}_{-0.85} \times 10^{10} \text{ cm}^{-3} \text{ s}$  for G292.0 + 1.8, and  $1.5 \pm 0.5$  keV and  $6.3^{+4.0}_{-2.0} \times 10^{10} \text{ cm}^{-3} \text{ s}$  respectively for W44. In addition, the abundances of the elements O, Ne, Mg, Si, S, Ar and Fe are determined.

For G292.0 + 1.8, numerical calculations of the nucleosynthesis expected for  $25 M_\odot$  progenitor agree best with the derived abundances. From the fitted emission measure and a simple geometric model of the remnant the mass of X-ray emitting plasma is estimated to be  $7.3^{+10.1}_{-5.4} M_\odot$ , for an assumed distance of  $3.6 \pm 1.5$  kpc. Clumping of the ejecta may, however lead to substantial errors on this estimate. G292.0 + 1.8 resembles the remnant Cas A (another product of a massive star supernova).

In the case of W44, the elemental abundances are consistent with a mixture of material having cosmic composition and ejecta from a 20 or  $25 M_\odot$  progenitor in the ratio of  $\simeq 4$  to 1. From a geometric model and the fitted emission measure we estimate the plasma density to be  $0.145 \text{ cm}^{-3}$ . Using the fitted  $n_e t$  value we obtain an 'age' of 14,000 yrs, which agrees with the pulsar characteristic age of  $\sim 20,000$  yrs.

★★★★★

## Instability of Gravitating Grainy Plasma

Bhavneet Kaur & G. L. Kalra *University of Delhi, New Delhi 110 063, India*

The instability of plasma in the presence of another minor component, variously referred to as grains, dust or suspended particles, which interacts with the plasma through collisions is of interest in the laboratory as well as geo- and astrophysical situations. The instability of compressible, gravitating, hydrodynamic fluid in the presence of interstellar grains was first investigated by Kalra & Talwar (1967).

Subsequently several authors carried out similar studies by including viscous effects of the compressible gravitating hydrodynamical fluid or plasma threaded by magnetic field. The present paper points out errors in the viscous term used by the earlier authors and employs correct equations to derive the dispersion relation. The discussion of the dispersion relation shows that the classical wavelength at which Jeans' instability sets in remains unaltered.

★★★★★

### **The Neutral Hydrogen Subsystem in the Milky Way: The Movements and the Structure**

I. V. Petrovskaya *St. Petersburg State University, 198904 St. Petersburg, Russia.*

The interpretation of 21-cm line profile gives the possibility to find the velocity field and density distribution of neutral hydrogen subsystem in our Galaxy. To obtain the rotation curve we use not only the tangential point but the whole 21-cm profile. We correct the confusion of outer rotation curve as a result of the warp of hydrogen layer. The structure of inner regions was investigated simultaneously with the rotation. We found the ring structure for  $0.4 < R/R_0 < 0.66$  and 4-arm spiral for  $0.66 < R/R_0 < 1$  ( $R_0$  – the distance of the Sun from the Galactic centre). The requirement of the best fitting of HI and HII rotation velocities gives  $R_0 = 7.5$  kpc.

★★★★★

### **The Effect of Time Dependent Tidal Forces on Molecular Clouds**

Mousumi Das & Chanda J. Jog *Department of Physics, Indian Institute of Science, Bangalore 560 012*

We present a study of the effect of the time varying tidal field on a molecular cloud. When a molecular cloud moves in epicyclic motion in the galactic disk potential, the tidal field across the cloud changes with time. The magnitude of the variation depends on the amplitude of the radial and vertical oscillations. Since a molecular cloud has internal dissipation, there will be a net exchange of energy between the cloud and the disk gravitational field. We have tried to determine the effect of this time dependent tidal field on cloud collapse and hence see whether it can act as a source of energy for a cloud.

A molecular cloud is taken to be a bound system of equal mass clumps moving in a tenuous interclump medium. The cloud mass is  $\sim 10^5 M_\odot$  and radius 50 pc (Falgarone & Puget 1986, *Astr. Astrophys.*, **162**, 235). An  $n$  body method was used to evolve the motion of the clumps within a cloud moving in the Galactic potential (Carlberg &

Innanen 1987, *Astrophys. J.*, **94**, 666). To take into account the internal dissipation, the equation of motion included a damping term proportional to the clump random velocity.

We find that the time dependent tidal field does not significantly delay the collapse of a cloud; both for the disk and nuclear region. Hence we conclude that the tidal field cannot support the internal motions of a molecular cloud.

★★★★★

## **Dynamics of Clumps in Molecular Clouds**

U. Gorti & H. C. Bhatt *Indian Institute of Astrophysics, Bangalore 560034, India.*

I. P. Williams *Queen Mary and Westfield College, London, England.*

The motion of clumps in a molecular cloud through the ambient inter-clump medium has been numerically analysed. The forces acting on an individual clump considered are the gravitational force due to the cloud, a drag force due to dynamical friction on the clumps by the gas, alongwith an increase in mass of the clump because of accretion. The clumps are initially given random positions and randomly oriented virial velocities. About a hundred clumps with masses according to a power law mass spectrum of index 1.5 are integrated over times typically of the order of a cloud lifetime. The dynamical drag acting on a particle is dependent on its mass, and thus clumps of different masses have in general different retardations. The most massive particles suffer the maximum decelerating effects and settle to the center in a shorter time than the lower mass clumps. Thus there is a clustering of the clumps towards the center, and a radial segregation of mass is established in the cloud. The timescale of the process is governed by the cloud parameters, and is shorter for denser and cooler clouds. Molecular clouds are thus expected to have the most massive clumps at the center. Such a structure is also expected for the highly dense cores from which stars form. If each of the cores forms a single star, then this cloud explains the mass segregation observed in many young clusters of pre-main sequence stars and YSOs.

★★★★★

## **Cosmic Rays and Interstellar Medium**

Sukumar Biswas *Tata Institute of Fundamental Research, Bombay 400005, India.*

Recent results on low energy cosmic rays obtained from spacecrafts in the interplanetary medium such as Voyager 1,2, Pioneer 10 and 11 and inside the magnetosphere e.g. Spacelab-3 have provided information on the following two new aspects of the interstellar medium: (1) The anomalous cosmic rays (ACR) were identified as being in singly ionized state in the Spacelab-3 Anuradha experiment and hence it is concluded that these originate from interstellar neutrals drifted into the heliosphere as in Fisk model. Thus the data on

the abundances of major components of ACR such as He, N, O, Ne have been used to derive the abundances of neutral atoms in the local ISM with calculated fractionations due to ionization and acceleration processes. (2) The Spacelab-3 Anuradha showed that a fraction of about 20% of low energy galactic cosmic rays are in partially ionized states at  $\sim 100$  MeV/N. These indicate that in ISM reacceleration has taken the place of the GCR heavy ions which captured electrons at  $1-10$  MeV/N energies. The implications are discussed.

★★★★★

## **Interplanetary Scintillation Measurements and Deformation of Heliospheric Current Sheet**

**B. Bala & S. R. Prabhakaran Nayar** *University of Kerala, Trivandrum 695 581, India*

The interplanetary medium is filled with solar coronal plasma and magnetic field driven from the Sun by the solar wind. The solar wind velocity distribution in the interplanetary medium is best represented in two dimensions in a v-map in the heliographic latitude and longitude. In this study, we have constructed v-maps on the source surface for the Carrington rotations 1787 to 1795 during 1987, using the interplanetary scintillation measurements. These v-maps are used to study the time evolution of low speed region in the heliosphere and to deduce the distribution of solar wind velocity on the heliospheric current sheet for these rotations. We found that the evolution of low speed belt is similar to that of neutral line and the velocity varied in the range  $300$  to  $580 \text{ km s}^{-1}$ , during the period of study. This velocity distribution on the current sheet has been found to distort the shape of the current sheet as it travels outward from the Sun. The magnitude of deformation increases with (1) the magnitude of gradient on the HCS and (2) the distance from the Sun.

★★★★★

## **Effects of Two Types of High Speed Solar Wind Stream on Cosmic Ray Intensity and on Geomagnetic Disturbances**

**Pankaj K. Shrivastava & R. P. Shukla** *New Science College, Rewa 486 001, India*

It is known that the High Solar Wind Streams (HSWS) originate from coronal holes or during solar flares. These two types of high solar wind streams have been separated with respect to their origin into two categories (Mavromichalaki *et al.* 1988). Their effects on cosmic ray intensity as well as on geomagnetic disturbances have been studied using the three method of superposed epoch. The high counting rate Deep River neutron monitor data have been used to observe the cosmic ray intensity variation during the declining phase of solar cycle 21. It is found that the flare generated streams are more effective to produce cosmic ray decreases and enhancement in geomagnetic activity.

★★★★★



## **A 327 MHz Interplanetary Scintillation Survey of Radio Sources over 6 Steradian**

**V. Balasubramanian & P. Janardhan** *Radio Astronomy Centre, Tata Institute of Fundamental Research, Udhagamandalam 643 001, India.*

**S. Ananthakrishnan** *National Centre for Radio Astrophysics, Tata Institute of Fundamental Research, Pune 411 007, India.*

A systematic interplanetary scintillation (IPS) survey has been initiated to detect compact components in all radio sources above 1.5 Jy at 327 MHz in the declination range  $-40^\circ < \delta < 40^\circ$  and 0 to 24 h in right ascension. However, at 327 MHz, the IPS method is useful only for solar elongation  $\epsilon$  in the range  $15^\circ$  to  $55^\circ$ , and hence the area covered is  $\approx 6$  steradian of the sky. The radio sources were selected from the Texas and Molongolo Catalogues.

The major objectives of the above survey of about 5000 radio sources are as follows:

- To rapidly produce a finding list of compact sub-arc second sources ( $< 100$  mas) for the space VLBI mission 'Radio astron' due for launch in 1996.
- To obtain a spatially well distributed list of scintillating sources around the ecliptic plane for mapping 'interplanetary weather'.
- To have a statistically viable sample for studying compact components in extra-galactic radio sources.

3500 sources have been observed from August 1992 to May 1993 and the survey is expected to be completed by October 1993. Of these, about 40% have compact scintillating components. A preliminary analysis shows that weak, medium and strongly scintillating sources constitute approximately 60, 25 and 15% of this sub sample. The majority of strongly scintillation radio sources have significant flux density ( $> 250$  mJy) in compact structures  $\leq 150$  mas at 327 MHz.

During the course of the survey, there were about 6 to 8 instances of enhanced scintillations on particular days; that is, the scintillation indices of some sources are much higher than expected. These enhancements were characterized by rapid onset and slow decay with time. A few of the cases were traceable to energetic events on the Sun.

★★★★★

## **Estimation of Solar Coronal Plasma Density by IPS Observations**

**Hari Om Vats & M. R. Deshpande** *Physical Research Laboratory, Ahmedabad 380 009, India*

Observations of several compact radio sources have been made since 1984 by an IPS telescope operating at 103 MHz. From these observations standard  $m$  vs  $\epsilon$  curves have been obtained. The data is used to calculate  $q$  values ( $m_{\text{date}}/\langle m \rangle$ ) which is the ratio of

the rms value of the observed scintillation to the expected average value of the scintillation at the same solar elongation angle  $\epsilon$ . The  $g$  value is empirically found to be related to the plasma density in the interplanetary medium. This empirical relation has been used to estimate plasma density in the interplanetary medium. Thus we obtain the plasma density at the point of closest approach for all the observations. These plasma densities are projected back to solar corona and also modified appropriately by inverse square of the distance away from the Sun. The results are presented and discussed.

★★★★★

### **The Geminga Supernova and the High and Intermediate Velocity Neutral Hydrogen Concentrations**

V. R. Venugopal *Inter University Centre for Astronomy and Astrophysics, Pune 411 007, India*

Recently Gehrels & Chen (1993, *Nature*, **361**, 706) have proposed that the hot cavity, the Local Bubble, was caused by the Geminga supernova. They have computed the galactic latitude of the supernova to be  $-11.7^\circ$  and they also find that the cavity has a large scale high-density boundary with the Perseus OB associations at galactic longitude  $145^\circ$ . This direction,  $145^\circ, -11.7^\circ$ , is close to the direction of the solar motion derived by Venugopal (1970, *Nature*, **228**, 44) for high and intermediate neutral hydrogen condensations (HVC and IVC) of the Berkeley Radio Astronomy Laboratory Survey (Dieter 1969, *Publ. astr. Soc. Pacific*, **81**, 186). In view of the agreement between these directions it is suggested that these condensations are caused by the Geminga supernova.

★★★★★

### **Infrared Emission from HII Regions: An Analysis of IRAS Data**

D. B. Vaidya & B. G. Anandarao *Physical Research Laboratory and Gujarat College, Ahmedabad, India.*

Infrared Astronomical Satellite (IRAS) survey includes a large number of galactic HII regions observed in both photometry and spectroscopy. From the IRAS-low resolution spectra (LRS) on HII regions we have selected about 10 sources with no discernable emission or absorption features but with only continuum in the range  $8-22\ \mu\text{m}$ . Using a radiative model (Anandarao *et al.* 1987, *Astr. Astrophys.*, **203**, 361) and assuming that a single O-B star is embedded in the HII region, we have determined dust parameters: temperature, optical depth, shell size and masses (given in Table 1). The absorption efficiencies of dust grains required in these computations were obtained using the optical constants given by Draine (1987, Princeton Observatory Preprint No. 213). We found that rather large grains ( $0.5-1.0\ \mu\text{m}$ ) are required to fit the observed

**Table 1.** Dust parameters in the HII regions selected.

Source	Dust temp.(K)	Extent(ster)	Optical depth	Dust mass ( $M_{\odot}$ )
AFGL 5182	122	2.2e-08	1.1e-03	4.1e-05
AFGL 890	114	3.5e-08	2.7e-03	1.5e-04
AFGL 961	138	1.7e-08	1.8e-03	5.0e-05
G294.5-01.6	128	1.5e-08	2.9e-04	2.4e-06
S40	150	8.0e-09	1.1e-03	1.4e-05
AFGL 2211	151	3.8e-09	4.9e-03	3.1e-05
AFGL 2492	138	2.7e-08	1.1e-03	5.0e-05
AFGL 2591	149	1.2e-07	1.0e-04	5.1e-04
S138	130	1.0e-08	1.7e-03	2.9e-05
S162	134	1.9e-08	2.7e-03	8.4e-05

data. Anomalous extinction ( $R = E(\lambda - V)/E(B - V) \sim 5.2$ ) found towards some HII regions (Cardelli *et al.* 1988, *Astrophys. J.*, **95**, 516) supports the presence of such larger grains. Earlier we have shown models (Vaidya & Anandarao 1993, *BASI*, in press) with core-mantle particles to fit the observed anomalous extinction towards the Orion region. Further work on these lines is in progress.

★ ★ ★ ★ ★

# **Stars and Stellar Physics**



## Mass Loss from Wolf-Rayet Stars

**Bambang Hidayat** *Department of Astronomy I.T.B. and Bosscha Observatory, I.T.B.,  
Lembang, Java, Indonesia.*

**Abstract.** The phenomenon of mass loss from Wolf-Rayet stars is briefly reviewed, with particular emphasis on its influence of Wolf-Rayet evolution and the role played by these stars in galactic chemical evolution.

**Key words.** Mass loss—Wolf-Rayet stars—chemical evolution.

### 1. Introduction

As early as in 1929, Beals (1929) argued that stars are losing matter in a more or less spherically symmetric way – now called stellar wind. But it was Adams & McCormack (1935) who showed observational evidence of matter flows from stars. The blueshifted components of low excitation lines of some metals, of some red giants spectra, were interpreted as the indication of material flow. P-Cygni line profiles were then used as the basis of measuring mass-loss rates.

It has been generally accepted now that most of the stars are losing matter. Analytical expressions relating the mass-loss rate and the basic stellar parameters are formally expressed as

$$\dot{M} = f(L, T_{\text{eff}}); \quad \text{or} \quad \dot{M} = (R, T_{\text{eff}}).$$

Theoretically derived prediction has been given by Abbott (1982) who used a radiation-driven model for early type stars. This, already, gave the basic relationship between the mass-loss rate and terminal velocity,  $V_{\infty}$ , and showed that almost all massive OB-stars suffer from mass-loss.

Like OB-stars, WR spectra show intense stellar wind. The rate at which WR-stars are losing mass was estimated of the order of  $10^{-5}$ – $10^{-4} m_{\odot}/\text{yr}$ . In recent years (see review by van der Hucht 1992), improvement in the formulation of mass-loss rate have accommodated considerations related to:

1. High carbon abundance, and a low ionization.
2. An outward decreasing degree of ionization.
3. Improved distances of WR-stars.

The above mentioned considerations, naturally, do not act independently nor produce the same effect.

Prinja *et al.* (1990) and Willis (1991) estimated respectively  $2$ – $10 \times 10^{-5} m_{\odot}/\text{yr}$  and overall mean WR mass-loss rate is  $5 \times 10^{-5} m_{\odot}/\text{yr}$ . The results on mass-loss rate cited above suffice to indicate that WR stars suffer high mass-loss rate which, in turn, should influence the evolution of these stars.

With the high mass-loss rate of WR-stars, it can be expected that the return of mass to the interstellar medium by WR winds is significant, despite the fact that WR-stars are

very rare. The stars constitute only 5% of the luminous stars within 3 kpc from the sun (van der Hucht *et al.* 1988). Abbott (1982) already (in 1982) has attached the importance of the contribution of WR-stars to the interstellar medium. Recent works which emphasized the significant impact of mass loss of massive stars to the galactic environment were given by Matteucci (1991) and Leitherer *et al.* (1992).

The purpose of this paper is to provide a review of the mass loss of WR-stars in 2 aspects: namely the influence on the WR evolution and, by inference, their final states and the role the WR-stars play in the galactic chemical evolution.

## 2. Measuring the mass loss

The calculation on mass loss indicates that the WR-stars show large mass-loss rate which has prompted Johnson (1973) to suggest a search for radio emission from WR-stars. Wendker *et al.* (1975) were able to detect a very weak source of HD 192163 (a WN6 star) at 5 GHz. But the first certain detection that refers to the brightest WR object was made by Seaquist (1976).

Mass loss rate can, in principle, be determined from the  $V_\infty$ , the terminal velocity of the wind and the free-free emission of these stars at radio wavelength. This emission arises at large distances from the star, where it can be thought that the wind has reached a constant terminal velocity. Wright & Barlow (1975) assumed a stationary and isotropic stellar wind arrived at mass-loss rate as:

$$\dot{M}/V_\infty = \frac{0.095 \mu S_\nu^{3/4} D^{3/4}}{z^{1/2} q^{1/2} \nu^{1/2}} \cdot m_\odot \nu^{-1} / \text{km},$$

where  $V_\infty$  is the terminal velocity of the wind in  $\text{km sec}^{-1}$ ;  $S_\nu$  is the observed radio flux in Jy;  $D$  is the distance to the stars in kpc. The other symbols,  $\nu$ ,  $q$ ,  $g$  and  $\mu$  respectively express the molecular weight per ion,  $z$  is the mean number of electrons per ion; the Gaunt factor; and frequency in Hz.  $Z_\infty$  the r.m.s. ionic charge.

Barlow *et al.* (1981) have derived mass-loss rates for 6 WC and 15 WN stars from the predicted flux at 5 GHz, which was computed on the basis of the measurement of the free-free fluxes at  $10 \mu$  and the average spectral index between infrared and radio frequencies of  $\gamma 2$  Vel and HD 192163. They obtained

$$\dot{M}(\text{WC}) = 4.7 \times 10^{-5} m_\odot / \text{yr}$$

$$\dot{M}(\text{WN}) = 3.2 \times 10^{-5} m_\odot / \text{yr}.$$

Radio observations of WR-stars at the frequency of 4.9 GHz conducted by Dickel *et al.* (1980) for HD 192163 (WN6 binary) give the value of  $\dot{M} = 2.6 \times 10^{-5} m_\odot / \text{yr}$ ; and the value of emitting region was found to be quite extended, around  $10^4 R_\odot$ .

Van der Hucht *et al.* (1986) elaborated the method of mass-loss rate determination by taking into account the enhanced abundances of carbon and oxygen in WC-stars. They also computed detailed ionization balance in both WN and WC stars. Higher value of mass-loss rates of  $1\text{--}1.5 \times 10^{-4} m_\odot / \text{yr}$  were obtained for WN7 and WC stars. This value is upto 3 times larger than that obtained from pure He-envelope consideration only. The results were confirmed by Schmutz & Hamann (1986) who calculated non-LTE model of the atmospheres of WR-stars.

In determining the mass-loss rate, information regarding terminal velocities of the winds of WR-stars plays an important role. The terminal velocities are generally determined from the absorption edge of P-Cygni lines in the uv. The extreme-violet edge velocities were already determined by Willis (1982) for ten WR-stars. Here the observed lines of higher ionized species yielded large edge velocities, and the relation between the velocity and the excitation potential is approximately linear. Recently, Nugis (1989) suggested that  $V_\infty$  depends on  $T_{\text{eff}}$  to the power between the limits from 1.5 to 2.2. There are some deviations from this prescribed formula, and are attributed to Alfvén waves (in the case of the Sun) and shell ejections in some other peculiar stars. Applying his 'Universal' formula, Nugis (1989) calculated  $\dot{M}$  for 50 WR-stars and obtained results which lie within the uncertainty limits (by a factor of 2).

Rigorous methods to obtain better estimates for mass-loss rate have been performed by William & Eenens (1989) and by Howarth & Schmutz (1992). High-quality near-infrared spectra of 24 galactic WR-stars (from  $0.97\ \mu\text{m}$  -  $12\ \mu\text{m}$ ) were used as the basis of the study by Howarth & Schmutz. Twelve other stars of known distance are added to the sample. The use of strong HeI, the 10830 Å triplets, ensured better determination of the density-related parameters which is a function of mass-loss rate and terminal velocity. One of the results which is important in the context of this review is that Howarth & Schmutz (1992) found that mass-loss rates depend only weakly on mass, but there is a statistically significant correlation between surface mass flux and temperature. Moreover it is found that the difference between the spectroscopic and radio (4.9 GHz) mass-loss rate is small, and there is no discernible difference between WC and WN subtypes. The results give confidence to applying spectroscopic mass-loss rates for distance WR-stars, where radio observation is not available.

Mass is effectively lost by the star if it travels uninterrupted through the envelope. What is effectively measured are density and velocity in only limited parts of the envelope, from which a mass-loss rate  $\dot{M}$  is derived. Implicitly  $\dot{M}$  is well defined and derived as long as the flow is spherically symmetric and is in a steady state. Abrupt change of wind velocities or densities must be dealt with separately. In his review van der Hucht (1992) cited the relative importance of clumping to the uncertainty of mass-loss rates. This factor alone can reduce the calculated mass-loss rates by a factor of 3 to 5.

One other possible explanation of high mass-loss rates is the fluctuation theory proposed by Andriesse (1980). The theory is based on the occurrence of statistical fluctuations of non-thermal energy in stellar atmospheres. It predicts a mass-loss rate for all types of stars. The yield was  $\dot{m}_{\text{WR}} \sim 9 \times 10^{-5} m_\odot/\text{yr}$ . The value shows that  $\dot{m}$  is sufficiently large, although the connection between the non-equilibrium of the stellar envelope and the mass loss is still to be explained.

Detailed modelling of extended atmosphere of luminous stars is still necessary, in order to discern more subtle features other than radiation-driven winds. At present we have learned that the radiation-driven winds theory can explain consistently mass-loss rates of WR-stars, but it cannot be shown that all WR-stars are losing mass through this mechanism only. In the formulation of Nugis (1989) for example, he indicates that his formula predicts a strong dependence of mass-loss rate on helium fractional abundances which shows that in helium-rich stars the mass loss is mainly caused by some sort of 'deep-seated process', which is able to amplify mass-loss.

A comparison of physical and dynamical problems in envelope of stars in late evolutionary stages may be appropriate at this point. As pointed out by de Jager *et al.*



(1988), the stars increase their mass-loss rates from solar-like values, that is  $10^{-14} m_{\odot}/\text{yr}$ , to much larger rates of  $10^{-5}$  to  $10^{-4} m_{\odot}/\text{yr}$  for WR within a time interval much smaller than their lifetime prior to m.s. phase. The picture that can be drawn from their analysis indicates that the chemically evolved stars have mass-loss rates larger than those of normal stars occupying the same positions in the HR diagram. The value for the WR-stars is 10 to 20 times larger than that of normal O-stars with T similar as WR stars.

### 3. Evolution

For a long time, metallicity was not considered to play a major role in massive star evolution. Maeder (1990) explained that the cause for not having included Z-factor was obviously due to:

1. Observations of population I WR in our solar neighbourhood essentially revealed stars of similar Z; and
2. The dominant opacity source in massive stars is electron scattering. This quantity is Z independent and therefore, the Z-effect was considered very small.

With the radial change of WN/O distribution in our galaxy, and the accumulation of WR stars in other galaxies of different Z the formerly hidden Z-influence on WR distribution became apparent. In the SMC, where Z is low, and so are the mass-loss rates, the WR population is strikingly different to that in the solar neighbourhood where Z is high and, therefore mass-loss rates are substantial. This is an observational evidence for Z-factor in the WR formation rate in that the evolutionary property on  $\dot{M}$  was found so strong that even a weak dependence of  $\dot{M}$  on Z would be able to account for the observed WR distribution (Maeder 1990).

For the presently observed mass-loss rates the consequences of the stellar winds on main sequence evolution are small. However mass-loss effect on the appearance of stars during the He-burning phase may be large. The lifetime of massive star during the He-burning phase is

$$t(\text{He}) = t(\text{BSG}) + t(\text{RSG}) + t(\text{WR}).$$

The value of the 3 stages depends very sensitively on  $M$  and  $\dot{M}$ . If large  $\dot{M}$  occurs in the RSG stage, the earlier the star will be peeled off and evolve to the phase of a bare core, which we generally identify as WR-stars. Spectroscopically, WR-stars are subclassified into WN late; WN early and WC stars whose distinctions are actually the reflection of the differences in the surface composition of the stars in each group.

The detailed discussion of the process will be left out from this review, but it may be sufficient to show that the generally adopted scenario of the massive star evolution, which lead to WR star formation (Maeder 1990) is the following. For initial masses  $M_1$  and  $M_2$  respectively  $50 m_{\odot}$  and  $35 m_{\odot}$ , the following route to form WR may be followed:

$$M > M_1 \rightarrow \text{O} - \text{Of} - \text{BSG} - \text{LBV} - \text{WR} - \text{SN}$$

$$M_1 > M > M_2 \rightarrow \text{O} - \text{BSG} - \text{YSG} - \text{RSG} - \text{WR} - \text{SN}$$

$$M_2 > M \rightarrow \text{O} - \text{RSG (with or without Cepheid Loop)} - \text{SN}.$$

At present new grids of models of massive stars evolution for  $Z = 0.002$  through  $0.040$  have been computed for the mass range between  $15 m_{\odot}$  and  $120 m_{\odot}$  (cf. Maeder 1991). The grids enabled one to immediately see the lifetimes, luminosities,  $T_{\text{eff}}$  and chemical compositions at various phases. This, in turn, serves as a tool to perform population synthesis and modelling of star bursts in galaxies. In order to reconcile the difference between the calculated WR luminosity, compared to that observed, average observed mass-loss rates are not used in the calculation. Instead, individual  $\dot{M}$ , which incorporated mass-loss rates for WNE and WC stars depending on the actual masses of WR were used.

Maeder also included core-overshooting effect and  $T_{\text{eff}}$  values of WR-stars which have been corrected for the optical thickness of the wind. This is supposed to be due mainly to electron scattering. The important finding of all these corrections on  $T_{\text{eff}}$  is that WNE and WC have unique tracks in the HR diagram, which are almost independent of their initial stellar masses. In a general sense the WR stars move downwards and towards the higher temperature in the HR diagram.

Langer (1991) while emphasizing also the metallicity effect on the massive stars evolution also applied mass-loss and semi convection as the mixing process to reveal the CNO products to the surface.  $\dot{M}$  as a function of  $M$  is obtained in this analysis.

Returning to Maeder's analysis (1991), he found that for  $Z \geq 0.02$  all stars with  $M_i \geq 25 m_{\odot}$  end their evolution with masses in the range of  $5 - 10 m_{\odot}$ , while the length of time the star remains on WR phase increases with metallicity and  $M$ . Moreover the scenario proposed by Maeder gives results which compare well with the observed number ratios of WR/O; WC/WR and WC/WN in our galaxy (van der Hucht *et al.*, 1988), for  $m > 35 m_{\odot}$ .

Discussions of the mass regime of WR predecessors have already been given by many authors. In this short review this will not be represented, but, instead we will present the possible connection between SNe as descendants of WR stars. The final outcome of WR path toward SNe seems to be determined by the absence or not of hydrogen in WR although the discrimination between hydrogen containing and hydrogenless WN star, as WNL and WNE is not always in general agreement with one another.

It is thought that for WR which contains hydrogen there exists a second independent region of nuclear energy generation besides that of the burning central energy source. Langer (1991) viewed that the duration of WNL phases may increase with increasing initial mass, making it possible that the WNL lifetime becomes comparable to that of He-burning stage. This implies that some massive stars would never lose their H-envelope completely, and this will raise consequence of their final stages.

The facts about SNII are very interesting in this connection. The presence of hydrogen in SNII is common. From the theoretical point of view no homogeneous SNII can be expected since both core and envelope masses may be originated in a wide range of presupernova stages (including RSG; BSG in case of SN 1987 A and Wolf-Rayet stars). Perhaps only WN with the highest mass can be a SN(II). The low mass WR end the final phase of their evolution in WNL.

For hydrogenless WR the situation is slightly different. Once a massive star has lost its hydrogen envelope completely, its internal structure becomes simple and, more or less, independent of its previous life. Langer (1989) showed the effect of mass dependent WNE and WC mass-loss rates. For stars of  $45 m_{\odot} \leq m \leq 100 m_{\odot}$  the final mass is almost the same for the whole range, and it is in the range of  $5 - 10 m_{\odot}$ . Since those stars lose their hydrogen envelope, it may be thought that they will give rise to type SNI.

Ensmann & Woosley (1988) found that the light curves of exploding low mass hydrogen-less WR-stars look similar to observation of SN of type Ib. The connection between type Ib SN and WR stars, if it can be strongly established, would support the concept of the mass dependence of WR mass-loss rates.

A recent treatise by Nomoto (1991) indicated that the maximum brightness and fast decline of typical Ib/Ic SN light curves can be explained in terms of helium star models with masses of  $3-5 m_{\odot}$ . This implies that only WR stars with  $3-5 m_{\odot}$  could become a type Ib/Ic progenitor. However, lots have to be bridged between the observed frequency of the type Ib/Ic SN and birth rate of massive stars which is still too small.

Metallicities have been shown to influence the formation of SN types from the original wide range of stellar masses. The range of initial masses leading to SN from WR stars is much shorter in low  $Z$  than at high  $Z$ . In this case the number of type Ib SN should be less in low  $Z$ , compared to that in large  $Z$  environment. More observational data are still needed to affirm the above mentioned consideration.

#### 4. WR-stars and interstellar medium

Although WR stars only have a lifetime of about 0.1 of the lifetime of their progenitors, their mass-loss is about 10 times more intense than the mass-loss of OB stars. The implication is that there is much contribution of mass and energy from WR stars into interstellar medium.

Based on the corrected mass-loss rates of O, B, A Sg and WR stars van der Hucht *et al.* (1986) obtained the following:

Parameter	WR	O	BA
$\dot{M}$	77%	19%	14%
$\dot{M} V_{\infty}$	74%	28%	2%
$1/2 \dot{M} V_{\infty}^2$	70%	28%	2%
$L$	8%	65%	27%

Here one can see that only the radiative energy input of WR stars is superseded by other types of stars. The other parameters, mass-loss rates by stellar wind, the wind momentum and the wind energy deposit are all dominating as compared to the same parameters of other stars.

The question which may arise is that whether the chemical enrichment of the galactic environment arises from WR stars or from nova and supernova. Using the data of the previous table, it can be shown that 95% of the total energy input into ISM comes from radiation. Abbott (1982) put forward an argument that the storage of energy by winds and supernova is more efficient than the deposit by radiation. The outcome would be that the stellar radiation dominates the heating of HII regions but SN are the dominating source of energy for the cloud motions.

Matteucci (1991), based on several line of arguments showed that if WR were the progenitors of type Ib SN, the galactic chemical evolution would not change substantially with respect to the case of white dwarfs (C-O) being the progenitors of type Ib SN.

Thus the results of abundance determinations may not be, as yet, used to decide the path of star evolution which lead to SN. But of course, given the number of WR (Maeder 1991) the enrichment of ISM by WR stars can be predicted. He argued that  $^{12}\text{C}$ ,  $^{16}\text{O}$  and  $^{22}\text{Ne}$  abundance increments is large ( $\approx 2$  order of magnitudes) at the transition from WN to the WC stage.

The formation of  $^{26}\text{Al}$ , as shortlived isotopes has been the subject of discussions in relation with the contribution of WR stars to the ISM. The decay of this isotope gives rise to a gamma photon that can be observed directly from satellites. On a time scale of a million years the decay of the isotope emits photon at 1.809 MeV. Deaborn & Blake (1985, 1988) considered the production of  $^{26}\text{Al}$  during core H-burning in massive stars, where it is formed by proton capture on  $^{25}\text{Mg}$ . For the massive stars, i.e.  $M = 100 m_{\odot}$ , they produced some  $10^{-6} m_{\odot}$  of  $^{26}\text{Al}$  per star. Prantzos *et al.* (1986) and Prantzos & Casse (1986) viewed that the production of  $^{26}\text{Al}$  in the convective core of massive stars, by including overshooting in their model calculations they obtained more  $^{26}\text{Al}$  than that predicted by Deaborn & Blake. The  $^{26}\text{Al}$  is injected in the interstellar medium by the mass-loss during the Of and WN phases. The estimated  $^{26}\text{Al}$  production, after taking into account the gradient of metallicity, is  $1.11 \times 10^{-4} M_{\odot}$  per WR star.

Signore & Dupraz (1993) showed that, contributions from type II SN and WR stars amount to  $1.35 m_{\odot}$  and  $0.35 m_{\odot}$  respectively, by assuming that the total galactic rate of core-collapse supernova is 4 per century.

### Acknowledgement

The author thanks Karel van der Hucht for his supply of publications on WR stars and for his comments on the text. He appreciates Mr. Narayana Sasrawiguna's help in typing this review. Part of the travel expenses was supported by the Leids-Kerkhoven-Bosscha Foundation, for which the author expresses his appreciation.

### References

- Abbott, D. C. 1982, *Astrophys. J.*, **253**, 282.  
 Adams, W. S., McCormack, E. 1935, *Astrophys. J.*, **81**, 119.  
 Andriesse, C. D. 1980, *Mon. Not. R. astr. Soc.*, **192**, 95.  
 Barlow, M. J., Smith, L. J., Willis, A. J. 1981, *Mon. Not. R. astr. Soc.*, **196**, 101.  
 Beals C. S. 1929, *Mon. Not. R. astr. Soc.*, **90**, 202.  
 Deaborn, D., Blake, J. B. 1985, *Astrophys. J.*, **288**, L2.  
 Deaborn, D., Blake, J. B. 1988, *Astrophys. J.*, **332**, 305.  
 Dickel, H. R., Habing, H. J., Isaacman, R. 1980, *Astrophys. J.*, **238**, L39.  
 de Jager, C., Nieuwenhuijzen, H., van der Hucht, K. A. 1988, *Astr. Astrophys. Suppl. Ser.* **72**, 259.  
 Ensmann, L. M., Woosley, S. E. 1988, *Astrophys. J.*, **333**, 754.  
 Howarth, I. D., Schmutz, W. 1992, *Astr. Astrophys.*, **261**, 503.  
 Johnson, M. H. 1973, in *Wolf-Rayet and High Temperature Stars* Eds. M.K.V. Bappu & J. Sahade (Reidel), p. 42.  
 Langer, N. 1989, *Astr. Astrophys.*, **220**, 135.  
 Langer, N. 1991, in *Wolf-Rayet Stars and Interrelations with other Massive Stars in Galaxies* Eds. K. A. van der Hucht & B. Hidayat (Dordrecht: Reidel) p. 431.  
 Leitherer, C., Robert, C., Drissen, L. 1992, *Astrophys. J.* **401**, 596.  
 Maeder, A., 1990, *Astr. Astrophys.*, **178**, 159.  
 Maeder, A., 1991, *Q. J. R. astr. Soc.*, **32**, 217.

- Matteucci, F. 1991, in *Wolf-Rayet Stars and Interrelations with other Massive Stars in Galaxies* Eds. K. A. van der Hucht & B. Hidayat (Dordrecht: Reidel) p. 625.
- Nomoto, K. 1991, in *Wolf-Rayet Stars and Interrelations with other Massive Stars in Galaxies* Eds. K. A. van der Hucht & B. Hidayat (Dordrecht: Reidel) p. 515.
- Nugis, T. 1989, *Tartu Astrof. Obs. Teated No.* 94.
- Prantzos, N., Casse, M. 1986, *Astrophys. J.*, **307**, 324.
- Prantzos, N., Doom, C., Arnould, M., de Loore, C. 1986, *Astrophys. J.*, **315**, 209.
- Prinja, R. K., Barlow, M. J., Howard, I. D. 1990, *Astrophys. J.*, **361**, 607.
- Schmutz, W., Hamann, W. R. 1986, *Astr. Astrophys.*, **166**, L111.
- Seaquist, E. R., 1976, *Astrophys. J. Lett.*, **203**, L35.
- Signore, M., Dupraz, C. 1993, *Astr. Astrophys. Suppl. Ser.*, **97**, 141.
- van der Hucht, K. A. 1992, *Astr. Astrophys. Rev.*, **6**, p. 123.
- van der Hucht, K. A., Cassinelli, J. P., Williams, P. M. 1986, *Astr. Astrophys.*, **168**, 111.
- van der Hucht, K. A., Hidayat, B., Admiranto, G., Supelli, K. R., Doom, C. 1988, *Astr. Astrophys.*, **199**, 217.
- Wendker, H. J., Smith, L. F., Israel, F. P., Habing, H. J., Dickel, H. R. 1975, *Astr. Astrophys.*, **42**, 173.
- Williams, P. M., Eenens, P. 1989, *Mon. Not. R. astr. Soc.*, **240**, 445.
- Willis, A. J. 1982, in *Wolf-Rayet Stars, IAU Symp. 99* Eds.: C.W.H. de Loore & A. J. Willis; (Dordrecht: Reidel) p. 87
- Willis, A. J. 1991, in *Wolf-Rayet Stars and Interrelations with other Massive Stars in Galaxies* Eds. K. A. van der Hucht & B. Hidayat (Dordrecht: Reidel) p. 515.
- Wright, A. E., Barlow, M. J. 1975, *Mon. Not. R. astr. Soc.*, **170**, 41.

## Evidence for Mass Loss in Close Binaries and its Implications

**Alan H. Batten** *Dominion Astrophysical Observatory, Herzberg Institute of Astrophysics, 5071, W. Saanich Rd., Victoria, B.C., Canada, V8X 4M6.*

We must distinguish between binary systems that are losing mass because they contain stars that would lose mass even if they were single, and binaries that are losing mass because their characteristics as binaries create circumstances in which mass will be lost at particular stages in the evolution of the system, even though similar single stars would not lose significant amounts of mass. The principal example of the first group, of course, would be a binary containing an early-type star. It is now well established that all such stars are losing mass through their stellar winds. This fundamental characteristic of such a star is not changed by its membership in a binary system. If the companion is a small star, without a very strong wind of its own, it will probably have little effect on the wind of the early-type component. Many binaries, however, contain two, often roughly similar, early-type components in relatively close proximity. Obviously the two winds are going to affect each other. There is now a body of both theoretical and observational papers on the subject of colliding or interacting stellar winds (Shore & Brown 1988; Gies & Wiggs 1991). The interested reader can find references to, and some discussion of them in papers by both Sahade and myself, presented two years ago (Sahade 1992a; Batten 1992). Shock waves are created in the region where the winds collide, and enough matter accumulates for emission features to become detectable in the far UV and X-ray regions. The wind itself may cease to be isotropic and become strongly directional. Systems which are currently believed to show evidence of such colliding winds include Plaskett's star, AO Cas,  $\gamma$  Vel, and possibly Y Cygni (Koch, private communication). Does this collision of the wind in any way affect the evolution of the stars from which they originate? I think that this still has to be explored, both observationally and theoretically. The collision, of course, occurs some distance away from either star, and its direct effect on the stars can only be small, if not negligible. The development of chaos theory, however, has made us all more aware of how a small perturbation may have disproportionately large effects, and it would be worthwhile for someone to investigate whether or not the evolution of early-type stars in binaries believed to have colliding winds is any different from that of similar single stars.

Obvious examples of stars whose loss of mass is a consequence of their being in binary systems are provided (we believe) by all novae and possibly some supernovae. I shall not discuss these phenomena in detail as I have little doubt that they will be dealt with by other speakers, who are better qualified than I am to do so. I would like to emphasize, however, that, whereas early-type stars losing mass through winds are releasing only their surface layers, unaffected by nuclear processing within their own interiors, supernovae, as is well known, are generating and releasing heavy nuclei. Even novae are probably releasing some processed material: although the nova explosion involves only the outer layers of a star, it is believed to be the result of mass transfer that has exposed deeper layers and that thermonuclear reactions do take place during the outburst.

The next group of binary systems to consider is the one with which I am most familiar: the Algol-type systems. These contain a moderately massive primary – usually of late B spectral type and a secondary component that is oversized and overluminous for its mass. Agreement is now very nearly universal that these systems are the result of large-scale mass-transfer from the erstwhile more massive component that has become the present-day secondary. When it first became possible to compute the effects of mass-transfer (Kippenhahn & Weigert 1967) it was necessary, in order to make any progress at all, to assume that the mass transfer was conservative (i.e. no mass lost from the system as a whole). At that time, the dimensions for Algol systems were only approximately known and, somewhat to everyone's surprise, the conservative approximation seemed to fit. It seemed that if only enough trial computations were made, it would be possible to deduce what the progenitors of Algol or U Cep, or some other system, must have been like. However, we were all aware that the conservative approximation was a computational convenience. It was not reasonable to suppose that one could pour several solar masses from one star to another without spilling some. As the number of computations increased, and our knowledge of Algol systems grew more precise, it finally became obvious that the conservative assumption would not work. Over twenty years ago, Plavec (1973) rejected it on theoretical grounds, and not long after, Kondo *et al.* (1980) found evidence, from IUE observations of the resonance lines of MgII and FeII, for mass loss from U Cep. Some estimates of mass-loss rates from Algol systems have been made (Sahade 1992b), and they lie in the same range as those for stellar winds from early-type stars, namely,  $10^{-8}$  to  $10^{-5}$  solar masses per year. We note that there is reason to believe that this mass will also be partially processed. If several solar masses are lost by the primary star, then layers in which thermonuclear reactions have been going on are likely to be exposed. There is some evidence for unusual CNO abundances in such systems (Plavec 1983), that would be compatible with the supposition that deeper layers had been exposed. Very little thought has been given to the possible effects of this on the interstellar medium. The only discussion I know of it is brief and unsatisfactory (Giuricin *et al.* 1983).

There is, of course, a wide variety of binary systems that are believed to have been formed by a combination of mass-transfer and mass-loss. Sahade (1992a) lists eight different groups, including the Algols and the cataclysmic variables. Some of them, such as the symbiotic stars (Kenyon 1992), he believes to be undergoing a second stage of mass-loss. In this group, mass is lost from a red-giant component through a stellar wind, which again is believed to lead to losses in the range of  $10^{-7}$  to  $10^{-5}$  solar masses per year. Another group that displays evidence for mass loss is the so-called RS CVn group (Rodono 1992). These systems contain two cool stars, main-sequence or sub-giant, at least one of which is chromospherically active. They appear to have strong magnetic fields associated with them, and these enhance the mass-loss considerably compared with the normal rate for solar-type stars.

Thus we find the concept of mass-loss, particularly in conjunction with that of mass-transfer, to be essential for our understanding of how close binary systems came to be the way they are. Quantitatively, at least, these concepts seem able to explain a wide variety of systems, and we are beginning to fill in the quantitative picture – although there is still a long way to go, and some of our ideas may be changed. It also becomes clear that binaries are an essential part of the mechanism by which stars and interstellar matter are kept in equilibrium. That is, binaries are, in many different ways, responsible for returning matter to the interstellar medium and that matter is often

enriched in heavy elements. Thus, binaries are an important constituent of galaxies, since they affect both the dynamical and chemical evolution of the latter.

### References

- Batten, A. H. 1992, in *Evolutionary Processes in Interacting Binary Stars*, IAU Symposium, No. 151, Eds. Y. Kondo, R. F. Sistero & R. S. Polidan, (Dordrecht: Kluwer) p. 235.
- Gies, D. R., Wiggs, M. S. 1991, *Astrophys. J.*, **375**, 321.
- Giuricin, G., Mardirossian, F., Mezzetti, M. 1983, *Astrophys. J. Suppl.*, **52**, 35.
- Kenyon, S. J. 1992, in *Evolutionary Processes in Interacting Binary Stars*, IAU Symposium, No. 151, Eds. Y. Kondo, R. F. Sistero & R. S. Polidan, (Dordrecht: Kluwer) p. 137.
- Kippenhahn, R., Weigert, A. 1967, *Zs. f. Ap.*, **65**, 251.
- Kondo, Y., McCluskey, G. E., Stencel, R. E. 1980, in *Close Binary Systems: Observations and Interpretation*, IAU Symposium, No. 88, Eds. M. T. Plavec, D. M. Popper & R. K. Ulrich, (Dordrecht: Reidel) p. 237.
- Plavec, M. 1973, in *Extended Atmospheric and Circumstellar matter in Close Binary Systems*, IAU Symposium, No. 51, Ed. A. H. Batten (Dordrecht: Reidel) p. 216.
- Plavec, M. 1983, *J. R. Astr. Soc.*, **77**, 283.
- Rodono, M. 1992, in *Evolutionary Processes in Interacting Binary Stars*, IAU Symposium, No. 151, Ed. Y. Kondo, R. F. Sistero & R. S. Polidan (Dordrecht: Kluwer) p. 71.
- Sahade, J. 1992a, in *Evolutionary Processes in Interacting Binary Stars*, IAU Symposium, No. 151, Eds. Y. Kondo, R. F. Sistero & R. S. Polidan, (Dordrecht: Kluwer) p. 3.
- Sahade, J. 1992b, in *The Realm of Interacting Binary Stars*, Eds. J. Sahade, G. E. McCluskey & Y. Kondo, (Dordrecht: Kluwer) p. 3.
- Shore, S. N., Brown, D. N. 1988, *Astrophys. J.*, **334**, 1021.





## Lithium Abundances as Clues to Stellar Mixing

Suchitra Balachandran<sup>1</sup> *Dept. of Physics and Astronomy, University of North Carolina, CB#3255 Phillips Hall, Chapel Hill NC 27599, USA*

**Abstract.** Observational data on the evolution of angular momentum during the pre-main sequence and early main sequence are summarized, and a possible connection between Li depletion and rotation is explored.

**Key words:** Stellar mixing    lithium abundances.

### 1. Introduction

Due to its fragile nature, Li is easily destroyed in the stellar interior. In the last decade, scores of observations in stars of various ages and evolutionary phases have revealed a complex pattern of Li abundances which must hold clues to mixing mechanisms that operate in the stellar interior. Due to the limited length of this article, I will not attempt to review all of the observations and theories referred to during my talk. Here I will elaborate on interesting observational evidence that appears to indicate a link between the rotational history of K dwarfs and the Li depletion that occurs in them.

### 2. Rotational evolution to the ZAMS

Rotational breaking of stars on the main sequence has only been known since the discovery of rapidly rotating K dwarfs in the Pleiades (van Leeuwen & Alphenaar 1982). Since then, through observations of clusters of different ages (see review by Stauffer 1991), it has been established that the timescale for spin-down increases towards later spectral types. Such mass-dependent spin-down can be broadly understood if the convective envelope of the star is assumed to decouple from the core so that the increasing fractional mass of the envelope from G to K to M dwarfs results in the longer spin-down timescale at later spectral types. The typical spin-down timescale for a K dwarf is about  $2-3 \times 10^8$  years. Since the age spread within the young clusters Alpha Persei and the Pleiades is only about 10 Myr (Prosser 1992; Soderblom *et al.* 1993a), K dwarfs in these clusters have not had time to spin down and the observed distribution of rotational velocities must be representative of the velocities with which they first arrived on the ZAMS. The observed rotational velocities indicate that a large fraction of the stars arrive as slow rotators on the main sequence having somehow lost most of the angular momentum they must have acquired during pre-main sequence (PMS) contraction. A smaller fraction appears to rotate rapidly on arrival on the ZAMS.

<sup>1</sup> Present address: Department of Astronomy, The Ohio State University, 174 West 18th Avenue, Columbus OH 43210, USA.

Recent observational studies by Bouvier *et al.* (1993) and Edwards *et al.* (1993) find that the rotational periods of classical T Tauri stars (CTTS) are typically long ( $\sim 8$  days), while weak-lined T Tauri stars (WTTS) show a large spread in rotational periods extending from periods typical of CTTS and to very short periods ( $\sim 2$  days). Since CTTS are thought to be associated with accretion disks, they suggest that CTTS do not spin up until they have dissipated their accretion disk and become WTTS, and the spread in rotational velocities may thus be related to the longevity of the accretion disk around the star.

### 3. Lithium abundances in young clusters

Observations of Li in K dwarfs in young clusters show a decline in Li abundances in stars cooler than about 5200 K with a spread in Li at a given  $T_{\text{eff}}$ . Rapid rotators lie preferentially along the upper envelope of Li abundances and the lower envelope is populated by slow rotators. This was first pointed out for the Alpha Persei cluster (Balachandran, Lambert & Stauffer 1988) and more extensive data in the Pleiades (Soderblom *et al.* 1993b) bear out these findings. PMS models are able to predict the upper envelope of Li abundances (e.g. D'Antona & Mazzitelli 1993) but, clearly, larger amounts of depletion have occurred and rapid rotation appears to inhibit this 'extra' depletion. Since the K dwarfs have not had time to spin-down by the age of the Pleiades and Alpha Per, this 'extra' depletion is not a result of rotational spin-down on the main sequence. Unless the correlation between Li depletion and rotation is entirely fortuitous (i.e., the 'extra' depletion occurs on the main sequence and the lack of 'extra' Li depletion in the rapid rotators is simply coincidental), this Li depletion pattern must have been established during the PMS phase, perhaps by the same processes which regulate the angular momentum of the star. This explanation is not as straightforward as it may seem because the correlation between the lack of 'extra' Li depletion and rapid rotation is not one to one; slow rotators *are* found along the upper Li- $T_{\text{eff}}$  envelope as well.

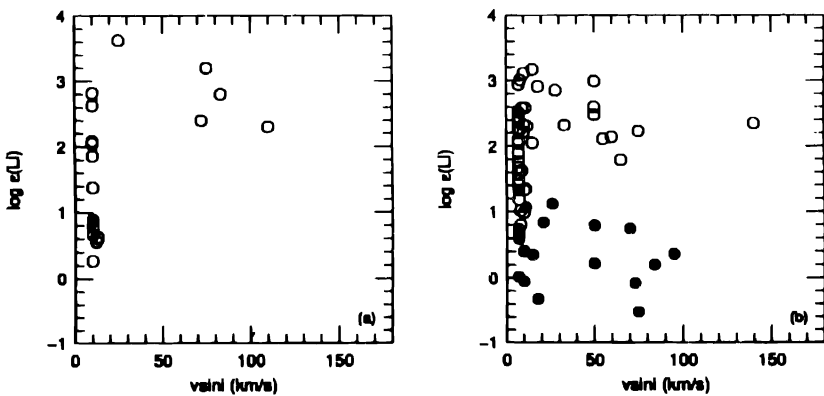


**Figure 1.** Lithium abundance as a function of rotational velocity ( $v \sin i$ ) in the **a)** Alpha Persei and **b)** Pleiades clusters. The data are taken from Balachandran, Lambert & Stauffer (1988); Soderblom *et al.* (1993b) and Garcia-Lopez, Rebolo, & Martin (1993). The open symbols represent stars with  $4400 \text{ K} < T_{\text{eff}} < 5200 \text{ K}$  and the filled symbols, stars with  $T_{\text{eff}} < 4400 \text{ K}$ .

Recent observations by Garcia-Lopez, Rebolo & Martin (1993) in the Pleiades have added another twist to this scenario. They point out that the correlation between Li depletion and rotation exists only in K dwarfs between  $0.7$  and  $0.9 M_{\odot}$  (5200 K–4400 K). At masses less than  $0.7 M_{\odot}$ , all stars show large Li depletions which appear to be independent of the rotational velocity of the star (see Fig. 1).

It is conceivable that main sequence depletion may become very effective in these lower-mass stars so that even though they arrive on the ZAMS with the same Li-rotation distribution as the early-K dwarfs, both rapid and slow rotators then deplete their Li so quickly that the Li-rotation distribution is no longer perceived by the age of the Pleiades. Alternatively, the PMS angular momentum regulation mechanism may become ineffective in controlling Li depletion in the low-mass stars. This finding prompts one to enquire if there are any significant differences in the rotational periods of WTTS and CTTS at masses above and below  $0.7 M_{\odot}$ . Unfortunately the present data samples of Bouvier *et al.* (1993) and Edwards *et al.* (1993) do not contain any CTTS with spectral types later than M0. The 6 low-mass stars in their samples are all WTTS with fairly large periods. It would be very useful to measure rotational periods in later spectral type T Tauri stars; the Li data appear to indicate that additional information may indeed prove to be quite exciting.

## References

- Balachandran, S., Lambert, D. L., Stauffer, J. R. 1988, *Astrophys. J.*, **333**, 267.  
 Bouvier, J., Cabrit, S., Fernandez, M., Martin, E. L., Matthews, J. M. 1993, *Astr. Astrophys.*, (in press).  
 D'Antona, F. D., Mazzitelli, L. 1993, *Astrophys. J. Suppl.*, (in press).  
 Edwards, S., Strom, S. E., Hartigan, P., Strom, K. M., Hillenbrand, L. A., Herbst, W., Attridge, J., Merrill, K. M., Probst, R., Gatley, I. 1993, *Astr. J.*, **106**, 372.  
 Garcia-Lopez, R. J., Rebolo, R., Martin, E. L. 1993, *Astr. Astrophys.*, (in press).  
 Prosser, C. F. 1992, *Astr. J.*, **103**, 488.  
 Soderblom, D. R., Jones, B. F., Balachandran, S., Stauffer, J. R., Duncan, D. K., Fedele, S. B., Hudon, J. D. 1993b, *Astr. J.*, **106**, 1059.  
 Soderblom, D. R., Stauffer, J. R., Hudon, J. D., Jones, B. F. 1993a, *Astrophys. J. Suppl.*, **85**, 315.  
 Stauffer, J. R. 1991, in *Angular Momentum Evolution of Young Stars* Eds. S. Catalano, & J. R. Stauffer (Dordrecht: Kluwer), p. 117.  
 van Leeuwen, F., Alphenaar, P. 1982, *ESO Messenger*, No. 18, p. 15.



## SN 1993J in M 81: Photometry and Spectrophotometry

T. P. Prabhu *Indian Institute of Astrophysics, Bangalore 560034, India*

**Abstract.** CCD photometric and spectrophotometric observations of the peculiar type IIb supernova 1993J in M 81 (NGC 3031) were made from Vainu Bappu Observatory, Kavalur during the first two months since the outburst of the supernova. The spectroscopic evolution was similar to other type II supernovae during the early phases, but lines of helium strengthened later indicating that the supernova was turning into type Ib like SN1987K. The lines due to Ba II and Sc II were weaker than in SN 1987A appeared together with lines of helium indicating that there was no significant mixing in the hydrogen envelope. We use the absorption velocities together with photometric radii to make an estimate of the distance to M 81 using the Baade-Wesselink (expanding photosphere) method.

**Key words:** Supernovae: spectra – supernovae: photometry – supernovae: distances – supernovae: SN 1993J – galaxies: M 81 (NGC 3031).

### 1. Introduction

Spectrophotometry in the ultraviolet, optical and infrared bands of radiation constitutes the most important data on supernova (SN) outbursts since most of radiation is emitted in these bands around the time of maximum. The classification of supernovae has also been based canonically on optical spectroscopic information. While the basic classification scheme of type I (without the lines due to hydrogen) and type II (showing hydrogen lines in emission) has survived over several decades since Zwicky's initial suggestion, deviants from this scheme are becoming apparent during the last decade. SN 1983N in M 83 (NGC 5236), type I according to the above definition, did not show the dip at 6150 Å attributed to blue-shifted absorption of Si II which was seen in all type I supernovae till then. Instead, it showed lines of helium (Richter & Sadler 1983; Prabhu 1985). This class of SN is growing in number and has now been termed type Ib. Type Ic has also been identified with the SN that shows lines due to oxygen instead of silicon. The early expectations on the homogeneity of type I SN have been growing thin even in the case of their light curves (Branch 1981), a fact that casts aspersions on their utility as distance candles.

Type II SN light curves have been classified into plateau-type (P) and linear-type (L). Though this class was never considered to be a homogeneous one, the subluminal type II SN 1987A in LMC with very large initial expansion velocity and a secondary maximum in the light curve, and SN 1987K which turned from type II near maximum to type Ib at late times, have shown the diversity of phenomena that can take place in SN II (Harkness & Wheeler 1990; Filippenko 1991). It is thus important to study individual SN in detail in order to understand the physical phenomena involved. The discovery of SN 1993J in a nearby M 81 by F. Garcia (Ripero 1993) on March 28, 1993

provided such an opportunity since it reached a maximum brightness of  $V \sim 10$ . Though the SN started as type II, as time progressed it became evident that it was peculiar with a good resemblance to SN 1987K. We will call this a type IIb SN following Woosley, Pinto & Ensmann (1988).

We present here a brief report on the results on SN 1993J based on observations obtained with the 1-m and 2.3-m telescopes at the Vainu Bappu Observatory (VBO), Kavalur. The detailed results will be published elsewhere.

## 2. Photometry

CCD images of the region around SN 1993J were obtained on a total of 11 nights between April 14 and May 23, 1993 at the prime focus of the 2.3-m Vainu Bappu telescope, generally in  $BVR$  bands and on two nights also through  $I$  band. The photometry was carried out differentially with respect to star B (Corwin 1993) as the comparison star and star A as the check star. The colour corrections were made using the transformation equations of Anupama *et al.* (1993). The corrections needed were negligible during the early days when the colours of SN were similar to those of star B, but became very significant as the SN became progressively redder. The results are plotted in Fig. 1 together with other magnitudes available through the nova network (T. Kato, personal communication) and IAU Circulars.

Based on pre-discovery and subsequent observations available in the literature we adopt the date of outburst as March 28, 1993. The initial rise was followed by a sharp drop to  $V = 11.9$  on April 5. The SN then brightened slowly to  $V = 10.8$  till April 18 and declined thereafter. This behaviour resembles the light curve of SN 1987A though the latter was about 1.4 mag fainter in absolute brightness in  $V$  band, and reached the

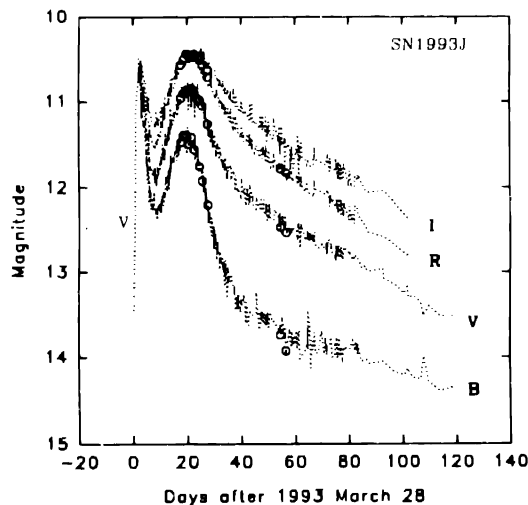


**Figure 1.** The light curves of SN 1993J in  $BVR$  bands. The dotted lines denote the observations from other sources available through the nova network and IAU Circulars. VBO observations are shown by open circles.

second peak  $\sim 90$  days since the outburst compared to only  $\sim 20$  days in the case of SN 1993J. The models of SN outburst constructed soon after the outburst of SN 1987A (cf., Woosley 1991) qualitatively explain such light curves and require a low-mass hydrogen envelope (Ray, Singh & Sutaria 1993). The SN according to this model brightens quickly due to the deposition of the shock energy. This is followed by a sharp drop as the expanding envelope cools adiabatically. When the temperature drops sufficiently to allow recombination of hydrogen the luminosity rises slowly and steadily to the secondary maximum due to the recombination radiation as well as due to the release of trapped radioactive energy of newly synthesized  $^{56}\text{Ni}$  and its daughter  $^{56}\text{Co}$ . The recombination front moves continuously inward until it hits the base of the envelope. The final decline is characterized by the decay of  $^{56}\text{Co}$ . It remains to be verified whether several other SN also have a similar light curve with the first maximum and rapid decline missed by observational selection (Woosley 1991).

### 3. Spectrophotometry

CCD spectrophotometric observations were carried out mostly with the 1-m Zeiss reflector, and in the early phase also with the 2.3-m VBT. The dispersions employed were about  $5 \text{ \AA}$  per pixel. Observations were obtained altogether on 16 nights between April 1 and May 18, 1993. Feige 34 was used as spectrophotometric standard and star B as comparison. The reductions were carried out using the RESPECT package at VBO (Prabhu & Anupama 1991).

The spectra on April 13, 14, May 17, 18 are shown in Fig. 2. These were the epochs when the best wavelength coverage could be obtained. The most prominent lines at the first epoch are,  $\text{H}\alpha$ ,  $\text{He I } \lambda 5876 + \text{Na I D}$ , and several lines of  $\text{Fe II } (\lambda\lambda 4568, 4924, 5018,$

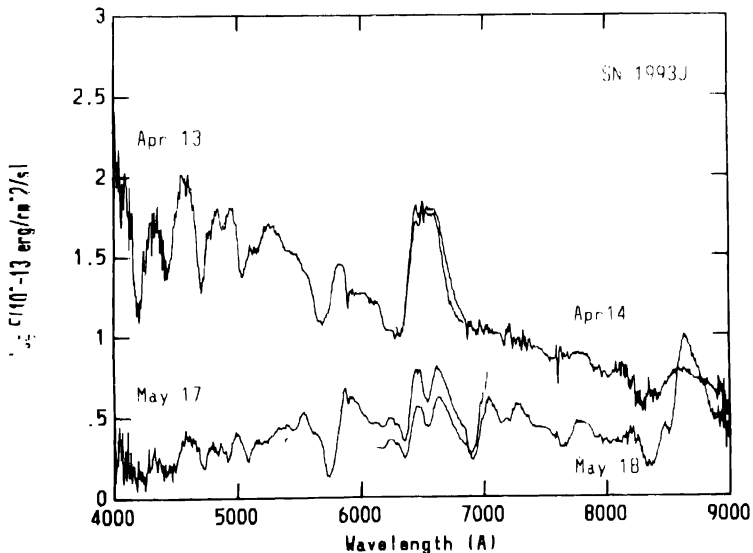


Fig. 2. Spectra of SN 1993J on 1993 April 13, 14, and May 17, 18.



the last two blended with  $H\beta$ ;  $\lambda 5169$  blended with  $Mg\ I\ \lambda 5183$ ; 5276, 5284, 5317, 5363 blended with each other). At the later epoch, the  $H\alpha$  line showed distinctly double structure. The emergence of  $He\ I\ \lambda 7065$  and strengthening of  $He\ I\ \lambda 5876$  imply that the structure in  $H\alpha$  is due to the superposition of the P-Cygni profile of  $He\ I\ \lambda 6678$ . The features near  $\lambda\lambda 4925, 5015$  should hence be identified with  $He\ I$  rather than  $Fe\ II$  at this stage. The lines  $O\ I\ \lambda 7774$  as well as  $Ca\ II$  infrared triplet are much stronger at the later phase. The emission at  $\lambda 5535$  is very likely due to  $[O\ I]\ \lambda 5577$ . This transition has a higher value of critical density and is generally present at relatively higher density diffuse matter. The blue shift of the centre of this line is suggestive of asymmetries in the envelope. The absorptions due to  $Ba\ II\ \lambda 6141$  and  $Sc\ II\ \lambda 6245$  are evident clearly on May 17 at  $\lambda\lambda 6078, 6170$ . These dips can be traced back with some difficulty till April 19. The s-process elements like  $Ba$  and  $Sc$  are expected in the helium layer and not in the  $H + He$  envelope. Their strength in the spectra of SN 1987A indicated mixing of the envelope matter with inner layers (see Dopita 1988). The emergence of these lines in SN 1993J during the phase when lines of helium strengthened imply that there was no extensive mixing.

#### 4. Spectroscopic distance to the supernova

The temperature and angular radius of the photosphere can be estimated from a black-body fit to the observed magnitudes (e.g. Ray, Singh & Sutaria 1993) or by comparing the colours with a supergiant (Ashoka *et al.* 1987). The absorption velocities due to lines formed near the photosphere give us the rate of change of photospheric radius in absolute units. A comparison of the spectroscopically determined radius with the observed angular radius gives us an estimate of the distance to the supernova.

Two sources of systematic error in such an estimate are known (Schmidt-Kaler 1991). First, the geometry of the photosphere need not be spherical as assumed. Spectropolarimetry of SN 1993J by Trammell, Hines & Wheeler (1993) is indicative of departure from spherical symmetry though both prolate and oblate models can explain the asymmetry. Depending on whether the actual geometry is prolate or oblate, Schmidt-Kaler (1991) had estimated in the case of SN 1987A that the derived distance needs to be multiplied by 1.05 or 0.95. The continuum polarization is higher for SN 1993J compared to SN 1987A and hence the correction factor would probably depart from unity by a larger amount.

Secondly the photosphere may not behave as a blackbody. The model calculations for SN 1987A indicated that the photosphere was grey and a correction factor of 0.95 needed to be applied to the derived distance during the secondary maximum (Schmidt-Kaler 1991). A similar correction factor may be applicable in the case of SN 1993J during the secondary maximum.

The velocities of absorption dips yield expansion velocities of the envelope. The velocities derived from different lines in SN 1993J show a similar trend as observed in SN 1987A (Ashoka *et al.* 1987). The  $H\alpha$  yields the highest velocity indicating that it is formed well above the photosphere. The weak lines like  $Fe\ II\ \lambda\lambda 4568, 4924, 5018, 5176, 5300$  yield the lowest velocities and are probably formed close to the photosphere. The velocities decrease as the photosphere recedes with respect to the matter. The decrease is sharp in the case of the weakest lines particularly after April 23 when the photosphere

has probably reached the bottom of the H + He envelope. We will use velocities derived from the weak lines till April 23 as indicative of photospheric velocities.

Counting time from March 28, the probable date of explosion, the observed velocities of Fe II lines between days 11 and 26 can be approximated by the parabola

$$V_{\text{exp}}(t_d) = 9260 - 4.668t_d^2,$$

where  $V_{\text{exp}}$  is in  $\text{km s}^{-1}$  and  $t_d$  is time since explosion in days. The angular radius of the photosphere should then vary as

$$\theta = \theta_0 + D^{-1} \int V_{\text{exp}}(t) dt$$

Using the estimates of angular size based on *UBVRIJHK* photometry (Ray, Singh & Sutaria 1993), we obtain from a least-squares fit to the above equation, a distance of  $4.2 \pm 0.2$  Mpc to the supernova. The best current estimate of the distance to M 81 is  $3.6 \pm 0.3$  based on the photometry of Cepheids using the Hubble Space Telescope (Freedman *et al.* 1993). A correction factor of 0.9 for possible oblateness and 0.95 for grey atmosphere would make the two distances agree exactly.

The accuracy of the expanding photosphere method does not depend on the distance at all. Hence, we conclude that even ignoring the effect of asymmetric explosion and grey atmosphere, it is possible to estimate distances to supernovae to an accuracy of 15–20%.

### Acknowledgements

Several observers using the facilities at Vainu Bappu Observatory have contributed to the photometric and spectroscopic monitoring of SN 1993J. I would like to thank all of them: K. K. Ghosh, Gopal-Krishna, S. K. Jain, N. Kameswara Rao, Y. D. Mayya, M. V. Mekkaden, G. Pandey, M. Parthasarathy, A. K. Pati, A. V. Raveendran, B. E. Reddy, Ram Sagar, K. P. Singh, A. Subramaniam and R. Surendiranath.

### References

- Anupama, G. C., Kembhavi, A. K., Prabhu, T. P., Singh, K. P., Bhat, P. N. 1993, *Astr. Astrophys. Suppl.*, (in press)
- Ashoka B. N., Anupama, G. C., Prabhu, T. P., Giridhar, S., Ghosh, K. K., Jain, S. K., Pati, A. K., Rao, N. K. 1987, *J. Astrophys. Astr.*, **8**, 195.
- Branch, D. 1981, *Astrophys. J.*, **248**, 1076.
- Corwin, H. C. 1993, *IAU Circ.*, 5742.
- Dopita, M. A. 1988, *Space Sci. Rev.*, **46**, 225.
- Filippenko, A. V. 1991, in *Supernovae and Stellar Evolution*, Eds A. Ray & T. Velusamy, (Singapore: World Scientific) p. 34.
- Freedman, W. L. *et al.* 1983, *Astrophys. J.*, (submitted).
- Harkness, R. P., Wheeler, J. C. 1990, in *Spectra of Supernovae*, Ed. A. G. Petschek, (New York: Springer-Verlag) p. 1.
- Prabhu, T. P. 1985, *Bull. astr. Soc. India*, **13**, 63.
- Prabhu, T. P., Anupama, G. C. 1991, *Bull. astr. Soc. India*, **19**, 97.
- Ray, A., Singh, K. P., Sutaria, F. K. 1993, *J. Astrophys. Astr.*, **14**, 53.

- Richter, T., Sadler, E. M. 1983, *Astr. Astrophys.*, **128**, L3.
- Ripero, J. 1993, *IAU Circ.*, 5731.
- Schmidt-Kaler, T. 1991, in *Supernova 1987 A and other Supernovae*, Eds U. J. Danziger & K. Kjär, (Munich: ESO) p. 311.
- Trammell, S. R., Hines, D. C., Wheeler, J. C. 1993, *Astrophys. J.*, **414**, L21.
- Woosley, S. E. 1991, in *Supernovae*, Ed. S. E. Woosley, (Springer-Verlag) p. 202.
- Woosley, S. E., Pinto, P. A., Ensmann, L. M. 1988, *Astrophys. J.*, **324**, 466.

## Observations of SN1993j in BAO

Li Qibin & Wang Lifan *Beijing Astronomical Observatory, 100080, Beijing, China*

**Abstract.** Photometric and spectroscopic observations of SN1993j in Beijing Astronomical Observatory from April 7 to August 9 are reviewed. The observations suggest that SN1993j is undergoing a change from type IIb to type Ib/c. Evidences for global instabilities in the explosion and asymmetric geometry of the ejecta are found from the observations.

**Key words:** Supernovae: SN1993j    photometry -- spectrography.

Continuous photometric and spectroscopic observations of SN1993j have been conducted in Beijing Astronomical Observatory since April 7. *U, B, V, R, I* photometry was made with  $2048 \times 2048$  CCD attached to 60/90 cm, Schmidt telescope. The spectroscopic data have been obtained with spectroscopy attached to the 2.16 m telescope of BAO. A  $512 \times 512$  CCD camera (1 pixel  $\approx 5.3 \text{ \AA}$ ) was used as the detector. The dispersion of the spectroscopy is  $195 \text{ \AA/mm}$ . We review preliminary results in this paper, in particular the spectra of the supernova SN1993j.

From early phase photometric observations, a second maxima of the SN1993j is found. The light curves of different bands are shown in Fig. 1. The time of the second maxima in the *U, B, V, R, I* bands, obtained from spline fitting, are as the following (Zhou *et al.* 1993).

Band	<i>U</i>	<i>B</i>	<i>V</i>	<i>R</i>	<i>I</i>
Days (in April, 1993)	15.9	16.6	18.1	18.5	18.5

The subsequent rapid fading of the SN is quite unusual for a typical type II SN, and has led several groups to conclude that SN1993j is a type IIb supernova like SN1987K.

Figures 2 and 3 show the wavelength calibrated spectra in arbitrary flux scale. The spectra are dominated by hydrogen Balmer lines in early phase, later by metal lines from He, Na, Fe and Sc. The behaviour of the P-Cygni profiles is seen in hydrogen Balmer lines as well as in He  $5876 \text{ \AA}$ /Na  $5893 \text{ \AA}$  line, which are typical in early photospheric spectra of supernova of type II. The behaviour of the  $5880 \text{ \AA}$  feature is, however, unusual, its strength increases even when the photospheric temperature decreased to about 6000 K. Absorption troughs in these lines are due to resonance scattering of photons from the supernova photosphere. The measurements of the strengths of hydrogen Balmer lines show a sharp increase in the first 20 days after explosion followed by a rapid decrease to  $1.00 \times 10^{-11} \text{ erg cm}^{-2} \text{ \AA}^{-1} \text{ s}^{-1}$  at a slower rate. After April 19, a double peak appeared in the H $\alpha$  line (Hu *et al.* 1993a, b, c). The profiles can be due to either asymmetries in the explosion, or non-thermal emissions of He I. After August 8, the structure of double peak in H $\alpha$  line disappeared. It shows that the SN1993j is turning to a type Ib supernova. All these features show that the

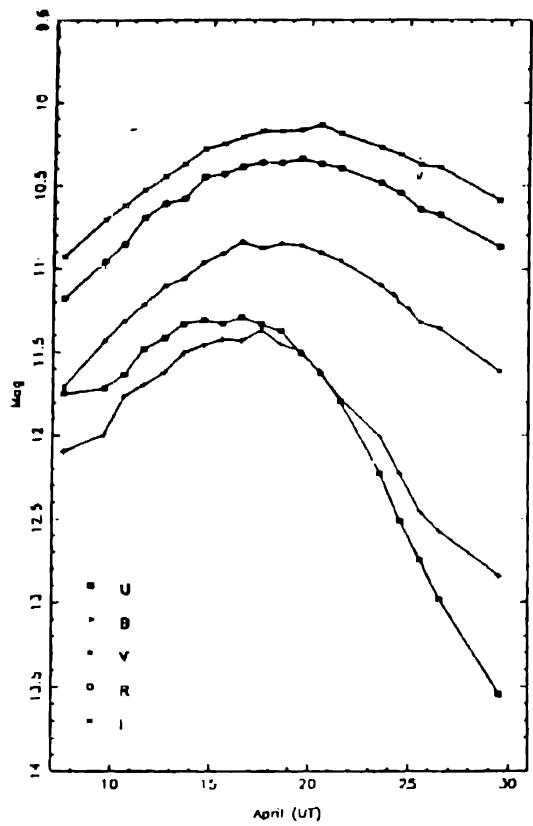


Figure 1. *U, B, V, R, I* magnitude of SN1993j.

supernova is not a typical type II supernova. Its late time behaviour is much more like a type Ib/c supernova than a type II supernova.

As the supernova debris expands and gets more transparent, nebular lines start to appear. Since April 24, [OI]5577 Å, [OI]6300, 6364 Å, was observed. The emission lines were formed primarily in the dense, deep metal rich layers of the ejecta. The profiles in this phase reflect the radial distribution of density structures and atomic level populations.

The [OI] 5577 Å line is strikingly stronger than the [OI] 6300, 6364 Å doublet. This is probably because the doublet happens to lie in the absorption trough of the P-Cygni profile of the H $\alpha$  line.

The flux ratio [OI] 6300/6364 Å  $\simeq 1$  is different from what is expected for forbidden lines. In fact, the ejecta can be so dense that the forbidden lines can be optically thick due to quadruple transitions (Wang *et al.* 1993; Wang & Hu 1993). This gives a measure of density

$$n \simeq 2 \times 10^{10}/\text{cm}^{-3}.$$

This number is in agreement with recent hydrodynamical calculations.

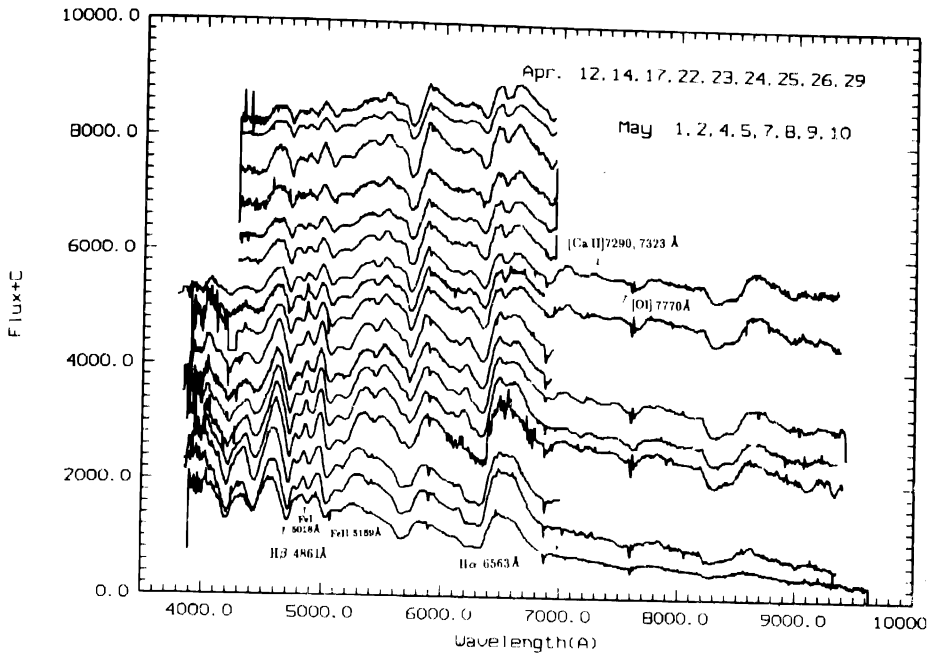


Figure 2. Spectra of SN1993j from April to May, 1993.

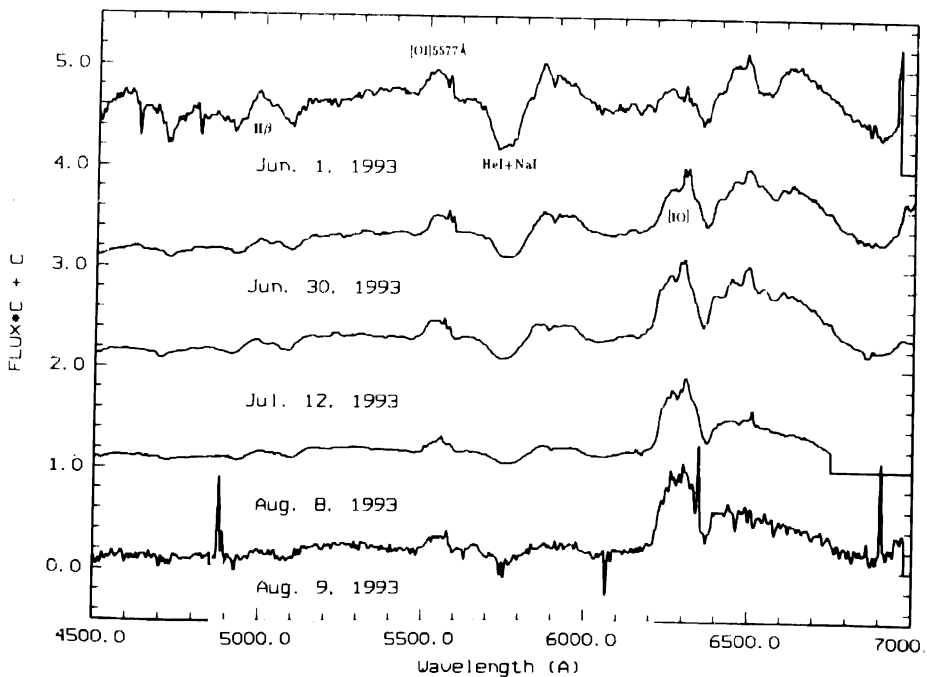


Figure 3. Some spectra of SN1993j from June to August 9, 1993.

In the recent spectra of August 8, both the [OI] 5577 and [OI] 6300, 6364 lines were fully developed and attained a ratio of about 0.25. The [OI] 5577, [OI] 6300, 6364 Å lines are blue shifted by about 1800 km/s about 30 days after explosion. This blue shift happens at such an early date that it is unlikely due to dust formation in the supernova ejecta. This may indicate that the supernova photosphere developed a complex irregular structure near maximum light, and heavy elements were brought up into the hydrogen rich layer due to strong dynamical instabilities and chemical mixing. Forbidden oxygen emission emerges from regions outside of the supernova photosphere and photons from the receding side are strongly shielded by the irregular photosphere and therefore give rise to the blue shifted line profiles (Wang & Hu 1993).

Another peculiar feature of SN1993j is that the hydrogen Balmer and oxygen lines are fine structured. This behaviour shows evidences of instabilities in supernova envelope, or clumpiness of the circumstellar medium.

To summarize briefly, we have the following conclusions:

- SN1993j is undergoing a change from type II to type Ib according to its light curve, early photosphere spectra and the disappearance of hydrogen Balmer lines;
- There are spectroscopic evidences for global instabilities and asymmetries in the explosion. The asymmetric nature of the ejecta is also firmly established by spectra polarimetric measurements of a TEXAS group.

## References

- Hu, J. Y., Wang, L. F. *et al.* 1993a, *Acta Astrophysica Sinica*, **13**, 295.  
Hu, J. Y., Wang, L. F. *et al.* 1993b, *IAU Circ.* No. 5783.  
Hu, J. Y., Li, Z. W. *et al.* 1993c, *IAU Circ.* No. 5577.  
Wang, L. F., Hu, J. Y. *et al.* 1993, *IAU Circ.* No. 5847.  
Wang, L. F. and Hu, J. Y., 1993, submitted to *Nature*.  
Zhou, X. *et al.* 1993, *Acta Astrophysica Sinica*, **13**, 293.

## Emission Line Spectrum of the Hot R Cr B Type Star MV Sgr

G. Pandey<sup>1</sup>, N. Kameswara Rao<sup>1,3</sup> & D. L. Lambert<sup>2,3</sup>

<sup>1</sup> Indian Institute of Astrophysics, Bangalore 560 034, India.

<sup>2</sup> Department of Astronomy, University of Texas at Austin.

<sup>3</sup> Visiting Astronomer Cerro Tololo Inter-American Observatory, operated by AURA under contract with National Science Foundation.

### 1. Introduction

MV Sgr is one of the hot R Cr B stars with  $T_{\text{eff}} = 15400 \pm 400$  K. (Drilling *et al.* 1984) which shows light variations of R Cr B type with magnitude range 12–16. The spectrum near maximum light has been described by Herbig (1964, 1975). In the UV (ultraviolet), the low excitation lines exist in absorption (Rao & Nandy 1982) indicative of low temperature gas seen against the continuum of the B-type star.

Higher resolution blue spectra obtained around light maximum have been analysed by Jeffery *et al.* (1988). They also discovered that the FeII emissions are split with peak separation of  $68.2 \text{ km s}^{-1}$  and FWHM of  $131 \pm 18 \text{ km s}^{-1}$ . The central minimum of the emission is nearly at line centre and therefore the mean emission line centre gives a radial velocity very close to the one given by the absorption lines. They attribute the line splitting to the large optical thickness in the line (Jeffery *et al.* 1988).

Forbidden lines of [S II] are observed in blue (Rao *et al.* 1990). Here we describe the emission line spectrum in the red region and the profiles of forbidden lines.

### 2. Observations

The observations were obtained in 1992 on May 22/23 with CTIO 4-m Echelle spectrometer. The wavelength region covered was from  $5500 \text{ \AA}$  to  $7000 \text{ \AA}$  with a resolution of  $0.08 \text{ \AA/pixel}$ . The wavelength calibration was obtained with a Th–Ar source. The spectrum reductions were done using the RESPECT package at VBO Kavalur.

### 3. Results and discussion

The spectrum is rich in emission lines predominantly due to FeII, SiII, OI, NI, Cl etc. The emission lines of HeI have superposed absorption components ( $5875 \text{ \AA}$  &  $6678 \text{ \AA}$ ). H $\alpha$  is in emission. The absorption lines due to CII, NII, SII, NeI etc. are present.

#### 3.1 Radial velocity

We have measured the radial velocity of absorption lines (NeI, NII, CII etc.) of MV Sgr as  $-94 \pm 4 \text{ km s}^{-1}$ .



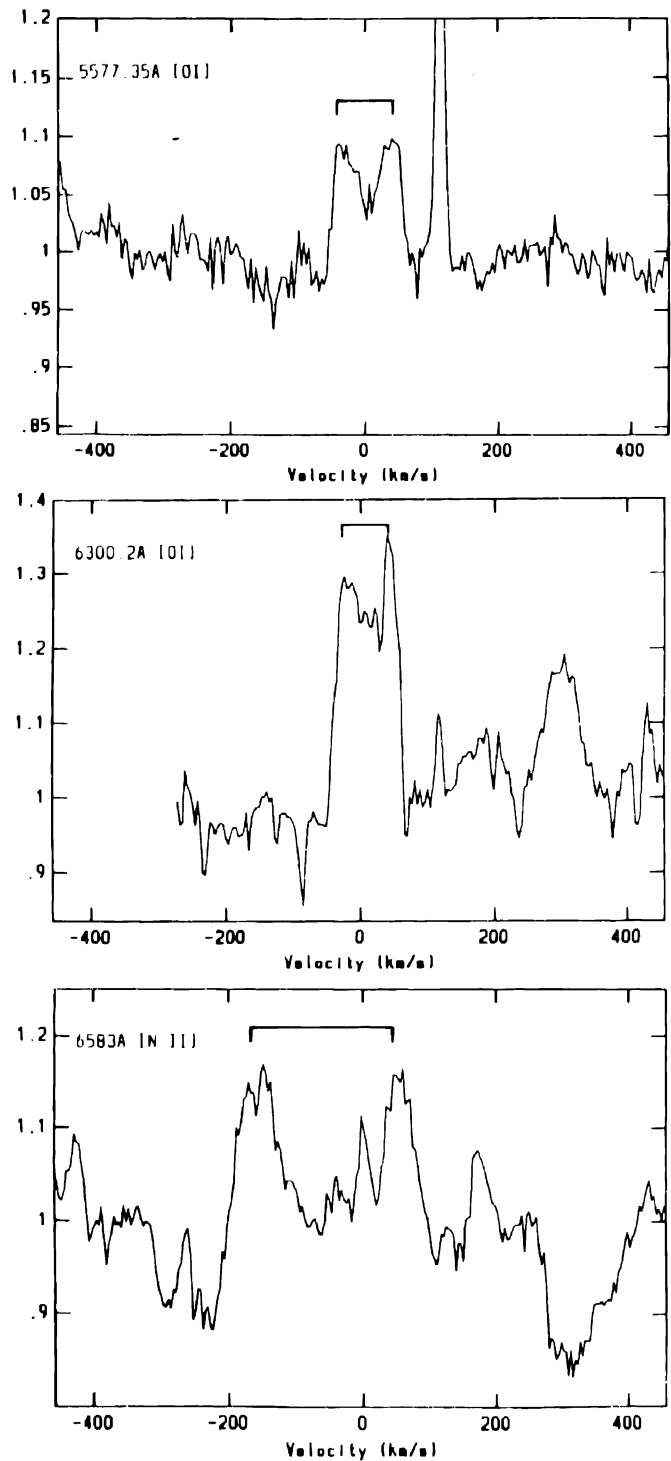


Figure 1.

### 3.2 The emission lines

The emission lines are mostly due to FeII, TiII, SiII, OI, NI, Cl etc. The forbidden lines of [OI] (6300, 6363 & 5577 Å) and [NII] (6583 & 5755 Å) are present though weak.

### 3.3 Radial velocities of emission lines

- Forbidden Lines: The [OI] (6300, 6363 & 5577 Å) are split with peak separation of  $\sim 72 \text{ km s}^{-1}$ . The central minimum of the emission is nearly at line centre and therefore the mean emission line centre gives a radial velocity very close to the one given by the absorption lines. The [NII] line (5755 Å) has a double structure and the central minimum of the emission is nearly at the line centre. (See Fig. 1).
- The FeII lines (6516, 6456, 6369, 6318 Å) are double structured with peak separation of  $68 \text{ km s}^{-1}$ . The central minimum of the emission is nearly centred on the absorption line velocity. Indicating the radial velocity of FeII consistent with stellar velocity.
- H $\alpha$  emission line has a double structure and the central minimum gives a radial velocity of  $\sim 98 \text{ km s}^{-1}$  which is consistent with  $(-94 \pm 4 \text{ km s}^{-1})$  stellar velocity.
- The central emission of HeI (5876 & 6678 Å) is red shifted and the absorption component is blue shifted showing complex profile.
- The line ratios of (6300 + 6365 Å)/5577 Å of [OI] and 6583/5755 of [NII] indicate  $n_e \approx 3.0 \times 10^6 \text{ cm}^{-3}$  and  $T_e \approx 1.6 \times 10^4 \text{ K}$ . Broad band magnitudes in *UBV* filters as given by Landolt (1979) are used with  $E(B - V) = 0.45$  to calibrate our spectra.

Since many of the nebular lines are double (well separated peaks), the line splitting cannot be attributed solely to optical thickness but also to the geometrical distribution of matter either as a ring (disc) or as bipolar flow.

### References

- Drilling, J. S., Schönberner, D., Heber, U., Lynas-Gray, A. F. 1984, *Astrophys. J.*, **278**, 224.  
 Herbig, G. H. 1964, *Astrophys. J.*, **140**, 1317.  
 Herbig, G. H. 1975, *Astrophys. J.*, **199**, 702.  
 Jeffery, C. S., Heber, U., Hill, P. W., Pollacco, D. 1988, *Mon. Not. R. astr. Soc.*, **231**, 175.  
 Landolt, A. R. 1979, *IAU Circ.* No 3419.  
 Rao, N. K., Nandy, K. 1982, *J. Astrophys. Astr.* **3**, 79.  
 Rao, N. K., Houziaux, L., Giridhar, S. 1990, *J. Astrophys. Astr.*, **11**, 37.



## Abstracts

### Infrared Spectroscopy of Accretion Disks in Young Stars

**John S. Carr** *Department of Astronomy, Ohio State University, 174 W. 18th Ave., Columbus, OH 43210 USA.*

**Alan T. Tokunaga** *Institute for Astronomy, University of Hawaii, 2680 Woodlawn Dr., Honolulu, HI 96822 USA.*

Accretion disks are considered to be central to the formation of stars and planetary systems, and they are likely to play a role in the generation of mass loss and perhaps in the regulation of stellar angular momentum in young stars. While the evidence for disks around young stars is compelling, it is largely indirect, and most of the inferred properties of disks (accretion rates, temperatures, masses) are derived by modeling broadband spectral energy distributions. It is clearly important to establish kinematic evidence for the existence of disks and to identify spectroscopic diagnostics of their physical properties. Towards this goal, we have been studying the circumstellar environment of young stellar objects (YSOs) through high-resolution infrared spectroscopy. Here we present the results of spectroscopy of the CO overtone emission in a number of young stars.

The CO molecule is a good probe of dense neutral gas near YSOs because the temperatures (2000–4500 K) and high densities required for vibrational excitation are those expected in the inner regions of circumstellar disks. Our data and disk modeling provide strong spectroscopic evidence for rotating circumstellar disks. The most dramatic case is the highly obscured young stellar object known as WL 16 (Carr *et al.* 1993, *Astrophys. J. Lett.*, **411**, L37). A Keplerian disk provides an excellent fit to the observed profile of the  $v = 2-0$  bandhead and requires a projected velocity ( $v \sin i$ ) for the CO emitting region of about  $250 \text{ km s}^{-1}$  at the inner radius and  $140 \text{ km s}^{-1}$  at the outer radius. The CO emission is marginally optically thick with a radial intensity distribution corresponding to a  $r^{-0.75}$  temperature law. The inner radius for the CO emission has an upper limit of  $8 R_{\odot}$ . In the young star 1548C27, the CO emission has a velocity dispersion about one-third that in WL 16. A Keplerian disk model fits the shape of the  $2-0$  bandhead with an inner  $v \sin i$  of  $90 \text{ km s}^{-1}$  and a  $r^{-0.75}$  temperature gradient. The minimum CO inner radius is  $11 R_{\odot}$ . Most young stellar objects with CO emission which have been observed at high-resolution show clear disk signatures or are consistent with disk origin. These include DG Tau, AS 353 A, and the BN object.

Keplerian disk models reproduce the observed shapes and fluxes of the CO bandhead emission in the majority of YSOs observed. Useful constraints can be placed on the properties of the gas in the disk, including the radial distribution of the temperature and column density, and the physical sizes. These results provide some of the best kinematic evidence for disks in the inner regions around young stellar objects.



## Polarization Variability in Isolated T Tauri Stars

M. V. Mekkaden *Indian Institute of Astrophysics, Bangalore 560 034, India.*

TW Hya and V4046 Sgr are two 'isolated T Tauri stars', in the sense that they are located far from any known dark or molecular cloud. TW Hya shows light variation with a 2.195 day period. The observed amplitudes in different wavelength bands suggest that the light variation is caused by the rotational modulation of hot regions (spots) on the stellar surface. We have found V4046 Sgr to have a 2.44 day photometric period. Observations of these objects over several seasons show that quite often they exhibit irregular light variations also.

As part of an ongoing program of polarimetric studies of T Tauri stars, TW Hya was observed in *UBVR* bands on nine nights and V4046 Sgr was observed in *BVR* bands on two nights with the 2.3 m Vainu Bappu Telescope at Kavalur during 1990-1992 with the PRL-polarimeter. The linear polarization ( $P\%$ ) and position angle ( $\theta$ ) obtained for TW Hya show large variations. The polarization observed on 24 March 1992 in B band was  $\sim 3\%$ , whereas those observed on other occasions were less than or close to 1%. The polarization does not show any appreciable dependence on wavelength on most of the occasions and hence the mechanism for polarization is most likely dust grain scattering. It is noticed that the position angles observed on two consecutive nights differ by  $\sim 80^\circ$ . There are observational evidences which show that TW Hya has active accretion disk. The rotation of the star would cause a variable illumination of the circumstellar material resulting in a net polarization.

V4046 Sgr is a classical T Tauri star with strong spectral emission features. It has a photometric period of 2.44 days. The polarization measurements were made for V4046 Sgr on 18 May 1991 and 15 March 1992. The position angles observed on these two nights remained more or less the same. But the wavelength dependence of polarization observed on 15 March 1992 was steeper than that observed on the other night. The mechanism of polarization in V4046 Sgr may be nonuniform illumination of its circumstellar envelope by a rotating spotted star.

A clear picture of the mechanism that causes the changes in polarization and position angle in stars with hot spots can be obtained by simultaneous photometry and polarimetry over a few rotation periods. These stars have active accretion disks and due to the accretion through the boundary layer hot spots are produced on the stellar surface. Polarimetric observations will help us to study the nature of the accretion disk, like the possibility of inhomogeneities in the accretion disk.

★★★★★

## Angular Diameter of Carbon Star TX Piscium from Lunar Occultation Observations in the Near Infrared

Sam Ragland, T. Chandrasekhar & N. M. Ashok *Physical Research Laboratory, Navrangpura, Ahmedabad 380 009, India.*

A program of High Angular Resolution observations of stars and their circumstellar regions using the technique of lunar occultations in the near infrared has been initiated

at Gurushikar, Mt. Abu, India (72° 47'E, 24° 39'N, 1680 m) and several occultations have been successfully observed in the K band (2.2  $\mu$ m). In this paper we discuss the observations and results from detailed analysis of a day time ( $\sim$  13:50 local time) disappearance lunar occultation of a carbon star TX Psc observed with a 14" telescope on 27th Jan 1993 at Gurushikar. A LN<sub>2</sub> cooled InSb based IR photometric system developed at PRL (Chandrasekhar *et al.* 1993) was used to record the light curve. The motivation for the present work came from a suggested world wide campaign by A. Richichi of observing TX Psc lunar occultations in the infrared in 1993-94.

A least-squares fit to the data involving source brightness, lunar velocity component in the direction of occultation and central time of occultation with a low order polynomial to simulate background light level has been carried out.

The angular diameter of a uniformly illuminated disk of TX Psc deduced from the best model fit has a value  $\phi_{LD} = 7.5 \pm 1$  milliarcseconds. The main source of error is due to the large scintillation noise present in the data due to the small telescope aperture (35 cm) and daytime observation. Our angular diameter value appears to provide a better fit to the model atmospheric calculations of this star (Eriksson *et al.* 1986) than the earlier optical occultation measurements which have a high noise content (Ridgway *et al.* 1977). We derive the stellar effective temperature from our angular diameter measurement as  $T_{\text{eff}} = 3390 \pm 200$  K.

There is no apparent signature in the occultation light curve for a circumstellar shell of extent 4-5 stellar radii at a flux level  $F_{\text{shell}}(2.2 \mu\text{m}) \geq \frac{1}{30} [F_{\star}(2.2 \mu\text{m})]$ .

### References

- Chandrasekhar, T., Ashok, N. M., Sam Ragland 1993, *Proc. of IAU Symposium No. 158, Very High Angular Resolution Imaging* (in press).  
 Eriksson, K., Gustafsson, B., Johnson, H. R., Querci, F., Querci, M., Baumert, J. H., Carlsson, M., Olofsson, H. 1986, *Astr. Astrophys.*, **161**, 305.  
 Ridgway, S. T., Wells, D. C., Joyce, R. R. 1977, *Astr. J.*, **82**, 414.



### CCD Photometry of the Young Open Cluster NGC 366

A. K. Pandey, B. C. Bhatt, V. Mohan, D. C. Paliwal & H. S. Mahra *Uttar Pradesh State Observatory, Manora Peak, Naini Tal 263 129, India.*

The open star clusters can be used to trace the evolution of the Galaxy and its present dynamical state. Open clusters are also good tools to analyse the large scale properties of the galactic disk and to test the theories of stellar and galactic evolution. To obtain fundamental information for such studies cluster's distance, age and interstellar extinction inside the star cluster are mandatory which can be derived from the colour-magnitude and colour-colour diagrams of star cluster. Such observations are lacking for most of the distant open star clusters. Therefore, we have started a systematic CCD photometric investigation of open clusters which have not been observed in

detail so far. Here we report the results of our investigations of the open cluster NGC 366.

The observations of NGC 366 were carried out in the  $U, B, V, R$  and  $I$  passbands using the Photometrics CCD 3000 system at  $f/13$  Cassagrain focus of the 104-cm reflector of the Uttar Pradesh State Observatory during October 1992 and January 1993. The multiple exposures were taken in order to achieve a total integration time of 60 minutes in  $U$ , 30 minutes in  $B$  and  $V$  and 5 minutes in  $R$  and  $I$  filters. The observations have been reduced using the Micro Vax II and Vax Stations installed with the ESO MIDAS software for image processing and DAOPHOT profile-fitting software for photometry. The photometric errors of observations ( $\pm \sigma$ ) are found to be 0.018, 0.023, 0.032, 0.017 and 0.024 mag in  $V, (B - V), (U - B), (R - I)$  and  $(V - I)$  respectively. The CCD photometry of the cluster NGC 366 in  $UBVRI$  photometric passbands down to 19.5 mag, manifests a true distance modulus of 11.66 mag corresponding to a distance of 2.15 kpc. The age of the cluster is estimated to be  $\sim 25$  Myr. The reddening in the cluster region is found to be variable having  $\Delta E(B - V) = 0.30$  mag.

The luminosity function (LF) of NGC 366 has been compared with the LFs of the other young open clusters and it is found that the luminosity functions agree fairly well towards the higher mass end. However, there is substantial variation towards the fainter end of the LF, because of a significant excess of low mass stars in NGC 366 as compared to other young clusters.

★★★★★

### Theoretical Models of Starspots\*

J. S. Park & H. S. Yun *Department of Astronomy, Seoul National University, Republic of Korea.*

In the present study a starspot is assumed to be single, circular and in magnetostatic equilibrium, whose field configuration is under the similarity law. A set of magnetostatic model starspots of late type stars ranging from G5V to K5V has been constructed that uses as parameters the ratio of effective temperature of starspots to that of its parent star  $T_{\text{eff}}^*/T_{\text{eff}} = 0.76$ , the total magnetic flux  $\Phi = 5 \times 10^{23} \text{ Mx}, 1 \times 10^{24} \text{ Mx}, 2 \times 10^{24} \text{ Mx}, 3 \times 10^{24} \text{ Mx}$  and the angle of inclination  $\psi_p = 75^\circ$  at the outer edge of the penumbra. The resulting models are summarized in Table 1.

It is demonstrated that the physical characteristics of starspots suggested by photometric, spectroscopic and magnetic observations can be accounted fairly consistently with our computed starspot models. It is found that the starspots have the total magnetic flux at least 10 ~ 100 times that of sunspots in order to maintain their sizes. The field strength is sensitive to spectral type, which increases with later spectral types. In contrast to the field strength, the area of starspots depends strongly on the total magnetic flux. Despite several differences in starspots and sunspots, it is found that they are qualitatively similar phenomena. Finally, it is hoped that the present study provides

\*This work is supported by Seoul National University Daewoo Research Fund (92-04-1047).

**Table 1.** Physical characteristics of computed model spots ( $T_{\text{eff}}^*/T_{\text{eff}} = 0.76$ ).

Parent stars	Sp. type	G5V	K0V	K5V						
	$T_{\text{eff}}(\text{K})$	5520	4900	4130						
Starspots	$T_{\text{eff}}^*(\text{K})$	4195	3720	3139						
	$\psi_p(^{\circ})$	75	75	75						
	Area(%)	1.5	4	11	1.5	4	11			
	$\Phi(10^{24}\text{Mx})$	0.56	1.2	2.6	0.68	1.5	3.2	0.82	1.8	4.0
	B(gauss)	1870	1530	1200	2670	2220	1760	4390	3580	2900



some theoretical basis for using starspots in interpreting the peculiar behaviours of stellar light curves.

★★★★★

### Effects of Differential Rotation and Tidal Distortion on the Periods of Small Adiabatic Oscillations of Stellar Models

V. P. Singh & M. K. Sharma *University of Roorkee, I.P.T., Saharanpur 247 001, India.*

We have analysed in this study, the effects of differential rotation and tidal forces on the periods of small adiabatic oscillations of Roche model of a star. The law of differential rotation of the type  $w = b_1 + b_2 s^2$ , has been assumed, where  $w$  is the angular velocity of rotation of a fluid element at a distance  $s$  from the axis of rotation,  $b_1$  and  $b_2$  are numerical constants. Terms up to second order of smallness in  $b_1$ ,  $b_2$  and  $q$  are retained. In this paper we use the approach of Mohan & Singh (1982, *Astrophys. Space Sci.*, **85**, 83) to obtain the effect of differential rotation and tidal distortion on the period of small adiabatic oscillations of a Roche model of the star. A comparison of these results with the corresponding results in which only rotational effects are considered shows that the eigen frequencies of differentially rotating Roche model increase (so that the corresponding periods of oscillations decrease in presence of tidal effects of companion star). However in absence of differential rotation the results show that with the increase in the mass of the companion star causing tidal distortion these eigen values decrease (so that the periods of oscillations increase). The value of  $\Gamma$  (ratio of specific heat) also affects eigen values; increase in the value of  $\Gamma$  increases the eigen value of the fundamental mode. The results show that compared to the undistorted model, the eigen frequencies decrease with the introduction of the angular velocity of rotation both for the case of solid body rotation as well as differential rotation. The decrease is larger in the case when angular velocity is increasing from axis of rotation to outwards compared to the case in which angular velocity decreases from axis of rotation to inwards. The cases where it partially increases and partially decreases are also presented. Our result shows that none of the models are found unstable as the fundamental modes in every case are positive.

★★★★★

### Stochastic Radial Pulsation of Gaseous Masses

Anunay K. Chaudhary<sup>1</sup>, M. K. Das<sup>2</sup>, R. K. Tavakol<sup>3</sup>, V. B. Bhatia<sup>1</sup>

<sup>1</sup>Department of Physics and Astrophysics, University of Delhi, Delhi 110 007, India

<sup>2</sup>Sri Venkateswara College, University of Delhi, Dhaura Kuan, New Delhi 110 021, India

<sup>3</sup>Queen Mary and Westfield College, London.

Recent studies of the photometric data of most of the variable stars suggest irregularity superimposed on the regular trend. The nonlinear theoretical modelling of stellar

**Table 1.** Statistical parameters obtained for stochastic pulsation equation (1).

Parameter	$\epsilon$	Method-I	Method-Ia	Method-II	FPE
$n = 1.5, A = -2.36058, B = 3.82764, \beta = 0.1$ and $\Gamma = 1.0$					
$E[X]$	0.05	0.11675618	0.11608376	0.11608376	0.11668377
	0.20	0.31021487	0.32692114	0.32692115	0.30789209
$E[X^2]$	0.05	1.03760470	1.01183360	1.01183360	1.03722220
	0.20	1.03397240	0.98219118	0.98219118	1.04914560
$n = 3.0, A = -0.990245, B = 1.45628, \beta = 0.1$ and $\Gamma = 1.0$					
$E[X]$	0.05	0.04867923	0.04880220	0.04880219	0.04867154
	0.20	0.15335832	0.15949124	0.15949124	0.15318644
$E[X^2]$	0.05	1.00091370	0.99636821	0.99636821	1.00087540
	0.20	0.96156988	0.93442869	0.93442869	0.96374422

variability has been proved to be of great help in analysing some of the intricate features. However, the nonlinear dynamical studies of a system are usually confined only to the predominant principal radial modes. Recently, inadequacy of the mean field equations describing a dynamical system has been pointed out in (Hoyng 1987, *Astr. Astrophys.*, **171**, 348; Moss *et al.* 1992, *Astr. Astrophys.*, **265**, 843). In view of the importance of higher degrees of freedom, though may be of smaller amplitudes, in shaping the observed systematics we simulate the effect of such terms by a random fluctuating term  $f(t)$ . In connection with stellar variability problems, we have considered the nonlinear radial pulsation of a simple polytropic model, described by the following equation:

$$\ddot{q} + \beta\dot{q} + q + A\lambda q^2 + B\lambda^2 q^3 = \Gamma f(t), \quad (1)$$

with the random fluctuating force, modelled by  $\delta$ -correlated white gaussian noise. Various statistical parameters, listed in Table 1, are obtained by using the following approximate techniques: Cumulant-Neglect Closure Technique (Das *et al.* 1993, in preparation) (fourth order closure: Method I and Gaussian Closure: Method Ia), Equivalent Linearization Technique (Chaudhary *et al.* 1993, in preparation) (Method II) and Fokker-Planck Method (FPE). The results obtained could be summarized as follows:

- For a given value of damping coefficient  $\beta$  and the nonlinearity factor  $\epsilon$ , and the noise strength  $\Gamma$ , the stationary values of the moments, e.g., mean and mean square displacement of the response decrease with an increase in the central condensation of the system.
- For a given polytrope,  $\Gamma$  and  $\beta$ , these moments decrease with an increase in  $\epsilon$ .
- Stationary Non-Gaussian response of the system differs considerably from the Gaussian response in polytropes with lower central condensation.

## Non-Linear Stability of a Cluster of Stars Sharing Galactic Rotation

**K. B. Bhatnagar & P. P. Hallan** *Department of Mathematics, Zakir Husain College, Delhi University, Jawaharlal Nehru Marg, New Delhi 110 002, India.*

In this paper the non-linear stability of an ellipsoidal cluster of stars sharing galactic rotation has been studied. Chandrasekhar (1942) considered the motion of a cluster of stars sharing galactic rotation and moving in a field having both an axis and a plane of symmetry. The Lagrangian function  $L$  for a star of mass  $m$  of the cluster is given by

$$L = T - mB - \Omega,$$

where  $T$  is the kinetic energy,  $B$  is the general gravitational potential and  $\Omega$  is the potential energy of the star. If the smoothed out distribution in the cluster is approximated to a homogeneous ellipsoid, then  $\Omega$  has the form

$$\Omega = -\frac{1}{2}m\beta_0 + \frac{1}{2}\left(\beta_1x^2 + \beta_2y^2 + \beta_3z^2\right),$$

where  $\beta_0, \beta_1, \beta_2, \beta_3$  are constants depending on the density  $\rho$  and the geometry of the ellipsoid, i.e.

$$\beta_i = \pi G \rho \beta'_i(a:b:c), \quad i = 0, 1, 2, 3.$$

$\beta'_i$  is a number depending on the ratios of the axis  $a, b$  and  $c$  of the ellipsoid;  $x, y, z$  are the coordinates of the star referred to a frame of reference  $C - XYZ$  rotating uniformly about  $Z$ -axis which is perpendicular to the galactic plane and  $X$ -axis is along  $OC$ , the line joining  $O$  (the centre of the galaxy) to  $C$  (the Centre of gravity of the cluster). Assuming that the dimensions of the cluster are small compared to  $\omega_0$  ( $\omega_0 = OC$ ) and neglecting all quantities of order more than one in  $x, y, z$ , it is found that the solutions of the linearized equations of motion are circular functions and therefore correspond to stable oscillations if  $\rho > \rho^*$ , where the critical value  $\rho^*$  of the density is given by (Chandrasekhar 1942)

$$\rho^* = \frac{0.165}{\beta'_1}.$$

Thus Chandrasekhar has considered the stability of the cluster of stars in the linear sense. In the present study the non-linear stability of the cluster is studied. This is done by applying Arnold's Theorem (1963) which states that if

- (i)  $K_1\omega_1 + K_2\omega_2 + K_3\omega_3 \neq 0$  for all triplet of integers  $K_1, K_2, K_3$  such that  $|K_1| + |K_2| + |K_3| \leq 4$  and
- (ii) determinant  $D \neq 0$  where  $\omega_1, \omega_2, \omega_3$  are the basic frequencies for the linear

dynamical system.

$$D = \det. \left( b_{ij} \right), \quad (i, j = 1, 2, 3, 4),$$

$$b_{ij} = \left( \frac{\partial^2 H}{\partial I_i \partial I_j} \right) I_i = I_j = 0 \quad (i, j = 1, 2, 3),$$

$$b_{i4} = b_{4i} = \left( \frac{\partial H}{\partial I_i} \right) I_i = I_j = 0 \quad (i = 1, 2, 3),$$

$$b_{44} = 0$$

$$H = \omega_1 I_1 + \omega_2 I_2 + \omega_3 I_3 + \frac{1}{2} \left( a I_1^2 + b I_2^2 + c I_3^2 + 2f I_2 I_3 + 2g I_3 I_1 + 2h I_1 I_2 \right)$$

is the normalized Hamiltonian with  $I_1, I_2, I_3$  as the action momenta coordinates, then the equilibrium is stable. The procedure followed is similar to that adopted by Bhatnagar & Hallan (1983). First of all first order normalization is done by the method given in Whittaker (1965). Then second order normalization is done for which Birkhoff's normalization is performed by expanding the coordinates  $x, y, z$  in double D'Alembert's series. While applying Arnold's Theorem (1963), we have assumed that  $\omega_1 > \omega_2 > \omega_3$ . The correct ordering of the frequencies  $\omega_1, \omega_2$  and  $\omega_3$  depends on the geometry of the ellipsoidal form of the cluster and ordering of the constants  $\beta_1, \beta_2$  and  $\beta_3$ . We have made the assumption  $\omega_1 > \omega_2 > \omega_3$  just to illustrate the procedure to be adopted for deciding the stability of the cluster.

We have found that the ellipsoidal cluster of stars sharing galactic rotation is stable in the non-linear sense for all densities  $\rho > \rho^*$  and for the range of linear stability except where Arnold's Theorem is not applicable.

### References

- Arnold, V. I. 1963, *Russian Math. Surveys* (London Math. Soc.) **18**, 86–101.  
 Bhatnagar, K. B., Hallan, P. P. 1983, *Celestial Mechanics*, **30**, 97–114.  
 Chandrasekhar, S. 1942, *Principles of Stellar Dynamics*, (New York: Dover Publications) pp. 213–223.  
 Whittaker, E. T. 1965, *A Treatise on the Analytical Dynamics of Particles and Rigid Bodies* (London: Cambridge University Press) pp. 427–430.

★★★★★

### Some Unidentified Features in the IRAS LRS Spectra of Cool Peculiar Stars

M. S. Vardya & K. S. Krishna Swamy *Tata Institute of Fundamental Research, Bombay 400 005, India.*

Generally, it is believed that M-spectral type stars evolve to S-type, which in turn

go to C-type. Normally, circumstellar shells formed due to mass loss show silicate features in M-type stars and silicon carbide in C-type stars. Recently, surprisingly, silicate emission features have been observed in some C-type stars as well. This has led to the suggestion that some M stars may evolve straight to C stars without the intermediate S phase. Low dispersion spectra are available of many of these and other peculiar stars from the IRAS. Many of these show a lot of weak features, identification of some of which may hopefully elucidate the true evolutionary nature of the stars. Our attempt in this direction has led us, in seven HCN stars, to tentatively identify 18 hydrogen recombination lines between 10.8 and 22.5  $\mu\text{m}$  wavelength range, originating from  $n = 7$  to 20, with  $\Delta n = 1$  to 10, as well as three features which may be due to helium.

★★★★★

### Short Time-Scale Monitoring of SiO Maser Sources

Antony Joseph & C. S. Shukre *Raman Research Institute, Bangalore 560 080, India*

With an aim to monitor the SiO maser emission from Mira variable stars at relatively short time intervals, starting in January 1993 dual polarization observations were done using the Raman Research Institute's 10.4 m millimeter wave telescope. Maser emission was observed at 86.243 GHz in the  $v = 1, J = 2-1$  transition of SiO for fifteen stars at about two weeks interval. This paper is a preliminary report of these observations from January–May 1993. The details about the observational system and method are given (Patel N. A. 1990, Ph.D. Thesis, Indian Institute of Science, Bangalore and Patel N. A., Joseph A., Ganesan R. 1992 *J. Astrophys. Astr.* **13**, 241). The system temperature (DSB) in each polarization on a good day was about 600 K, leading to an RMS of 0.11 K for an integration of 600 sec.

The sources selected were TX Cam, R Leo, VY Cma, OMC-1, VX Sgr, RX Boo, U Ori, U Her, R Cas, R Aqr, Omicron Ceti, Mu Cep, W Hya, R Cnc, S Crb, Chi Cyg, R Dor, S Per, WX Psc, AH Sco, NML Tau and RT Vir. Here we report only on four sources R Leo, RX Boo, TX Cam, and U Ori.

Generally the line profiles, width and line centres did not vary much in the monitoring interval. Our observations agree with previous observations of R Leo and TX Cam (Martinez A., Bujarrabal V., Alcolea J. 1988, *Astr. Astrophys. Suppl.*, **74**, 273). For RX Boo which is a SRB star the peak in SiO maser emission is seen at phase = 0.08. The rise in antenna temperature in about one day is a factor of 3 (more than 6 sigma). Values of parallactic angles also indicate substantial changes in polarization over the same time interval. A second maximum is seen at phase 0.33, curiously enough a quarter of the period after the first one. In both Rx Boo and TX Cam close to 100% linear polarization was seen on some days. In U Ori the SiO maser maximum seems to occur at phase = 0.18 and variations in both intensity and polarization with phase are indicated by observations.

★★★★★

## Coulomb Excitation and Production of P-Elements

H. L. Duorah<sup>1,2</sup> & K. Duorah<sup>1</sup>

<sup>1</sup>*Department of Physics, Gauhati University, Guwahati 781 014, Assam, India.*

<sup>2</sup>*Inter University Centre for Astronomy and Astrophysics, Ganeshkhind, Pune 411 007, India.*

In a  $Z$ - $N$  plot of the elements one observes that certain elements are proton-rich and are by-passed in the slow and rapid neutron capturing chains. These proton-rich elements are supposed to have been processed via rapid proton-capturing chain in the super-nova envelope (Duorah 1968). They are also thought to be produced via  $(\gamma, n)$  reactions. Neutrino interactions are also being considered. Till now the abundance distribution of these elements has not been explained in a satisfactory manner. An attempt is made here to examine the Coulomb dissociation of the pre-existing s-elements in a hot astrophysical environment. The nuclei are accelerated in the Coulomb field of other charges where pulses of virtual quanta are emitted. These high frequency pulses result from the Coulomb de-excitation of the nuclei and they break up the neutron-rich elements. There was a suggestion by Migdal (1973) that in neutron-rich elements there was the possibility of two neutrons forming a cluster. Depending on their binding in the nuclei, they may get dissociated under the action of the high frequency pulse leaving behind the proton-rich elements. We assume here that the s-elements undergo Coulomb acceleration in the field of a proton and they move in such a way that only electromagnetic interaction is effective. We then try to examine the abundance of p-elements resulting from the  $(\gamma, 2n)$  reaction on the s-elements.

The photodisintegration reaction  $B(\gamma, X)A$  is the inverse of the radiative capture reaction  $A(X, \gamma)B$ . The photodisintegration cross-section  $\sigma_{\text{photo}}$  is always favoured over  $\sigma_{\text{cap}}$  (Rolf & Barnes 1990) under the circumstances. The high flux spectrum of virtual photons are produced by the time-varying electromagnetic field. The copious source of virtual photon offers a promising way to study the disintegration process, where the cross-section for Coulomb dissociation is obtained approximately from

$$d\sigma_{\text{diss}}/dE_{\gamma} = N_{\gamma}(E_{\gamma})d\sigma_{\text{photo}}(E_{\gamma}). \quad (1)$$

We consider large impact parameter to ensure that there is no influence of the strong nuclear field. The minimum of the impact parameter is taken after Cline (1986)

$$R = 1.25(A_p^{1/3} + A_t^{1/3}) + 5, \text{ fm} \quad (2)$$

where  $A_p$  and  $A_t$  represent the mass numbers of the projectile and the target respectively in the case in point. The virtual photons in the high frequency limit are calculated from Jackson (1974). Using the expression for the Coulomb dissociation cross-section from Bertulani & Baur (1988), we have found that this lies between 1 and 10 millibarns. The photon number per unit energy interval is then found to lie between  $2-3 \times 10^4$ . The production rate of p-elements is then obtained. The abundances of the elements so obtained are then normalized to the abundance of  $^{122}\text{Te}$ , which was in turn normalized to  $\text{Si} = 10^6$ .

A comparison between the calculated and observed values show that the agreement is sufficiently good. It shows that production of p-element due to Coulomb dissociation in certain astrophysical setting is quite likely. We have mainly considered here the

( $\gamma, 2n$ ) type of reactions. The Coulomb excitation due to electron in the high temperature conditions may be crucial and it is suggested that a comprehensive study of Coulomb excitation is called for the understanding of this element build-up process in astrophysics. A detailed version of the work will be published elsewhere.

### References

- Bertulani, C. A., Baur G., 1988, *Nucl. Phys. A* **480**, 615.  
Cline, D. 1986, *Ann. Rev. Nucl. Part. Sci.* **36**, 363.  
Duorah, H. L. 1968, *Indian. J. Pure Appl. Phys.* **6**, 289.  
Jackson, J. D. 1974, *Classical Electrodynamics*, (John Wiley and Sons).  
Migdal, A. B. 1973, *Soviet J. Nucl. Phys.* **16**, 238  
Rolf, C., Barnes, C. A. 1990, *Ann. Rev. Nucl. Part. Sci.* **40**, 45.

★ ★ ★ ★ ★

# **Sun and the Solar System**





## Probing the Solar Interior

**S. M. Chitre** *Tata Institute of Fundamental Research, Homi Bhabha Road, Bombay 400 005, India*

**Abstract.** The internal layers of the Sun are not directly accessible to observations, but the powerful handles provided by the measurement of solar neutrino flux and by the helioseismic data have considerably enhanced our knowledge of the physical conditions prevailing inside the Sun. The standard solar model appears to describe the profiles of internal density and temperature reasonably well. It is suggested that a cooler solar core is not a viable solution of the solar neutrino puzzle, the answer to which should probably be sought in the realm of particle physics.

**Keywords:** Solar interior – solar neutrino – solar models and seismology.

### 1. Introduction

The interior of our Sun is clearly not accessible to direct observations; nevertheless, it is possible to construct a reasonable picture of its inside. This is accomplished through a combination of theory and observations. It is a triumph of the theory of stellar structure that with the help of a set of mathematical equations governing the mechanical and thermal equilibrium of stars together with the boundary conditions provided by observations, one can infer the conditions prevailing inside the Sun. The central problem of the theory of stellar structure is to determine the density, pressure and temperature, particularly, their radial variation throughout the solar interior.

### 2. Basic structure equations and input physics

#### 2.1 Governing equations

The structure of stars is governed by conditions of mechanical and thermal equilibrium. The mechanical equilibrium condition ensures that the pressure at any point in the interior is adequate to support the weight of the overlying layers. For a spherical star, we can express the mechanical equilibrium by the following equations,

$$\frac{dP(r)}{dr} = -\frac{Gm(r)}{r^2} \rho(r),$$

$$\frac{dm(r)}{dr} = 4\pi^2 r \rho(r).$$

Here  $P(r)$  is the pressure,  $\rho(r)$ , the density and  $m(r)$  the mass interior to radius  $r$ .

For thermal equilibrium, the energy loss at the surface as measured by its luminosity must be compensated by the energy released by nuclear processes in the stellar interior:

$$-\frac{dL(r)}{dr} = 4\pi^2 r \rho \epsilon,$$

where  $L(r)$  is the luminosity and  $\epsilon$  is the energy generation rate per unit mass. The condition that the flux of energy must be transported from the region where it is generated to the surface from which it is radiated determines the temperature gradient in the star. In much of the solar interior, for example, the energy is transported by radiative processes and the flux of radiation,  $F_{\text{rad}}$  is related to the temperature gradient by the equation:

$$F_{\text{rad}} = -K_{\text{rad}} \frac{dT}{dr},$$

where the radiative conductivity,  $K_{\text{rad}} = (4acT^3/3\kappa\rho)$ . Here  $c$  is the speed of light,  $a$  the Stefan-Boltzmann constant and  $\kappa$  is the opacity so defined that  $(\kappa\rho)^{-1}$  is the mean free path of a photon. If the temperature gradient becomes too steep, the layer becomes unstable towards convection and the energy is transported mainly by convective motions and partly by radiative processes. The instability condition for the onset of convection is  $\nabla > \nabla_{\text{ad}}$ , where  $\nabla = d \ln T / d \ln P$  and  $\nabla_{\text{ad}} = (\partial \ln T / \partial \ln P)_s$ . Such a condition obtains in the outer layers of the Sun where the temperature is upwards of  $10^4$  K and consequently in the hydrogen ionization zone the opacity increases rather sharply in the process causing the temperature gradient to steepen. The convective flux,  $F_{\text{conv}}$  is written as

$$F_{\text{conv}} = -K_{\text{turb}}(\nabla - \nabla_{\text{ad}}) \frac{1}{H_p} \quad (H_p = \text{pressure scale - height}),$$

where an approximate expression for the turbulent conductivity is provided by a mixing-length theory.

These structure equations need to be supplemented by auxiliary equations incorporating the input physics which describes the thermodynamic state of the gas through the equation of state, the opacity and the nuclear energy generation rate:

$$P = P(\rho, T, X, Y, Z),$$

$$\kappa = \kappa(\rho, T, X, Y, Z),$$

$$\epsilon = \epsilon(\rho, T, X, Y, Z).$$

Here  $X, Y, Z$  are respectively the hydrogen, helium and heavy element concentrations by mass.

The computations of stellar models depend on the assumed physical inputs of matter in the star: the equation of state, the opacity and the nuclear reaction rates. The conventional approach in stellar evolutionary calculations is to adopt a homogeneous initial chemical composition and the mass of the star and then evolve the star to yield its luminosity and the radius at its present age. In practice, however, for evolving the Sun,

it is convenient to adjust the initial helium abundance,  $Y_0$  and the mixing-length parameter,  $\alpha$  ( $=$  mixing length/ $H_p$ ) to fit the solar radius and luminosity. Thus, it is customary in such 'standard' stellar models to neglect effects of microscopic diffusion, overshoot from convective envelopes or cores, mass loss or accretion of material and mixing arising from rotational instabilities, the presence of rotation and magnetic fields and the consequent departure from spherical symmetry.

## 2.2 State of matter

In a large part of the solar interior (particularly, at temperatures exceeding  $10^7$  K and densities exceeding  $100 \text{ g cm}^{-3}$ ) the material is essentially completely ionized. An ideal gas law is then the simplest approximation to the equation of state and the pressure is given by

$$P = \frac{k_B}{m_H \mu} \rho T = \frac{R}{\mu} \rho T,$$

( $k_B$ , Boltzmann constant,  $m_H$  mass of hydrogen atom) where  $R = (k_B/m_H)$  is the gas constant. When the number of nuclei and electrons contributed by hydrogen, helium and heavy elements are taken into account, the mean molecular weight,

$$\mu = \frac{1}{2X + \frac{3}{4}Y + \frac{1}{2}Z}$$

Clearly, this simple description of the state of matter is inadequate in the outer parts of the Sun. In these regions, both hydrogen and helium undergo various stages of ionization before getting essentially completely ionized at temperatures exceeding 200,000 K. Furthermore, ionization also leads to a local decrease of  $\nabla_{\text{ad}} = (\partial \ln T / \partial \ln P)_s$  and  $\Gamma_1 = (\partial \ln P / \partial \ln \rho)_s$  in different zones in the stellar atmosphere. This is displayed in Fig. 1 for the solar envelope where  $\Gamma_1$  is lowered from its ideal value of 5/3 to about 1.21 in H and HeI ionization zones, whereas in the HeII ionization zone  $\Gamma_1$  falls only to about 1.58.

The ionization equilibrium is described by the Saha equation which for a simple hydrogen plasma (without molecules) takes the form

$$\frac{n_H}{n_H + n_e} = \frac{h^3}{(2\pi m_e k_B T)^{3/2}} \sum_i g_i e^{-E_i/k_B T}.$$

Here  $n_H$ ,  $n_H + n_e$  are respectively the number densities of neutral hydrogen atoms, protons, electrons and  $g_i$  and  $E_i$  are the statistical weight and the (negative) energy of the internal states of the hydrogen atom. In the simplest approximation, the equation of state avoids the problem of the divergence in the sum by including only the ground state. The Saha equation then becomes

$$\frac{n_e - n_H}{n_H} = 2 \frac{(2\pi m_e k_B T)^{3/2}}{h^3} e^{-I/k_B T},$$

where  $I = -E_0$  is the ionization potential of hydrogen.

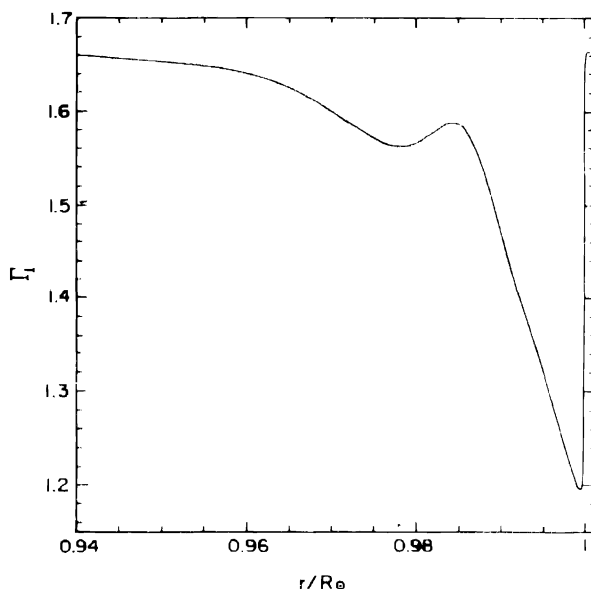


**Figure 1.** Adiabatic index,  $\Gamma_1 = (\partial \ln P / \partial \ln \rho)$  as a function of the fractional solar radius.

Additional corrections to the ideal gas law include the effects due to pressure ionization, electron degeneracy, core packing, plasma screening and Coulomb free energy between the charged particles (cf. Eggleton, Faulkner & Flannery, 1973; Mihalas, Hummer & Däppen, 1988; Rogers & Iglesias, 1992). These have now been incorporated and tables of the equation of state are available as a function of density, temperature and chemical composition.

### 2.3 Opacity

The opacity of solar material depends on a host of atomic processes involving many elements and several stages of ionization. The solar material prevents the radiant energy from streaming out unhindered – part of it is absorbed and part scattered, and the opacity basically incorporates this interaction between matter and radiation. In computations of stellar models it has been customary to use opacity tables given as a function of density, temperature and the chemical composition. The calculations have been based largely on the Los Alamos opacities tabulated by Cox & Tabor (1976). Recently, it has been demonstrated that the opacity of stellar material at moderate temperatures  $T \gtrsim 10^5$  K) had previously been underestimated. The detailed opacity calculations including the contribution from the line sources (Fe, Mg etc) has made a substantial difference to the opacity values (hereafter referred to as OPAL Opacities) (cf. Rogers & Iglesias 1992). It is evident from Fig. 2 that the OPAL opacities are larger than the Los Alamos opacities by as much as a factor of 2–3 in the temperature-range  $10^5$ – $10^6$  K and this is caused when the line sources arising from Fe etc. are included in the opacity calculations.

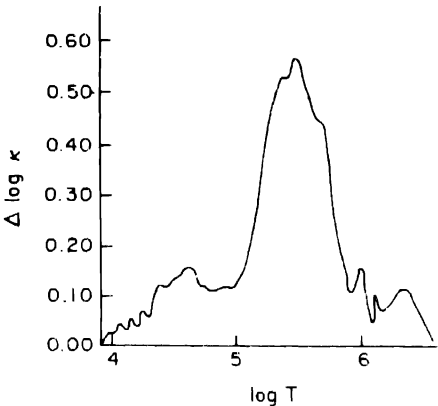


**Figure 2.** Opacity increase in the OPAL calculations of Rogers & Iglesias (1992) over the corresponding Los Alamos opacity computations of Cox & Tabor (1976).

2.4 Nuclear reactions

The basic energy source for the Sun is the fusion of four protons to form one helium atom having a mass that is less than the combined mass of the original four protons by 0.8 per cent. This mass-defect when converted into energy provides the source for the Sun to shine with almost unvarying brightness. The Sun derives nearly 99 per cent of its energy from the proton–proton chain which is shown in Table 1. An additional minor (about 1 per cent) contribution comes from the CNO cycle, which constitutes another route whereby hydrogen can be converted into helium.

**Table 1.**

Reaction	Neutrino energy (MeV)
$p + p \rightarrow {}^2\text{H} + e^+ + \nu_e$	$\lesssim 0.42$
or	
$p + e^- + p \rightarrow {}^2\text{H} + \nu_e$	1.44
${}^2\text{H} + p \rightarrow {}^3\text{He} + \gamma$	
${}^3\text{He} + {}^3\text{He} \rightarrow {}^4\text{He} + 2p$	
or	
${}^3\text{He} + {}^4\text{He} \rightarrow {}^7\text{Be} + \gamma$	
${}^7\text{Be} + e^- \rightarrow {}^7\text{Li} + \nu_e$	0.86
${}^7\text{Li} + p \rightarrow 2{}^4\text{He}$	
or	
${}^7\text{Be} + p \rightarrow {}^8\text{B} + \gamma$	
${}^8\text{B} \rightarrow {}^8\text{Be}^* + e^+ + \nu_e$	$\lesssim 14.6$
${}^8\text{Be}^* \rightarrow 2{}^4\text{He}$	

In the nuclear reaction involving the fusion of four protons into one helium atom, the number of leptons must, of course, be conserved and this leads to the production of two neutrinos. It is clear from the proton-proton chain that the fusion of hydrogen may proceed through a number of different paths, and the average neutrino losses in the three branches amount to 0.26 MeV, 1.06 MeV and 7.46 MeV respectively. The total amount of energy liberated in the reaction leading to the formation of a helium atom from the fusion of four protons is 26.73 MeV less the energy carried away by neutrinos. Nearly all of the neutrinos from the  ${}^8\text{B}$  decay originate in the inner 5 per cent of the solar mass, while the flux of neutrinos from the proton-proton reaction which generates the solar luminosity occurs in the intermediate region between 5 per cent and 40 per cent of the solar mass. The detection of solar neutrinos released by the nuclear reaction network operating in the Sun's core provides a valuable diagnostic of physical conditions in the central region of the Sun.

### 3. Probes of the solar interior

These are three possible methods available for probing the interior of the Sun

- a) Solar quadrupole moment.
- b) Solar neutrinos.
- c) Solar seismology.

#### (a) *Solar quadrupole moment*

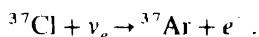
This method makes use of the possible gravitational quadrupole moment of the Sun due to rapid rotation or intense magnetic field in the solar interior. Both these force-fields are expected to contribute a higher-order term to the gravitational quadrupole moment. One of the most important aspects of rotation is that it provides a crucial test of Einstein's general theory of relativity. The test depends on measurements of planetary orbits which should be ellipses under Newton's inverse square law of gravity. After correcting for the planetary interactions, the residual orbit of planet Mercury turns out to be a rotating ellipse that precesses about the Sun at 43 seconds of arc per century. The excellent agreement between theoretical expectations of general relativity and observations of the precession of the perihelion of Mercury and other independent evidence from the gravitational deflection of starlight grazing the Sun have lent support to the validity of GTR. This suggests that there is no substantial quadrupole moment associated with the Sun.

It is now well established that the precession of the orbit of planet Mercury is well explained by the general theory of relativity; this explanation is based on the assumption that the Sun is spherically symmetrical. But the presence of rotation or magnetic field will cause a bulging at the equator and a flattening at the pole and such an oblateness will modify the Sun's gravitational field by contributing a higher-order term to the potential. This could perturb the objects in the vicinity of the Sun in such a way as to induce a precession of Mercury's orbit of the kind that is observed. Unfortunately, to account for the full observed precession of 43 seconds of arc per century would require the Sun to be much more oblate than what was observed. From the shape of the visible surface, the solar oblateness has been measured by Dicke, Kuhn & Libbrecht (1987) to be less than 2 parts in  $10^5$ .

## (b) Solar neutrinos

This probe requires the exceedingly difficult measurement of neutrinos resulting from the nuclear reactions taking place in the solar core. Under conditions prevailing in the solar interior the photons have a mean free path of less than a cm, thus requiring over 10 million years for radiation to flow from the centre to the surface, while the electron neutrinos have a mean free path of the order of several A.U and traverse the solar body under 3 seconds. Thus, the neutrinos emitted in a number of nuclear reactions occurring in the energy-generating regions of the Sun enable us to 'see' into the depths of the solar core. The measurement of the flux of solar neutrinos is, therefore, expected to provide a direct handle on the physical conditions prevailing in the central regions of the Sun. The capture rate of solar neutrinos are expected to provide us with stringent boundary conditions for constructing detailed models. As a result of the strong temperature-dependence of the nuclear reaction rate ( $T^{18}$  for  $^8B$  neutrinos), a measurement of this flux even to an accuracy of some 50 per cent is likely to determine the central temperature of the Sun to better than 5 per cent.

The Homestake experiment of Davis has been operating for over 25 years and has a tank containing 615 tons of liquid perchloroethylene ( $C_2Cl_4$ ), located some 4850 feet underground. In this  $^{37}Cl$  nuclei are the solar neutrino absorbers according to the reaction (threshold of 0.814 MeV):



The predicted capture rate for the chlorine experiment calculated by Bahcall & Pinsonneault (1992) for a standard solar model adopting OPAL opacities in units of the Solar Neutrino Unit (SNU) defined as  $10^{-36}$  captures per target atom in the detector per second is:

$$(\Phi_\nu)_{Cl}^{pred} = 7.2 \pm 2.7 \text{ SNU}.$$

The various capture rates from different neutrino-sources are listed in Table 2.

Clearly, for the chlorine experiment the capture rate is dominated by the  $^8B$  neutrinos, with the  $^7Be$  neutrinos making a significant contribution.

It turns out that the calculated neutrino fluxes are critically dependent on the input physics. For example, the capture rates are particularly sensitive to the relatively modest changes in iron abundance and the reaction rate of  $^7Be + p$ . Thus, the

**Table 2.**

Neutrino source	Capture rate (SNU)	
	(Chlorine experiment)	(Gallium experiment)
$(\Phi_\nu)_{pp}$	0	70.8
$(\Phi_\nu)_{pep}$	0.2	3.1
$(\Phi_\nu)_{^7Be}$	1.2	35.8
$(\Phi_\nu)_{^8B}$	6.2	13.8
$(\Phi_\nu)_{^{13}N}$	0.1	3.0
$(\Phi_\nu)_{^{15}O}$	0.3	4.9



uncertainty in the cross-section of  ${}^7\text{Be} + p \rightarrow {}^8\text{B} + \gamma$  reaction causes a difference of 1.7 SNU for Cl, making the result between the predicted and measured neutrino fluxes more discrepant, while the change in the iron abundance from the photospheric to a lower meteoritic value leads to a decrease in the neutrino capture rate of about 1.3 SNU.

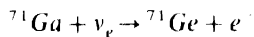
The measured neutrino capture rate reported for the chlorine experiment averages to

$$(\Phi_\nu)_{\text{Cl}}^{\text{obs}} = 2.26 \pm 0.24 \text{ SNU},$$

which is evidently inconsistent with the predicted rate, being about 31 per cent of the expected flux.

A second experiment, the Kamiokande II, consists of a water detector located about 1000 m underground in the Kamioka mine. The entire tank, containing 3000 tons of water, out of which only the inner 680 tons are used for the solar neutrino experiment. In the Kamioka facility, charged particles are detected by measuring Cerenkov light and has a threshold of 7.5 MeV. The experiment is thus exclusively sensitive to the  ${}^8\text{B}$  neutrinos, but it provides the advantages of  $(\nu - e)$  scattering measurements including record of accurate spectral times of all events and directionality of the recoil electrons. As in the case of the chlorine experiment, the measured rate of neutrino events recorded by the Kamiokande set up is also deficient and is about 60 per cent of the theoretically predicted values.

We note that the chlorine and Kamiokande experiments are insensitive to the lower energy neutrinos ( $E_\nu \lesssim 0.42 \text{ MeV}$ ) which are emitted in the basic  $p + p$  reaction dominantly responsible for generating the solar luminosity. It is, therefore, of great interest to carry out measurements that are sensitive to the neutrino flux from the  $p + p$  reaction. The only detectors currently capable of capturing the lower end of the solar neutrino spectrum are based on gallium and the measurements make use of the reaction



with a threshold of 0.233 MeV. It is this low threshold energy that makes possible the detection of neutrinos produced by the  $p + p$  reaction. There are two such radio-chemical experiments using the gallium detector: Soviet-American Gallium Experiment (SAGE) and GALLEX. The results of the counting rate reported by the two experiments are as follows:

$$\text{SAGE(1992): } 85_{-33}^{+22}(\text{stats}) \pm 20(\text{system})\text{SNU}$$

$$\text{GALLEX(1992): } 97_{-22}^{+24}(\text{stats})_{-7}^{+6}(\text{system})\text{SNU}.$$

The predicted neutrino capture rate for  ${}^{71}\text{Ga}$  detector on the other hand, is

$$(\Phi_\nu)_{\text{Ga}} = 127_{-16}^{+19}\text{SNU}.$$

The SAGE measurement gives neutrino capture rate which is about 66 per cent of the predicted flux, while the GALLEX capture rate is nearly 79 per cent of the expected neutrino flux.

The high-energy detection rate depends sensitively on details of the solar model and the high temperature dependence of the  ${}^7\text{Be}$  neutrino rate ( $\alpha T^8$ ) and of the  ${}^8\text{B}$  neutrino

rate ( $\propto T^{18}$ ) implies that in order to reduce the expected capture rate to the observed values would need a reduction in the central temperature of the Sun by only about 5 per cent, while, naturally, maintaining the required solar luminosity. There have been a number of ingenious suggestions to explain the observed solar neutrino deficit: for example, partial mixing in the solar core which brings additional hydrogen, helium fuel to the centre, thus maintaining the energy production rate at a slightly lower temperature and leading to a lower neutrino capture rate; the presence of a small admixture of Weakly Interacting Massive Particles (WIMPS) in the solar core increasing the thermal conductivity and in the process diminishing the temperature gradient required to transport the flux and again leading to a reduction in the central temperature; the centrally concentrated magnetic fields, the rapidly rotating solar core or lower heavy element abundance can also lead to a reduction in the central temperature and hence cause a lowering of the neutrino flux.

Out of the 127 SNU expected from the  $^{71}\text{Ga}$  detector, nearly 70 SNU flux comes from the proton-proton fusion reaction. The recent GALLEX measurement of nearly 97 SNU, may have captured most of this low energy neutrino flux and it is very likely that the reduction in the measured counting rate is mostly contributed by the high-energy neutrinos. A possible solution is the so-called by MSW effect (cf. Wolfenstein 1978; Mikheyev & Smirnov 1985; see also Bahcall & Bethe 1990). This effect is based on neutrinos having mass, whereby the electron neutrinos generated in the nuclear reaction network in the solar core may be transformed, during their transit through the solar body, into neutrinos of different flavours which are, of course, not detected by the current experiments.

In order to resolve the solar neutrino puzzle we have to await results of further measurements from the gallium detectors, but the indications from the current experiments are that it is the high-energy neutrinos generated in the nuclear reactions in the Sun which are mainly depleted. Does this mean that it is the adiabatic oscillation, in which the high-energy electron neutrinos get largely converted into other types of neutrinos, that is responsible for the observed deficit in the capture rate! Or, is it that the input physics (e.g. opacity, equation of state) is still inadequate? Or, perhaps, there is partial mixing in the solar energy-generating region which keeps the nuclear reactions operating at a slightly lower temperature! But then is a cooler solar core a viable solution of the solar neutrino puzzle! These and other questions have prompted solar physicists to look for another independent means to determine conditions in the interior of the Sun.

### (c) *Solar seismology*

This tool, provided by a rich spectrum of velocity fields observed at the solar surface, probes the Sun's interior with extraordinary precision. Since the early 1960s it has been noticed that the Sun undergoes a series of mechanical vibrations which appear as radial displacements imprinted as shifts of the spectral lines at the solar surface. These Doppler shifts oscillate through a cycle with a period around five minutes; when viewed through absorption lines, the effect manifests as periodic intensity fluctuations as the absorption feature shifts in and out of the bandpass of the narrow bandwidth filter. When imaged through such filters, the entire solar disk shows a rhythmically vibrating pattern of dark and light regions; even in the integrated light where the Sun is viewed as a star, the oscillations are revealed with an approximately five-minute period.

Thus, this approach attempts to detect and identify normal modes of global solar oscillations arising from internal processes. These pulsations characterize phenomena in which dynamical processes operating in the solar interior can cause visible manifestations on the Sun's surface.

These oscillations are triggered at many different places in the solar body and hence the Sun very much resembles a gong that is being sounded. The observed oscillations reveal information about the Sun in much the same manner as the study of terrestrial seismic waves generated by earthquakes has helped us to learn about the interior of the earth. The study of solar oscillations has, therefore, been called helioseismology, and it is expected to provide us with a complementary tool to probe the opaque layers of the Sun which would otherwise be inaccessible to direct observations.

The solar oscillations were detected over thirty years ago by Leighton, Noyes & Simon (1962). Later observations revealed that these oscillations occur as a very large number (over a million) of individual modes, each with its own frequency and wavenumber. The amplitude of individual modes is of the order of a few  $\text{cm s}^{-1}$ , but when superimposed, they produce velocity fluctuations as large as a fraction of  $\text{km s}^{-1}$  at the surface. Solar oscillations may be regarded as a super-position of many standing waves and their frequencies depend on the average internal physical properties like the temperature, density, chemical composition of the solar material. Each mode is characterized by three integers: the radial order,  $n$ ; the angular degree,  $l$  and the azimuthal order,  $m$ . There are two main classes of waves generated inside the Sun: high frequency acoustic modes which are controlled by pressure forces and low frequency gravity modes for which the major force responsible is the buoyancy. The frequencies of the solar normal modes of oscillations reflect the internal properties of the Sun and in principle, with a sufficient number of modes, it should be possible to unravel its internal structure.

Waves excited in the solar interior have a complicated propagation pattern. Thus, while propagating inside the solar body into the layers of increasing temperature, the path of an acoustic wave excited near the surface will be affected by the rising sound speed with depth. The deeper parts of the advancing wavefront will travel faster and the wave will eventually be refracted back towards the surface. The high degree p-modes propagate nearly horizontally and are trapped in the subsurface layers, while the low-degree modes penetrate practically into the core of the Sun. Thus, the solar p-mode oscillations with  $l = 0$  correspond to rays that propagate radially and pass through the centre of the Sun. The behaviour of low-degree ( $l = 0, 1, 2$ , say) modes differs only in the central region and it is expected that the frequency-difference between two such modes would provide information about the core.

The penetration depth of a given p-mode depends on its wavelength—a short wave-length wave is confined within a shallow cavity below the surface, while larger the horizontal wavelength of an acoustic wave, the more readily it propagates into the interior. In the  $(k_h - \omega)$  diagram, where  $k_h$  is the horizontal wavenumber and  $\omega$  is the frequency, these p-modes lie along discrete ridges (cf. Fig. 3); the different curves correspond to different values of the radial order,  $n$ . From this simple picture, we can conclude the following:

If the top of the cavity is nearly the same for all the p-modes and the bottom of the cavity is defined by the position where  $c_s = \omega/k_h$ , then the p-modes in different regions of the  $(k_h - \omega)$  diagram, with the same value of  $\omega/k_h$  are trapped in an identical cavity, and the sound travel time across such a cavity will be the same for different modes.

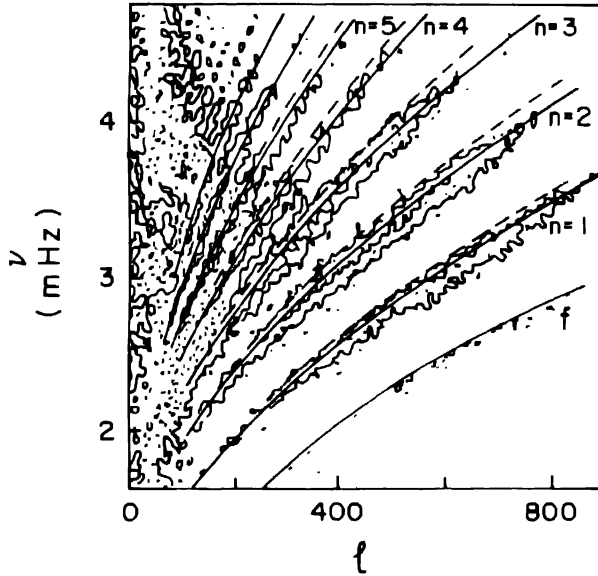


**Figure 3.** The  $(k_n - \omega)$  diagram of solar  $p$ -mode oscillations with the ridges, in the two-dimensional power spectrum, designated by the radial order,  $n$  of the mode.

A convenient form for analyzing  $p$ -modes was introduced by Duvall (1982) who showed that if the quantity  $\pi(n + \alpha(\omega))/\omega$  is plotted against  $\omega/k_n$ , then the ridge structure should collapse onto a single curve. Here  $\alpha(\omega)$  is a phase-shift factor that arises from the reflection of the internal acoustic wave from the surface layers. In fact, both the observed and computed frequencies of  $p$ -mode oscillations satisfy the Duvall relation  $\pi(n + \alpha(\omega))/\omega = F(\omega/\sqrt{l(l+1)})$  quite accurately.

The rich spectrum of  $p$ -modes provided by helioseismology enables us to derive a considerable amount of information about the solar interior, since the oscillation frequencies depend on the detailed structure of the Sun; in particular, the frequencies of acoustic modes are largely determined by the speed of sound,  $c_s$ , in the solar interior. We define the adiabatic sound speed,  $c_s$  as given by

$$c_s^2 = \frac{\Gamma_1 p}{\rho} = \frac{k_B \Gamma_1 T}{\mu m_H},$$

assuming the ideal gas law and  $\Gamma_1 = (\partial \ln p / \partial \ln \rho)_s$ .

The frequencies of solar oscillations have been measured with extraordinary precision, to better than one part in  $10^3$ . The helioseismic data may be analyzed in two ways:

- Direct model fitting
- Inversion

In the direct method, we can use the stellar structure equations to construct a set of solar models with different values of one or more adjustable parameters of the theory. The equilibrium model may then be perturbed to determine the eigenfrequencies of

solar oscillations in the linear theory. In principle, we can find the values of those parameters that best fit the helioseismic data, but in practice, the fit of the theoretically computed frequencies with the observed data does not turn out to be so good. However, there have been some distinct indications from the comparison of observed and theoretically computed frequencies.

The depth of the solar convection zone is  $\simeq 200,000$  km and the helium abundance by mass in the solar envelope  $\simeq 0.25$ . It has also been noticed that the inclusion of Coulomb effects in the equation of state led to a significant improvement in the agreement between calculated and observed p-mode frequencies. An analysis of the oscillation frequencies further indicated that the adopted opacities near the base of the convection zone were too low, a result which has later been confirmed by the recent Livermore opacity calculations. Thus, helioseismic data has led to improvements in the input physics required to compute stellar models.

The direct method has had only a limited success and it was felt desirable to employ the inversion technique, whereby the solar structure may be inferred directly from the helioseismic data. One of the major achievements of the inversion method has been a determination of the sound-speed profile through the bulk of the solar interior, save the innermost region ( $r \leq 0.01 R_{\odot}$ ) of the solar core. This follows from the Duvall relation,

$$\frac{\pi(n + \alpha(\omega))}{\omega} = F(W) = \int_r^R \left(1 - \frac{a^2}{W^2}\right)^{1/2} \frac{1}{a} \frac{dr}{r},$$

where  $W = (\omega/l + 1/2)$ ,  $a = c_{s,r}$ ,  $\alpha(\omega) =$  phase-shift factor,  $n =$  radial order of the mode and  $\omega$  its frequency, and  $r_t =$  radius at the lower turning point at which  $a = c_{s,r} = W$ . This equation can be inverted (Gough 1986) to give

$$r = R \exp \left\{ -\frac{2}{\pi} \int_{a(R)}^a (W^2 - a^2)^{-1/2} \frac{dF}{dW} \right\}$$

and the use of the relation,  $c_s = a(r)r$  then determines the sound-speed profile from a knowledge of the observed p-mode frequencies (i.e.,  $\omega, l, n$ ). Figure 4 shows the exact sound speed indicated by a continuous curve, as a function of fractional solar radius for a standard solar model while the dotted curve is the sound speed, inferred from the Duvall relation, using computed frequencies of over 2000 p-modes. (cf. Basu & Antia 1993). It is remarkable that the difference between the actual and inferred sound speeds of the model Sun comes out to be less than about half a per cent down to a radius of  $0.1 R_{\odot}$ . We can thus obtain a reasonably reliable estimate of the sound speed within the Sun and hope to determine the central temperature quite accurately. The observed accurate oscillation frequencies have been profitably employed to infer the helium abundance in the solar envelope to be  $\sim 0.252 \pm 0.003$  from studying variations in the adiabatic index of solar material in the second helium ionization zone (cf. Antia & Basu 1993; Dziembowski, Pamyatnykh & Sienkiewicz 1991; Däppen *et al.* 1991; Vorontsov, Baturin & Pamyatnykh 1992). This demonstrates that a direct seismological measurement of the helium abundance in the solar envelope is possible from studying a variation of  $\Gamma_1$  in the ionization zones.

Another quantity of interest is the function  $W(r) = (dc_s^2/dr/Gm/r^2)$  which represents ratio of acoustic to gravitational acceleration (cf. Gough 1984). The function  $W(r)$  for

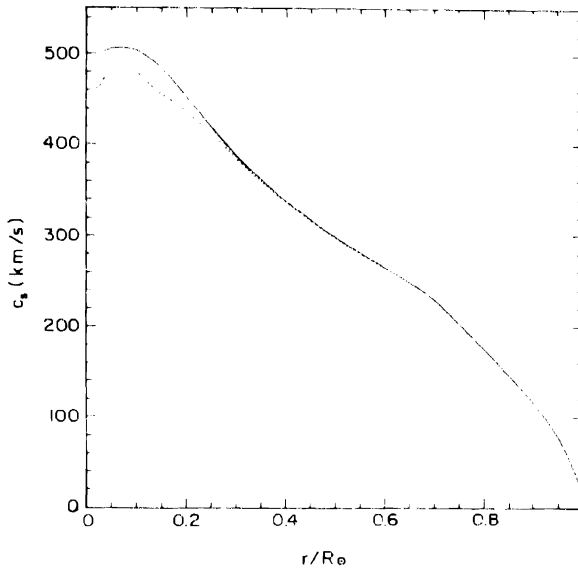


**Figure 4.** Model sound speed profile through the solar interior shown by a full line and the inverted profile of the sound speed obtained from the observed  $p$ -mode frequencies, indicated by a dotted line.

a model Sun shows two distinct humps just below the surface – one hump corresponding to the hydrogen and first helium ionization zones around  $r \gtrsim 0.99 R_{\odot}$  and a smaller hump at  $r \simeq 0.98 R_{\odot}$  corresponding to the second helium ionization zone. It should be noticed that  $W(r)$  rises abruptly beneath the base of the convection zone a property that can be effectively used to measure the depth of the convection zone. Figure 5 shows the model profile of  $W(r)$  as well as the inverted profile as a function of the fractional solar radius. The depth of the convection zone is found to be about 200,000 km (Christensen-Dalsgaard, Gough & Thompson 1991).

In similar analysis, Monteiro, Christensen-Dalsgaard & Thompson 1992 and Basu, Antia & Narasimha (1993) set an upper limit of 0.1 Hp on the extent of overshoot below the base of the convection zone. This is done by analyzing the characteristic oscillatory component introduced in the frequencies of  $p$ -modes by the discontinuity in the temperature gradient at the lower boundary of the convection zone.

Solar seismological measurements enable us to surmise the internal angular velocity of the Sun. The surface of the Sun rotates with a period of about 25 days at the equator and nearly 33 days at the poles. The  $p$ -mode oscillations pervade the deep solar interior and therefore, experience the rotation beneath the visible surface. In the absence of rotation, one of the resonant modes which the Sun can exhibit is a standing wave with its crests and troughs always aligned with the longitudes. For a completely spherical distribution, the eastward and westward moving waves would have identical frequencies and would, as a result, be indistinguishable. The rotation would break this symmetry and there will be a slight difference in the frequencies of the waves travelling with the direction and against the rotation. This is the rotational splitting of eigenfrequencies which is a weighted average of the internal solar angular

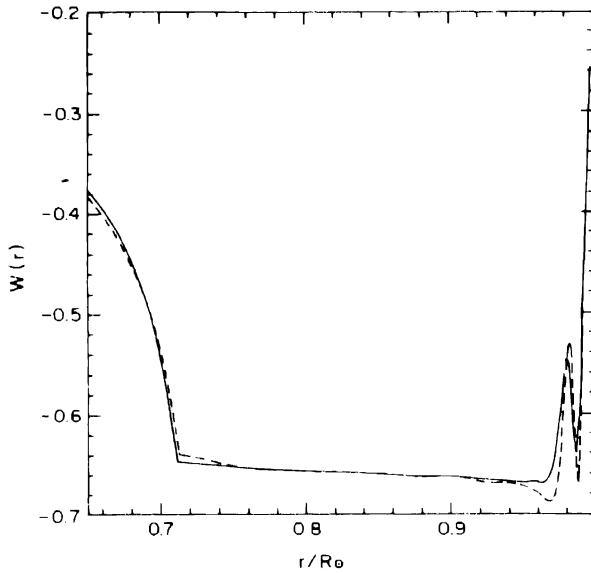


**Figure 5.** Function  $W(r) = (dc_s^2/dr/Gm/r^2)$  plotted against the fractional solar radius showing the abrupt increase at the base of the convection zone; the solid line displays  $W(r)$  obtained from the model, while the broken line represents  $W(r)$  given by the inversion. (Antia & Basu 1993).

velocity, the weighting being different for different resonant oscillations. Thus, by observing the rotational splitting of several  $p$ -modes, we can learn about the distribution of angular velocity throughout the solar body. It turns out that the latitudinal differential rotation observed at the solar surface in fact persists at least through most of the convection zone (Duvall, Harvey & Pomerantz 1986; Brown & Morrow 1987). With a knowledge of the angular velocity distribution in the solar interior, it is straightforward to calculate the oblateness produced by the centrifugal force and deduce the distortion produced in the gravitational field and the resultant contribution to the precession of the orbit of Mercury. It now appears that a little more than one percent of the intrinsic precession of the orbit of the planet arises from the centrifugal flattening of the Sun – a result consistent with the prediction of General Relativity.

#### 4. Conclusion

- The structure of the standard solar model is basically correct in describing the profiles of the internal density and temperature.
- The solution of the solar neutrino puzzle should be sought in the realm of neutrino physics.
- With the help of accurate information available from the observed oscillations at the surface of the Sun, helioseismology can provide valuable information about conditions in the solar interior and thus contribute to the use of the Sun as a laboratory for particle physics.

### Acknowledgements

I am grateful to H. M. Antia and D. Narasimha for valuable and stimulating discussions. Thanks are due to Antia and Basu for supplying their results in advance of publication.

### References

- Antia, H. M., Basu, S. 1993, *J. Astrophys. Astr.* (submitted).  
 Basu, S., Antia, H. M., Narasimha, D. 1994, *Mon. Not. R. astr. Soc.* **267**, 209.  
 Basu, S., Antia, H. M. 1993, *Astrophys. J.*, (submitted).  
 Bahcall, J. N., Bethe, H. A. 1990, *Phys. Rev. Lett.* **65**, 2233.  
 Bahcall, J. N., Pinsonneault, M. H. 1992, *Rev. Mod. Phys.* **64**, 1885.  
 Brown, T. M., Morrow, C. A. 1987, *Astrophys. J.*, **314**, L21.  
 Christensen-Dalsgaard, J., Gough, D. O., Thompson, M. J. 1991, *Astrophys. J.*, **378**, 413.  
 Cox, A. N., Tabor, J. E. 1976, *Astrophys. J.*, **S31**, 271.  
 Däppen, W., Gough, D. O., Kosovichev, A. G., Thompson, M. J. 1991, in *Challenges to theories of the structure of moderate-mass stars*, Eds. D. O. Gough & J. Toomre, (Heidelberg: Springer).  
 Dicke, R. H., Kuhn, J. R., Libbrecht, K. G. 1987, *Astrophys. J.*, **318**, 451.  
 Duvall, T. L. 1982, *Nature*, **300**, 242.  
 Duvall, T. L., Harvey, J. W., Pomerantz, M. A. 1986, *Nature* **321**, 500.  
 Dziembowski, W. A., Pamyatnykh, A. A., Sienkiewicz, R. 1991, *Mon. Not. R. astr. Soc.*, **249**, 602.  
 Eggleton, P. P., Faulkner, J., Flannery, B. P. 1973, *Astr. Astrophys.*, **23**, 325.  
 Gough, D. O. 1984, *Mem. Soc. Astr. Ital.*, **55**, 13.  
 Gough, D. O. 1986, in *Seismology of the Sun and Distant Stars*, Ed. D. O. Gough, (Dordrecht: Reidel) p. 125.  
 Leighton, R. B., Noyes, R. W., Simon, G. W. 1962, *Astrophys. J.*, **135**, 474.  
 Mihalas, D., Däppen, W., Hummer, D. G. 1988, *Astrophys. J.*, **331**, 815.  
 Mikheyev, S. P., Smirnov, A. Yu. 1985, *Soviet J. Nucl. Phys.* **42**, 913.  
 Monteiro, M. J. P. F. G., Christensen-Dalsgaard, J., Thompson, M. J. 1992, in *Proc. GONG: Seismic Investigation of the Sun and Stars*, Ed. T. M. Brown.  
 Rogers, F. J., Iglesias, C. A. 1992, *Astrophys. J.*, **S79**, 507.  
 Vorontsov, S. V., Baturin, V. A., Pamyatnykh, A. A. 1992, *Mon. Not. R. astr. Soc.*, **257**, 32.  
 Wolfenstein, L. 1978, *Phys. Rev.* **D17**, 2369.





## Physics of the Solar Corona and Flares Revealed by *Yohkoh*

Takeo Kosugi *National Astronomical Observatory, Mitaka, Tokyo 181, Japan.*

**Abstract.** The Japanese *Yohkoh* satellite was launched on August 30 1991, for investigating the solar corona, especially high-temperature and high-energy phenomena occurring there in the X-ray and  $\gamma$ -ray ranges such as flares. Thanks to a set of X-ray imagers as well as spectrometers with advanced capabilities, *Yohkoh* has been revealing various new aspects of coronal plasma dynamics, of which one of the most important is the topological change of coronal magnetic fields through reconnection and its relation to flares. Essence of new observations are briefly reviewed, with emphasis upon the results from soft X-ray imaging observations.

**Key words:** Sun: corona – sun: flares – sun: magnetohydrodynamics.

### 1. Introduction to the *Yohkoh* satellite

The Sun is the only star that can be observed with moderate, though far from sufficient, spatial resolution to investigate physical processes involved in stellar activities. In these activities magnetic energy storage and release in stellar coronae play a dominant role. A large solar flare, the most powerful explosion occurring in the solar corona, releases as much as  $10^{32}$ -erg magnetic energy over a relatively short period of time (minutes to hours) in forms of relativistic and nonrelativistic particle acceleration, plasma heating, bulk mass motion, and shock waves, and triggers disturbances propagating outwards through the interplanetary space. However, little has been known about the fundamental mechanisms for energy release as well as particle acceleration. This is probably because no relevant information has been available on the magnetic field structure in the corona! We need to observe changing topology of magnetic fields during the energy release.

For achieving this goal a space observatory project named SOLAR-A was planned by Japanese scientists in mid-1980's as a successor of their successful, first solar flare mission, *Hinotori*. It was clear that the plan should be developed to include international collaboration in order to have a best set of instruments onboard a single satellite. After a long preparation and integration period, the SOLAR-A satellite was launched into an orbit around the Earth by the Institute of Space and Astronautical Science (ISAS) on August 30 1991, and since then SOLAR-A, now given a new name *Yohkoh*, which means 'sunlight' or 'sunbeam' in English, has been continuously observing the solar corona.

The *Yohkoh* satellite (Ogawara *et al.* 1991) carries two imagers, namely the Hard X-ray Telescope (HXT; Kosugi *et al.* 1991) and the Soft X-ray Telescope (SXT; Tsuneta *et al.* 1991), and two types of spectral analysis instruments, namely the Wide Band Spectrometer (WBS; Yoshimori *et al.* 1991) and the Bragg Crystal Spectrometer (BCS; Culhane *et al.* 1991). The two imagers have advanced capabilities in comparison with

their predecessors, i.e., soft X-ray imagers on *Skylab* in the case of SXT and hard X-ray imagers on *SMM* and *Hinotori* in the case of HXT. The sensitivity of BCS is greatly improved by typically an order of magnitude from those carried by *P 78-1*, *SMM*, and *Hinotori*, and WBS has advantages in its increased number of channels in the hard X-ray pulse-height analysis as well as in its improved sensitivity for detecting  $\gamma$ -rays above  $\geq 10$  MeV. Note that among the four instruments only SXT is so designed as to provide images of soft X-ray 'quiet' corona as well as those of flares. The other instruments are for flare observations alone. Both HXT and WBS are pure Japanese experiments, while SXT and BCS are under Japan–U.S. and Japan–U.K.–U.S. collaborations, respectively. The details of the satellite and the instruments are given in the papers cited above.

## 2. Highlights of observations by Yohkoh

Since launch *Yohkoh* has been revealing many new aspects of solar coronal physics. Some of them from the initial-period observations have been reviewed by Acton *et al.* (1992), Uchida (1993), Tsuneta & Lemen (1993), Tsuneta (1993a, b), and Kosugi (1993). Also a series of letter papers were edited as 'Initial Results from Yohkoh' (special feature of *Publ. Astr. Soc. Japan*, Vol. 44, No. 5, 1992; note in the following that papers from this special feature are marked in citation with an asterisk symbol after the author name and published year and not included in the References). Those who are interested in this subject are advised to refer to these articles. Thus in the following the author will try to pick up several phenomena which he believes interesting and discuss their implications. The selection is quite biased towards imaging observations with SXT, because the HXT results are discussed in a separate paper (Kosugi 1994).

### 2.1 Coronal structures and dynamics

It has been known since *Skylab* in 1973–74 that the solar corona seen in soft X-rays is highly inhomogeneous, divided into three portions, namely active regions, loops connecting active regions (or 'quiet corona'), and coronal holes, with tiny X-ray bright points appearing sporadically everywhere. *Yohkoh*/SXT has revealed, thanks to its higher spatial resolution as good as  $\sim 2.5$  arcsec, much smaller X-ray scattering in its telescope optics, and higher time cadence of image acquisition with better time coverage, that it is full of marvelous complexity and dynamical behavior.

Active regions are filled with many long, thin loops, which are believed to trace magnetic flux tubes or bundles of field lines. Much longer but similarly thin loops connect two active regions whose separation is sometimes greater than the solar radius. Some of the loops are twisted or S-shaped; some others show even a kink-like shape. It is astonishing to see a loop whose diameter is much smaller than its length but has an almost constant cross-sectional area along the loop (Klimchuk *et al.* 1992\*). This cannot be interpreted as a current-free magnetic loop; instead it suggests current flowing along the loop. Relatively frequently we see loops to continually expand outwards, but only rarely to shrink. It is noteworthy mentioning that, although no precise estimate has been done, the rate of mass loss due to this kind of 'magnetic expansion' may not be negligibly small in comparison with the steady solar wind flow (Uchida *et al.* 1992\*). Also it is to be noted that the temperature of coronal holes is

estimated from SXT images taken with several different filters to be  $\sim 2$  MK, which is as high as that in the quiet corona (Hara *et al.* 1993).

One of the most spectacular findings by Yohkoh/SXT is that the X-ray corona drastically changes its topology through 'magnetic field reconnection', which we will discuss below.

## 2.2 Gigantic arcade formation

A large-scale restructuring of coronal magnetic fields takes place in association with the disappearance of a filament in a style of 'propagating arcade formation', in which a closed-loop arcade is formed progressively from one end to the other in an open-field area. One of the largest was observed on November 12 1991 near the north pole when a polar crown filament disappears, which is shown in Fig. 1 (Tsuneta *et al.* 1992\*a). The arcade formation began at  $\sim 00:00$  UT, propagated westwards ( $v = 20\text{--}40$  km s $^{-1}$ ), and reached the west limb at  $\sim 12:00$  UT, when the process is still in progress as revealed by increasing height and footpoint separation ( $v = 2\text{--}4$  km s $^{-1}$ ). The arcade which reached the west limb showed a cusp shape (marked by an arrow in the frame at 13:06 UT), which, together with the increasing height and footpoint separation, is suggestive that the magnetic field reconnection was still in progress.

In Fig. 1 we see another arcade formation, though much smaller and more quickly changing, between 18:53 UT and 23:00 UT near the center of each image. Thus this type of magnetic field restructuring is not a rare phenomenon; it covers a size scale from an active-region size to more than a solar radius and a propagation velocity from several km s $^{-1}$  to several tens of km s $^{-1}$ .

It is to be noted that, when we see such an arcade formation in soft X-rays, the H $\alpha$  filament associated with it has already disappeared, or more rigorously already erupted into the corona to more than 10,000 km above the photosphere. For a beautiful example, see Enome *et al.* (1993). Thus it is phenomenologically quite clear that the eruption of filament triggers the arcade formation. Extensive studies on this phenomenon from various viewpoints are in progress (Ta. Watanabe *et al.* 1992\*; McAllister *et al.* 1992\*; Hanaoka *et al.* 1993).

## 2.3 Long-duration, cusp-shaped flares

The arcade formation mentioned above has a large size and may cause a major interplanetary disturbance. However, it is not necessarily so intense in soft X-ray emission as flares, although the classification of an actually observed phenomenon into the two categories is not so unambiguous.

Sometimes, though not frequently, we observe flares lasting for more than one hour in the GOES X-ray intensity plot. Such flares are called LDEs or Long Duration Events. When an LDE occurs near the solar limb, which makes it easier to examine the vertical structure, we see in the late phase of the event a soft X-ray bright loop with a cusp at the apex of the loop, which is similar to that found in the arcade formation. A typical example is shown in Fig. 2. It can be pointed out that the cusp part, especially its outer boundary portion, has the higher temperature than the other parts of the loop, and that the whole loop increases its height and footpoint separation with time (Tsuneta *et al.* 1992\*b; Tsuneta 1993a, b). Again this may be regarded that we observe the reconnection process going on. Note that the magnetic configuration involved is

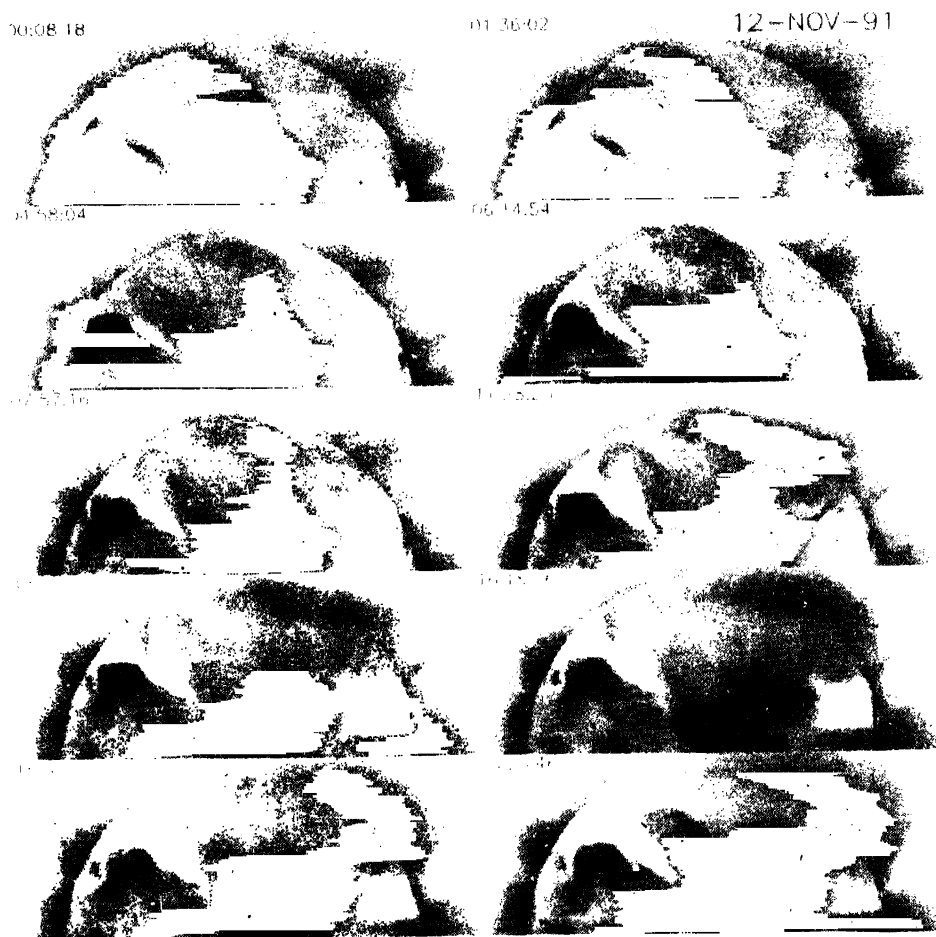


**Figure 1.** Two propagating arcade formations on November 12 1991. One is seen propagating from east (left) to west (right) during the interval between  $\sim 00:00$  UT and  $\sim 23:00$  UT near the north pole (top), where a polar crown filament disappears. The other is seen near the center of the 18:53 UT and 23:00 UT images (after Tsuneta *et al.* 1992\*a).

just homologous to what was previously proposed by several theoreticians or modellers (e.g., Hirayama 1974; Kopp & Pneuman 1976).

#### 2.4 Soft X-ray jets

A different type of manifestation of reconnection can be seen as 'jets' (Shibata *et al.* 1992\*; see also Shibata *et al.* 1993). An X-ray jet has a typical length  $5 \times 10^3$ – $4 \times 10^5$  km, velocity 30–300 km s $^{-1}$ , and kinetic energy  $10^{25}$ – $10^{28}$  erg. Many of the jet are associated with X-ray bright points or with flaring activity in emerging flux regions. The suggested reconnection morphology for the case of emerging-flux-associated events is shown in Fig. 3.

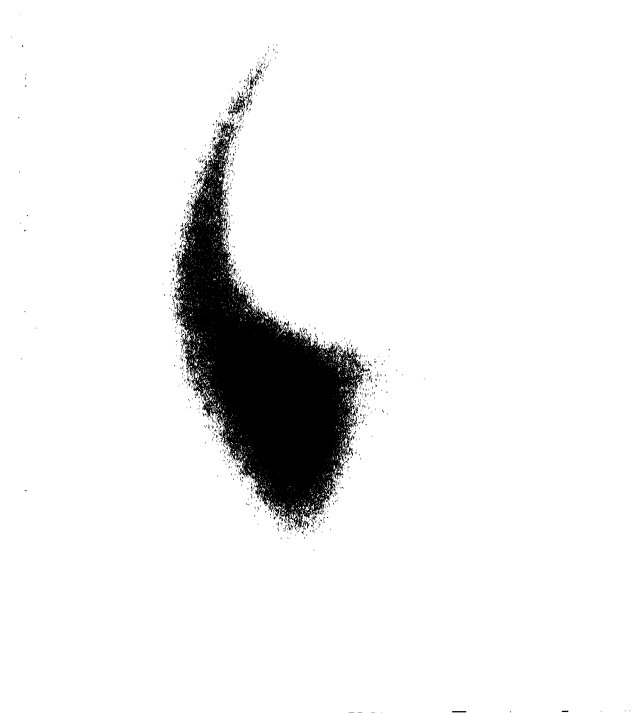


**Figure 2.** Long-duration, cusp-shaped soft X-ray flare on February 21 1992. This flare was a GOES M3.2-class event which occurred behind the east solar limb, commencing at  $\sim 02:45$  UT and lasting for more than 7 hours. For more details, see Tsuneta *et al.* (1992\*b).

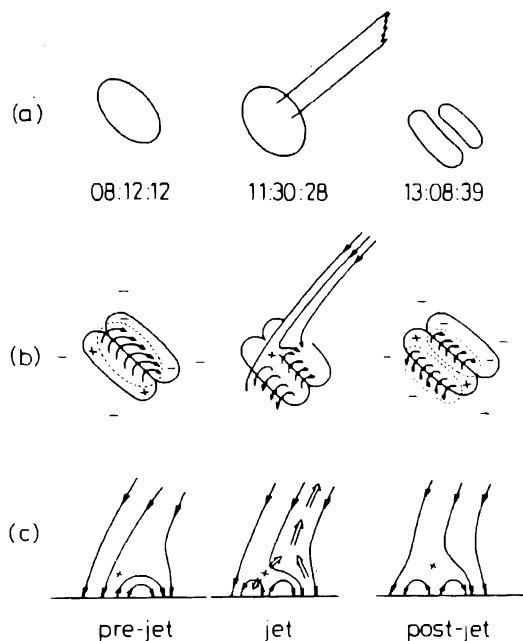


**Figure 3.** (a) Schematic drawing of an active region with a jet observed with SXT on November 12 1991 at pre-jet (08:12 UT), during-jet (11:30 UT), and post-jet (13:08 UT) stages. (b) Magnetograms and inferred magnetic field lines from them. (c) Side view of inferred magnetic field lines (after Shibata *et al.* 1992\*).

### 2.5 Transient brightenings or microflares

Many tiny flaring activities, which have been overlooked due to their small amount of energy released in an event, are found to occur quite frequently in active regions (Shimizu *et al.* 1992\*). These are seen as small enhancements in the GOES time plots, and maybe accompanied by quite weak hard X-ray emission such as 'microflares' observed by Lin *et al.* (1984) with a balloon-borne, high-sensitivity hard X-ray detector. Each of the microflares releases much less than  $10^{29}$  erg, but the occurrence frequency reaches once every  $\sim 3$  min in an 'active' active region while it is once every  $\sim 1$  hour in a 'quiet' active region. Thus the total amount of energy released cannot be negligibly small in comparison with that from rarely-occurring major flares. Rather there may be a possibility that an assembly of huge number of microflares explains a long-lasting enigma how the solar corona is heated up to millions K.

### 2.6 Single loop flares vs. loop-loop interaction flares

A further study by Shimizu *et al.* (1993) on the morphology of microflares observed with SXT has revealed that simultaneous *multiple* loop brightenings are more often seen than single loop brightenings, and further that they tend to brighten from their footpoints and/or the apparent contact point in the initial phase, followed by the brightening of the entire loops.

We believe this finding of crucial importance for investigating the solar flare energy release mechanism. Similar morphological studies for 'normal-sized' flares are in progress but unfortunately in a style of individual case studies, and the results are just case-by-case; in some cases we see typical single-loop flares and in others multiple-loop 'interaction' flares.

### 2.7 Energetic flares with hard X-ray emission

Now a question arises as to where the main energy release site of flares is, or more specifically where (and how) particles are accelerated to nonrelativistic (or sometimes relativistic) energies; is it at the cusp-shaped reconnection point seen in long-duration soft X-ray events, at the contact point of the interacting magnetic loops, or inside a strongly sheared single magnetic loop?

Although some theoretical approaches on the possible particle acceleration mechanism have been made starting from the soft X-ray observations of long-duration, cusp-shaped flares (e.g., Tsuneta 1993a), it is noteworthy that the morphological study of microflares by Shimizu *et al.* (1993) mentioned in the previous subsection seems to suggest the loop-loop interaction as the most plausible cause of the main energy release. The relevant data for this problem from the hard X-ray observation side are summarized in a separate paper (Kosugi 1994), some of which seems to support the idea that particle acceleration takes place inside a single loop. Thus any conclusions are premature; no definitive answer has been given. We expect that this problem will be challenged in the near future by synthetic studies using well-coaligned sets of images for many flares taken with HXT and SXT simultaneously in cooperation with BCS and WBS spectral data from *Yohkoh*, as well as in cooperation with ground-based observations.

### 2.8 $\gamma$ -ray flares

The Gamma-Ray Spectrometer of WBS has detected four  $\gamma$ -ray line flares occurring in 1991 just after the launch (Yoshimori *et al.* 1992\* a, b). Their characteristics in comparison with intense flares without any  $\gamma$ -ray emission have been examined. Also detailed studies based upon the line spectroscopy are in progress on the ion acceleration as well as their propagation and interaction with ambient plasmas.

## 3. Summary and remarks

This review is not intended to cover the whole fields of the *Yohkoh* science. Instead it concentrates upon topics that match the author's personal interest. Nevertheless the author has tried to let the reader feel the excited atmosphere in the *Yohkoh* team. The major results are as follows:

- *Yohkoh* has observed that the coronal global structure drastically changes through magnetic field reconnection in a style of propagating arcade formation.
- *Yohkoh* has confirmed that the long-duration soft X-ray flare is a manifestation of on-going reconnection at the cusp point above the closed loop.
- *Yohkoh* has pointed out several possible magnetic field configurations maybe responsible for the main energy release in solar flares, i.e., the neutral sheet at the cusp, the



loop-loop interaction, and the highly sheared single magnetic loop. Further studies are highly desirable to clarify the roles of the individual configurations in a solar flare.

### Acknowledgements

The author is mainly involved in the HXT experiment, not in the SXT experiment, therefore he is indebted to his colleagues, especially S. Tsuneta and K. Shibata for reviewing SXT-related topics. The *Yohkoh* project is a team effort, including not only Japanese but also many U.S. and U.K. colleagues. ISAS, NASA, and SERC have been continuously supporting the *Yohkoh* operation. The attendance of the author at the 6th Asian-Pacific Regional Meeting of IAU held at Pune, India was supported by a grant from IAU.

### References\*

- Acton, L., Tsuneta, S., Ogawara, Y. *et al.* 1992, *Science* **258**, 618.  
 Culhane, J. L., Hiei, E., Doschek, *et al.* 1991, *Solar Phys.* **136**, 89.  
 Enome, S., Nakajima, H., Shibasaki, K. *et al.* 1993, in *The Magnetic and Velocity Fields of Solar Active Regions* Eds. H. Zirin *et al.* (A.S.P. Publ.), pp. 310–320.  
 Hanaoka, Y., Kurokawa, H., Enome, S. *et al.* 1993, *Publ. astr. Soc. Japan*, (submitted).  
 Hara, H., Tsuneta, S., Acton, L. A., Lemen, J. R., Ogawara, Y. 1993, in *Proc. International Yohkoh Science Meeting held in 1993 February in Japan* (in press).  
 Hirayama, T. 1974, *Solar Phys.*, **34**, 323.  
 Kopp, R. A., Pneuman, G. W. 1976, *Solar Phys.* **50**, 85.  
 Kosugi, T. 1993, in *Physics of Solar and Stellar Coronae* Eds. J. Linsky & S. Serio (Kluwer Academic Publ.) pp. 131–138.  
 Kosugi, T. 1995, (in this issue).  
 Kosugi, T., Makishima, K., Murakami, T., Sakao, T., Dotani, T., Inda, M., Kai, K., Masuda, S., Nakajima, H., Ogawara, Y., Sawa, M., Shibasaki, K. 1991, *Solar Phys.* **136**, 17.  
 Lin, R. P., Schwartz, R. A., Kane, S. R., Pelling, R. M., Hurley, K. C. 1984, *Astrophys. J.* **283**, 421.  
 Ogawara, Y., Takano, T., Kato, T., Kosugi, T., Tsuneta, S., Watanabe, T., Kondo, T., Uchida, Y. 1991, *Solar Phys.* **136**, 1.  
 Shibata, K., Ishido, Y., Acton, L., *et al.* 1993, in *The Magnetic and Velocity Fields of Solar Active Regions* Eds. H. Zirin *et al.* (A.S.P. Publ.), pp. 343–346.  
 Shimizu, T., Tsuneta, S., Acton, L. W., Lemen, J. R., Ogawara, Y., Uchida, Y. 1993, *Astrophys. J.* (in press).  
 Tsuneta, S. 1993a, in *The Magnetic and Velocity Fields of Solar Active Regions* Eds. H. Zirin *et al.* (A.S.P. Publ.), pp. 239–257.  
 Tsuneta, S. 1993b, in *Proc. Fourth International Toki Conference on Plasma Physics and Controlled Nuclear Fusion* held in 1992 November in Japan (in press).  
 Tsuneta, S., Acton, L., Bruner, M., Lemen, J., Brown, W., Carvalho, R., Catura, R., Freeland, B., Jurcevich, B., Morrison, M., Ogawara, Y., Hirayama, T., Owens, J. 1991, *Solar Phys.* **136**, 37.  
 Tsuneta, S., Lemen, J. R. 1993, in *Physics of Solar and Stellar Coronae* Eds. J. Linsky & S. Serio (Kluwer Academic Publ.) pp. 113–130.  
 Uchida, Y. 1993, in *Physics of Solar and Stellar Coronae* Eds. J. Linsky & S. Serio (Kluwer Academic Publ.) pp. 97–111.  
 Yoshimori, M., Okudaira, K., Hirasima, Y., Igarashi, T., Akasaka, M., Takai, Y., Morimoto, K., Watanabe, T., Ohki, K., Nishijima, J., Yamagami, T., Ogawara, Y., Kondo, I. 1991, *Solar Phys.* **136**, 69.
- \*Papers which appeared in 'Initial Results from Yohkoh' (special feature of *Publ. astr. Soc. Japan*, Vol. **44**, No. 5, pp. L41–L214, 1992), marked with an asterisk in the text, are not included.

## Solar Flare Observations with the *Yohkoh* Hard X-ray Telescope

Takeo Kosugi *National Astronomical Observatory, Mitaka, Tokyo 181, Japan.*

**Abstract.** Hard X-ray imaging observations of solar flares with the *Yohkoh* Hard X-ray Telescope (HXT) are reviewed. Thanks to its high sensitivity HXT has so far detected more than 800 flares. General characteristics of different types of hard X-ray sources, i.e., those of double-footpoint sources, loop-top thermal sources, and super-hot thermal sources, are discussed together with their interrelation and implication.

**Key words:** Sun: flares — sun: hard X-rays — particle acceleration.

### 1. The HXT instrument and experiment

The Hard X-ray Telescope (HXT; Kosugi *et al.* 1991) onboard the *Yohkoh* satellite (Ogawara *et al.* 1991) is an advanced hard X-ray imager for solar flare observations. Its objectives are to clarify the mechanisms of particle acceleration and magnetic energy release through hard X-ray imaging observations. The main advantages of HXT over its predecessors are: i) simultaneous imaging in four energy bands, namely, the L-band (13.9–22.7 keV), M1-band (22.7–32.7 keV), M2-band (32.7–52.7 keV), and H-band (52.7–92.8 keV); ii) angular resolution of  $\sim 5$  arcsec with a wide field of view covering the whole Sun; iii) basic temporal resolution of 0.5 s; and iv) high sensitivity with a total geometrical aperture of  $\sim 60$  cm<sup>2</sup>. Onboard the same satellite we have the Soft X-ray Telescope (SXT; Tsuneta *et al.* 1991) and spectrometers; this is another advantage because HXT and SXT are especially complementary to each other in that the former looks at nonthermal electrons while the latter magnetic loop structures, where the electrons are energized.

Since the start of routine observations in 1991 October, the HXT instrument has been working well. So far HXT has detected more than 800 flares, including a dozen X-class and about 200 M-class events. More than two thirds of the  $\sim 800$  flares are intense enough for us to synthesize images. The performance of HXT in orbit and some initial results are briefly discussed in a series of letter papers (Kosugi *et al.* 1992; Sakao *et al.* 1992; Matsushita *et al.* 1992) which appeared in 'Initial Results from *Yohkoh*' (a special issue of *Publ. astr. Soc. Japan*, Vol. 44, No. 5). See also Takakura *et al.* (1993). A preliminary review is already given by Kosugi (1993), so that in this paper we will try to update it by including as new results as possible.

### 2. A preliminary summary of observations

Several interesting characteristics of hard X-ray sources revealed with HXT have been summarized as follows (Kosugi *et al.* 1992; Kosugi 1993):

- The hard X-ray flares observed in the HXT L-band (13.9–22.7 keV) usually show one or more long, thin structures which seem to trace magnetic loops. In fact hard X-ray images generally resemble the corresponding soft X-ray images taken with SXT.
- In the higher energy band (M1-, M2- and H-band) images, the sources become more compact and patchy. Typically two separate sources are observed at both ends of the long, thin structure seen in the L-band, which suggests that the electrons (possibly accelerated near the loop top) propagate along the magnetic loops and stream into the lower atmosphere at their footpoints.
- Correspondingly the average height of hard X-ray sources decreases with increasing photon energies (Matsushita *et al.* 1992).
- Sometimes a sudden shift of the hard X-ray source is observed from one location to another during impulsive peaks, suggestive of successive flaring of adjacent loops.

Subsequent observations have supplemented the contents by many details.

### 3. Double-footpoint sources in the impulsive phase

Even in the era of the first hard X-ray imaging experiments made by *SMM* and *Hinotori* more than a decade ago, it was recognized that *some* impulsive flares are characterized by the double-source structure, and it was claimed that this is evidence for precipitating nonthermal electrons towards both ends of a single flaring loop (e.g. Hoyng *et al.* 1981; Duijveman *et al.* 1982). Although this conclusion may be correct as shown below, there was no firm observational base which unambiguously supports this; the X-ray energy range was below  $\sim 20$  keV where contamination from thermal emission is not negligible, and also the temporal resolution was not sufficient as to confirm the expected simultaneity between the two sources (e.g. MacKinnon *et al.* 1985).

The HXT observations have drastically changed the situation. Sakao *et al.* (1992) have revealed, in the case of the X-class flare of November 15, 1991, that the double-source structure is most pronounced at X-ray energies  $\gtrsim 30$  keV at the times of individual peaks, whereas hard X-rays at  $\lesssim 30$  keV at the valleys between the peaks originate from near the apex of the flaring loop. This may be interpreted by the DC electric field – runaway acceleration model (Benka & Holman 1992), in which electron acceleration takes place together with direct heating. Or this may be explained by the trap-plus-precipitation model (Melrose & Brown 1976) with a strong scattering process operating. Note that the white-light flare brightenings (Hudson *et al.* 1992), which were coincident with the hard X-ray double sources (Sakao *et al.* 1992), support the electron-precipitation interpretation. In this event, a systematic increase of the separation between the double sources was also found together with a systematic increase of the angle sustained by the line connecting the double sources and the magnetic neutral line, suggestive of multiple loop system flaring successively from strongly sheared loops to less sheared ones with rising energy release site.

Subsequent analyses of a few dozens of impulsive flares by Sakao (1993) have confirmed (i) that the double-source structure can be found in more than one third of the events examined, (ii) that double sources almost simultaneously vary in intensity with time lags less than a fraction of a second, (iii) that the brighter source tends to correspond to a footpoint where the magnetic field is the weaker (irrespective of the sense of the magnetic field), and (iv) that the brighter source tends to show the harder

hard X-ray spectrum than the other source. These findings, together with the above-mentioned case study of the November 15, 1991 flare, strongly suggest that electrons are accelerated near the apex of a loop or system of loops, that the electrons precipitate towards the two footpoints with preference towards the weaker magnetic field footpoint, and that individual accelerations take place in different loops. We believe these are important findings to pose a strong constraint upon the acceleration mechanism.

#### 4. Loop-Top Sources in the Gradual Phase and Chromospheric Evaporation

Apart from spikes, we see in most of flares that the lower-band time history is dominated by a gradually-varying component upon which spikes are superposed. Correspondingly, L-band hard X-ray sources are frequently located in between the double footpoint sources seen in the higher-energy bands. This type of source becomes pronounced as time goes on after the impulsive phase ceases, and is characterized by a very steep hard X-ray spectrum which is typical for thermal emission from an optically thin plasma with temperatures ranging from 20 to 30 MK. Indeed hard X-ray sources resemble the corresponding soft X-ray sources which represent  $\sim 10$ -MK plasma.

Then a question arises as to how this thermal plasma is created, i.e., whether it is due to direct heating from magnetic energy release or due to evaporated material rising up from the chromosphere, and if the latter is the case, whether the energy is supplied by nonthermal electrons or by heat conduction. These problems are now challenged by several authors (Culhane *et al.* 1993; Inda-Keide *et al.* 1993; Wülser *et al.* 1993) using HXT and SXT data together as well as the Bragg Crystal Spectrometer (BCS) data.

#### 5. Super-hot thermal sources

When magnetic energy is released in solar flares, it is primarily converted into forms of nonthermal particle acceleration, plasma heating, bulk mass motion, and shock waves, among which it is difficult to clearly separate the first two, because nonthermal particle energies are easily thermalized. One of the key observations to determine the acceleration efficiency in the primary energy release should be, in addition to examining the energetics involved in the chromospheric evaporation, to examine positional relationship between the footpoint and loop-top sources whether they belong to a single loop or not.

An opportunity to study this point can be provided by super-hot thermal flares, characterized by dominant  $\geq 30$ -MK thermal plasma emission in hard X-rays (Tanaka *et al.* 1982; Tsuneta *et al.* 1984). Here we discuss one example which occurred on February 6, 1992 near the west limb (Kosugi *et al.* 1993). The flare was composed of two loops. The southern loop was a normal flaring loop; its hard X-rays lasted for less than a few minutes, originated mainly from the two footpoints, and showed a power-law spectrum. On the contrary, the northern loop showed typical super-hot thermal flare characteristics: a gradual broad peak lasting for longer than 10 min, a thermal hard X-ray spectrum with temperatures exceeding 30 MK, and lack of associated microwave burst. In this loop the hard X-ray source first appeared near the loop top and then gradually expanded downwards, maybe due to direct heating as a result of primary

energy release. At the same time a soft X-ray source, representing  $\sim 10$ -MK plasma, brightened first at one of the two footpoints and gradually expanded upwards, maybe tracing the chromospheric evaporation process due to heat conduction from the super-hot plasma. Thus in this northern loop no efficient particle acceleration took place; it seems that the ambient plasma density in the flaring loops caused the different behavior between the northern and southern loops.

Many other further studies are now in progress.

### Acknowledgements

The author wishes to express his thanks to his colleagues in the HXT experiment. The *Yohkoh* project is a team effort, including not only Japanese but also many U.S. and U.K. colleagues. ISAS, NASA, and SERC have been continuously supporting the *Yohkoh* operation. Part of this work is financially supported by the Scientific Research Fund of the Japanese Ministry of Education, Science, and Culture under Grant No. 02452011. The attendance of the author at the 6th Asian-Pacific Regional Meeting of IAU held at Pune, India was supported by a grant from IAU.

### References

- Denka, S., Holman, G. D. 1992, *Astrophys. J.*, **391**, 854.
- Culhane, J. L., Phillips, A. T., Inda-Koide, M., Kosugi, T., Fludra, A., Kurokawa, H., Makishima, K., Pike, C. D., Sakao, T., Sakurai, T., Doschek, G., Bentley, R. D., 1993, (in preparation).
- Duijveman, A., Hoyng, P., Machado, M. E. 1982, *Solar Phys.*, **81**, 137.
- Hoyng, P., Machado, M. E., Duijveman, A., Boelee, A., de Jager, C., Fryer, R., Galama, M., Hoekstra, R., Imhof, J., Lafleur, H., Maseland, H. V. A. M., Mels, W. A., Schadee, A., Schrijver, J., Simnett, G. M., Svestka, Z., van Beek, H. F., van Tend, W., van der Laan, J. J. M., van Rens, P., Werkhoven, F., Willmore, A. P., Wilson, J. W. G., Zandee, W. 1981, *Astrophys. J. Lett.*, **244**, L153.
- Hudson, H. S., Acton, L. W., Hirayama, T., Uchida, Y. 1992, *Publ. astr. Soc. Japan*, **44**, L77.
- Inda-Koide, M., Makishima, K., Kosugi, T., Sakao, T. 1993, in *Proc. International Yohkoh Science Meeting* held in 1993 February in Japan (in press).
- Kosugi, T. 1993, in *Physics of Solar and Stellar Coronae*, Eds. J. Linsky & S. Serio, (Kluwer Academic Publ.), pp. 131–138.
- Kosugi, T., Makishima, K., Murakami, T., Sakao, T., Dotani, T., Inda, M., Kai, K., Masuda, S., Nakajima, H., Ogawara, Y., Sawa, M., Shibasaki, K. 1991, *Solar Phys.*, **136**, 17.
- Kosugi, T., Sakao, T., Masuda, S., Makishima, K., Inda, M., Murakami, T., Ogawara, Y., Yaji, K., Matsushita, K. 1992, *Publ. astr. Soc. Japan*, **44**, L45.
- Kosugi, T., Sakao, T., Masuda, S., Hara, H., Shimizu, T., Hudson, H. S., Sterling, A. C. 1993 (in preparation).
- MacKinnon, A. L., Brown, J. C., Hayward, J. 1985, *Solar Phys.*, **99**, 231.
- Matsushita, K., Masuda, S., Kosugi, T., Inda, M., Yaji, K., 1992, *Publ. astr. Soc. Japan*, **44**, L89.
- Melrose D. B., Brown, J. C. 1976, *Mon. Not. R. astr. Soc.*, **176**, 15.
- Ogawara, Y., Takano, T., Kato, T., Kosugi, T., Tsuneta, S., Watanabe, T., Kondo, T., Uchida, Y. 1991, *Solar Phys.*, **136**, 1.
- Sakao, T. 1993, *Ph.D. thesis* (University of Tokyo).
- Sakao, T., Kosugi, T., Masuda, S., Inda, M., Makishima, K., Canfield, R. C., Hudson, H. S., Metcalf, T. R., Wuelser, J. -P., Acton, L. W., Ogawara, Y. 1992, *Publ. astr. Soc. Japan*, **44**, L83.

- Takakura, T., Ina, M., Makishima, K., Kosugi, T., Sakao, T., Masuda, S., Sakurai, T., Ogawara, Y., 1993, *Publ. astr. Soc. Japan*, **45**, 737.
- Tanaka, K., Watanabe, T., Nishi, K., Akita, K. 1982, *Astrophys. J. Lett.*, **254**, L59.
- Tsuneta, S., Nitta, N., Ohki, K., Takakura, T., Tanaka, K., Makishima, K., Murakami, T., Oda, M., Ogawara, Y. 1984, *Astrophys. J.*, **284**, 827.
- Tsuneta, S., Acton, L., Bruner, M., Lemen, J., Brown, W., Carvalho, R., Catura, R., Freeland, B., Jurcevich, B., Morrison, M., Ogawara, Y., Hirayama, T., Owens, J. 1991, *Solar Phys.* **136**, 37.
- Wülser, J. -P., Canfield, R. C., Acton, W. A., Culhane, J. L., Phillips, A., Fludra, A., Sakao, T., Masuda, S., Kosugi, T., Tsuneta, S. 1993, *Astrophys. J.* (in press).



## Dynamical Structures of Uranian Rings

Yoshihide Kozai *National Astronomical Observatory, Mitaka, Tokyo 181, Japan.*

**Abstract.** In this paper the observed dynamical structures of Uranian rings are explained by actions of unknown inner and outer shepherding satellites for each ring. In fact it is assumed that only the outer satellite has an appreciable proper eccentricity and inclination and that the observed eccentricities and inclinations for the ring particles as well as those for the inner satellite are forced ones produced by the outer satellite. Therefore, it is reasonable to conclude that the apsidal and precessional motions of the ring particles are identical to those for the outer satellite. Then the masses, the eccentricities and the distances to the ring of the satellites to fit the observed quantities are derived and are found to be in reasonable limits.

**Key words:** Shepherding satellites – rings – Uranus.

The rings of Uranus were discovered in March, 1977 when an occultation of Uranus by a star was observed. Since then as both ground-based and Voyager spacecraft observations have been made extensively for the rings, their structures have been made clear. Namely, their widths are very narrow, 5 to 100 km, their orbits are eccentric with slightly increasing eccentricity with the semi-major axis, and the apsidal motions are common for all particles in the same ring. The precession rates of the orbital planes are also believed to be common for all the particles, since although the orbital planes are inclined, a few arc minutes, to the equator of Uranus they are very thin, a few hundred meters thick.

Table 1 lists for the three typical rings,  $\alpha$ -,  $\beta$ - and  $\epsilon$ -rings, the semi-major axes ( $a$ ), their mean widths ( $\delta a$ ), the eccentricities ( $e$ ), the ratios ( $f$ ) of  $e$  at the outer and inner edges, the inclinations ( $i$ ) with respect to the equator of Uranus, the mean motions ( $n$ ) and the masses of the rings ( $m$ ) as well as apsidal and precessional motions ( $\dot{\omega}$  and  $\dot{\Omega}$ ) computed by the oblateness parameters derived from the motions of satellites.

The apsidal and precessional motions for ring particles are mainly due to the effect of the oblateness of Uranus, and, therefore, they depend on the semi-major axes of the orbits and take different values from place to place inside the rings. In fact the directions of the major axes and the nodal lines differ by more than 100 degrees between the two edges after 10 years if the motions are mainly due to the oblateness of Uranus even though they happen to be on lines at one epoch. Therefore, the observed structures seem to be very strange.

There are several papers for explaining such phenomena, however, it seems to the author that none of them is convincing. Therefore, in this paper the author tries to explain the phenomena by assuming two shepherding satellites, one inside and one outside. In fact it is believed that the two shepherding satellites are necessary to keep the widths of Uranian rings very narrow. And since it is reported that the



**Table 1.** Dynamical parameters of three rings.

Ring	$\alpha$	$\beta$	$\varepsilon$
$a(\text{km})$	44 718	45 661	51 149
$\delta a(\text{width in km})$	7.4	8.8	58.1
$e \times 10^3$	0.761	0.442	7.936
$f$	1.079	1.140	1.100
$i(\text{deg})$	0.015	0.005	0.0002
$n(\text{deg/day})$	1262.2	1223.3	1031.4
$\dot{\omega}(\text{deg/day})$	2.1833	2.0292	1.3623
$\dot{\Omega}(\text{deg/day})$	-2.2033	-2.0468	-1.3719
mass( $10^{15}$ kg)	0.042	0.038	6.1

Voyager spacecraft discovered all the satellite larger than 15 km, the unknown satellites should be smaller than 15 km.

Here it is assumed that the orbit of the outer shepherding satellite has appreciable values of proper eccentricity and inclination. By this way only the increase of the eccentricity as the semi-major axis can be explained. It is also assumed that the proper eccentricities and inclinations of the inner satellite and the ring particles are very small, much smaller than the proper values of the outer satellite. Then it can be concluded that the observed eccentricities and inclinations listed in Table 1 for the ring particles as well as those for the inner satellite are forced ones produced by strong actions due to the outer satellites. The mass and the equatorial radius of Uranus are assumed to be, respectively,  $8.67 \times 10^{25}$  kg and 26 200 km.

For such cases the apsidal and precessional motions of the inner satellite and all the ring particles are equal to those of the outer satellite which are due to the oblateness and the actions of the rings and of the inner satellite. Moreover, their pericenter longitudes and the nodal lines are always in phase for the two satellites and all the ring particles.

If the problem of a pendulum is considered, its frequency is usually its proper one depending on its length and mass. However, if the amplitude of the free oscillation is very small, there may be a case that only the forced oscillation with the frequency of the acting force is observable. The author considers that the problem treated here for Uranian rings is similar to this case.

In the two papers (Kozai 1992, 1993) the author tried to derive the masses and the distances to the ring of the two shepherding satellites as well as the eccentricity and the inclination of the outer one so as to fit the observed eccentricities and their gradients of the ring particles as well as the inclination, that is,  $e$ ,  $f$  and  $i$  in Table 1. By using very rough theory of secular perturbations among test particles at the inner and outer edges of the ring and the inner and outer satellites as well as the rings the author could derive solutions, in which the masses and the distances to the edge of the ring of the shepherding satellites are, respectively, of the order of  $10^{15}$  kg (10 km in diameter) and 25 km. Then it is believed that the mechanisms explained above can work for the rings if there are shepherding satellites.

Therefore, according to the author's view the ring systems of Uranus together with the two shepherding satellites are axial symmetric with respect to the major axes and the nodal lines of the orbits.

### **References**

- Kozai, Y. 1992, *Publ. astr. Soc. Japan*, **44**, 135–139.  
Kozai, Y. 1993, *Publ. astr. Soc. Japan*, **45**, 263–267.



## Structures in Saturn's Magnetosphere

J. C. Bhattacharyya *Indian Institute of Astrophysics, Bangalore 560 034, India*

*Key words:* Planets—Saturn—occultation.

### 1. Introduction

During the Pioneer XI and Voyager passes by Saturn, it was noticed that at specific distances from the planet, the ion probe results displayed prominent dips (Lazarus *et al.* 1982). These dips were noticed in all the three passes, and at approximate locations where the dipole model magnetic field of the planet intersects its equatorial plane at 14 and 19 radii. One possible explanation offered was that there are distributed particulate matter at those locations which affect the ion recombination co-efficient and cause these dips. Such clouds, if present, could be detected during events when the planet Saturn with its complete environment of rings, satellites and plasma, occults a reasonably bright star.

Possibilities of such events were computed from planetary ephemerides (Mink 1983). One of the events was ideally suitable for investigation from the longitudes of India when both the eastern and western regions at 14 L occultated an 8.5 magnitude star on two successive nights of 24 and 25 March 1984 with the object conveniently located for observations. A continuous watch with a high speed photometer was maintained on both nights which indicated possible presence of such clouds, probably in the form of a set of rings or tori.

### 2. Observations

#### 2.1 The 14 L region

The telescope used was the 1 metre telescope at Kavalur Observatory ( $15^{\circ}15'19^{\circ}.6\text{E}$ ,  $+12^{\circ}34'1.58$ ) (now named as Vainu Bappu Observatory), with a photometer and a pulse counting arrangement with 1 second integration. The observations were taken on the nights of 24th and 25th March 1984. Both the nights enjoyed photometric skies during the 3 hour observation period each. To maximise signal to noise ratio, no filter was employed on 24th night, but a Johnson B filter was used on 25th night, with a slight reduction in the S/N ratio.

The same event was also observed from Nainital Observatory ( $5^{\circ}17'49^{\circ}.71\text{E}$ ,  $+29^{\circ}21'1.65$ ) with a slightly different recording arrangement. They, however, had mixed luck about the observing conditions; while being able to record a substantial part of 24th event, clouds frustrated their efforts on 25th. All the records show dips due to increased extinction at instants which could be connected to the passage of star beams through the circumplanetary clouds (Vasundhara *et al.* 1984). Five major dips were noticed in both the Kavalur records, and three in the Nainital record of 24th. The position is shown in Fig. 1.

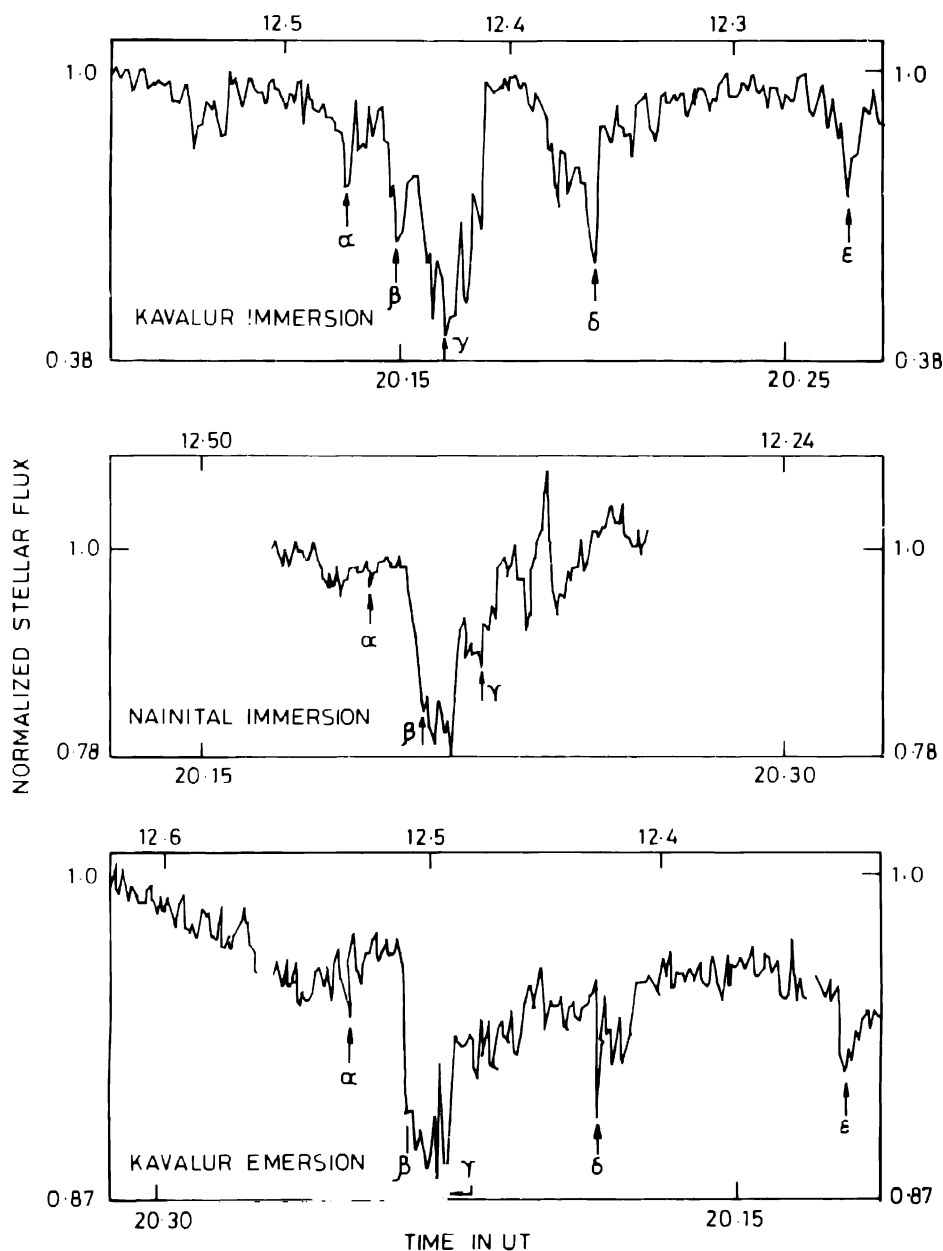


**Figure 1.** Occultation of an 8.5 magnitude star by Saturn.

For estimation of the distances of these clouds from the planet's centre, a simplified model has been assumed. In the model the extinction clouds have been assumed to be contained in a thin equatorial ring, as in the case of the visible rings of the planet. The physical orientation and the ephemerides of the planet being known the time scale

cloud be directly related to the planetocentric distances; according to these schemes all the dips in the three records were found to have occurred when the starbeam crossed regions between 12.2 to 12.8 Saturn-radii. Relative depths of minima as displayed in the three records were found to be consistent, thereby suggesting the presence of well marked clouds in those regions.

Since these clouds have been found on both the east and west sides of the planet, at almost the same distances, we can assume that this is in the form of a set of complete rings. Some variations in the depths, widths and locations have been noticed, but the data being meagre, detailed calculations to ascertain the shape and stability will be fruitless.

An attempt was made to confirm the existence of such a structure through another occultation event. The event was not observable in India, so the help of a foreign observatory was sought. The record was not a clean one, but again after scaling the data, comparing with our old records, some features could be seen to be repeated at almost the same planetocentric distances.

Another attempt to reinvestigate the region of magnetosphere at 12.5 Saturn radius was made by enlisting the help of a large number of observatories in the eastern hemisphere on 2–3 July 1989 when the Saturn system occulted 28 Sgr. Poor sky conditions at most places precluded a systematic comparison of the records. Two of the observers reported negative results at the predicted times.

## 2.2 The 19 L region

In May 1984, another event was observable from India, when the 19 L feature was predicted to be occulted. This time, bad weather was encountered at Kavalur, but at Nainital they could obtain a record from which certain features of this outer system could be found (Mahra *et al.* 1985). The data from Kavalur, was noisy, but still some features could be seen in this record. But the locations as calculated from the adopted equatorial shell model and the timings of dip-events did not match Nainital findings, so that the findings remain unconfirmed till date.

## 3. Attempts for direct detection

As the occultations are few and far between and subject to vagaries of weather, some attempts were made to do area photometry of the concerned regions. The first attempt was made by Baron & Elliot (1983), who employed a CCD camera for detecting any abnormality in these regions. The experiment was marred by a very strong gradient of scattered illumination from the planet, and no definite conclusions could be drawn. An attempt was made at VBO, by employing the 'Diffuse Masking' technique developed by Dave Malin (1977) but the results were vitiated by unforeseen artifacts of the technique. Fresh attempts, however, are being planned.

## 4. Discussions

The results of the occultation experiments have been, however, criticised by Cheng *et al.* (1985) on grounds of negative results of space probes and disagreement between

different occultation records. The latter comment can be traced to rather uncritical examination of observational results, while the former is not free from controversies (Schardt *et al.* 1984).

The results of the occultation experiments on 24 and 25 March 1984 have been critically examined as regards the possibility of their spurious origin, but nothing could be found which may cast a doubt about their reality. The only weak point about the analysis is perhaps the assumption of their containment in a thin ring in the equatorial plane; for if these are composed of fine dust mixed with plasma in Saturn's magnetosphere, the electromagnetic forces are bound to play an important role in their dynamics. In all probabilities, they cannot be contained in a thin equatorial ring, but will have considerable spread along the magnetic lines. Some of the observed characteristics of the dip minima suggests such lateral spreads of the clouds (Bhattacharyya & Vasundhara 1985). The negative results of occultation of 28 Sgr on 3rd July at the predicted time would possibly be attributed to an error in prediction which was based on an equatorial model.

It is now necessary to tackle the question from two different angles: More observations and predictions of occultation events should be continued, and attempts to do the faint photometry by suitable methods should be renewed; and the dynamics of charged dust particles in the circumplanetary magnetic field must be better understood.

### References

- Baron, R. L., Elliot, J. L. 1983, *Astr. J.*, **88**, 562–564.  
 Bhattacharyya, J. C., Vasundhara, R. 1985, *Curr. Sci.*, **54**, 601.  
 Cheng, A. F., Lanzerotti, L. J., MacLennan 1985, *Nature*, **317**, 508–509.  
 Lazarus, A. J., Hasegawa, T., Bagenal, F. 1982, *Nature*, **302**, 230.  
 Mahra, H. S., Pandey, A. K., Mohan, V., Sanwal, B. B. 1985, *Nature*, **313**, 38–39.  
 Malin, D. F. 1977, *AAS Photo Bulletin No. 16*, **10**.  
 Mink, D. G. 1983, *Astr. J.*, **88**, 4.  
 Schardt, A. W., Behannon, K. W., Lepping, R. P., Carbary, J. F., Eviator, A., Siscoe, G. L. 1984, *Saturn, Space Sciences Series* (Ed. T. Gehrels), p. 416.  
 Vasundhara, R., Bhattacharyya, J. C., Santhanam, P., Pande, A. K., Vijay Mohan, Mahra, H. S. 1984, *Nature*, **312**, 621–623.

## Abstracts

### **A Study of Active Region Magnetic Field Structure Using VLA-Radio, Yohkoh X-ray and Mees-Optical Observations**

**N. Gopalswamy** *Department of Astronomy, University of Maryland, College Park, MD 20742, USA*

We have discovered two interesting phenomena in solar active regions, using the Very Large Array: Transient microwave brightenings (TMB) in the sunspot umbra-penumbra boundary and 3 minute oscillations in the umbra. These observations were made during April–May 1992 during the coronal magnetic field structure observing campaign. The TMBs occurred as compact sources at many places around the sunspot umbra. The peak intensity of the TMB's was rather small, typically, 0.01 sfu. The TMBs are associated with brightenings in Yohkoh soft X-rays. The TMBs were located at one footpoint of the X-ray loop. Comparison with magnetogram data shows that the soft X-ray loop connects the sunspot to a neighboring site of opposite polarity, thus supporting the idea of a magnetic loop. These observations will be helpful in understanding the heating of the active region corona through microflares and to derive the magnetic properties of the loops.

The sunspot associated emission shows variability over a time scale of minutes. To our knowledge, this is the first time such rapid variability has been observed in microwaves from a sunspot. The radio emission from umbra consisted of several compact sources with a size less than 4 arcsec. The time evolution of the peak flux of one of these sources showed periodic time variations with a period of approximately 3 min, similar to that of intensity and Doppler shift oscillations observed in optically thin, transition region lines such as C IV in sunspot umbrae. A detailed investigation of this phenomena will provide additional diagnostics in the sunspot atmosphere. The details of these findings will be published elsewhere.

★★★★★

### **H $\alpha$ Intensity Oscillations Observed in Solar Flares**

**Rajmal Jain & S. C. Tripathy** *Udaipur Solar Observatory, 11 Vidya Marg, Udaipur 313 001, India.*

It is known that solar chromosphere oscillates with a period of 120–300 s. In this paper, we report the detection of H $\alpha$  intensity oscillations in two extended flares of 15 November 1989 and 20 April 1991. The H $\alpha$  filtergrams of these flares after digitization were re-registered pixel to pixel using IRAF to remove guiding jitters. The intensities at many different locations including flare kernels ( $I$ ) and background chromosphere ( $I_{ch}$ ) were determined after applying proper corrections for various non-solar effects. The



relative intensity variation  $((I - I_{ch})/I_{ch})$  with time in flare kernels and background chromosphere was then determined. These time sequences were subjected to Fourier Transform (FT) to obtain the oscillation modes. Our analysis showed predominant 5 and 3 minute modes unambiguously in chromosphere and flares.

Our results mark the first detection of the prominent 5 and 3 minute modes in flares. The frequency deviation in oscillation modes in chromosphere and flares observed by us from those determined at the center of the disk by Elliott (1969); Kneer & Uexkull (1983) and Harvey *et al.* (1993), may be an effect of higher magnetic field and location of the measurements in chromosphere. Further, the reduction in frequencies of the order of  $100 \mu\text{Hz}$  observed in flare oscillations as compared to the background chromosphere may be due to the high temperature in flare regions as predicted by Evans & Roberts (1990).

★★★★★

## **2-Dimensional Velocity Field Measurement of Eruptive Prominence Observed on January 14, 1993**

A. Bhatnagar & S. C. Tripathy *Udaipur Solar Observatory, 11 Vidya Marg, Udaipur 313 001, India.*

On January 14, 1993, a quiescent prominence was observed from the Udaipur Solar Observatory on the south-east limb of the sun which suddenly erupted between 05:11 and 07:13 UT, displaying a huge mass ejection. Two dimensional velocity measurement of several knots of the eruptive prominence were made. Except for one fast moving knot, the whole prominence material rose with an initial average velocity of  $90 \text{ km/s}$  and with increasing height the velocity increased to  $720 \text{ km/s}$ . Within 49 minutes the prominence material reached upto a height of  $5.5 \times 10^5 \text{ km}$  from the limb. A conspicuous increase in the acceleration by two orders of magnitude suggests an imbalance between the magnetic, gravitational and kinetic energy. A remarkable new phenomenon of quasi-periodic velocity oscillations with height in prominence knots has been observed.

★★★★★

## **Three-Dimensional Velocity Structure of Surge and Quiescent Prominences**

Nandita Srivastava & Shibu K. Mathew *Udaipur Solar Observatory, 11 Vidya Marg, Udaipur 313 001, India.*

We report here measurements of three-dimensional velocity field structure of a surge prominence observed on May 26, 1993 and a quiescent prominence observed on June 7,

1993, from Udaipur Solar Observatory through a multislit spectrograph in H $\alpha$  in conjunction with a 15 cm Coude telescope.

From the measurements of the Doppler shifts of H $\alpha$  line, we found that the maximum line-of-sight velocities in the surge prominence were of the order of 20–40 km s<sup>-1</sup>. Combining the radial and sky-plane velocities, the resultant velocity in the surge is found to lie in the range  $\sim 120$ –300 km s<sup>-1</sup>. The orientation of the surge on the solar surface has also been obtained by calculation of the angle of inclination which the surge makes with respect to the vertical of the solar surface. It is found that the surge is nearly vertical to the solar surface. The temporal evolution of the angle of inclination shows an increase from 4° to 15° in a duration of 5 minutes. It is suggested that the surge material falls back on the solar surface, as time progressed.

In the case of quiescent prominence, the measured Doppler shifts were smaller and hence the line-of-sight velocities were lesser in the range  $\sim 0$ –7 km s<sup>-1</sup>. Since negligible sky-plane velocities were observed in the case of quiescent prominence, the resultant velocities were also found to lie in the range 0–7 km s<sup>-1</sup>.

★ ★ ★ ★ ★

### Direct Observational Evidence for the Heating of the Solar Chromosphere

R. Kariyappa & K. R. Sivaraman *Indian Institute of Astrophysics, Bangalore 560 034, India.*

M. N. Anandaram *Department of Physics, Bangalore University, Bangalore 560 056, India.*

A 35-minute time series of photographic spectra in the CaII H line obtained at the Vacuum Tower Telescope (VTT) of the Sacramento Peak Observatory, New Mexico at high spatial, spectral and the temporal resolution on a quiet region around the centre of the solar disc has been analysed to provide data on the range of line profile variations. We have derived line profiles at the sites of the inner network bright points. From the temporal changes seen in these profiles we have studied the dynamical processes associated with the evolution of these structures. We find that the bright points can be grouped into three classes based on their evolution pattern. We have discussed the similarities and differences in behavior of the bright points among the three classes. It is argued that the differences in the behavior of the bright points in the three classes are directly linked with the differences in the underlying photospheric magnetic field co-spatial with them. The plots of the intensity of  $H_{2v}$  parameter versus time (light curves) for the entire 35-minute duration of the sequence show that the mode of excitation in the bright points starts with a 'main pulse' which is followed by smaller pulses with exponentially decreasing brightness. The histogram plots and the power spectrum analysis of these pulses show that their intensity oscillates with a period around 190 s. The period of oscillations is independent of the amplitudes of the wave pulses.

We have also estimated the total energy dissipated at the site of the bright points using their line profiles over the entire sun and this energy flux together with that contributed by the network boundary regions matches well with the emission by the CaII ions estimated in the model calculations. Thus the bright points are the sites where substantial heating takes place and the main pulse transports this energy. We have discussed the physical nature of the wave propagation in the three classes of bright points.

★ ★ ★ ★ ★

## **Spectroscopic Analysis of Prominence H $\alpha$ CaII H & K and HeI 10830 Lines**

**Y. D. Park** *Korea Astronomy Observatory, Korea.*

**H. S. Yun** *Astronomy Department, Seoul National University, Korea.*

**K. Ichimoto** *National Astronomical Observatory, Japan.*

Quiescent prominence spectra of H $\alpha$ , CaII H & K and HeI 10830 lines have been taken with GI CCD camera attached to 25 cm coronagraph at the Norikura solar station, the National Astronomical Observatory of Japan from August 10 through October 13, 1992. In the present study, we have analysed a set of spectra of H $\alpha$ , CaII H & K taken from a quiescent prominence (P.A. = 110°) that appeared on the 16th of August 1992. In taking these spectra the slit was placed parallel to the solar limb at 7 different heights on the prominence, each being separated by 10 arcsec. The spectral resolution is 0.023 Å/pixel and the spatial resolution is 0.6 arcsec/pixel. Each spectra was taken 30 seconds apart for about half an hour, during which time the slit was kept fixed. The projected maximum height of the prominence was about 42,000 km.

The quantitative analysis has been made on the observed H $\alpha$ , CaII H & K lines to determine the temperature and turbulent velocity of the prominence by measuring their Doppler half widths. The final analysis shows that the temperature ranges from 7300 to 8800 K with an average turbulent velocity of 7 km/s. The column density of CaII and H are found to be  $N(\text{CaII}) = 10^{13}$  and  $N(\text{H}) = 5 \times 10^{18}$  respectively, which are in good agreement with those of Gallegos & Machado (1973, *Solar Phys.*, **31**, 427) and Engvold (1976, *Solar Phys.*, **49**, 283).

In order to examine the oscillatory nature of prominences we have taken time sequential spectra of HeI 10830 lines by placing the slit at a fixed position over two hours each for two quiescent prominences, which appeared on the 23rd of August (P.A. = 270°) and on the 3rd of October (P.A. = 80°). The spectral resolution is 0.054 Å/pixel for HeI 10830. The peak intensities of the observed HeI 10830 lines have been measured to obtain their intensity variations with time. From the measured intensity variations the power spectra of these two quiescent prominences were generated by using the method of Carbonell *et al.* (1992, *Astr. Astrophys.*, **264**, 350). The resulting power spectra show that both the prominences have definitive oscillatory motions with a nearly identical set of periods of 66, 40 and 30 minutes.

★★★★★

## **Solar Observations using Lithium Niobate Fabry-Perot Etalon**

**A. Bhatnagar, Debi Prasad C. & Shibu K. Mathew** *Udaipur Solar Observatory, 11 Vidya Marg, Udaipur 313001, India.*

Solar physicists have been using the Lyot birefringent filters for the narrowband ( $\delta\lambda = 0.5 \text{ \AA}$ ) imaging of solar chromospheric activities. The limitations of these filters are lower throughput, smaller usable aperture, higher temperature sensitivity and

higher cost. During the last few years Fabry-Perot (FP) etalon based filters have been used in solar astronomy in order to overcome some of these difficulties. In particular, the use of Lithium Niobate ( $\text{LiNbO}_3$ ) based FP etalons have opened new avenues to design excellent tunable narrowband filters. These FP etalons can be made by cutting a wafer parallel to Z or Y axis of  $\text{LiNbO}_3$  crystal, two surfaces of which are polished and coated with dielectric material. The refractive index of the crystal can be varied by applying voltage, which serve the purpose of tuning the wavelength. At the Udaipur Solar Observatory, USO, we are using a 60 mm aperture Z-cut  $\text{LiNbO}_3$  FP etalon filter, made by the CSIRO, Australia. The free spectral range and finesse of this etalon at  $6122 \text{ \AA}$  is  $4.6 \text{ \AA}$  and 29 respectively, which gives a band pass of  $0.15 \text{ \AA}$ . The filter can be tuned with a sensitivity of  $0.57 \text{ \AA}$  per 1000 volt. This filter is being used at USO to take monochromatic H $\alpha$  solar observations. The same filter will be used in video magnetograph being built at USO, using  $6122 \text{ \AA}$  line of CaI. Comparing the H $\alpha$  observations taken through the  $0.5 \text{ \AA}$  passband birefringent filter and those taken through the  $\text{LiNbO}_3$  filter, the FP yields about 50% higher transmission through  $0.15 \text{ \AA}$  passband. However, this FP has a smaller field of view (acceptance angle) and the instrumental profile is an Airy function, while the birefringent filter is a Sinc function. This leads to higher continuum leakage in case of FP. We have completed the bench test of the filter and used it at the f/40 beam of the USO Spar telescope in a telecentric arrangement.

★★★★★

### **Study of Solar Flares Observed in Hard X-ray and Soft X-ray Emissions**

V. K. Verma & M. C. Pande *Uttar Pradesh State Observatory, Manora Peak, Naini Tal 263129, India.*

The study of over 400 solar burst data observed by the X-ray polychrometer and the hard X-ray bursts spectrometer (aboard SMM satellite) during solar flares is reported here. The study shows that 30% solar flares show hard X-ray (HXR) emissions earlier than the soft X-ray (SXR) emissions, while 70% solar flares show HXR emissions that occur later than the SXR emissions. Since the SXR emissions and the HXR emissions originate at different heights in the solar atmosphere, therefore these events seem to represent two different types of flares. In the first case, the triggering starts from the place of origin of hard X-rays i.e. lower chromosphere or photosphere, while in the other case, the flare triggering starts from the place of origin of soft X-rays i.e. the solar corona. The possible cause for this type of behaviour is also discussed in the paper.

★★★★★

### **Eruptive Prominence Associated with Limb Flare of 25 January 1991**

Wahab Uddin & V. K. Verma *Uttar Pradesh State Observatory, Naini Tal 263129, India.*

We have observed an eruptive prominence on 25 January 1991 which started earlier

than 06 23 UT and was associated with a limb flare (S16 E90) of class 1B/X10. The eruptive prominence ejected out with a maximum speed of about  $1300 \text{ km sec}^{-1}$  and its huge mass attained height upto 150,000 km and finally faded/disappeared in the corona. During the ascending phase there was an unscrewing of the loop system associated with the eruptive prominence. The type II, III, and IV radio bursts were also reported during the eruptive prominence. The high flux of sudden ionospheric disturbances and the solar radio emissions on fixed frequencies (245-15400 MHz) were also recorded. The eruptive prominence associated with limb flare also shows increase in proton flux ( $\geq 10 \text{ MeV}$ ) during its occurrence. In the paper we have analysed the observed data and compared it with the theoretical model of the solar flare.

★★★★★

### **Eruption of Helical Prominence of December 15, 1992**

Wahab Uddin, V. P. Gaur & M. C. Pande *Uttar Pradesh State Observatory, Naini Tal 263 129, India.*

We present an analysis of a dynamical helical loop prominence of December 15, 1992 which was observed with the help of a 15-cm coude refractor and Bernard Halle H-alpha filter on the south-east limb. The observations cover complete evolution of the prominence from quiescent phase to eruptive phase. Prominence rise and eruption was noticed when one footpoint evolved with a complex multiloop structure. The prominence shows a strong activation with dynamic expansion. The velocities of bright knots of the prominence show gradient of velocity with respect to height. The maximum height attained by the prominence loop as per our observations was  $0.48 R_{\odot}$  above the limb. After attaining this height, the top portion of the loop erupted out with a velocity of about  $600 \text{ km/sec}$ . Dynamic behaviour of the prominence shows characteristics of disaripation brusque. Possible mechanisms for activational and morphological evolution of the prominence are also discussed.

★★★★★

### **Eruption of a Large Quiescent Prominence on January 14, 1993**

Wahab Uddin & K. R. Bondal *Uttar Pradesh State Observatory, Naini Tal 263 129, India*

Analysis of a large quiescent prominence, which erupted on January 14, 1993 is carried out. The prominence made its first appearance on January 12, 1993 at the East limb, showed a flare-like brightening on January 13, attaining a maximum volume with twisted structure. The eruption was caused probably by a plage brightening in the nearby active region, imparting a maximum velocity of about  $1400 \text{ km sec}^{-1}$  to the prominence before it disappeared. The morphology and evolution of the prominence is given in the light of existing models and some physical parameters calculated.

★★★★★

## **Recurrent Surge Activity from Active Region NOAA 6368**

**Wahab Uddin, V. K. Verma & M. C. Pande** *Uttar Pradesh State Observatory, Naini Tal 263 129, India.*

We report here a study of 8 solar surges observed in H $\alpha$  emissions on the west solar limb in active region (AR) NOAA 6368 on 26, 27 and 28 November 1990. Three surges were observed on 26 November of durations 35, 86 and 40 min at time intervals of 20 and 25 min respectively for successive events. Two solar surges of durations 56 and 101 min on 27 November at an interval of 10 min in same AR. Three surges were also observed on 28 November of durations 25, 138 and 95 mins at time intervals of 10 and 20 min respectively for successive events. Using photographic observations, we have studied the morphological behaviour and estimated the height, mass, radial velocity and mechanical energies associated with the 8 surges. The X-ray and radio data observed during the surges are also included in the study. The various parameters estimated from the observed data are discussed in the light of solar surge theories.

★★★★★

## **Mass Transfer and Surge Activity of 14 May 1993**

**V. K. Verma & Wahab Uddin** *Uttar Pradesh State Observatory, Manora Peak, Naini Tal 263 129, India.*

An analysis of the mass transfer from the quiescent prominence to nearby active center and two solar surges observed in H-alpha emissions during 01:30–05:00 UT (14 May 1993) are presented here. The mass transfer from the quiescent prominence to the nearby active center X took place with an average velocity of 134 km/s for 55 min duration. During this period, the prominence lost its 75% mass which transferred to the nearby active center X. The two surges ejected from the active center Y which is about 5 arcmin distance from the active center X. The two surges attain maximum heights/velocity  $37 \times 10^3$  km/160 km/s and  $77 \times 10^3$  km/300 km/s, respectively. In the paper we have also estimated height, mass, mechanical energy and magnetic field associated with all surges. The parameters obtained for the mass transfer from prominence and two surges are discussed in the light of existing theories.

★★★★★

## **On the Periodicity of Solar Wind Phenomena**

**V. K. Verma & G. C. Joshi** *Uttar Pradesh State Observatory, Manora Peak, Naini Tal 263 129, India.*

We have investigated the rate of occurrence of solar wind phenomena observed between 1972–1984 using power spectrum analysis. The data have been taken from the

high speed solar wind (HSSW) streams catalogue published by Mavromichalaki *et al.* (1988). The power spectrum analysis of HSSW events indicate that HSSW stream events have a periodicity of 9 days. This periodicity of HSSW events is 1/3 of the 27 days period of coronal holes which are the major source of solar wind events. In our opinion the 9 days period may be the energy build up time to produce the HSSW stream events.

★★★★★

## Coronal Mass Ejections and the Critical Ionization Velocity Phenomenon

E. Golbraikh, M. Filippov & R. Steinitz *Ben-Gurion University, Physics Department, Beer-Sheva, Israel.*

The critical ionization velocity (CIV) mechanism was introduced by Alfvén (1954) in his theory of the origin of the Solar system. Alfvén postulated that rapid ionization of neutral gas occurs, when it moves through magnetized plasma with velocity  $V_0$ , whose component perpendicular to the magnetic field exceeds a critical value

$$V_0 > V_c = (2C_i/M_n)^{1/2},$$

where  $C_i$  and  $M_n$  are the ionization energy and mass of the neutral particle, respectively.

Here we propose a new mechanism for Coronal Mass Ejection (CME) formation in the solar corona. We suggest that the origin of a CME is connected with high-speed movement in the transition zone or lower. The high-speed flows of neutral gas are able to produce explosive events and jets in the chromosphere by the CIV mechanism.

These can be the sources of eruptive prominences. In this case CIV results in ion and electron heating up to tens eV. In turn high-energy electrons can cause weak flares. The eruptive prominences generate CMEs with velocities  $> 100 \text{ km s}^{-1}$ .

Thus, the following chain of events appears to form the observed CME: high-speed movement of neutral gas – its ionization due to CIV – eruptive prominence (weak flare) – Coronal Mass Ejection.

★★★★★

## Masked Coronal Mass Ejections: An Attempt to Demask Them

M. Filippov, E. Golbraikh & R. Steinitz *Ben-Gurion University, Physics Department, Beer-Sheva, Israel.*

Coronal mass ejections from the Sun (CMEs) are observed as bright emissive structures of the solar corona ( $r < 10R_\odot$ ) by means of Earth-orbiting coronagraphs.

The white light observations just provide a particular view of mass ejection, projected onto the plane of the sky, as viewed from Earth. From these observations we are not able to determine the exact location of the CME on the sun, yet observed CMEs

are classified according to their two-dimensional, apparent, morphologies. We unify the existing elaborate classification system applied to CMEs. This is possible because one and the same phenomenon – i.e., mass ejection – is projected on the plane of the sky. We suggest therefore that only one three-dimensional structure of CME exists. Just looking at such a structure in different projections one can see various coronal forms. We conclude that it is not necessary to have ten different morphological classes of CME's, when in fact they represent one and the same structure, seen in different aspects.

★★★★★

## **Diamagnetic Abundance Differentiation**

**Raphael Steinitz & Estelle Kunoff** *Physics Department, Ben Gurion University of the Negev 84105, Beer Sheva, Israel.*

It is well established that there is chemical abundance differentiation between material in the photosphere, and material in the corona or the solar wind. It appears that this effect is according to first ionization potential (FIP) only, and does not depend on mass or charge. We explore the possibility that this differentiation is the result of strong diamagnetic effects experienced by ions in the chromosphere – corona transition zone, in the presence of diverging magnetic structures.

★★★★★

## **Misconceptions Concerning the Vanishing Average of the Diamagnetic Effect**

**Raphael Steinitz** *Physics Department, Ben Gurion University of the Negev 84105, Beer Sheva, Israel.*

It has been argued in the past that while the diamagnetic effect (DME) is apparent for single particles (i.e. motion of charged particles in the earth's ionosphere), it is not relevant for fluid descriptions of plasmas. We show that this is a misconception which is due to a wrong averaging procedure.

It is easy to show that when charged particles move in a magnetic field that changes its intensity along the field, the time average over such a particle motion and the ensemble average are not equal. Thus, the Gibbs condition is violated and the ensemble average cannot replace the time average. The DME does not therefore vanish for a plasma.

Taking into account the DME and gravity, we obtain speed filters. They, in turn, function as heat and momentum pumps, resulting in cool sunspots, hot coronae and stellar winds.

★★★★★



## Diamagnetic Acceleration of the Solar Wind

**B. Sekeles & R. Steinitz** *Department of Physics, Ben Gurion University, Beer Sheva 84105, Israel.*

We develop a new model to account for proton acceleration in the solar wind. Acceleration is a direct result of the diamagnetic effect on the charged particles, and hence on their velocity distribution. Our basic assumptions are: a collisionless plasma, energy conservation and magnetic moment conservation.

Through numerical simulations we explore the changes in bulk speed between 0.3 AU and 1 AU. We find that the diamagnetic effect account for the observed velocity increase in bulk speed.

Since any form of wave-particle interactions is excluded from our simulations, but they fit well the observations, we suggest that the diamagnetic effect also accounts for wind expansion in early type stars, i.e. for stars without convective energy available at their surface.

★ ★ ★ ★ ★

## Energy Transport to the Solar Corona by Magnetic Kink Waves

**Arnab Rai Choudhuri<sup>1</sup>, Mausumi Dikpati<sup>1,2</sup> & Dipankar Banerjee<sup>2</sup>**

<sup>1</sup> *Department of Physics, Indian Institute of Science, Bangalore 560012, India.*

<sup>2</sup> *Indian Institute of Astrophysics, Bangalore 560034, India.*

We show that the magnetic kink waves generated by the motions of photospheric footpoints of the coronal flux tubes can supply adequate energy for heating the quiet corona, provided there are occasional rapid motions of these footpoints as found in recent observations (Vigneau *et al.* 1992, preprint). Choudhuri, Auffret & Priest (1992, *Solar Phys.*, **143**, 49; hereafter Paper I) modelled the solar corona as an isothermal atmosphere and showed that these rapid footpoint motions are much more efficient for transporting energy compared to the slow footpoint motions taking place most of the time. We extend these calculations for a two-layer atmosphere, with the lower layer having chromospheric thickness and temperature, and the upper layer having coronal temperature. Even in the presence of such a temperature jump, we find that the rapid footpoint motions are still much more efficient for transporting energy to the corona and the estimated energy flux is sufficient for quiet coronal heating, i.e. we reinforce the conclusions of Paper I.

In addition to presenting results for the solar corona, we discuss the general problem of the propagation of kink pulses in a two-layer atmosphere for different possible values of the basic parameters. We find a fairly complicated behavior which could not be anticipated from the analysis of a pure Fourier mode. For pulses generated by rapid footpoint motions, the energy flux decreases due to reflection at the transition layer. For pulses generated by slow footpoint motions, however, the behavior of the system is

governed by modes, which are evanescent in the lower layer, but can tunnel through it. The energy flux carried by such pulses can actually increase when there is a temperature jump in the atmosphere.

★★★★★

## **The Evolution of Weak Magnetic Fields of the Sun in Relation to Dynamo Theory**

**M. Dikpati & A. R. Choudhuri** *Department of Physics, Indian Institute of Science, Bangalore 560 012, India*

We present here a model to explain how the weak large-scale diffuse magnetic fields of the sun migrate poleward in contrast to the sunspots which migrate equatorward with the progress of the solar cycle. We study the evolution of the sun's poloidal field in the convection zone by assuming that it is produced by an equatorward-propagating dynamo wave at the base (Choudhuri 1990, *Astr. J.*, **355**, 733) of the convection zone and is subject to turbulent diffusion and a meridional circulation with a poleward surface flow. The magnetic fieldlines in the lower part of the convection zone first move towards the equator where they are pushed upward by the upwelling meridional flow there to form magnetic bubbles by joining with their opposite hemisphere counterparts. After reaching the surface, these bubbles drift to higher latitudes with the poleward meridional flow. Our model incorporates the three-dimensional vector character of the magnetic field, whereas the previous model of Wang *et al.* for the poleward drift of weak fields treated the magnetic field as a scalar on the two-dimensional solar surface.

★★★★★

## **Magneto-Convection in Sunspot Penumbra**

**S. G. Tagare & P. Murali** *School of Mathematics, University of Hyderabad, Hyderabad 500 134, India.*

The original motivation for studying the magneto-convection arose from the attempts to explain the origin of sunspots. Here we analyze the effect of horizontal magnetic field on Rayleigh-Bénard convection in a region where

$$\frac{k}{\eta} = \frac{\sigma_2}{\sigma_1} < 1 \text{ for any } Q,$$

and

$$\frac{k}{\eta} = \frac{\sigma_2}{\sigma_1} > 1 \text{ for } Q \leq Q_c = \frac{(1 + \sigma_1)(\pi^2 + q_c^2)^2}{q_c^2(\sigma_2 - \sigma_1)}$$

Here  $k$  denotes thermal diffusivity,  $\eta$  denotes magnetic diffusivity,  $\sigma_1$  denotes thermal Prandtl number,  $\sigma_2$  denotes magnetic Prandtl number,  $Q$  denotes Chandrasekhar number and  $q_c$  is a critical wave-number corresponding to onset of stationary convection. The magnetic field in umbral region of sunspots is vertical (typically around 3000 gauss), spreading outward to the nearly horizontal in the penumbral region (typically around 1000 gauss). In the region of sunspot penumbra where above limits are satisfied, Hopf bifurcation (oscillatory convection) is absent and the principle of exchange of instability is valid leading to pitchfork bifurcation (cusp bifurcation) for  $Q < Q_c$  and Takens-Bogdanov bifurcation (saddle-node bifurcation) for  $Q = Q_c$ . We have derived nonlinear time-dependent one-dimensional equation near the onset of stationary convection at supercritical pitchfork (cusp) bifurcation and nonlinear second-order ordinary differential equation near the onset of stationary convection at supercritical Takens-Bogdanov (saddle-node) bifurcation. We have obtained the steady-state solution of the Landau-Ginzburg equation as well as solution of the nonlinear second-order ordinary differential equation which describes behaviour near the onset of stationary convection.

★★★★★

### **Helioseismic Determination of Sound Speed in the Sun**

**Sarbani Basu & H. M. Antia** *Tata Institute of Fundamental Research, Homi Bhabha Road, Bombay 400 005, India.*

We present an asymptotic method for inferring the speed of sound within the Sun using solar  $p$ -mode oscillation frequencies. The method has been tested on solar models. We show that addition of higher order terms to the Duvall Law leads to substantial improvement in the results. The relative difference between the actual and inferred sound speeds of the solar models is found to be less than 0.5% between radii of  $0.05R_\odot$  and  $0.99R_\odot$ . Using the differential technique we can get much better results, even without the higher order terms. With this method it is possible to get similar accuracy down to a radius of  $0.01R_\odot$ . Results for frequencies with random errors added show that the method is not very sensitive to errors in the frequencies, and hence the sound speed within the Sun can be estimated quite reliably. The sound speed in the Sun is found to be within 1% of that in a standard solar model with a convection zone depth of 200000 km.

★★★★★

### **On the Relation of AAA Asteroids and Comets**

**Suryadi Siregar** *Department of Astronomy, Institute of Technology of Bandung, Indonesia.*

By using the Minor Planet Data Base of the National Astronomical Observatory, Tokyo, we investigated the origin of the Apollo-Amor-Aten (AAA) asteroids. This

study concluded that the AAA asteroids are double than three years ago, the percentage of both classes remains constant. Statistically, the Tisserand invariant,  $T$ , of AAA objects spread in the range from 2 to 7.6 with strong concentration at  $T \geq 3$ , meanwhile comets have the Tisserand invariant of  $T \leq 3$ . The present status of Tisserand invariant of comets and AAA asteroids are briefly described, the AAA asteroids appear unusual, as compared with main-belts objects. The precise physical mechanism that might explain the differences remains a mystery. The current studies estimate that some 60% of the Earth-crossing objects are supplied from some other reservoirs. At present the short period comets are the only identified reservoir that can fill that gap. The present status of possible Comet-like Asteroid and Asteroid-like Comet are briefly described.

There is as yet no conclusive evidence that any of the asteroids are extinct or dormant cometary nuclei. But there is a tantalizing body of evidence which we have presented here, which suggests that some near Earth asteroids plus several others have cometary properties, either dynamically or physically in particular are identified as cometary. At the same time many of the likely cometary candidates have physical properties which are inconsistent with our current understanding of cometary nuclei such as high albedos and (or) unusual spectra. Thus it is not yet possible to put together a coherent picture or to conclusively identify any specific asteroids as an extinct cometary nucleus.

★★★★★

### **Formation and Regression of the Martian North Polar Cap in 1992–1993 from Image Processed CCD and Photographic Images and Drawings**

**K. Iwasaki** *Kyoto Gakuen University, Nanjo, Sogabecho, Kameoka, Kyoto 621, Japan.*

**S. M. Larson** *Lunar and Planetary Laboratory, University of Arizona, Tucson, Arizona 85721, U.S.A.*

**E. Panjaitan & I. Radiman** *Bosscha Observatory, Institute of Technology of Bandung, Lembang, Indonesia.*

**T. Akabane** *Hida Observatory, Kyoto University, Kamitakara, Gifu 506-13, Japan.*

**S. Ebisawa** *Planetary Research Observatory, Hirayama, Hino, Tokyo 191, Japan.*

The problem of when the north polar cap forms has not yet been solved observationally. The 1992–1993 apparition was favorable to observe the season of the formation and the regression of the north polar cap. The cooperation works of the observations of Mars in 1992–1993 were executed with the 49-cm reflector at the Planetary Research Observatory, with the 60-cm double refractor at the Bosscha Observatory, with the 65-cm refractor at the Hida Observatory, and with the 154-cm reflector at the Catalina Station, Steward Observatory, University of Arizona. The CCD and photographic images and the drawings obtained by those observations have been image processed and measured with a new measuring system of Martian polar cap. In this method, we use image display routine (SAO image) in the IRAF to display images of Mars on the screen of the SUN work stations.

In our observations in 1992, red filter images taken in the period before  $L_s = 0^\circ$  ( $L_s$  is the areocentric longitude of the Sun) revealed dark surface features of the northern high latitudes, when blue filter images show the extensive polar hood. The latitude of the northernmost feature observed was about  $64^\circ\text{N}$ . Similar to our observations in 1975–1976, a widespread north polar cap, which is predicted by most of the existing models and the Viking observations, was not observed in our observations in 1992.

After  $L_s = 0^\circ$ , the north polar cap in the 1992–1993 apparition hesitated to shrink until  $L_s = 40^\circ$ , and then it started to shrink in our observations. The mean latitude of the edge of the cap was near  $60^\circ\text{N}$ , and was too big compared with the earlier observations. The color of the north polar cap before  $L_s = 40^\circ$  was a little bit bluish. Therefore, there is a possibility that the north polar hood remained until  $L_s = 40^\circ$  in this apparition and we observed the edge of the polar hood instead of the edge of the polar cap. After  $L_s = 45^\circ$ , the size of the north polar cap in 1993 appears to have been similar to those in earlier years.



## On the Dust Torus around the Orbit of Phobos

A. V. Krivov & V. B. Titov *Astronomical Institute, St. Petersburg University, Stary Peterhof, 198904 St. Petersburg, Russia.*

Impact ejecta from the surfaces of some small planetary satellites (such as Martian moon Phobos) should give rise to dust belts surrounding the satellites' orbits. The mechanism of dust belt formation is as follows. A satellite is subjected to impacts of meteoroids with encounter velocities of about  $10\text{ km second}^{-1}$ . The total mass of the ejecta is 3 to 4 orders of magnitude greater than the mass of a projectile. A great number of excavated particles is thrown to planetocentric trajectories close to the satellite orbit. This results in the generation of a dust toroid with an axial line coinciding with the orbit of the parent body. Simultaneously the grains are removed from the torus by the satellite. For not very small grains, their removal by the satellite is the major loss mechanism, so that the matter injection into the torus and the re-accretion come to a dynamical equilibrium at the increased density level.

We construct the model of a dust torus and apply it to the Phobos case as the most typical and important in view of the Martian space missions planned for the near future. Under some plausible assumptions, we come to the following estimates. The total mass of the Phobos dust belt is several times  $10^4\text{ kg}$ . The lifetime of a particle inside the torus should be about 1 yr. The matter density reaches a maximal value at the Phobos orbit, being  $10^6$  times the background density of the interplanetary medium. All estimations are probably within one order of magnitude accuracy due to the physical data uncertainties and errors of the simulation.

Our results are valid for macroscopic particles, greater than about  $100\text{ }\mu\text{m}$  in size. The fine-dust component of the belt, affected strongly by radiative forces and charging, should be the subject of a separate study.

Ways to refine the model and directions for further investigation are discussed.



## Imaging Polarimetry of Comet Austin

U. C. Joshi, J. S. Chauhan, M. R. Deshpande & A. K. Sen *Physical Research Laboratory, Ahmedabad 380 009, India.*

A. K. Bhatnagar *Positional Astronomy Centre, Calcutta 700 053, India.*

Comet Austin was observed during April and May 1990 when its phase was between 106 and 110 degrees to study its polarization behaviour. Observations were made at Mt. Abu on April 30 and May 1–3, 1990 with a Celestron-14 telescope equipped with an image intensifier placed at the focal plane. A polaroid sheet was placed in front of the primary mirror. Kodak-2515 film was used for photographic recording. Three exposures of comet Austin were taken in three different orientations (0, 120 and 240 degrees) of the optic axis of the polaroid sheet with respect to the celestial NS axis. Polarization of individual pixel was calculated using the method discussed in Sen *et al.* (1990, *Icarus*, **86**, 248). In this paper we have presented the results based on the observations made on April 30, 1990.

Polarization image shows the regions of high (16%) and low (0–2%) polarization. Near the nucleus polarization is almost zero; in the near vicinity the value is 4–6%. There is a small feature south of comet nucleus showing relatively high polarization (8%). High polarization (16%) in the outer region in the form of a shell is seen. The mean distance of the shell from the nucleus on the west side is 450 arcsec. The high polarization may be due to scattering by smaller dust grains (implying segregation of grains). The total molecular emission in the outer region may be low.

Strong jets or other unusual activity, as observed in comet Halley (Eaton *et al.* 1988, *Icarus*, **76**, 270) is not seen in the polarization map. Mild streaming is however seen on the western side. Segregation of dust particles is expected in the tail direction due to solar radiation pressure. The plate scale of the telescope being 68 arcsec per mm and the pixel size of the digitized image being 60 micron, each pixel corresponds to 4.08 arcsec of comet i.e. a linear size  $\sim 1700$  km on the comet on April 30. The mean distance of the high polarization region on the west side from the nucleus is estimated to be about 190,000 km.

★★★★★

## Physical Structure and Stability of Cometary Nuclei

B. S. Sandhu & M. Šolc *Institute of Astronomy, Charles University, Prague, Czech Republic.*

Whipple's icy conglomerate model of cometary nucleus enjoyed wide acceptance and a long successful life. Considerable changes were brought to it, based on the guidance of observational evidences and theoretical considerations. After the fractal model and the rubble pile model, icy glue model brought major alterations. But the concept of porous refractory boulders of the icy glue model seems to be quite unrealistic and inexplicable. Viewing minutely the process of cometary formation, the boulder complex model is proposed. It explains cometary splitting as the breaking free of a single complex of boulders or more. Breakage of boulders at a small scale may explain the issue of cometary outbursts. An extreme case of global breakage of boulders may even explain the complete disruption of a comet.

★★★★★



# **Instrumentation**





# New Observing Facilities and Recent Progress in China

Ye Shuhua *Shanghai Observatory, Chinese Academy of Sciences.*

**Abstract.** Developing and upgrading the observing facilities in China have been emphasized to provide the foundation of observational astronomy. Most of the instruments were designed and made in domestic factories and observatories. The Nanjing Astronomical Instrument Research and Manufacturing Center has played an important role in the application of these advanced techniques and detectors such as self-adaptive optics, fiber optics, CCD cameras, computer image processing system, etc.

This paper gives a brief survey on the new progress in recent years. All the facilities are available to domestic and foreign astronomers and scientific cooperations are highly welcome.

*Key words:* Telescope – observation.

## 1. Optical telescopes

### 1.1 2.16 m Reflector (Location: Xinglong Station, Beijing Observatory)

This telescope is equipped with two CCD cameras, the red sensitive one with  $578 \times 384$  pixels, corresponding to a  $2'.34 \times 1'.56$  field, while the blue sensitive one with  $512 \times 512$  pixels and a  $2'.23 \times 2'.44$  field. As spectrograph is located on the F/9 Cass. focus, with grating of 300 lines/mm, and  $80 \times 100$  mm area, the dispersion being 195 Å/mm. The telescope is being used in both single and multi-object observing mode with fiber optics system. A new spectrograph will be installed in the F/45 focus this year.

### 1.2 1.56 m Astrometric reflector (Location: Sheshan Station, Shanghai Observatory)

This telescope is also equipped with a CCD camera on the F/10 focus, the CCD is a red sensitive one with  $1024 \times 1024$  pixels, corresponding to a  $4' \times 4'$  field. A photoelectric photometer with time resolution to 1 ms is used for occultation observation.

### 1.3 1.26 m IR Telescope (Location: Xinglong Station, Beijing Observatory)

The Cass. focus of F/30 with a field  $14'$  is used for this telescope. For 1 minute integration time, the photometer can reach

J	H	K	L	M	band
12.5	12.5	12.5	8.5	7.0	magnitude

#### 1.4 69/90 cm Schmidt telescope (Location: Xinglong Station, Beijing Observatory)

By using 17 filters on the F/3 focus and with a CCD camera of  $2048 \times 2048$  pixels, the Beijing-Arizona Multi-colour Survey Project is being performed on this telescope for stars down to 20th magnitude.

### 2. Solar observing facilities.

#### 2.1 Solar Magnetic field telescope (Location: Huairou Station, Beijing Observatory)

The performances of the telescope are as follows:  $A = 35$  cm,  $f = 228$  cm with vacuum tube, dual observing channels: 5324.19Å and 4861.34Å by using specially designed birefringent filter with 3 KDP electro-optic modulators and CCD with  $512 \times 512$  pixels. The solar photosphere and chromosphere can be observed simultaneously. The resolution is as follows:

Magnetic field (longitudinal)	1G.
Velocity field	10 m/s.
Time	1 minute.
Spatial	$0.5 \times 0.7$ arcsec.

A terminal of 9 channels will be installed to replace the dual channels soon.

#### 2.2 Photometric solar seismograph (Location: Yunnan Observatory, Kunming)

The instrument was developed by the Santa Catalina Lab. for Experimental Relativity by Astrometry as a cooperative project between the University of Arizona and Yunnan Observatory. This instrument is used to observe solar oscillations by determining changes in the intensity of the continuum of the solar disk with spatial resolution of about 50 arcsec.

The performance of the telescope is as follows:

Coelostat mirror	20 cm.
Primary mirror	7.0 cm, $f = 200$ cm.
Two detector systems:	— 19 mm solar image at disk center. — 28 mm solar image at solar limb.

#### 2.3 Spectra-spectroheliograph and scanning stokes polarimeter (Location: Yunnan Observatory, Kunming)

The spectra-spectroheliograph can scan 2 lines simultaneously from 3600–11000Å, with spatial resolution  $1-2''$ .

The performance is as follows:

Telescope:  $A = 50$  cm,  $f = 12.5$  m, solar diameter = 116 cm

Spectrograph: Grating 630 lines/mm,  $320 \times 300$  mm area, dispersion 1.2Å/mm

Polarimeter: 3 mechanical modulations

Electronics: CCD array,  $515 \times 512$  pixels,  $6 \times 6$  mm

#### 2.4 *Solar fine structure telescopes (Location: Yunnan Observatory, Kunming and Wusan Station, Purple Mt. Observatory)*

The two telescopes are of the same design, both are 26 cm binocular vacuum tube telescope to observe the Sun on  $H\alpha$  band and white light simultaneously.

#### 2.5 *Solar radio telescope group (Location: Yunnan Observatory, Kunming)*

Four small dishes working on 7.5, 10.6, 15, 21 cm and a 10 m antenna with a radio acoustic-optical spectrograph working at 230–300 MHz are involved in this group. The Sun is observed with all these telescopes simultaneously with time resolution of 1 ms.

#### 2.6 *High resolution observing network for solar burst*

Besides the solar radio telescope group in Yunnan Observatory, the network consists of the dishes at the following locations:

Shahe Station, Beijing Observatory:	observing on 3.10 cm
Purple Mt. Observatory:	3.13 cm
Nanjing University:	3 cm
Beijing Normal University:	2 cm

The time resolution of all the receivers is 1 ms and the time synchronization among all the stations is 1 ms.

### 3. Radio telescope

#### 3.1 *25 m Telescope (Location: Sheshan Station, Shanghai Observatory and Urumqi Astronomical Station)*

The two stations are mainly working on VLBI, but can also be used as single dish. The Sheshan Station is newly equipped with a VLBA terminal of 14 channels. The MK II terminals and MK II correlator are in operation. The Urumqi Station will be equipped with a MK III A terminal with 14 channels and MK II terminal and the station will be in operation next year.

#### 3.2 *13.7 m Telescope (Location: Delingha Station, Purple Mt. Observatory)*

13 mm receiver is in operation and 2.6 mm one will be used soon. The telescope is being used to observe cosmic molecular lines as well as high resolution solar burst.

#### 3.3 *Meter-waveband aperture synthesis radio telescope (Location: Miyun Station, Beijing Observatory)*

The telescope is an E–W array of 28 elements 9 m antenna and is operating on 232 and 327 MHz. The 28 elements are under modification of phase linking to be used as a single dish telescope with equivalent diameter of 47 m.

#### 4. Astrometric instrument

##### 4.1 *Danish-Chinese Meridian Telescope (DCMT) (Location: Lintong, Shanxi Observatory)*

The DCMT is under operation between Shanxi Observatory and the Copenhagen University Observatory. It is a horizontal meridian telescope of automatic observing mode, the limiting magnitude is 14.

##### 4.2 *MK III Photoelectric astrolabe (Location: Xinglong Station, Beijing Observatory)*

The performance of the astrolabe is as follows:

Aperture 26 cm,  $f = 500$  cm, single image  
Autocollimation  
Dual photo counting record system in V, B band  
Dual zenith angle, 36 and 55 degrees  
Automatic mode, limiting magnitude 13

##### 4.3 *H-maser clock (Location: Shanghai Observatory)*

Two types of H-maser clocks have been developed

Mobile H-maser clock, Type II,      Wt. 200 kg  
Portable H-maser clock, Type III,    Wt. 50 kg

All the clocks have stability better than  $10^{-14}$ . They are used to support the VLBI observation as well as keep the atomic time scale.

##### 4.4 *Satellite laser ranging network (Location: Sheshan Station, Shanghai Observatory; Changchun Satellite Observing Station; Wuhan Station)*

All stations are equipped with third generation SLR system: Aperture 60 cm, YAG: nd mode-locked laser, 120 ps pulse width, computer controlled automatic tracking. All the laser satellites are being tracked, and daylight tracking has been conducted in Shanghai.

#### 5. New techniques

##### 5.1 *Adaptive optical system on 1.2 m telescope (Location: Yunnan Observatory, Kunming)*

The telescope has a clear aperture of 106 cm,  $f = 14$  m, tracking accuracy =  $1''$ , pointing accuracy of a few seconds; wave front detector: sheer interferometer; control bandwidth: 65 Hz, 21 Units; deformation mirror: 158 mm, driving by piezoelectric ceramics separately and deformation range  $\pm 1$  mm.

In 1990-1992, four testing observations were conducted jointly by the Yunnan Observatory and the Chengdu Institute of Optics and Electronics. The central part ( $\phi$  375 mm) of the telescope was used. Images of 4th magnitude were detected with resolution of 0."5. Further experiments will use the whole aperture of the telescope to detect star of 11th magnitude with resolution of 0."1 (visible) and 0."2 (IR). Hartmann wave front detector of 73 units will be used.

### *5.2 Optical interferometer*

Testing units of the interferometer are under construction in Nanjing by the Shanxi Observatory and Nanjing Astronomical Instrument Research and Manufacture Center.



## Plans for a Large Indian Telescope

S. N. Tandon *Inter-University Centre for Astronomy and Astrophysics, Post Bag 4, Ganeshkhind, Pune 411 007, India.*

**Abstract.** In order to meet the growing demands for optical observational facilities, it is proposed to develop a 4 m class modern telescope. The telescope would have a fast and low mass primary mirror, an altitude-azimuth mounting, and would incorporate active optics to get sub-arc second images. The telescope would mainly be used for optical and near infrared observations, and good seeing conditions would be an important criterion for the design and site selection. One of the prospective sites is Devasthal – a peak near Nainital at a height of  $\approx 2300$  m; however a final selection of the site would be made by monitoring more sites in Himalayas. It is hoped that the Department of Science and Technology would provide adequate support for setting up such a telescope.

*Key words:* Telescope — site selection.

### 1. Introduction

In India the interests of observational astronomers span a wide range, from the highest energy particles of cosmic-rays to the lowest energy photons of radio-waves. If a division is to be made, the maximum number of astronomers would fall in the category of optical astronomers. There are four one meter class telescopes in India – one each at Abu (lat.  $24^{\circ}39'N$ , long.  $72^{\circ}47'E$ ), Kavalur (lat.  $12^{\circ}35'N$ , long.  $78^{\circ}50'E$ ), Nainital (lat.  $29^{\circ}22'N$ , long.  $79^{\circ}27'E$ ), and Rangapur (lat.  $17^{\circ}06'N$ , long.  $76^{\circ}14'E$ ) – and one 2.34 m telescope at Kavalur. For several years, a need for a larger modern telescope has been felt by the astronomy community. As a first step towards the planning of such a telescope, the Department of Science and Technology appointed a group of astronomers and engineers to make recommendations for such a telescope. In this paper the main features of the 4 m class telescope recommended by this group are presented. As the technology is going through very active evolution, we have to make choices from the possible solutions which are not proven yet. As we go along, the reasons for our choices would be mentioned and I would be grateful for any comments/criticism concerning these choices.

### 2. The telescope

The telescope would be of 4.2 m aperture, and would be capable of giving sub-arc second images in the optical and near-infrared bands. Consistent with these requirements we are looking for the most economical implementation.



## 2.1 Optics

A classical Cassegrain configuration is selected with a  $f/2$  primary mirror, and two foci of  $f/8$  and  $f/13$  respectively. A field corrector would be incorporated for the  $f/8$  focus, to get a  $30'$  field for wide field work. The  $f/13$  focus would be used mainly for the near infrared work, and the secondary mirror would be optimised for minimal background. Prime and Nasmyth foci are not proposed, and the advantages of these have been given up in exchange for the simplifications in the mechanical design.

## 2.2 Primary mirror

There are two possible choices for light weight mirrors: pyrex mirror with a honeycomb core, and thin solid meniscus of ultra-low expansion glass. A comparison of the two mirrors is presented in Table 1. The most important advantage of the honeycomb mirror is its higher rigidity which would simplify the support system, and its main disadvantage is its sensitivity to the temperature gradients.

We have chosen the solid meniscus option, because it appears to be already proven for obtaining sub-arc second images, limited by seeing at a level of  $< 0.5''$ .

## 2.3 Supports for the primary mirror

The solid meniscus mirror necessarily needs axial supports every 40 cm or so, and these supports need to balance the forces of gravity with a precision of about 1 part in  $10^4$ . The supports would be hydraulic type, divided in three groups (each covering a  $120^\circ$  sector of the mirror) of interconnected supports and these groups are servoed to give zero reaction forces on the three position defining points. In addition to these hydraulic supports, which act effectively as whiffle tree (see Angel 1988), individual active force actuators would be used on each of the axial supports (see Enard 1988) for the purpose of active correction. With such an arrangement, the interconnected hydraulic supports adjust themselves to the systematically changing load due to the variation in elevation, and the active actuators only need to correct for the remainder errors in forces. The

**Table 1.** Comparison of ULE meniscus mirror and pyrex honeycomb mirror.

Parameter	Meniscus (20 cm thick)	Honeycomb (5 cm thick face plates and 60 cm total thickness).
Temperature gradients	Insensitive	Sensitive, gradients to be below $\sim 0.1^\circ\text{C}$ .
Temperature changes	Resulting distortions can be corrected by active optics	Resulting distortion not easy to correct.
Thermal time constant	Few hours	Less than an hour if the core is ventilated.
Wind gusts	Very susceptible to distortions	Relatively insensitive.
Costs	More	Less

radial support would be passive astatic type, and no active correction would be needed for these.

## 2.4 Active optics

In order to ensure sub-arc second images, active optic control based on the development of this technique at ESO would be used (Tarenghi & Wilson 1989). The principle of the active optic control is illustrated in Fig. 1. In order to analyse aberrations of the optics, the image analyser in effect has to divide the wavefront into a few hundred small parts, and the image in each of these is averaged over more than ten seconds (to filter out the perturbations due to the atmospheric variations) to derive the corresponding tilt. The tilts of the wavefront are then used to calculate the force and position corrections required to be applied on the primary and secondary mirrors respectively. In order to be able to get sufficient photons to get an accuracy of  $< 0.1''$  from the wavefront analyser, a star brighter than  $m_v \approx 16$  is required - such a star would be easily available if a field of  $20'$  is accessible.

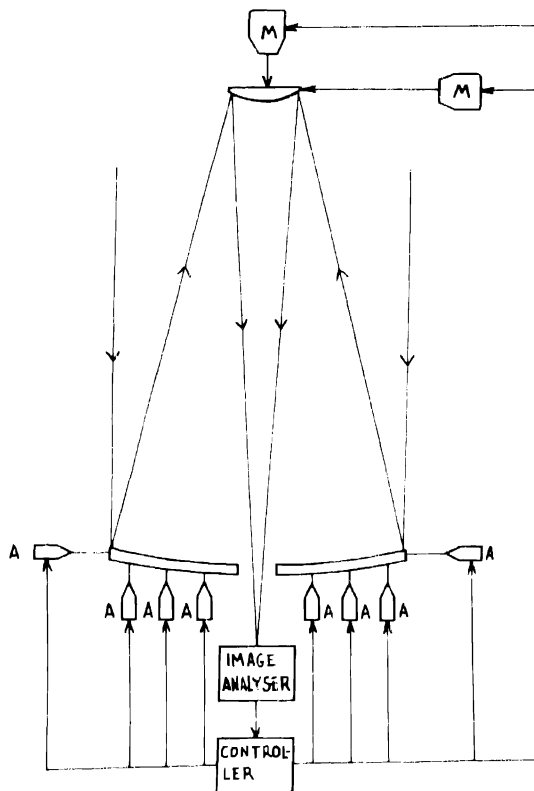


**Figure 1.** Principle of active optic control is illustrated as developed at ESO. The forces to correct the primary mirror figure are applied by actuators represented as 'A', and the secondary is moved by motors represented as 'M' for focus, alignment, and tilt corrections.

### 2.5 *Wind loads on the primary mirror*

The primary mirror is extremely flexible and unless the forces due to the wind are well balanced by the supports a serious distortion of the surface would occur. The forces of a steady wind are corrected by the active part of the supports, as the wavefront analyser would be able to provide the required feedback. However, a fluctuating wind force is much more difficult to handle because of the rather large response time ( $> 10$  s) of the active optics. For example a sudden change in the wind speed from zero to 1 m/s would lead to a pressure change on the mirror's face of  $1 \text{ N/m}^2$ , and this pressure, if unbalanced, would lead to unacceptably large forces on the three position defining axial supports. The interconnected hydraulic supports automatically adjust themselves to such changing loads (see Knohl 1988) and ensure that the load is countered uniformly by the supports. Further, division of the supports into three interconnected groups ensures that the wind force is independently balanced in each third of the mirror, and therefore any spatial gradients in the wind pressure would only generate unbalanced forces over a scale much smaller than the aperture.

### 2.6 *Structure*

The mechanical structure would be an alt-azimuth configuration, incorporating friction drives and roller bearings on the two axes (see Fig. 2). The use of roller bearings simplifies the construction at the cost of increased friction. The friction torque on the azimuth bearing can be quite substantial and become a source of trouble if the full diameter of the azimuth ring ( $\sim 4.5$  m) is used for it; the friction torque can be reduced if the bearing diameter is reduced. In principle a constant frictional torque would not affect the pointing and tracking performance. However, roller bearings are also associated with some amount of ripple torque and this affects the pointing and tracking.

The frictional torque in the azimuth roller bearing would be about 100 N-m (for a mass of  $6 \times 10^4$  kg) and if it has a 10% part as fluctuating at 1 Hz the corresponding ripple in the pointing would be about  $2''$ . Such a ripple in tracking is unacceptably large, however if this ripple can be detected by the incremental shaft encoder then a correction can be made for it by tilting the secondary mirror appropriately.

### 2.7 *Pointing and tracking*

The drive for the two axes would be friction drive on disks of about 2 m radius. The pointing would be based on absolute shaft encoders of  $1''$  resolution, and the tracking would be guided by incremental tape encoders mounted on the drive disks and by star sensors in the focal plane. The incremental encoders would have a resolution of  $0.05''$ , and these could be also used to detect any errors arising due to the fluctuating frictional or wind torques; fast corrections can then be made through tilt of the secondary mirror.

## 3. *The enclosure*

The enclosure would be a simple structure with double skinned plane surfaces (see Fig. 3), and having a minimum volume. The enclosure would be actively cooled during

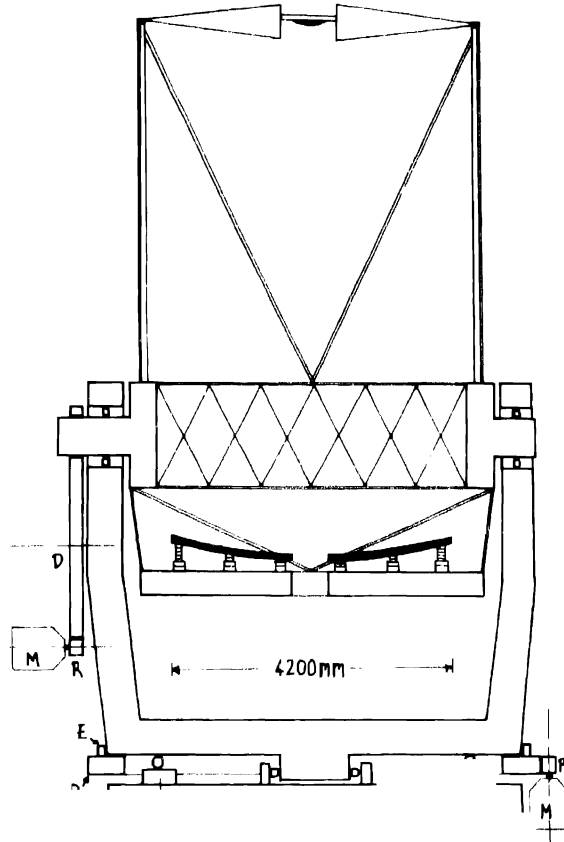


**Figure 2.** The mechanical configuration of the telescope is shown. The friction drive disks are indicated by 'D' and the corresponding motors and rollers are indicated by 'M' and 'R' respectively. The tape incremental encoder for the azimuth axis is also indicated as 'E'.

the day, and would be ventilated actively during the observations to minimise the effects of thermal perturbations. The service buildings would be far away from the enclosure, and all the sources of heat would be isolated from the telescope floor.

#### 4. The site

In India, cloud cover is minimal in the central part of the country, and it increases to the south and to the north. However, in the Himalayas there are relatively sharp variations due to effect of the mountain ranges and good high altitude sites are likely to exist there.

The Uttar Pradesh State Observatory of Nainital has carried out a survey of possible sites in that region, and have studied one of the promising sites in detail. This site, called Devasthal, is at an altitude of 2330 m and is located at lat.  $\sim 29.5^\circ\text{N}$ , long.  $79^\circ\text{E}$ . The observations show that about 200 nights/year are useful for observations, the wind speed is generally  $< 10\text{ km/hr}$ , the temperature variations during the night are  $< 1^\circ/\text{hr}$ ,

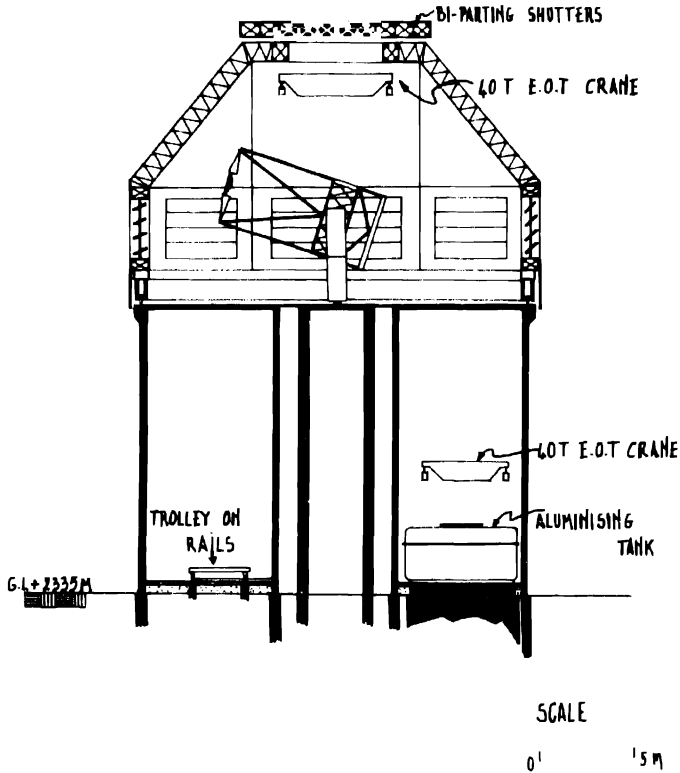


**Figure 3.** The enclosure for the telescope is shown. Windows with controllable opening area are provided for ventilation during the observations, and occupancy of the building is minimised for easing the thermal control.

the seeing is better than 1" for 40% of the time, and the precipitable water vapour is  $< 2$  mm for 20% of the nights. Whereas this is not an excellent site, better and higher sites are likely to exist in Himalayas.

### 5. Prospects

The Department of Science and Technology is very interested in promoting the realisation of this large telescope. The total cost of realising the observatory is estimated to be about Indian rupees  $6 \times 10^8$ , and due to the budgetary constraints support to the project is not yet approved, but we are hoping for such an approval in the near future.

### Acknowledgements

This presentation is based on the report on the study sponsored by the Department of Science and Technology, Government of India.

### **References**

- Angel, J. R. P. 1988, *Very Large Telescopes and their Instrumentation*, Ed. M. H. Ulrich, ESO Conference and Workshop Proceedings No. 30, p. 281.
- Enard, D. 1988, *Very Large Telescopes and their Instrumentation*, Ed. M. H. Ulrich, ESO Conference and Workshop Proceedings No. 30, p. 301.
- Knohl, E. D. 1988, *Very Large Telescopes and their Instrumentation*, Ed. M. H. Ulrich, ESO Conference and Workshop Proceedings No. 30, p. 505.
- Tarengi, M., Wilson, R. N. 1989, *Active Telescope Systems*, Ed. F. J. Roddier, SPIE Proceedings No. 1114, p. 302.



## Subaru: An 8-m Optical/IR Telescope Project

Norio Kaifu *National Astronomical Observatory, Mitaka, Tokyo, Japan 181.*

**Abstract.** The concepts of the Japanese 8.2 m optical and IR telescope project, Subaru, are summarized. Subaru aims at the highest achievements of ground based telescope in the optical and IR wavelength region. The status of the construction is also reported.

**Key words:** Telescope: optical and IR—instruments.

### 1. Basic design

Subaru is an 8.2 m diameter new technology telescope for optical and infrared astronomy being built by the National Astronomical Observatory, Japan. The main concepts of the project are (1) large monolithic mirror, (2) very good image quality, (3) wide coverage of observable wavelength, and (4) high data-taking ability. The name “Subaru” was given after the old Japanese word for Pleiades.

The Subaru project is now at nearly one-third of its 9-years’ schedule; the construction started in 1991, and will be completed in 1999. The Subaru telescope site is the 4200-m high Mauna Kea summit in Hawaii island, one of the best sites for the ground-based astronomical observations (Fig. 1).

The basic design of Subaru can be summarized as follows.

- 8.2-m effective aperture, thin-meniscus ULE mirror.
- 264 active supporting structures.
- Alt-azimuth mounting with oil bearings and direct driving system.
- Air-flushing type enclosure with temperature control (in daytime only).
- Cassegrain, prime and two Nasmyth foci.
- Aims observations through 0.3 to 30  $\mu\text{m}$  wavelength region.

The scientific target of Subaru is wide, including the Solar system, external planetary system, star formation, interstellar matter, stellar physics, evolution of galaxies, AGN, proto-galaxies, and cosmology.

### 2. Primary mirror and active supporting system

The 8.2 m main mirror of the Subaru is designed to obtain the best possible image, by adopting active supporting system. The error budget of the FWHM image size of the main mirror is as follows:

Diffraction limit (at 0.5 $\mu\text{m}$ )	0.013 arcsec
Figuring error	0.07 arcsec
Active support error	0.07 arcsec



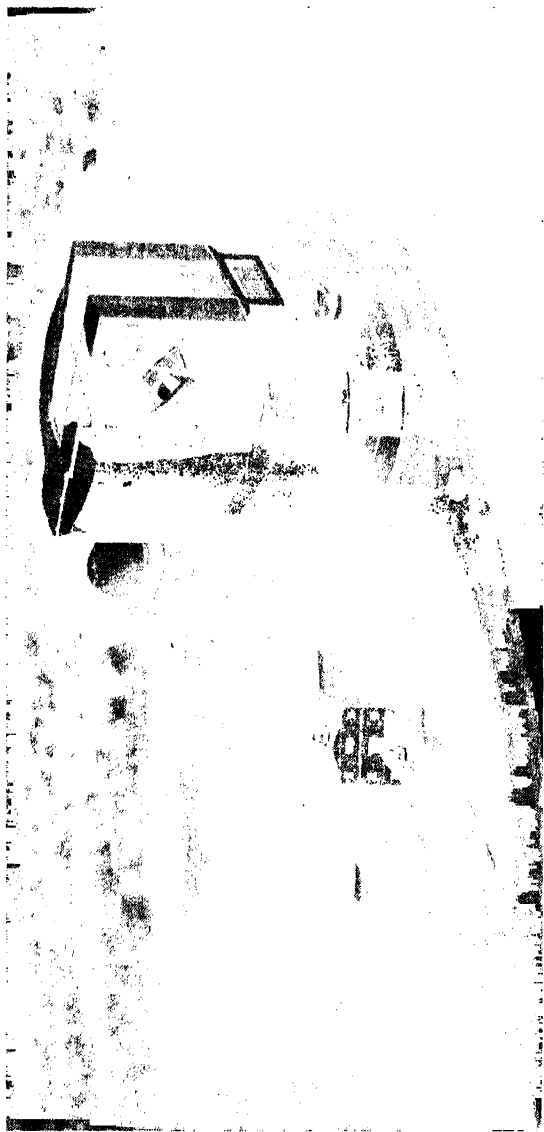
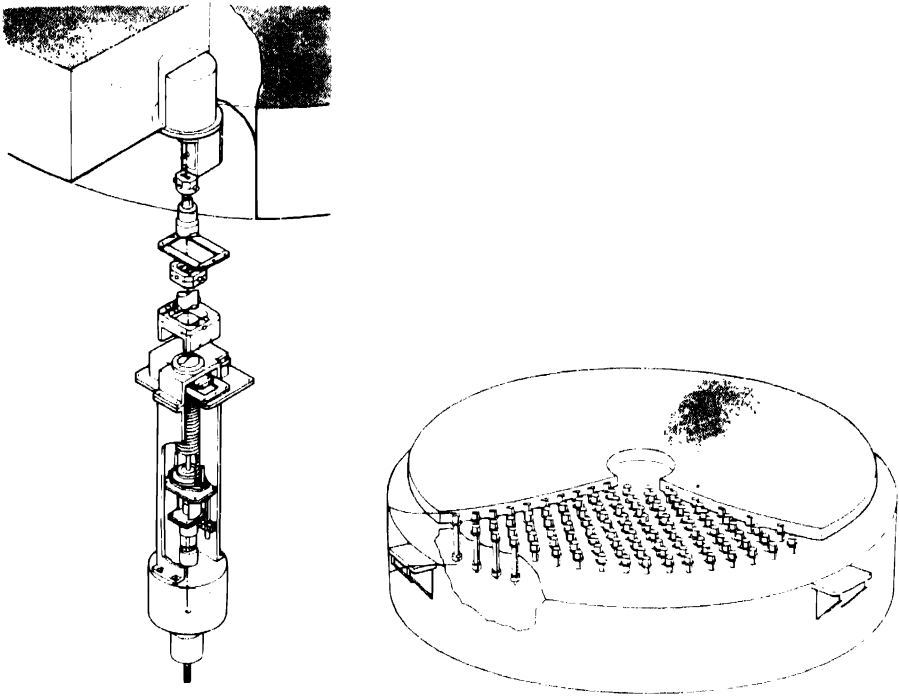


Figure 1. Artist's impression of Subaru on Mauna Kea.



**Figure 2.** Concept of active-supporting system of Subaru main mirror.

Shack-Hartmann measurement error	0.02 arcsec
Overall	0.10 arcsec

The main mirror is a thin-meniscus type, 20-cm thickness ULE (ultra-low expansion glass developed by the Corning Glass Company). It will be supported by 264 precision actuators which keep the mirror surface within the accuracy of 20-nm rms at any elevation angle of the telescope higher than 15 degrees. This active supporting system will also keep the surface accuracy against the temperature change, and to some extent, against the wind (Fig. 2).

So far all of the 44 ULE hexagonal units have been finished in the Corning factory at Canton, USA. Measured coefficient of thermal expansion of the ULE materials were satisfactory. The whole ULE hexes will be arranged so that the best temperature performance of the mirror is attained, and then be fused together in a large rotating furnace and be sagged down to get proper convex shape. The construction of the large furnace has almost been completed. The delivery of the finished glass material to the polishing site is scheduled in middle 1994. The construction of the polishing machine has just started, and the polishing process will take another three years.

The actuators to support main mirror are now being fabricated and will be tested for their accuracy at Amagasaki factory of the Mitsubishi Electric Company (MELCO). Very accurate force sensor for the actuator had also been successfully developed.

### 3. Telescope, mounting and tracking

As shown in Fig. 3, the telescope tube adopts a simple truss structure, and the mounting is a stable alt-azimuth system. By using accurate hydrostatic bearings and direct driving system, the tracking accuracy of the telescope is designed to achieve 0.12 arc sec or better in the auto-guiding mode. The overall FWHM image size of the Subaru telescope is estimated as shown in the error budget below.

Optics	0.11 arcsec
Tracking	0.12 arcsec
Local seeing	0.12 arcsec
Miscellaneous	0.11 arcsec
Overall	0.23 arcsec

Above error budget of the optics includes those of the secondary and tertiary mirrors. The local seeing will be discussed in the following section.

The telescope has four focusing positions; Primary focus with F-number of 1.8, Cassegrain focus with F-numbers of 12 and 35, and two Nasmyth foci with F-numbers of 12 and 35, respectively. Each focusing position will be equipped with heat-pipes, helium gas tubes and data acquisition systems. The second mirrors and primary focus instruments will be changed by using a remote-controlled auto-changer system (Fig. 4).



Figure 3. A computer-drawn structure of Subaru telescope.

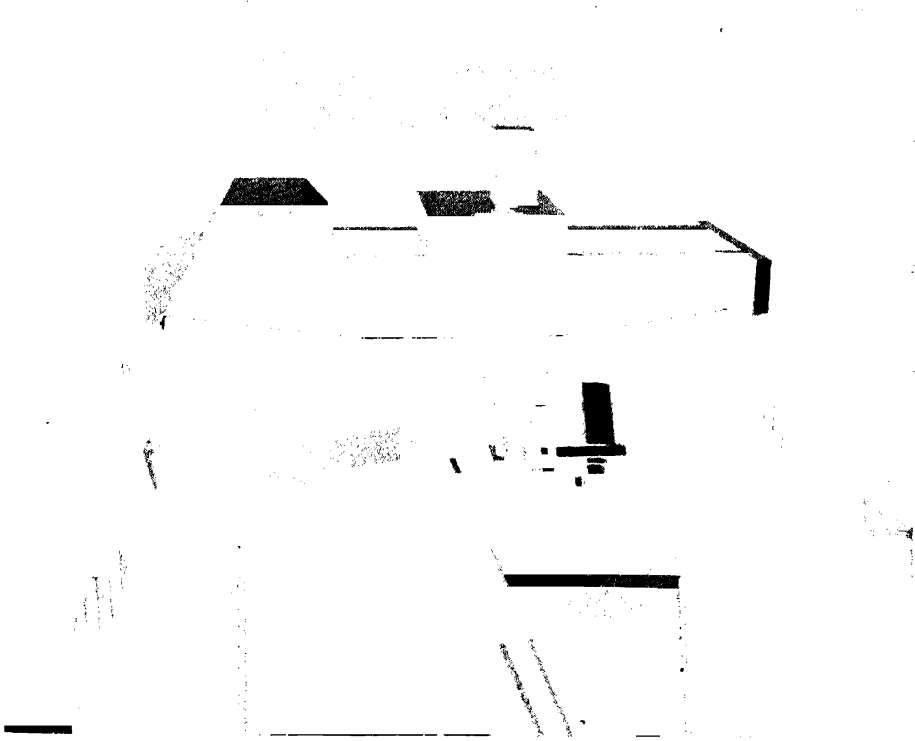


**Figure 4.** A computer-drawn prime focus instrument auto-changer of Subaru.

#### **4. Enclosure**

The enclosure of Subaru is a co-rotating, air-flushing type with front, back and side ventilators, which will enable achieving the temperature equilibrium between the telescope and the air, and also between the room floor and the air, to suppress the artificial seeing effect to a very low level. The enclosure will be equipped with the front and top wind shields, which act as the light shields too. To realize as good performance of the inside air flow as possible, detailed three-dimensional calculations to simulate the hydrodynamic behavior have been made (Fig. 5). A similar technique was also used to design the air conditioning system in the enclosure to keep the daytime temperature of the telescope and room floor near to the predicted night temperature. The elevation of the ground level is 4139 m, and the dome height is designed to be 44 m. The telescope elevation axis will be put at the height of 24 m from GL, to avoid the turbulent surface air and dust.

#### **5. Construction on the Mauna Kea summit**

The start of summit construction of Subaru was celebrated by 150 participants from Hawaii, USA, and Japan on July 6, 1992. So far the works are going on schedule; the

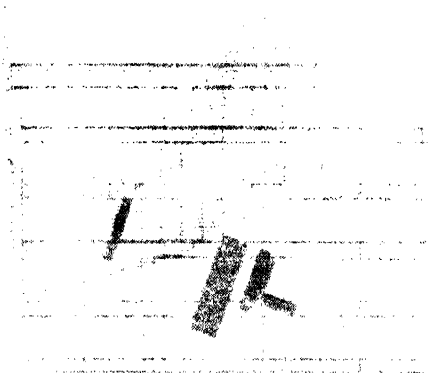


**Figure 5.** A sample result of the hydrodynamic simulation of air-flow in the Subaru enclosure.

telescope pier is almost completed after the grading works for the dome and control building area and road, and the soil improvements by soil-cement method (Fig. 6). This year the construction of the lower fixed part of the enclosure will start. The whole enclosure and control building will be completed in 1995.

## **6. Observing instruments of Subaru**

About 10 preliminary proposals were proposed for the first-phase Subaru instruments, which will be used for the test and early-phase observations (from 1998), as follows. Detailed design, developments and experiments of some of the prototype models have started this year. Larger and long-term instruments are also being considered in parallel. Collaboration and informal proposals with other countries both for first phase and long-term instruments are welcome.

## **PROPOSED SUBARU INSTRUMENTS**

### **FOCAS (Faint Object Camera and Spectrograph)**

Iye, Ohtani, Sasaki *et al.*

Cassegrain, visual (+ IR), multipurpose for faint galaxies and other objects.

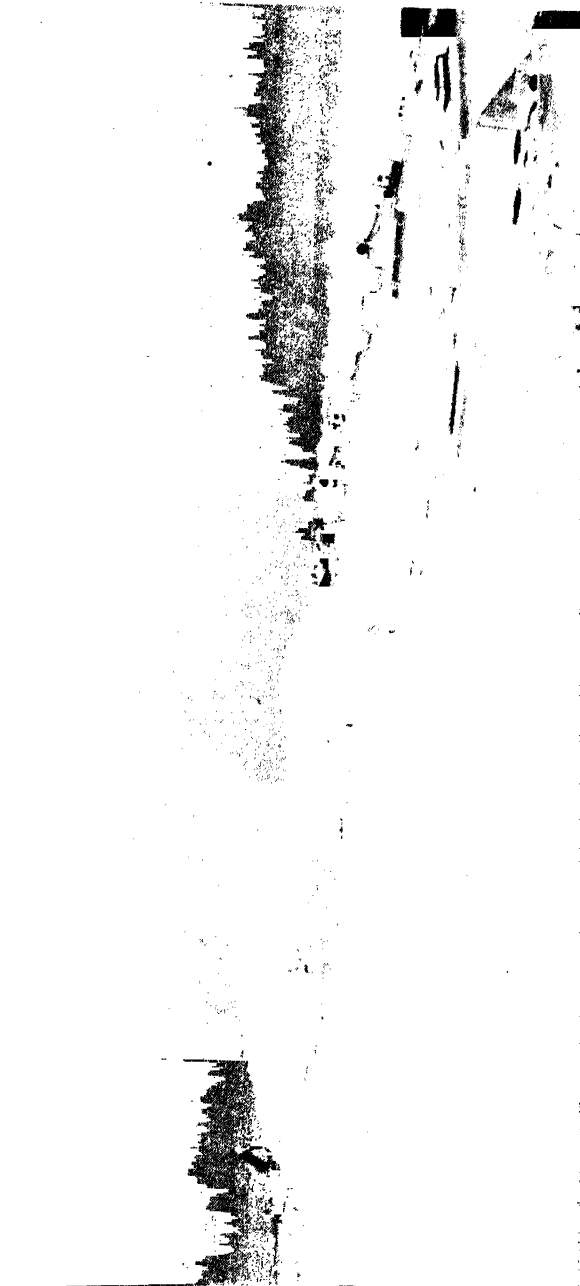


**Figure 6.** Construction of the telescope pier, enclosure, and control building on Mauna Kea summit.

**CIAO (Coronagraph Imager with Adaptive Optics)**

Kaifu, Takami, Tamura *et al.*

Cassegrain, aims 0.2" occulting disk and 0.1" imaging, K-band optimized.

**IRCS (IR Camera and Spectrograph)**

Tokunaga *et al.* (UH-SUBARU collaboration)

Cassegrain, 1–5 micron, cooled, high resolution imaging and spectroscopy.

**MIRS (Middle IR Spectrograph)**

Yamashita, Shibai, Onaka, Nishimura *et al.*

Cassegrain, 10 & 20 micron, imager & spectrometer.

**High Speed Mosaic IR Camera**

Ueno *et al.*

Cassegrain, sift-and-add mosaic array system with 12 K × 12 K PtSi pixels. Wide field.

**Mosaic CCD Camera**

Okamura, Sekiguchi *et al.*

Prime focus, 30–40 min. field of view with 8 K × 8 K CCD pixels.

**Fiber Optics Multi Object Spectrograph**

Karoji, Noumaru, *et al.*

Prime focus, 1000 or more objects.

**OHS (OH Suppression Spectrograph)**

Maihara *et al.* (UH-SUBARU)

Nasmyth, H & J bands, R = 5600. A prototype was completed.

**HDS (High Dispersion Spectrograph)**

Ando *et al.*

Nasmyth, visual + near IR (uncooled), R = 100,000.

To support the developments of instruments the Astronomical Engineering and Development Center has been established at NAO (Mitaka). A small-size (1.5-m) telescope and optical simulators for the test of instruments, machine shop, electronics and optical labs, and design center will be organized here.

## 7. Long-term schedule

The main schedule of Subaru construction is shown below. The total budget and schedule was almost defined. The final budgetary year of the Subaru project is 1999. We plan to get the first-light and to make test observations with the Cassegrain focus in 1998.

1993–1994	Complete 8.3-m mirror blank.
1994–1996	Mirror polishing.
	Hilo Facility completed.
	Complete enclosure.
1997	Telescope erection on Mauna Kea.
1998	First light.
	Start test observations.
2000	Start operation.

The plan for high capacity (0.5 to 1 Gbps) network which connects the summit and the Hilo facility (Subaru headquarters, planned to be completed in 1997) via optical fibers is considered, and this will make the remote observations from Hilo (sea-level) possible.

## Concept and Status of the ESO Very Large Telescope Project

D. Enard *European Southern Observatory, Karl-Schwarzschild-Str. 2, D-85748 Garching, Germany.*

**Abstract.** The ESO VLT was first presented in April 1984 and its construction decided in December 1987. The VLT program consists of an array of four telescopes of 8 m diameter capable of working independently or in a combined mode, in which case it provides the collecting power of a 16 m telescope. It foresees an interferometric mode where the telescope beams are phased. Smaller size auxiliary telescopes can also be used in this mode.

This paper gives the present status of the construction of the 8 m unit telescopes.

*Key words:* Telescope.

### 1. Concept of unit telescopes

Each 8 m 'unit telescope' (UT) has an Alt-Azimuthal mount (Fig. 1) and is designed around an 8.2 m diameter monolithic, actively corrected, primary mirror with an  $f$ /ratio of 1.8. All optical elements remain in place although their position may change according to the focal station selected (Fig. 2). Each UT has a Cassegrain, two symmetrical Nasmyth foci and a coudé focus located in the base of each telescope and from where the image is relayed to the combined focus. The optical combination is of the Ritchey-Chrétien type and is optimised for the Nasmyth focus.

At the Cassegrain focus which is about 2.5 m closer to the secondary mirror than the Nasmyth focus there is – after correction of about 26 microns of spherical aberration by the active primary mirror – some uncorrected coma which remains however acceptable for a field of less than about 15 arcminutes. The aperture at the Nasmyth focus is  $F/15$  and  $F/13.6$  at the Cassegrain. The secondary mirror is 1.16 m diameter and is to be used as a servo mirror to correct small guiding errors as well as for chopping in the IR. As a consequence the pupil is set on the secondary mirror. For observation at the Cassegrain the tertiary mirror is moved into a vertical plane so that it does not obstruct the beam.

The unvignetted field is 20 arcminutes at the Nasmyth and 15 arcminutes at the Cassegrain. The coudé focus of each UT is obtained by inserting a small pick-up mirror before the Nasmyth focus. The Nasmyth focal plane is relayed by 2 elliptical and 2 flat mirrors to the coudé focus. The field of view at the coudé foci is 2 arcminutes.

The active optics must compensate for static or slowly varying deformations such as manufacturing errors, thermal effects, remaining errors of the lateral support, as well as for random effects such as wind buffeting. The active axial support is also used to compensate the spherical aberration generated at the Cassegrain focus because of the shift of position with respect to the Nasmyth focus.



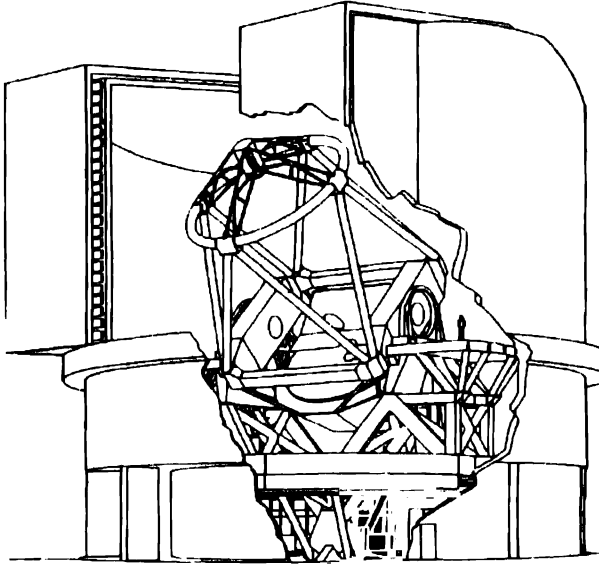


**Figure 1.** Architecture of the VLT Unit Telescopes.

The bandwidth of the active optics loop is limited by the need to integrate out the seeing which is not correlated between the centre of the field and the location of the reference star used for the wavefront sensing. Averaging of seeing will need integration time of a few seconds at least. Working at higher rates may induce some errors that will have to be balanced out with the advantage of correcting fast varying effects such as wind buffeting. The wavefront sensor is a CCD Shack-Hartmann sensor and will be integrated together with an imaging CCD used for field acquisition and auto-guiding. Both sensors will share the same offset star.

## **2. The primary mirrors**

The primary mirrors consist of glass ceramic thin meniscuses. Their thickness is 175 mm and their mass about 23 tons. The first blank has been delivered on June 25th, 1993 (Fig. 3) and the grinding and polishing started. The three other blanks of the VLT are at various stages of finish and will be delivered before 1995.

The axial supporting of the primary mirror is ensured by a passive hydraulic whiffletree which consists of 150 supports distributed in three 120 degrees sectors. To each passive hydraulic support is attached an active force actuator which allows to modify the distribution of actual forces on the 150 support points. The supports are connected to the mirror through 3 legs pads which compensate partially the local sag between support points. The residual RMS wavefront error is about 15 nm (Fig. 4).

The frequency of correction of the active forces is essentially determined by the possible need to correct for wind buffeting. Several schemes to measure in real time the mirror deformation are being analysed.

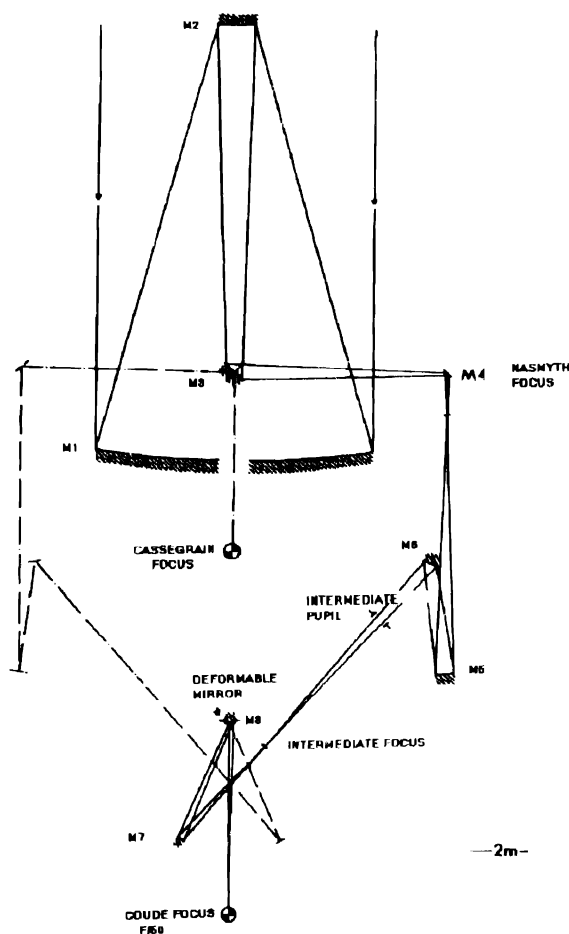


Figure 2. Optics lay out of the VLT Unit Telescopes.

The lateral supporting system consists of 64 supports located only at the outer edge of the mirror. The distribution has been determined so as not to introduce a deformation of the surface. Only inaccuracies on the exact location and values of the forces will have to be corrected with the active axial support. Lateral forces are distributed into 4 pushing or pulling sectors and are inclined with respect to both the plane of the mirror defined as the plane passing by the mid-edge, and the vertical symmetry plane. The axial components of the lateral forces are determined to balance the moments with respect to the centre of mass and all lateral forces are tangent to the average mirror surface and inclined with respect to the mirror plane. Each support consists of an oil pad. The pulling and pushing set of pads corresponding to each half of the mirror are hydraulically connected and generate two virtual fixed points. The mirror lateral position can be adjusted by controlling the volume of oil in each of the two hydraulic circuits.

The coating of the primary mirrors will be done outside the telescope in a specialised facility. The process selected for the aluminization is sputtering which allows to significantly decrease the dimension of the coating chamber.



Figure 3. Delivery of the first 8 m mirror blank.

## *Concept and Status of the ESO Very Large Telescope Project*

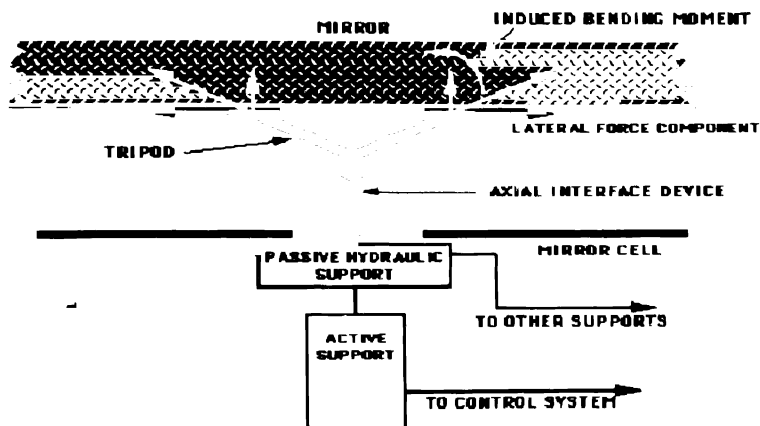


**Figure 4.** Principle of axial supports of the active primary mirror.

### **3. Secondary mirrors**

The secondary mirror has five degrees of freedom. It can move along the 3 main axes to ensure focusing and collimation and can be tilted around its vertex in any direction. The tilt function can be used for two different operating modes: chopping and rapid guiding. Chopping is essentially used for IR observing at wavelength above 5 microns. The chopping frequencies are 0.1 to 5 Hz and the maximum amplitude 30 arcseconds.

Rapid guiding consists of correcting high frequency guiding errors originating from the limited bandwidth of the control system and from wind buffeting on the telescope structure. Atmospheric image motion can also be corrected if the instrument can generate the error signal at the appropriate sampling frequency.

In order to achieve the dynamic performance required for the chopping and rapid guiding modes, the secondary mirrors are lightweighted. The technologies envisaged are Silicon Carbide and Beryllium. Feasibility studies have shown that the mass of a 1.2 m mirror made of SiC or Beryllium will not exceed 25 kg.

### **4. The coudé foci and beam combination**

Each unit telescope has a coudé focus fed by two symmetric coudé optical trains that are essentially relay optics. Each coudé train consists of a pick-up mirror located before the Nasmyth focus, 2 relay elliptical mirrors and two flats (Fig. 2). The optical design has been optimised in order to limit polarisation effects and to have an image of the pupil of adequate dimension located on a flat mirror. This flat mirror will effectively be a deformable mirror, part of an adaptive optics system to be used for high spatial resolution imaging at the coudé focus. The two beams are optimised for different spectral ranges.

Adaptive optics can only work over a small field of view and requires at least one intermediate pupil image where to locate the deformable mirror. This implies

a relatively complex optical system. This is the reason why it is only foreseen at the coudé focus since there is no penalty because the number of mirrors one would have at the Nasmyth of Cassegrain would be roughly the same. The Adaptive Optics system of the VLT is foreseen to provide quasi diffraction limited images at 2.2 microns. It will have about 256 correcting elements. Two wavefront sensors can be used, one in the visible, the other one in the near IR depending on the nature of the observed object or of the reference star.

## **5. The mechanical structures**

The detailed design of the mechanical structures is completed and the manufacturing has begun. Each structure is a framework optimised for maximum stiffness. The lowest eigenfrequency is close to 10 Hz. The drive locked rotor frequency is 8 Hz and the moving mass about 260 tons. The top ring is placed lower than the secondary mirror which provides a better stability along the optical axis and lower wind loads. A platform attached to the fork covers the two tracks and provides a safe and easy access to the Cassegrain area.

The azimuth and elevation bearings are hydrostatic. The azimuth bearing consists of two separate tracks of 9 and 18 m diameter. The encoder, drive and radial bearing are located at the inner track.

The drives consist of directly coupled torque motors which do not introduce any friction or backlash and allow a high resonance frequency and control bandwidth.

The elevation drive consists of two motors of 2.4 m diameter on each side of the elevation axis. The azimuth motors have a diameter of about 9.5 m.

The encoders are based on a novel principle, the LDDM (Laser Doppler Displacement Meter). Each encoder consists of a double beam laser interferometer which essentially converts an angular displacement of a reference mirror located on the structure into a variation of pathlength between the two interferometer beams. The differential sensitivity of this system is about 1.2 nm which for a distance between the two beams of 25 mm gives an angular sensitivity of 0.01 arcsec. A number of flat mirrors are disposed on the structure in order to cover the necessary range (90 degrees for elevation and 360 degrees for azimuth).

## **6. The telescope enclosures**

Two types of enclosure have been considered for the VLT. The first type called the inflatable dome has been pursued for several years and a 15 m diameter demonstration model has been built and erected at La Silla Observatory in 1988. This model has demonstrated the validity of the concept in particular with respect to the resistance of wind loads. The second solution was a more conventional steel dome designed for maximum controlled natural ventilation. The steel dome has been finally selected because of the lower risk involved in its construction and of a better control of the wind on the primary mirror. The selected enclosure has a cylindrical geometry (Fig. 1). The rotating part has two doors and a permeable wind screen which can be raised when the wind faces the opening. At the rear of the cylinder a number of openings allow control of the flow inside the enclosure.

### **7. VLT site and site activities**

The site selected for the VLT is Cerro Paranal at about 2650 m elevation. It is located at about 10 km from the Pacific ocean but well above a very stable inversion layer which maintains the clouds at a lower elevation. Meteorologic and atmospheric seeing parameters have been regularly recorded at Cerro Paranal since 1985. The seeing measurements at both sites are recorded with seeing monitors based on differential image motion. Very low seeing values down to 0.25 arcsecond have been measured for short periods, values below 0.5 arcsecond are not uncommon. Paranal is superior to any other identified site for the number of clear nights and low humidity. The civil works have already begun at Paranal. A platform of about  $150 \times 200$  m has been created and excavations for the four 8 m telescopes completed. Effective construction will start at the beginning of 1994.



## The Giant Metrewave Radio Telescope

**S. Ananthakrishnan** *National Centre for Radio Astrophysics, Tata Institute of Fundamental Research, Poona University Campus, Pune 411 007, India.*

**Abstract.** The Giant Metrewave Radio Telescope (GMRT), which will be the most sensitive radio telescope facility in the world in the 30–1500 MHz frequency range, is at an advanced stage of construction 80 kms north of the city of Pune in India. GMRT will consist of 30 fully steerable parabolic dishes, of 45 m diameter each. Twelve antennas form a random array in a central 1 km  $\times$  1 km area and the remaining 18 are equally distributed along the 3 arms of an approximate ‘Y’ configuration resulting in a maximum baseline separation of about 25 km. GMRT will initially operate at six frequency bands around 50, 150, 233, 327, 610, and 1420 MHz.

Low noise amplifiers are fitted at the back of each feed near the focus to keep the sensitivity high. Analog wideband optical fibre links connect all the antennas, for distributing local oscillator, intermediate frequency, telemetry and voice communication signals. An ‘FX’ correlator system will provide a total of 238,080 complex channels including 256 spectral channels for each of the 435 baselines and the self correlation products.

*Key words:* GMRT—electronics—system parameters.

### 1. Introduction

The basic aim was to build a very sensitive aperture synthesis radio telescope in the decimeter and metre wavelength range that will be complimentary to both Arecibo and VLA telescopes for investigating many outstanding problems in astrophysics. The advantages in building large antennas at low frequencies are that (i) they can be made at lower cost, due to the lower surface accuracy requirement, (ii) electronics is relatively inexpensive and (iii) moderate resolution is sufficient for many astrophysical problems that are best studied at longer wavelengths because the emission comes from diffuse extended regions. However, there are some disadvantages; (i) sky back ground noise is higher, (ii) man made interference is higher and (iii) the distortion of radiowaves due to the ionosphere increases with wavelength. India has the advantage that man made noise is relatively quite low as yet; the absence of snow in most parts of India also helps in the design of lighter antenna structures as the wind forces can be reduced by using mesh surfaces. Further, the experience of the TIFR group in constructing and operating the Ooty Radio Telescope and the Ooty Synthesis Radio Telescope at 327 MHz during the 1965–1985 period was extremely valuable in the GMRT design. Lastly, the development of self calibration techniques now allows almost complete elimination of ionospheric distortions.

In the original proposal (Swarup 1984), 34 parabolic cylinders, similar in design to the Ooty radio telescope, but with dual polarization, were to be built with a total



effective area of  $70,000\text{ m}^2$  for operating upto 600 MHz. Considering the many advantages of parabolic dishes and a break-through in the design of low-cost dishes for metrewavelengths, the proposal was revised in 1985 to replace the cylinders with dishes of 45 m diameter. The 30 dishes enable an effective area of  $\sim 30,000\text{ m}^2$  to be obtained, which is comparable to that of the Arecibo facility. The reduction in collecting area compared to the original proposal is however compensated for, by the reduced system temperatures and cross polarizations, wider bandwidth, frequency and sky coverage obtainable and by the greater versatility of the facility. In the final design, operation at six frequency bands at 50, 150, 233, 327, 610 and 1420 MHz has been provided for.

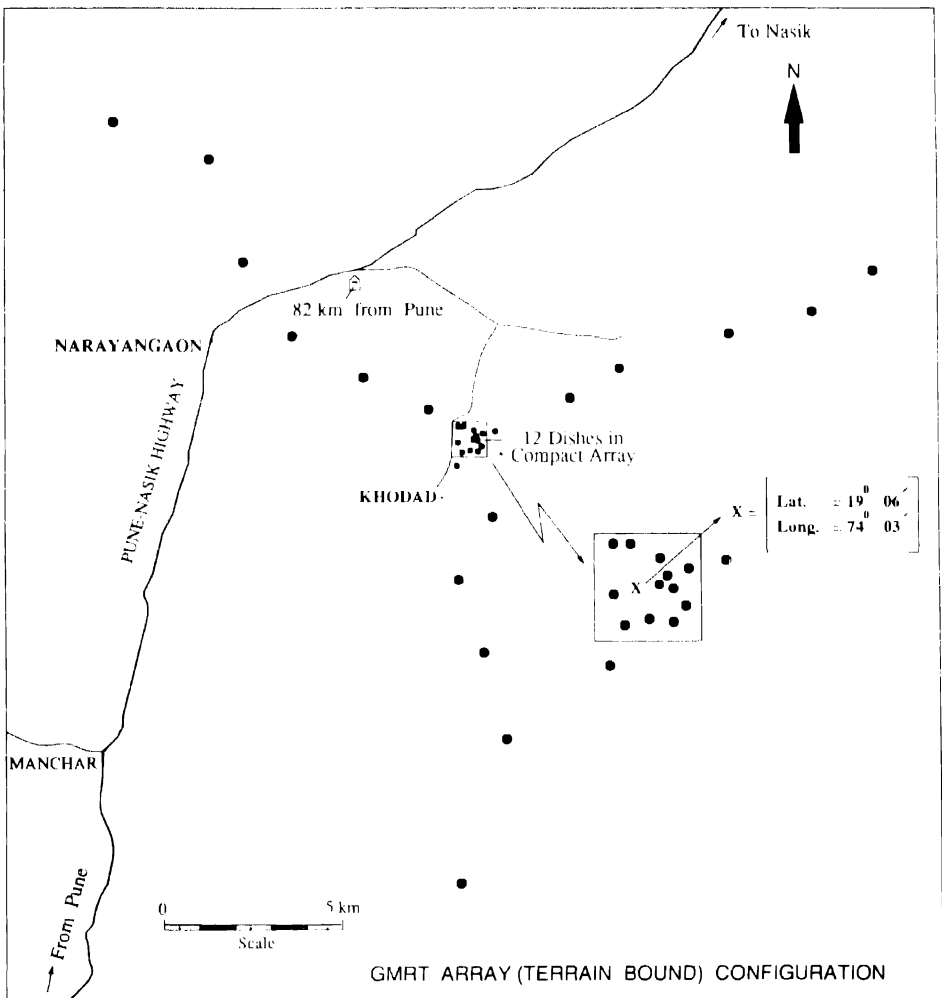


**Figure 1.** Location and configuration of the GMRT array. The existing rural roads have been advantageously used in placing the antennas.

## 2. Array configuration and 45 m dishes

Figure 1 shows the location and configuration of the array, in which 12 antennas form a random cluster in a central  $1 \text{ km} \times 1 \text{ km}$  area and the remaining 18 antennas are distributed equally in the 3 arms of a 'Y' configuration with a maximum baseline separation of 25 km. As is well known from the Very Large Array (VLA) experience, the 'Y' configuration gives a good u-v coverage at both high and low declinations. The compact array, which is comparable to the VLA C-D configurations but with larger collecting area, has been designed to provide sensitivity to large extended sources. The 'Y' array antennas provide angular resolutions of about 2 arcsec and 20 arcsec at 1420 and 150 MHz respectively. Thus the hybrid configuration of GMRT gives good u-v coverage and sensitivity for both compact and extended sources (Swarup *et al.* 1991).

The new design concept used in the GMRT dishes is called SMART -- an acronym for Stretched Mesh Attached to Rope Trusses (Fig. 2). The conventional (heavy) backup structure is replaced by a series of 4 mm and 2 mm diameter stainless steel (SS)

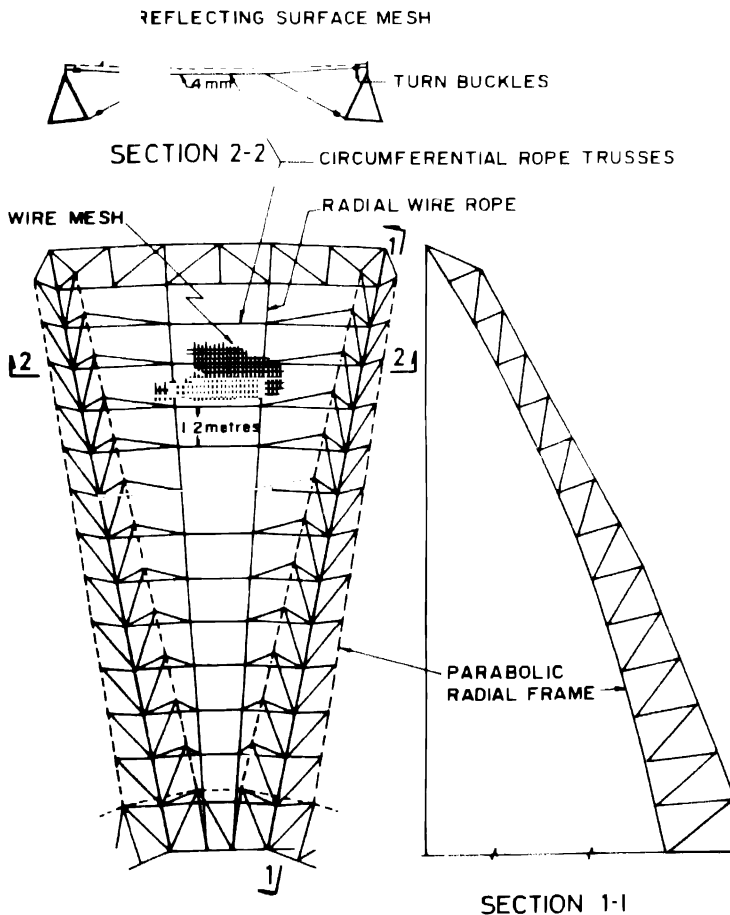


Figure 2. The SMART concept (Swarup 1990).

wire rope trusses stretched between 16 parabolic frames made of tubular steel. The ropes are tensioned to form 360 plain facets over which mesh panels made of 0.55 mm diameter SS wires are stretched. 1200 turnbuckles are used in each dish for tensioning and shaping the facets. The mesh size varies from 10 mm  $\times$  10 mm near the central part of the dish to 20 mm  $\times$  20 mm near the outer edges.

The low solidity of the mesh surface ( $\sim 7\%$ ) greatly reduces the wind forces on the antenna. The total tonnage of the 45 m dish is thus only  $\sim 80$  tonnes, in contrast to  $\sim 250$  tonnes for a conventional 25 m dish. A counter-torque servo system using a pair of 5 KVA DC servo motors connected to azimuth and elevation axes is able to slew the dish at speeds upto  $30^\circ/\text{min}$  in azimuth and  $20^\circ/\text{min}$  in elevation at wind speeds of upto 80 kmph. The dishes are designed for survival upto 133 kmph. At low winds, the pointing accuracy is better than 1 arcmin rms. More details about the dishes are given in Swarup (1990) and Swarup *et al.* (1991). Some of the erected GMRT antennas are shown in Fig. 3.

### 3. Electronics system

A simplified block diagram of the receiver system is shown in Fig. 4. All the six frequencies have dual polarized feeds (Sankar *et al.* 1995, this issue) at the prime focus of the antenna mounted on a rotating turret (Fig. 5) which is controlled by a D.C servo

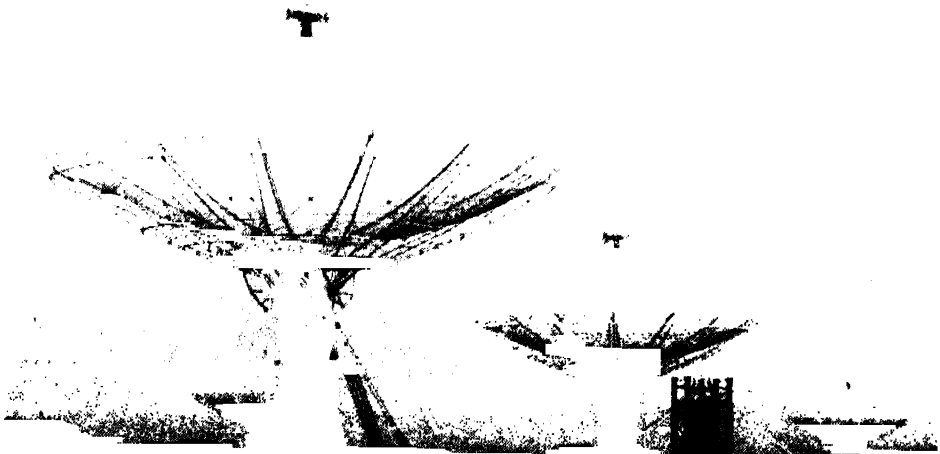


**Figure 3.** GMRT dishes in the 'central square' at Khodad.

# Block diagram of GMRT Receiver system

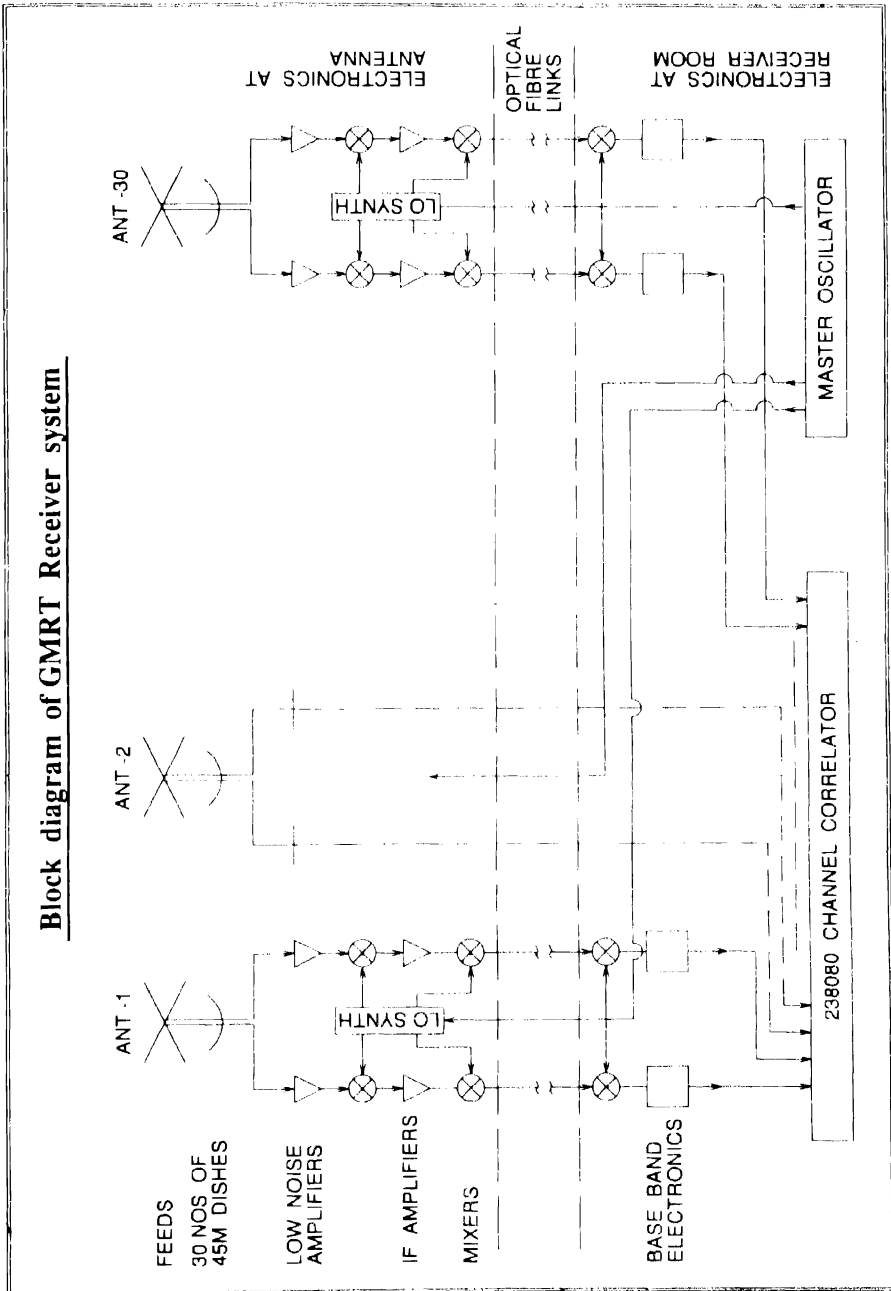


Figure 4. Block diagram of the GMRT receiver system.

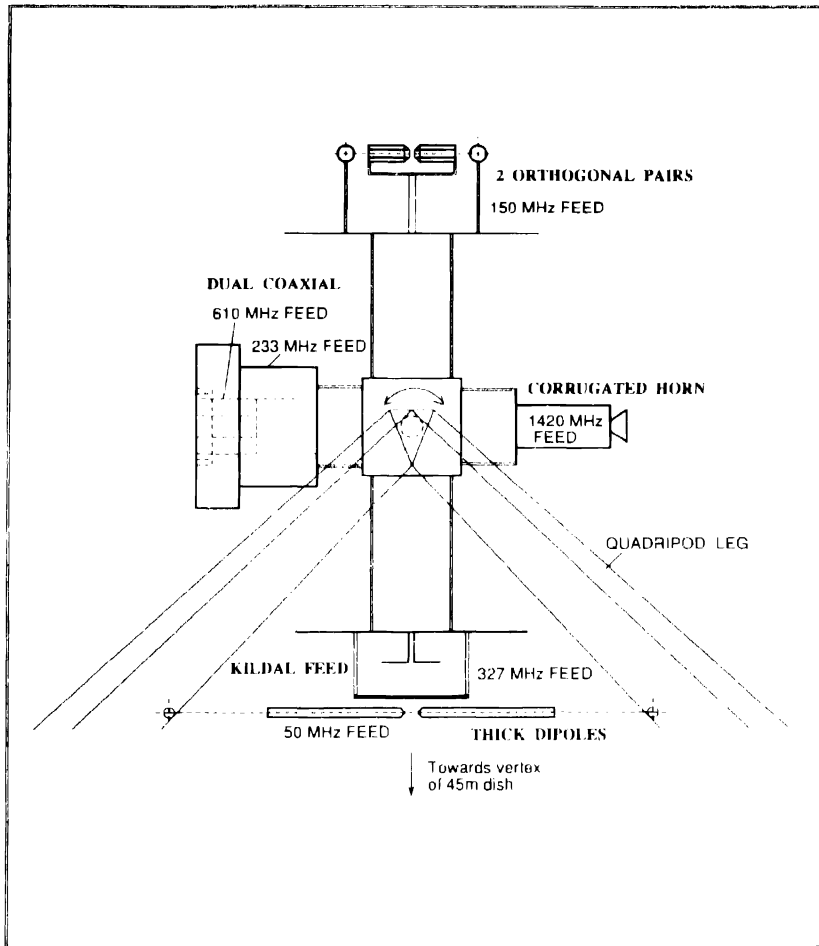


Figure 5. Configuration of feeds on the rotating turret at prime focus.

motor and encoder for precise positioning of the feeds. While the five lower frequency feeds and front-ends are being made by NCRA at Pune, the 1420 MHz system is being built by the Raman Research Institute at Bangalore.

Features of the receiver system include:

- Simultaneous observation at two frequencies (i.e., 2 frequency, 1 polarization or vice-versa).
- Low-noise uncooled RF amplifiers (A. Praveen Kumar *et al.* 1994, this issue).
- Phase switching using Walsh functions to minimize coupling between antenna electronics.
- A flexible Local Oscillator System (Venkatasubramani *et al.* 1994, this issue).
- Low-loss analog fibre optic link between the Central Electronics Building and the antennas (Sivaraj *et al.* 1994, this issue).

- Maximum IF bandwidth of 32 MHz.
- SAW filters at 70 MHz IF for good rejection of out-of-band interference signals.
- The 32 MHz IF signals down converted to two baseband signals of 16 MHz each.
- Video filters from 62.5 KHz to 16 MHz in binary steps.
- Frequency and time referencing using crystal oscillators, GPS and Rubidium standards.

The control and monitor system positions the 30 antennas with full steerability over  $\pm 270^\circ$  in azimuth and  $+15^\circ$  to  $+110^\circ$  in elevation; sets the various receiver parameters such as frequency, bandwidth and noise calibration steps and monitors the health of the systems. It further provides voice communication between the central computer and the antennas (Balasubramanian *et al.* 1994, this issue).

The receiver backend includes:

- An Fx type correlator that uses 1650 high speed FFT/multiplier chips developed by National Radio Astronomy Observatory (NRAO), USA for the Very Long Baseline Array (VLBA).
- A 256 spectral channel cross correlator for the 30 antennas giving  $(30 \times 31/2) \times 256 \times 2 \text{ pol.} = 2,38,080$  correlated outputs including self correlation products. Each of the complex outputs can be averaged over integration times selectable from 0.04s to 10s (Subrahmanya *et al.* 1994, this issue). The special purpose hardware for GMRT includes a phased array mode for Pulsars, VLBI, IPS and Lunar Occultation observations. A pulsar search machine is being designed in collaboration with the Raman Research Institute. An S2 recorder system, specially developed for the space antenna Radioastron by the Canadian scientists, will be used for both VLBI and Pulsar observations.

#### 4. Scientific studies

GMRT will be a very versatile instrument capable of investigating a variety of astrophysical objects and phenomena. These include:

- Continuum studies of the Solar System, HII regions, planetary nebulae, SNRs, Radio stars, Pulsars, metre wavelength variability, mapping of extragalactic radio sources and cosmological investigations.
- Spectral line studies involving neutral hydrogen surveys, search for protoclusters, deuterium line and recombination lines.
- VLBI observations with Ooty and other radio telescopes for pulsar parallaxes and other high resolution studies.

#### 5. System parameters

The aperture efficiency of GMRT dishes would be about 65% at frequencies between 150 and 610 MHz and about 40–45% at 50 and 1420 MHz. Table I gives the estimated values of total system temperatures at various frequencies and the resulting rms thermal noise in  $\mu\text{Jy}$  ( $1 \text{ Jy} = 10^{-26} \text{ W m}^{-2} \text{ Hz}^{-1}$ ).

**Table 1.** GMRT system parameters (30 nos. 45m dishes).

Frequency (MHz)	Primary beam (Deg)	Synthesised beam (Arcsec)	T <sub>sys</sub> (°K)	S <sub>min</sub> <sup>*</sup> (μJy)
50	9.0	60	8170	4300
150	3.0	20	578	300
233	2.0	13	234	120
327	1.4	9	108	56
611	0.7	5	102	53
1420	0.3	2	98	67

\*5 RMS over 10 hrs integration.

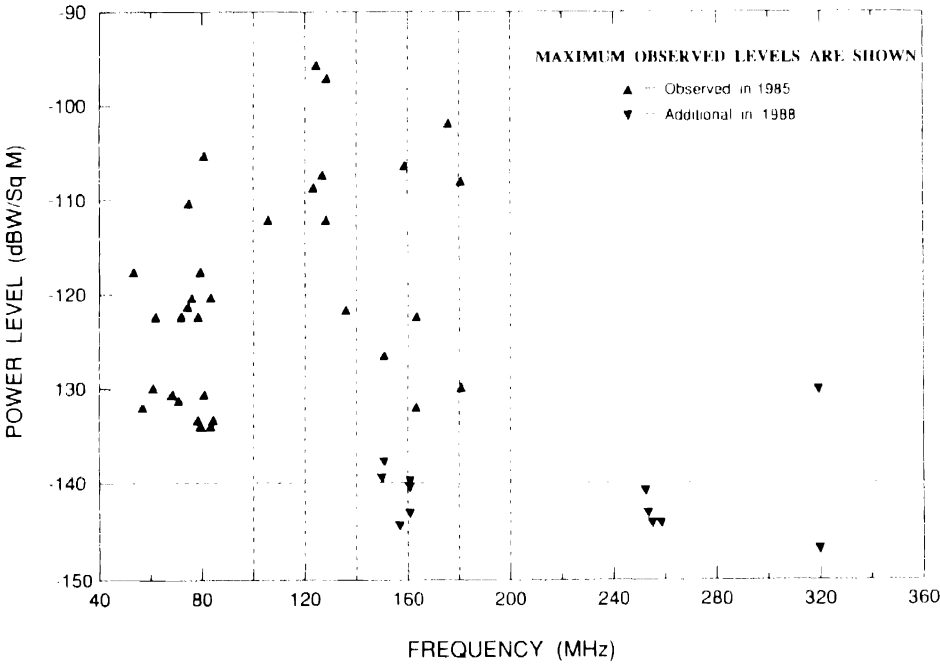


**Figure 6.** RFI survey at the GMRT site (Swarup & Venkatasubramani 1991).

A comparison of the effective areas and resolutions provided by VLA, Arecibo and GMRT facilities shows that GMRT should provide as high a sensitivity as the partially steerable Arecibo dish in the 150–600 MHz range of frequencies, while it has angular resolution comparable to the fully steerable VLA in its mid frequency range. The radio interference levels at the GMRT site are however expected to be  $\sim 10^5$  times lower than at VLA in the metre wavelength range (Fig. 6). This should make GMRT an outstanding radio astronomical facility at metre wavelengths.

### Acknowledgements

The progress made on GMRT owes a great deal to the untiring efforts of a team of 15 scientists, 35 engineers and other scientific, technical and administrative staff. I would like to thank the leader of the team, Prof. Govind Swarup for his constant guidance and support in crossing major hurdles faced by the project team. I would also like to thank colleagues at the Raman Research Institute, Bangalore for their enthusiastic support and participation in the project. Tata Consulting Engineers, Bombay have provided the engineering design of the dishes and the Reactor Control Engineering group of Bhabha Atomic Research Centre, Bombay have been associated with the servo design and fabrication of the first ten servo systems. I thank Prof. V. K. Kapahi for many helpful comments on the manuscript.

### References

- Balasubramaniam, R., Asodekar, C., Ramakrishna, A., this issue, p. 452.  
Praveen Kumar, A., Chiplunkar, A. C., Nayak, S., Sreedharan, N. G., this issue, p. 451.  
Sankar, G., Swarup, G., Ananthakrishnan, S., Sankararaman, M. R., Suresh Kumar, S., Izhak, S. M., this issue, p. 450.  
Sivaraj, D. S., Sankararaman, M. R., Suresh Kumar, this issue, p. 452.  
Subrahmanya, C. R., Dutta, A., Tatke, V. M., Puranik, U. S., Dixit, A., Joardar, S., this issue.  
Swarup, G. 1984, *Giant Metrewave Radio Telescope - A Proposal* (Radio Astronomy Centre, Ootacamund).  
Swarup, G. 1990, *Indian J. Rad. Sp. Phys.*, **19**, 493.  
Swarup, G., Venkatasubramani, T. L. 1991, *Proc. IAU Symp. 112: Light Pollution, Radio Interference and Space Debris*.  
Swarup, G., Ananthakrishnan, S., Kapahi, V. K., Rao, A. P., Subrahmanya, C. R., Kulkarni, V. K. 1991, *Curr. Sci.*, **60**, 95.  
Venkatasubramani, T. L., Ajithkumar, B., Somashekar, R., Saini, K. S., Chattopadhyay, G., this issue, p. 451.





## New Nobeyama Radioheliograph

H. Nakajima<sup>1</sup>, M. Nishio<sup>1</sup>, S. Enome<sup>1</sup>, K. Shibasaki<sup>1</sup>, T. Takano<sup>1</sup>,  
Y. Hanaoka<sup>1</sup>, C. Torii<sup>1</sup>, H. Sekiguchi<sup>1</sup>, T. Bushimata<sup>1</sup>, S. Kawashima<sup>1</sup>,  
N. Shinohara<sup>1</sup>, Y. Irimajiri<sup>2</sup>, H. Koshiishi<sup>1,3</sup>, T. Kosugi<sup>1</sup>, Y. Shiomi<sup>1</sup>,  
M. Sawa<sup>1</sup> and K. Kai\*

<sup>1</sup>*Nobeyama Radio Observatory, National Astronomical Observatory, Nobeyama, Minamisaku, Nagano 384-13, Japan.*

<sup>2</sup>*Communication Research Laboratory, Koganei, Tokyo 184, Japan.*

<sup>3</sup>*Department of Astronomy, School of Science, The University of Tokyo, Bunkyo-ku, Tokyo 113, Japan.*

**Abstract.** The New Nobeyama Radioheliograph at 17 GHz, dedicated to solar observations, was constructed and started daily routine observations in late June, 1992. It consists of eighty-four 80-cm antennas arranged in T-array extending 490 m in east-west and 220 m in north-south. It provides us with both circular polarization images of the full disk with a spatial resolution of 10 arcsec and the minimum temporal resolution of 50 ms. An image quality better than 20 dB is attained by excellent performance in hardware and software.

Hundreds of flares have been observed so far with the Nobeyama radioheliograph. Some initial new results are presented.

*Key words:* Microwave interferometer—sun—solar flare.

### 1. Introduction

A new radioheliograph at 17 GHz, dedicated to solar observations, started routine observations in June 1992. This radioheliograph provides us with high spatial and temporal resolution images of the whole Sun with high image quality.

In this paper, we briefly introduce this new radioheliograph and some initial new results from it. Details of this instrument are described in a separate paper (Nakajima *et al.* 1993a).

### 2. Outline of the Nobeyama Radioheliograph

#### 2.1 Major characteristics

Major characteristics of the Nobeyama radioheliograph are as follows:

(a) The radioheliograph operates at 17 GHz (simultaneously at both 17 and 34 GHz in near future). The receiver bandwidth is 33.6 MHz. (b) Both circular polarization components are measured with accuracy better than 1%. (c) The field of view of 40' arc, which covers the whole Sun to catch flares whenever those occur. (d) The spatial resolution is about 10" arc. The temporal resolution is usually 1 s and 50 ms for selected

\* Passed away in March, 1991.

events. (e) The dynamic range of images is about 25 dB for snapshots (Koshiishi *et al.* 1993). This high dynamic range is crucial to reveal the whole structure of flares. (f) The observing period is 4 hours per day before and after the local meridian time (about 0245 UT). (g) The sensitivity of the radioheliograph is very high. The minimum detectable flux density and brightness temperature in rms are  $4.4 \times 10^{-3}$  sfu and 1300 K, respectively, for 1 s snapshots of the Sun.

## 2.2 Antenna configuration

The array configuration of the Nobeyama radioheliograph is a multiply-equally-spaced T-array, extending 488.96 m in the east-west and 220.06 m in the north-south, as shown in Fig. 1. Eighty-four parabolic antennas are arranged with increasing antenna spacings of  $d$  (the fundamental),  $2d$ ,  $4d$ ,  $8d$ ,  $16d$  from the center of the T-array, where  $d$  is chosen to be 1.528 m corresponding to the field of view of about  $40'$ . This array configuration has a great advantage in image processing in that the FFT algorithm can be directly applied without gridding.

Each parabolic antenna of 80-cm diameter is supported by an alt-azimuth mount driven by stepping motors, which are controlled from the observation building. The half-power beam width of the element antenna is  $87'$ . The overall antenna pointing accuracy is better than  $\pm 1.5'$  arc.

## 2.3 Receiver

The RF signal at 17 GHz is amplified by an uncooled HEMT amplifier with an average noise temperature of 180 K, which is installed behind a circular polarization switch. The amplified signal is mixed with an 8.4 GHz local signal and is down-converted to a single sideband IF signal at 200 MHz, using a harmonic mixer. The IF signal transmitted from the frontend box to the observation building is mixed with a 200 MHz local signal (second local signal) and is down-converted to a video signal with a bandwidth of 16.8 MHz, using a double-sideband mixer. In the backend, complex correlations are calculated for all antenna pairs of 3486 combinations of 84 antennas, using one-bit correlators which can be assembled with simple digital logic and yield great stability to the backend.

The receivers of the radioheliograph are designed to keep the phase and gain stability in rms as good as less than  $3^\circ$  and 0.2 dB, respectively, and also phase and gain errors, especially correlator-base errors, as small as less than  $\pm 1^\circ$  and  $\pm 1\%$ , respectively.

In order to keep good phase stability, the 8.4 GHz local signal is phase-locked to a reference signal of 525 MHz which is distributed through phase-stable optical fiber cables (temperature coefficient: 0.2 ppm/ $^\circ$ C) from the observation building to each antenna.

In order to stop the fringe, the phase rotator is inserted on the second local signal line of each antenna system. The phase is changed in steps of  $0.36^\circ$  with the overall accuracy less than  $\pm 0.6^\circ$ . The delay compensation is performed in the digital backend by a step of 1 ns with accuracy less than 1 ns.

All data with 1-s time resolution are stored in optical disks of 5 Gbytes. On the other hand, all 50-ms data are stored in a high-density MT of 20 Gbytes once every day, and after the end of daily observations, a small part of flare data are selected under some criterion to be stored in the optical disks.

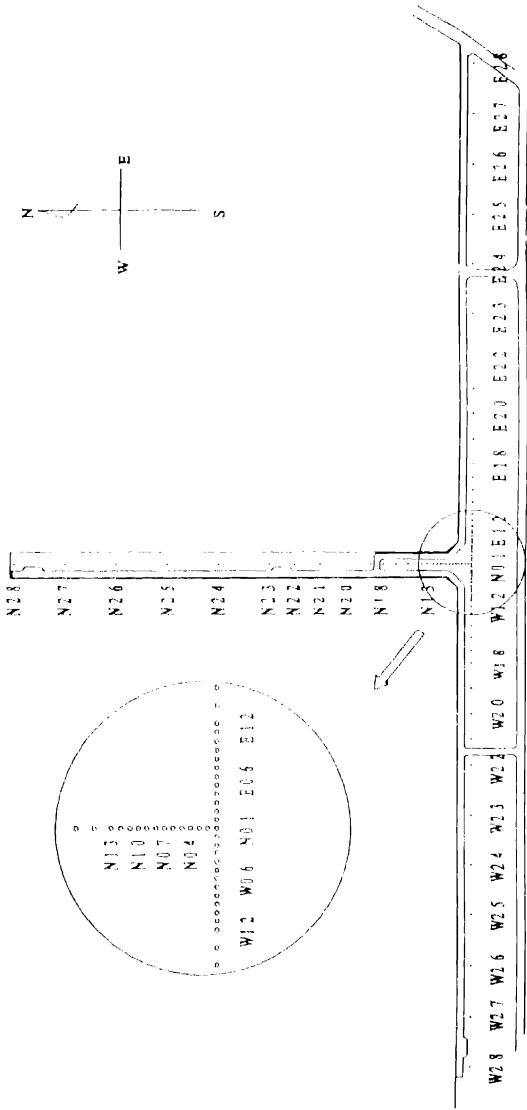


Figure 1. Array configuration of the Nobeyama radioheliograph.

Real-time images are synthesized every 10 s, and displayed on a monitor CRT as well as recorded on a video tape.

### *2.4 Calibration and image restoration*

The multiply-equally-spaced T-array has many redundant antenna combinations, which provides a useful phase and gain calibration method using the Sun itself as a calibrator. After the phase and amplitude errors included in measured Fourier components are corrected, the radio image (the dirty map) of the whole Sun are synthesized by applying the inverse FFT. Then, a model disk component convolved with the dirty beam is extracted from the dirty map, and a CLEAN algorithm is applied to the remaining map. The restored image of the Sun is given by the combined map of the cleaned map and the model disk convolved with the clean beam.

### **3. Initial results**

Hundreds of solar flares have been observed with the Nobeyama radioheliograph since late June 1992. Some pieces of information such as event lists and time profiles are publicized to outside users through 'anonymous ftp' utility of the Unix operating system at IP address of 133.40.76.80. Various solar activities have been analysed and

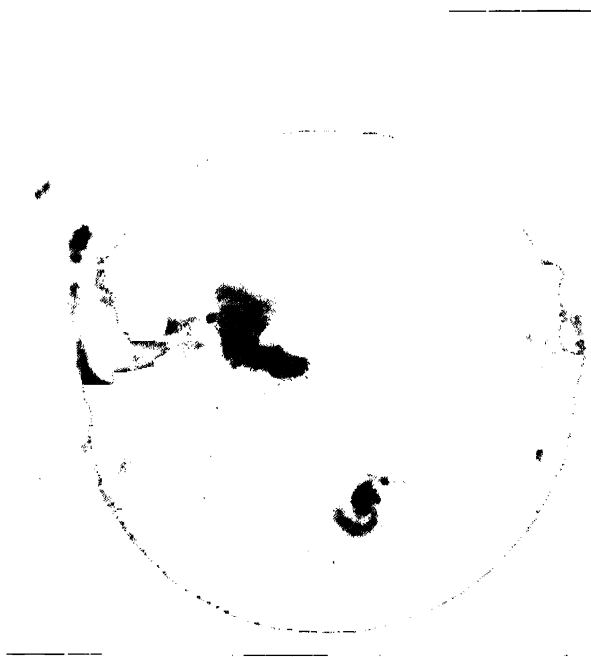


**Figure 2.** An eruptive prominence and formation of a flare arcade on July 31, 1992. This is a composite of three radio images above the solar disk, covering about 1.5 hours, and a negative disk image from Yohkoh/SXT at a later phase of the arcade formation. The flare arcade in soft X-ray forms below the eruptive prominence in radio.

## 1992.06.28 M-class Flare



**Figure 3.** Time evolution of a gradual flare observed with the Nobeyama radioheliograph on June 28, 1992. The field of view of the images is  $315'' \times 315''$ .

initial new results are obtained (Enome *et al.* 1993a, b; Hanaoka *et al.* 1993; Nakajima *et al.* 1993b; Nishio *et al.* 1993; Shibasaki *et al.* 1993; Takano *et al.* 1993). Next, we present only two examples from these initial results.

Figure 2 shows a composite of radioheliograph images at three different times above the disk and a Yohkoh/SXT image of the disk in negative form. The quiet prominence began to rise at about 2345 UT, and continued to ascend with a speed of about 10 km/s as clearly seen in the radio image in Fig. 2. After the onset of the prominence eruption, a weak thermal flare in the form of an arcade was observed below the eruptive prominence with the Yohkoh/SXT, as shown in the soft X-ray image of the disk in Fig. 3. These observations clearly show how the flare is triggered by the prominence eruption. Details of this event are given by Hanaoka *et al.* (1993).

Figure 3 shows radio images at 17 GHz of a gradual flare which occurred on the east limb on June 28, 1992. In the beginning of the flare (0228:44 UT), a polarized compact source appeared just on the limb, corresponding to the impulsive emission. Slightly after that (0242:58 UT), an unpolarized component elongated upward from the polarized compact source with a speed of 170 km/s, corresponding to the gradual emission. These observations suggest that the nonthermal emission from the polarized compact source and the thermal emission from the unpolarized elongated source are connected by a single loop, and that the upward motion of the microwave source is an indication of evaporation of the chromospheric matter heated by high-energy electrons. Details of this event are given by Nishio *et al.* (1993).

### References

- Enome, S *et al.* 1993a, *Proc. of IAU Colloquium No. 141 on the Magnetic Fields of Solar Active Regions*, Beijing, Sept. 1992.  
 Enome, S *et al.* 1993b, *Publ. astr. Soc. Japan*, (submitted).

- Hanaoka, Y et al. 1993, *Publ. astr. Soc. Japan*, (submitted).
- Koshiishi, H et al. 1993, *Publ. astr. Soc. Japan*, (submitted).
- Nakajima, H et al. 1993a, *Special Issue of the Proceedings of the IEEE on the Design and Instrumentation of Antennas for Deep Space Telecommunications and Radioastronomy*, (accepted).
- Nakajima, H et al. 1993b, *Publ. astr. Soc. Japan*, (submitted).
- Nishio, M et al. 1993, *Publ. astr. Soc. Japan*, (submitted).
- Shibasaki, K et al. 1993, *Publ. astr. Soc. Japan*, (submitted).
- Takano, T et al. 1993, *Publ. astr. Soc. Japan*, (submitted).

## Abstracts

### Project GRACE – A New Ground-Based Facility for Gamma-Ray Astrophysics Cerenkov Experiments

C. L. Bhat, R. Koul, R. C. Rannot, M. L. Sapru & A. K. Tickoo *Bhabha Atomic Research Centre, Nuclear Research Laboratory, Trombay, Bombay 400 085, India.*

A new observing facility (GRACE), based on the atmospheric Cerenkov technique, is being created for carrying out high-sensitivity investigations in the field of TeV and PeV  $\gamma$ -ray astrophysics at Gurushikar (24.65° N, 72.78° E,  $\sim 1700$  m a.s.l.). Situated close to Mt. Abu in Western India, Gurushikar can offer an average observing time of 1150 h per calendar year (Sapru *et al.* 1993). The location of the place will allow carrying out concurrent investigations with other  $\gamma$ -ray experiments at Ooty, Pachmarhi and Tien-Shan and also multi-spectral band observations with the 1.2 m infra-red telescope at Gurushikar (Deshpande, these proceedings).

Detailed studies of  $\gamma$ -ray candidate objects in the TeV energy bracket (0.2–10 TeV) will be undertaken through the Cerenkov imaging  $\gamma$ -ray telescope, TACTIC (Bhat *et al.* 1993). This generation-II instrument involves  $4 \times 10^2$  m<sup>2</sup> area alt-azimuth-mounted optical reflectors which are suitably instrumented to provide a high-rejection factor ( $> 99.9\%$ ) for the background cosmic ray events, leading to  $5\sigma$  flux sensitivity of  $\sim 7 \times 10^{-11}$  photons cm<sup>-2</sup> s<sup>-1</sup> (1 CRAB) above 0.5 TeV in  $\sim 1$  hour of observations. Unlike other imaging systems, TACTIC will attempt to record images of on- and off-source Cerenkov events concurrently. For this purpose, one telescope unit will deploy a Cerenkov Light Imaging Camera, comprising 349 photomultiplier pixels covering an overall field of  $\sim 7.2^\circ \times 7.2^\circ$  with a pixel resolution of  $0.36^\circ \times 0.36^\circ$ . The other 3 telescope units, arranged in a triangular configuration around the Imaging Unit, will generate event triggers and also spectral and timing data of the recorded events. These data, along with the event image details, will be deployed for efficiently rejecting cosmic-ray background events and achieving the stipulated detection sensitivity factor  $Q \sim 26$ .

Another experiment, Mystique, is being set up to extend the range of these investigations to the hitherto largely-unexplored, albeit promising, energy bracket of 10 TeV – 0.1 PeV (Bhat *et al.* 1991). Here, an array of upto 100 wide-angle, large-area Cerenkov light detectors will be spread over a physical area of 0.25 km<sup>2</sup>. The arrival of the conical Cerenkov wavefront will be timed to reconstruct the event arrival direction with an accuracy of  $\sim 0.2^\circ$ . This mode of operation will substantially augment the detection sensitivity, apart from keeping the cost of the Mystique array significantly low. The project work, starting in 1992, is likely to be over by 1997.

### References

- Bhat, C. L. *et al.* 1991, NRL Technical Report No. 2/91.  
Bhat, C. L. *et al.* 1993, *Proc. Towards a Major Atmospheric Cerenkov Detector-II*, Calgary, (in press)  
Sapru, M. L. *et al.* 1993, *Bull. astr. Soc. India*, **21**, 515.



## 1.2 m Infra-red Telescope at Gurushikar

**M. R. Deshpande**, *Physical Research Laboratory, Navrangpura, Ahmedabad 380 009, India.*

Near-Infra-red is one of the important windows of the electromagnetic spectrum for the study of relatively cool celestial objects. Realising the importance of the IR studies, Physical Research Laboratory decided to build an IR Observatory. Accordingly a site was selected at Gurushikar, Mt. Abu, Rajasthan at an altitude of 5650 feet. Gurushikar is the highest peak between Himalayan Ranges and Nilgiri hills. Also Gurushikar offers large number of clear nights (about 200) with low precipitable water vapour (about 3 mm) and easy accessibility. These features make Gurushikar a good site for an IR observatory.

The telescope has an aperture of 1.2m with three secondary mirrors, (i) f/13 nonvibrating secondary (ii) f/45 vibrating secondary and an (iii) f/45 coude secondary, for various applications. In addition, nodding provision for the primary mirror is also incorporated. Surface accuracy of all the mirrors is designed for the operation of the telescope in the optical region, so that the telescope can be used for optical as well as IR work. The observatory is expected to be commissioned by the end of March 1994.

Considerable parallel efforts have gone in at PRL to build back end instruments. In the optical region a state-of-the-art photopolarimeter, a CCD camera, high resolution F-P Spectrometer, a high speed photometer etc. have already been commissioned and successful scientific programmes are going on. In the near IR we have a photometer, a CVF photometer, a fast photometer, an F-P spectrometer. In the next year a near-IR FTS, a polarimeter and a CCD camera are likely to be operational.

With the above host of instruments and the observatory we look forward for exciting scientific work in the field of astronomy & astrophysics.

★★★★★

## Lucifers: A Photoelectric Radial-Velocity Spectrometer at Mt John University Observatory

**J. B. Hearnshaw, L. C. Watson & D. M. Ward** *Mt John University Observatory, University of Canterbury, Christchurch, New Zealand.*

Lucifers is a fibre-fed échelle radial-velocity spectrometer operating on the 1-m telescope at Mt John University Observatory. It produces in real time the cross-correlation function of an oscillating mask (with 2447 transmitting slots based on the spectrum of  $\alpha$  CenA (G2V) with a late type stellar spectrum. The instrument can measure the radial velocities of F, G, K and M stars with a precision of about 300 m/s. Some technical data are tabulated below:

Échelle Spectrograph	
Ruling	79 grooves/mm
Blaze angle	63° 26' (arctan 2)
Dispersion	1.75 Å/mm
in order	46
of nominal centre	502.0 nm
Mask	
Size	67 × 20.3 mm
Number of slots	2447
Wavelength range	398.1–577.3 nm
in orders	40–58
Oscillation	
Oscillation frequency	2.25 Hz
Max. range in coarse mode	6.818 ± 0.001 mm
Used range	5.932 ± 0.001 mm
Corresp. velocity range	603.2 ± 0.1 km/s
Max. range in fine mode	893 ± 0.3 μm
Used range	779 ± 0.3 μm
Corresp. velocity range	79.2 ± 0.03 km/s
Photomultiplier Tube	
Type	EMI 9924A bialkali (Cs, Sb)
Number of dynodes	11
Maximum quantum efficiency at	400 nm
H.T. used	1400 volts
Cooling method	water-cooled Peltier
Operating temperature	typically ~ -13 °C

★★★★★

## High Angular Resolution Imaging Using a Rotational Shear Interferometer

J. K. Rajagopal & N. Udayashankar *Raman Research Institute, Bangalore 560 080, India.*

Achieving diffraction-limited imaging using ground based telescopes is an area of great interest in modern optical astronomy. Of the various techniques used towards this end,

pupil plane interferometry is perhaps the one with maximum theoretical advantages. We have fabricated a Rotational Shear Interferometer (an instrument which uses the pupil plane technique) and have used it to observe bright stars, mainly at the 2 m telescope at the VBO, Kavalur.

We present the details of fabrication and use of the instrument, along with preliminary results obtained. Analysis of the present data should yield resolutions significantly better than the limits imposed by atmospheric seeing. Proposed modifications to the instrument, including an 'adaptive' tilt-correcting mirror currently being developed, are also presented.

★★★★★

### **Image Restoration by Blind Iterative Deconvolution: Results Obtained from VBT**

S. K. Saha & P. Venkatakrishnan *Indian Institute of Astrophysics, Bangalore 560 034, India.*

The blind iterative deconvolution technique was employed to deconvolve the atmospheric point spread function from specklegrams of two binaries, HR 5138 and HR 5747 obtained at the Cassegrain focus of the VBT. The residual noise in the deconvolved result is less than 5%. The position angle and separations of the binary components were seen to be consistent with results of the autocorrelation technique.

★★★★★

### **An Imaging Polarimeter for Astronomical Observations**

A. K. Sen & S. N. Tandon *Inter-University Centre for Astronomy and Astrophysics, Pune 411 007, India.*

The complexity of the structure of many astronomical objects (viz. galaxies, nebulae, comets etc.) is such that details of polarization frequently requires seeing limited resolution. A two channel imaging polarimeter has been described here which can provide seeing limited spatial resolution and highly accurate values of linear polarization by minimising the harmful effects of atmospheric variations. This can be achieved by using a Wollaston prism analyser to split a telescope image into two polarized components and simultaneously comparing them to eliminate effect due to atmospheric scintillation. The introduction of a grid at the focal plane, prevents the overlapping of o and e images on the CCD plane, where the image is refocussed. In order to keep the orientation of the two polarized components fixed in the instrument frame, the polarization vector of the image is modulated by mechanically rotating a half wave plate and readings are taken for several positions of the half wave plate to derive the polarization.

After building the polarimeter we plan to use it at the Cassegrain plane of the Vainu Bappu 2.3 m telescope (f/13 beam) to carry out imaging polarimetry of extended astronomical objects. With 10 minutes exposure time for each frame, on the GEC/EEV

P8603A CCD chip, one should be able to measure polarization values with an uncertainty of 0.7 percent, for the Seyfert N1068 ( $m_p = 17.2$  per square arc sec) when observed in  $V$  band. This uncertainty is mainly dominated by photon count statistics.

★★★★★

### **Sheikh Tahir Astronomical Centre: The Birth of an Idea and Beyond**

**M. Ilyas** *The Astronomy and Atmospheric Research Unit, University of Science Malaysia, Malaysia and Sheikh Tahir Astronomical Centre, Penang.*

The idea for the establishment of an astronomical research observatory in Penang was first presented in 1985. By early 1986, formal discussions were underway and by 1987 the concept was transformed into a broader centre. In June 1988, the project had been accepted by the State Government and the Foundation Laying Ceremony was held during a regional conference. This was also reported in the IAU General Assembly Newspaper in Baltimore. Subsequently, the concept was further expanded to establish a broad research centre including atmospheric science as well but with certain priority areas. The construction of the first phase, consisting of a 3-storey building block (including a small guest house, exhibition area and laboratories) was completed and officially launched in October 1991. Arrangements between the University and State Authorities for its long-term development and expansion were completed a year later in September 1992. The University of Science Malaysia was formally charged with the responsibility of its day to day administration and scientific development in collaboration with other State Agencies in October 1992.

The infrastructure development is now in progress and by the end of 1993, the centre is expected to be ready for observational work. To optimize the use of limited space at the Centre, the University has provided a spacious 2-storey building on the main campus housing support facilities and offices of staff. The observatory, located about 20 km on the western side of the Penang Island hill range has road access and overlooks the Indian Ocean. A rather modest facility at present, it nevertheless offers a tremendous potential for the progress of astronomical science development and education in this region. We hope that it will also be used by researchers from overseas and we look forward to their support and contribution to this small but important venture.

★★★★★

### **The Mauritius Radio Telescope**

**K. Golap, N. H. Issur & R. Somanah** *University of Mauritius, Reduit, Mauritius.*

**R. G. Dodson, M. Modgekar, S. Sachdev & N. Udayashankar** *Raman Research Institute, Bangalore 560 080, India.*

**Ch. V. Sastry** *Indian Institute of Astrophysics, Bangalore 560 034, India.*

The Mauritius Radio Telescope (Latitude  $-20^\circ$ ) is an aperture synthesis Instrument, with a 2 km long East–West arm and a 1 km long North–South arm. The E–W arm has

1024 helices with an interelement spacing of 2 m. The 1024 helices are divided into 32 groups, each having 32 helices. The groups are at 14 different heights. The maximum height difference being 35 m. The 1 km long N-S arm will be synthesized by observations spread over 64 days using 16 trolleys, each mounted with four helices. A 1024 channel correlation receiver is used to correlate the E-W arm outputs with the southern elements.

A monofilar left-handed peripheral feed helix having 3 turns and a pitch angle of  $13^\circ$  forms the basic element. Each helix has a primary beam of  $60^\circ$  and a collecting area of 4 sq. metres at 150 MHz. These elements are mounted with a tilt angle of  $20^\circ$  to the local zenith so that the instrumental zenith is  $-40^\circ$ .

In the E-W arm, 32 helices in each group are connected using a branched feeder system. To preserve the SNR, a low noise preamplifier with a high-pass filter is used at the junction of every four helices.

In the N-S arm 4 helices on each trolley are also connected using a branched feeder system and the signal from each group is amplified using a low noise amplifier. Signals in all the 48 groups are heterodyned to 30 MHz and sent to the lab. The Local Oscillator (LO) required for heterodyning (Frq. = 180 MHz) is distributed along the array using low loss Helix cable.

The 30 MHz signals are further heterodyned with a LO of 40 MHz to produce a 1nd IF at 10 MHz. After further filtering, the signals pass through an AGC to optimize SNR in the two bit three level correlators. Four IF bandwidths 3, 1.5, 0.75 and 0.15 MHz are selectable. The 10 MHz output of each receiver channel is sampled at a frequency of 12 MHz, digitally delayed and then cross correlated.

The 1024 channel correlation receiver (from Clark Lake Radio Observatory) comprises of 64 correlator boards each having 16 cross-correlators plus a self-correlator. Multiplication and pre-integration are performed by custom made asic chips developed for VLA correlator system. To avoid overflow of the accumulator, the counter is reset every  $2^{13}$  clock periods after transferring the sum into a 12 bit shift register. The sum is serially transferred into a microprocessor which accumulates it in 16 bit registers.

The correlator outputs from the 512 simultaneous interferometers are transferred to a PC via a Data Acquisition System (DAS) built around 80186 processor. The DAS controls the correlator and sets the integration time in the PC before transferring data to a SUN work station for storage and further processing.

The NS trolleys are moved along a 1 km rail track and correlations are to be recorded on 64 days. This results in 32 K complex visibilities per integration time. These are to be Fourier transformed to obtain an image of the sky with a resolution of  $4' \times 4'$  (approximately) and a point source sensitivity of 100 mJy (Dec range:  $-10^\circ$  to  $-70^\circ$ , R. A range: 24 hours).

The installation of the telescope has recently been completed. Observations to estimate the array efficiency, phase stability of the system and to study the ionospheric effects are in progress.

★★★★★

## Gauribidanur Radio Heliograph

K. R. Subramanian, M. S. Sundara Rajan, R. Ramesh & Ch. V. Sastry  
*Indian Institute of Astrophysics, Bangalore 560 034, India.*

A radio heliograph operating in the frequency range of 40 to 150 MHz is being constructed at the Gauribidanur radio observatory. This heliograph will produce images of the solar corona at several frequencies in the range of 40 to 150 MHz for coronal studies.

This heliograph located at Gauribidanur (Latitude  $13^{\circ}26'12''\text{N}$  and Longitude  $77^{\circ}26'07''\text{E}$ ) is a 'T' shaped array with the long arm along the East West direction and the short arm along the South. The dimensions of the array are 1.3 km along the East West direction and 0.45 km along the South direction. This array consists of 192 Log periodic dipoles, 128 in the East West arm and 64 in the South arm. The East West arm is divided into 32 groups of 4 elements each. In a group the signal from each element is passed through a high pass filter and a broadband amplifier. The signal from 4 elements are combined using power combiners and RG8U cables. In the South arm 64 elements are divided into 16 groups of 4 elements each. In a group the filtered, amplified and delay shifted signals from 4 elements are combined using power combiners and cables. The signal from 32 East West groups and 16 South groups will be brought to the receiver building by open wire transmission lines.

The RF signal from each group is converted into an IF at 10.7 MHz after double mixing. The 32 outputs from the East West arm and 16 outputs from the South arm will be correlated in a 1024 channel digital correlator system. Multifrequency operation is achieved by time sharing with each frequency being sequentially observed for about 100 milliseconds. This is achieved by time multiplexing the first local oscillator in the receiver system.

This radioheliograph will have a resolution of  $5' \times 8'$  and produce  $10 \times 8$  pixel image of the sun at 150 MHz. The field of view and angular resolution are frequency dependent. The zenith angle coverage will be  $\pm 45$  degrees. It is planned to track the sun for about  $\pm 2$  hours around the zenith everyday. The sensitivity is  $\approx 25 \text{ Jy}$  at 150 MHz for 1 MHz bandwidth and 10 sec integration.

All the log periodic dipoles in the East West and South arm are installed. In the East West array 8 group outputs are brought to the receiver building by open wire transmission lines. One dimensional scans of the sun at 55 MHz obtained using analog correlation receivers are being processed at present.

★★★★★

## IPS Radio Telescopes at Thaltej and Rajkot

Hari Om Vats, M. R. Deshpande, A. D. Bobra, K. S. Lali, N. S. Nirman & P. Venat *Physical Research Laboratory, Ahmedabad 380 009, India.*

Radio astronomers at PRL, Ahmedabad are exploiting the phenomenon of interplanetary scintillations for investigating (1) the density deviation and the scale sizes of the plasma irregularities in the interplanetary medium, (2) the solar wind velocity by comparing the spatial fluctuations of the pattern as it drifts across, (3) the angular size of radio sources in the range 0.1–1 arcsec. and (4) the variation of radio fluxes.

There are two large radio telescopes operating at 103 MHz at Thaltej (near Ahmedabad) and Rajkot. In fact there was one more at Surat and three telescopes were

operated simultaneously and gave some results on objective (2), but Surat telescope suffered many failures due to rain, local radio interference and security. This telescope had to be abandoned and PRL radio astronomers are planning for a better site for the third telescope. Each radio telescope consists of five sub-systems; Antenna arrays, Preamplifiers, Beamforming network, Receiver, and Data Acquisition System. The details of these are given in Vats & Deshpande (1993, *BASI*, **22**, 165). There are 64 arrays in each radio telescope. The physical collecting area of the telescope is  $5,000\text{ m}^2$  and  $20,000\text{ m}^2$  at Rajkot and Thaltej respectively. Thaltej telescope initially had a collecting area of  $5,000\text{ m}^2$  which was increased to  $20,000\text{ m}^2$  in two phases. An individual array is laid along East–West and consists of full wave dipoles separated by half wavelength. The dipoles are alternately transposed so that the signal from two dipoles add in phase. There are 16 and 64 dipoles in each array at Rajkot and Thaltej respectively. To increase the efficiency of the dipoles, there is a reflecting wire mesh at  $\lambda/4$  distance below the dipoles. The telescopes are operated in the interferometric mode and their interferometric fringes are placed in North South direction. Each telescope has two sets of 32 beams in the form of a fan with the phase centre separated by  $32\lambda$ .

These telescopes have been used for the investigations of plasma tails of comets, solar, interplanetary medium and pulsars. The studies of pulsar 0950 + 08 indicated a unique burst phenomenon on July 29, 1992. The radio burst seems to be associated with an X-ray burst from the pulsars. Similarly study of plasma tail of the comets (Halley and Austin) provided for the first time the estimates of plasma density and scale size of the irregularities in the cometary tails. The solar wind measurements provide that the coronal holes are the site for high speed plasma flow, whereas giant bipolar magnetic regions and neutral line structures emit plasma at low speed. There have been some attempts to investigate the interstellar scattering and the scale size of the plasma irregularities in the interplanetary medium.

★★★★★

## Prime Focus Feeds for GMRT Antennas

G. Sankarasubramanian, G. Swarup, S. Ananthakrishnan, M. R. Sankararaman, S. Suresh Kumar & S. M. Izhak *National Centre for Radio Astrophysics, TIFR, Pune 411 007, India.*

The chosen frequencies in the metre-wave band are six separate ones, centered at 50, 150, 233, 327, 610 and 1420 MHz. All the feeds at these frequencies provide dual, circularly-polarized outputs. The various designs chosen to fulfil the objectives of the antenna are outlined. Performance characterisation of feeds for 150, 327, 233 & 610 MHz are given. This includes principal plane patterns, cross-polar levels, SWR plots and bandwidth measurements. The feeds are mounted on the four faces of a rotating turret and the observing frequency is chosen by positioning the requisite feed at the prime focus. Estimates of aperture efficiencies of the various feeds are also provided.

★★★★★

## **Low Noise Multi-Frequency Front-Ends for the Giant Metrewave Radio Telescope (GMRT)**

**A. Praveen Kumar, A. C. Chiplunkar, S. Nayak & N. G. Sreedharan**  
*National Centre for Radio Astrophysics, TIFR, Pune 411 007, India.*

The low-noise multi-frequency front end for the Giant Metrewave Radio Telescope consists of six two-channel low-noise receivers for the six operating bands at 50, 150, 235, 327, 610 and 1420 MHz and a Common RF electronics system for band selection and further processing. Each receiver converts the two linear orthogonally polarised signals received by the antenna feeds to right-handed and left-handed circularly polarised signals (RHCP and LHCP) using low loss quadrature hybrids and amplifies them using low-noise GaAsFET amplifiers (LNA). These LNAs typically have noise temperatures of 30 Kelvin at room temperature. Phase switching is done after the amplification in order to minimise any cross-talk between the antenna electronics. The receivers can be calibrated at approximately 10%, 40% 100% or 400% of the system noise temperature ( $T_{sys}$ ) using switchable calibrated noise sources. The band selection scheme provides flexibility to observe dual circular polarisation at a single frequency band or single circular polarisation at two frequency bands simultaneously in some cases. The system also incorporates switchable attenuators for solar observations. The front-ends have a typical gain of 55 dB and a spurious-free dynamic range of 45 dB.

★★★★★

## **Local Oscillator, IF and Baseband Systems for the Giant Metrewave Radio Telescope (GMRT)**

**T. L. Venkatasubramani, B. Ajithkumar, R. Somashekar, K. S. Saini & G. Chattopadhyay**  
*National Centre for Radio Astrophysics, TIFR, Pune 411 007, India.*

The features of the Local Oscillator (LO), Intermediate Frequency (IF) & Baseband (BB) systems of the Giant Metrewave Radio Telescope (GMRT) are described. These systems form part of the frequency agile receiver being built for the GMRT.

The LO system employs phase locked loops (PLLs) & synchronous counters using 'Pulse Swallow' techniques to generate phase-coherent LO signals at all antennas, referenced to a 5 MHz source with a typical RMS phase jitter of  $< 5^\circ$ . Any differential phase variation due to path length changes are to be corrected by measuring the round-trip phase.

The IF system uses the coherent LO signals thus generated, to convert the output of the front-end system in the VHF and UHF band to a common IF band. The frequency agility of the LO, together with the high selectivity of the surface acoustic wave (SAW) filters used helps in taking care of the radio frequency interference. The dynamic range is better than 25 dB for a two-tone third order IMD specification of  $-30$  dBc. The IF signals are brought to the Central Electronics Building (CEB) by an analog optical fibre link for further processing.



The baseband system at the CEB makes these IF signals compatible to the sampler in the correlator. Each of the IF signals is translated to two video bands, by Single Sideband (SSB) conversion techniques. The Baseband system offers a wide choice of video bandwidths, from 64 KHz to 16 MHz, in octave steps.

★★★★★

## **Analog Optical Fibre Network for the Giant Metrewave Radio Telescope**

**D. S. Sivaraj, M. R. Sankararaman & S. Sureshkumar** *National Centre for Radio Astrophysics, TIFR, Pune 411 007, India*

The GMRT receiver system at the Central building (CEB) and the remote antenna sites are being linked by two way optical fibre cables, using analog communication scheme. In one direction the local oscillator and antenna control signals are transmitted from CEB to an antenna site; the intermediate frequency (IF) signals and the monitored information from the site are sent to the CEB in the other direction. The intensity of a laser diode is modulated directly by the signals (analog modulation) and detected by PINFET receivers. Compared to the digital modulation schemes, analog transmission scheme simplifies electronics at remote antennas and requires less bandwidth. Each of the sites is connected by an independent pair of fibres. The requirements of the communication links for GMRT are:

- To enable synchronising and maintaining the phase of LO systems at each antenna location and down converting the received signals in range 38–1420 MHz to two IF bands, corresponding to two polarisations.
- Transmitting the IF signals to the CEB for signal processing.
- Controlling and monitoring the antennas from the CEB.
- Establishing voice communication between the nodes.

The specifications for the optical fibre communication system are:

- |                               |  |
|-------------------------------|--|
| Channel bandwidth             | 100–200 MHz.                                     |
| Linearity                     | – 65 dBc at optical modulation depth of 3.       |
| Signal to noise ratio         | 30 dB in 100 MHz with 20 km of fibre.            |
| ■ Phase stability             | : $2^\circ/\text{km}/^\circ\text{C}$ at 100 MHz. |
| ■ Phase error (rms)           | : $3^\circ$ (1 KHz bandwidth).                   |
| ■ Reflections from connectors | : – 60 dB.                                       |

★★★★★

## **Control and Monitor System for GMRT**

**R. Balasubramaniam, C. Asodekar & A. Ramakrishna** *National Centre for Radio Astrophysics, TIFR, Pune 411 007, India.*

The control and monitor system for the GMRT project caters to the following:

- Controls and monitors the position of all the 30 antennas in azimuth and elevation.
- Sets and controls the receiver configuration like selection of frequency of observation, selection of IF bandwidth, noise calibration etc.
- Monitors the health of various electronic systems.
- Provides digital voice communication between central electronics building and antennas.

Advanced microcontroller based electronic systems have been developed for master and remote station systems. A Sun workstation located at the master station handles the positioning of all the antennas and the setting of various receiver parameters for carrying out any astronomical observations.

The system uses noncoherent FSK techniques for data transmission over optical fibre links at 256 K baud rate in SDLC format with polynomial error detecting capabilities. This system provides a bit error probability of  $10^{-12}$ .

★★★★★

### **The Correlator System for the Giant Metrewave Radio Telescope**

C. R. Subrahmanya, A. Dutta, V. M. Tatke, U. S. Puranik, A. Dixit & S. Joardar *National Centre for Radio Astrophysics, Tata Institute of Fundamental Research, Pune 411 007, India.*

The Correlator System of the Giant Metrewave Radio Telescope (GMRT) employs the 'FX' scheme for providing the cross power-spectra of signals from all antenna pairs. It handles a total of 120 analog signals (4 from each antenna) with a bandwidth of 16 MHz, which are digitised at 32 MHz, compensated for path-length differences between antennas, and routed to the FX system. The FX system consists of a set of 120 FFT engines – each sustaining the continuous input samples at 32 MHz, followed by a multiplier-accumulator (MAC) system. The MAC performs self and cross-correlations for each spectral channel (maximum of 256) resulting from the FFT engines. It provides an equivalent of a total of 238080 complex channels, with a typical time-resolution of 64 ms which could be enhanced to 8 ms for specific high time-resolution observations. The MAC section is followed by a long-term-accumulator (LTA) which reads the 238080 Complex numbers every 64 ms and provides user-selectable integration options before recording the data on 8 mm (Exabyte) tape recorders. A control system consisting of a set of microprocessors and special hardware circuitry provides synchronisation between various subsections of the correlator system. Provision also exists for self-test and diagnostic capabilities, as well as online monitoring of selected visibility channels.

The delay system performs the operations relevant to Walsh switching and online system-temperature calibration using noise reference sources injected at the front-end. The FFT system performs the operations necessary for phasing of the antennas and also provides additional inputs to the GMRT Array combiner (part of the Pulsar Machine which is being built in collaboration with Raman Research Institute). It is also planned to provide support to VLBI using the S2-recorders.

The correlator control and the functions related to online monitoring of visibilities will be performed using a SPARC-based single-board-computer (Sun1e) which is networked to the online file-server.

★★★★★



# **Astronomy in Antarctica**



## Discussion Meeting on Astronomy in Antarctica

R. D. Cannon *Anglo Australian Observatory, Epping, NSW 2121, Australia.*

*Key word.* Antarctica—astronomical sites.

As a consequence of their location, Australian astronomers are very interested in the development of astronomy in Antarctica. An energetic working group has been set up with eighteen members from eight different institutions. This group has generated a fairly detailed scientific case for doing astronomy in Antarctica; a report, edited by Dr Michael Burton at the University of New South Wales (UNSW), will be published soon in the Proceedings of the Astronomical Society of Australia. The basis of the case is the expectation that the central ice plateau may well provide the best sites on earth for doing astronomy, particularly at infrared and sub-millimetre wavelengths. The plateau reaches heights of over 4000 m, with the atmospheric pressure equivalent to altitudes of 5000 m elsewhere; it is extremely cold, averaging  $-50^{\circ}\text{C}$  and going as low as  $-90^{\circ}\text{C}$  in winter; and the precipitable water vapour ranges from 0.4 mm down to 0.1 mm. Furthermore, in contrast to the situation near the edges of the continent, the weather is very stable with low wind velocities averaging about 5 m/s. Combined with the negligible diurnal temperature change, this is expected to produce conditions of extraordinarily good seeing and led Peter Gillingham to suggest that Antarctica might also provide exceptional sites for optical astronomy.

However, the primary interest in going to Antarctica is to make infrared and sub-millimetre observations. Other speakers here will elaborate on the case, but calculations show that a 2.5 m telescope in Antarctica will gain about a magnitude over the 3.9 m AAT in the near infrared and should be about as powerful as an 8 m telescope in Mauna Kea in the mid-infrared. For sub-millimetre work, Antarctica gives access to wavelengths and hence to molecular transitions which cannot be observed from anywhere else on earth. As a first step, a team of astronomers at UNSW is preparing some infrared site-testing equipment to be used at the South Pole base during 1994. The first of these will employ a near-infrared photometer, a modified version of a detector formerly used on the Anglo-Australian Telescope, to monitor the night sky brightness; this project is being done in collaboration with the CARA group at the University of Chicago, who plan eventually to establish an international observatory in Antarctica. The second experiment will be to make microthermal measurements, initially on a 30 m high mast and later with a tethered balloon, following the techniques developed by Jean Vernin in France. Both experiments are due to go to the South Pole in January and to run through the 1994 winter.

My personal interest is particularly in optical work. Here too Antarctica offers great promise. The key considerations in this case are the quality of the 'seeing' and the amount of cloud cover. Neither of these seems to be well-known at any inland Antarctic site so the first step should be to set up site testing equipment, preferably at the Russian base at Vostok since this is closest to the centre of the plateau, or at Dome C if that site is opened up. However, there are also some drawbacks which must not be ignored even if the conditions there are superb. The biggest is that although Antarctica offers very long

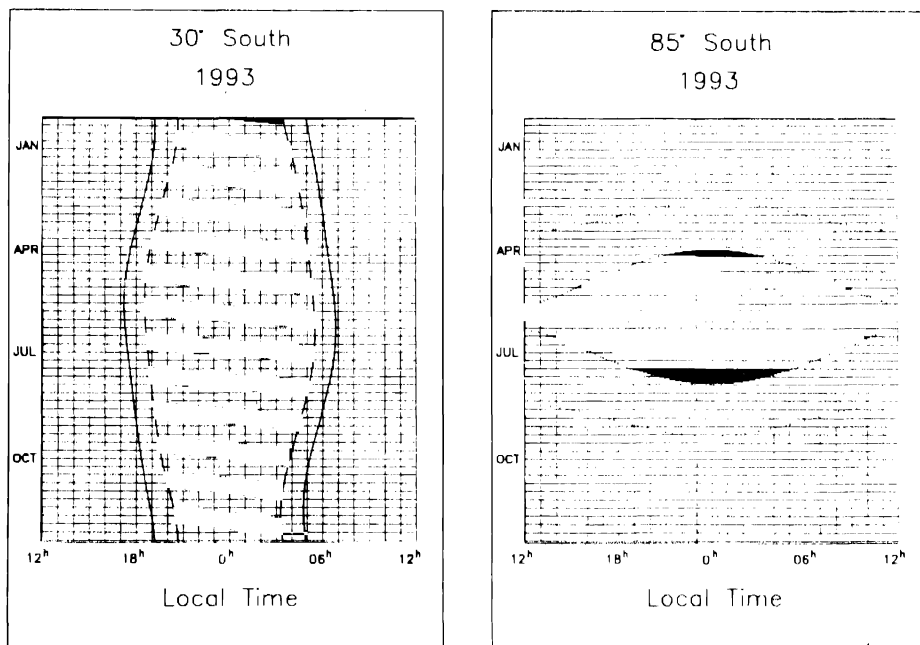


Figure 1.

nights and the prospect of continuous observing runs for 100 hours or more, there is not in fact a great deal of truly 'dark' time, defined as being when the sun is more than  $18^\circ$  below the horizon. For example, at  $-85^\circ$  there are only about half as many dark hours in a year as at  $-30^\circ$  and those hours are concentrated into just three months. Fig. 1, prepared by Steve Lee (AAO), shows the distribution of dark time throughout 1993, from January at the top to December at the bottom. The time of day runs from midday to midday across the plot, with midnight in the centre; the curved lines represent sunset, the end of evening twilight, the start of dawn and sunrise, while the dark bars indicate when the moon is also below the horizon. Of course, this problem affects only optical astronomy, not infrared work. A second hazard for optical work is the aurora, which is likely to affect all Antarctic sites to varying degree. Finally, while Antarctica offers the possibility for long observing runs and year-round accessibility of targets, as a corollary it also provides only a limited view of the sky. From  $-85^\circ$ , only about a quarter of the celestial sphere can be seen at airmasses of less than two, whereas in the course of a year three-quarters of the sky can be seen from sites at around  $30^\circ$  latitude.

My conclusion is that for infrared and sub-millimetre work, Antarctica may be so much better than anywhere else on earth as to become the major centre of the future, despite the obvious difficulties and costs of working at such an inhospitable and inaccessible site. It may also be the best place for certain types of optical observations, although it is not likely to supplant the best sites at intermediate latitudes since the gains are not so spectacular as at longer wavelengths and there are some losses.

## **Astronomy in Antarctica – India's First Attempt**

**G. S. D. Babu** *Indian Institute of Astrophysics, Bangalore 560 034, India.*

*Key words.* Antarctica—Sun.

### **1. Introduction**

During the early part of 1989, the astronomers in India and the Indian Government mutually agreed to include the programmes related to Astronomy for the first time in the on-going Indian Scientific Expeditions to Antarctica. However, since the polar night, as seen from the approximately 70°S latitude of the Indian station in Antarctica, is filled with a long spell of twilight, it was considered to be not-dark-enough for any long term observations of stars or for that matter, any other night time celestial objects. This resulted in turning the attention to solar programmes so that the polar day may be used more fruitfully. At this juncture, though an experiment related to helioseismology which needs the long term continuous and stable observations of the Sun, was thought of as the most appropriate one, the time available for its preparation turned out to be too short. So, a simpler programme involving the study of the lifetimes of the solar surface supergranules was taken up. Further, this also offered a chance for a first hand assessment of the site for astronomical observations. Thus started the first ever Indian venture of carrying out an astronomical experiment in Antarctica that was included in the IX Indian Scientific Expedition which sailed off from India on 30 November 1989 on board the ice-class ship MV/Thuleland and returned on 27 March 1990.

### **2. Instrumentation and observational programme**

The choice of an uncommon programme that required the continuous 24-hour tracking of Sun demanded some special features in its instrumentation. The heliostat which was designed exclusively for the latitude (70° 45' S) of the Indian permanent station Maitri, incorporated two 6-inch (15-cm) flats as the first and the second mirrors along with a 4-inch (10-cm) achromat lens of 10-ft (300-cm) focal length to form a 28 mm image of the sun on the blue sensitive fine grain Kodak SO-115 film of 35 mm format. The first mirror was mounted on a wheel which could rotate freely over full 360° in order to track the sun continuously for a complete 24 hour period. A Ca-K line daystar filter with a passband of 1.2 Å was fitted just in front of the camera. It was carefully fabricated at the IIA workshops in such a way that it was totally manageable under the hostile weather conditions of Antarctica. The installation of the telescope, the maintenance and the upkeep of the instrument, the actual observations and all other related tasks were carried out by just the three astronomers on site – Jagdev Singh and G. S. D. Babu of Indian Institute of Astrophysics and Wahabuddin of Uttar Pradesh State Observatory, who happen to be the very first Indian astronomers to have set foot on the icy continent of Antarctica.





**Figure 1.** An example of the Ca-K line filtergram of the sun, taken on 8 January 1990 from the Indian permanent station Maitri in Antarctica using the IIA made heliostat. The network pattern can be seen clearly alongwith other features associated with solar activity.

Each frame of the sun's picture was carefully photographed after ascertaining that the image was properly centered onto the aperture of the filter and thereby on the film that was loaded in the camera having the date/time facility. Exposures of adequate timings were taken at intervals of 10 minutes over a period of about 100 hours that remained continuously clear during the second week of January 1990. Some photographs were taken at very short intervals also for studying the evolution of flares.

It is known that besides many other features, the convective flow in the solar atmosphere gives rise to supergranulation. This phenomenon was discovered in 1959 by Leighton and others at Mt. Wilson Observatory in the dopplergrams of the sun's photospheric surface. The counterparts of these convective cells can be more easily observed in the chromospheric level, where they can be seen conspicuously in the monochromatic photographs of the sun, like the ones obtained in this programme. In these photographs, a network pattern can be seen all over the solar surface, which in turn bears a one-to-one correspondence with the supergranulation cells. Presently, these photographs are being analysed to study the temporal features of the convection cells in order to obtain their lifetimes. This is an important parameter in the evolution and decay of these cells for an understanding of their dynamics. In addition, the data acquired also contain enough material for studying the organisational processes of active regions on the sun.

### **3. Sky conditions and other related aspects**

During the period of observations, which was summer in Antarctica, the temperatures at the Indian station Maitri ranged between  $-5^{\circ}\text{C}$  and  $-30^{\circ}\text{C}$ . Only occasionally it crossed over into the  $+ve$  side. But whenever the wind speed increased, the wind chill factor brought down the temperatures effectively upto a very miserable  $-40^{\circ}\text{C}$  and below. However, as the acclimatisation to the low temperatures was fairly complete, the members of the expedition could easily work outdoors as long as the wind chill factor was not too bad.

Bad weather in Antarctica generally means a blizzard, with heavy drifting of snow along with winds upto about 100 to 200 km/hr speeds. Sometimes, the pre-blizzard period may be for about a week or so during which time the sky will remain mostly overcast. There are also times when a blizzard sets on within one day of cloudiness. Each blizzard would last for a few days, sometimes extending upto a week. Then the sky slowly clears and the clear sky would continue for some days. This is almost cyclical, but not necessarily at regular intervals. But whenever there are no clouds, the transparency of the sky appears to be excellent. During the period of observations, the sun's image was generally very stable and on many occasions the sharp demarcation of the solar limb could be clearly seen.

The moisture content in the Antarctic air is very less. It does not rain in Antarctica and the snow fall is minimal. With no other pollution in the atmosphere, the region is perhaps more suitable for infrared and millimeter wavelength observations. However, some specific programmes in the optical region like the location dependent events of eclipses, occultations and so on may be worth taking up.

### **4. Conclusions**

The first ever attempt of conducting an astronomical experiment in Antarctica by the Indian astronomers was a part of the IX Indian Scientific Expedition during the

southern summer of 1989-90. The pioneering three Indian astronomers who were included in the expedition installed a heliostat at the Indian permanent station Maitri and with that instrument observed the sun continuously for about 100 hours in Ca-K line in order to study the evolution and lifetimes of the solar surface supergranules.

The sky conditions in Antarctica are intermittently good for astronomical observations, giving excellent transparency during the cloudless spells. The humidity is very low and there is no pollution in the atmosphere. The prevailing conditions appear to be more suitable for IR and mm wavelength observations. Some location dependent events like eclipses, occultations, etc. may be taken up in the optical region in addition to any short-term phase dependent programmes.

### **Acknowledgements**

India's astronomy programme in Antarctica was first conceptualised by the Late Prof. M. K. V. Bappu. Then, it was Prof. J. V. Narlikar who took the initiative and continued the efforts in this direction. The eventual inclusion of astronomy in the on-going Indian Expeditions to Antarctica owes its origin to him. The opportunity of carrying out this first astronomical programme was given to the Indian Institute of Astrophysics by the Department of Ocean Development (DOD) of the Government of India. The programme was most efficiently co-ordinated by Prof. J. C. Bhattacharyya and Prof. K. R. Sivaraman of IIA.

## On the possibility of 200 $\mu\text{m}$ Observations in Antarctica

G. B. Sholomitskii *Space Research Institute, 84/32 Profsoyuznaya St. 117810, Moscow, Russia.*

**Key words.** Antarctica – sub-millimetre astronomy

It is a paradox that the large sub-millimeter telescopes of 10 to 15 m diameter are not very effective at the shortest wavelengths determined by their design and cost. The atmospheric water vapor blockage is strong even at the highest observatories: for example the winter transmission in 460 and 350  $\mu\text{m}$  windows at the 4350 m site in Shorbulak, Eastern Pamirs during our observations there with the 0.7 m Pulkovo telescope amounted to between 1 and 30% (Maslov *et al.* 1989; Sholomitskii & Maslov 1993). This, with an additional deterioration due to the sky noise makes sub-millimeter astronomers to look for better places on the Earth, namely in Antarctica (Stark 1990; Lynch 1991; Burova *et al.* 1986).

Situated between the Dome A and Dome C (discussed as the candidate sites for AAO) – 78° 27' south latitude and 106° 52' east longitude and 3488 m altitude is the Russian station Vostok, one of the most appropriate in Antarctica. Its general characteristics for 33 years are given in Table 1. Besides the very low temperatures the peculiarity of Vostok is a short 'warm' period in December–January and a diurnal cold one in April–October. During the day the temperature stability is very high: in winter – within 0.3 °C per 6 hours between separate measurements as compared to 7 °C in summer.

The pressure is between  $P = 618$  mb in September and  $P = 635$  mb in January (instrumental and temperature corrections were applied).

The stable wind blowing mainly from the south-west (70% of the time) is about 5 m/s. The variance during the day is about 1 m/s. Both small and large values are rare (4%) and the probability for the wind to surpass 15 m/s is about 1%.

The mean yearly precipitations are only 28 mm, most of them during the winter. The prevailing forms are the ice needles (about 50%). The visual estimates of cloudiness show clear sky (0–20% of the sky area covered by clouds) for more than half the time. One more peculiarity is the presence of a soft haze connected with the inversion layer.

The problem of aerological humidity measurements at low temperatures is well known to meteorologists. In Russia they use the intestinal film of animals and calibrate each sensor (Balagurov & Fridzon 1989). Though the uncertainty of humidity measurements at Vostok temperatures can amount to larger than 50%, we considered it useful to extend our 5 years estimates of precipitable water (Burova *et al.* 1986) to the entire period of Vostok activity from 1958 and to calculate more accurately the anticipated water vapor transmission there.

The amount of precipitable water was obtained by integrating the radio sounding balloon measurements over the pressure down to 300 mb. The mean yearly value for more than 30 years (the period recommended by WMO as the most trustful) is 0.31 mm with the very small rms of 0.02 mm. About 20% belongs to the inversion layer. The

**Table 1.** Climatic conditions at Vostok during 1958–1991.

	Value	
	Summer	Winter
Mean temperature, t (C)	– 31.9 Dec.	– 68.0
Extreme monthly	– 22.9	– 80.9
Extreme absolute	– 13.3 Jan.	– 88.3
Max mean change/6 h	– 7.0 Jan. (19 01 GMT)	0.3 July (19 01 GMT)
Pressure (mb)	635 Dec.	621
Wind speed, m/s	4.6 Jan.	5.8
Precipitation, mm	0.6 Dec.	3.8 June
Cloudiness	0.39 Jan.	0.28 July
Time of clear sky	0.53	0.62

mean winter value for 7 months between April and October is 0.19 mm thus approaching the aircraft (7.5 km) value of 0.14 mm measured by us in the middle northern latitudes (Gromov 1983). The minimal PW is 0.16 mm (August) while another extremum is 0.69 mm (January) that is still less than in the best months at Pamirs (Sholomitskii *et al.* 1982; Kanaev *et al.* 1983).

The sub-millimeter transmission of the water vapor is calculated for the average height profiles in January and July 1989 (this year was not atypical). The empirical correction for the difference in the window transmission from the theoretical one (Naumov & Zinicheva 1993) was not applied nor other atmospheric species other than WV were included. Both corrections may be unnecessary as our Pamir experience in 350  $\mu\text{m}$  and 460  $\mu\text{m}$  windows (Sholomitskii *et al.* 1982; Kanaev *et al.* 1983; Maslov *et al.* 1989; Sholomitskii *et al.* 1990; Sholomitskii & Maslov 1993) did not reveal any disagreement larger than about 30%.

The anticipated transmission at Vostok in 350 and 460  $\mu\text{m}$  windows can be 40% in the summer for the airmass  $M = 1$  (20% for  $M = 2$ ) and hence larger than that in winter time at Eastern Pamirs (Shorbulak site, 4350 m altitude). In winter the corresponding values are predicted to reach 80% and 60%, respectively. Moreover the windows at 225 and 200  $\mu\text{m}$  are expected to appear with  $M = 1$  and 2 air mass transmissions of about 35% and 10% respectively.

The astroclimatic representation of the place will be incomplete however without knowledge of a sky noise. According to our observations with the small aperture (0.7 m) telescope at Eastern Pamirs, a sky noise correlated with the atmospheric absorption is present at an important quarter-degree scale (Sholomitskii & Maslov 1993). The reason of this kind of noise is unclear but it can belong to a larger number of turbulent cells on the line of sight within the dryer atmosphere and may be expected also in Antarctica.

An expected partial transmission of the atmosphere above Vostok at 200  $\mu\text{m}$ , though requiring confirmation, makes it a unique base allowing to approach the IRAS 100  $\mu\text{m}$  band with ground based instrument observing young stars, protoplanetary nebulae, b Pic-like disks, protogalaxies, etc. in the immediate vicinity of their spectral maxima. The  $J = 13-12$  rotational transition of CO at 200  $\mu\text{m}$  and the fine structure line of NII at 205  $\mu\text{m}$  fall into this window and can be observed with a moderate size telescope of

1 m class and an uncooled superheterodyne receiver. Redshifted lines can be observed, may be OI 63  $\mu\text{m}$  line of the protogalaxy F1014 + 4724 at  $z = 2.29$  near 1207  $\mu\text{m}$ . Bright hydrogen recombination lines of the solar chromosphere falling just into windows at 460 and 350  $\mu\text{m}$  respectively are interesting for solar research.

To avoid a lot of constraints for big instruments a two element interferometer with about 10 m baseline seems to be very promising for such a research extending the angular resolution of large submm telescopes to shorter wavelengths. The brightness temperature sensitivity of superheterodynes for 1 km/s velocity resolution goes as 1 (Moran *et al.* 1984) nearly compensating the rising mixer noise temperature and atmospheric losses. Besides superheterodyne receivers, the direct interferometer with the telescopes at rigid bench as a meridian or as a fully steerable instrument is very attractive. Then due to the equal atmospheric transparency in 460 and 350  $\mu\text{m}$  windows, only moderate variances of the resulting interference 'beam' at 25.8 cm are expected from the winter to summer time.

The activity at Vostok will probably continue but because of the severely limited funding of scientific research in Russia, astronomical projects can only be realized by close international collaboration. The optical system for a wide temperature range is under study by the State Optical Institute, St. Petersburg (Russia).

## References

- Balagurov, A. M., Fridzon, M. B. 1989, *Meteorologiya i Gidrologiya* No. 5, 114.  
Burova, L. P., Gromov, V. D., Luk'yanchikova, N. A., Sholomitskii, G. B. 1986, *Pis'ma v Astron. Zhurnal* **12**, 657.  
Gromov, V. D. 1983, PhD thesis, Space Research Institute, Moscow.  
Kanaev, I. I. *et al.* 1983, *Sov. Sci. Reviews: Astrophysics and Space Phys.* **3**.  
Lynch J. T. 1991, *Report of IAU Joint Commission Meeting No. 4*, (Buenos Aires: The Development of Antarctic Astronomy) p. 16.  
Maslov, I. A. *et al.* 1989, *Pis'ma v Astron. Zhurnal* **15**, 757.  
Moran, J. M. *et al.* 1984, A submm-wavelength telescope array: scientific, technical and strategic issues, SAO, USA  
Naumov, A. P., Zinicheva, M. B. 1993, personal communication.  
Sholomitskii, G. B. *et al.* 1982, *Astron. Zhurnal* **59**, 594.  
Sholomitskii, G. B. *et al.* 1990, *Internal Report N314.305* (Moscow: Space Res. Institute)  
Sholomitskii, G. B., Maslov, I. A. 1993, *Astron. circular* **N1555**, 27.  
Stark A. A. 1990, in *Proc. 29th Liege Int. Astrophys. Colloq. "From the ground-based to space-borne sub-mm astronomy"*, **307**.



# **Regional Co-operation in Astronomy**





## Regional Co-operation in Astronomy and Astrophysics

The panel discussion on regional cooperation was chaired by J. V. Narlikar (India) and included R. D. Cannon (Australia), Y. Kozai (Japan), Li Qibin (China), Y. Sobouti (Iran), H. S. Yun (Republic of Korea) and G. Swarup (India) as speakers. Ch. V. Sastry from India also presented a brief account of the Indo-Mauritius joint project. The following is a brief account of the presentations made by speakers on the occasion.

### J. V. Narlikar

The Asia-Pacific Region is less developed with regard to A & A infrastructure, manpower and interaction, compared to North America and Europe. Keeping in view the various constraints the following steps may help improve the situation.

- a) *Facilities*: Special efforts may be made to facilitate the usage of astronomical facilities in the Asia-Pacific region by the member countries. Where new facilities, e.g. a large optical telescope, are planned serious thought may be given towards sharing the costs of a joint venture with the premium on a 'good site'.
- b) *Training schools and workshops*: There is a good case for holding regular schools for research students of the region to bring them up-to-date in the latest developments in A & A. These schools might be sponsored by the IAU and could be held annually at different venues. There is also a case for small regional workshops to bring together workers in a specific topic. Such workshops will provide wider perspective to those working in isolation.
- c) *Exchanges of academics*: The IAU programme of exchange of astronomers could be specially focussed to encourage visits of active scientists from one country of the Asia-Pacific region to another. The adhering national organizations (to the IAU) could be approached to provide more avenues for such exchanges.

★★★★★

### R. D. Cannon

#### *An Australian perspective*

- a) *The Asian-Pacific region*: Defined by the IAU to include Africa and most of what used to be known in English as the Middle East, this is an exceedingly large and diverse region. A number of parameters affect the level at which each country can undertake astronomical research, particularly research which involves the use of expensive advanced instrumentation. These include the Gross Domestic Product, the total population, the per capita GDP and of course the level of interest in astronomy, as measured for example by the number of members of the IAU. Each of these parameters varies by more than two orders of magnitude between different countries in the region. There are also differences in culture and in the level of technological development which are harder to quantify. The result is that a few

countries in the region, like India and China with their enormous populations, Australia with its high level of technological development and Japan which is both rich and populous, have a wide variety of astronomical facilities. But many of the countries have neither the wealth nor the population to build or maintain large modern telescopes, or like South Korea have only just begun to do so, so it is essential to consider co-operative projects. Given our geographical separation and cultural differences, it is going to be harder for us to work together than it was for the European countries when they set up ESO. Nevertheless there are some very encouraging examples. For example only yesterday a group of us got together for informal discussions about setting up a coordinated site-testing programme for the whole region.

- b) *Facilities in Australia:* Most of the observatories in Australia lie along an axis which is on average 200 km inland from the east coast and stretches from Narrabri in the north of New South Wales to Canberra some 550 km further south. The two main organisations for optical astronomy are the Mount Stromlo and Siding Spring Observatories of the Australian National University, which operates 2.3 m, 1.9 m and half a dozen smaller telescopes on two separate sites, and the Anglo-Australian Observatory, funded equally by the two Governments, which operates the 3.9 m AAT and the 1.2 m UK Schmidt Telescope on Siding Spring Mountain. The two principal groups for radio astronomy are the Australia Telescope National Facility of the CSIRO, which operates the six-element 6 km Compact Array near Narrabri, the Parkes 210-foot antenna and a long baseline array combining both of these with another 22 m antenna near Siding Spring; and the University of Sydney which operates the Molonglo Observatory Synthesis Telescope near Canberra. Then there are some special facilities, such as the Sydney University Stellar Interferometer (SUSI) near Narrabri and two gamma ray telescopes in South Australia, operated by the University of Adelaide and a Japanese group. There are also a number of smaller optical and radio observatories in the other states, mostly run by university groups.

Thus astronomy is particularly strongly developed in Australia, to a greater degree than many other sciences, for a mixture of historical, geographical and cultural reasons. We are well supported by the public, the media and politicians, which is just as well since astronomers do not generate a great deal of wealth directly so that we are almost totally dependent on public funding.

- c) *New facilities:* Significant enhancements to some existing facilities are being developed. The AAT has just acquired some remarkable new optics which gives it a good two-degree field of view at the prime focus, including full atmospheric dispersion compensation. This will be used with a new robotic fibre optic system allowing simultaneous spectroscopy of up to 400 objects, the whole assembly being designed for large scale cosmological redshift surveys. Plans are well advanced to extend the ATNF radio telescope in two ways, by adding more antennas across Australia and by incorporating higher frequency receivers.

Australian astronomers are also very involved in plans for new large optical telescopes. The situation is a bit similar to that in India, in that we have some quite good sites but none as good as the best in Chile or Hawaii. There is much discussion as to whether we should build a moderately large telescope in Australia or seek partners for a very large telescope at a superb site overseas. We are also actively looking at the possibilities of doing astronomy in Antarctica, especially in the infrared and sub-millimetre bands.

- d) *Possibilities for cooperation:* It may sound boastful, but given the excellent facilities in Australia there is not a great deal to attract our astronomers to work in other countries in the region, with a couple of notable exceptions like the unique GMRT here and the Japanese 8.2 m telescope, Subaru. But there is a great deal of scope for collaborative research projects whereby visiting astronomers can come to Australia to observe with Australian colleagues. In some areas of astronomy our equipment is now so powerful, for example with large optical CCDs and multi-object fibre feeds, that we can collect enough data in a few nights to keep an astronomer busy for a year. Thus we are becoming manpower limited and it would be to our mutual benefit to have astronomers from other countries spend time in Australia; the Australian astronomers would make faster progress and the visitors would become proficient in the latest observing and data reduction techniques. All we need is some source of funds to pay for the travel and living expenses of the visitors; fortunately there are quite a number of inter-governmental exchange agreements which we can and should exploit.

We already hold quite a few educational meetings in Australia, for example the annual Winter School for new PhD students organised by the Astronomical Society of Australia. This is held in a different venue and based on different themes each year. There are also special workshops from time to time on a variety of topics, both astronomical and instrumental. I realise that it can be difficult for students from some countries in the region to come to Australia, given the high cost of travel and of living in Australia, but again we have to learn to exploit existing agreements as well as seek new sources of funds.

In general I can say that Australians have recently become much more aware of their neighbours in Asia, although the ties back to Europe remain strong, and that there is a lot of Governmental encouragement for the development of closer links with countries in the Asian-Pacific region. We astronomers should take advantage of this; astronomy is a science which politicians like to support since it is interesting and relatively understandable, and it has no serious economic, environmental or strategic consequences. In the immediate future, we are very willing to welcome visitors to Australia, be they students, postdocs or senior astronomers on sabbatical. In the longer term I believe that there is a real possibility that we will be able to get together to establish new international facilities at a level which would be beyond the resources of any of us as individual nations.

★★★★★

## Y. Kozai

- a) *Space and ground-based observing facilities in Japan:* Projects for space astronomy are going on smoothly. In fact Yohkoh satellite for observing the sun by X-ray was launched in August 1992 and has detected several new phenomena already as Dr. Kosugi reported here. The 4th X-ray astronomy satellite, ASCA, was launched in February 1993 and when the operation started the supernova 1993J appeared and it could observe it in its early stage.

For a future project it is scheduled to launch VSOP satellite in 1996 with on-board 8 m radio telescope for VLBI observations together with world-wide ground-based telescopes. The analysis center for correlation computations of their observations will be in operation at the National Astronomical Observatory, Mitaka.

As you heard from Dr. Nakajima at this meeting the radio heliograph was completed at Nobeyama and has been operating since May, 1992. Now they use only 17 GHz, however, they are trying to add 34 GHz receivers to it. The observed data are available for international community by request. For the Nobeyama 5 element interferometer one more 10m dish has been added to increase its ability. At Mizusawa a 10m radio telescope has been completed mainly for geodetic project and has participated in IRIS-P (earth rotation monitoring VLBI observations in the Pacific area) network to determine parameters of the earth rotation. The Subaru project to construct an 8m optical-infrared telescope with a single meniscus mirror at Mauna Kea, Hawaii is going on as you heard from Dr. Kaifu at this meeting.

The Super-Kamiokande which will be ten times more powerful to detect neutrino flux from the sun and supernovae than the present one will be completed in 1996. A group to develop gravity wave detector was set up and is now trying to build a detector of  $2 \times 300$  m length by using very sensitive laser interferometer technique. Even theoreticians are interested in making hardware devices and have constructed a device to compute reciprocal mutual distance which quite frequently appears in N-body problem and they have used the devices for many-body numerical simulation problems.

Also smaller facilities such as the 60 cm sub-millimeter telescope Dr. Hasegawa explained here and the 4m millimeter radio telescope of the Nagoya University have made very exciting contributions and are seeking for good sites in southern hemisphere.

All the projects have been completed or in progress by international cooperations in every sense and are open for international participations. It is true also for any other facility which is not mentioned here. Already many astronomers have come to Japan to use the Nobeyama 45 m millimeter-wavelength telescope. Although no funds for their trips are available by a regulation for astronomers who come from abroad to use such facilities, we will try to find some for those whose proposals are adopted by the program committees and who could not find any funds for their trips to Japan in their home institutes.

- b) *International co-operations:* Several international co-operation programs have been in progress and this summer 10 Korean and Chinese graduate students came to Japan to attend a summer school for astronomy organized by a group of Japanese graduate students. It is very good news for us, as it was the first attempt of this kind.

Every two years astronomers in the field of star formation research hold meetings for Chinese including those coming from Taiwan, Japan and Korea. The meetings were held in China and Korea. As an outcome of the meetings, an idea of North East Asia Observatory came out and a group of astronomers will make site tests for it in western part of China in this fall. If they find a very good site they intend to bring small telescopes of infrared and/or submillimeter of special design to make observations.

International co-operation for astronomy is quite useful and helpful for Japanese astronomers on isolated islands where no good observing sites are available. Also, since I heard many of my colleagues complaining about shortage of scientists and technicians in their groups, we would appreciate it very much if astronomers come to Japan from abroad to participate in various projects

**Li Qibin**

- a) *Collaboration*: To promote the collaboration between the astronomers in Asian-Pacific region, Beijing Astronomical Observatory would like to offer two fellowships to the astronomers in our region. The objective of the program is to provide the opportunity for observational researches on solar activity, unstable stars, AGN's and large scale structure of the universe with the solar magnetic field telescope and 2.16 m telescope. The duration of the fellowship is a period of 3-6 months.
- b) *Site testing group*: Dr. Cowsik proposed to build an Asian Telescope and talked about the site testing for the scheduled telescope in a workshop yesterday. Recently, a group of astronomers from China, Japan and Korea proposed to build a North-east Asian Observatory and they will go to west China for site survey in the next month. In consideration of the common interest in the observation site testing, I suggest to establish a working group on site testing in A-P region for exchanging data, discussing the techniques and results and organizing joint survey.
- c) *X-ray satellite*: My colleague, Dr. Li Tipei and I have developed a concept on hard X-ray imager based on an image restoration method. As well known, Einstein Observatory and ROSAT have done the imaging observation in soft X-ray band. In the hard X-ray band, COMPTEL equipped on Compton GRO images the sky in the energy band higher than 700 KeV. Due to the difficulty in technology, a serious gap between 10-700 KeV remained poorly explored. My colleagues Drs. Li Tipei and Wu Mei have developed a method of image restoration with which X-ray sources can be imaged by scanning of mechanical collimator. Based on this concept, we propose to construct a hard X-ray astronomical satellite. The Hard X-ray Imager consists of a  $5^\circ \times 0.5^\circ$  collimator and a 850 cm NaI + CsI detector working in 10-300 KeV band with  $10'$  resolution and  $1'$  source location approaching. We propose the mission as a joint project APXAS-Asian-Pacific X-ray Astronomy Satellite and call for participation of the astronomers in our region. Please contact me if any one is interested in the details of the proposal.

★★★★★

**Y. Sobouti**

*Astronomy in Iran – trends and prospects*: There are of the order of 15-20 astronomers with research records and another 30-40 with substantial education in astronomy and astrophysics. Geographically, astronomical and astrophysical research is concentrated, mainly, at Shiraz University, Sharif University of Tehran (cosmology and gamma-ray astronomy), Tabriz University, and Meshed University. The Institute for Advanced Studies in Basic Sciences of Zanjan is in its developing phase. Three of its founding members, however, are established astrophysicists and cosmologists. Therefore, the Institute is expected to play a noticeable role in the promotion of astronomy in the country.

Observational facilities consist of a 20" Cassegrain and a number of smaller telescopes and photometers at Biruni Observatory of Shiraz. One 16", one 24" Cassegrain and one small solar telescope at Tabriz University Observatory. Shaheed Bahonar University of Kerman is likely to take a leap and venture the building of an observatory with a sizeable telescope. There is a significant endowment from a

benefactor to be spent for the creation of an observatory. Moreover, Kerman is a wealthy province and Kermanis have shown to be supportive of their University and its projects.

The B.Sc. curriculum of physics in Iranian Universities includes astronomy and astrophysics on an optional basis. Ten physics departments offer such options. Astrophysics at M.Sc. level is also taught within physics departments. The research record of the astronomical community of Iran is best summarized by saying that of the order of 10–15 papers based on research work in Iran find their way to international journals, and twice as much get published in Farsi language research journals.

Since five years a very respectable monthly, called 'Nojum', meaning 'astronomy' is being published. It has a wide readership among university and high school students and teachers as well as the immense number of amateur astronomers.

At present the Physical Society of Iran is the custodian of astronomy and astrophysics. It has a chapter and a committee for astronomy within itself; sets up meetings, workshops and seasonal schools for astronomers, awards prizes to young astronomers, and takes other promotional measures.

So far as the regional cooperation is concerned, there already exists a traditional exchange of knowhow between India and Iran. Many Indian scientists and technologists of all walks of life have worked and are working in Iran. Many Iranian students have always been present in Indian universities. With a minimum amount of coordination this road could be passed for astronomical collaboration between the two countries.



### G. Swarup

*Astronomy in India:* During the last 25 years a number of facilities have been established in India for astronomical observations at  $\gamma$ -rays, X-rays, optical, infrared and radio waves. Some of these facilities are briefly described below. India will welcome collaborative programmes with other observatories in the Asia-Pacific region.

a) *Optical Astronomy:* The Indian Institute of Astrophysics at Bangalore imported a 1 m Carl-Zeiss telescope in 1972 and a 2.3 m aperture Vainu-Bappu telescope at Kavalur was built in India during 1980s. These are being used for a variety of programmes in galactic and extragalactic research. IIA also operates the well known Kodaikanal Observatory for solar research. IIA has been identified as a nodal agency for a 3.5 to 4 m optical telescope to be built over the next 5–7 years.

A 1.2 m optical telescope at Japal Rangapur Observatory is used by the Osmania University for stellar observations. A 1 m Carl-Zeiss telescope is operated by the Uttar Pradesh State Observatory at Naini Tal for studies of eclipsing binaries, stellar spectra and active galaxies. UPSO has also several facilities for solar research. A 1.2 m Infra-red Telescope is being built in India for installation at Mount Abu by the Physical Research Laboratory, Ahmedabad. PRL also operates the Udaipur Solar Observatory having several facilities for solar research. The observatory is collaborating with the Global Oscillation Network Group for studying solar oscillations.

b) *Radio Astronomy:* A large 530 m  $\times$  30 m steerable radio telescope operating at 327 MHz was set up in 1970 by the Tata Institute of Fundamental Research at Udthagamandalam (Ooty) in South India for obtaining arcsec resolution using the

method of lunar occultation. It has also been used for a variety of other studies. TIFR is now constructing a Giant Metrewave Radio Telescope consisting of 30 numbers of 45 m dia dishes located over a region of about 25 km. When completed in 1995 it will become the world's largest radio telescope in the frequency range of 38–1430 MHz. It has several outstanding astrophysical objectives.

The Indian Institute of Astrophysics and the Raman Research Institute have built a Tee-shaped array (1.45 km EW and 0.45 km NS) for operation at 34.5 MHz. A Tee array (2 km EW and 1 km NS) is being built in Mauritius by RRI, IIA and the University of Mauritius for operation at 150 MHz. RRI has also set up a 10.4 m parabolic dish for observations at mm wavelengths.

- c) *Space Astronomy*: TIFR has an excellent facility at Hyderabad for launching balloon borne telescopes specially at X-ray and Infra-red wavelengths. TIFR is also collaborating with Russia for constructing a gamma-ray telescope (NATALYA II) for launch in 1994 and a 327 MHz receiver is being built for the RADASTRON VLBI mission.

It is clear that there is considerable scope for many valuable collaborative programmes in the Asia-Pacific region.

★★★★★

### H. S. Yun

*Astronomy today in Korea*: The formal introduction of modern astronomy to Korea dates back to 1957 when the Sputnik event took place. The exciting event has eventually led to the establishment of Department of Astronomy and Meteorology at Seoul National University in 1958. Ten years later Yonsei University joined in to set up Department of Astronomy and Meteorology. These two universities carried out the burden to bring up most of the young Korean astronomers today.

In 1965 the Korean Astronomical Society was founded to promote astronomical activities in Observatory (NAO). The NAO was inaugurated in 1974 as a research institute under the Ministry of Science and Technology. The NAO has been reorganized a couple of times, ending up with the Korean Astronomy Observatory (KAO) today.

There are now 7 universities with astronomy program, among which 5 universities have opened in the past several years. About one-fifth of the undergraduates continue on astronomy at the master's level. About half of the students who complete their master's work tend to go abroad for further advanced study, mostly to the U.S. since the last 15 years.

Starting with the first Ph.D. in 1965, the number of Korean Ph.D.s increased steadily at a very slow rate until 1985. Since then it grew with a much faster pace. Now the number reaches 58. When we classify them in terms of their speciality, 16% of them belong to pure theoretical group, 29% to so-called 'analysis group' (who analyse data and interpret them theoretically) and 55% to observation group. In terms of the wavelength range of their interest, 14% are involved in the radio, 10% in the IR, 66% in the optical and 10% in the UV and high energy astrophysics.

There are now in various universities two dozens of telescopes with aperture ranging from 15 cm to 75 cm, among which two 61 cm and two 75 cm reflectors are in use for research, mostly devoted to stellar photometry. The KAO has a 61 cm and a 14 m radio telescope. The 61 cm reflector was set up in 1974 on the top of Mt. Sobaek (1384 m



above sea level), but 150 kms southeast of Seoul. The radio telescope, installed in 1986 at Daeduk near Daejeon, operates at 80–120 GHz, 35–55 GHz and 150 GHz.

The KAO is constructing a new astronomical observatory at Mt. Bohyun to accommodate 3 new telescopes (1.8 m and 1 m reflectors and a solar flare telescope). The 1.8 m telescope has alt-azimuth mounting with two Cassegrain foci of F/8 and F/15 to be used for CCD direct imaging and intermediate dispersion spectroscopy. The 1 m robotic telescope is designed for automatic and intermediate dispersion spectroscopy. The 1 m robotic telescope is designed for automatic CCD imaging and photometry. The solar flare telescope comprises two 20 cm (F/8) and two 15 cm (F/15) refractors mounted on a single platform, almost identical to the one at Mitaka of the Optical Astronomical Observatory of Japan.

The Korean astronomy has made steady progress for the last 20 years. It seems that she just got out of the preparatory period to put a firm basis for active researches. Vigorous programs are being planned in the KAO and various universities. International participation is increasing at all levels. Planning for international collaboration is being considered and discussed seriously among the young colleagues. When the KAO 1.8 m, 1 m and solar telescopes are set up by 1994, the level of research activities will be greatly enhanced.

★★★★★

#### Ch. V. Sastry

*Indian Mauritius radio telescope project:* Since 1986 a Regional Collaboration program in astronomy training and research is in progress between India and Mauritius. Under this program we have built a large radio telescope for galactic centre observations at Mauritius. This is a joint project of the University of Mauritius (UOM), Indian Institute of Astrophysics and the Raman Research Institute. The details of the telescope are already presented by my colleague, Kumar Golap of UOM. We have also initiated teaching of introductory astronomy and astrophysics at the B. Sc. level at UOM. Several staff members of the UOM were trained in India in astronomy and they are now working for the Ph. D. degree of UOM.

This is perhaps the first time two developing countries got together in a major program of fundamental research. This successful south-south collaboration augurs well for future similar ventures.

★★★★★

# **Teaching of Astronomy**



## Star Watching Programme: An Effective Way to Teach the Importance of Astronomy

Syozo Isobe *National Astronomical Observatory, Mitaka, Tokyo, Japan.*

Twinkling stars under a dark night sky look very beautiful. Experience of gazing at stars could be as pleasing and refreshing as looking at a beautiful flower. However we astronomers are interested and concerned with the composition and working of heavenly bodies and the universe as a whole. This is why we would like to use beauty of stars to attract young talent in our discipline.

In our daily life astronomy plays a very little role. The common man is concerned with the calendar whose accuracy upto a few days in a year is quite tolerable. On a deeper level one could however ask the questions like the beginning of the universe, where it came from, how is the life created and evolved in the universe and so on? These questions till very recently fell in the realm of philosophy and religion. Now they have become very pertinent and valid in astronomy. Hence the study of astronomy can touch the people's imagination at a much deeper level as well.

In 1987 a global network of observing night sky brightness was undertaken in Japan in strong collaboration with an Environmental agency that proposed to find an index of air pollution in different places in Japan. Astronomers joined this programme and many local governments extended their support for this project. It ran from the summer of 1987 to the winter of 1993. Our concern was to measure the light pollution. There were large numbers of local governments and other agencies that joined our star watching programme. The idea was basically to photograph the night sky over the entire country and from there to prepare the night brightness map of Japan. There is a long zone connecting Tokyo through Nagoya to Osaka (Tokaido Megalopolis) which contains a large fraction of population, several cities and intensive industries, highways and so on. In this zone the brightness is sometimes brighter than 17 magnitude per square second of arc and people have completely lost sight of celestial objects in this zone. Fortunately there do exist some zones in Japan that are fainter than 21 magnitude per square seconds of arc.

Looking at a famous map of 'Earth at Night' brightness produced by W. Sullivan, III you can find cities shining brightly. Since this map was obtained from a satellite, light detected was mainly emitted to the sky. This energy was totally lost without illuminating the objects for which it was intended.

It is interesting to note that the brightness distribution map obtained from our star watching programme agrees very well with that of the satellite observation. This is very encouraging and exciting for all the people who participated in this programme because they feel they have made a scientifically valid observation. Thus our star watching programme has been very successful and has provided very useful data. Besides this has also, very important fall out in terms of astronomical education and creating interest in astronomy for people of all age groups. Some of them do ask questions about energy source for stars, galaxies and universe at large. This is good enough to arouse curiosity.

This programme had very strong support from the mass communication media as well, including radio, TV, newspapers, public journals and astronomical journals. It is hoped that astronomers in other countries will emulate our example and involve people at large in making a night brightness map of the earth. This will create awareness and interest in astronomy of global proportion.

# Author Index

- Ajithkumar, B., 451  
 Akabane, T., 393  
 Alladin, S. M., 204, 208  
 Anandaram, M. N., 383  
 Anandarao, B., 147  
 Anandarao, B. G., 299  
 Ananthakrishnan, S., 298, 427, 450  
 Anantharamaiah, K. R., 261, 265, 269, 273, 293  
 Anosova, J., 147, 149, 207  
 Antia, H. M., 392  
 Anupama, G. C., 206  
 Ashok, N. M., 332  
 Asodekar, C., 452  
 Athreya, R. M., 125, 203  
  
 Babu, G. S. D., 457  
 Bagchi, J., 131, 202  
 Bagla, J. S., 77  
 Bailes, M., 209  
 Baker, J. C., 125, 185  
 Bala, B., 297  
 Balachandran, S., 313  
 Balasubramanian, R., 452  
 Balasubramanian, V., 298  
 Ballabh, G. M., 208  
 Banerjee, D., 390  
 Banerji, S., 99  
 Banhatti, D. G., 149, 150  
 Basu, S., 392  
 Batten, A. H., 309  
 Bharadwaj, S., 69  
 Bhat, C. L., 148, 252, 443  
 Bhat, P. N., 195  
 Bhat, R., 251  
 Bhatia, V. B., 235, 336  
 Bhatnagar, A., 382, 384  
 Bhatnagar, A. K., 395  
 Bhatnagar, K. B., 338  
 Bhatt, B. C., 333  
 Bhatt, H. C., 296  
 Bhattacharya, D., 99, 231, 249  
 Bhattacharyya, J. C., 377  
 Biswas, S., 296  
 Bobra, A. D., 253, 449  
 Bondal, K. R., 386  
 Bramwell, D., 203  
 Breugel, van W., 125, 203  
 Burbidge, G., 87  
 Bushimata, T., 437  
  
 Cannon, R. D., 455  
 Carilli, C. L., 163  
 Carr, J. S., 331  
 Chandra, Harish, 253  
 Chandrasekhar, T., 332  
 Chattopadhyay, G., 451  
 Chaudhary, A. K., 336  
 Chauhan, J. S., 395  
 Chervon, S. V., 65  
 Chiplunkar, A. C., 451  
 Chitre, S. M., 342  
 Choudhuri, A. R., 390, 391  
 Cornwell, T. J., 265  
  
 Dadhich, N., 93  
 Das, M. K., 336  
 Das, Mousomi, 295  
 Das, P. K., 147  
 Davis, E. R., 293  
 Deshpande, A. A., 225, 275, 293  
 Deshpande, M. K., 207  
 Deshpande, M. R., 206, 253, 298, 395, 444, 449  
 deVorkin, D., 35  
 Dikpati, M., 390, 391  
 Dixit, A., 453  
 Dodson, R. G., 447  
 Duorah, H. L., 341  
 Duorah, K., 341  
 Dutta, A., 453  
  
 Ebisawa, S., 393  
 Edelson, R., 206  
 Elvis, M., 206  
 Enard, D., 419  
 Enome, S., 437  
 Erickson, W. C., 261  
  
 Filippov, N., 388  
  
 Gaur, V. P., 386  
 Gehrels, T., 1  
 Ghosh, K. K., 189  
 Ghosh, P., 171  
 Girimaji, M., 239  
 Golap, K., 447  
 Golbraikh, E., 388  
 Gopal Krishna, 153  
 Gopalswamy, N., 381  
 Gorkom, van J. H., 259

- Gorti, U., 296  
 Goss, W. M., 273  
 Gothoskar, P., 265, 289  
 Gottlöber, S., 59  
 Green, Richard, 206  
 Guhathakurta, P., 119, 259  
 Gupta, P. D., 141  
 Gupta, Y., 243, 251  
  
 Hallan, P. P., 338  
 Hanaoka, Y., 437  
 Hearnshaw, J. B., 444  
 Hibbard, John E., 259  
 Hidayat, B., 301  
 Hoyle, F., 87  
 Hughes, J. P., 294  
 Hunstead, R. W., 103, 125, 185, 204  
 Hwang, Jai-chan, 100  
  
 Ichimoto, K., 384  
 Ilyas, M., 447  
 Indrani, C., 277  
 Irimajiri, Y., 437  
 Isobe, S., 473  
 Issar, N. H., 447  
 Iwasaki, K., 393  
 Iyer, S., 149  
 Izhak, S., 243  
 Izhak, S. M., 450  
  
 Jain, R., 381  
 Janardhan, P., 253, 298  
 Joardar, S., 453  
 Jog, C. J., 295  
 Joseph, A., 340  
 Joshi, G. C., 387  
 Joshi, U. C., 206, 395  
  
 Kai, K., 437  
 Kaifu, N., 411  
 Kalra, G. L., 294  
 Kantharia, N. G., 261, 269  
 Kapahi, V. K., 125, 131, 185, 202, 203  
 Kariyappa, R., 383  
 Kaul, R. K., 252  
 Kaur, Bhavneet, 294  
 Kawashima, S., 437  
 Kembhavi, A. K., 195, 205, 206, 207  
 Khare, P., 137, 181  
 Konar, Sushan, 249  
 Korchagin, V., 207  
 Koshiishi, H., 437  
 Kosugi, T., 359, 367, 437  
 Koul, R., 443  
 Kozai, Y., 373  
 Krishna Swamy, K. S., 339  
 Krivov, A. V., 394  
 Kumar, A., 83  
 Kumar, Praveen A., 451  
 Kumar, Suresh S., 450, 452  
 Kunoff, E., 389  
  
 Lali, K. S., 449  
 Lambert, D. L., 327  
 Larson, S. M., 393  
 Lifan, Wang, 323  
 Lockman, F. J., 269  
  
 Mahabal, Ashish, 206  
 Mahra, H. S., 333  
 Mar, David P., 103  
 Markandeyulu, G., 239  
 Mathew, S. K., 382, 384  
 Mayya, D., 207  
 Mayya, Y. D., 281  
 McCarthy, P. J., 125, 203  
 McConnell, D., 293  
 McCulloch, P. M., 293  
 Mekkadon, M. V., 332  
 Miri, Jahan M., 231  
 Mishra, S., 235  
 Mishra, V. D., 146  
 Mitra, A. K., 148  
 Modgekar, M., 447  
 Mohan, V., 205, 333  
 Mückel, J. P., 59  
 Murali, P., 391  
  
 Nakajima, H., 437  
 Narasimhan, K. S. V. S., 204, 208  
 Narlikar, J. V., 87  
 Nayak, S., 451  
 Nayar, S. R. P., 297  
 Nirman, M. S., 449  
 Nishio, M., 437  
  
 Padmanabhan, T., 47, 77, 83  
 Paliwal, D. C., 333  
 Panchapakesan, N., 235  
 Pande, M. C., 385, 386, 387  
 Pandey, A. K., 333  
 Pandey, G., 327  
 Pandey, S. K., 205  
 Panjaitan, E., 393  
 Park, J. S., 334  
 Park, Y. D., 384  
 Parui, R. K., 251  
 Patel, L. K., 93, 99  
 Payne, H. E., 261  
 Petrovskaya, I. V., 295  
 Pettini, Max, 103  
 Prabhu, T. P., 195, 207, 317  
 Prabu, T., 239  
 Prasad, Debi C., 384  
 Puranik, U. S., 453

- Qibin, Li, 323  
 Qingkang, Li, 204
- Radiman, I., 393  
 Ragland, S., 332  
 Rajagopal, J. K., 445  
 Ramakrishnan, A., 452  
 Ramaprakash, A. N., 141  
 Ramesh, R., 448  
 Ramkumar, P. S., 239  
 Rana, N. C., 137  
 Rannot, R. C., 252, 443  
 Rao, A. P., 289  
 Rao, N. K., 327  
 Rawat, H. S., 252  
 Ray, A., 215  
 Rickett, B. J., 251  
 Roshi, A. D., 269, 293
- Sachdev, S., 447  
 Saha, S. K., 446  
 Sahai, R., 255  
 Sahni, V., 73  
 Sahu, Devendra, 205  
 Saini, K. S., 451  
 Sandhu, B. S., 395  
 Sankaraman, M. R., 450, 452  
 Sankarasubramanian, G., 450  
 Sapre, A. K., 146  
 Sapru, M. L., 252, 443  
 Saravanan, T. P., 275  
 Saripalli, Lakshmi, 204  
 Sastry, Ch. V., 447, 448  
 Sathyaprakash, B. S., 73  
 Sato, K., 37  
 Sawa, M., 437  
 Schweizer, F., 259  
 Sekeles, B., 390  
 Sekiguchi, H., 437  
 Sen, A. K., 395, 446  
 Senecha, V. K., 252  
 Shandarin, S. F., 73  
 Sharma, M. K., 336  
 Shibasaki, K., 437  
 Shinohara, N., 437  
 Shiomi, Y., 437  
 Sholomitskii, G. B., 461  
 Shrivastava, P. K., 297  
 Shuhua, Ye, 397  
 Shukla, R. P., 297  
 Shukre, C. S., 340  
 Singh, K. P., 195, 206, 294  
 Singh, V. P., 336  
 Siregar, S., 392  
 Sivaraj, D. S., 452  
 Sivaraman, K. R., 383  
 Sole, M., 395  
 Somanah, R., 447
- Somasekhar, R., 451  
 Soundararajaperumal, S., 189  
 Spoelstra, Th. T. A., 201  
 Sreedharan, N. G., 451  
 Sreekumar, P., 285  
 Srikanand, R., 181  
 Sridharan, T. K., 277  
 Srinivasan, G., 275  
 Srivastava, N., 382  
 Steinitz, R., 388, 389, 390  
 Subrahmanya, C. R., 125, 185, 203, 243, 453  
 Subrahmanyam, R., 111, 204  
 Subramanian, K., 83  
 Subramanian, K. R., 448  
 Sundara Rajan, M. S., 448  
 Swarup, G., 450
- Tagare, S. G., 391  
 Takano, T., 437  
 Tandon, S. N., 403, 446  
 Tatke, V. M., 453  
 Tavakol, R. K., 336  
 Thakur, Neeharika, 205  
 Tickoo, A. K., 252, 443  
 Tikekar, R., 93, 99  
 Titov, V. B., 394  
 Tokunaga, A. T., 331  
 Torii, C., 437  
 Tripathy, S. C., 381, 382
- Udayashankar, N., 445, 447  
 Uddin, Wahab, 385, 386, 387  
 Urpın, Vadim, 249
- Vaidya D. B., 299  
 Vardya, M. S., 339  
 Varma, R. K., 149  
 Vats, Hari Om, 253, 298, 449  
 Velusamy, T., 293  
 Venat, P., 449  
 Venkatakrishnan, P., 446  
 Venkatasubramani, P. L., 451  
 Venugopal, V. R., 204, 299  
 Verma, V. K., 385, 387  
 Viallefond, F., 275  
 Vivekanand, M., 247, 251  
 Vyas, G. D., 253
- Ward, D. M., 444  
 Watson, L. C., 444  
 Williams, I. P., 296  
 Wilson, W. E., 293
- Xizhen, Zhang, 145, 201
- Yi, Tong, 204  
 Yumin, Wang, 201  
 Yun, H. S., 334, 384
- Zhao, Jun-Hui, 273









